

209487 .

NASA
Technical Memorandum 109040, Volume 3

ATCOM
TR-93-A-012 , Volume 3

384 p.

Investigation of the Aerodynamic Environment for an Advanced Lightweight Rotor in Forward Flight

*Volume 3: Laser Velocimeter Inflow Data, Advance
Ratio of 0.37, Thrust Coefficient of 0.0064 and Hover
Tip Speed of 603 Ft/Sec*

*W. Derry Mace
Lockheed Engineering and Sciences Co.
Hampton, Virginia*

*Joe W. Elliott
Aeroflightdynamics Directorate
JRPO
NASA-Langley Research Center
Hampton, Virginia*

*Martin A. Peryea, Albert G. Brand and Tom L. Wood
Bell Helicopter Textron Inc.
Fort Worth, Texas*

November 1993



(NASA-TM-109040-Vol-3)
INVESTIGATION OF THE AERODYNAMIC
ENVIRONMENT FOR AN ADVANCED
LIGHTWEIGHT ROTOR IN FORWARD
FLIGHT. VOLUME 3: LASER VELOCIMETER
INFLOW DATA, ADVANCE RATIO OF 0.37,
THRUST COEFFICIENT OF 0.0064 AND
HOVER TIP SPEED OF 603 FEET/SECOND
(Diskette Supplement) (NASA)

N94-26497

Uncles

G3/02 0209487

384 p

National Aeronautics and
Space Administration

Langley Research Center
Hampton, Virginia 23681-0001

Summary

An Advanced Lightweight Rotor (ALR) model was tested in high speed forward flight in the 14- by 22-Foot Subsonic Tunnel at the NASA Langley Research Center. The pressure instrumented rotor, provided by Bell Helicopter, was a four-bladed, Mach-scaled, bearingless, soft-in-plane design. Rotor performance data were acquired from Bell's Powered Force Model (PFM) test stand, and the blade airloads were obtained using 92 unsteady pressure transducers. A two-component laser velocimeter was used to obtain azimuthally dependent velocities in the inflow region and in the wake of the rotor. The laser velocimeter acquired inflow data are presented in this report without analysis. To facilitate the use of the data, they are also provided on 1.4 Megabyte 3.5-inch floppy disks in Microsoft MS-DOS format.

Introduction

Investigators have worked on various phases of identifying the wake structure and how it relates to blade airloads (references 1-4). A key element of these studies has been the establishment of the wake geometry, whether defined from flow visualization or other measurements. Comparisons of available rotor performance test data with various analyses show improved correlations at high advance ratio when a free wake model is used in the analysis. Harris (reference 5) noted that the free wake analysis model included in CAMRAD (reference 6) predicts substantial induced drag for a rotor operating at high advance ratio and thrust, particularly over the aft portion of the rotor disk. Understanding the physical processes responsible for the high induced drag requires detailed information concerning the unsteady blade airloads and the surrounding unsteady flow field. Extensive measurements (references 7-9) have documented the induced inflow variations for a model rotor in forward flight. Blade surface pressure measurements have also been obtained in separate efforts, such as the works indicated by Hooper in reference 10, or more recently the pressure instrumented model rotor test at the German-Dutch Wind Tunnel DNW (reference 11). Such measurements serve as a needed vehicle for the validation of existing and emerging aerodynamic computer prediction codes, but comprehensive measurements of the rotor blade loads and rotor flow field nevertheless remain relatively sparse. In particular, a complete simultaneous measurement of inflow velocities, wake velocities, and blade pressures from a single test configuration in forward flight has not been available. Better insight into the validity of the free-wake blade load computations could be gained by combining experimental measurements of blade airloads with flow field velocity data for a single rotorcraft configuration. Variations of the rotor tip speed could serve to address questions that have been raised regarding the impact of tip speed on the rotor wake structure (reference 12).

A joint government/industry test program was initiated which concentrated on four flight conditions. The purpose of the test was to investigate the aerodynamic environment of a rotor operating at high advance ratio, high thrust, and with a significant degree of propulsive force. Data concerning flow field velocities and blade pressures for two tip speeds and two thrust coefficients were acquired. The data base provided by this volume includes the induced inflow velocities above the rotor plane, rotor forces and moments, as well as the model operating conditions for one of the four flight conditions tested. There were no velocity data acquired in the wake of the rotor for this flight condition. Two other flight conditions are reported in separate volumes, while the induced inflow velocities and blade pressure measurements at an advance ratio of 0.37, thrust coefficient of 0.0081 and hover tip speed of 710 ft/sec are contained in reference 13. References 14 and 15 provide the first analyses utilizing portions of this data base.

Notation

A	rotor disk area, πR^2 , ft ²
A_0	constant term in Fourier series of blade feathering (collective) at $r/R = 0.7125$, deg
A_1	coefficient of cosine term in Fourier series of blade feathering at $r/R = 0.7125$, deg

B_1	coefficient of sine term in Fourier series of blade feathering at $r/R = 0.7125$, deg
b	number of blades
C_P	blade pressure coefficient, $(P - P_\infty)/(0.5\rho V_{\text{local}}^2)$
C_P	rotor power coefficient, $p/\rho AV^3_{\text{tip}}$
C_X	rotor propulsive force coefficient, uncorrected, $X/\rho AV^2_{\text{tip}}$
C_{Xc}	rotor propulsive force coefficient, corrected for hub tare, $C_X + 0.0001198$
C_Q	rotor torque coefficient, $Q/\rho ARV^2_{\text{tip}}$
C_T	rotor thrust coefficient, $T/\rho AV^2_{\text{tip}}$
c	rotor blade chord, in
EI	bending stiffness, lb-in ²
GJ	torsional stiffness, lb-in ²
P	rotor power, ft-lb/sec
P	local static pressure, lb/in ²
P_∞	free stream pressure, lb/in ²
Q	rotor torque, ft-lb
q	dynamic pressure, lb/ft ²
r	local radius of a rotor blade cross section, ft
R	rotor radius, ft
T	thrust produced by the rotor, perpendicular to the tip path plane, lb
U	streamwise component of velocity, positive downstream, ft/sec
U_∞	free stream velocity, positive downstream, ft/sec
u_i	induced component of velocity parallel to the tip path plane, positive downstream, ft/sec
V	vertical component of velocity, positive up, ft/sec
V_{local}	flow velocity relative to blade, $\Omega r + U_\infty \sin\psi$, ft/sec

V_{tip}	rotor blade tip velocity, ΩR , ft/sec
v_i	induced component of velocity normal to the tip path plane, positive up, ft/sec
X	rotor propulsive force, positive forward (wind axis), lb
x/c	chordwise position, percent
y/c	vertical distance from the chord line, percent
x	distance from the rotor center of rotation, measured along the x coordinate axis, positive downstream, in
y	distance from the rotor center of rotation, measured along the y coordinate axis, positive to right, in
z	distance from the rotor center of rotation, measured along the z coordinate axis, positive up, in

Symbols

α	angle between tip path plane and free stream velocity, positive nose up, deg
λ	inflow ratio normal to tip path plane, positive up, $(U_\infty \sin \alpha + v_i)/V_{tip}$
λ_i	induced inflow ratio normal to tip path plane, positive up, v_i/V_{tip}
μ_∞	rotor advance ratio, $U_\infty \cos \alpha / V_{tip}$
μ	inflow ratio parallel to tip path plane, positive downstream, $(U_\infty \cos \alpha + u_i)/V_{tip}$
μ_i	induced inflow ratio parallel to tip path plane, positive downstream, u_i/V_{tip}
σ	standard deviation
Ω	rotor rotational speed, radians/sec
ψ	rotor azimuth measured from downstream position, positive counterclockwise as viewed from above, deg
ρ	air density, slug/ft ³
σ	rotor solidity, $bc/\pi R$
θ	blade pitch angle at specified azimuth, positive nose up, $r/R = 0.7125$, $\theta = A_0 - A_1 \cos \psi - B_1 \sin \psi$, deg
\overline{xx}	mean values

Experimental Apparatus

The experiment was conducted in the NASA Langley Research Center 14- by 22-Foot Subsonic Tunnel using Bell Helicopter Textron's Powered Force Model (PFM), a pressure-instrumented Advanced Lightweight Rotor (ALR) and a two-component laser velocimeter (LV).

The 14- by 22-Foot Subsonic Tunnel is an atmospheric, closed-circuit wind tunnel of conventional design with enhancements for the testing of powered and high-lift configurations (reference 16). The tunnel is pictured in figure 1 and is shown schematically in figure 2. This investigation was conducted with the walls and ceilings raised leaving a solid floor and a flow collector at the rear of the test section. The maximum tunnel velocity in this configuration is approximately 170 knots. This configuration was selected because it provided the LV system with unrestricted optical access to the test section.

Powered Force Model

Bell Helicopter Textron's Powered Force Model (PFM) is a general purpose rotor test stand designed to test Mach-scaled rotors. Figure 3 shows the PFM installed in the forward part of the test section. The PFM can accept rotors from 4 to 10 feet in diameter and operate at a maximum of 3000 RPM. As shown in figure 4, the PFM is comprised of an input quill assembly, pitch change mechanism, yaw change mechanism, test stand dynamic isolator unit, a five component rotor balance and swash plate for blade pitch controls. The input quill accepts two variable frequency electric motors rated at 75 HP each. Rotor pitch rotation takes place about the input quill axis by a pitch change actuator mechanism. Yaw rotation of the rotor pylon occurs above the input quill along the drive shaft axis. The test stand isolator consists of four rubber dampers that can be adjusted or locked-out depending on the rotor frequency requirements.

The non-metric fairing, shown in figure 5, was designed to minimize test stand aerodynamic interference with the rotor. The cross-sectional shape utilizes a NACA 0033 airfoil shape. The five component balance can resolve the rotor forces into conventional forces and moments. Mast torque is measured by a separate strain gauge located below the rotor hub attachment point. The rotor mast is driven through a flex-coupling designed to eliminate transmission of extraneous loads into the balance. The rotor cyclic and collective control are mounted above the rotor balance.

Advanced Lightweight Rotor System

The Mach-scaled Advanced Lightweight Rotor is a four-bladed, bearingless, soft-inplane design. Two stacked fiberglass flex-beam yokes and four composite rotor blades with integral cuffs and elastomeric shear dampers comprise the rotor system. The rotor characteristics are summarized below and airfoil coordinates are summarized in table 1.

ALR and Blade Characteristics

Hub Type	Flex Beam
Number of Blades	4
Root cut-out, inches	9.00
Geometric pitch-flap angle, deg	51.71
Twist Linear, deg	-8.0

Radius, inches	48.00
Airfoil chord, inches	3.720
Geometric solidity, σ	0.098674
Weight (per blade), lb	1.699
Flapping Inertia, slug-ft ²	0.2151
Lead/Lag damping, in-lb/deg/sec	182.4

The airfoil coordinates shown in table 1 are defined at a specific radius or over a range on the blade. Linear interpolation was used to transition between subsequent values given in the table. The blade twist distribution is shown in figure 6 and the blade structural properties are tabulated in table 2.

The PFM data acquisition system uses an HP3852A Data Acquisition and Control Unit that receives and stores data from several sources, including the test control computer, the Rotor Synchronized Digitizer (RSD) and NASA's Static Data Acquisition System. The data acquisition system is shown schematically in figure 7. The RSD is a 32 channel sample and hold analog to digital converter. The sampling is triggered by an optical shaft angle encoder that is also used by the LV system.

Laser Velocimeter (LV) System

The LV system used in this investigation was designed to measure the instantaneous components of velocity in the longitudinal (streamwise) and vertical directions as described in reference 17. The system is comprised of four subsystems: optics, traverse, data acquisition, and seeding. The optics subsystem, shown in figure 8, operates in backscatter mode and at high power (4 watts in all lines) in order to accommodate the long focal lengths needed to scan the wide test section. The transmitting and receiving optics packages are augmented by a zoom lens system consisting of a 3-in. clear aperture negative lens and a 12-in. clear aperture positive lens. Bragg cells in each optical path provide a directional measurement capability. The velocity measurements are made at a point in space where the four beams cross, called the sample volume. The length of the sample volume (transverse to the flow direction) increases as the sample volume is moved away from the optics assembly. Over the 10 to 20 foot focal length the sample volume is less than 1 cm long with a nearly constant diameter of 0.2 mm.

The traverse subsystem provides five degrees of freedom in positioning the sample volume and is controlled by the same computer that is used for data acquisition. Translation of the sample volume in the horizontal and vertical directions is accomplished by displacing the entire optics platform. Translation along the lateral axis is accomplished by displacing the negative lens location in the zoom lens assembly, thus refocusing the sample volume along the axis of optical transmission. The other two degrees of freedom, pan and tilt, are implemented by rotating the final mirror about its vertical and horizontal axis in order to change the direction of optical transmission. The total inclusive range of the traversing system is 7 feet vertically, 6 feet streamwise, 16.5 feet laterally, and 7 degrees in both pan and tilt. Measurements can be made outside of this envelope by repositioning the optics platform, which is mounted on wheels to facilitate such relocations. For this study, the traversing system was positioned to the left of the test section when looking downstream as shown earlier in figure 3.

The LV data acquisition subsystem, shown schematically in figure 9, interfaces with the optical signal processing equipment to receive two channels of raw LV data and up to five channels of auxiliary data. In this investigation, the tunnel and model parameters were passed from the 14- by 22-foot Tunnel Static Data Acquisition System (SDAS) and Bell's Model Data Acquisition System (MDAS). Two of the auxiliary channels (one each for the U and V components) measured the azimuthal position of the rotor shaft. The system converts the raw LV data to engineering units and determines the statistical characteristics of the

data so that the preliminary test results can be evaluated during the acquisition process. The raw data which is acquired from the buffer interface device and the 64 parameters which are acquired from the SDAS and MDAS are written to magnetic tape for later analysis. Another function performed by the data system is to interface with and control the five degree-of-freedom traversing subsystem.

The seeding subsystem, shown schematically in figure 10, is a solid particle, liquid-dispensing system (reference 18). Solid polystyrene latex microspheres are suspended in 100 proof Ethanol and dispensed into the tunnel flow. Polystyrene particles are used because of their low density, high reflectivity and precise particle size. The particles used in this investigation were 1.7 microns in diameter with a standard deviation of 0.0239 microns. The particle mixture is pumped to an array of nozzles where compressed air is used to atomize the mixture. These nozzles are mounted on a frame in the settling chamber of the tunnel as shown in figure 11. The position of the frame is remotely controlled by the laser operator during the data acquisition process. The low vapor pressure of the mixture allows it to evaporate as it travels the 85 feet from the settling chamber to the test section. This process provides isolated single particles in the flow field whose velocities are measured as they pass through the sample volume. The local fluid velocity is inferred from the seed particle velocity.

Error Analysis

The overall LV system error is obtained by summing the error of all of the components that contribute to an error in the velocity measurement. The error sources are summarized in table 3 and are defined in references 19 and 20. They result in a velocity bias error of -0.32 to 0.84 percent and a random error of 0.37 percent. Taking the square root of the sum of the squares of these values yields a total system error of 0.49 to 0.92 percent of the measured velocity.

Test Procedures

Inflow Velocities

Inflow velocity measurements were taken along radials spaced azimuthally by increments of 30 degrees from the downwind position. The inflow measurement points were kept a constant 3.72 in. (one chord length) above the rotor tip path plane. Note that the tip path plane was derived from the blade coning and first harmonic flapping motion. Measurement points along each radial were selected to coincide with the radial location of the pressure transducers mounted in the instrumented rotor blades and extended from $r/R = 0.2$ to a point outside the blade tips at $r/R = 1.10$. Figure 12 shows the inflow measurement locations superimposed on the rotor disk. The rotor tip path plane was set at -5.8 degrees relative to the free stream to produce a propulsive force coefficient of 0.0003. The tip path plane was maintained at -5.8 degrees by setting the shaft angle to -5.8 degrees and zeroing the first harmonic of the yoke beam bending at station 0.15. The operating rotor speed was approximately 1445 RPM, the nominal tunnel speed was 224 ft/sec resulting in an advance ratio of 0.37. The model RPM and tunnel speed were set to achieve a constant advancing tip Mach number, which for this test condition was 0.525. The nominal rotor thrust coefficient, C_T , was 0.0064.

The LV data acquisition process consisted of placing the sample volume at the location to be measured and acquiring 4096 individual velocity measurements for both the U and V components. This process typically requires less than two minutes per measurement point. During this time, conditional sampling techniques were employed to measure the azimuth of the rotor. Each of the 4096 instantaneous velocity measurements were thus permanently identified with a known rotor azimuth angle so that the data could

be cycle averaged. At the conclusion of this process, the measurement location was changed and the acquisition process repeated.

Wake Velocities

There were no wake velocity data acquired for the $C_T = 0.0064$, $V_{tip} = 603$ ft/sec flight condition. The wake data which were acquired for the other flight conditions are reported on figures 13 and 14 of Volumes 1 and 2 of this report. Figures 13 and 14 of Volume 3 are intentionally left blank.

Data Reduction

Velocity Measurements

Each velocity measurement has associated with it an encoder signal indicating the position of the blades when the measurement was made. This information was used to sort the velocities into 128 bins, each 2.81 degrees wide, encompassing the 360 degrees of blade rotation. This sorting process was required to present the data that required up to two minutes (2900 rotor revolutions) to acquire in a format of a single rotor revolution. The velocity value assigned to each of the 128 azimuthal intervals used in the azimuth dependent reconstruction is the arithmetic mean of all velocity measurements which occurred within the specified azimuthal interval.

Experimental Results

Rotor Performance

The rotor parameters of thrust, X-force and power for each particular inflow point may be determined from the plotted performance data presented in figure 15. These results depict the values of C_T , C_X and C_P that occurred while the LV data were being acquired and are presented by a fixed symbol marker as indicated in the legend. These data show that there was a shift in the nominal operating conditions of the rotor between some measurement locations, resulting in basically two separate operating conditions for the rotor. Because the LV system needed to be relocated to acquire data at the forward portion of the rotor disk, the tunnel and model were brought off-line. Upon returning on-line, the parameters were not precisely brought back to nominal conditions. The measurement locations at each of the two operating conditions is shown schematically in figure 12 and graphically in figure 15. The nominal rotor performance parameters obtained during the inflow measurement process is presented in table 4. The values for the uncorrected propulsive force shown in table 4 and figure 15 include the effects of the hub. The hub tares were not measured in this test, but the results obtained in an earlier investigation conducted at 163 knots were used to correct the propulsive force on this test. The correction consisted of adding 0.0001198 to the uncorrected propulsive force.

Velocity Measurements

The mean and standard deviation of the two components of the induced inflow ratio are given in table 5. Also included are the number of measurements comprising the statistical values for each case. In figure 16, the mean induced inflow ratio (longitudinal), $\bar{\mu}_l$, with a band of \pm one standard deviation is plotted

versus radius for each radial scan. Figure 17 presents in the same format the mean induced inflow ratio (normal), $\bar{\lambda}_i$. The \pm one standard deviation is not indicative of error in the measurements but rather the unsteady nature of the flow. The error of 0.92 percent is approximately equal to the size of the symbols in figures 16 and 17. The same data, without the one standard deviation, is presented in a contour plot format for $\bar{\lambda}_i$ in figure 18, and for $\bar{\lambda}_i$ in figure 19, for the two operating conditions to show the distribution of the mean induced inflow over the whole disk (viewed from above). Shown in figures 20 through 186 are the time dependent induced inflow ratios. These figures show the induced inflow ratio with the mean removed versus azimuth at the top of the figure, the number of measurements that went into determining the mean for each bin in the center, and an order ratio analysis of the time dependent data at the bottom of each figure. The plotted data presented in figures 20 through 186 are contained on 3.5 inch floppy disks in Microsoft Corporation MS-DOS format labelled "original disk - b66" (see pocket inside rear cover). The details of the data format and file structure are located in the file "README.DOC".

The figure numbers for the azimuthal and radial locations are indicated below. Locations where no measurements were made are indicated by an "xx".

r/R	Azimuth											
	0	30	60	90	120	150	180	210	240	270	300	330
0.20	20	34	48	62	76	89	103	117	131	145	159	173
0.32	21	35	49	63	77	90	104	118	132	146	160	174
0.50	22	36	50	64	78	91	105	119	133	147	161	175
0.58	23	37	51	65	79	92	106	120	134	148	162	176
0.69	24	38	52	66	80	93	107	121	135	149	163	177
0.73	25	39	53	67	81	94	108	122	136	150	164	178
0.75	26	40	54	68	82	95	109	123	137	151	165	179
0.81	27	41	55	69	xx	96	110	124	138	152	166	180
0.86	28	42	56	70	83	97	111	125	139	153	167	181
0.90	29	43	57	71	84	98	112	126	140	154	168	182
0.94	30	44	58	72	85	99	113	127	141	155	169	183
0.96	31	45	59	73	86	100	114	128	142	156	170	184
1.00	32	46	60	74	87	101	115	129	143	157	171	185
1.10	33	47	61	75	88	102	116	130	144	158	172	186

Concluding Remarks

An Advanced Lightweight Rotor (ALR) model was tested in high speed forward flight in the 14- by 22-Foot Subsonic Tunnel at the NASA Langley Research Center. The pressure instrumented rotor, provided by Bell Helicopter, was a four-bladed, Mach-scaled, bearingless, soft-in-plane design. Rotor performance data were acquired from Bell's Powered Force Model (PFM) test stand, and the blade airloads were obtained using 92 unsteady pressure transducers. A two-component laser velocimeter was used to obtain azimuthally dependent velocities in the inflow region and in the wake of the rotor. The laser velocimeter acquired inflow data are presented in this report without analysis. To facilitate the use of the data, they are also provided on 1.4 Megabyte 3.5-inch floppy disks in Microsoft MS-DOS format.

References

1. Landgrebe, A.J.; and Johnson, B.V.: Measurement of Model Helicopter Rotor Flow Velocities with a Laser Doppler Velocimeter. *Journal of the American Helicopter Society*, Volume 19, July 1974, pp. 39-43.
2. Biggers, James C.; Chu, Sing; and Orloff, Kenneth L.: Laser Velocimeter Measurements of Rotor Blade Loads and Tip Vortex Rollup. Pre-Print No. 900, 31st Annual Forum of the American Helicopter Society, Washington, D.C., May 1975.
3. Tangier, James L.: Schlieren and Noise Studies of Rotors in Forward Flight. Pre-Print 77.33-05, 33rd Annual Forum of the American Helicopter Society, Washington D.C., May 1977.
4. Biggers, James C.; Lee, Albert; and Orloff, Kenneth L.: Measurement of Helicopter Rotor Tip Vortices. Pre-Print 77.33-06, 33rd Annual Forum of the American Helicopter Society, Washington, D.C., May 1977.
5. Harris, F.D.: Rotary Wing Aerodynamics-Historical Perspective and Important Issues. Presented at the AHS National Specialists Meeting on Aerodynamics and Aeroacoustics, Arlington, TX, February 25-27, 1987.
6. Johnson, W.: A Comprehensive Analytical Model of Rotorcraft Aerodynamics and Dynamics. NASA TM-81182, June 1980.
7. Elliott, J.W.; Althoff, S.L.; and Sailey, R.H.: Inflow Measurements Made With a Laser Velocimeter on a Helicopter Model in Forward Flight, Volume I- Rectangular Planform Blades at an Advance Ratio of 0.15. NASA TM-100541, April 1988.
8. Elliott, J.W.; Althoff, S.L.; and Sailey, R.H.: Inflow Measurements Made With a Laser Velocimeter on a Helicopter Model in Forward Flight, Volume II- Rectangular Planform Blades at an Advance Ratio of 0.23. NASA TM-100542, April 1988.
9. Elliott, J.W.; Althoff, S.L.; and Sailey, R.H.: Inflow Measurements Made With a Laser Velocimeter on a Helicopter Model in Forward Flight, Volume III- Rectangular Planform Blades at an Advance Ratio of 0.30. NASA TM-100543, April 1988.
10. Hooper, W.E.: The Vibratory Airloading of Helicopter Rotors. *Vertica*, Volume 8, 1984. Also: paper No. 46, Ninth Annual European Rotorcraft Forum, September 13-15, 1983.
11. Lorber, P.F.: Aerodynamic Results of a Pressure Instrumented Model Rotor Test at the DNW. Presented at the 46th Annual Forum of the American Helicopter Society, Washington, D.C., May 1990.
12. Althoff, S.L.: Effect of Tip Speed on Rotor Inflow. *Journal of the American Helicopter Society*, Volume 34, No. 4, October 1989.
13. Elliott, J.W.; Peryea, M.A.; Brand, A.G.; and Wood, T.L.: Induced Inflow Velocity and Blade Surface Pressure Measurements for a Helicopter in Forward Flight, Volume 1- Advance Ratio of 0.37, Thrust Coefficient of 0.0081 and Hover Tip Speed of 710 Ft/Sec. NASA TM-104224, April 1992.
14. Wood, T.L.; Brand, A.G.; and Elliott, J.W.: An Experimental Investigation of Rotor Blade Airloads and Wake Structure at High Advance Ratio. Presented at the 46th Annual Forum of the American Helicopter Society, Washington, D.C., May 21-23, 1990.
15. Yen, G.J.; Yuce, M.; Chao C.F.; and Schillings, J.: Validation of Vibratory Airloads and Application to Helicopter Response. *Journal of the American Helicopter Society*, Volume 35, No. 4, pp. 63-71, October 1990.

16. Applin, Z. T.: Flow Improvements in the Circuit of the Langley 4- by 7-Meter Tunnel. NASA TM-85662, December 1983.
17. Sellers, W.L.; and Elliott, J.W.: Applications of a Laser Velocimeter in the Langley 4- by 7-Meter Tunnel. Proceedings on the Workshop on Flow Visualization and Laser Velocimetry for Wind Tunnels, NASA CP-2243, March 1982, pp. 283-293.
18. Elliott, J.E.; and Nichols, C.E.: Seeding Systems for Use With a Laser Velocimeter in Large Scale Wind Tunnels. NASA CP-2393, March 1985, pp. 93-103.
19. Young, W.H.; Meyers, J.F.; and Hepner, T.E.: Laser Velocimeter Systems Analysis Applied to a Flow Survey Above a Stalled Wing. NASA TN D-8408, August 1977.
20. Dring, R.P.: Sizing Criteria for Laser Anemometry Particles. Journal of Fluid Engineering, Volume 104, March 1982, pp. 15-17.
21. Peryea, M.: Test Plan for the 1/5 Scale Pressure Instrumented ALR Rotor/Laser Velocimeter Wind Tunnel Test at NASA Langley. Bell Helicopter Textron Inc. Report No. 699-199-014, May 1989.

Table 1.- ALR Rotor Airfoil Coordinates

Station 10.7 inches		Thickness 22%	
<u>Upper Coordinates</u>		<u>Lower Coordinates</u>	
x/c	y/c	x/c	y/c
0.000000	0.000000	0.000000	0.000000
0.001220	0.012950	0.003140	0.011900
0.006200	0.025980	0.010650	0.023150
0.014570	0.038320	0.021860	0.033650
0.025980	0.049900	0.036200	0.043390
0.039990	0.060680	0.053170	0.052320
0.056350	0.070600	0.072420	0.060500
0.074710	0.079640	0.093690	0.067870
0.094860	0.087820	0.116660	0.074490
0.116540	0.095100	0.141170	0.080330
0.139590	0.101490	0.166930	0.085400
0.163810	0.107020	0.193760	0.089680
0.189030	0.111640	0.221380	0.093180
0.215040	0.115390	0.249580	0.095860
0.241580	0.118210	0.278120	0.097760
0.268450	0.120130	0.306870	0.098810
0.295570	0.121120	0.335870	0.099060
0.322910	0.121190	0.365250	0.098490
0.350590	0.120360	0.395300	0.097130
0.378760	0.118620	0.426570	0.094970
0.407610	0.116000	0.459690	0.091990
0.437330	0.112500	0.495590	0.088090
0.468080	0.108110	0.535620	0.083270
0.499980	0.103170	0.580850	0.077380
0.533000	0.098000	0.631770	0.070480
0.567030	0.092460	0.689310	0.062420
0.602170	0.086510	0.747400	0.054100
0.638900	0.080040	0.795870	0.046940
0.679610	0.072570	0.838160	0.040040
0.736040	0.061700	0.870240	0.034030
0.781000	0.052620	0.893380	0.029290
0.819440	0.044540	0.912620	0.025080
0.864810	0.034660	0.929830	0.021090
0.892040	0.028540	0.945600	0.017240
0.911860	0.024090	0.960300	0.013500
0.929350	0.020090	0.974180	0.009760
0.945260	0.016420	0.987380	0.006000
0.960080	0.012810	1.000000	0.002090
0.974060	0.009370		
0.987310	0.005670		
1.000000	0.002090		

Table 1. - Continued

Station 15.70 to 36.70 inches		Thickness 10 %	
<u>Upper Coordinates</u>		<u>Lower Coordinates</u>	
x/c	y/c	x/c	y/c
0.000000	0.000000	0.000000	0.000000
0.000490	0.004200	0.000150	0.001950
0.002890	0.010640	0.002290	0.007350
0.007080	0.016980	0.006780	0.011990
0.012840	0.023070	0.013280	0.015870
0.019850	0.028860	0.021360	0.019150
0.027950	0.034230	0.030760	0.021840
0.036960	0.039160	0.041290	0.023960
0.046740	0.043610	0.052830	0.025550
0.057240	0.047580	0.065300	0.026630
0.068410	0.051090	0.078880	0.027300
0.080230	0.054150	0.093900	0.027580
0.092760	0.056820	0.111230	0.027550
0.106040	0.059110	0.134510	0.027230
0.135280	0.062810	0.160910	0.026800
0.168990	0.065510	0.183280	0.026610
0.208730	0.067580	0.205070	0.026610
0.231160	0.068450	0.227670	0.026790
0.254970	0.069190	0.252350	0.027160
0.279130	0.069810	0.281730	0.027750
0.302810	0.070280	0.320600	0.028590
0.325590	0.070560	0.352370	0.029230
0.347420	0.070670	0.379770	0.029670
0.368450	0.070600	0.405350	0.029960
0.388890	0.070310	0.429860	0.030120
0.428520	0.069130	0.453700	0.030110
0.467480	0.067080	0.500750	0.029630
0.479280	0.066280	0.524590	0.029150
0.499170	0.064720	0.549160	0.028500
0.519100	0.062920	0.575060	0.027680
0.544020	0.060380	0.603240	0.026670
0.573880	0.056970	0.635430	0.025390
0.593790	0.054490	0.675830	0.023720
0.633630	0.049080	0.718460	0.021910
0.673460	0.043120	0.751940	0.020450
0.708180	0.037630	0.780510	0.019100
0.777400	0.026830	0.806450	0.017770
0.816630	0.021270	0.831000	0.016370
0.836320	0.018670	0.855010	0.014860
0.875820	0.013820	0.879280	0.013170
0.895650	0.011560	0.901560	0.011490
0.915490	0.009430	0.918490	0.010150
0.930390	0.007920	0.932090	0.009010
0.945280	0.006480	0.944000	0.007970
0.965130	0.004690	0.954830	0.006990
0.975060	0.003850	0.974320	0.005040
0.985040	0.003050	0.983290	0.004030
0.995020	0.002270	0.991850	0.002980
1.000000	0.001880	1.000000	0.001880

Table 1.- Continued

Station 43.70 inches Thickness 8 %

<u>Upper Coordinates</u>		<u>Lower Coordinates</u>	
x/c	y/c	x/c	y/c
0.000000	0.000000	0.000000	0.000000
0.001600	0.005040	0.000350	0.004690
0.004760	0.009670	0.002990	0.008460
0.009410	0.013880	0.007710	0.011370
0.015390	0.017760	0.014130	0.013780
0.022590	0.021370	0.022200	0.015820
0.030880	0.024760	0.031950	0.017620
0.040110	0.027920	0.043460	0.019280
0.050140	0.030830	0.056690	0.020880
0.060830	0.033500	0.071380	0.022400
0.072090	0.035910	0.087120	0.023810
0.083880	0.038080	0.103610	0.025110
0.096180	0.040000	0.120770	0.026280
0.109000	0.041690	0.138580	0.027340
0.122380	0.043170	0.157120	0.028290
0.136330	0.044460	0.176430	0.029140
0.150870	0.045550	0.196530	0.029910
0.166010	0.046470	0.217360	0.030580
0.181760	0.047220	0.238860	0.031170
0.198080	0.047800	0.260930	0.031660
0.232300	0.048510	0.283480	0.032080
0.268340	0.048610	0.306440	0.032400
0.306060	0.048130	0.329770	0.032640
0.345650	0.047100	0.353430	0.032800
0.387590	0.045530	0.377390	0.032870
0.432470	0.043420	0.425930	0.032770
0.480990	0.040770	0.474680	0.032340
0.533810	0.037570	0.522640	0.031590
0.591580	0.033810	0.568960	0.030540
0.655500	0.029420	0.613430	0.029150
0.690490	0.026950	0.656520	0.027410
0.728250	0.024300	0.699080	0.025270
0.769570	0.021410	0.742450	0.022660
0.811070	0.018460	0.788840	0.019450
0.846730	0.015870	0.843600	0.015320
0.878030	0.013540	0.876000	0.012790
0.901390	0.011770	0.900990	0.010800
0.921140	0.010180	0.914890	0.009680
0.940890	0.008440	0.935550	0.007970
0.960620	0.006510	0.952510	0.006490
0.980330	0.004340	0.960180	0.005790
1.000000	0.001880	0.981150	0.003700
		1.000000	0.001880

Table 1.- Concluded

Station 45.90 to 48.00 inches		Thickness 6 %	
<u>Upper Coordinates</u>		<u>Lower Coordinates</u>	
x/c	y/c	x/c	y/c
0.000000	0.000000	0.000000	0.000000
0.000380	0.002760	0.000220	0.001690
0.002360	0.007150	0.002420	0.005210
0.006010	0.011000	0.006750	0.007860
0.011120	0.014330	0.012950	0.009870
0.017550	0.017260	0.020880	0.011600
0.025200	0.019890	0.030660	0.013130
0.043670	0.024410	0.042320	0.014560
0.065310	0.027990	0.070230	0.017190
0.089390	0.030630	0.101880	0.019370
0.116100	0.032420	0.137100	0.021150
0.146610	0.033560	0.176300	0.022630
0.183180	0.034250	0.218970	0.023810
0.227410	0.034630	0.264430	0.024720
0.274670	0.034730	0.311780	0.025340
0.320940	0.034520	0.359630	0.025680
0.367390	0.033990	0.407270	0.025710
0.415380	0.033130	0.455250	0.025450
0.465380	0.031940	0.504860	0.024890
0.517010	0.030450	0.556950	0.024030
0.569690	0.028680	0.610330	0.022910
0.622850	0.026660	0.662610	0.021580
0.675790	0.024400	0.713070	0.020040
0.727890	0.021950	0.761690	0.018290
0.778480	0.019300	0.807940	0.016330
0.826160	0.016540	0.850920	0.014190
0.848350	0.015150	0.871010	0.013040
0.869380	0.013740	0.889940	0.011860
0.889260	0.012310	0.905580	0.010800
0.905400	0.011070	0.927930	0.009100
0.917610	0.010080	0.945640	0.007580
0.927360	0.009250	0.961000	0.006130
0.937110	0.008380	0.968120	0.005420
0.949700	0.007210	0.974930	0.004700
0.962280	0.005970	0.981510	0.003990
0.968570	0.005330	0.987860	0.003290
0.974860	0.004670	0.994020	0.002580
0.981150	0.003990	1.000000	0.001880
0.987430	0.003310		
0.993720	0.002600		
1.000000	0.001880		

Table 2.- ALR Blade Structural Properties

RADIAL STATION (IN)	WT/IN (LB/IN)	EI*10 ⁻⁶ (LBF-IN ²)		CENTER OF GRAVITY OFFSET (IN)		GJ*10 ⁻⁶ (LBF-IN ²)	SHEAR CENTER OFFSET (IN)		NEUTRAL AXIS CENTER OFFSET (IN)	
		BEAM	CHORD	BEAM	CHORD		BEAM	CHORD	BEAM	CHORD
0.900	0.2818	2.7579	7.027	0.000	0.000	0.149	0.000	0.000	0.000	0.000
1.500	0.0244	0.0089	0.390	0.000	0.000	0.001	0.000	0.000	0.000	0.000
1.900	0.0179	0.0045	0.297	0.000	0.000	0.002	0.000	0.000	0.000	0.000
2.300	0.0252	0.0037	0.254	0.000	0.000	0.002	0.000	0.000	0.000	0.000
2.700	0.6237	0.0035	0.212	0.000	0.000	0.002	0.000	0.000	0.000	0.000
3.200	0.0144	0.0039	0.169	0.000	0.000	0.001	0.000	0.000	0.000	0.000
5.200	0.0080	0.0036	0.063	0.000	0.000	0.000	0.000	0.000	0.000	0.000
6.530	0.0065	0.0044	0.031	0.000	0.000	0.000	0.000	0.000	0.000	0.000
7.862	0.0054	0.0051	0.013	0.000	0.000	0.000	0.000	0.000	0.000	0.000
8.119	0.0090	0.0072	0.009	0.000	0.000	0.001	0.000	0.000	0.000	0.000
9.000	0.3164	0.0115	0.053	0.000	0.000	0.002	0.000	0.000	0.000	0.000
10.700	0.0625	0.1363	1.220	0.012	0.225	0.146	0.008	-0.122	-0.010	0.127
12.900	0.0260	0.0521	0.823	0.020	0.272	0.038	0.004	0.043	-0.017	0.110
14.050	0.0211	0.0287	0.677	0.015	0.274	0.016	0.012	0.056	-0.011	0.077
16.040	0.0251	0.0225	0.627	0.020	0.169	0.013	0.014	0.062	-0.011	0.052
18.030	0.0245	0.0210	0.570	0.022	0.148	0.012	0.011	0.015	-0.014	0.011
20.020	0.0239	0.0196	0.513	0.022	0.137	0.011	0.011	-0.022	-0.014	-0.020
22.010	0.0233	0.0182	0.457	0.022	0.116	0.010	0.012	-0.069	-0.014	-0.062
24.000	0.0227	0.0167	0.400	0.021	0.095	0.009	0.012	-0.116	-0.014	-0.103
26.000	0.0253	0.0148	0.358	0.030	-0.149	0.009	0.008	-0.141	-0.014	-0.149
26.900	0.0237	0.0114	0.322	0.032	-0.137	0.008	0.011	-0.116	-0.016	-0.141
28.750	0.0235	0.0111	0.319	0.032	-0.122	0.008	0.013	-0.107	-0.017	-0.133
30.600	0.0235	0.0111	0.319	0.032	-0.102	0.008	0.013	-0.087	-0.017	-0.113
32.450	0.0235	0.0111	0.319	0.032	-0.082	0.008	0.013	-0.067	-0.017	-0.093
34.300	0.0235	0.0111	0.319	0.032	-0.062	0.008	0.013	-0.047	-0.017	-0.073
36.200	0.0233	0.0108	0.320	0.033	-0.045	0.008	0.010	-0.047	-0.019	-0.067
38.100	0.0228	0.0103	0.321	0.035	0.000	0.007	0.003	-0.036	-0.022	-0.044
39.320	0.0222	0.0095	0.320	0.038	0.025	0.007	-0.006	-0.037	-0.027	-0.035
40.000	0.0289	0.0087	0.321	0.041	-0.089	0.007	-0.014	-0.008	-0.031	-0.033
42.000	0.0350	0.0077	0.320	0.044	-0.170	0.006	-0.024	0.027	-0.036	-0.017
43.800	0.0321	0.0060	0.312	0.050	-0.122	0.005	-0.039	0.046	-0.045	0.023
45.600	0.0284	0.0039	0.301	0.056	-0.066	0.004	-0.052	0.073	-0.054	0.067
48.000	0.0268	0.0030	0.296	0.059	-0.020	0.003	-0.058	0.107	-0.059	0.109

Table 3.- Laser Velocimeter System Error Summary

Error Source	Bias Percent	Random Percent
Cross Beam Angle Measurement	± 0.48	None
Divergent Fringes	A	A
Time Jitter	N/A	N/A
Clock Synchronization	0.26	± 0.26
Quantization	A	± 0.26
Velocity Bias	B	B
Bragg Bias	B	B
Velocity Gradient	B	B
Particle Lag	± 0.10	B
Total , %	-0.32 to 0.84	0.37
SYSTEM ERROR , %	0.49 to 0.92	

A - Not Measured

B - Negligible

N/A - Not Applicable

Table 4.- Nominal Rotor Parameters During LV Measurements

Tip Path Plane Angle of Attack, α, deg	-5.875
Collective Angle, A_0, deg	10.41
Lateral Feathering, A_1, deg	-1.63
Longitudinal Feathering, B_1, deg	8.46
Blade Coning Angle, deg	1.40
Blade Lag Angle, (mean), deg	0.75
Advance Ratio, μ_∞, non-dimensional	0.37
Uncorrected Propulsive Force, C_X	0.000319
Corrected Propulsive Force, C_{Xc}	0.000438
Rotor Thrust, C_T, non-dimensional	0.00640
Rotor Power, C_P, non-dimensional	0.000417
Tunnel Velocity, V, knots	132.79
Tip Speed, V_{tip}, ft/sec	606.12
Tip Mach Number, M_{tip}, non-dimensional	0.5250

Table 5.- Inflow Velocity Summary

Ψ	r/R	$\bar{\mu}_i$	σ_μ	Number	$\bar{\lambda}_i$	σ_λ	Number
0	0.20	0.0093	0.0108	3224	0.0049	0.0091	3322
0	0.32	0.0057	0.0092	3071	-0.0086	0.0098	3239
0	0.50	-0.0029	0.0080	2929	-0.0126	0.0068	3103
0	0.58	-0.0056	0.0079	2921	-0.0132	0.0060	3070
0	0.69	-0.0068	0.0074	2896	-0.0140	0.0058	3208
0	0.73	-0.0063	0.0072	2931	-0.0145	0.0057	3241
0	0.75	-0.0066	0.0074	2889	-0.0145	0.0058	3274
0	0.81	-0.0067	0.0070	2928	-0.0145	0.0057	3235
0	0.86	-0.0075	0.0069	2873	-0.0146	0.0056	3300
0	0.90	-0.0067	0.0075	2794	-0.0140	0.0060	3085
0	0.94	-0.0076	0.0074	2861	-0.0155	0.0058	3194
0	0.96	-0.0083	0.0074	2913	-0.0160	0.0056	3237
0	1.00	-0.0081	0.0074	2877	-0.0161	0.0057	3258
0	1.10	-0.0091	0.0078	2971	-0.0169	0.0052	3391
30	0.20	0.0112	0.0099	2889	-0.0012	0.0074	3513
30	0.32	0.0044	0.0103	2810	-0.0043	0.0076	3078
30	0.50	0.0038	0.0079	3062	-0.0162	0.0050	3513
30	0.58	0.0003	0.0076	2987	-0.0161	0.0050	3468
30	0.69	-0.0007	0.0075	2944	-0.0155	0.0052	3393
30	0.73	-0.0016	0.0076	2992	-0.0157	0.0053	3395
30	0.75	-0.0023	0.0098	2660	-0.0121	0.0069	2814
30	0.81	-0.0032	0.0105	2558	-0.0119	0.0083	2627
30	0.86	-0.0064	0.0073	2816	-0.0122	0.0060	3243
30	0.90	-0.0083	0.0070	2724	-0.0124	0.0060	3296
30	0.94	-0.0086	0.0071	2808	-0.0116	0.0056	3224
30	0.96	-0.0101	0.0072	2716	-0.0115	0.0056	3258
30	1.00	-0.0100	0.0068	2833	-0.0119	0.0055	3333
30	1.10	-0.0100	0.0076	2939	-0.0109	0.0045	3375
60	0.20	0.0033	0.0105	3006	0.0048	0.0054	3374
60	0.32	0.0049	0.0099	3035	-0.0021	0.0059	3324
60	0.50	0.0014	0.0096	2986	0.0010	0.0060	3164
60	0.58	-0.0002	0.0097	2921	0.0042	0.0056	2979
60	0.69	0.0018	0.0096	2944	0.0075	0.0055	3053

Table 5.- Continued

Ψ	r/R	$\bar{\mu}_i$	σ_μ	Number	$\bar{\lambda}_i$	σ_λ	Number
60	0.73	-0.0002	0.0086	3016	0.0081	0.0055	3369
60	0.75	0.0000	0.0083	3026	0.0088	0.0056	3376
60	0.81	-0.0007	0.0085	3060	0.0115	0.0056	3350
60	0.86	-0.0030	0.0082	2995	0.0139	0.0055	3377
60	0.90	-0.0040	0.0106	2430	0.0165	0.0063	1979
60	0.94	-0.0086	0.0093	2644	0.0199	0.0041	2697
60	0.96	-0.0088	0.0092	2646	0.0211	0.0038	2690
60	1.00	-0.0113	0.0089	2602	0.0215	0.0038	2633
60	1.10	-0.0109	0.0068	2913	0.0215	0.0030	3200
90	0.20	-0.0023	0.0095	2855	0.0084	0.0047	3189
90	0.32	-0.0021	0.0091	2918	0.0074	0.0049	3205
90	0.50	-0.0064	0.0093	2844	0.0131	0.0047	3103
90	0.58	-0.0051	0.0093	2953	0.0169	0.0043	3119
90	0.69	-0.0077	0.0088	2899	0.0216	0.0041	3052
90	0.73	-0.0099	0.0087	2814	0.0229	0.0041	3001
90	0.75	-0.0096	0.0088	2866	0.0238	0.0043	3060
90	0.81	-0.0135	0.0081	2938	0.0250	0.0045	3114
90	0.86	-0.0152	0.0080	3036	0.0255	0.0047	3282
90	0.90	-0.0146	0.0075	3062	0.0223	0.0043	3098
90	0.94	-0.0147	0.0072	2999	0.0197	0.0040	2990
90	0.96	-0.0142	0.0071	3077	0.0181	0.0039	3021
90	1.00	-0.0153	0.0070	3040	0.0158	0.0036	2997
90	1.10	-0.0184	0.0061	3114	0.0123	0.0024	3198
120	0.20	-0.0077	0.0112	3004	0.0135	0.0049	1739
120	0.32	-0.0057	0.0099	3246	0.0116	0.0059	2590
120	0.50	-0.0127	0.0107	2861	0.0184	0.0053	2758
120	0.58	-0.0164	0.0101	2781	0.0200	0.0051	2583
120	0.69	-0.0147	0.0100	2912	0.0228	0.0061	2771
120	0.73	-0.0163	0.0099	2710	0.0202	0.0050	2399
120	0.75	-0.0172	0.0098	2799	0.0219	0.0054	2626
120	0.86	-0.0193	0.0100	2760	0.0188	0.0045	2420
120	0.90	-0.0208	0.0094	2796	0.0175	0.0041	2667
120	0.94	-0.0193	0.0094	2848	0.0163	0.0039	2707
120	0.96	-0.0228	0.0081	2897	0.0157	0.0034	2947

Table 5.- Continued

Ψ	r/R	$\bar{\mu}_i$	σ_{μ}	Number	$\bar{\lambda}_i$	σ_{λ}	Number
120	1.00	-0.0224	0.0080	2874	0.0145	0.0031	2944
120	1.10	-0.0211	0.0072	3069	0.0128	0.0027	3142
150	0.20	-0.0138	0.0113	2083	0.0186	0.0060	2419
150	0.32	-0.0187	0.0123	2015	0.0123	0.0067	2222
150	0.50	-0.0135	0.0113	2190	0.0161	0.0058	2214
150	0.58	-0.0152	0.0110	2124	0.0179	0.0062	2431
150	0.69	-0.0170	0.0111	2168	0.0185	0.0062	2545
150	0.73	-0.0186	0.0113	2160	0.0178	0.0058	2493
150	0.75	-0.0188	0.0111	2119	0.0172	0.0056	2396
150	0.81	-0.0209	0.0111	2208	0.0165	0.0053	2436
150	0.86	-0.0225	0.0102	2478	0.0158	0.0058	2376
150	0.90	-0.0242	0.0093	2580	0.0168	0.0049	2084
150	0.94	-0.0249	0.0084	2952	0.0174	0.0039	2631
150	0.96	-0.0249	0.0074	2904	0.0166	0.0037	3133
150	1.00	-0.0259	0.0071	2945	0.0152	0.0035	3100
150	1.10	-0.0235	0.0073	3023	0.0135	0.0031	3132
180	0.20	-0.0177	0.0112	2260	0.0200	0.0066	2153
180	0.32	-0.0165	0.0122	1547	0.0175	0.0060	2224
180	0.50	-0.0181	0.0095	2709	0.0168	0.0061	2495
180	0.58	-0.0195	0.0099	2626	0.0165	0.0066	2585
180	0.69	-0.0202	0.0101	2765	0.0167	0.0060	2684
180	0.73	-0.0212	0.0099	2710	0.0163	0.0057	2736
180	0.75	-0.0210	0.0099	2754	0.0162	0.0054	2687
180	0.81	-0.0221	0.0097	2800	0.0162	0.0052	2707
180	0.86	-0.0236	0.0099	2743	0.0150	0.0046	2706
180	0.90	-0.0224	0.0096	2798	0.0147	0.0050	2710
180	0.94	-0.0238	0.0096	2713	0.0135	0.0047	2680
180	0.96	-0.0249	0.0098	2606	0.0121	0.0046	2567
180	1.00	-0.0254	0.0100	2583	0.0112	0.0046	2521
180	1.10	-0.0250	0.0096	2807	0.0129	0.0047	2803
210	0.20	-0.0179	0.0091	2989	0.0229	0.0059	2696
210	0.32	-0.0187	0.0096	2935	0.0192	0.0058	2693
210	0.50	-0.0206	0.0102	2851	0.0166	0.0078	2581
210	0.58	-0.0198	0.0101	2807	0.0161	0.0080	2556

Table 5.- Continued

Ψ	r/R	$\bar{\mu}_i$	σ_{μ}	Number	$\bar{\lambda}_i$	σ_{λ}	Number
210	0.69	-0.0191	0.0107	2696	0.0154	0.0069	2348
210	0.73	-0.0208	0.0106	2712	0.0158	0.0065	2481
210	0.75	-0.0195	0.0102	2699	0.0153	0.0061	2452
210	0.81	-0.0197	0.0103	2700	0.0156	0.0057	2451
210	0.86	-0.0190	0.0100	2679	0.0153	0.0051	2440
210	0.90	-0.0207	0.0100	2837	0.0153	0.0046	2670
210	0.94	-0.0201	0.0098	2823	0.0148	0.0043	2623
210	0.96	-0.0201	0.0097	2866	0.0148	0.0043	2648
210	1.00	-0.0210	0.0096	2879	0.0146	0.0040	2630
210	1.10	-0.0211	0.0097	2823	0.0124	0.0039	2592
240	0.20	-0.0168	0.0091	3082	0.0238	0.0062	2824
240	0.32	-0.0181	0.0098	3038	0.0194	0.0068	2772
240	0.50	-0.0153	0.0123	2925	0.0153	0.0083	2675
240	0.58	-0.0167	0.0108	2997	0.0141	0.0095	2816
240	0.69	-0.0158	0.0106	2925	0.0132	0.0091	2775
240	0.73	-0.0151	0.0103	2868	0.0129	0.0085	2711
240	0.75	-0.0152	0.0101	2856	0.0131	0.0084	2733
240	0.81	-0.0150	0.0095	2648	0.0133	0.0067	2557
240	0.86	-0.0157	0.0095	2817	0.0144	0.0072	2658
240	0.90	-0.0163	0.0094	2932	0.0149	0.0064	2678
240	0.94	-0.0167	0.0087	2859	0.0149	0.0057	2606
240	0.96	-0.0167	0.0080	2839	0.0146	0.0044	2645
240	1.00	-0.0154	0.0097	2949	0.0144	0.0046	2753
240	1.10	-0.0174	0.0095	2919	0.0135	0.0043	2677
270	0.20	-0.0112	0.0088	2931	0.0248	0.0056	3200
270	0.32	-0.0095	0.0094	2986	0.0194	0.0067	3306
270	0.50	-0.0096	0.0107	3111	0.0134	0.0084	3382
270	0.58	-0.0078	0.0107	3127	0.0106	0.0089	3476
270	0.69	-0.0074	0.0104	3036	0.0075	0.0084	3335
270	0.73	-0.0070	0.0107	3114	0.0083	0.0097	3404
270	0.75	-0.0068	0.0106	3083	0.0066	0.0094	3395
270	0.81	-0.0068	0.0104	3137	0.0061	0.0099	3416
270	0.86	-0.0077	0.0100	3223	0.0061	0.0109	3463
270	0.90	-0.0078	0.0093	3109	0.0080	0.0097	3380

Table 5.- Concluded

Ψ	r/R	$\bar{\mu}_i$	σ_μ	Number	$\bar{\lambda}_i$	σ_λ	Number
270	0.94	-0.0083	0.0089	3000	0.0097	0.0076	3196
270	0.96	-0.0084	0.0084	2936	0.0105	0.0064	3179
270	1.00	-0.0101	0.0084	2974	0.0121	0.0059	3213
270	1.10	-0.0125	0.0081	2977	0.0138	0.0050	3133
300	0.20	-0.0054	0.0092	2814	0.0241	0.0052	3011
300	0.32	-0.0066	0.0098	2779	0.0186	0.0054	2992
300	0.50	-0.0039	0.0105	2837	0.0131	0.0072	3106
300	0.58	-0.0026	0.0101	2775	0.0101	0.0069	3064
300	0.69	-0.0020	0.0096	2844	0.0062	0.0055	2995
300	0.73	-0.0024	0.0096	2823	0.0047	0.0056	3022
300	0.75	-0.0024	0.0095	2736	0.0039	0.0056	3033
300	0.81	-0.0022	0.0095	2646	0.0027	0.0056	2930
300	0.86	-0.0032	0.0094	2768	0.0006	0.0061	2963
300	0.90	-0.0037	0.0095	2782	-0.0004	0.0058	2970
300	0.94	-0.0023	0.0086	2779	-0.0017	0.0052	2985
300	0.96	-0.0034	0.0091	2827	-0.0031	0.0061	3024
300	1.00	-0.0050	0.0085	2655	-0.0032	0.0061	2943
300	1.10	-0.0061	0.0094	2554	0.0043	0.0056	2660
330	0.20	0.0023	0.0093	2899	0.0200	0.0047	3248
330	0.32	0.0002	0.0090	2822	0.0152	0.0045	2178
330	0.50	-0.0024	0.0094	2724	0.0118	0.0052	2606
330	0.58	-0.0030	0.0091	2741	0.0093	0.0054	2809
330	0.69	-0.0037	0.0089	2642	0.0062	0.0054	2881
330	0.73	-0.0037	0.0090	2671	0.0060	0.0053	2838
330	0.75	-0.0035	0.0090	2634	0.0056	0.0054	2790
330	0.81	-0.0033	0.0096	2621	0.0046	0.0059	2721
330	0.86	-0.0054	0.0094	2678	0.0036	0.0067	2772
330	0.90	-0.0035	0.0096	2666	0.0014	0.0077	2835
330	0.94	-0.0034	0.0095	2671	-0.0002	0.0082	2739
330	0.96	-0.0028	0.0098	2694	-0.0017	0.0085	2869
330	1.00	-0.0045	0.0096	2716	-0.0031	0.0086	2923
330	1.10	-0.0062	0.0100	2819	-0.0049	0.0082	3061

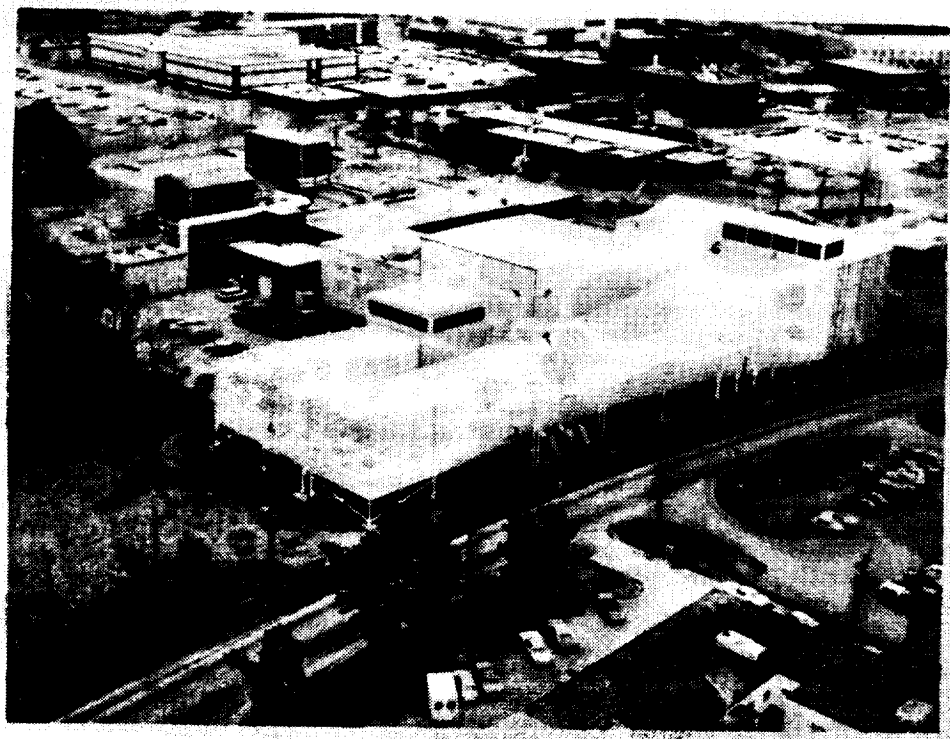


Figure 1.- NASA Langley 14- X 22- Foot Subsonic Wind Tunnel.

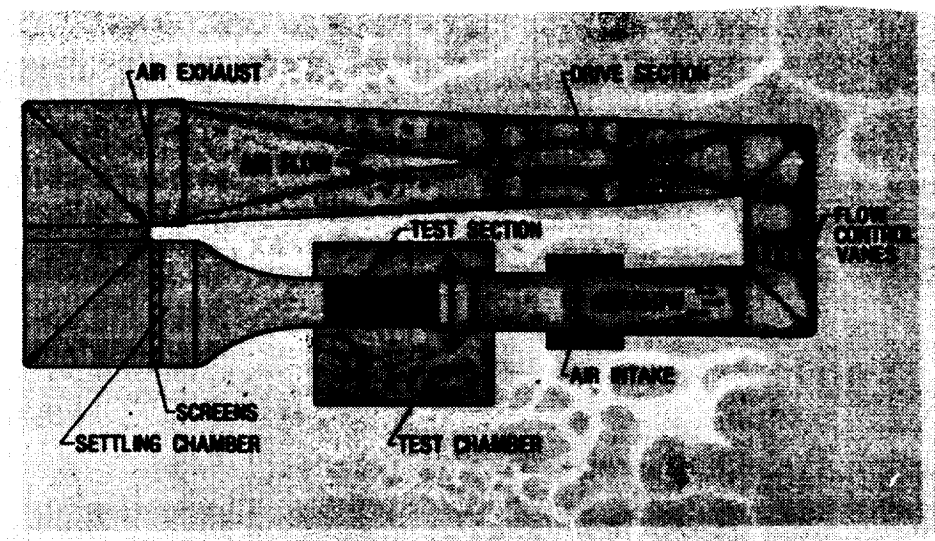


Figure 2.- Schematic view of wind tunnel.

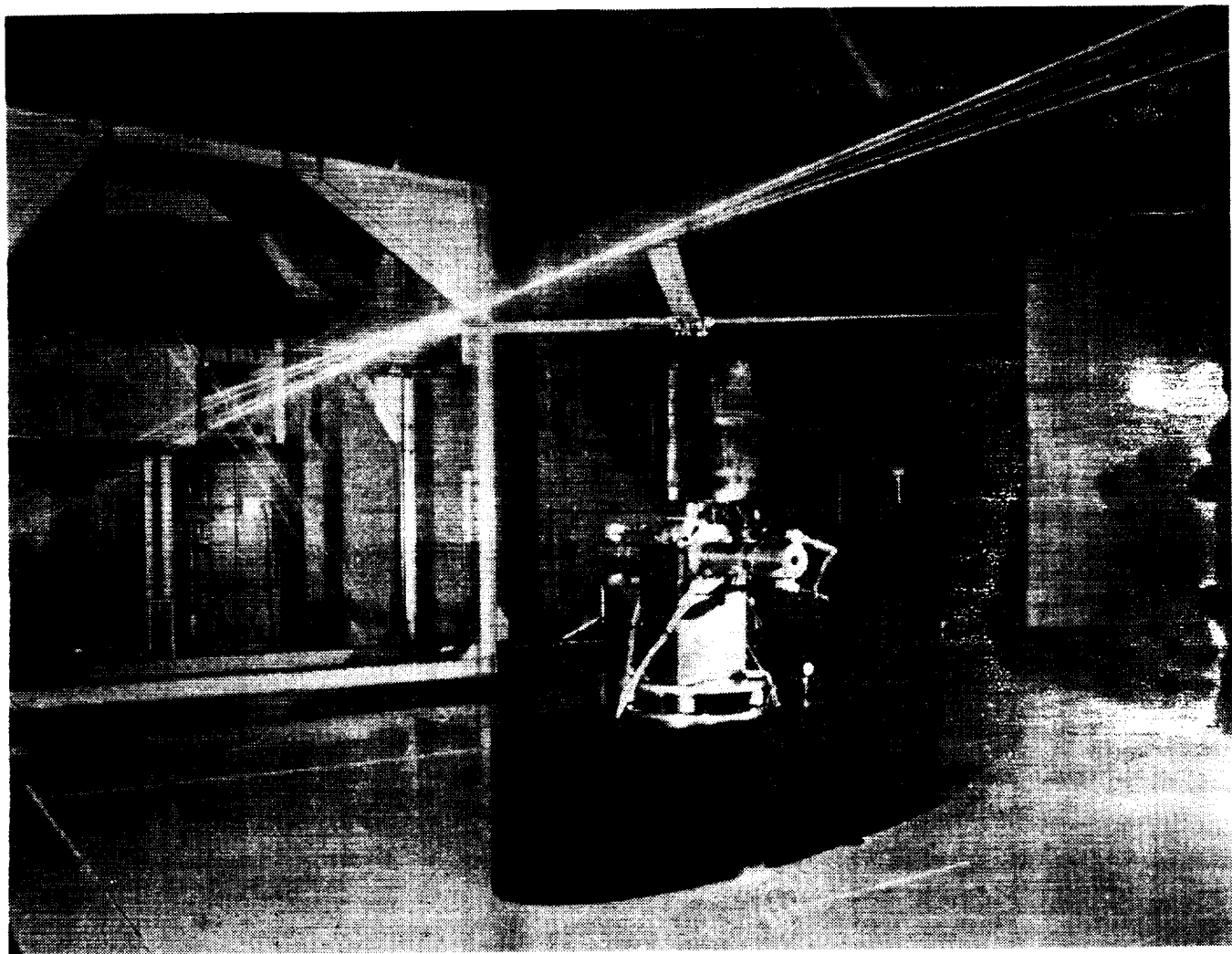


Figure 3.- PFM Test Stand and ALR installed in the test section with the LV and Traversing Platform in the background.

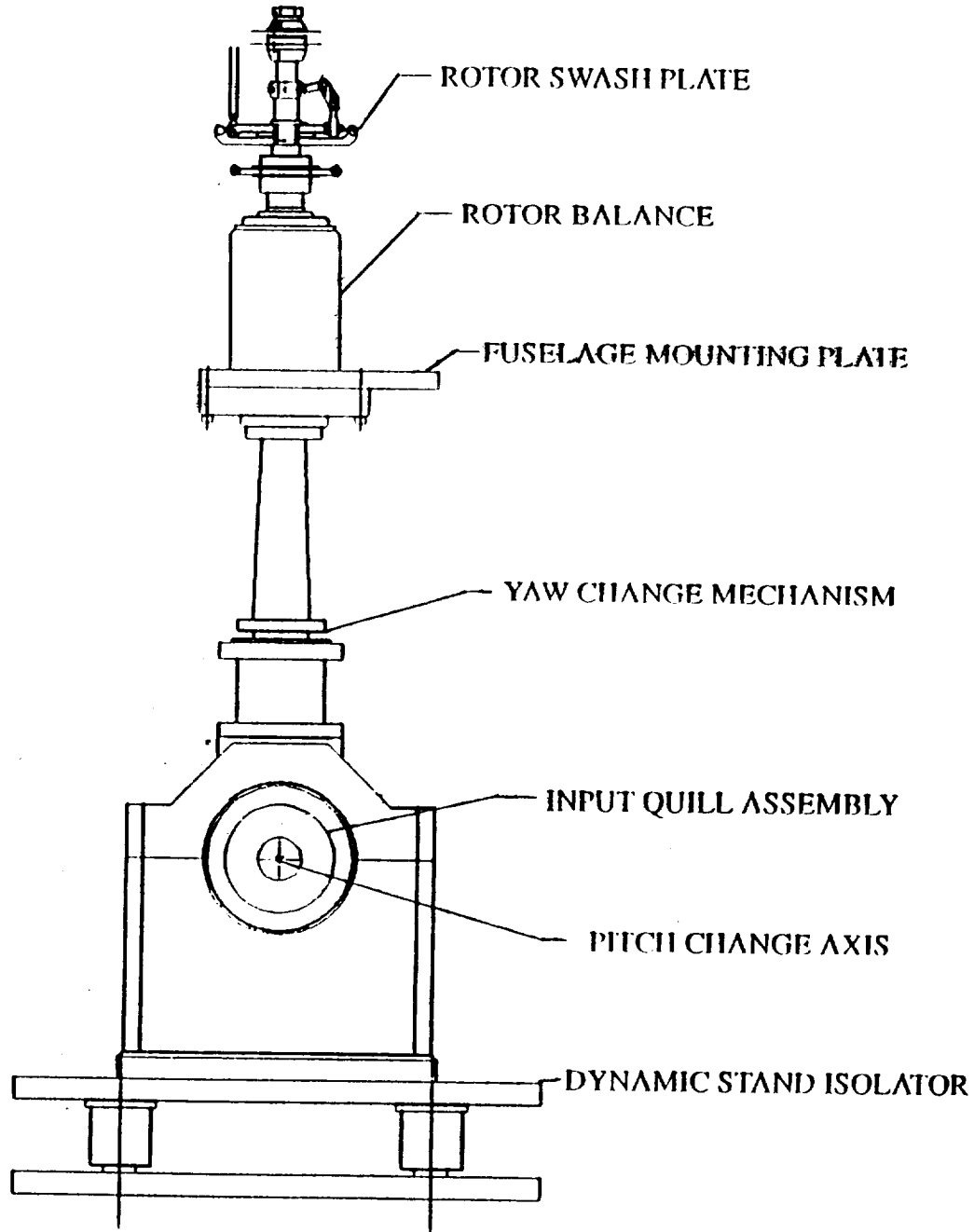


Figure 4.- BHTI Powered Force Model (PFM).

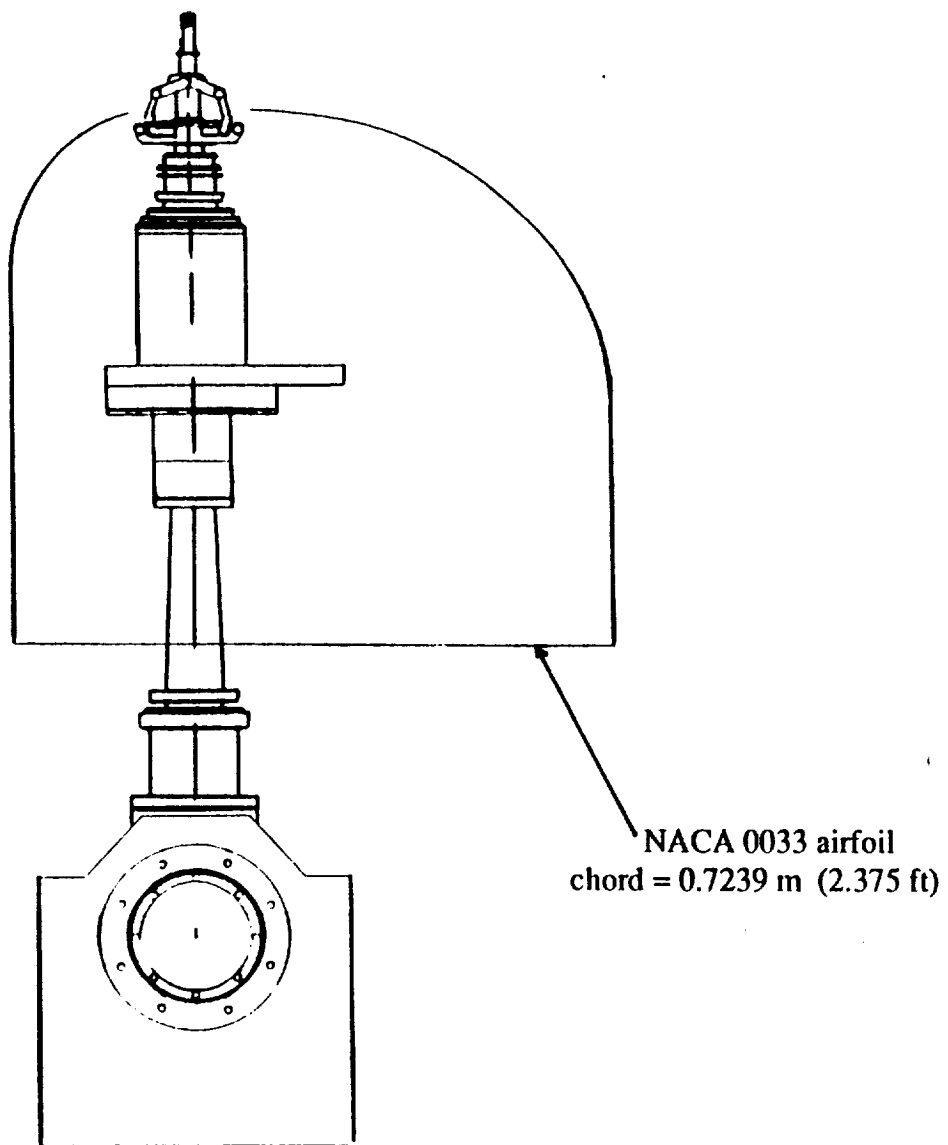


Figure 5.- PFM rotor test stand fairing.

ALR ROTOR BLADE TWIST DISTRIBUTION

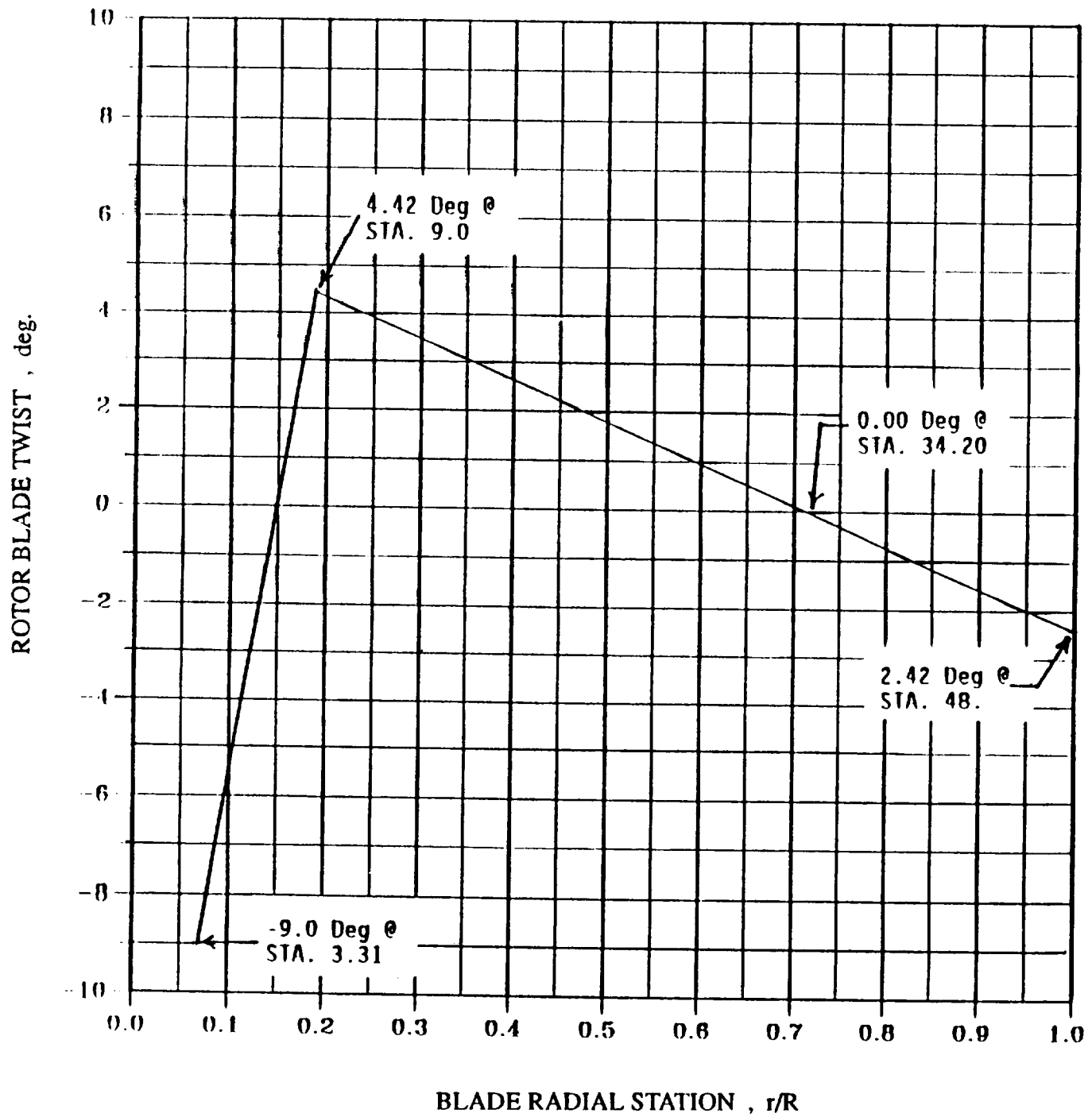


Figure 6.- ALR rotor blade twist characteristics.

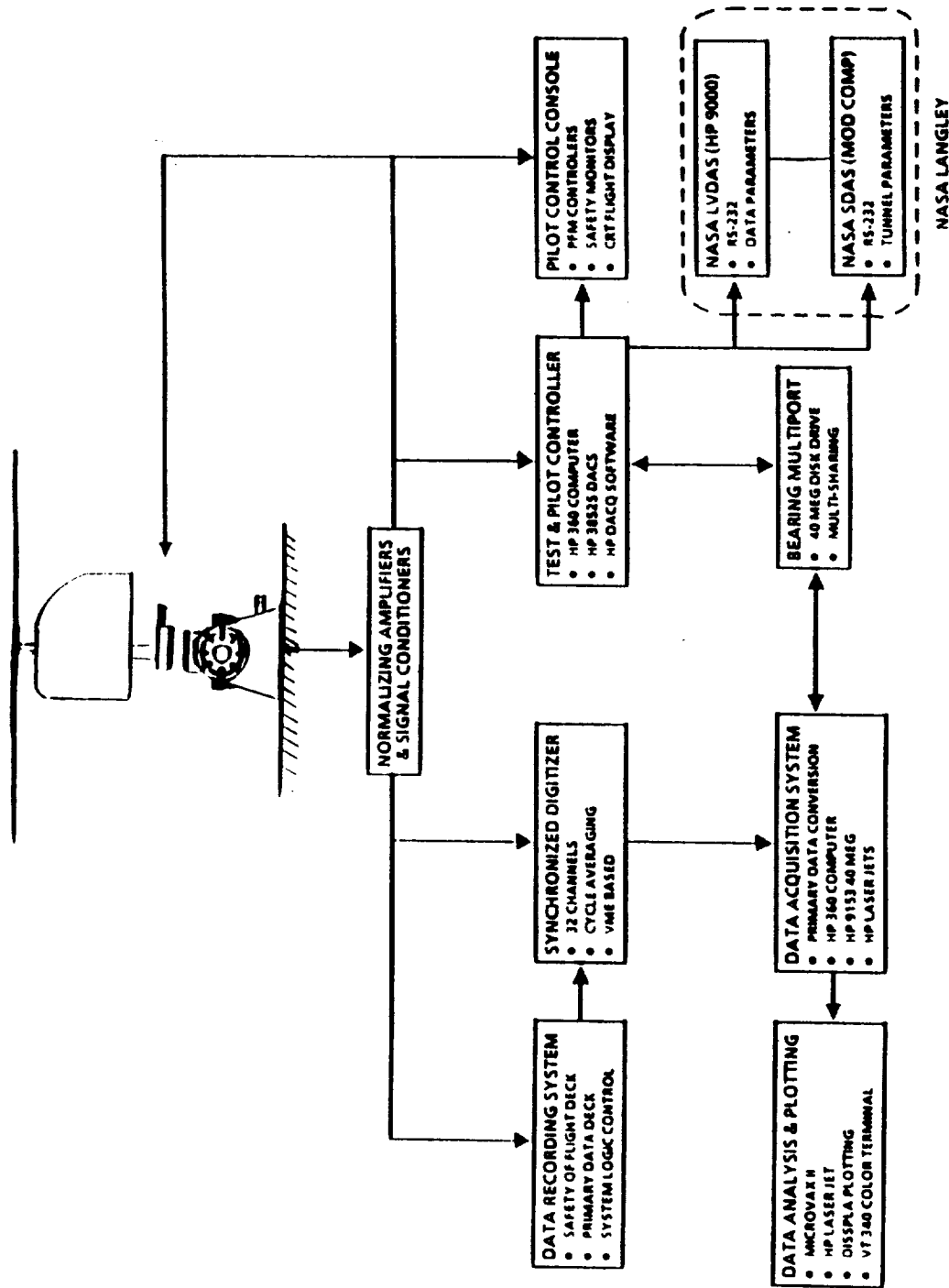


Figure 7.- PFM model data acquisition system.

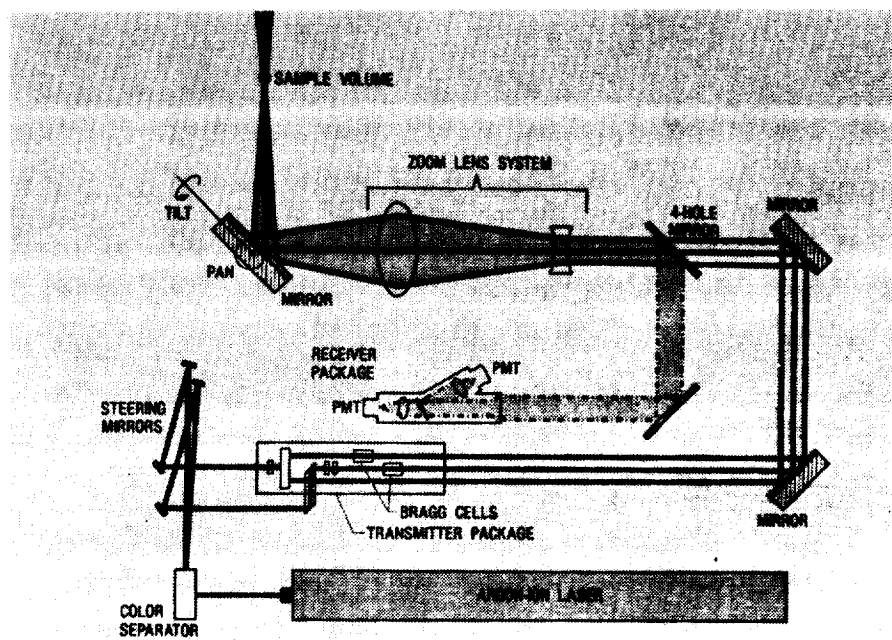


Figure 8.- Schematic diagram of LV optics subsystem.

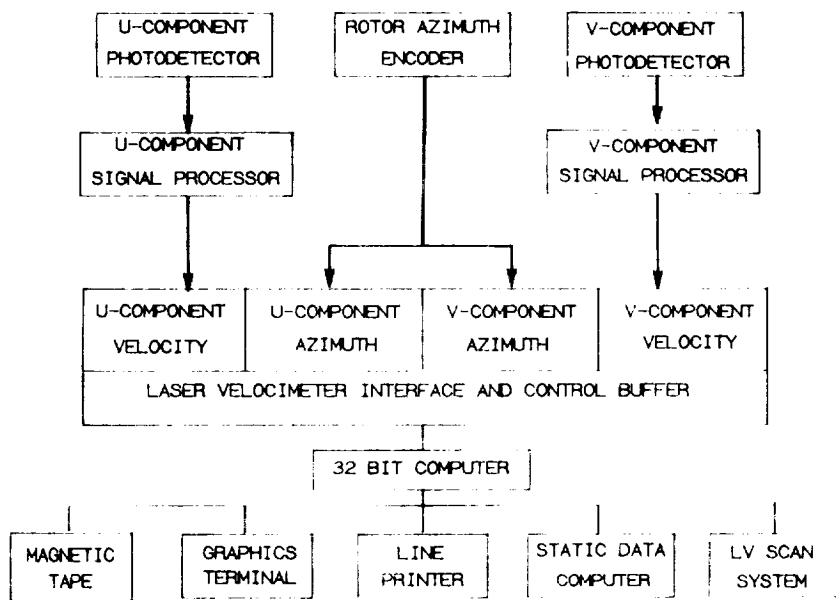


Figure 9.- Schematic diagram of LV data acquisition and control subsystem.

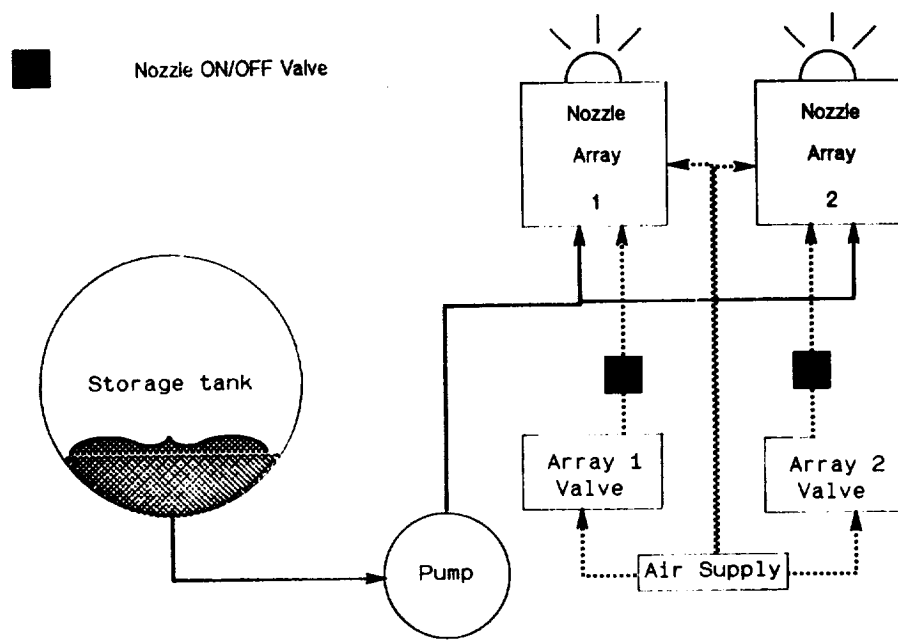


Figure 10.- Schematic of LV seeding subsystem.

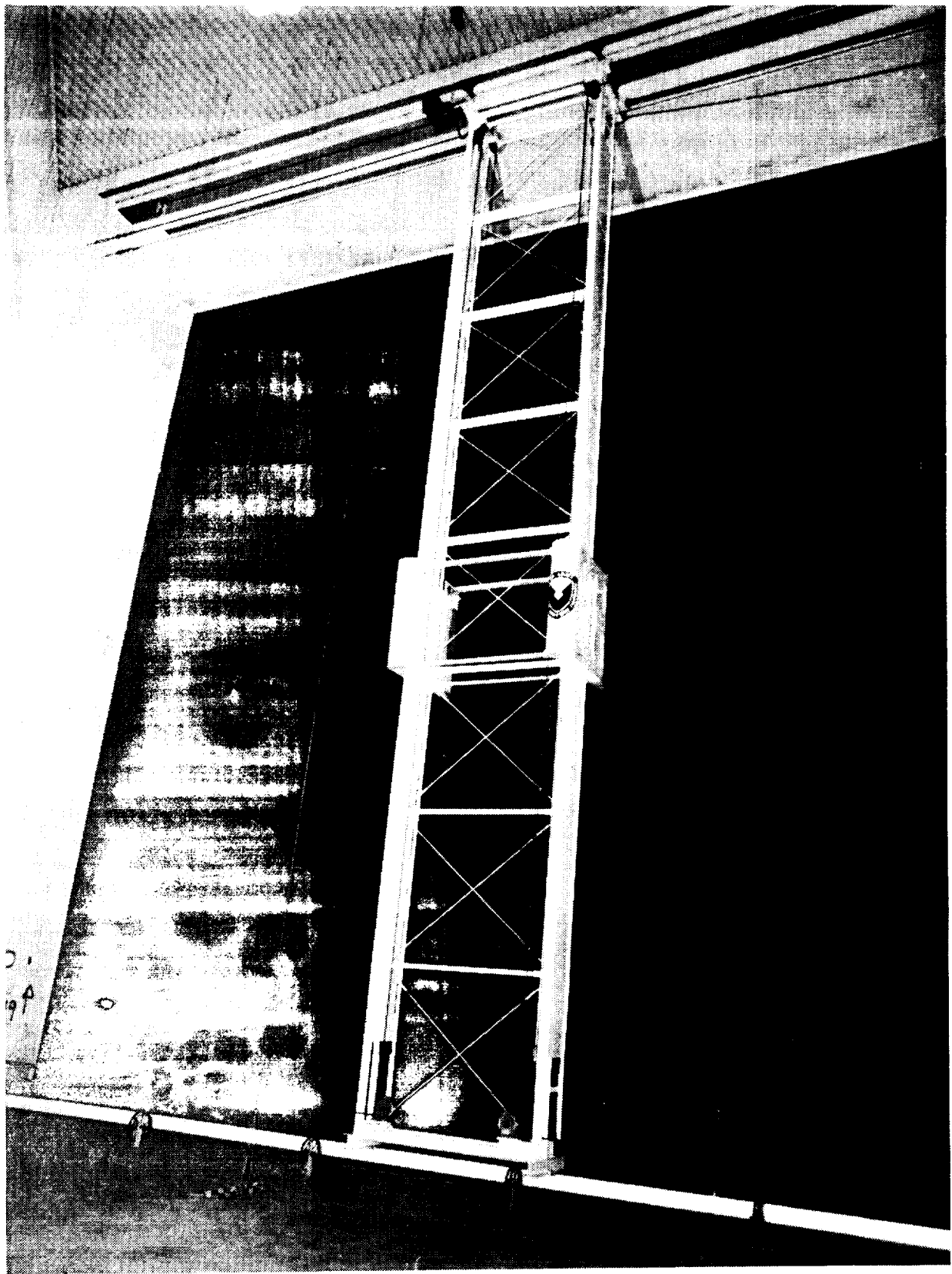


Figure 11.- Traverse assembly for LV seeding subsystem shown in the settling chamber of the tunnel.

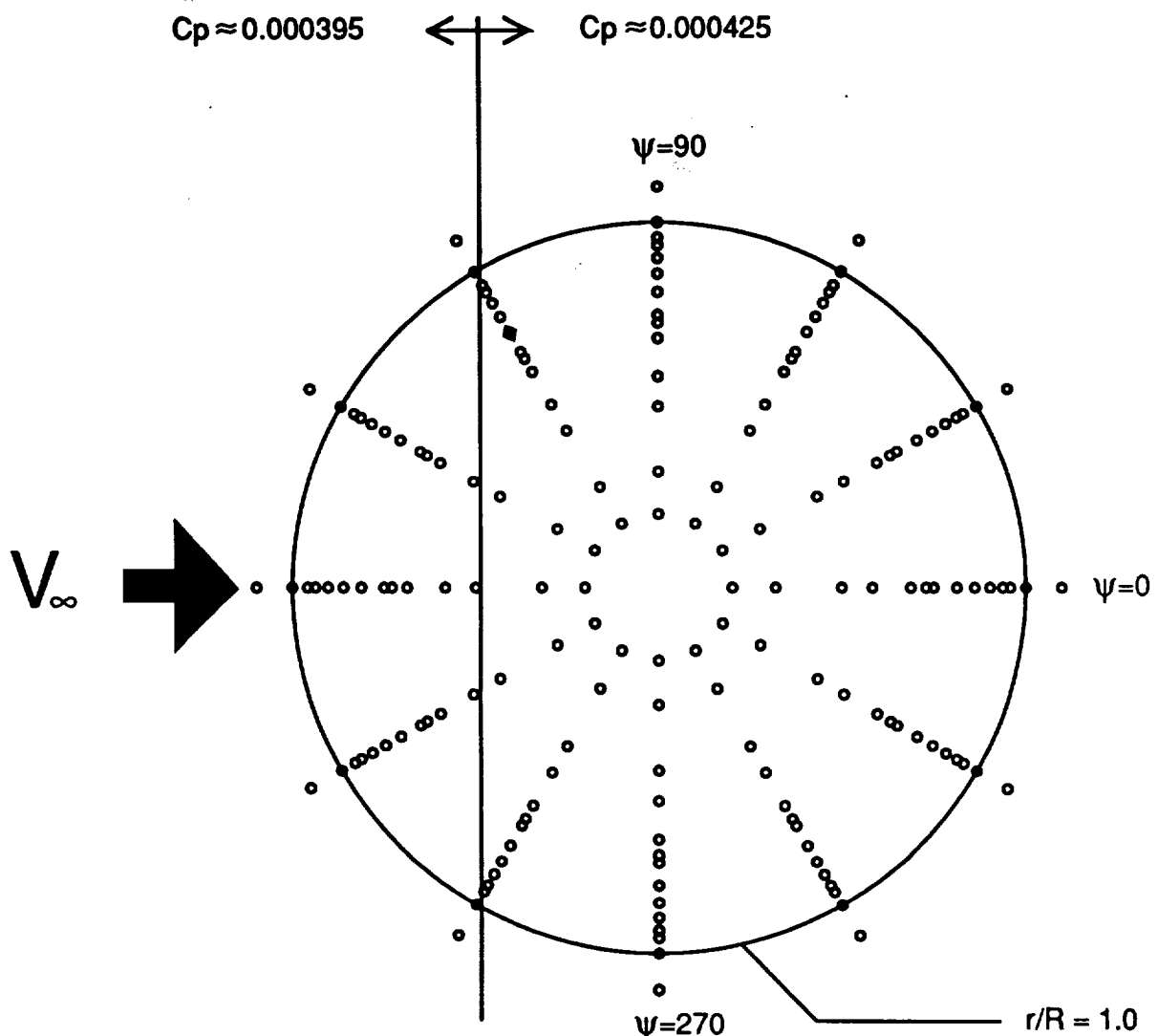


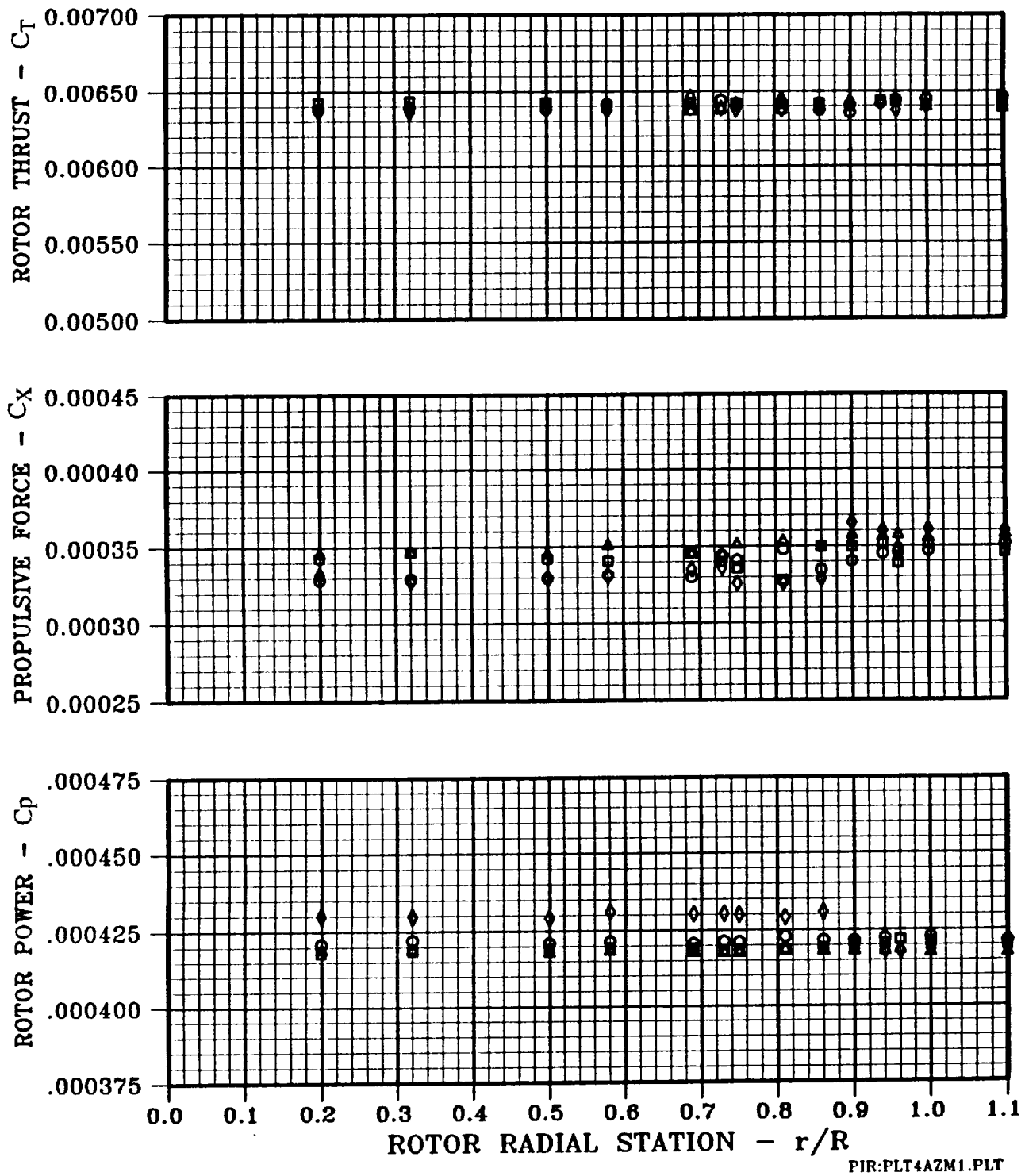
Figure 12.- Locations of the Inflow Measurement points,
3.72 inches above rotor tip path plane.

**There were no wake measurements made for this flight condition.
This figure is left intentionally blank.**

Figure 13.- Location of the wake measurement points.

There were no wake measurements made for this flight condition.
This figure is left intentionally blank.

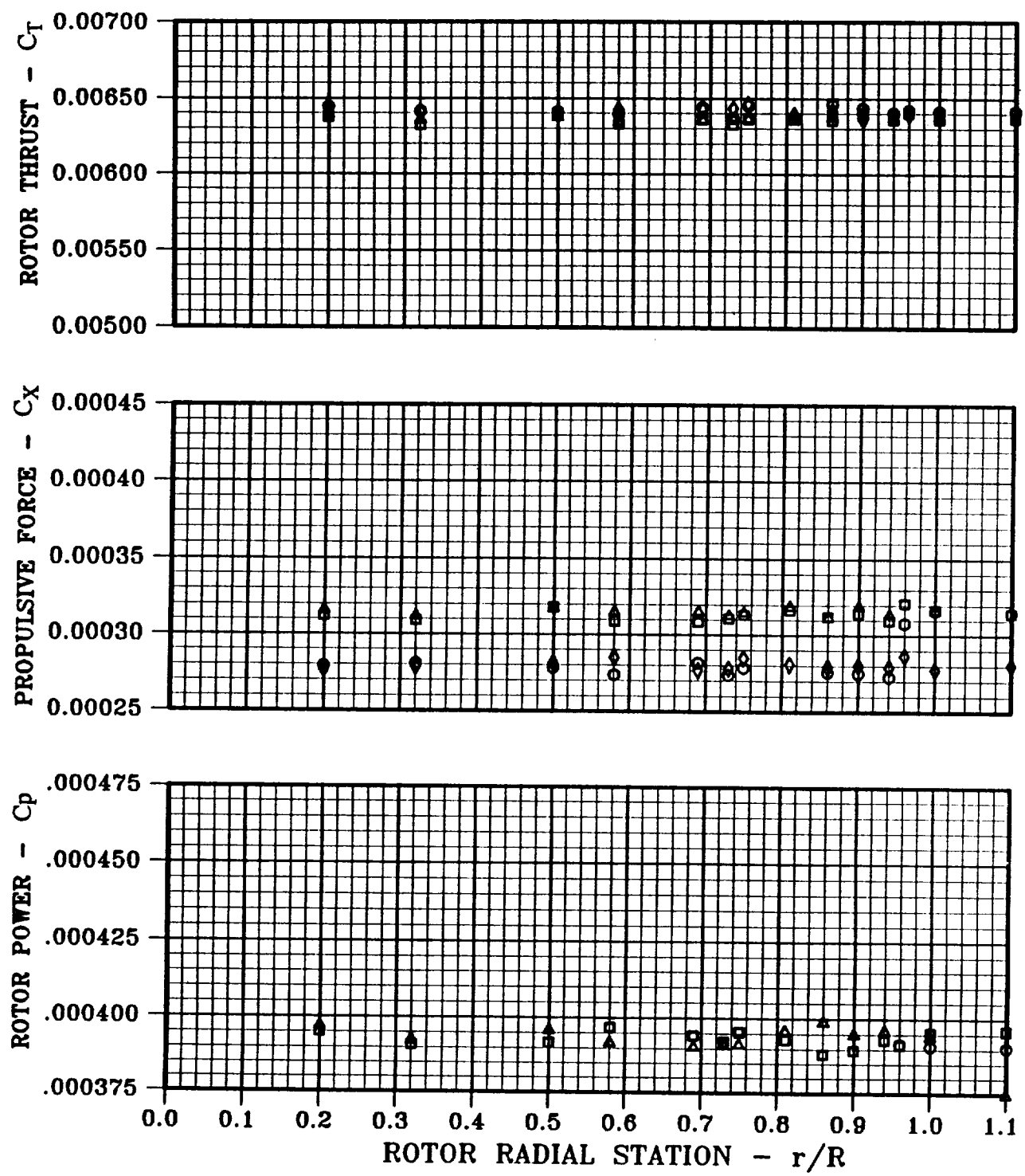
Figure 14.- Wake measurements at $V_{tip} = 603$ fps ; $C_T = 0.0064$



PIR:PLT4AZM1.PLT

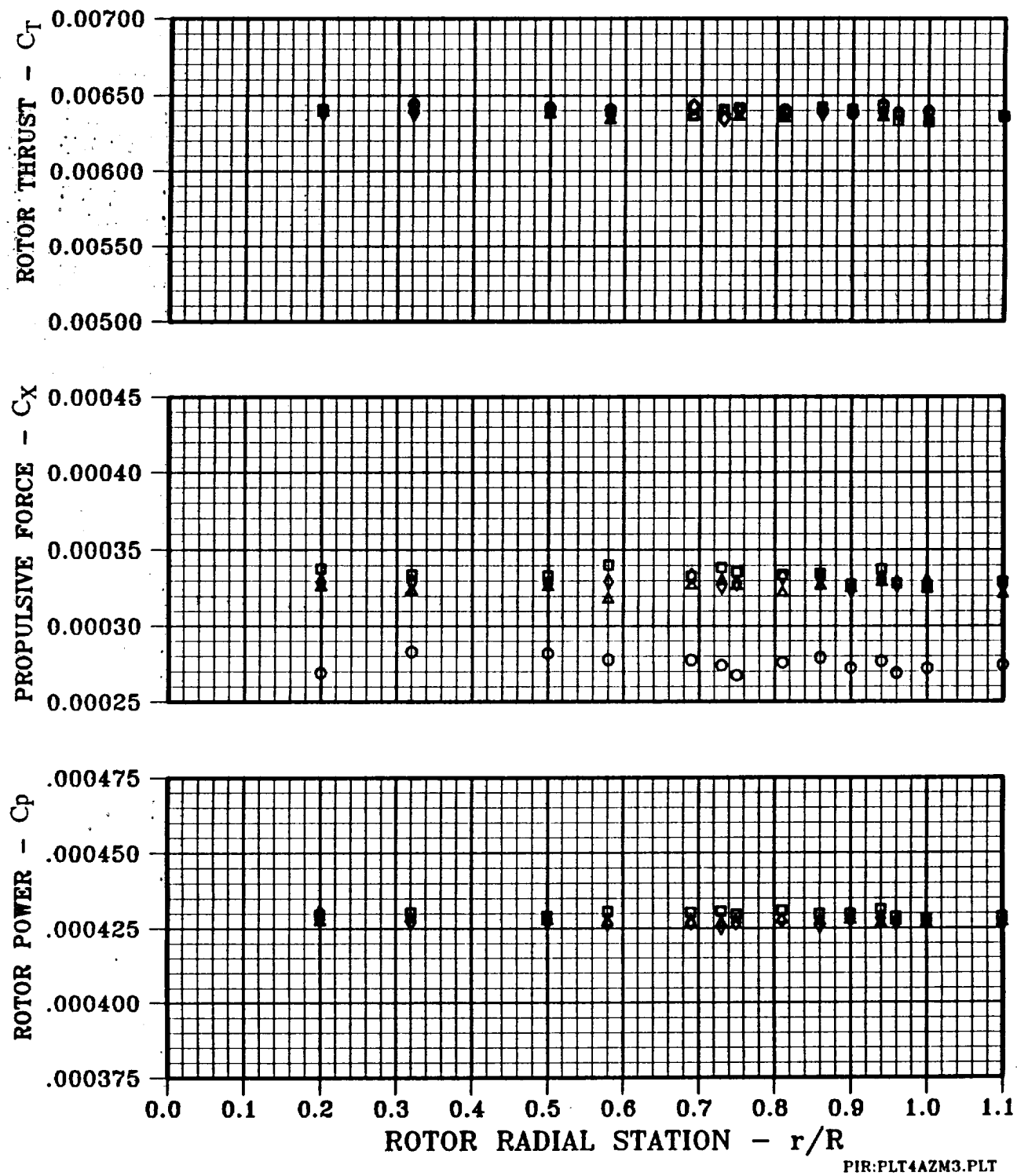
RADIAL	
○	0 DEG
□	30 DEG
△	60 DEG
◊	90 DEG

Figure 15.- Rotor performance parameters during LV measurements.



RADIAL
 ○ 120 DEG
 □ 150 DEG
 ▲ 180 DEG
 ♦ 210 DEG

Figure 15.- Continued.



RADIAL

- 240 DEG
- 270 DEG
- △ 300 DEG
- ◊ 330 DEG

Figure 15.- Concluded.

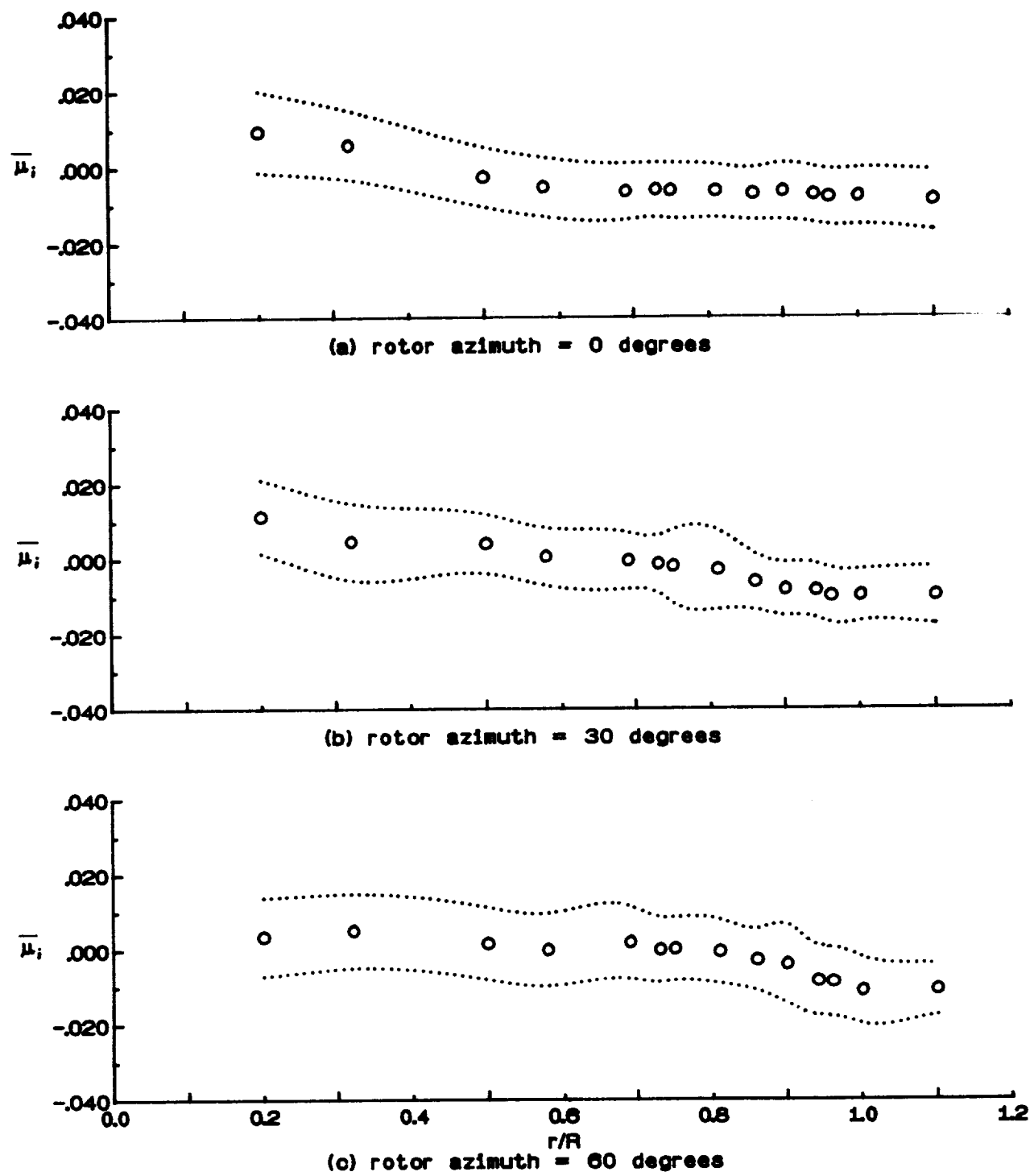
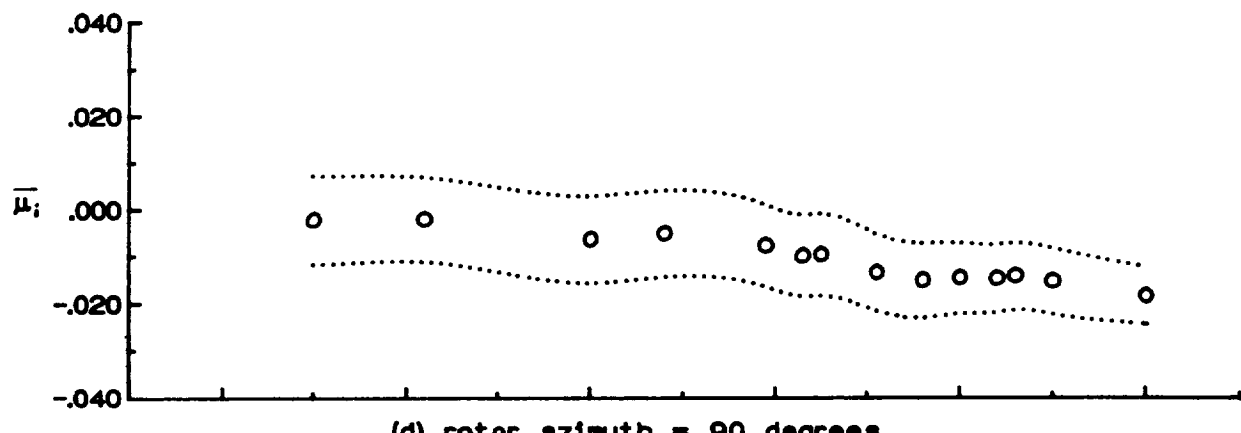
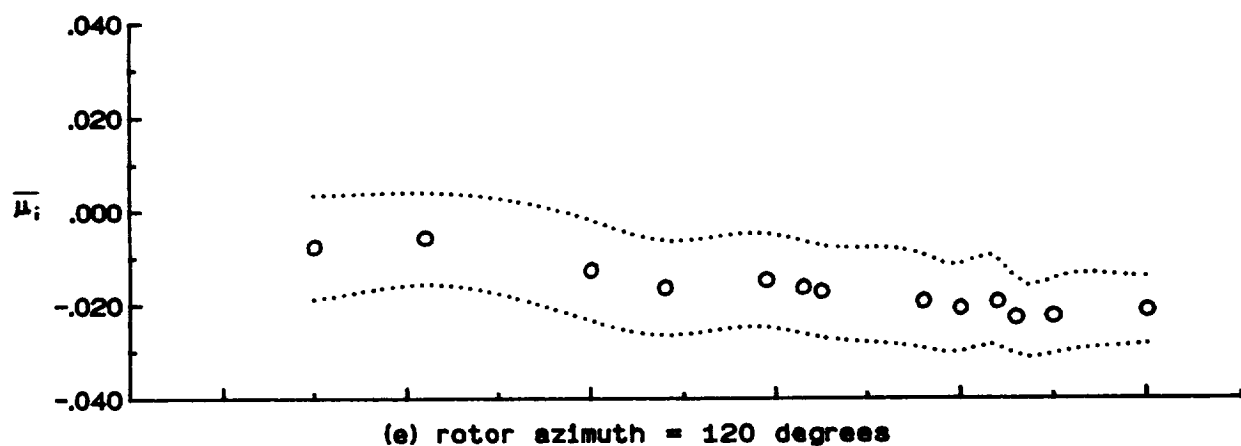


Figure 16.- Radial distribution of mean induced inflow ratio , $\bar{\mu}_i$.



(d) rotor azimuth = 90 degrees



(e) rotor azimuth = 120 degrees

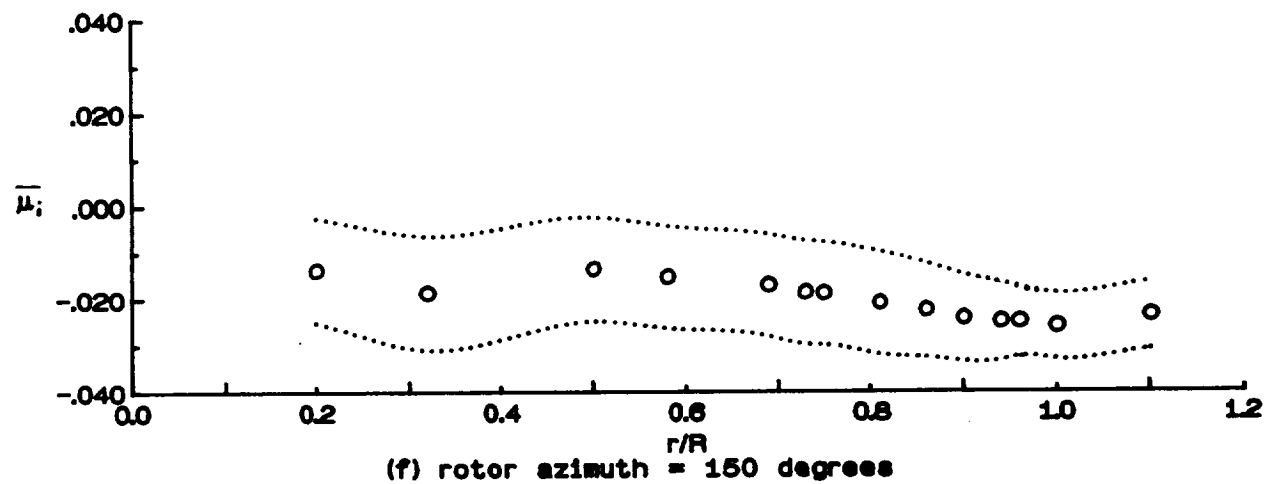


Figure 16.- Continued.

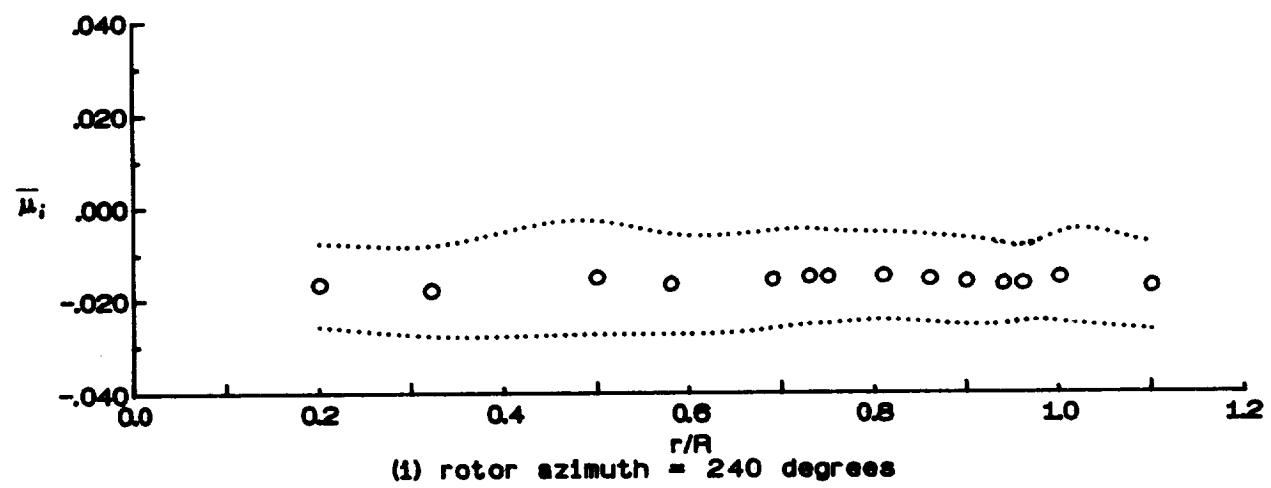
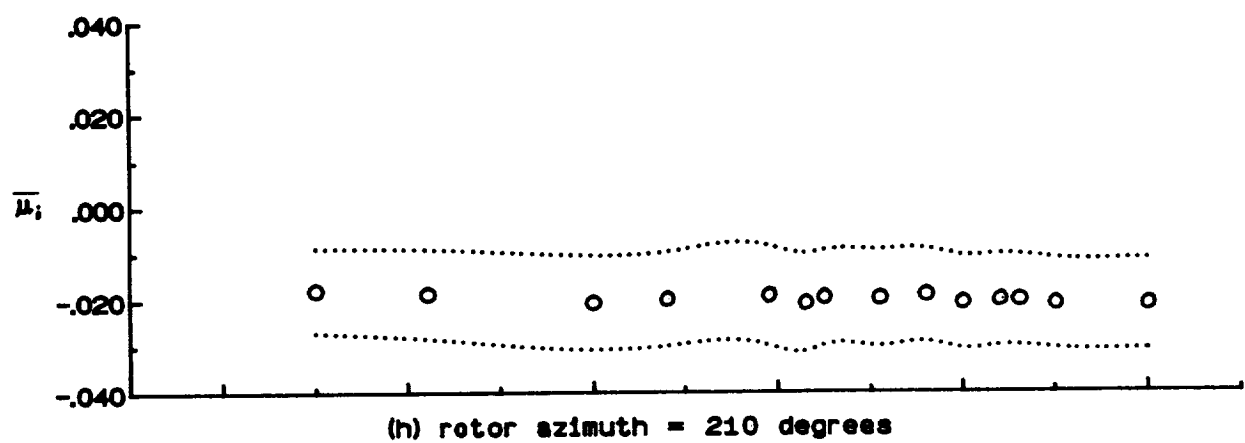
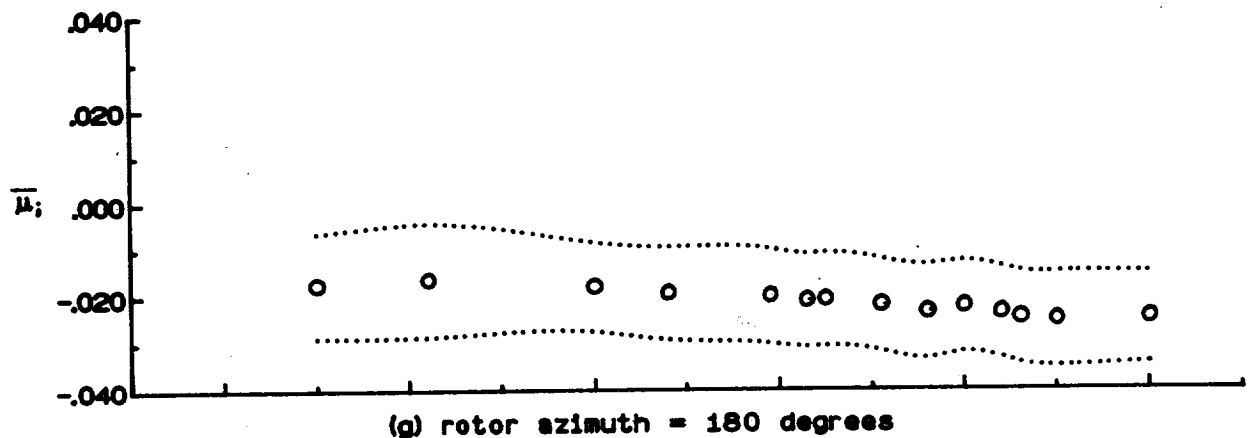
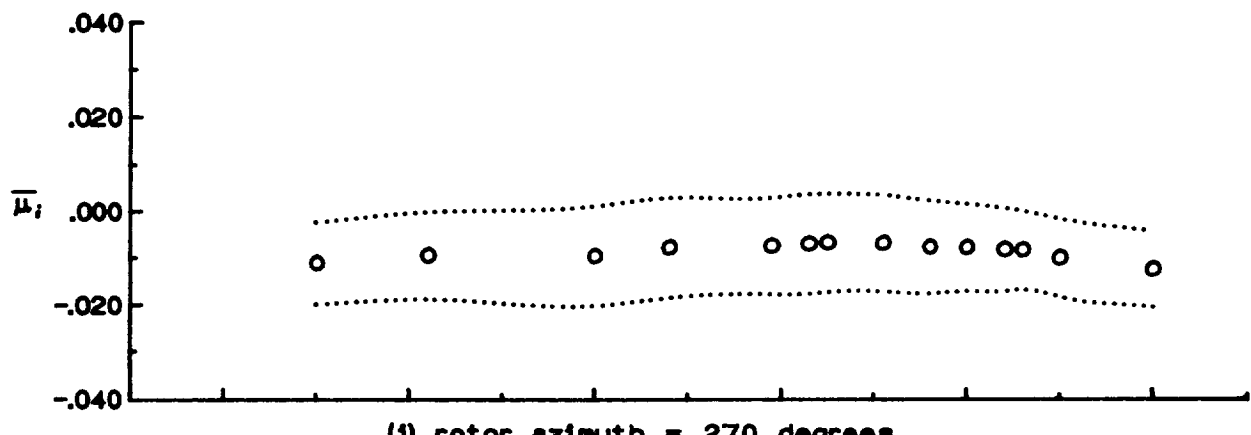
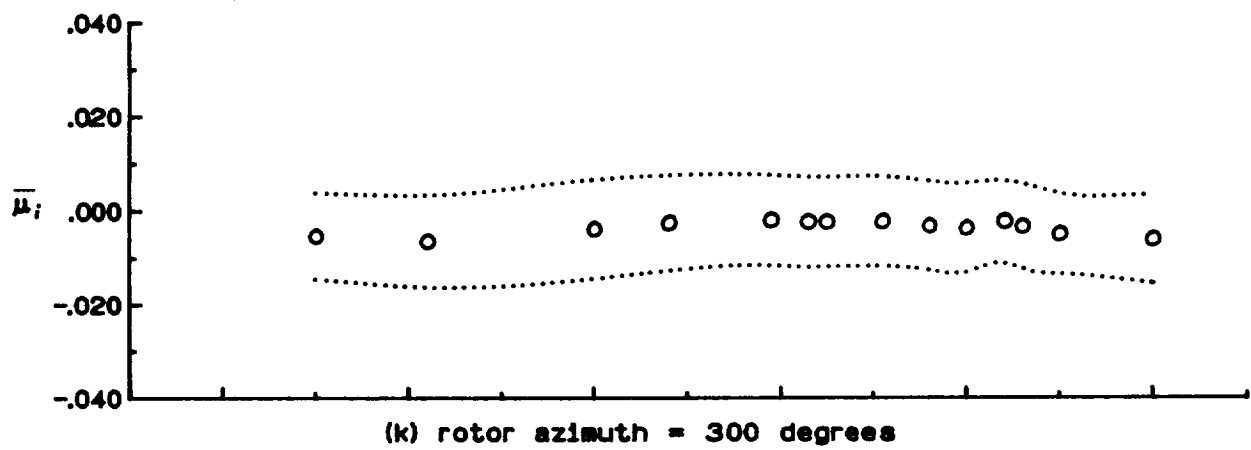


Figure 16.- Continued.



(j) rotor azimuth = 270 degrees



(k) rotor azimuth = 300 degrees

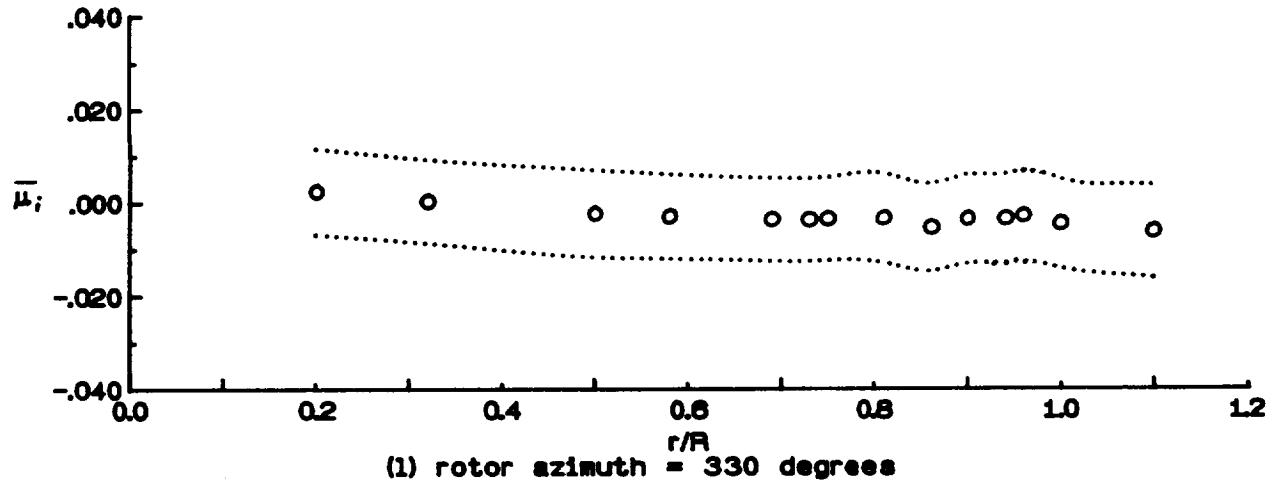


Figure 16.- Concluded.

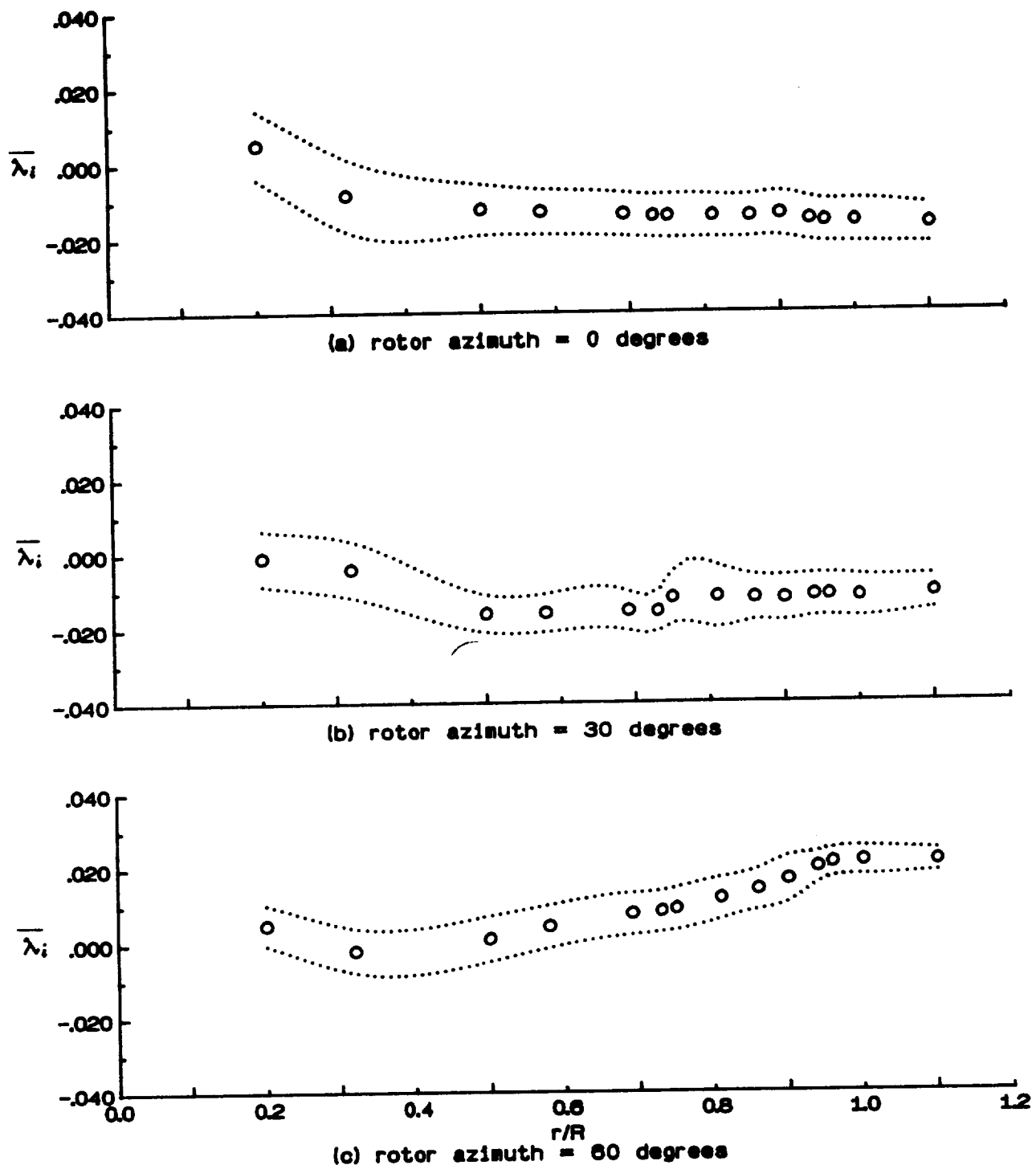


Figure 17.- Radial distribution of mean induced inflow ratio , $\bar{\lambda}_i$.

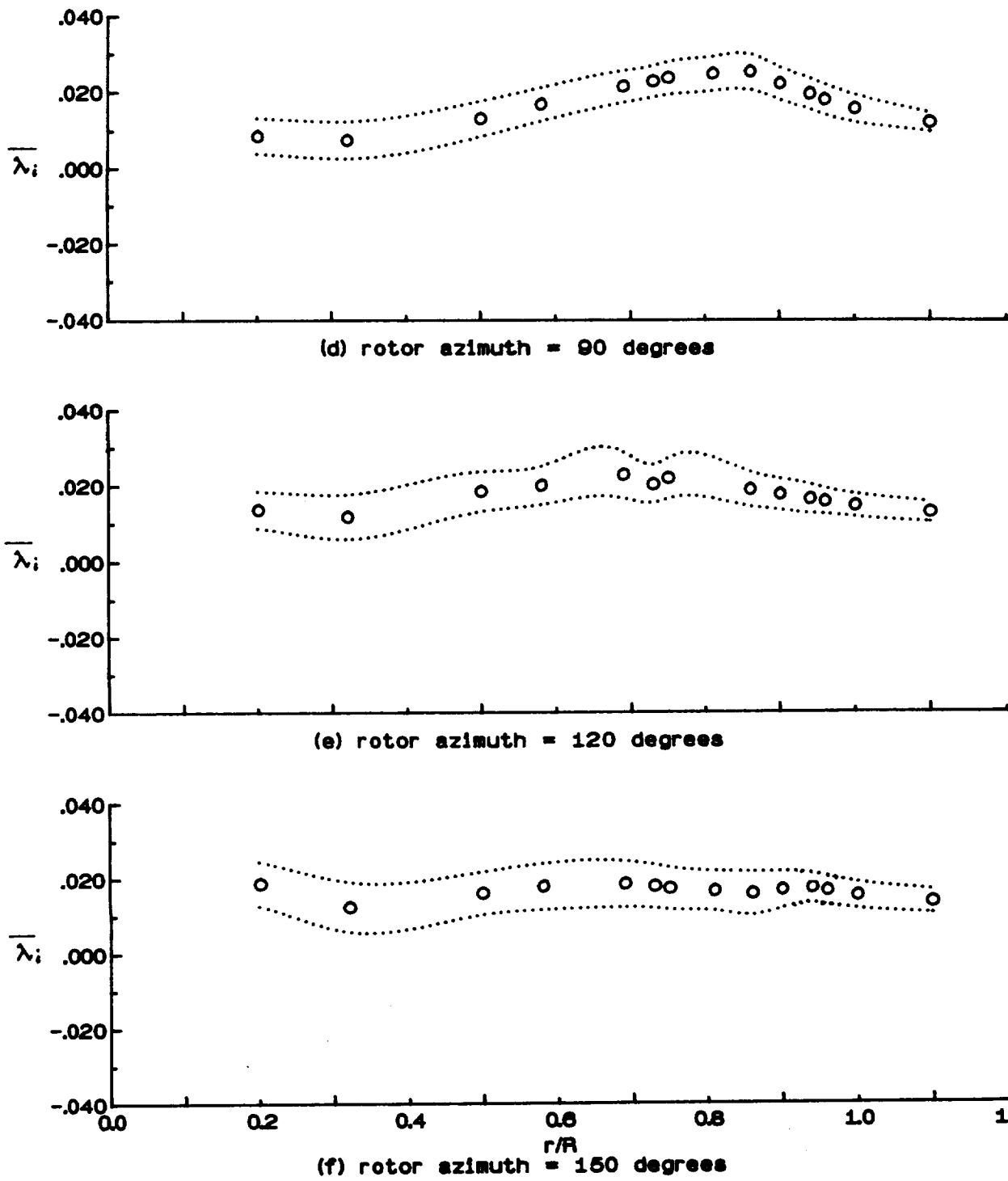


Figure 17.- Continued.

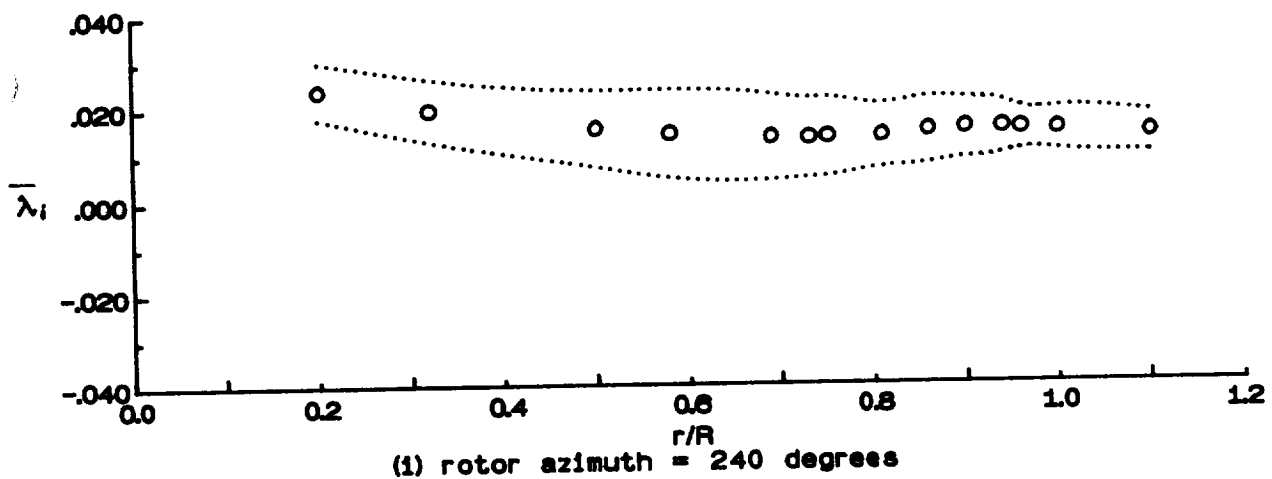
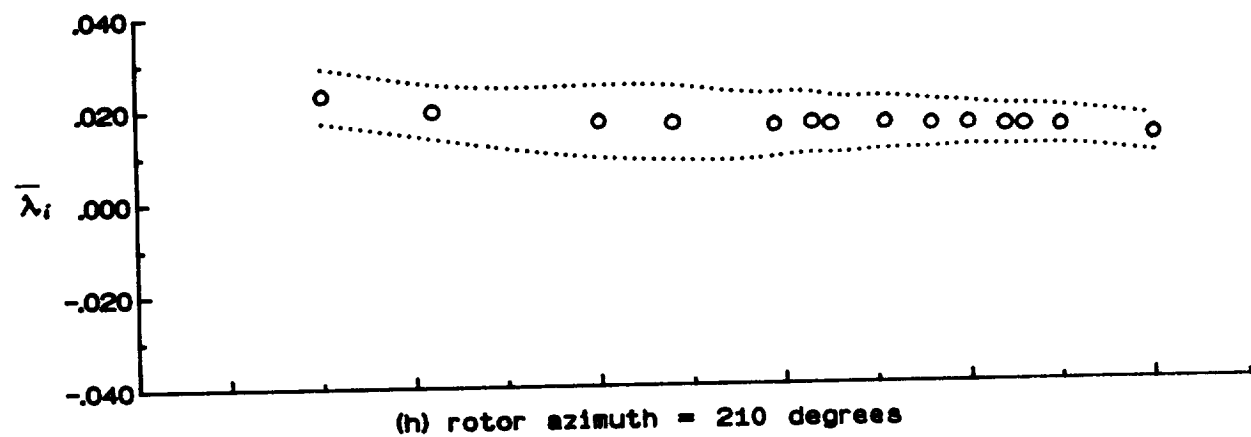
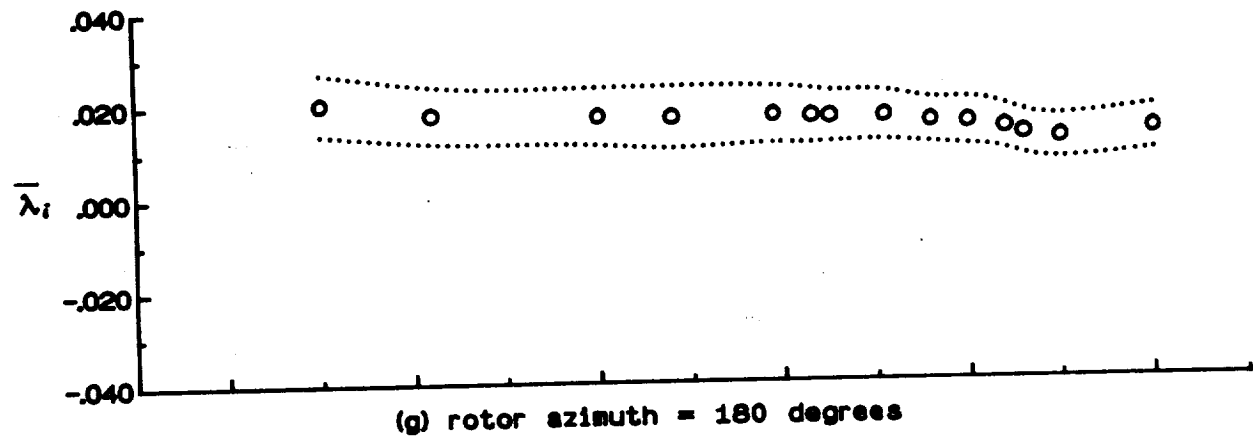
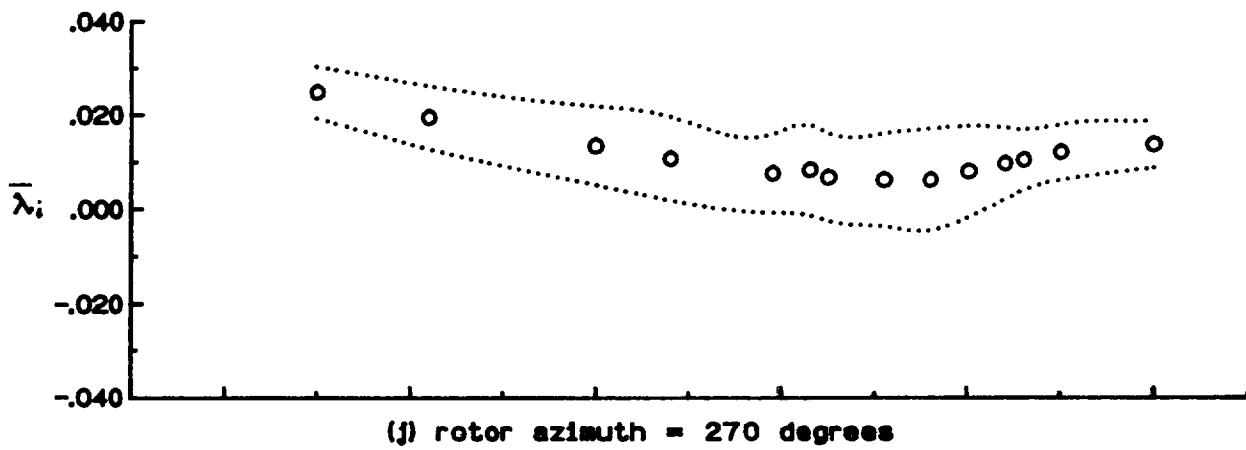
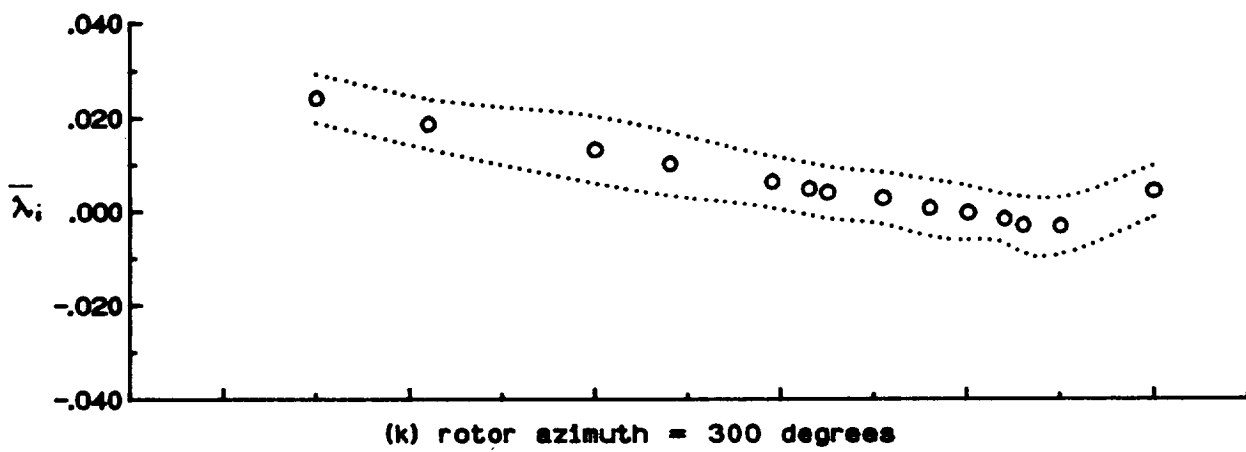


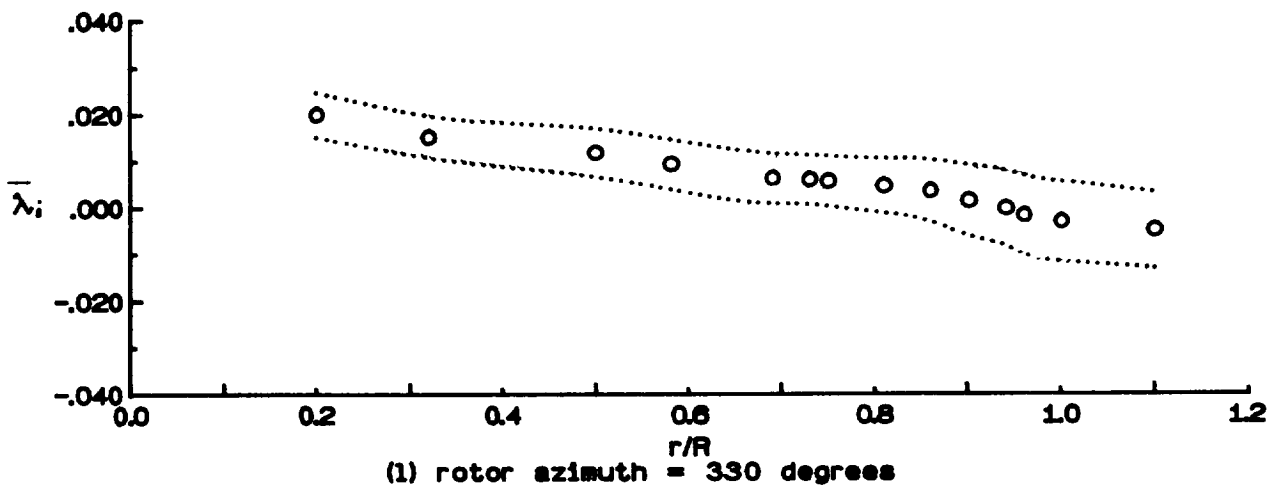
Figure 17.- Continued.



(j) rotor azimuth = 270 degrees

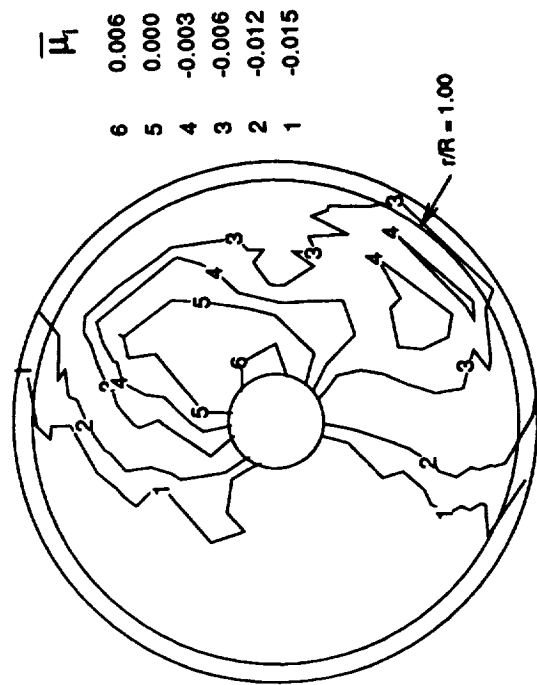


(k) rotor azimuth = 300 degrees

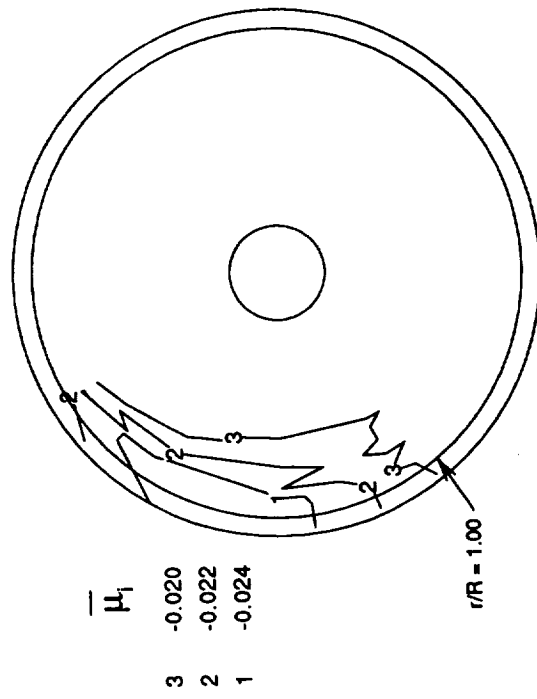


(l) rotor azimuth = 330 degrees

Figure 17.- Concluded.

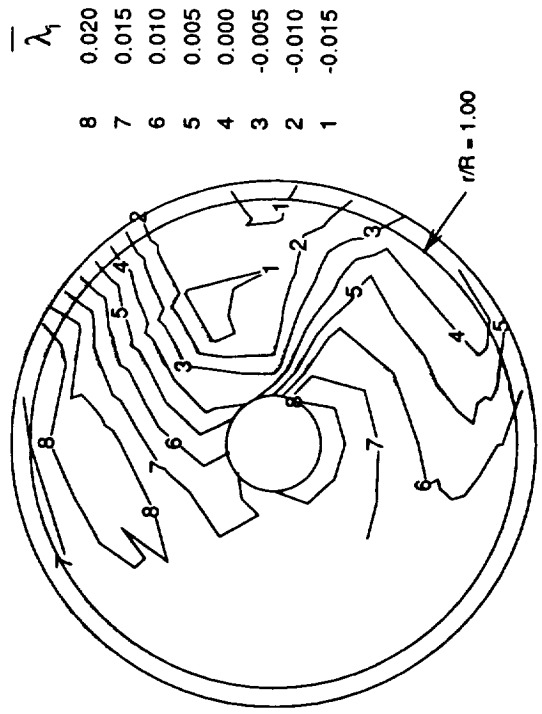


$$C_p \approx 0.000425$$



$$C_p \approx 0.000395$$

Figure 18.- Contour plot of mean induced inflow ratio, $\bar{\mu}_i$.



$V_\infty \Rightarrow$

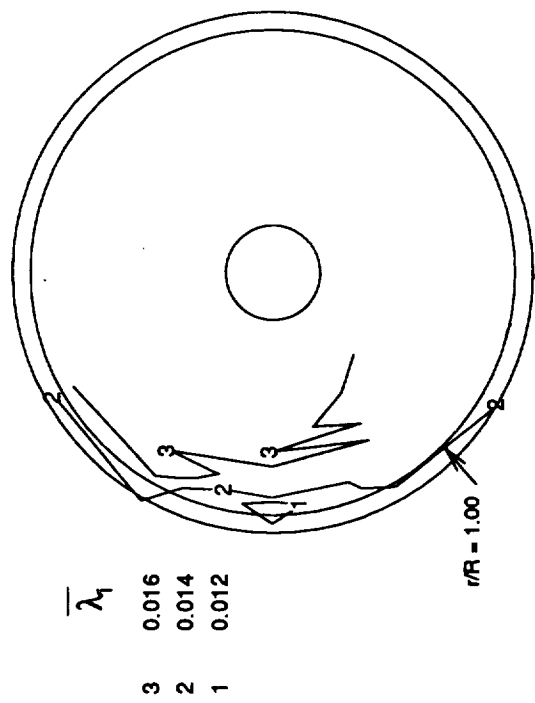


Figure 19.- Contour plot of mean induced inflow ratio, $\bar{\lambda}_1$.

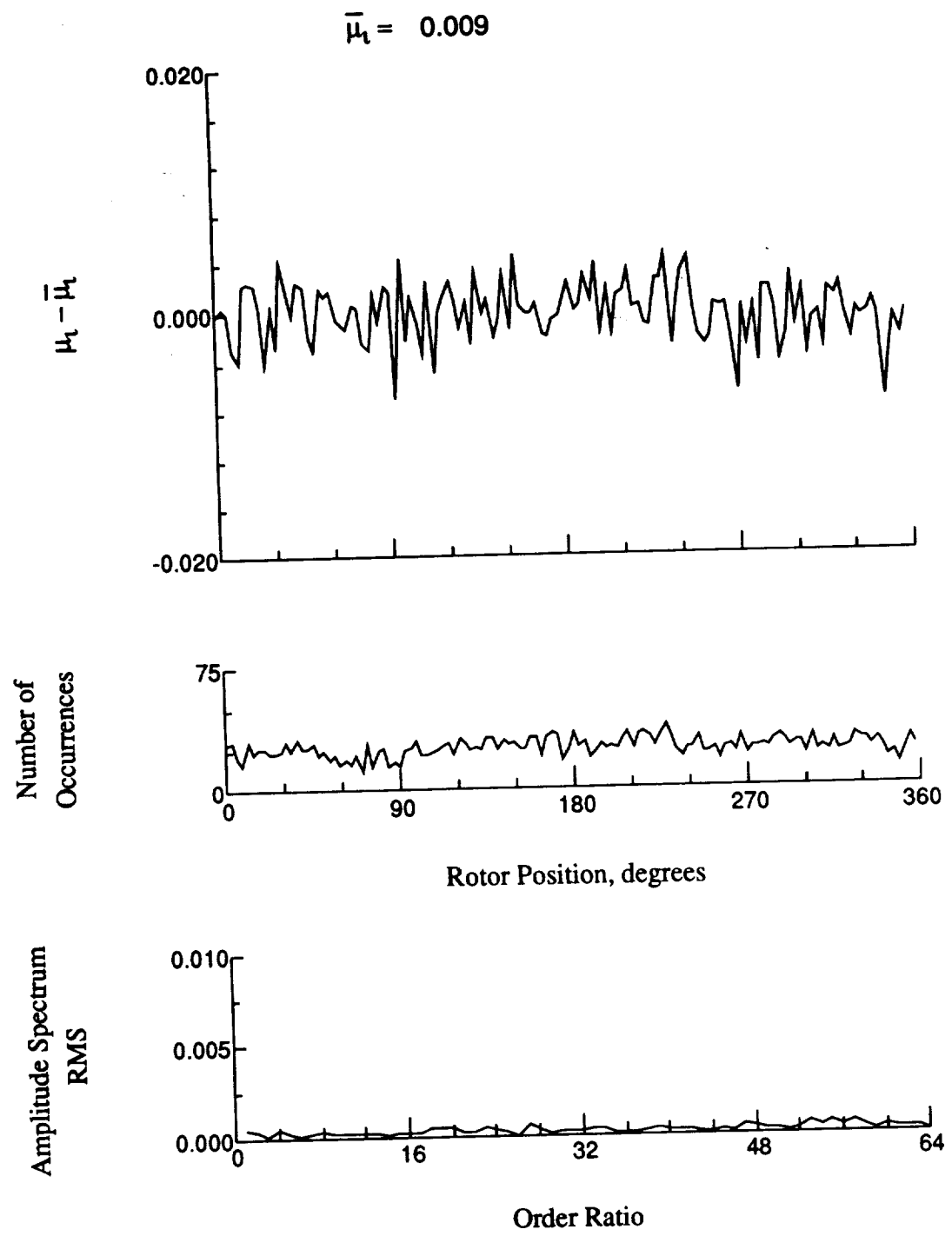


Figure 20.- Induced inflow velocity measured at 0 degrees and r/R of 0.20.

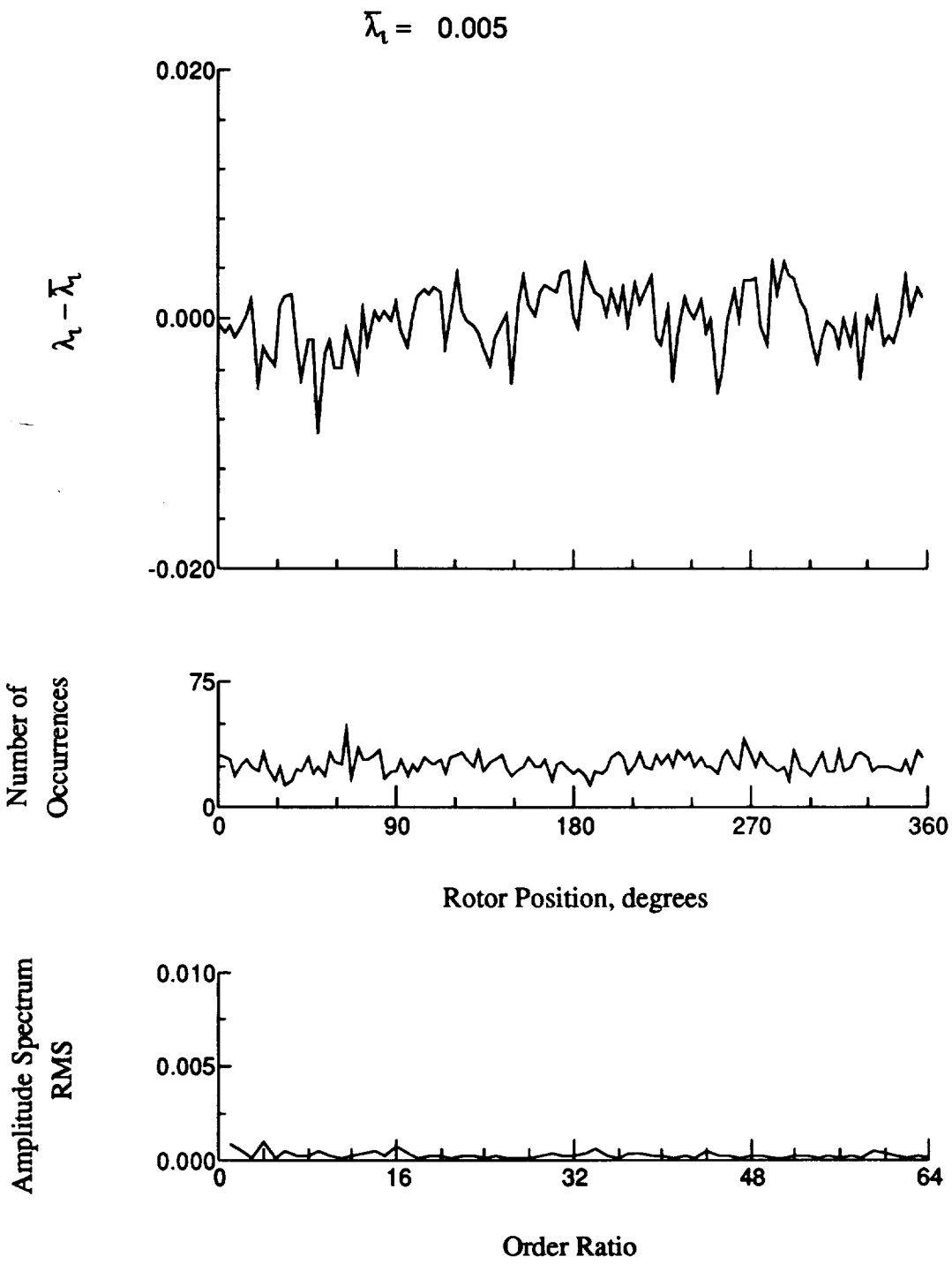


Figure 20.- Concluded.

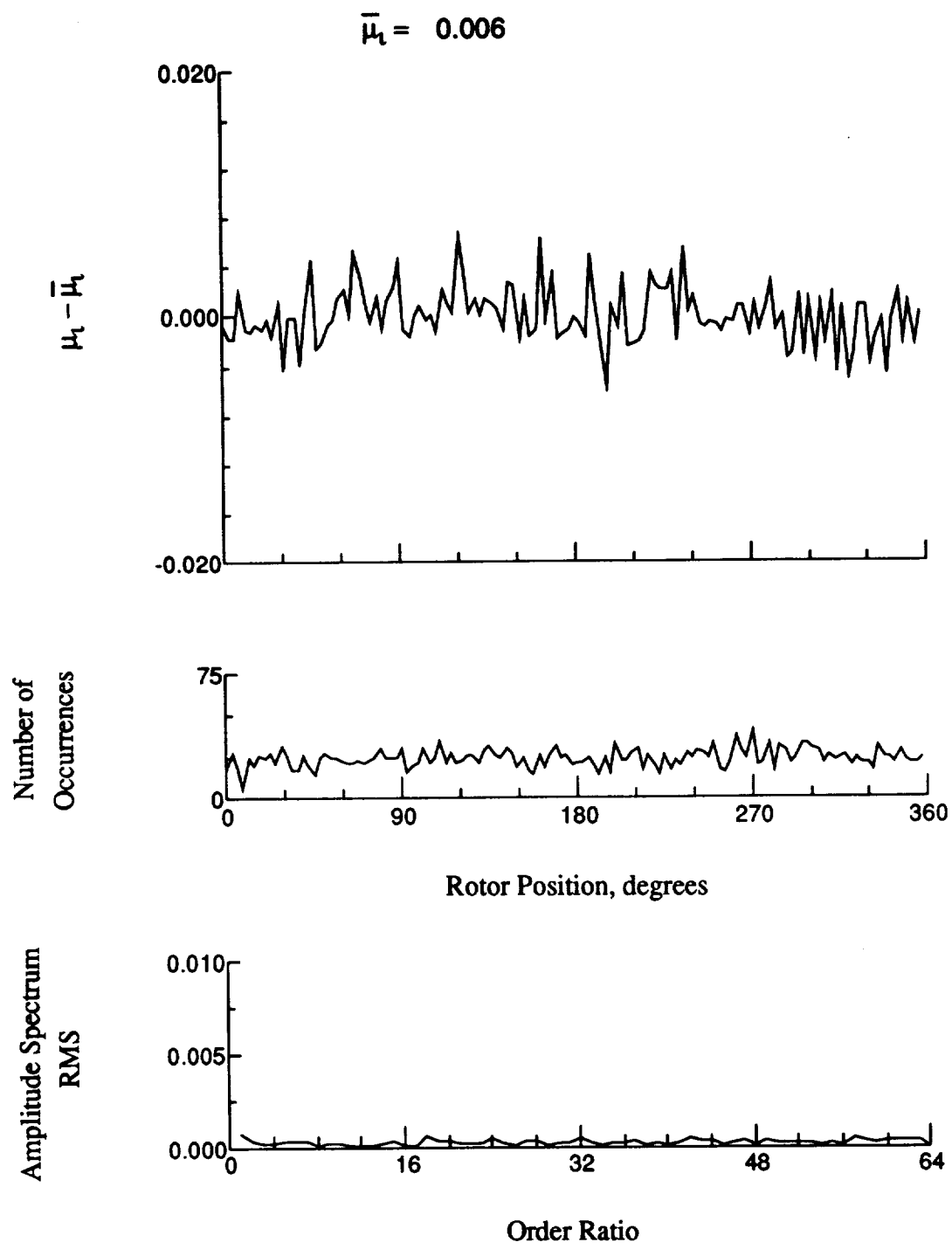


Figure 21.- Induced inflow velocity measured at 0 degrees and r/R of 0.32.

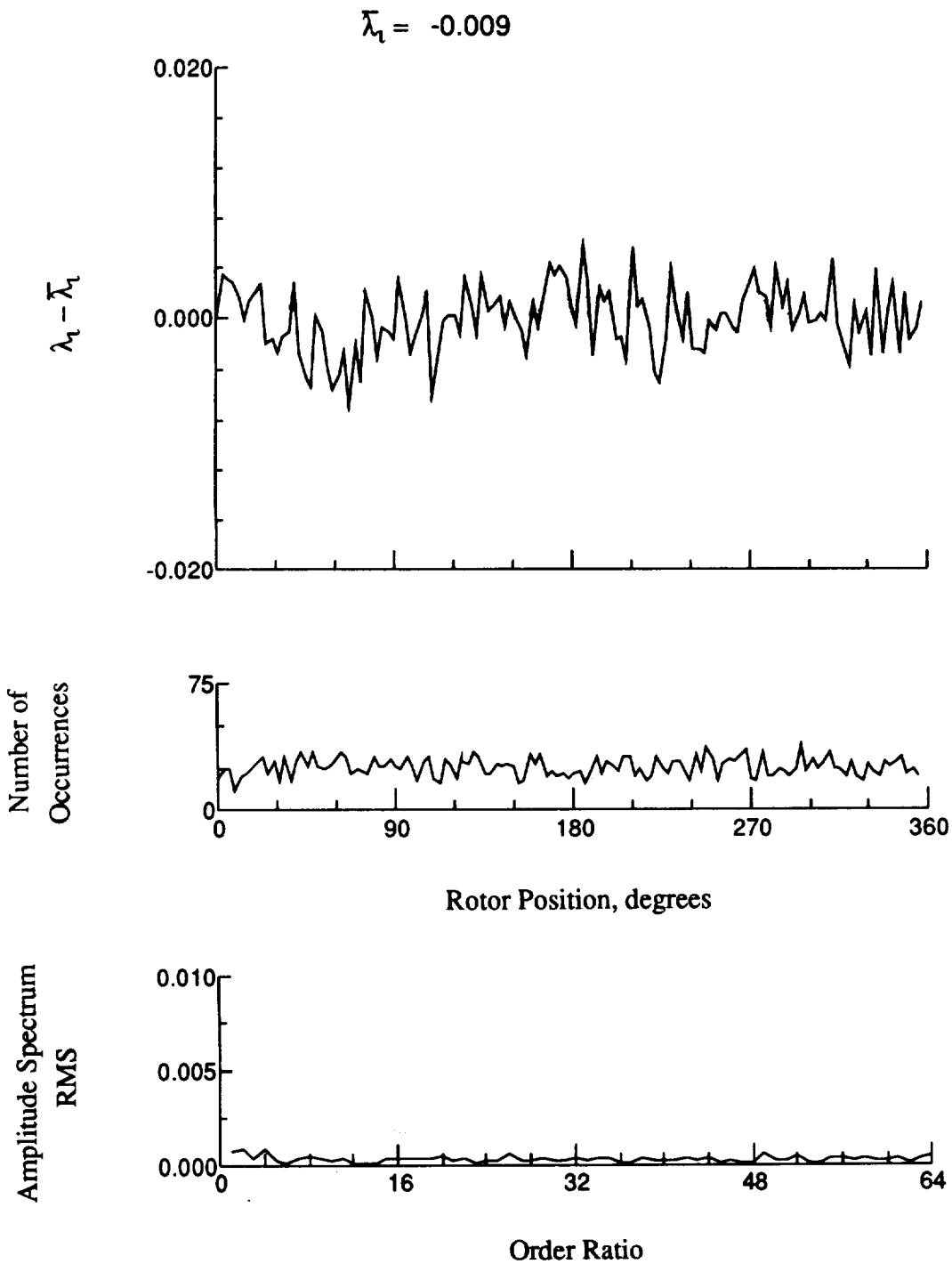


Figure 21.- Concluded.

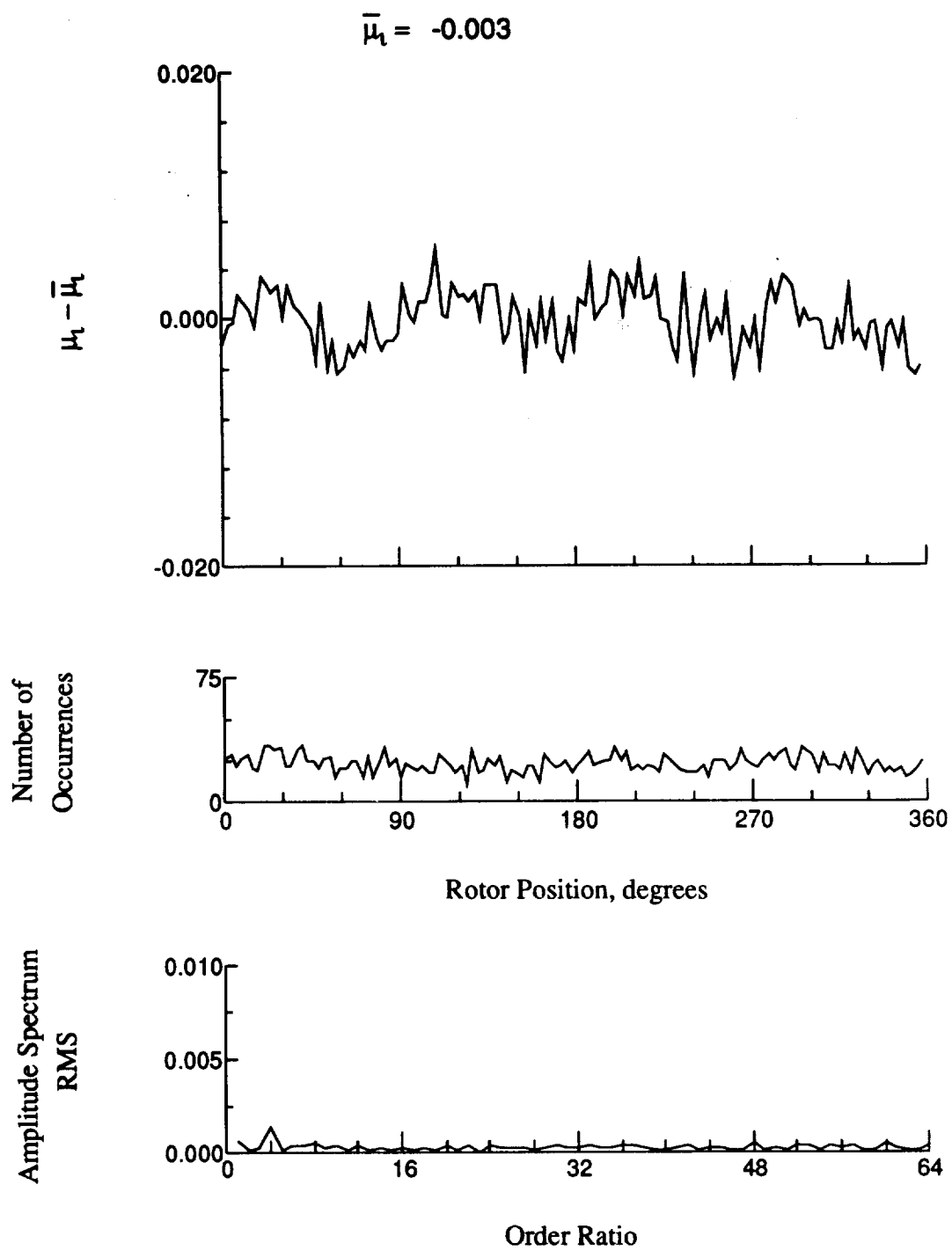


Figure 22.- Induced inflow velocity measured at 0 degrees and r/R of 0.50.

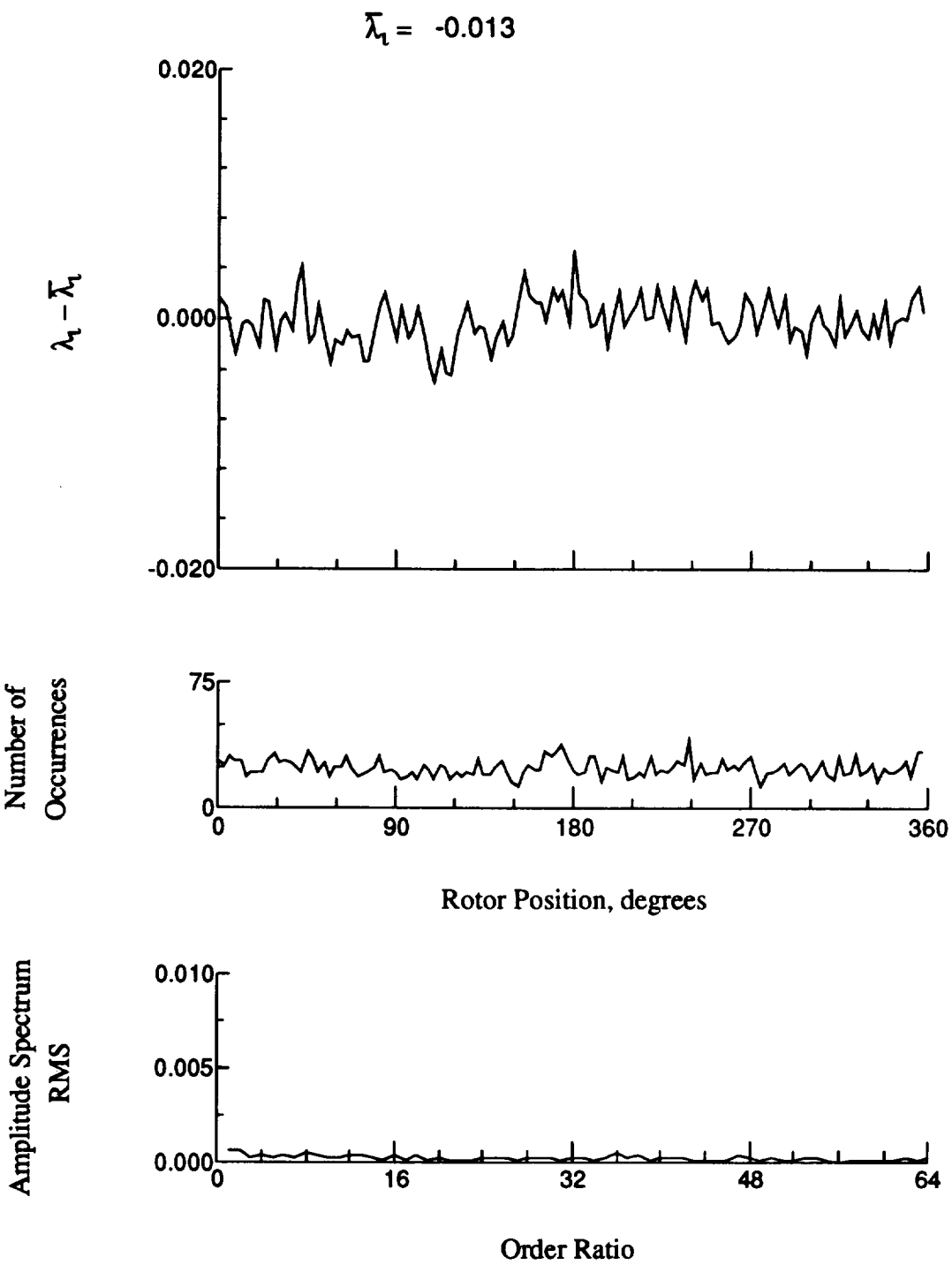


Figure 22.- Concluded.

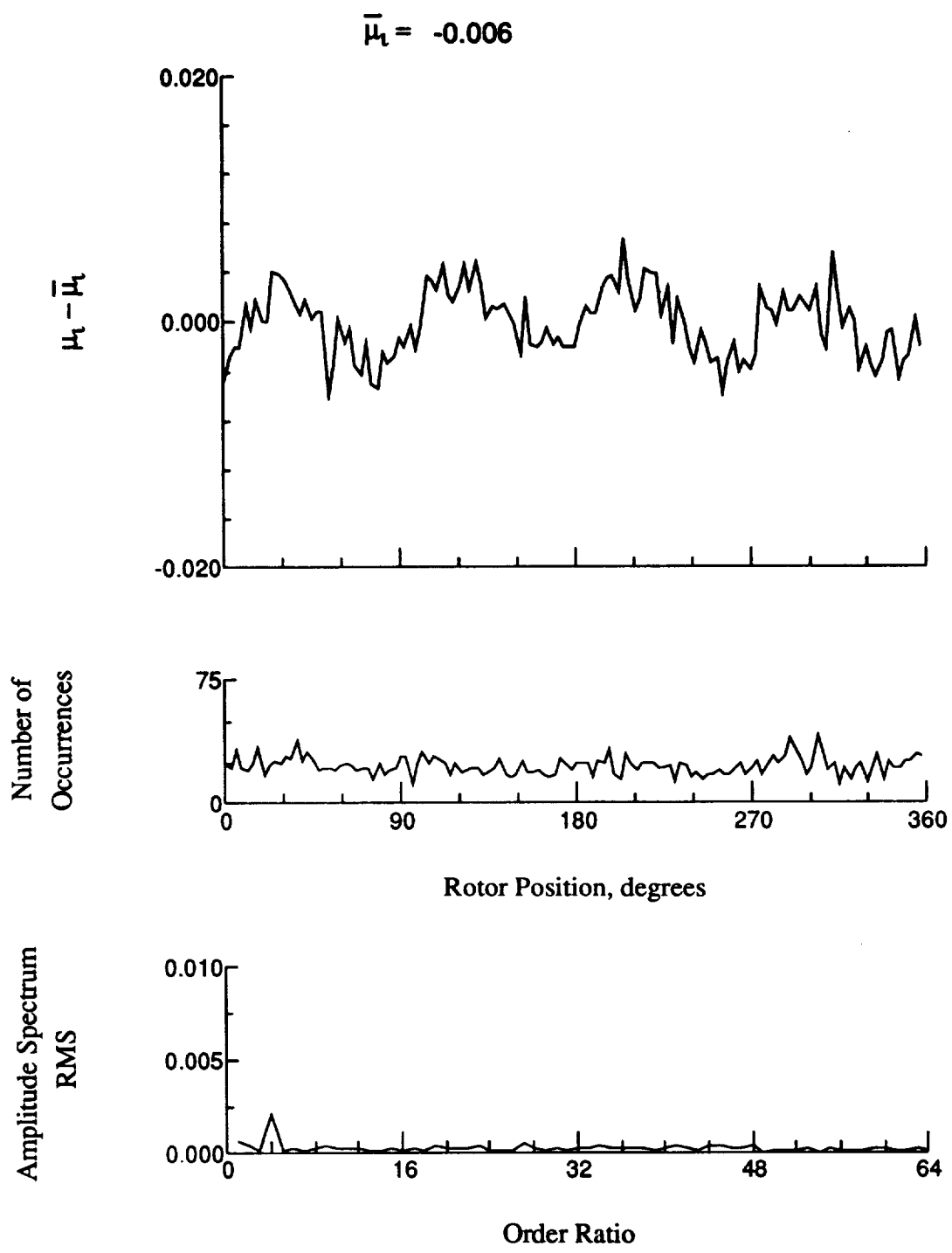


Figure 23.- Induced inflow velocity measured at 0 degrees and r/R of 0.58.

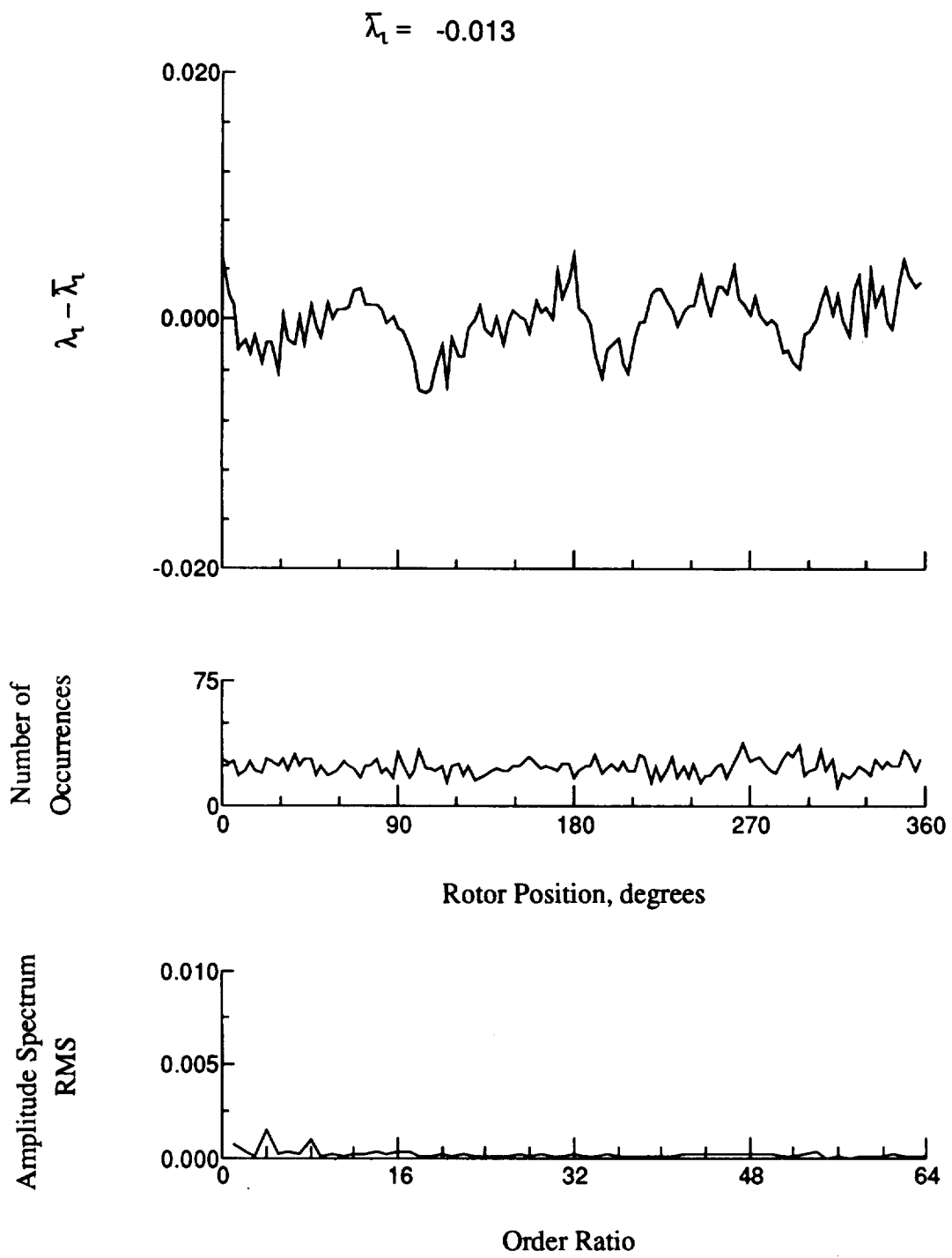


Figure 23.- Concluded.

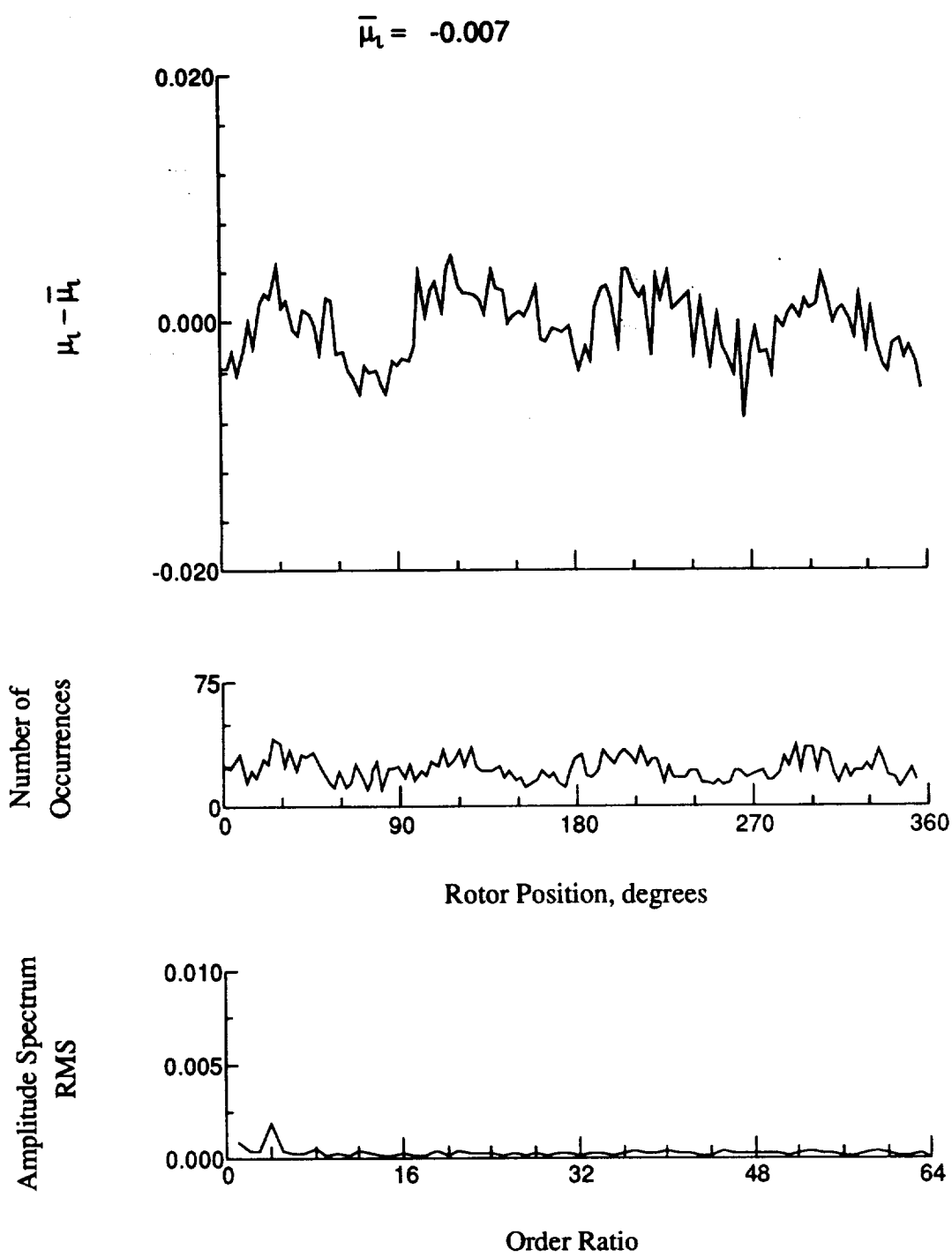


Figure 24.- Induced inflow velocity measured at 0 degrees and r/R of 0.69.

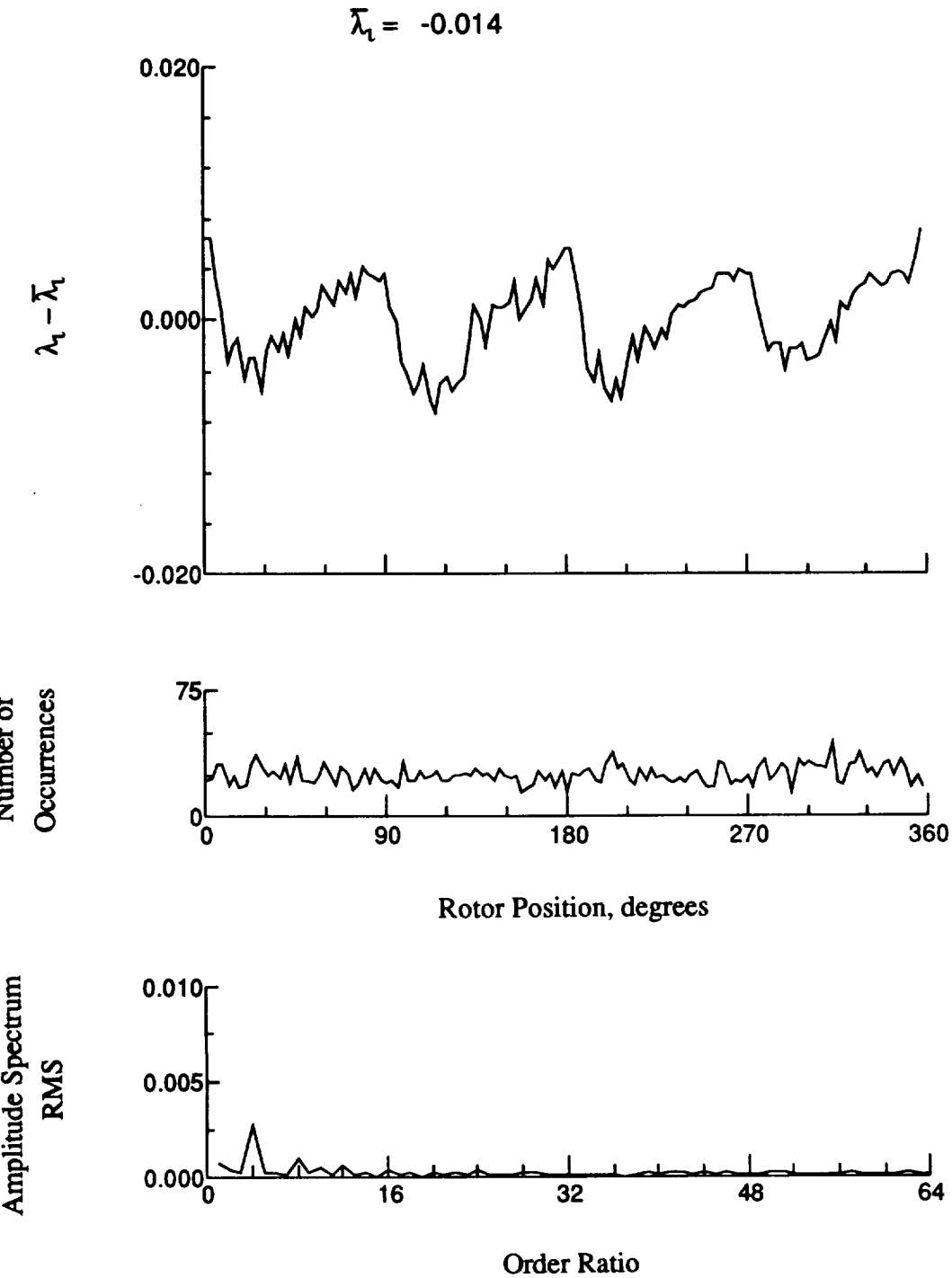


Figure 24.- Concluded.

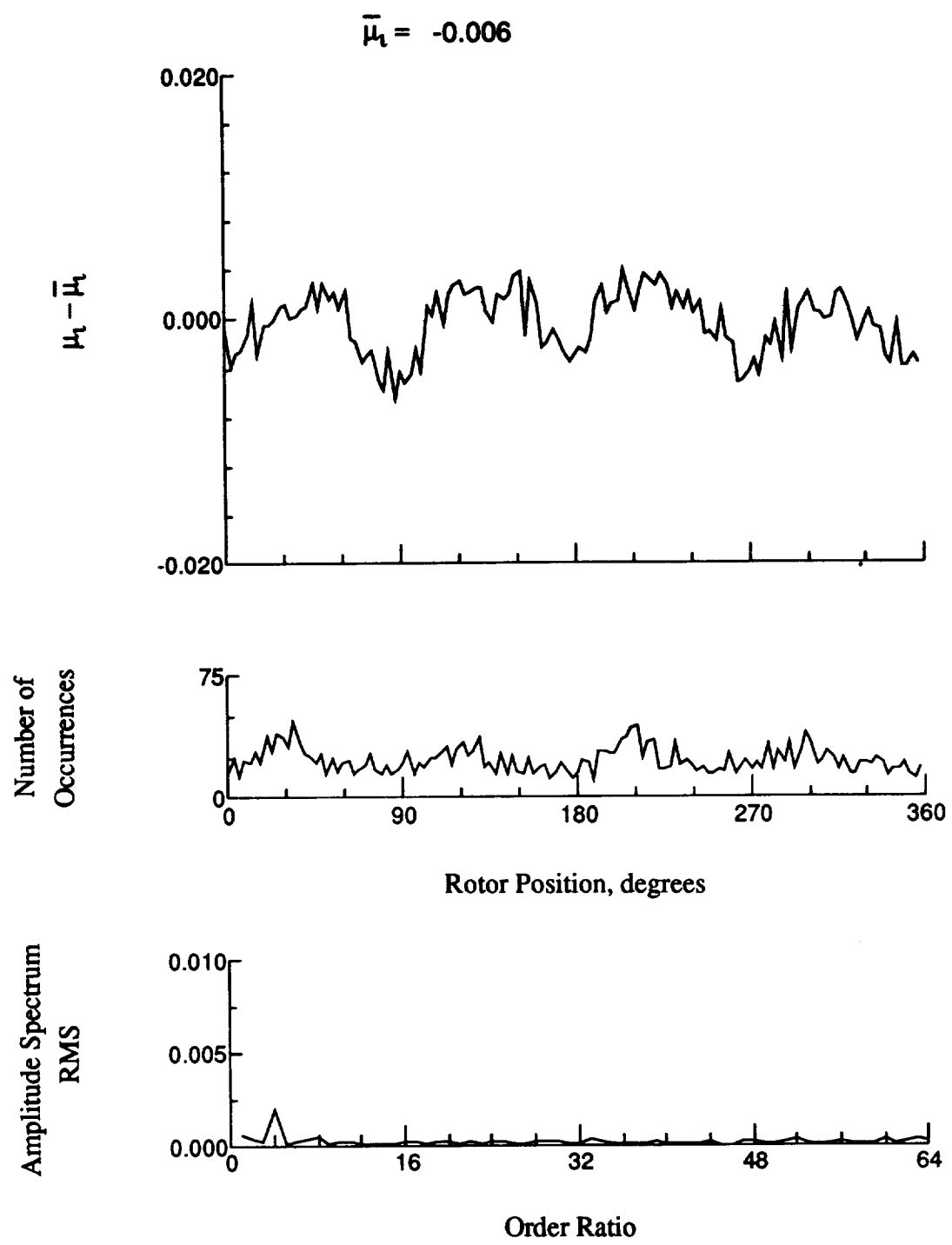


Figure 25.- Induced inflow velocity measured at 0 degrees and r/R of 0.73.

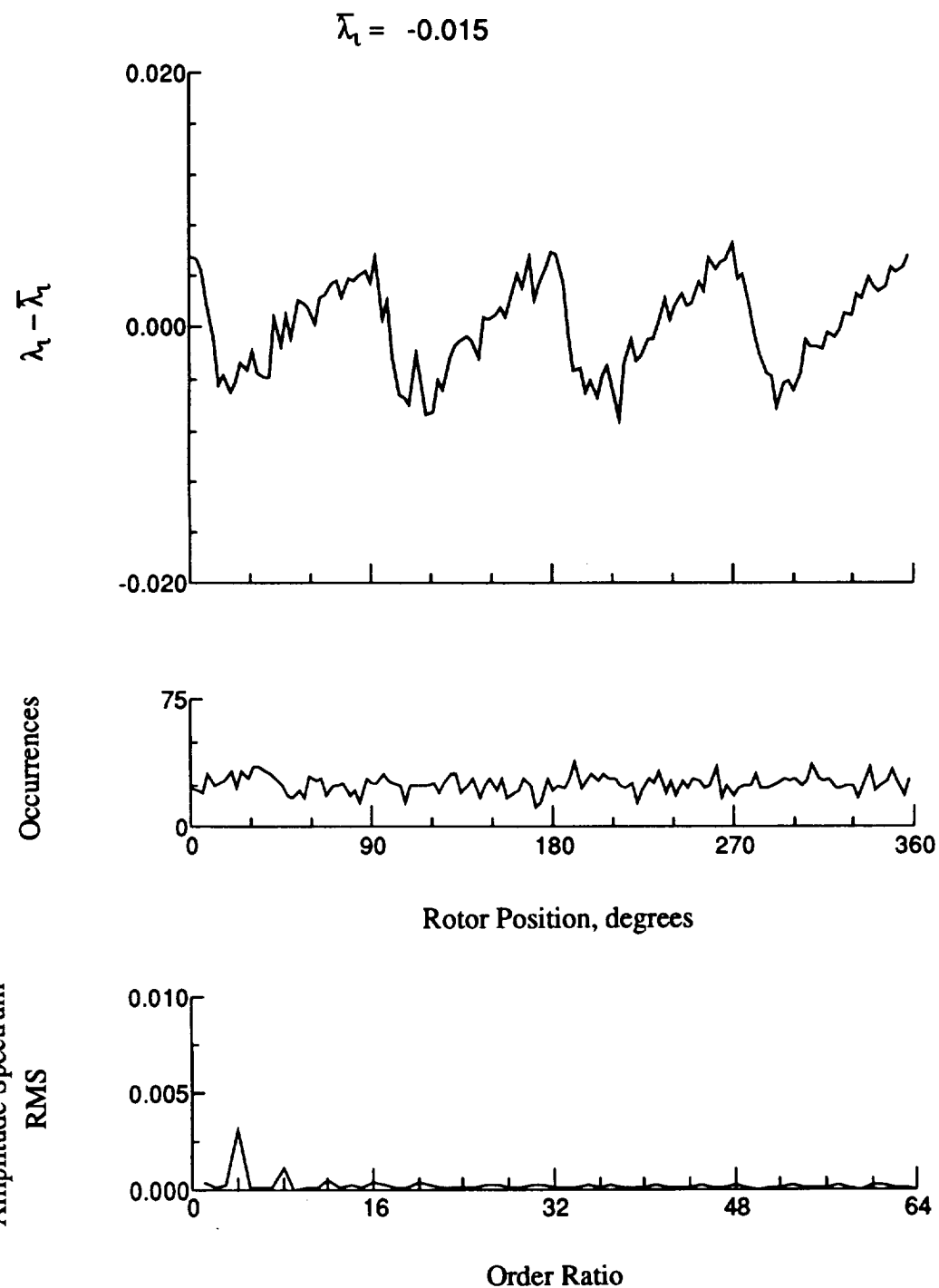


Figure 25.- Concluded.

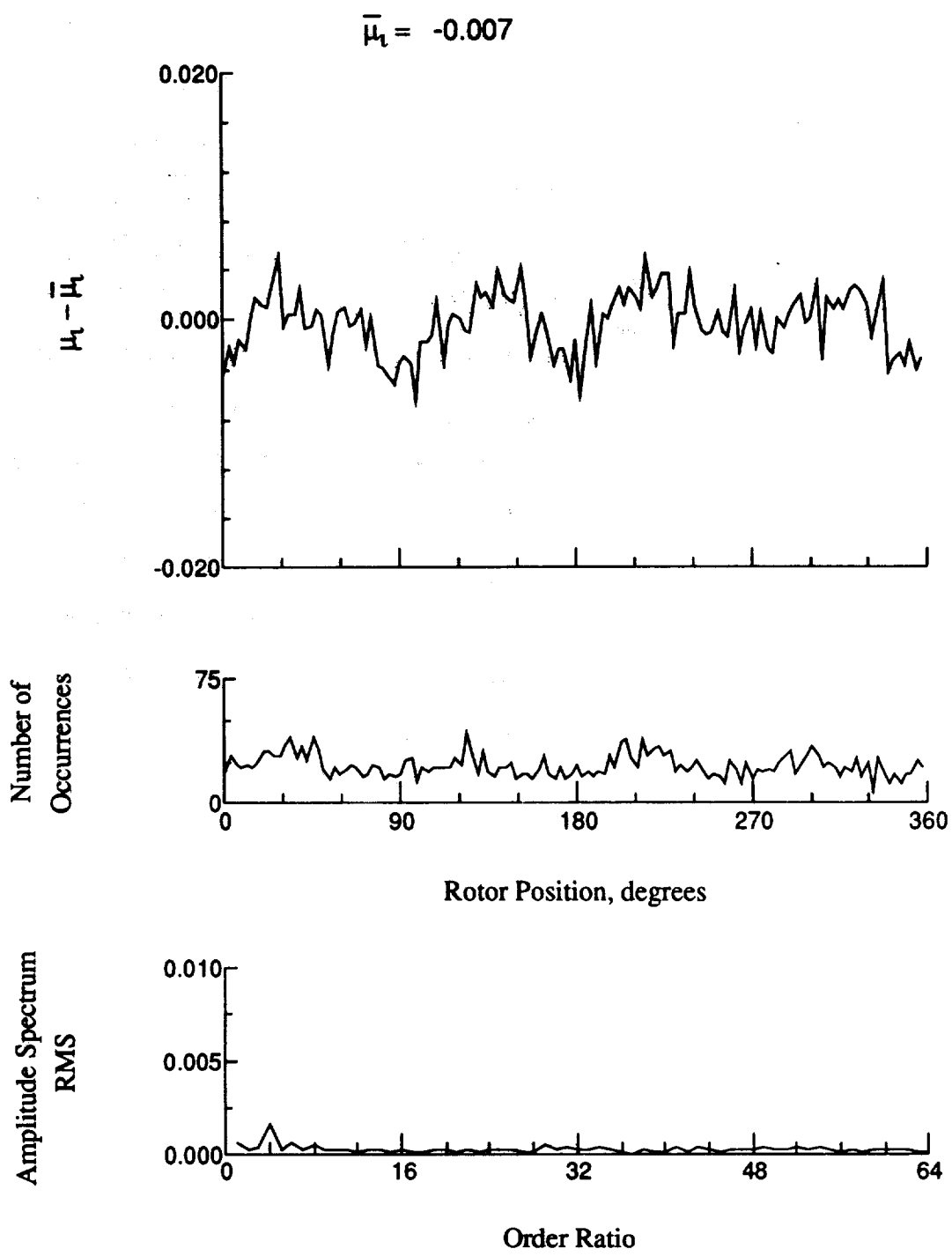


Figure 26.- Induced inflow velocity measured at 0 degrees and r/R of 0.75.

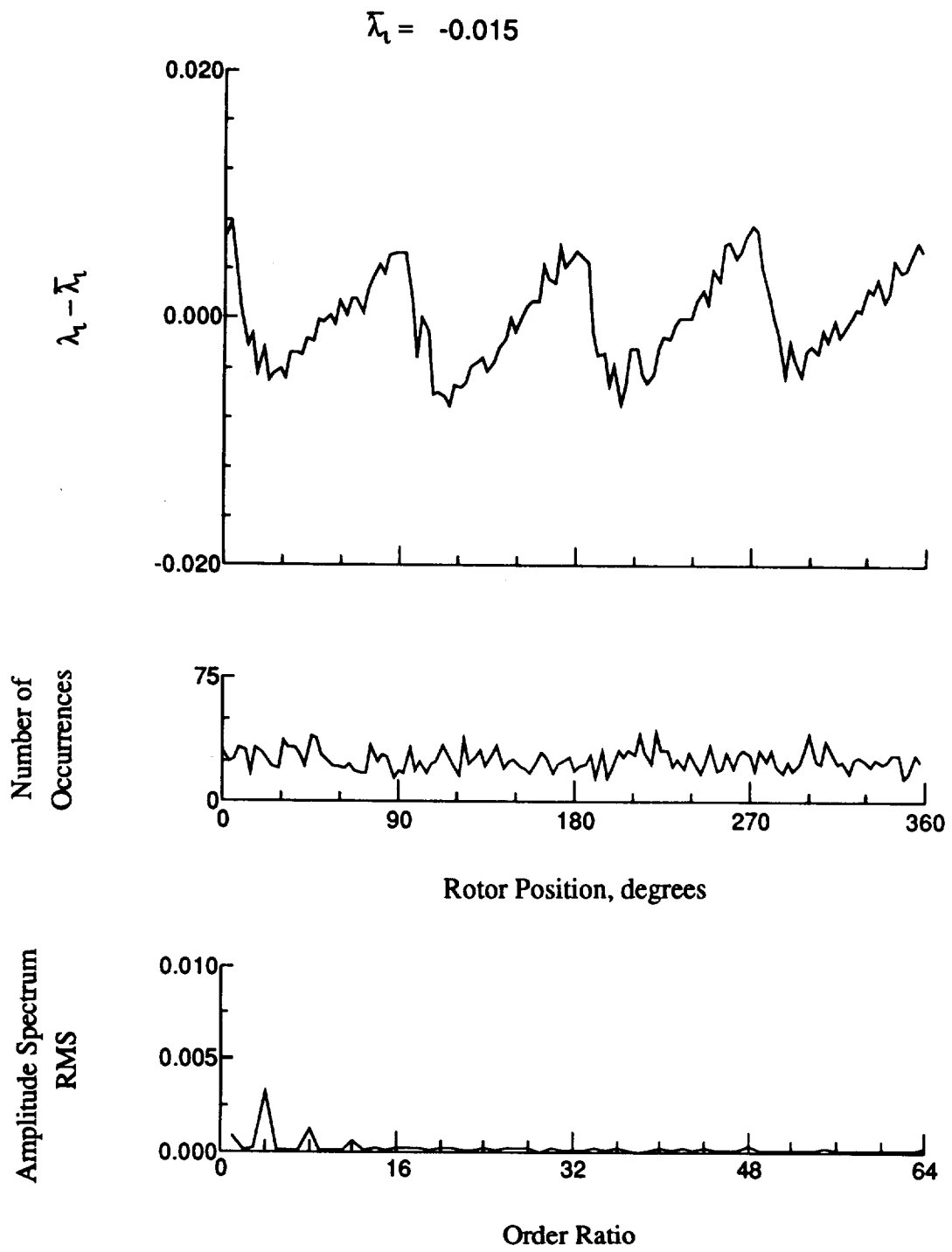


Figure 26.- Concluded.

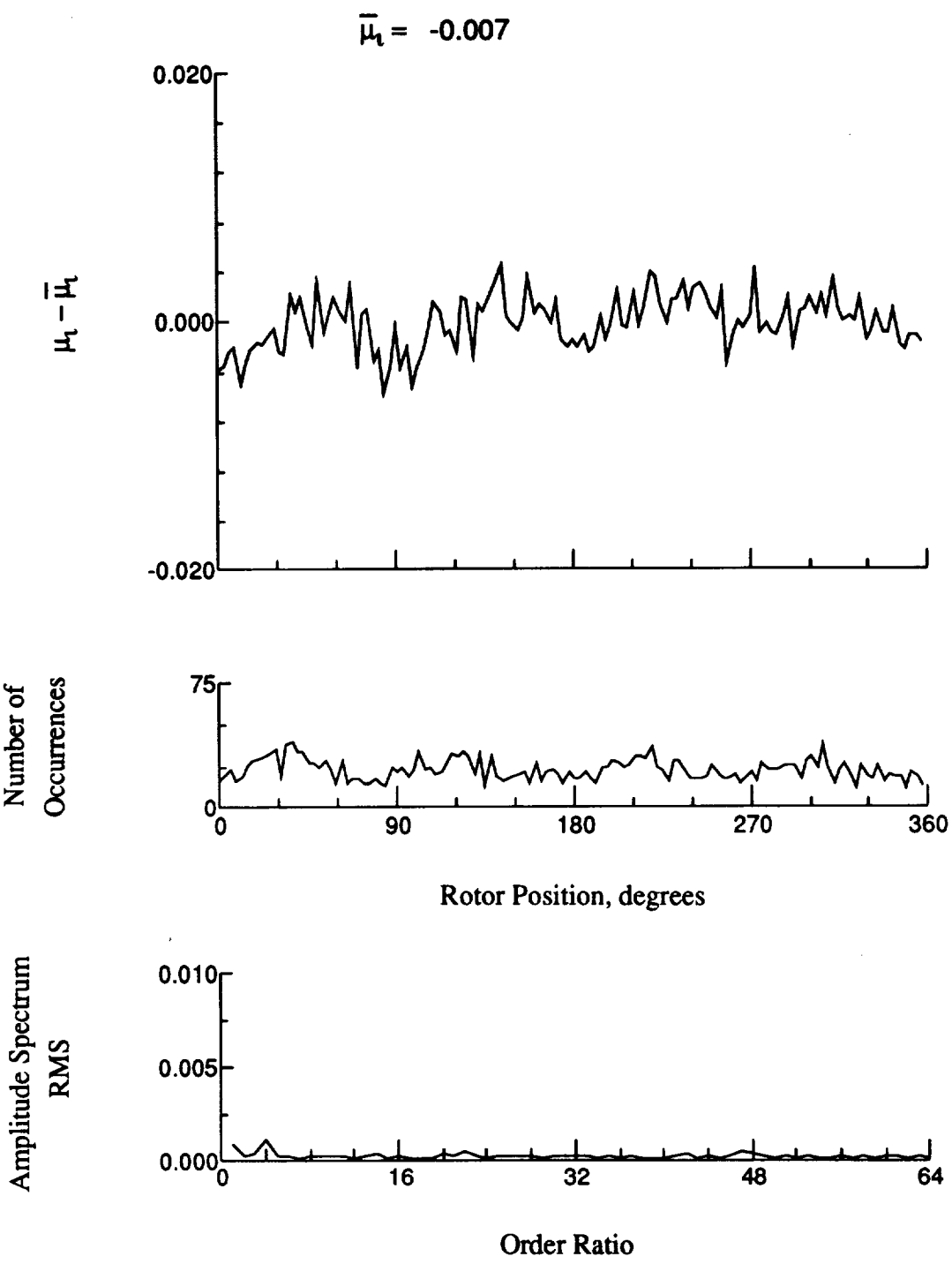


Figure 27.- Induced inflow velocity measured at 0 degrees and r/R of 0.81.

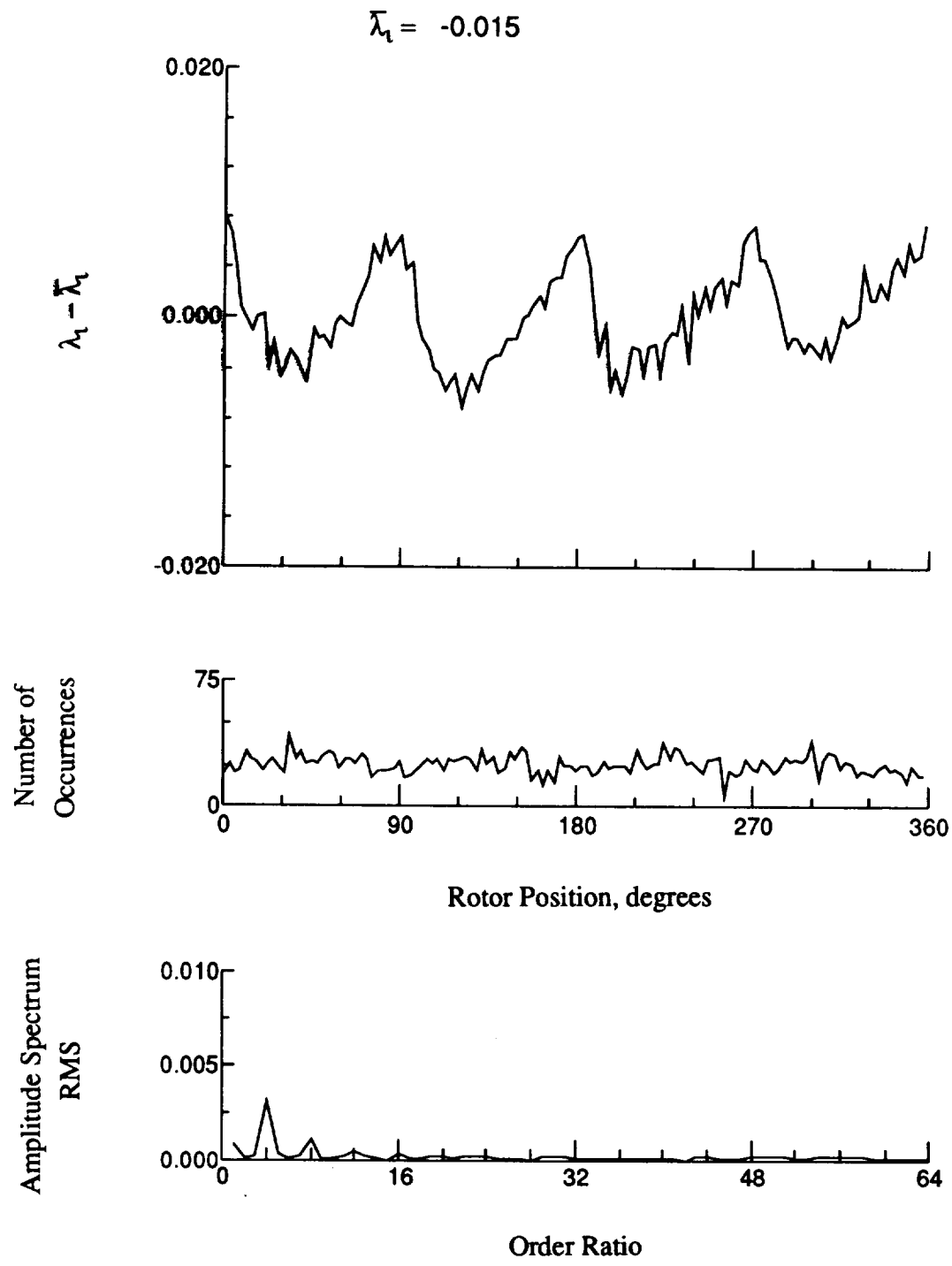


Figure 27.- Concluded.

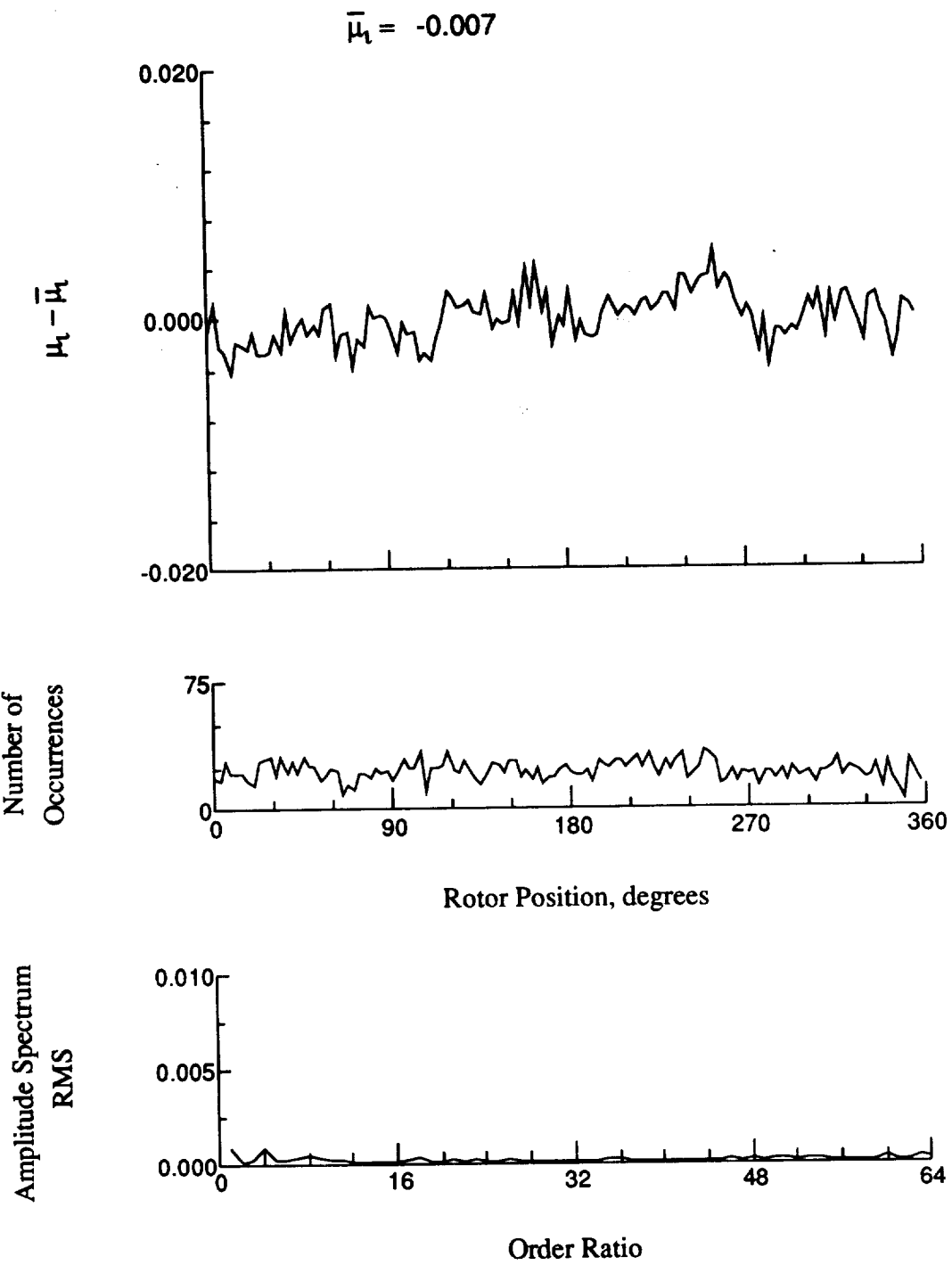


Figure 28.- Induced inflow velocity measured at 0 degrees and r/R of 0.86.

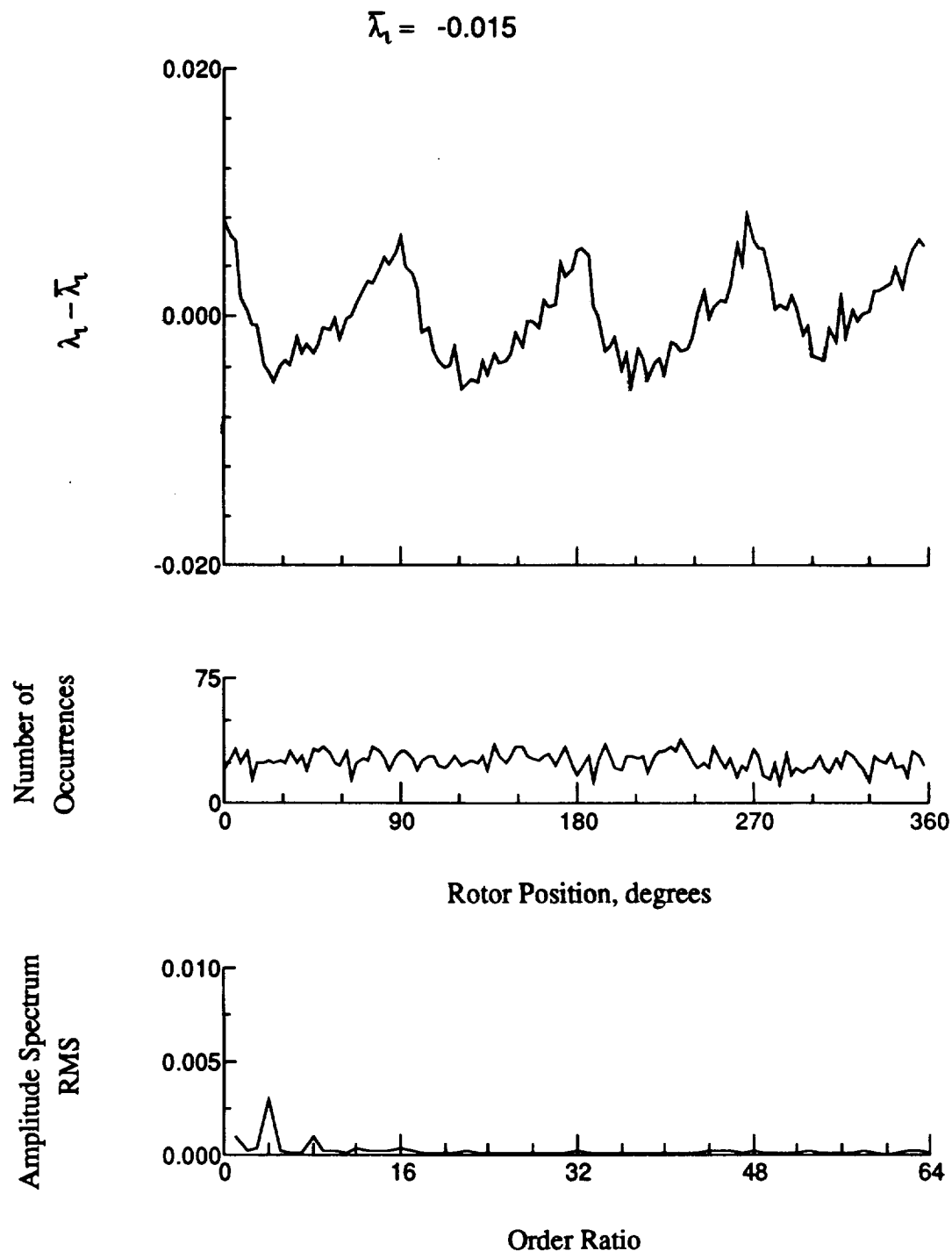


Figure 28.- Concluded.

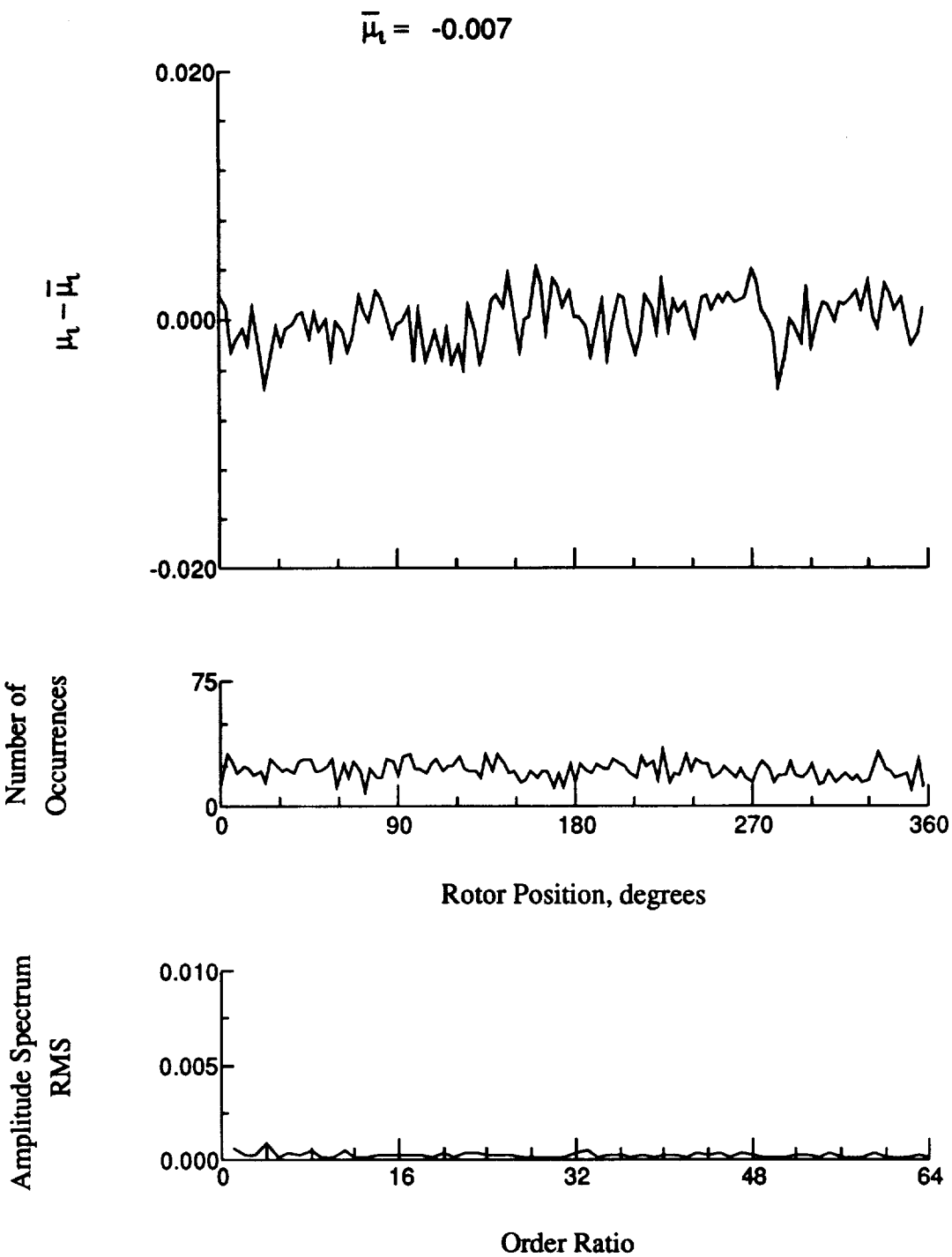


Figure 29.- Induced inflow velocity measured at 0 degrees and r/R of 0.90.

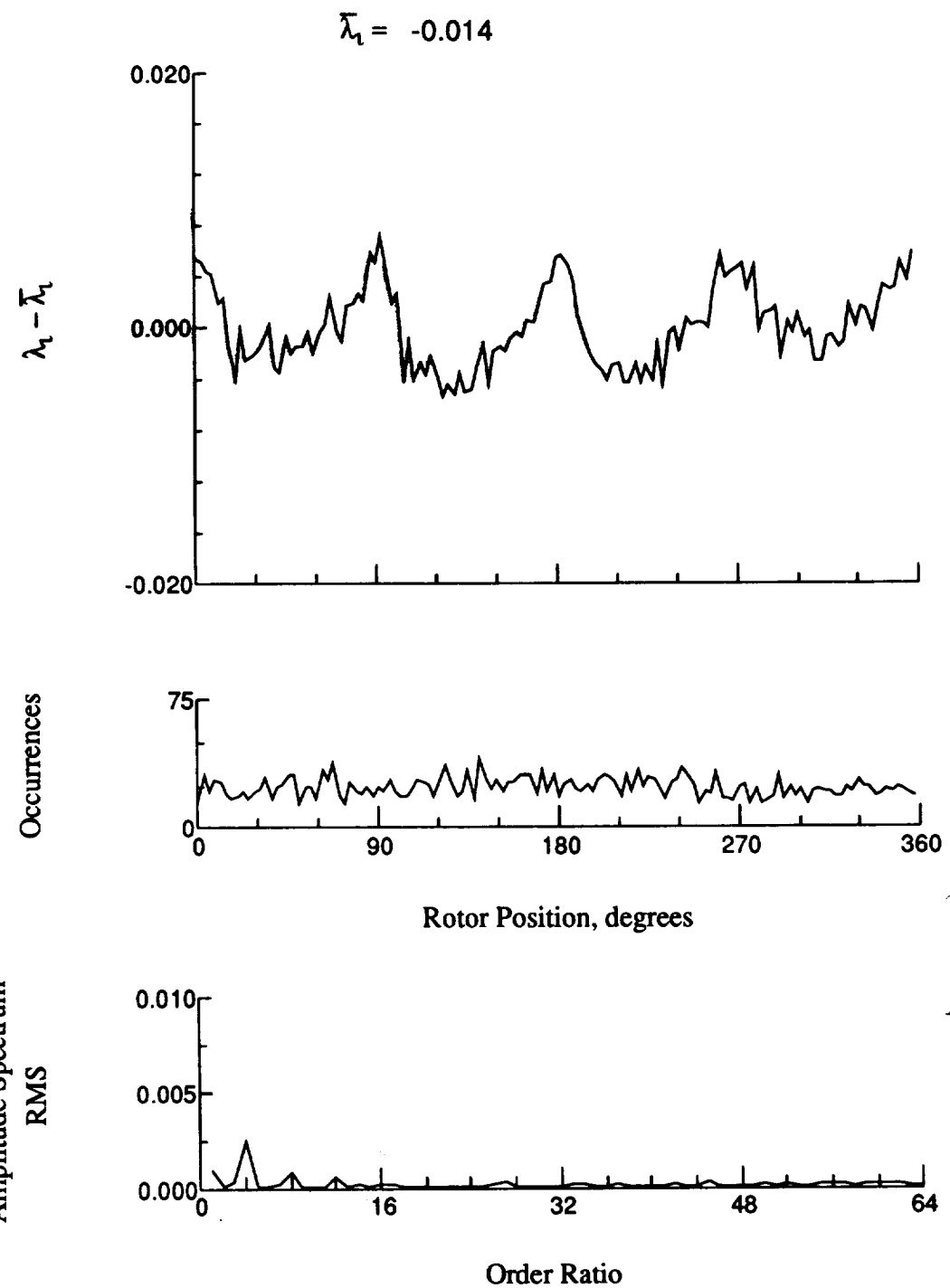


Figure 29.- Concluded.

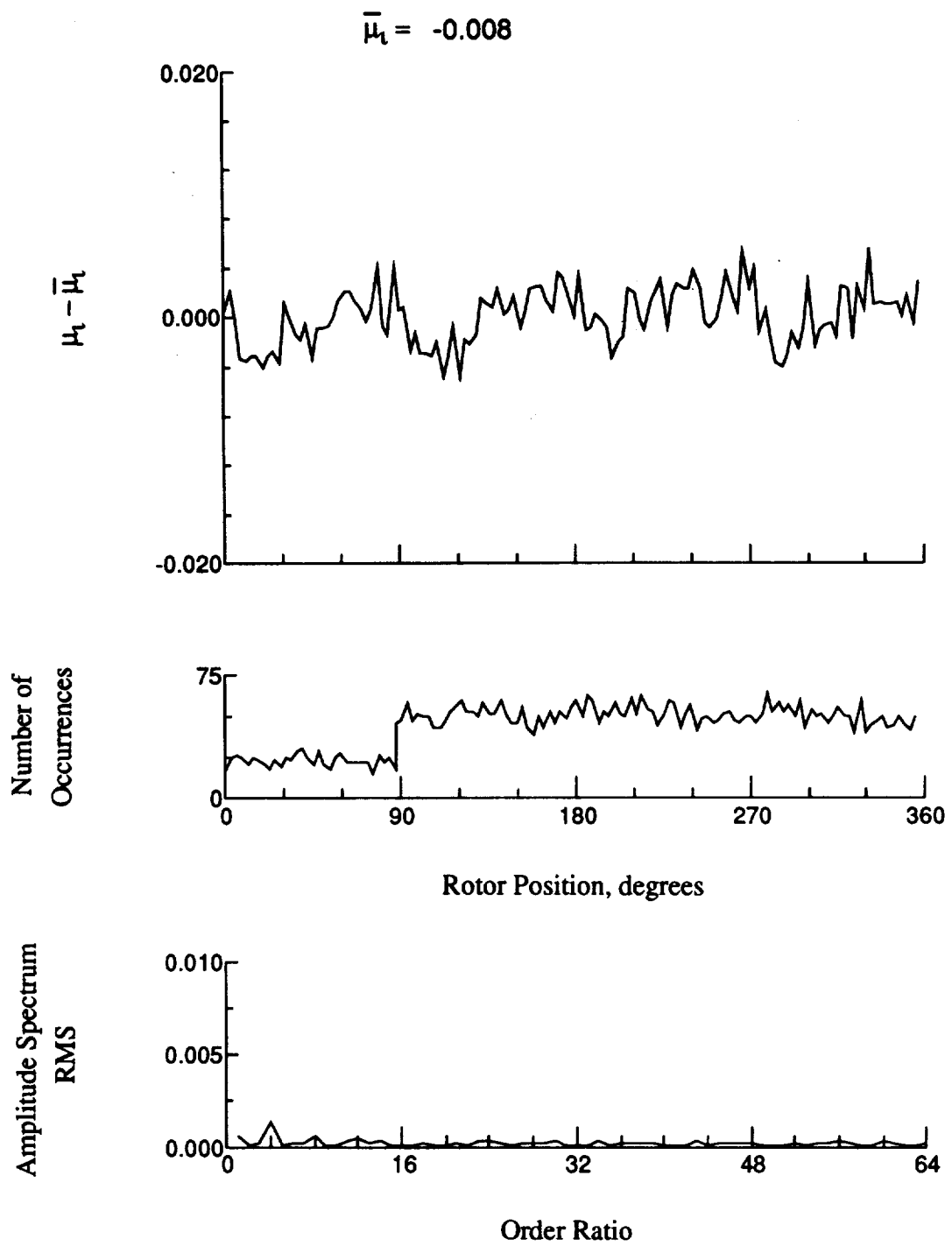


Figure 30.- Induced inflow velocity measured at 0 degrees and r/R of 0.94.

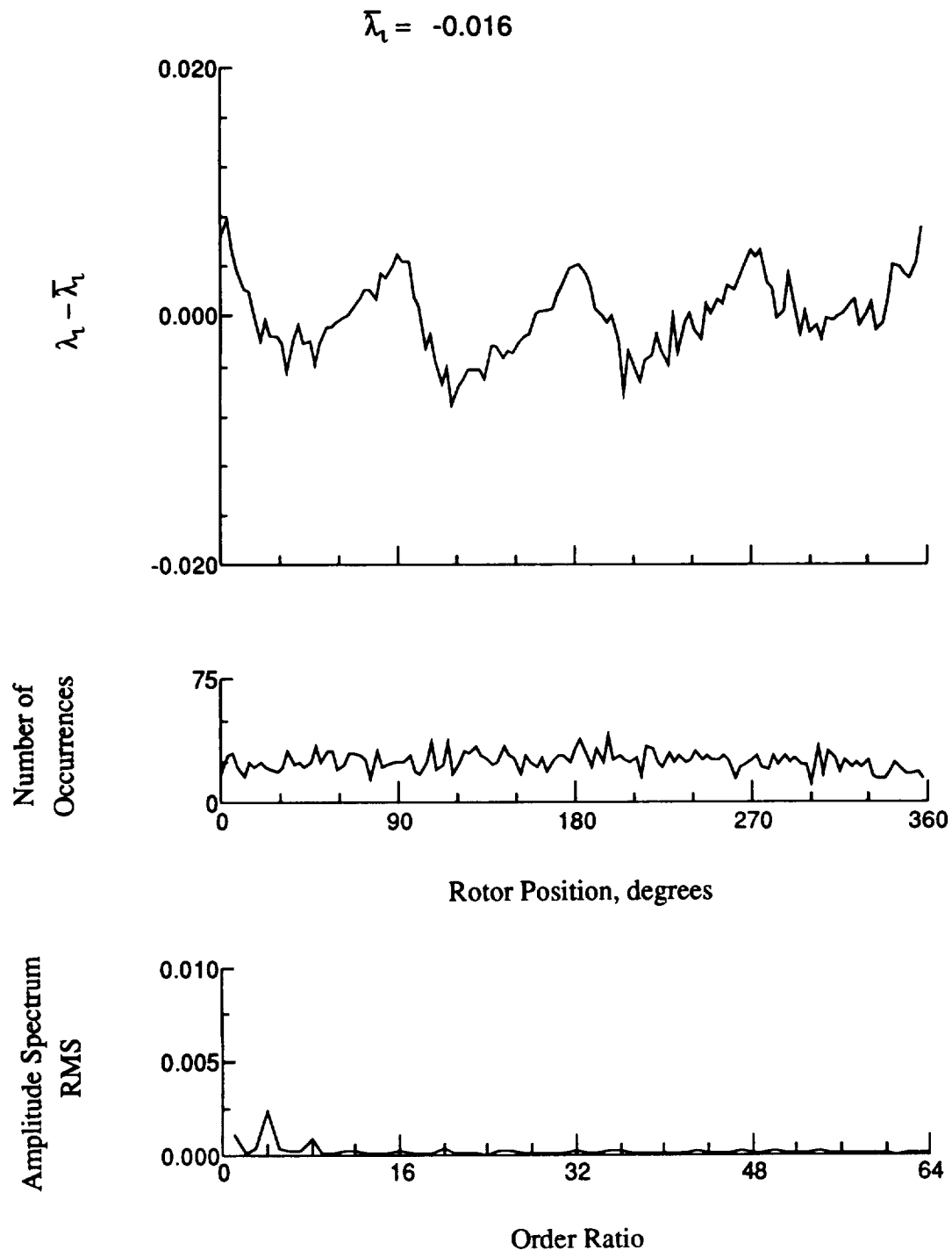


Figure 30.- Concluded.

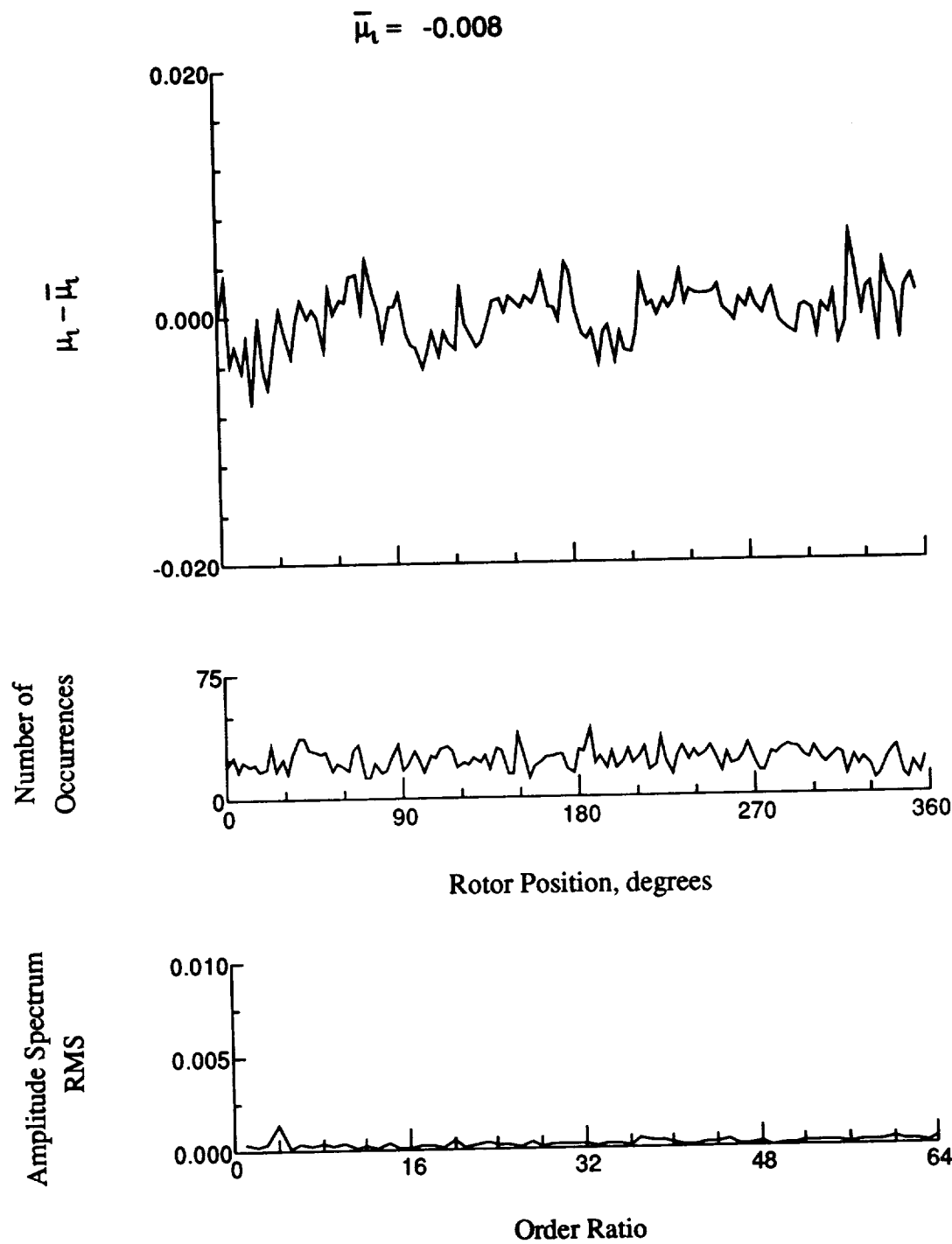


Figure 31.- Induced inflow velocity measured at 0 degrees and r/R of 0.96.

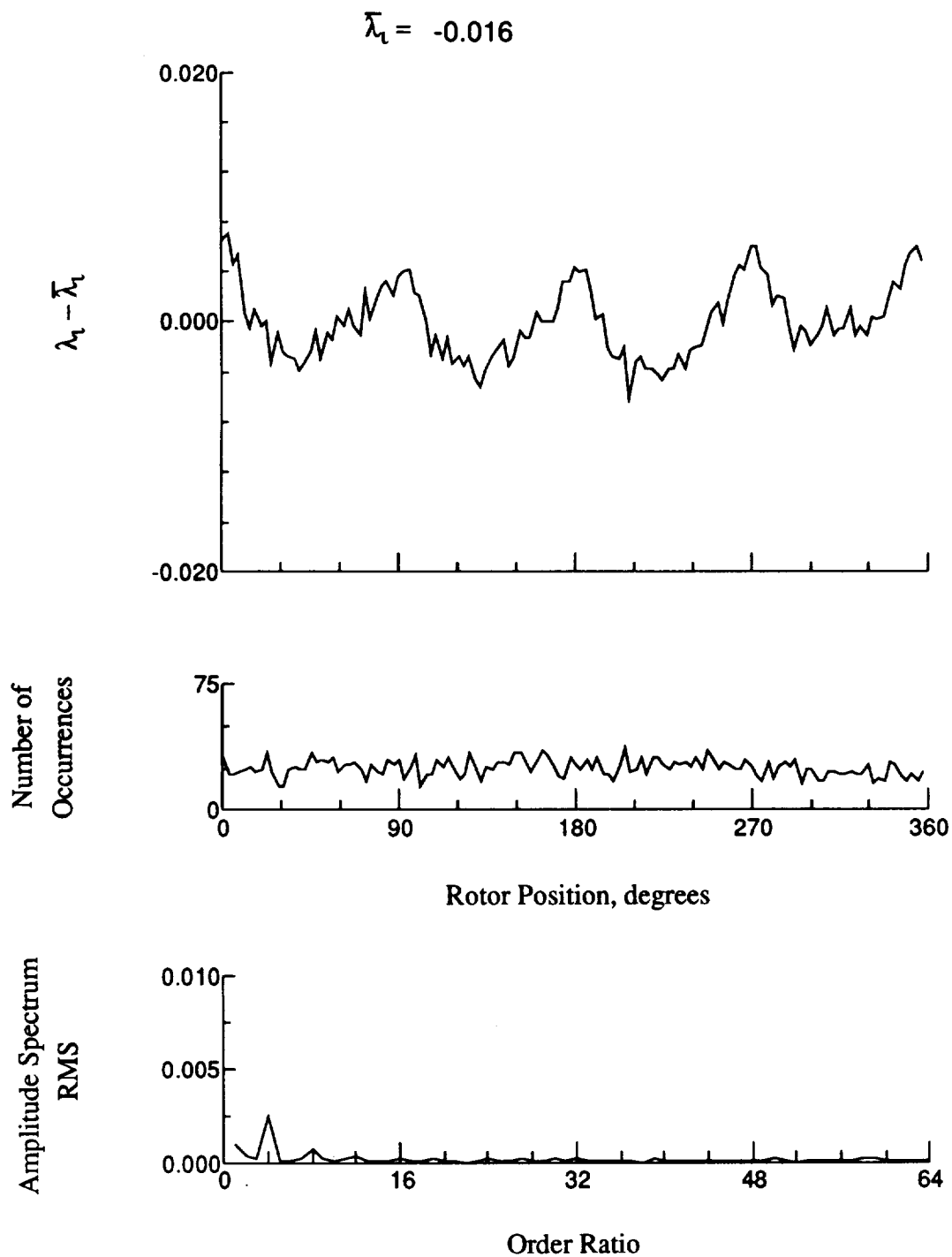


Figure 31.- Concluded.

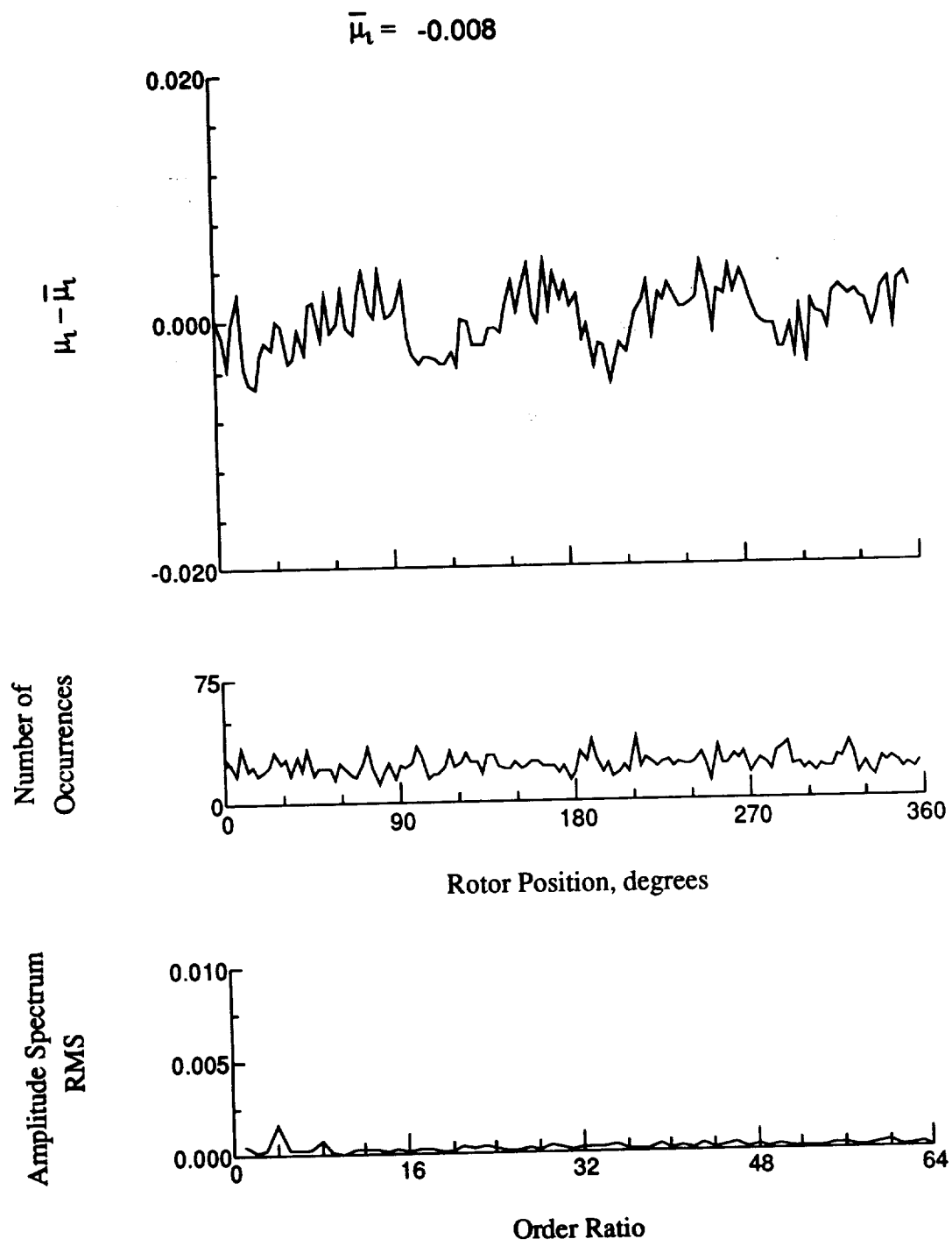


Figure 32.- Induced inflow velocity measured at 0 degrees and r/R of 1.00.

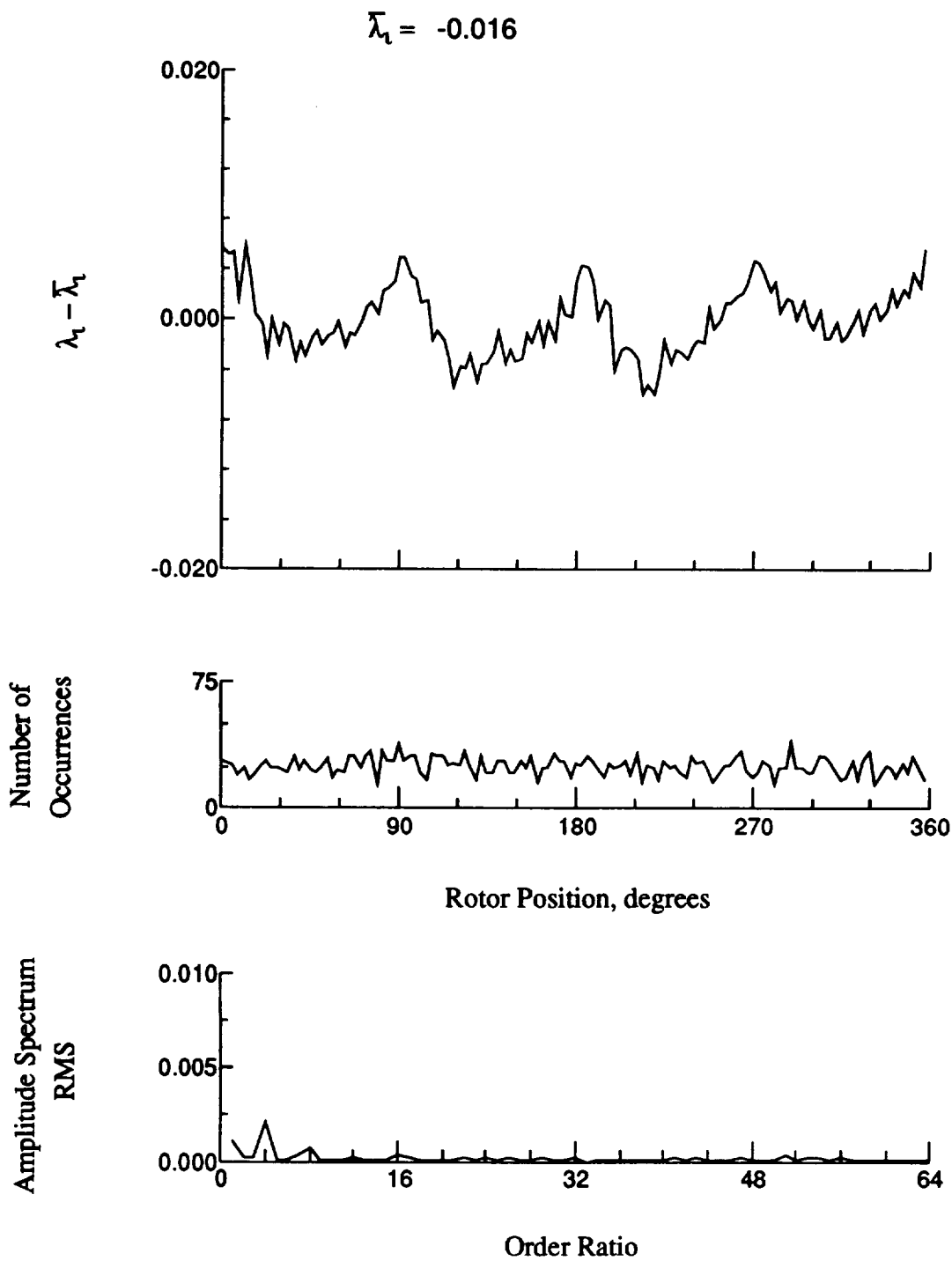


Figure 32.- Concluded.

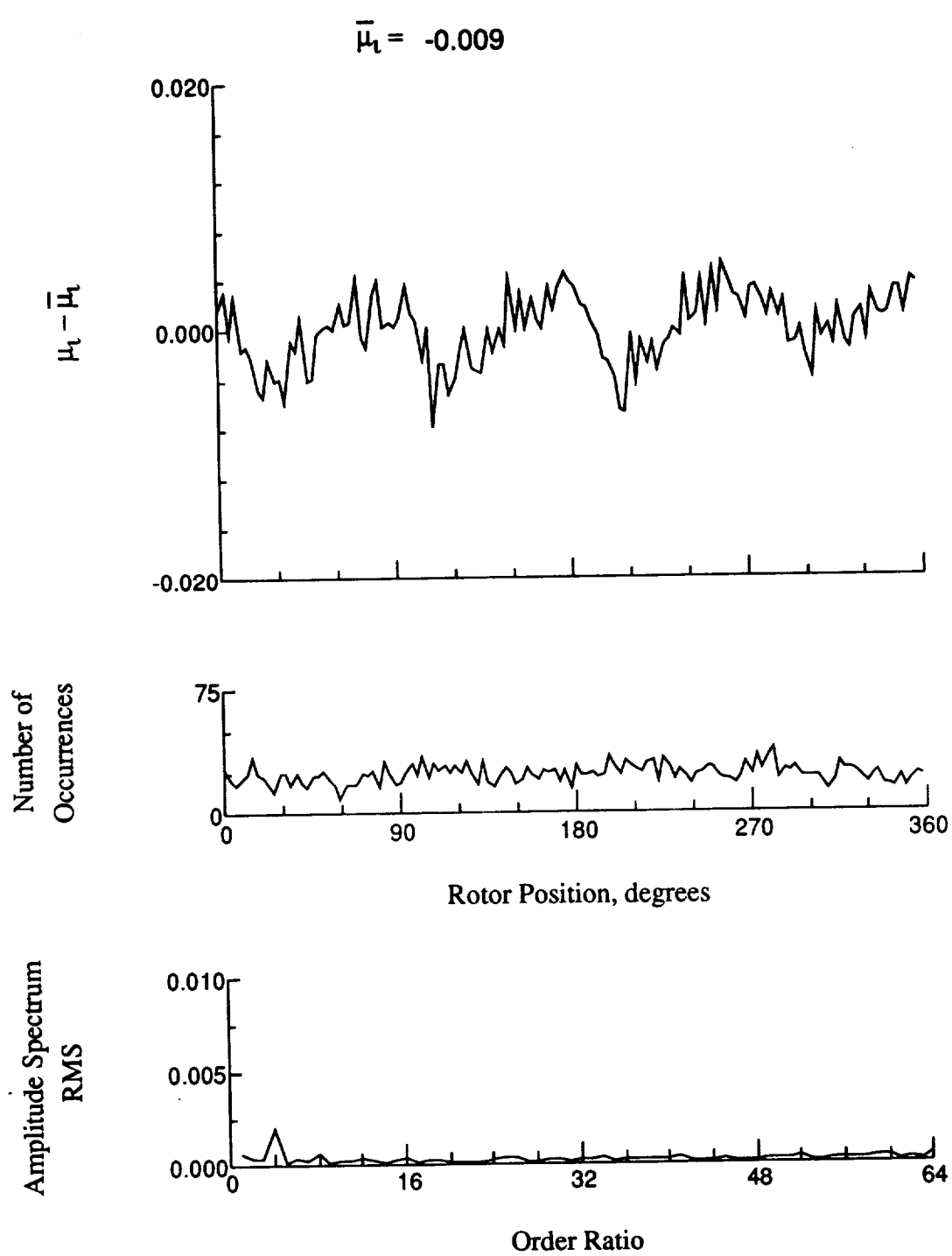


Figure 33.- Induced inflow velocity measured at 0 degrees and r/R of 1.10.

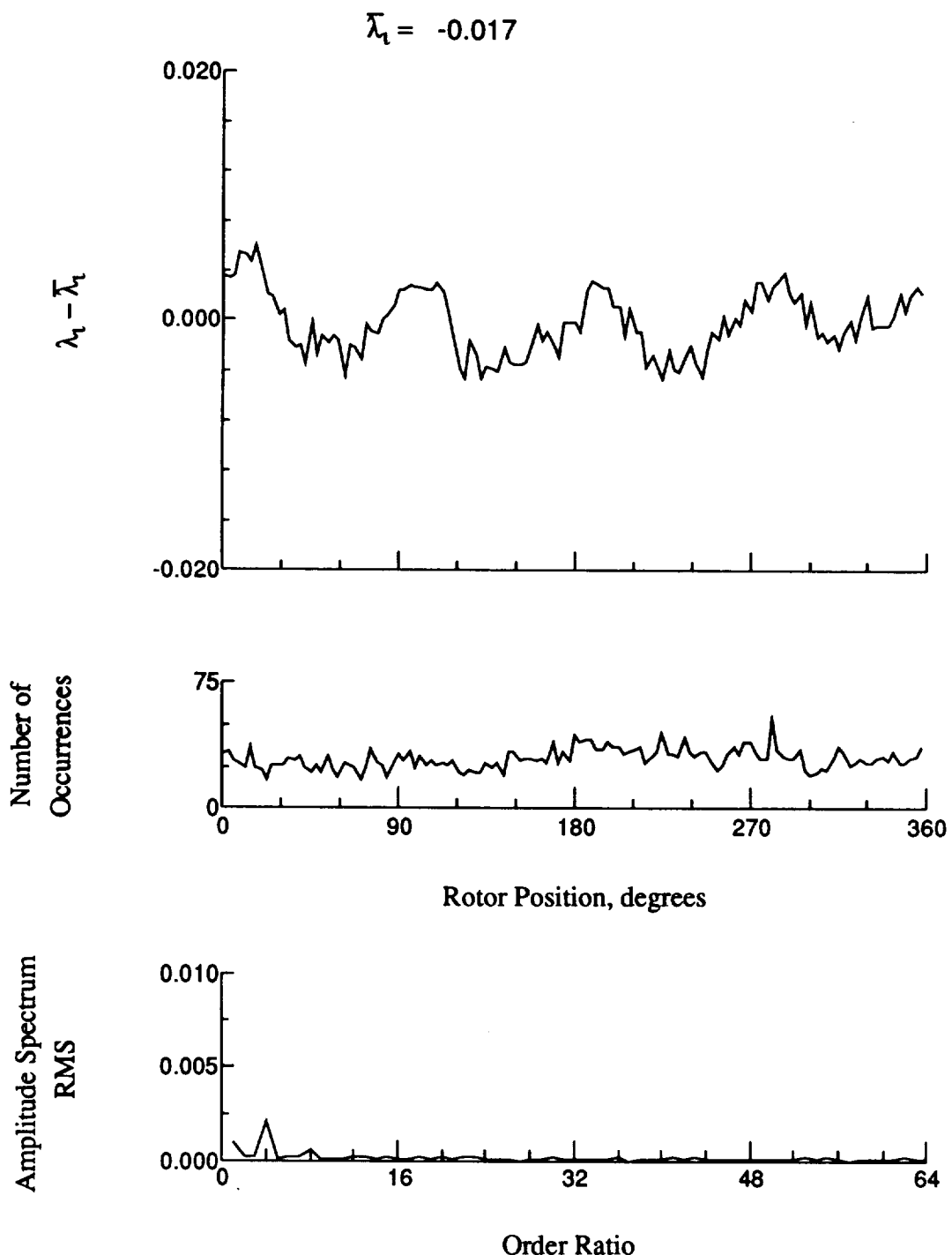


Figure 33.- Concluded.

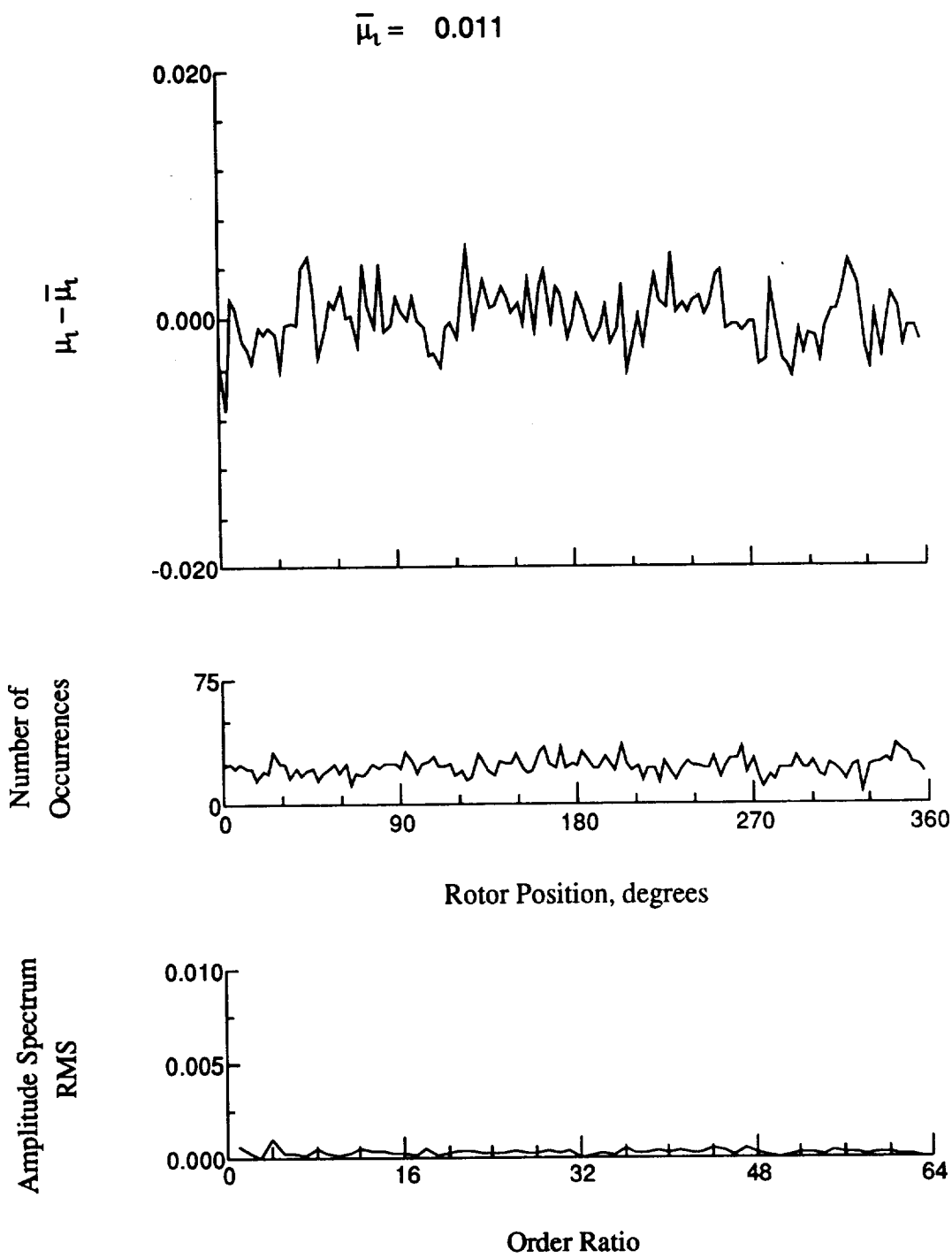


Figure 34.- Induced inflow velocity measured at 30 degrees and r/R of 0.20.

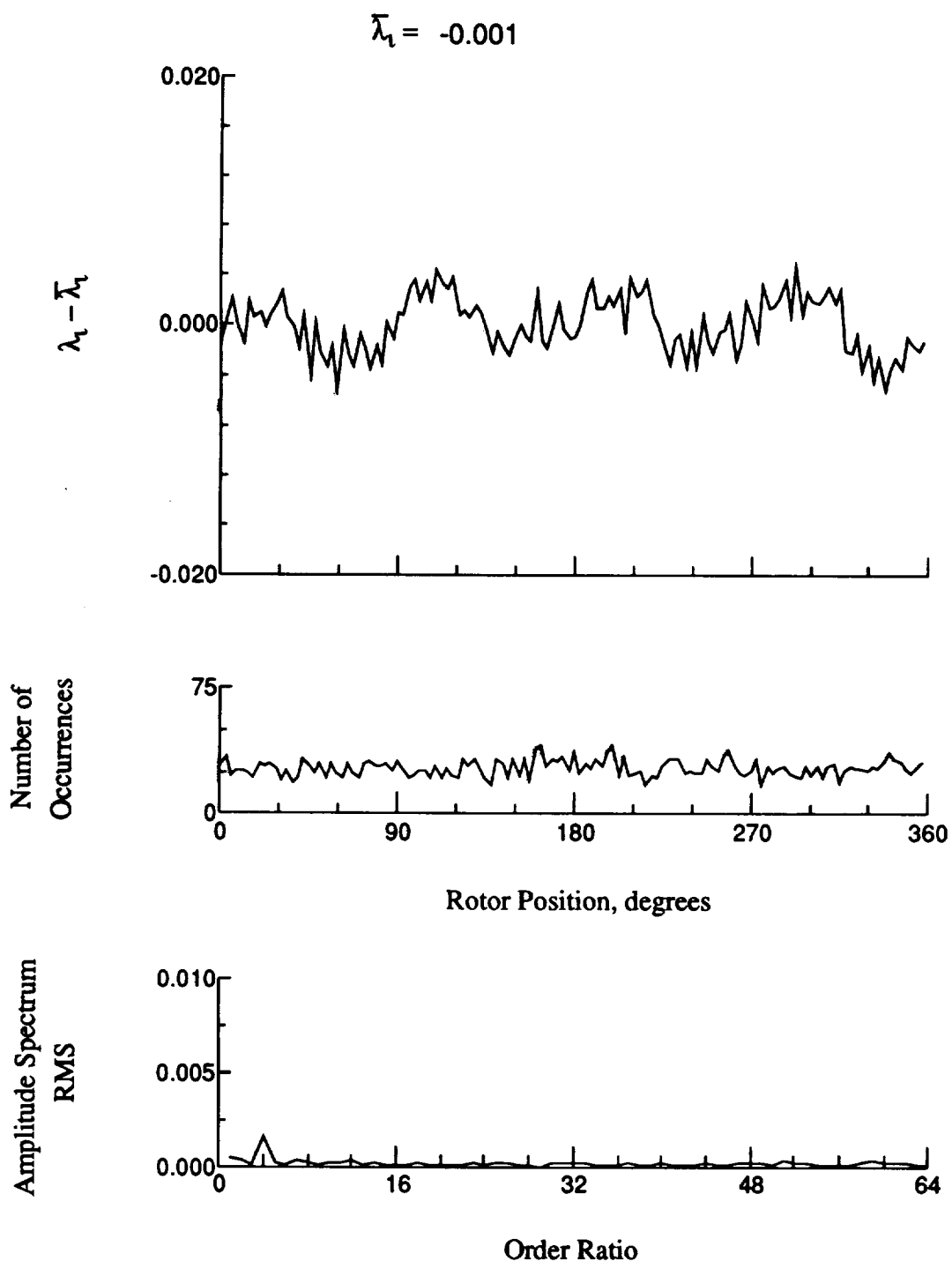


Figure 34.- Concluded.

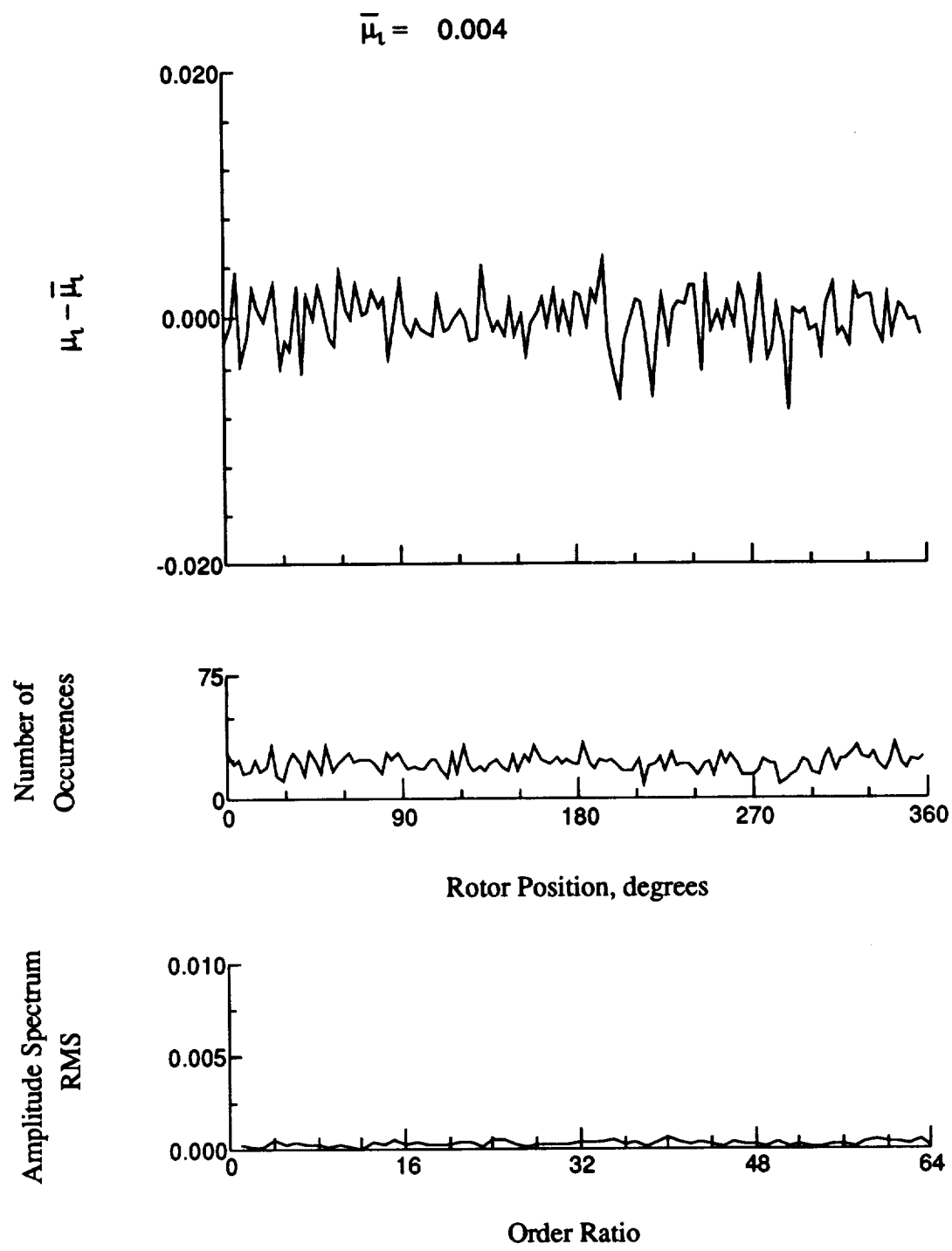


Figure 35.- Induced inflow velocity measured at 30 degrees and r/R of 0.32.

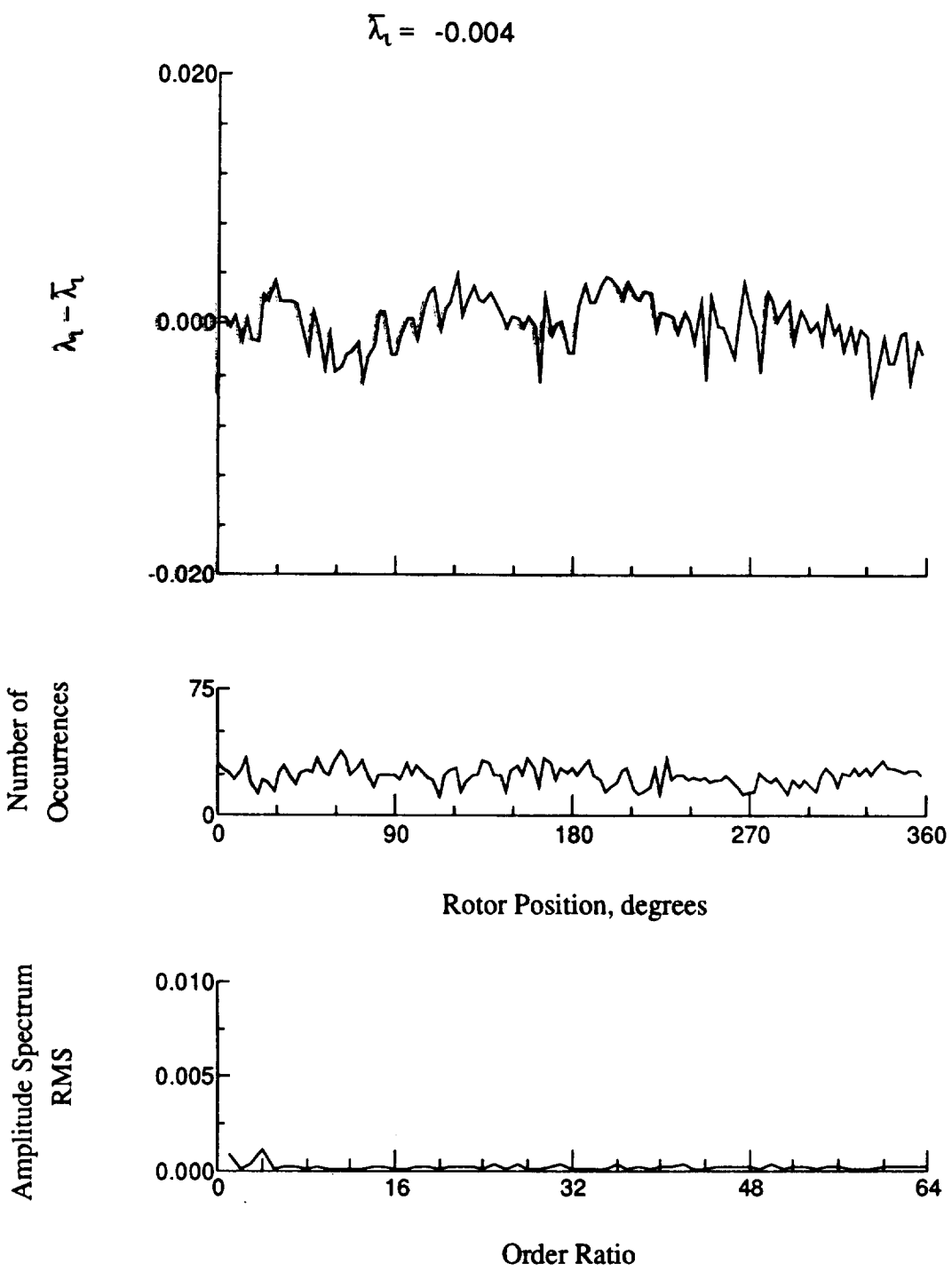


Figure 35.- Concluded.

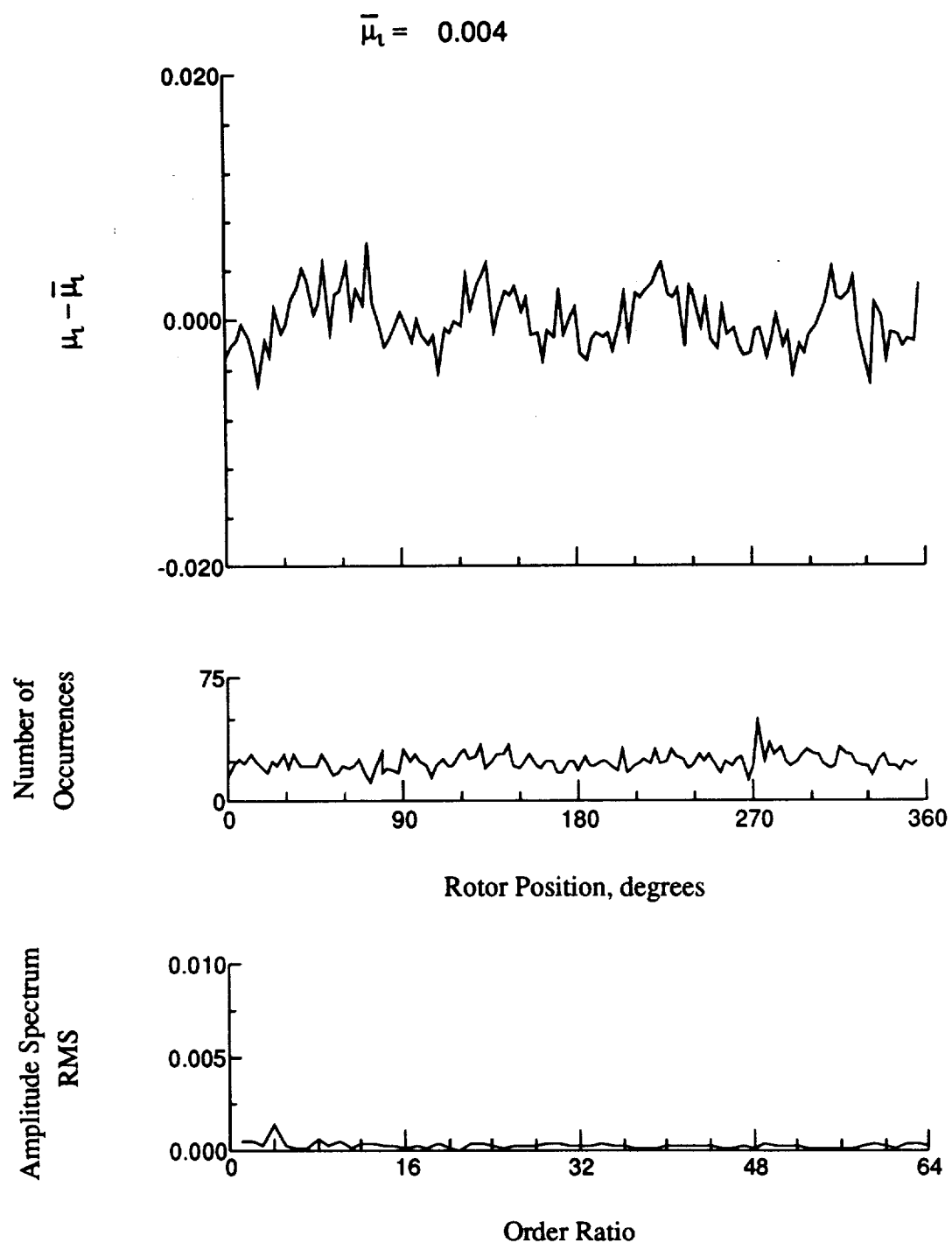


Figure 36.- Induced inflow velocity measured at 30 degrees and r/R of 0.50.

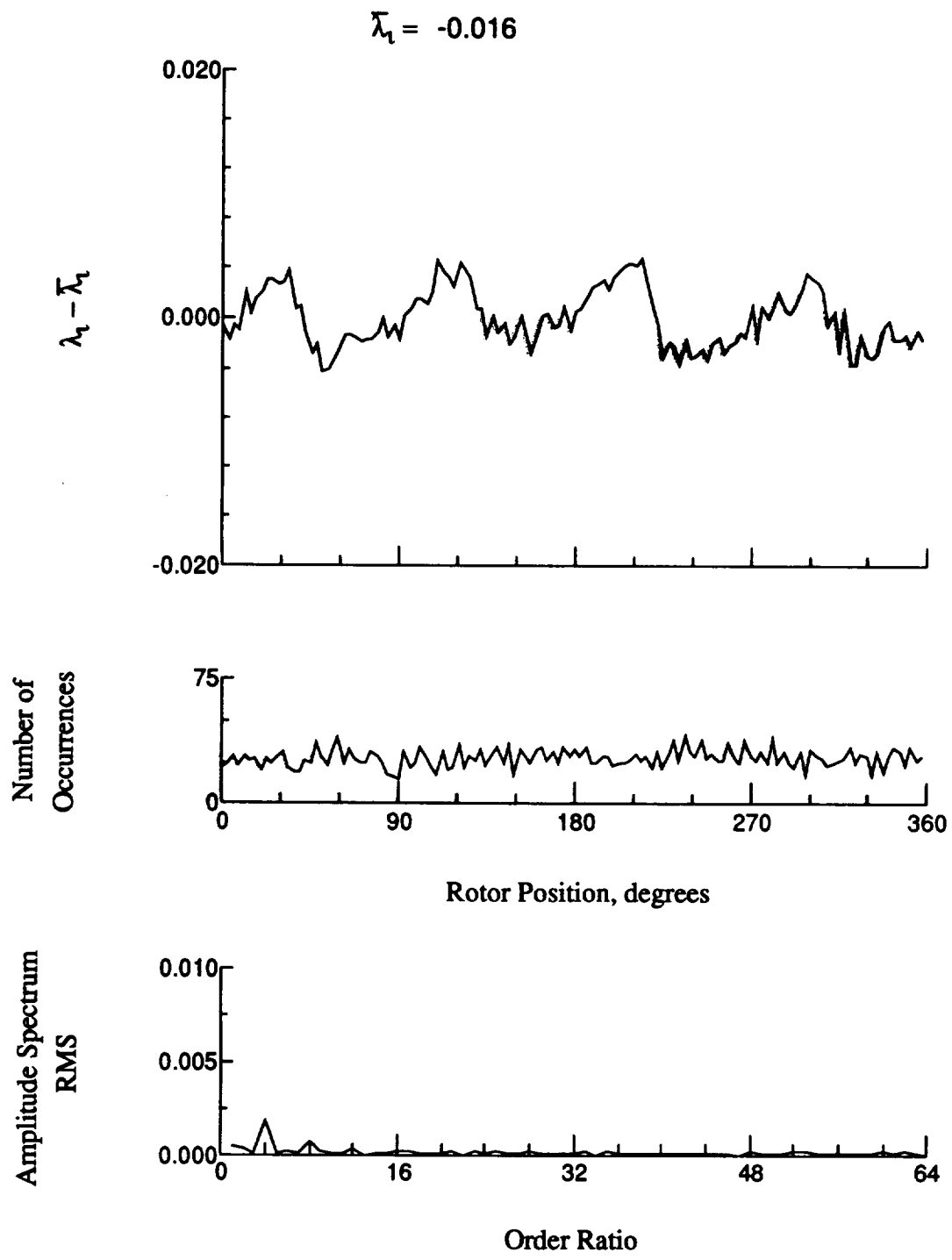


Figure 36.- Concluded.

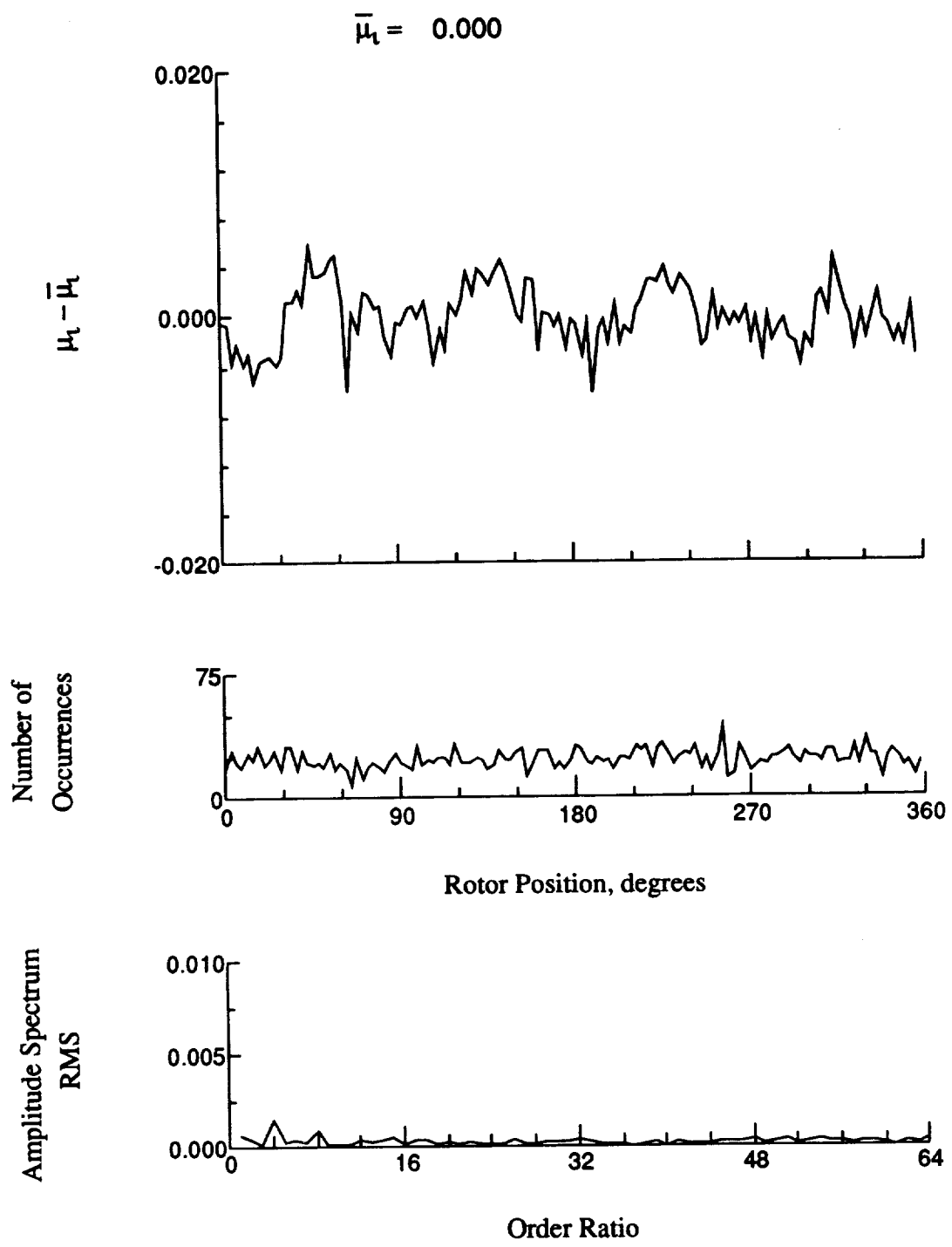


Figure 37.- Induced inflow velocity measured at 30 degrees and r/R of 0.58.

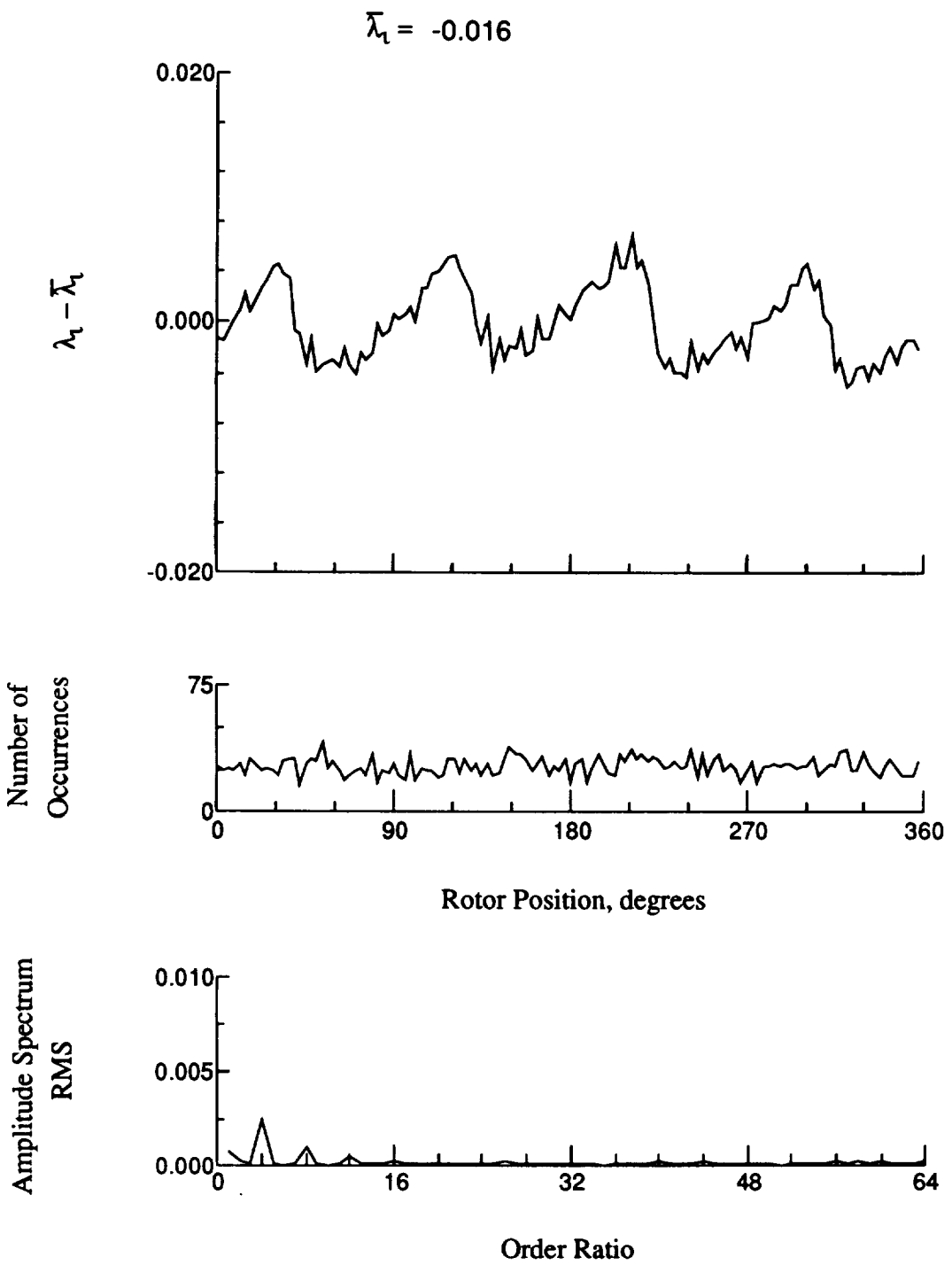


Figure 37.- Concluded.

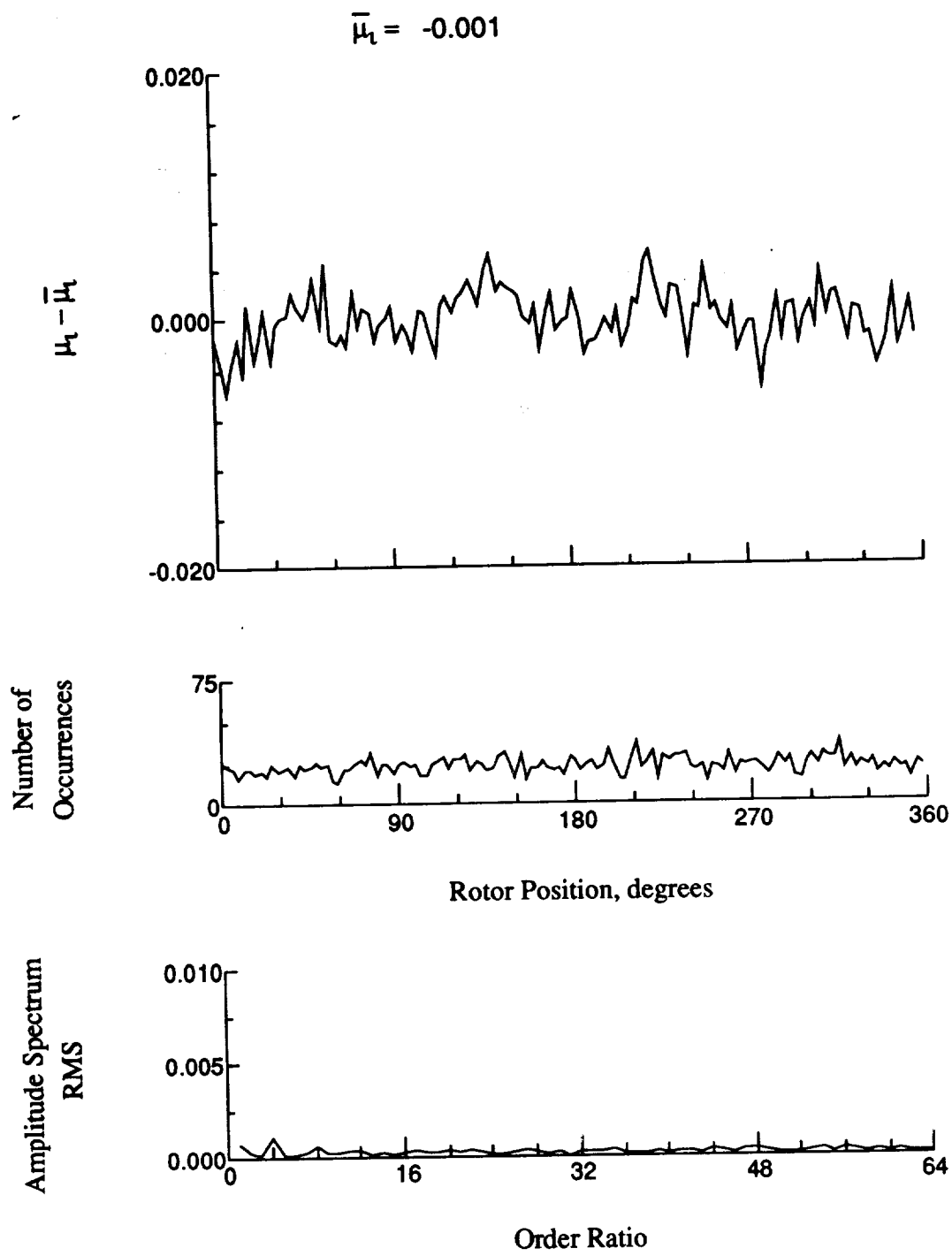


Figure 38.- Induced inflow velocity measured at 30 degrees and r/R of 0.69.

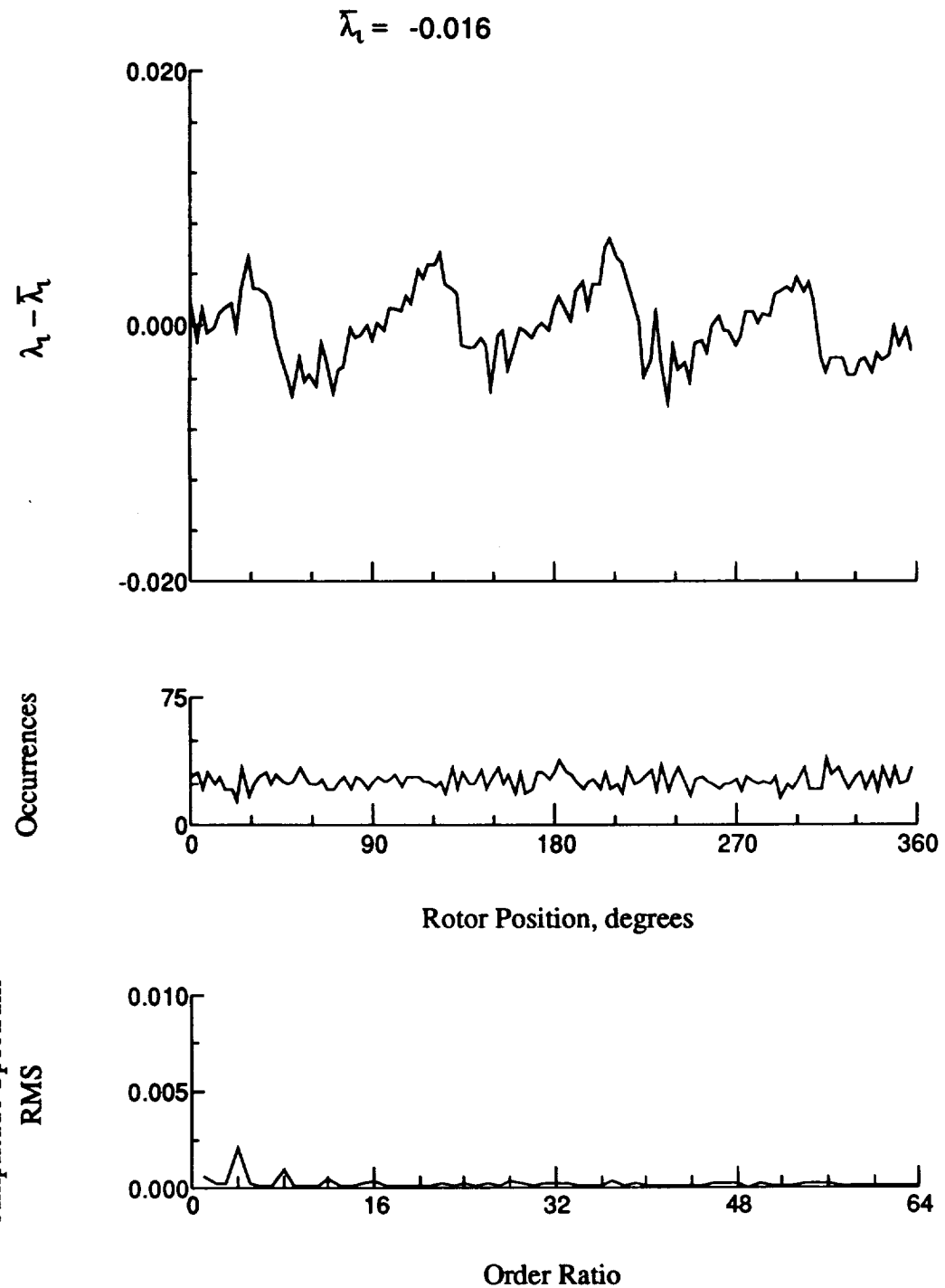


Figure 38.- Concluded.

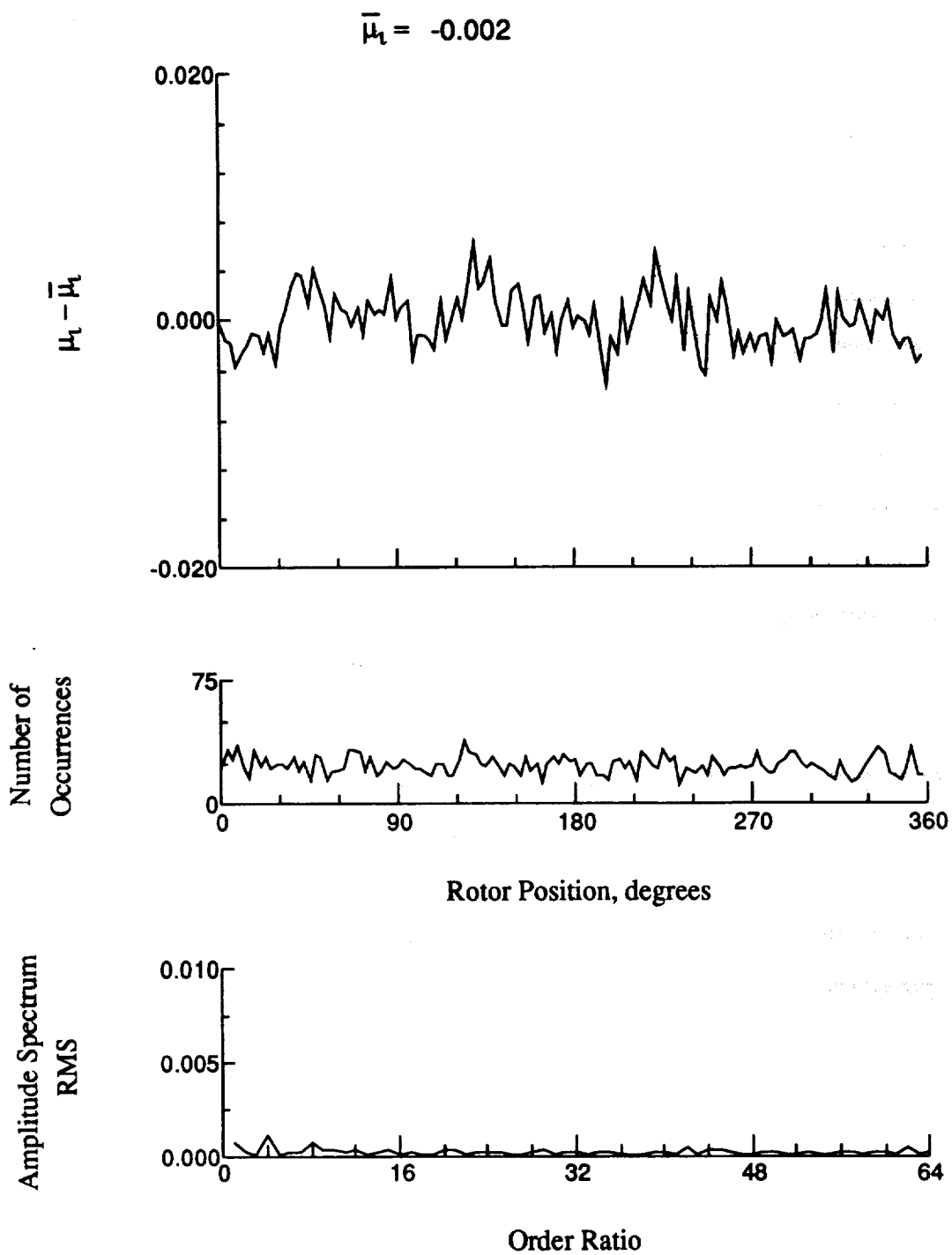


Figure 39.- Induced inflow velocity measured at 30 degrees and r/R of 0.73.

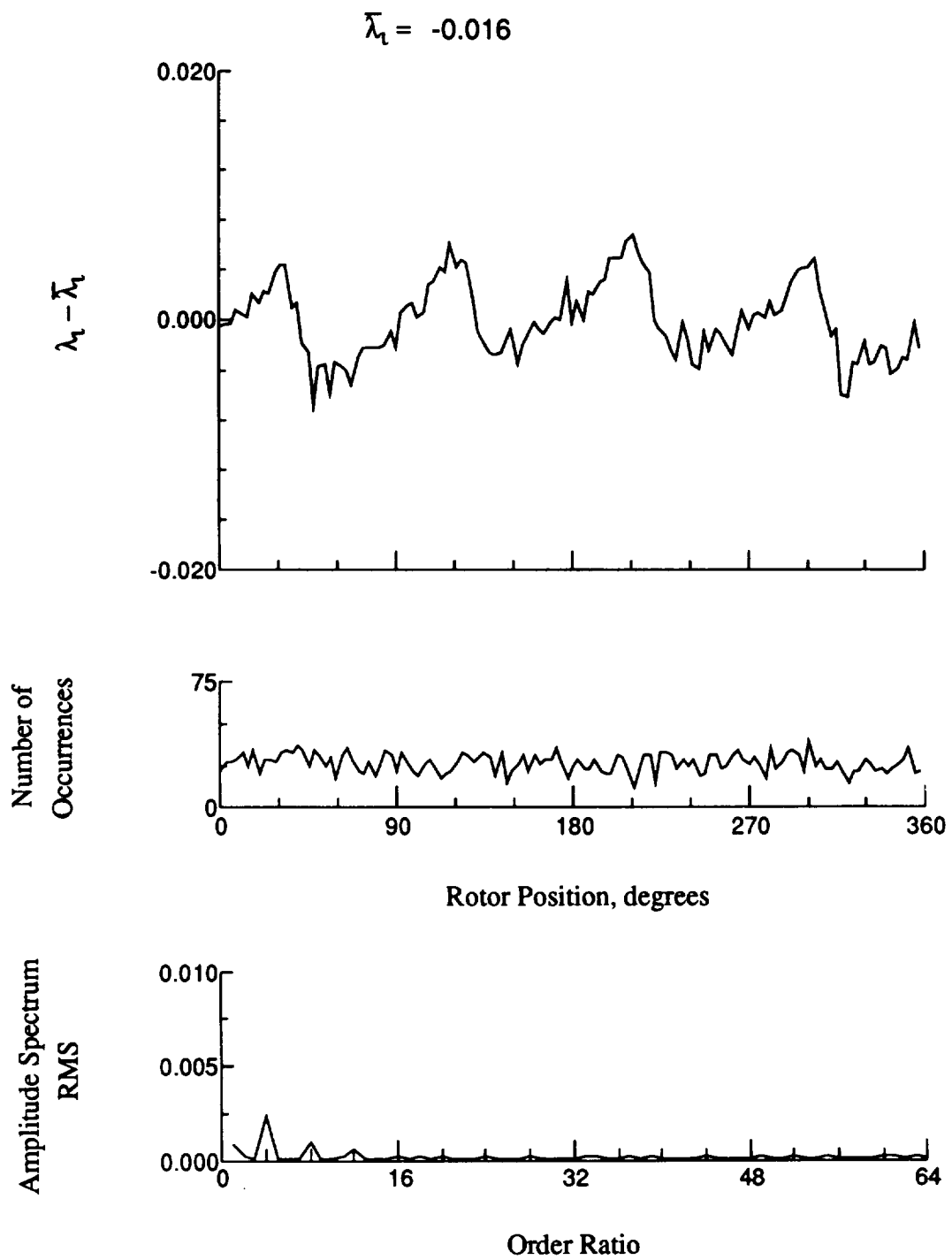


Figure 39.- Concluded.

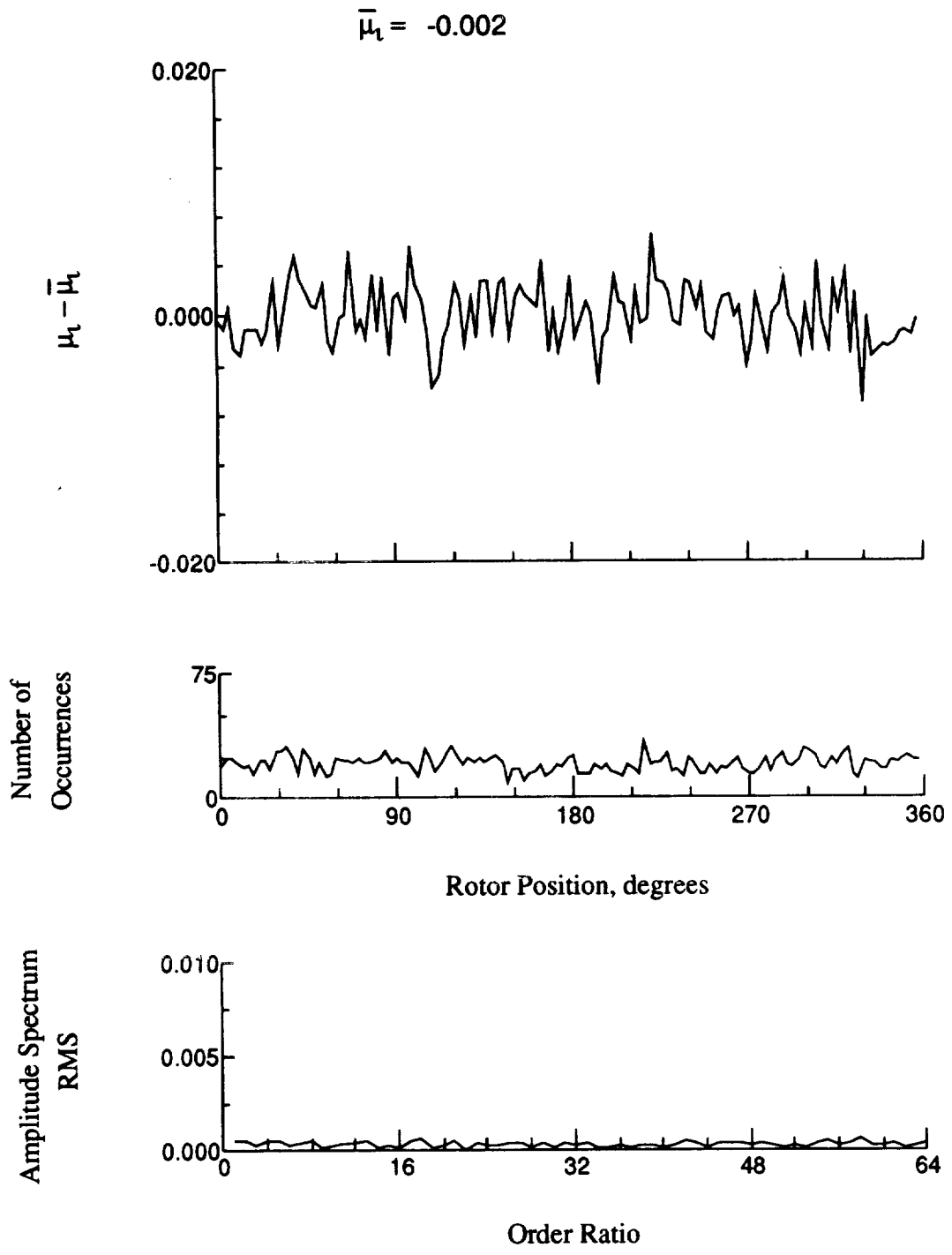


Figure 40.- Induced inflow velocity measured at 30 degrees and r/R of 0.75.

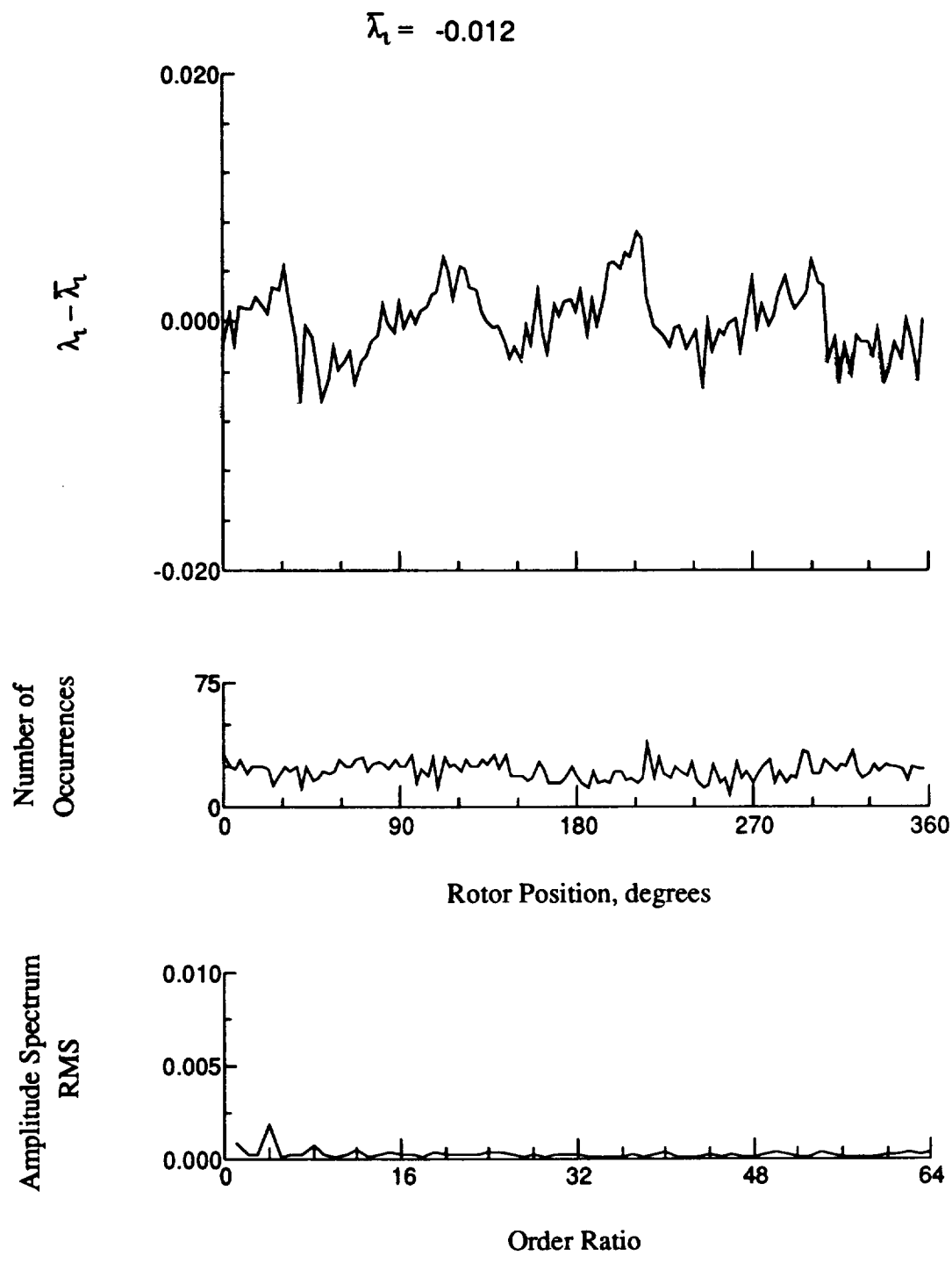


Figure 40.- Concluded.

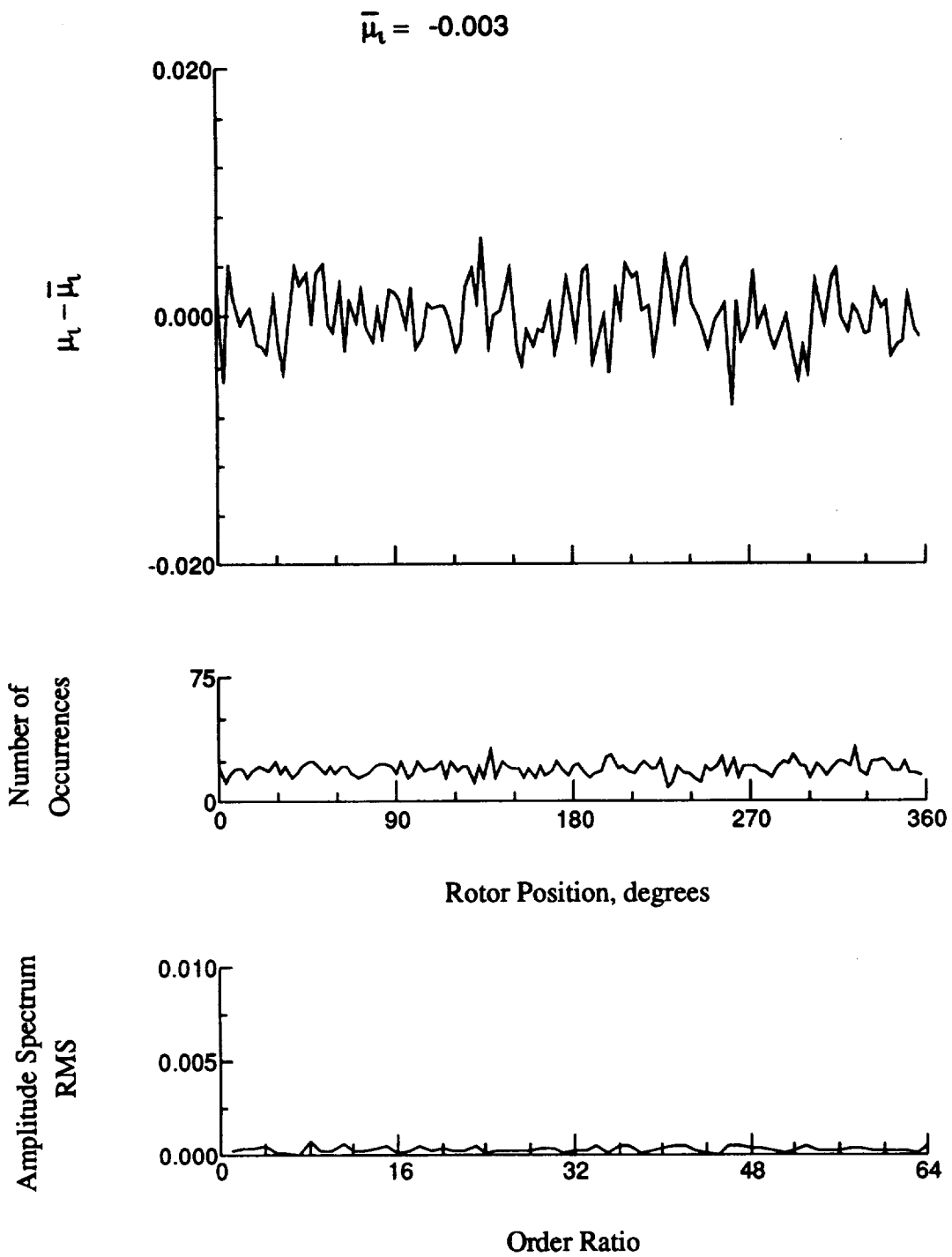


Figure 41.- Induced inflow velocity measured at 30 degrees and r/R of 0.81.

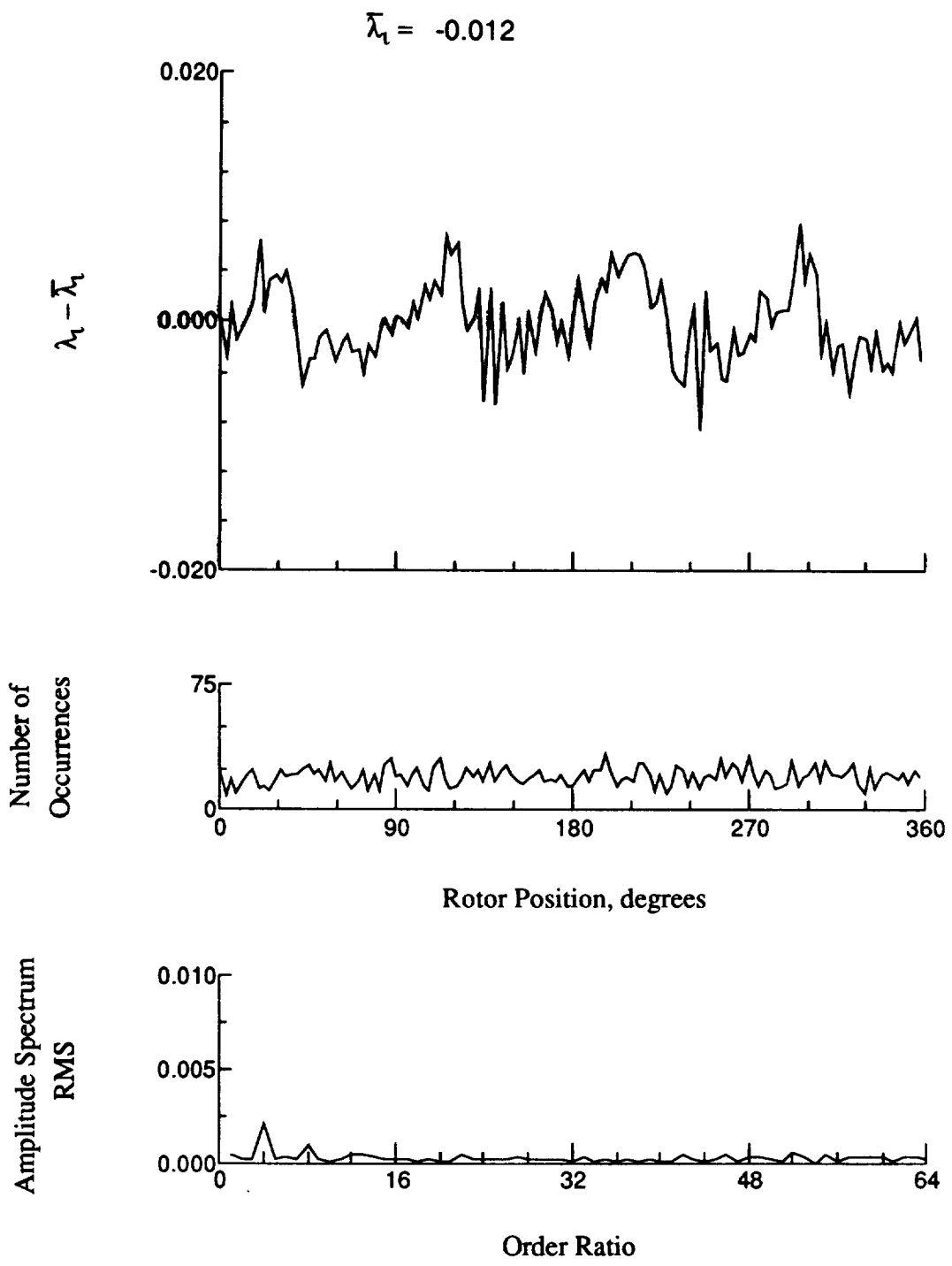


Figure 41.- Concluded.

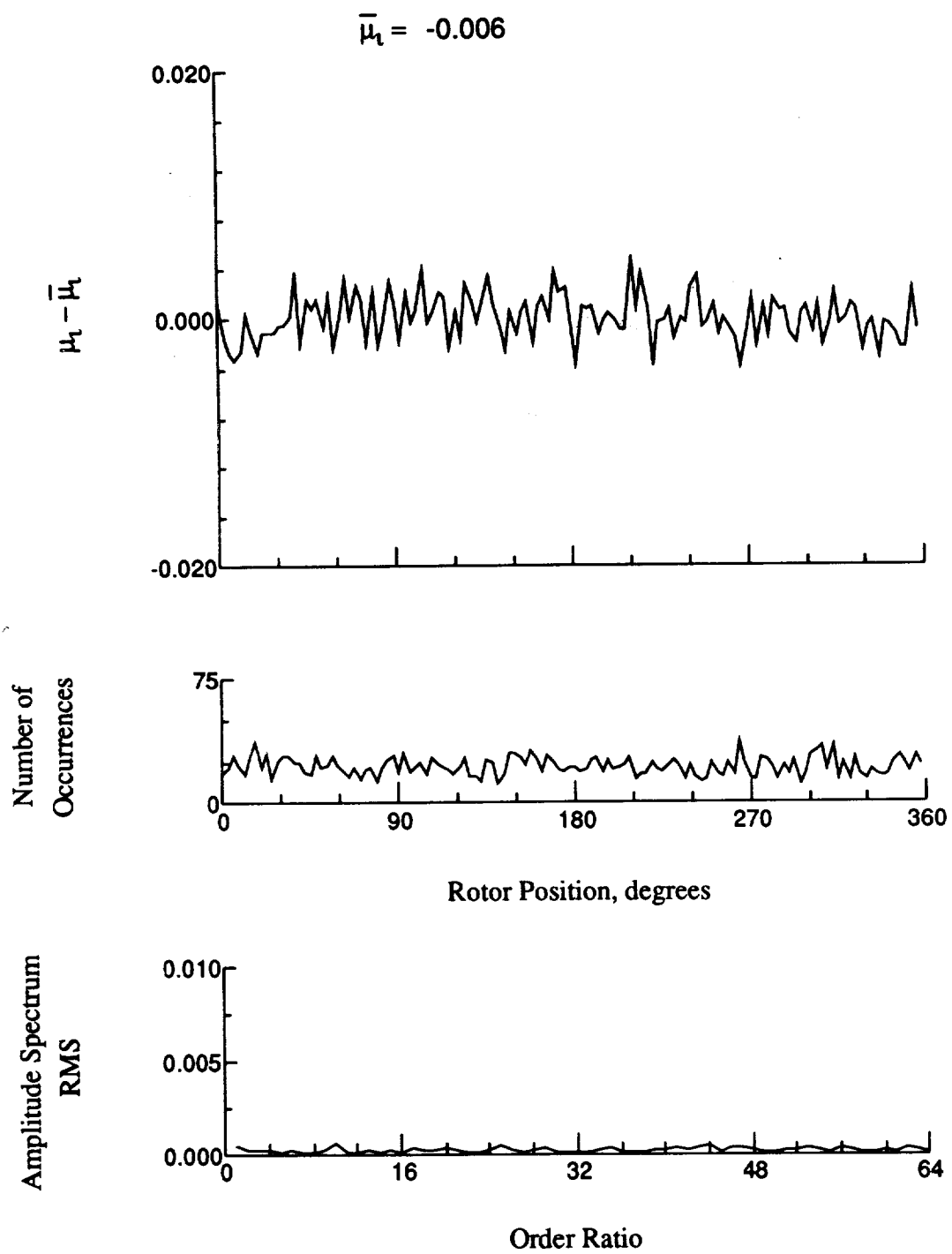


Figure 42.- Induced inflow velocity measured at 30 degrees and r/R of 0.86.

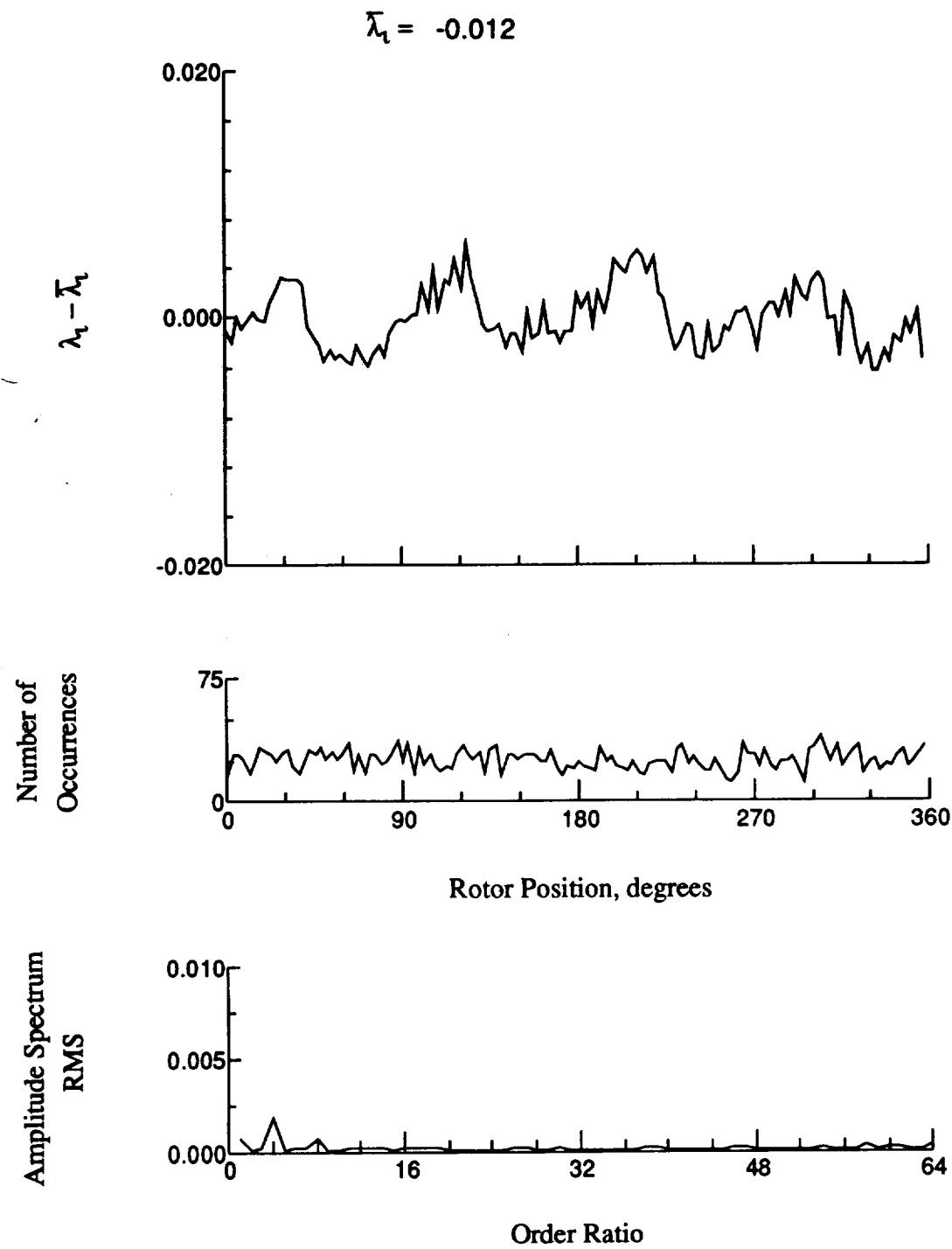


Figure 42.- Concluded.

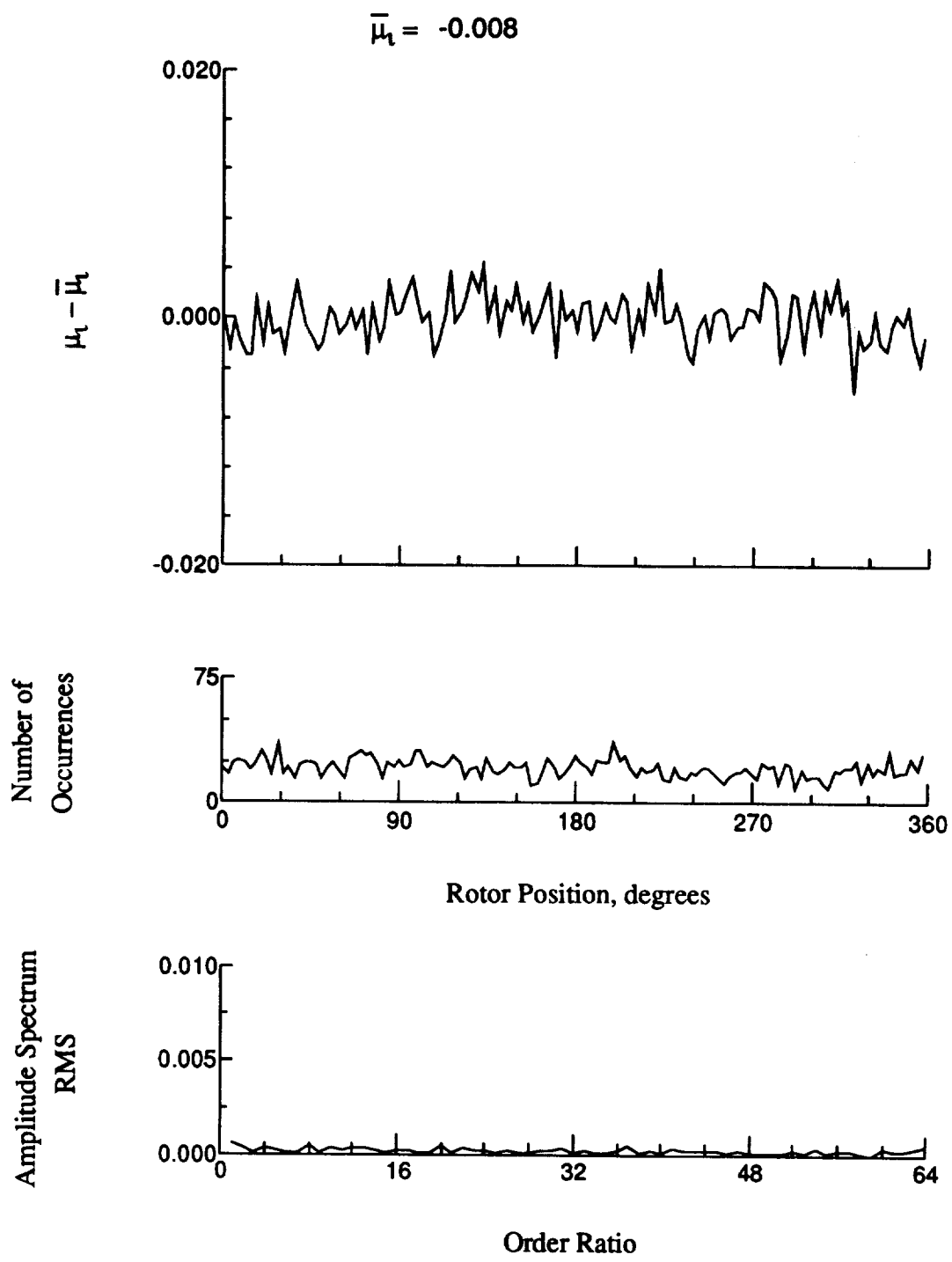


Figure 43.- Induced inflow velocity measured at 30 degrees and r/R of 0.90.

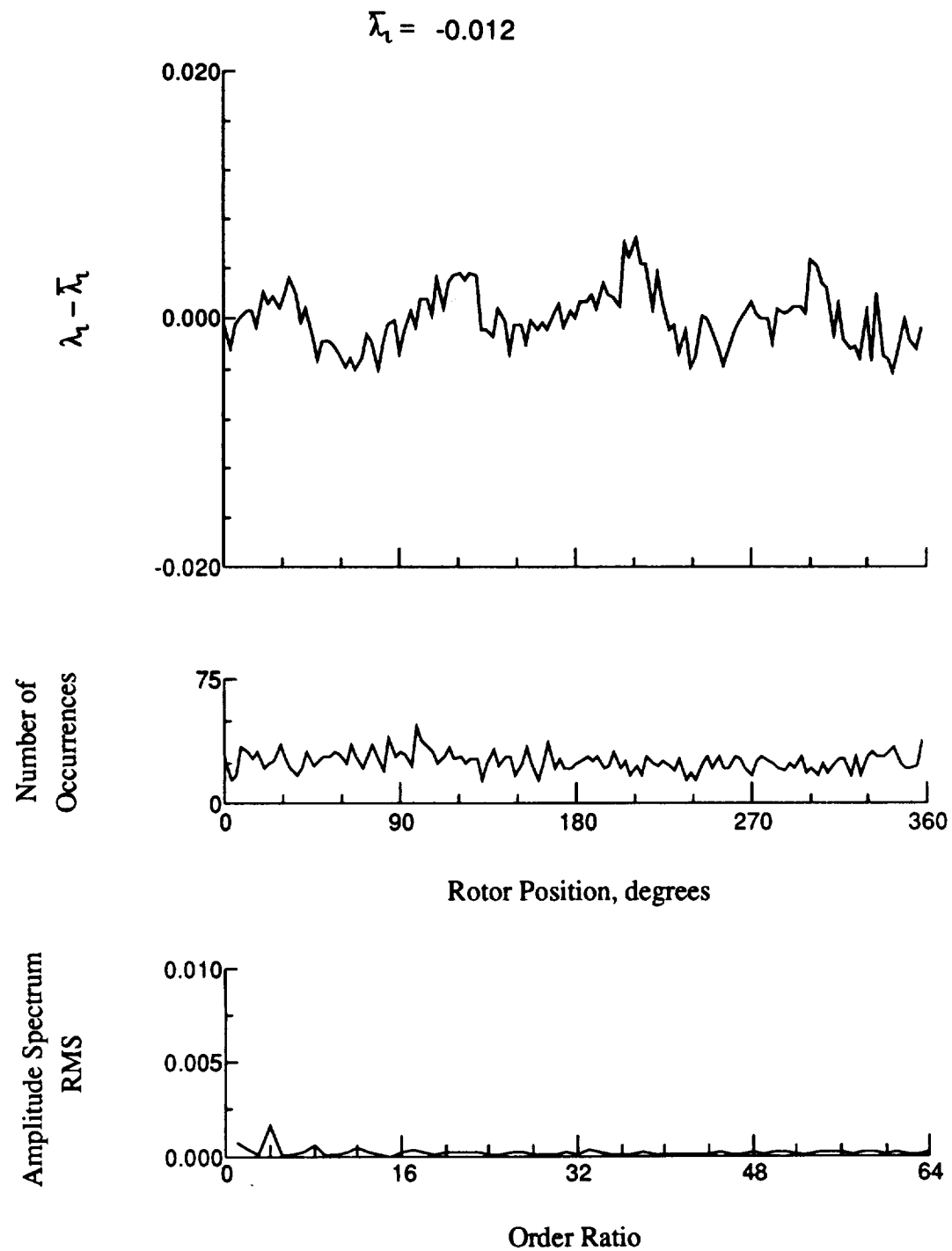


Figure 43.- Concluded.

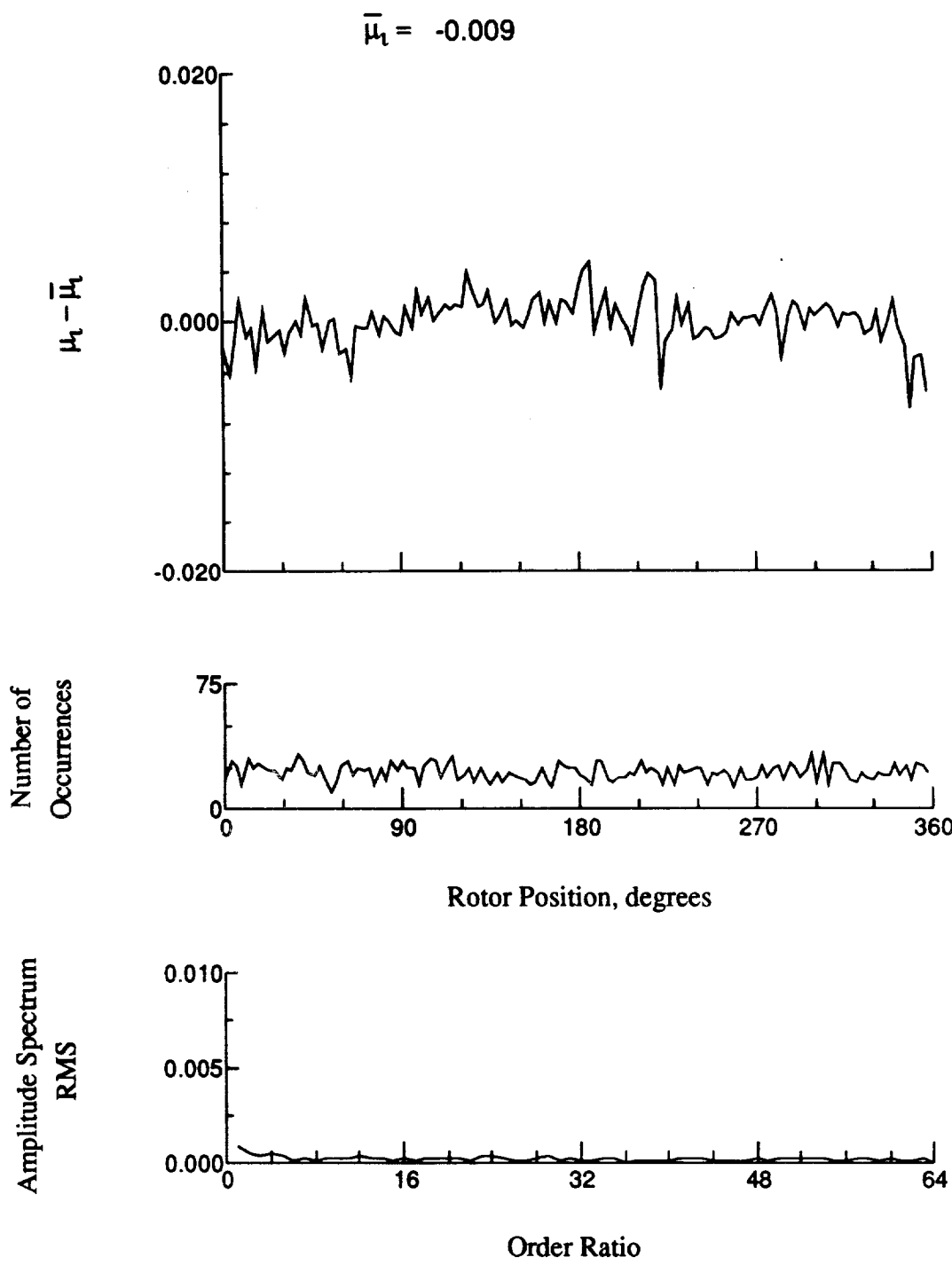


Figure 44.- Induced inflow velocity measured at 30 degrees and r/R of 0.94.

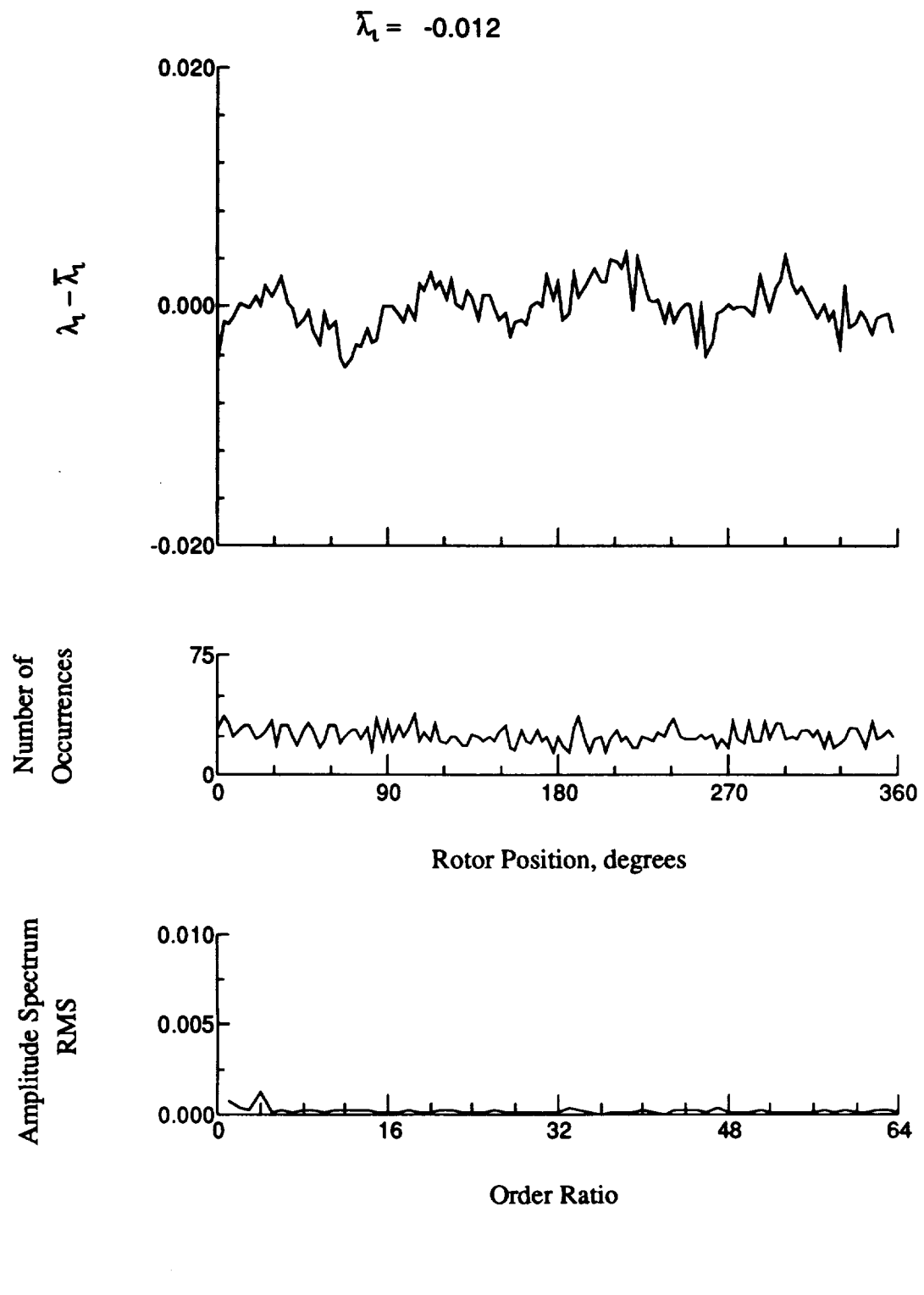


Figure 44.- Concluded.

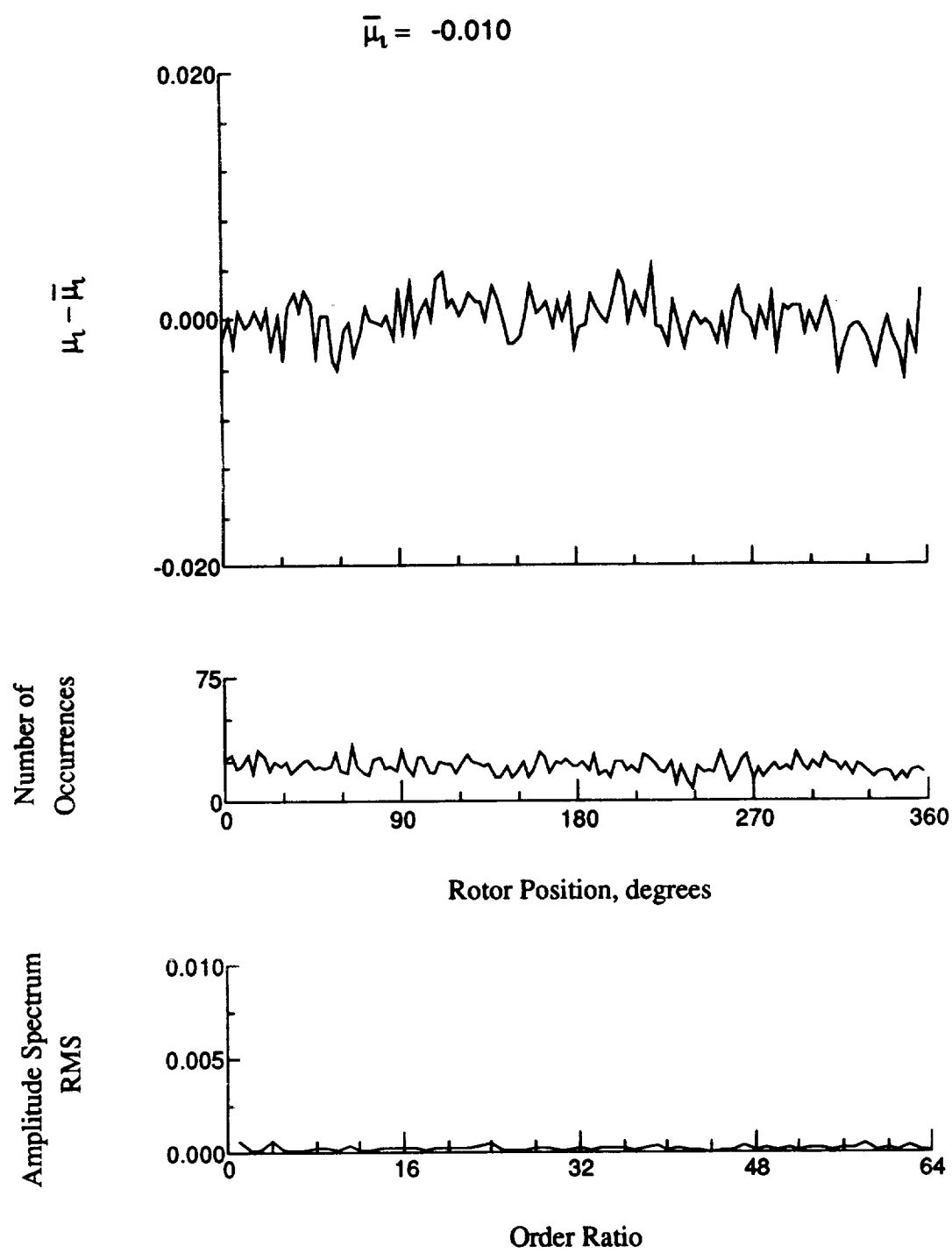


Figure 45.- Induced inflow velocity measured at 30 degrees and r/R of 0.96.

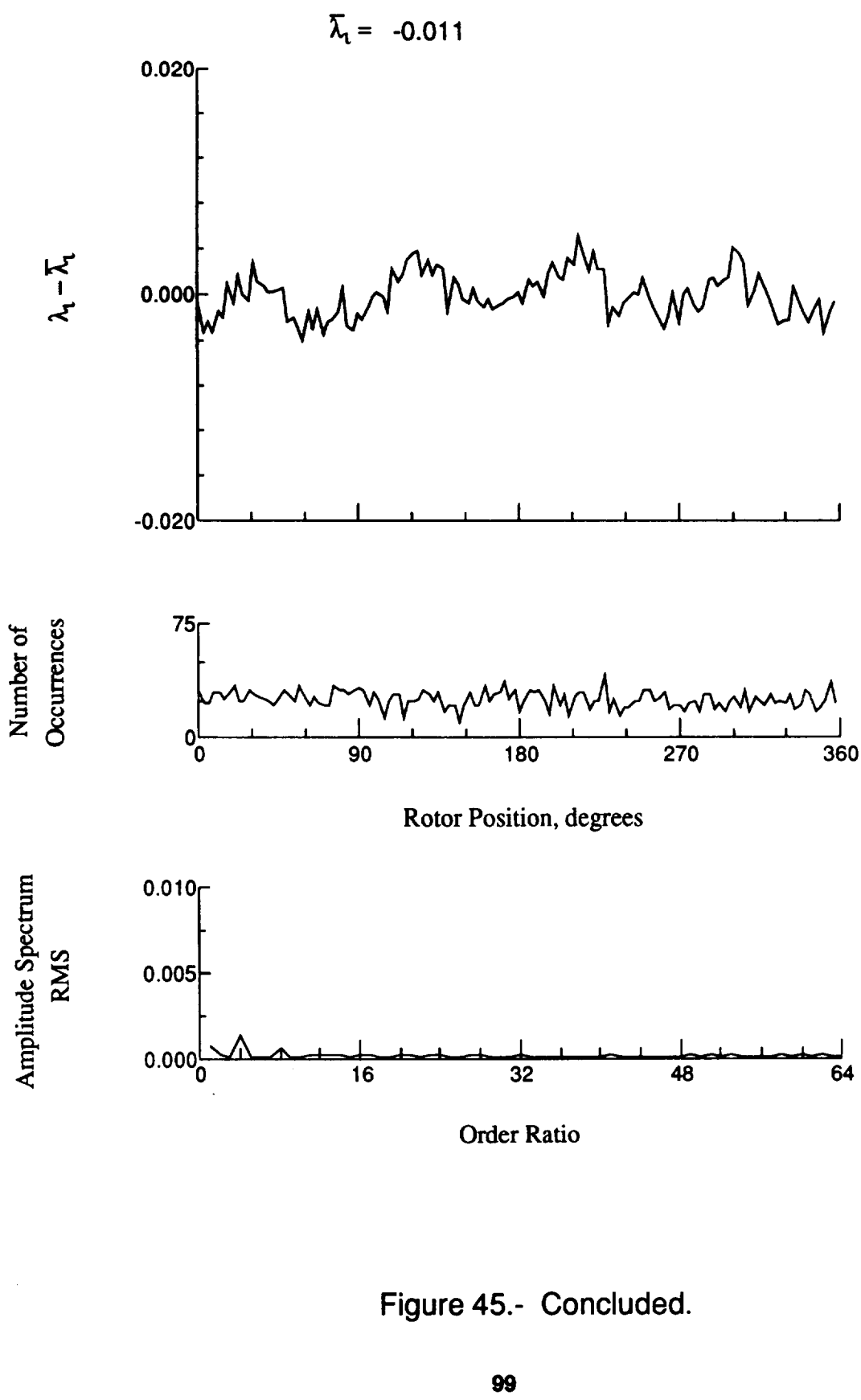


Figure 45.- Concluded.

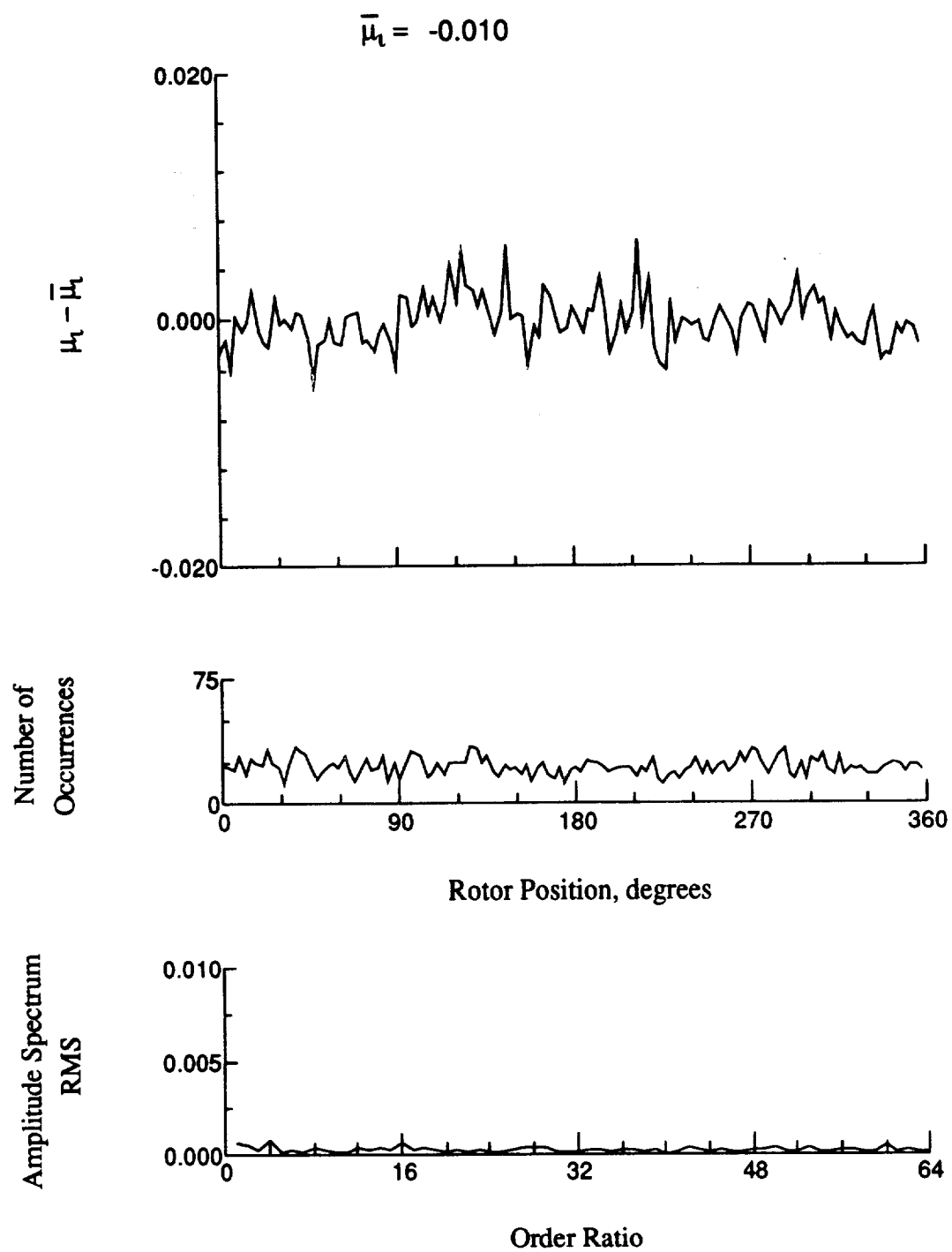


Figure 46.- Induced inflow velocity measured at 30 degrees and r/R of 1.00.

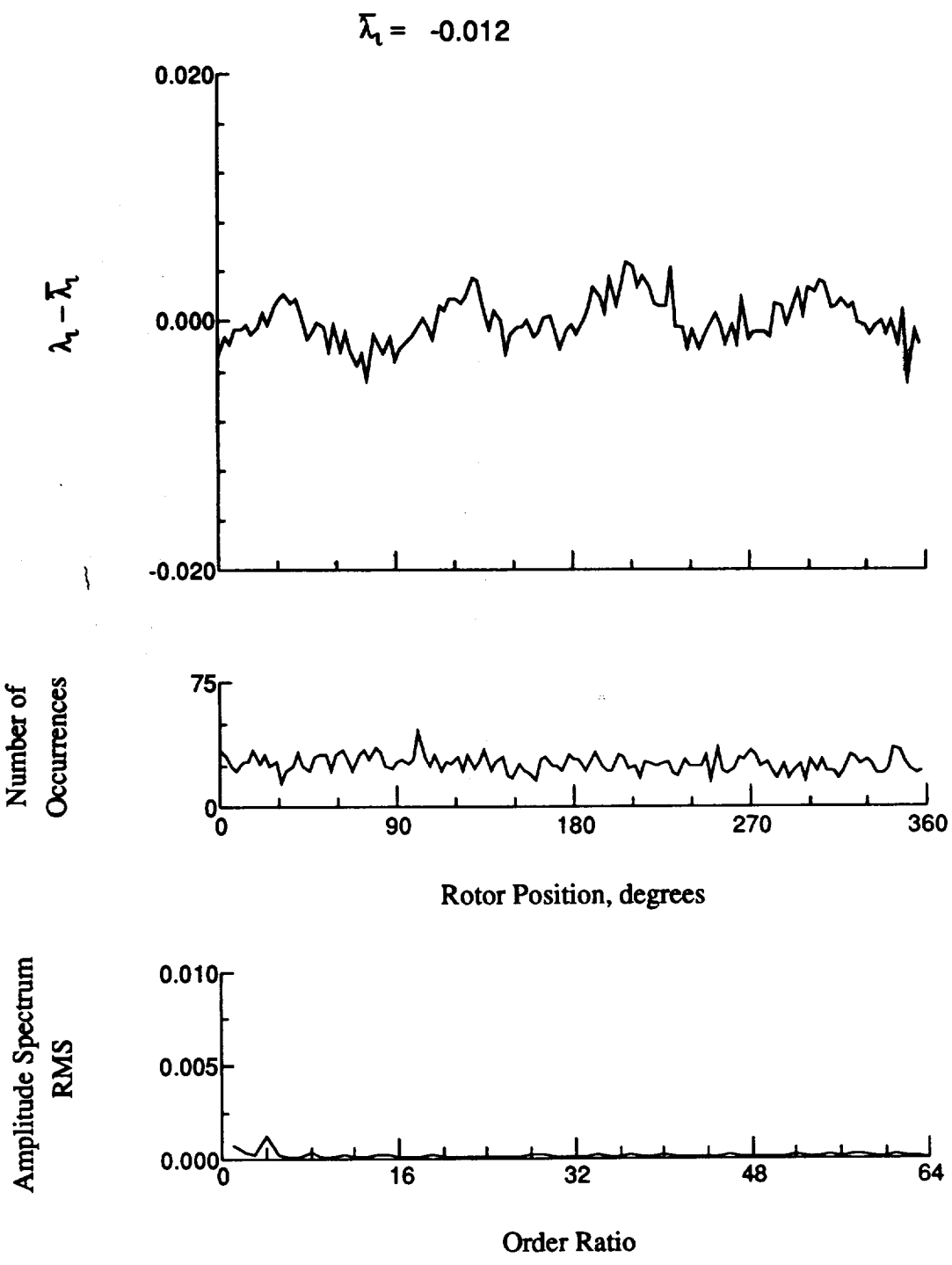


Figure 46.- Concluded.

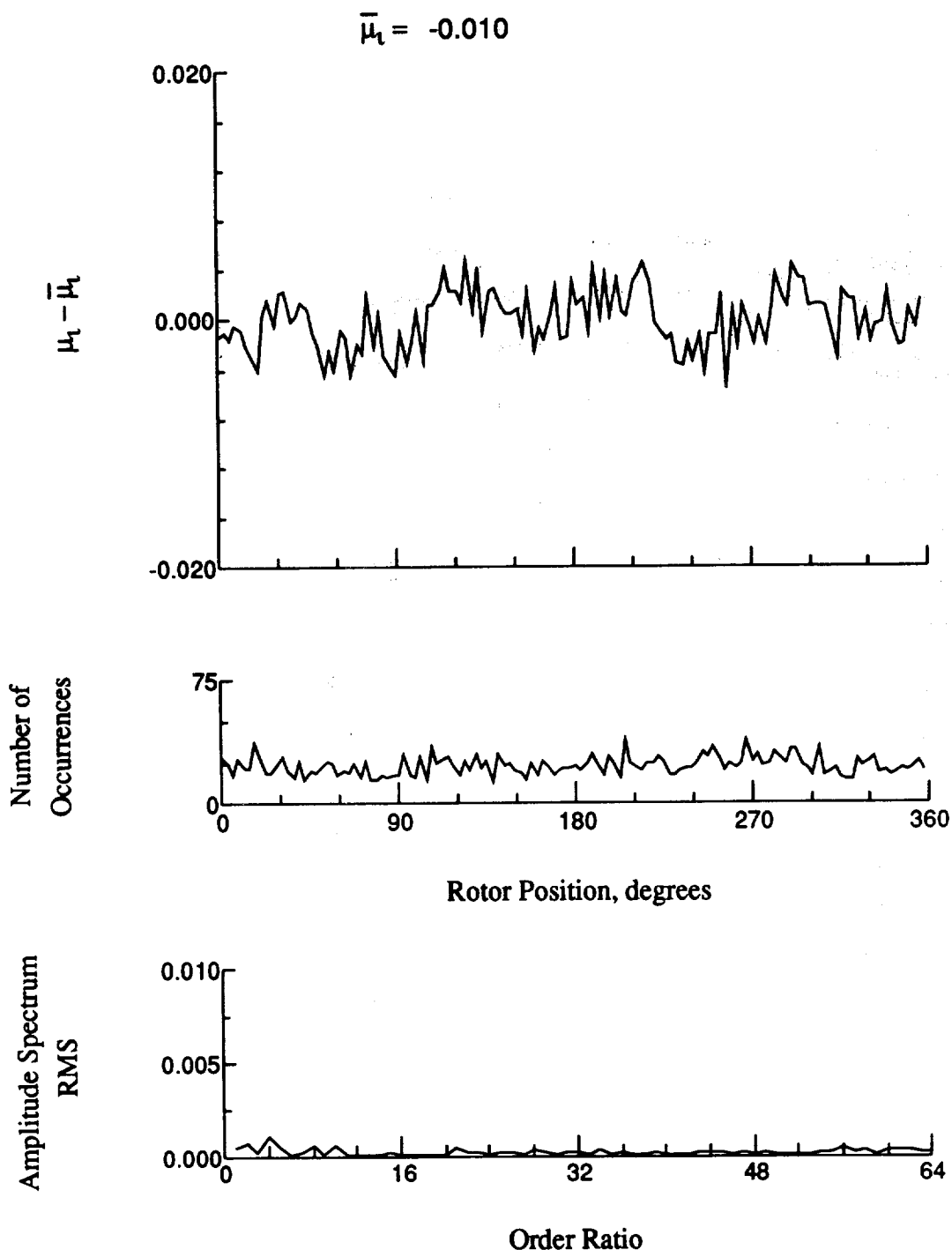


Figure 47.- Induced inflow velocity measured at 30 degrees and r/R of 1.10.

$$\bar{\lambda}_1 = -0.011$$

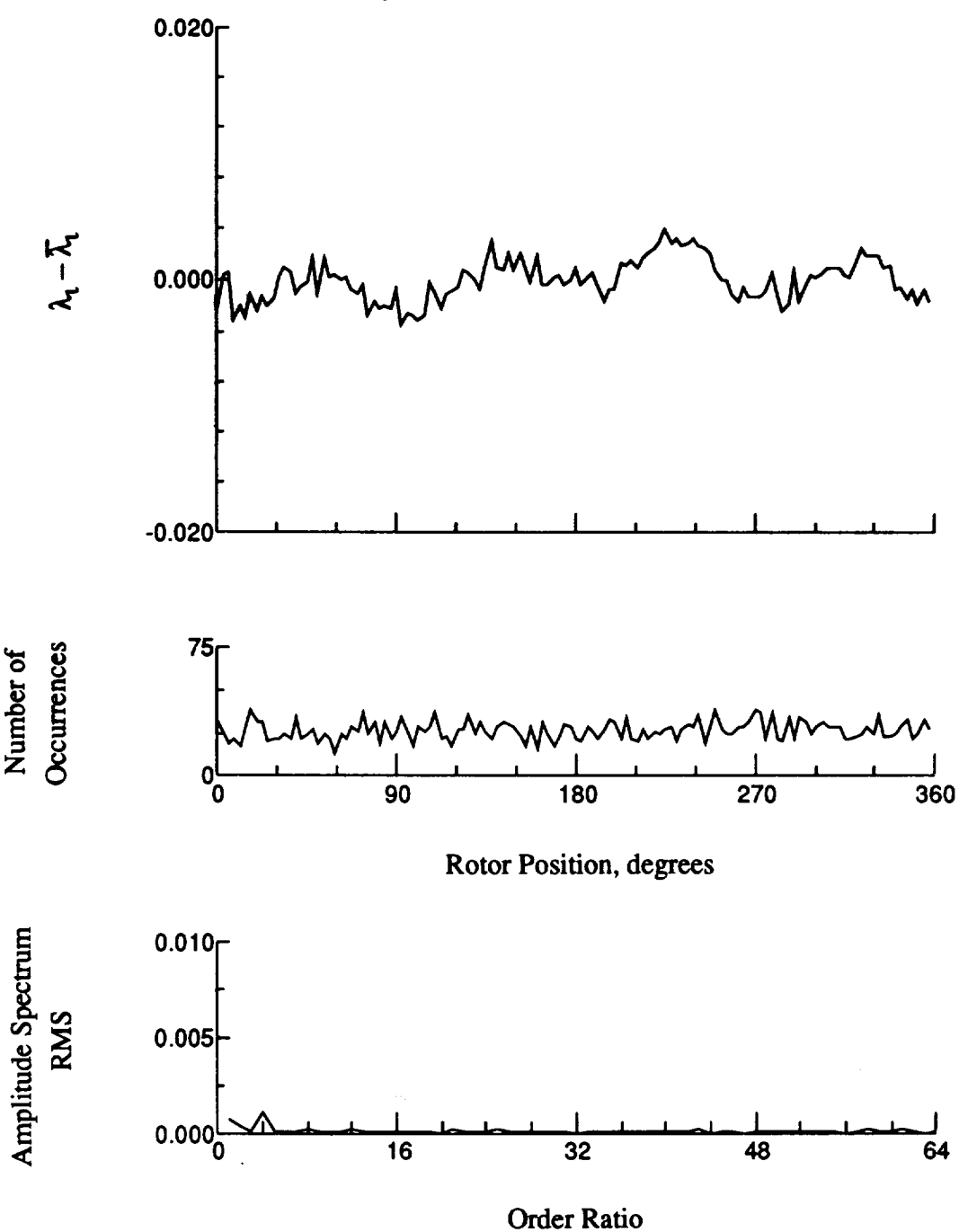


Figure 47.- Concluded.

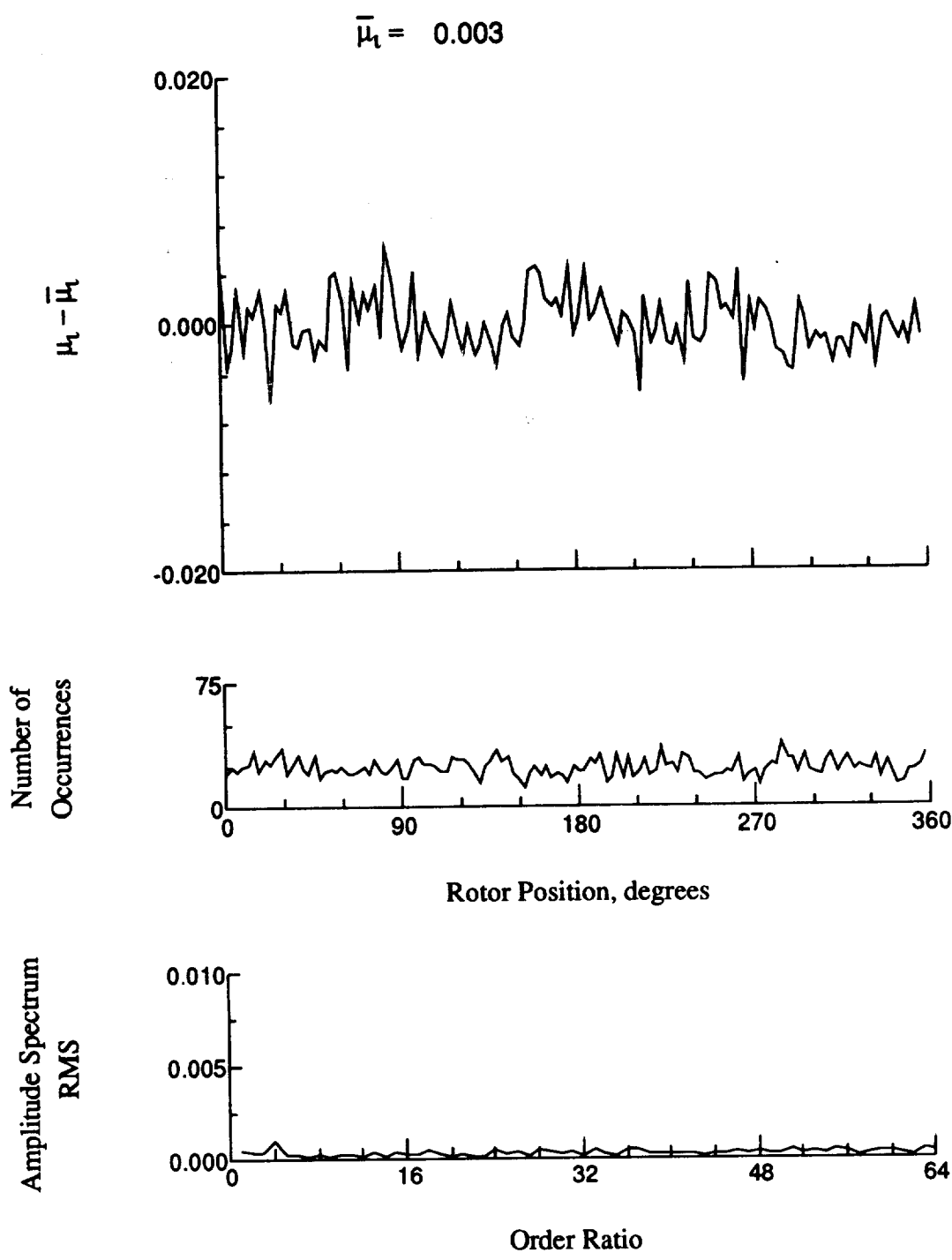


Figure 48.- Induced inflow velocity measured at 60 degrees and r/R of 0.20.

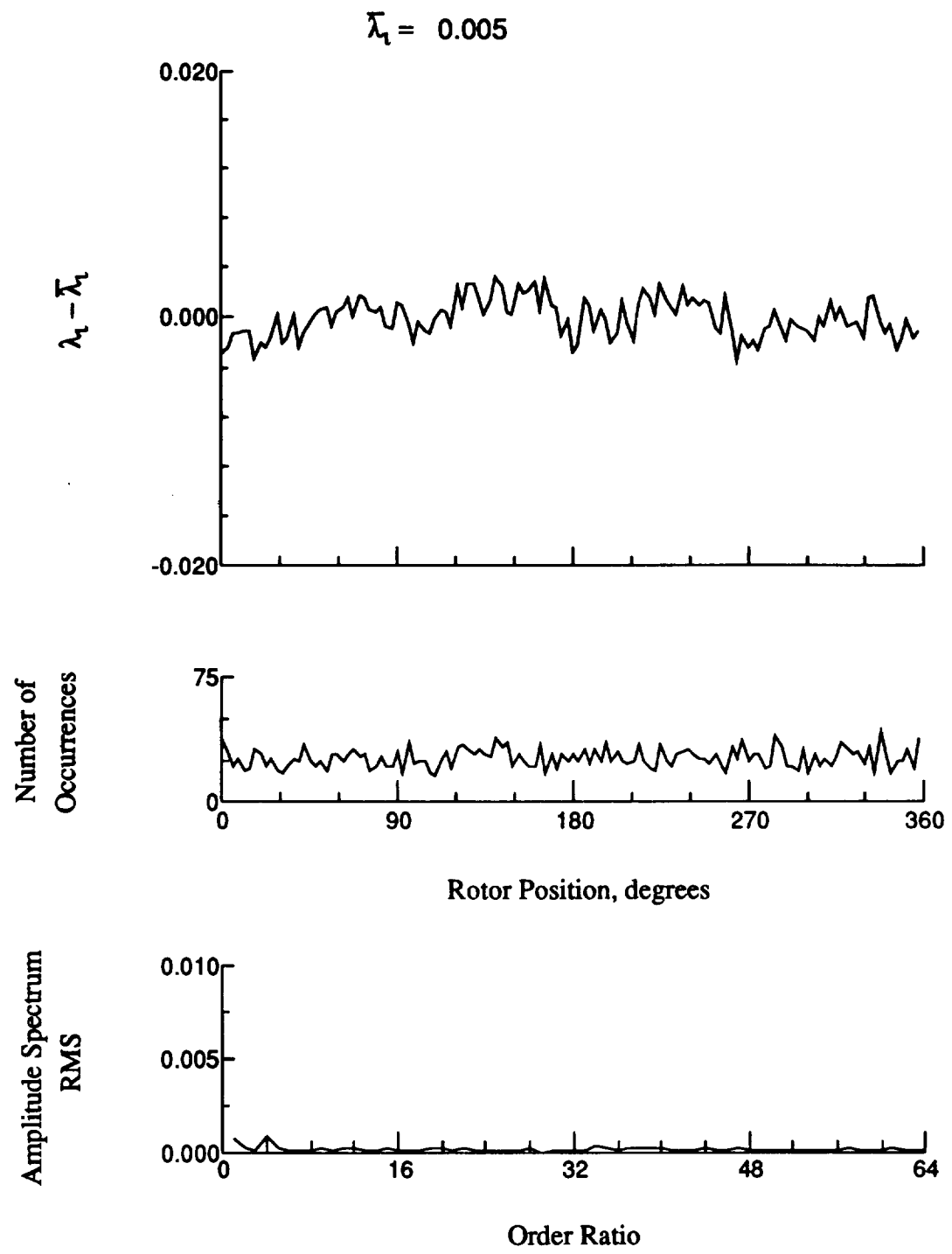


Figure 48.- Concluded.

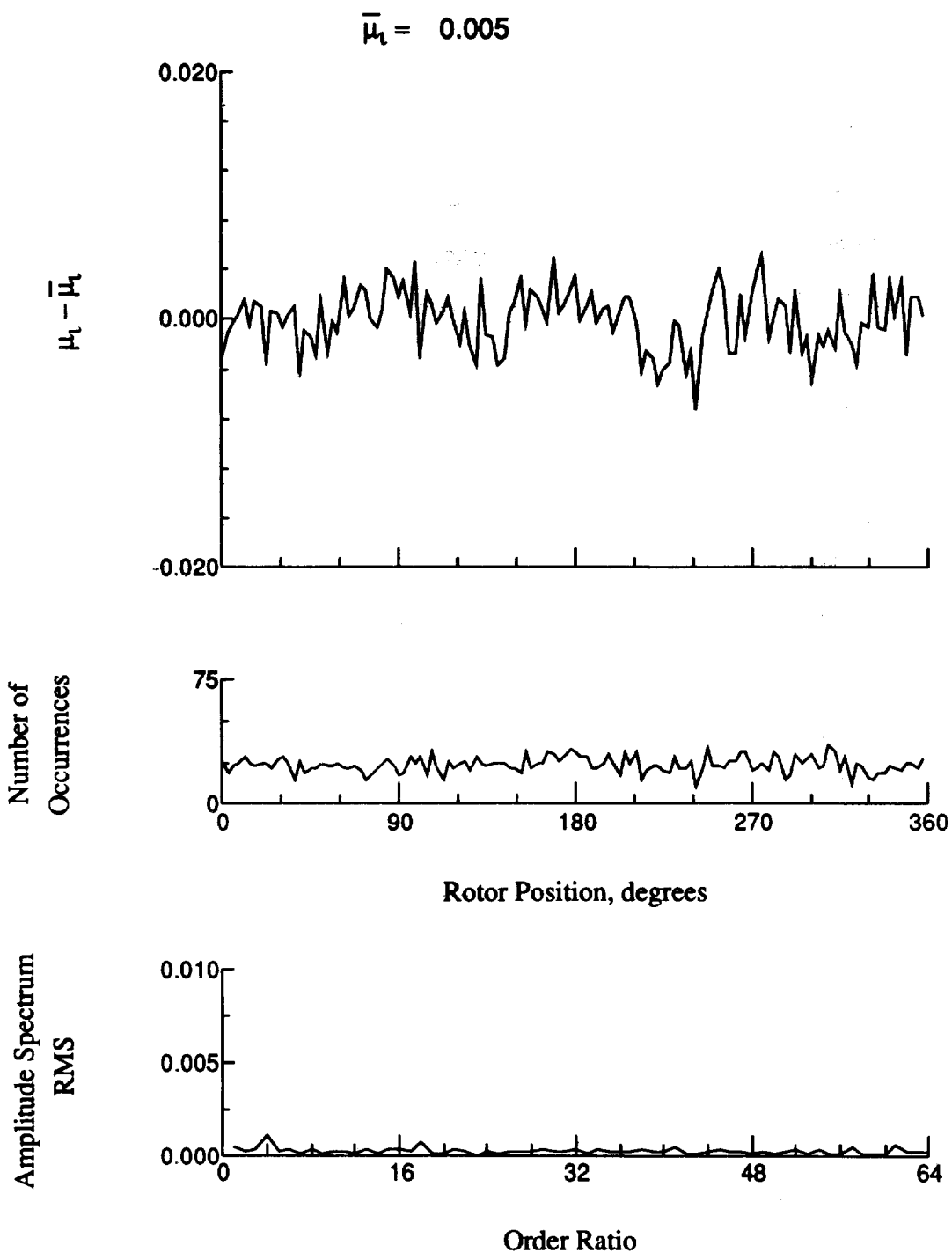


Figure 49.- Induced inflow velocity measured at 60 degrees and r/R of 0.32.

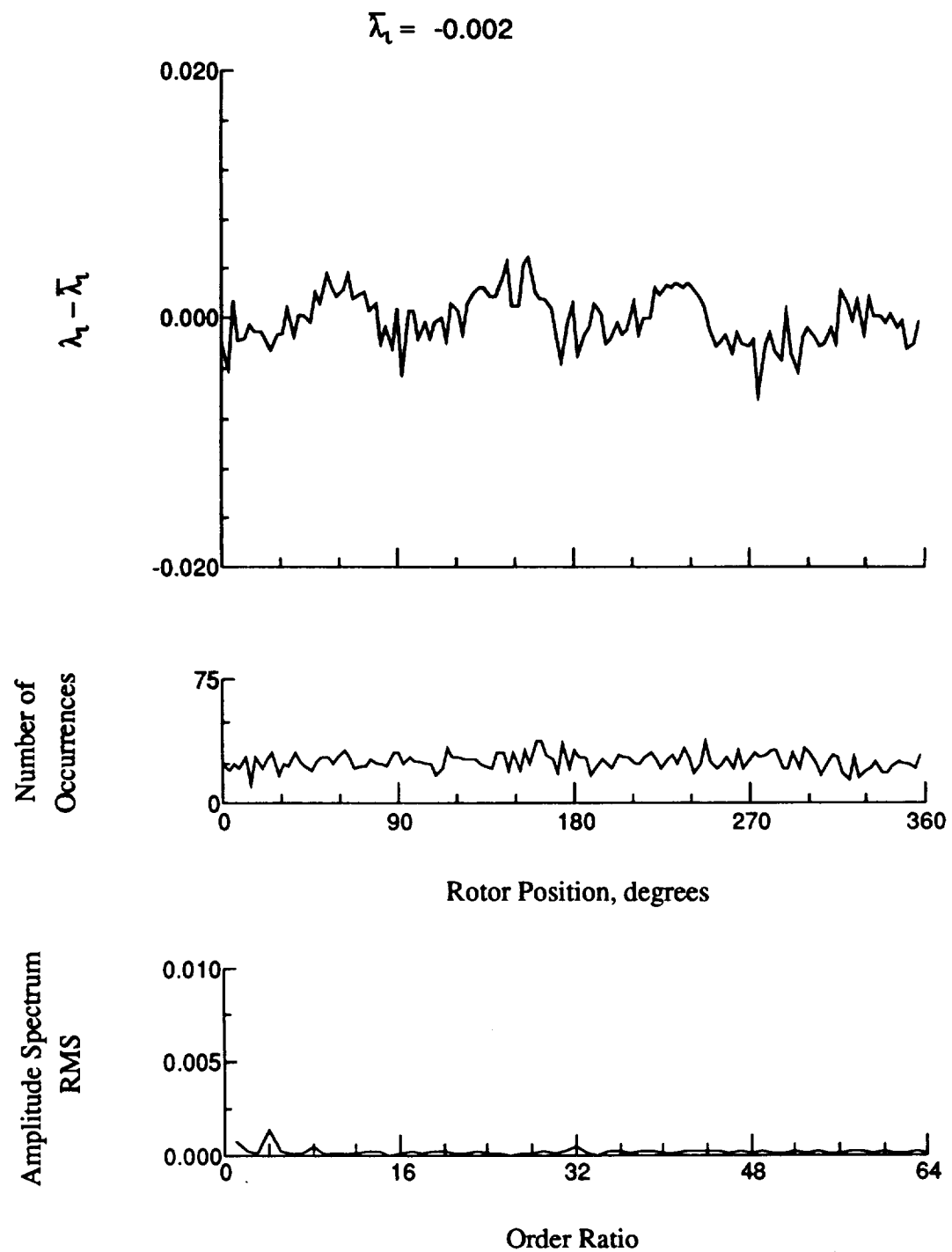


Figure 49.- Concluded.

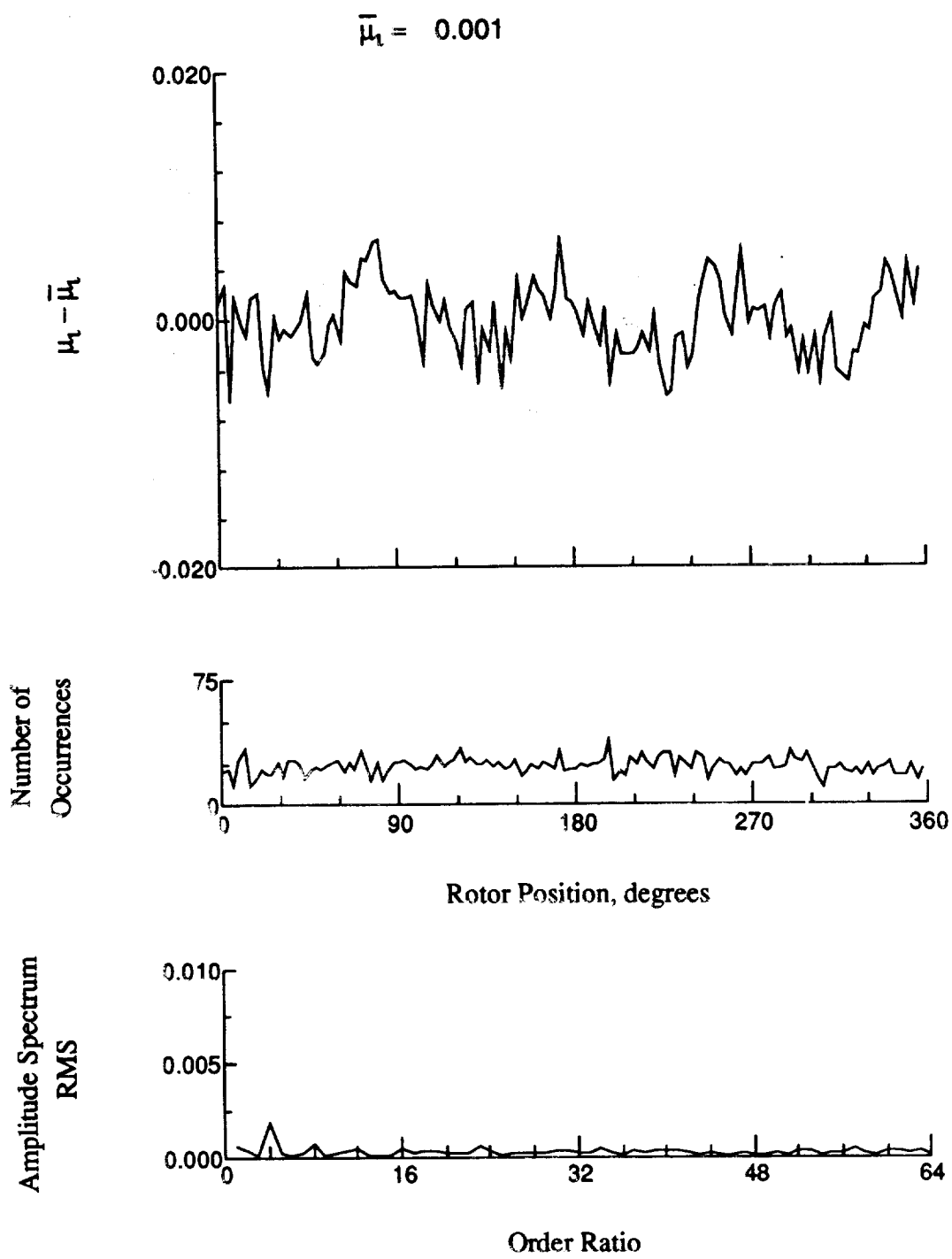


Figure 50.- Induced inflow velocity measured at 60 degrees and r/R of 0.50.

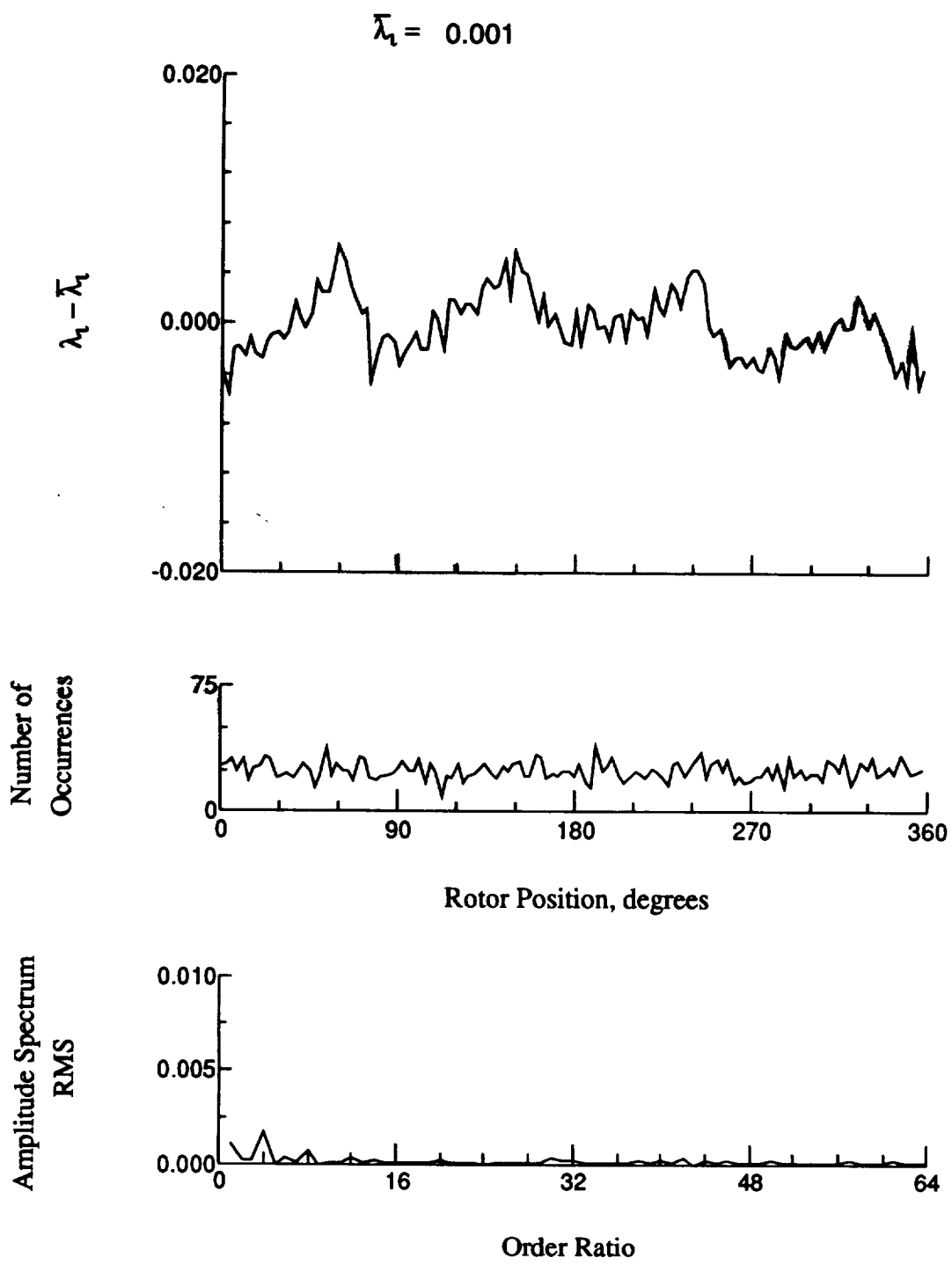


Figure 50.- Concluded.

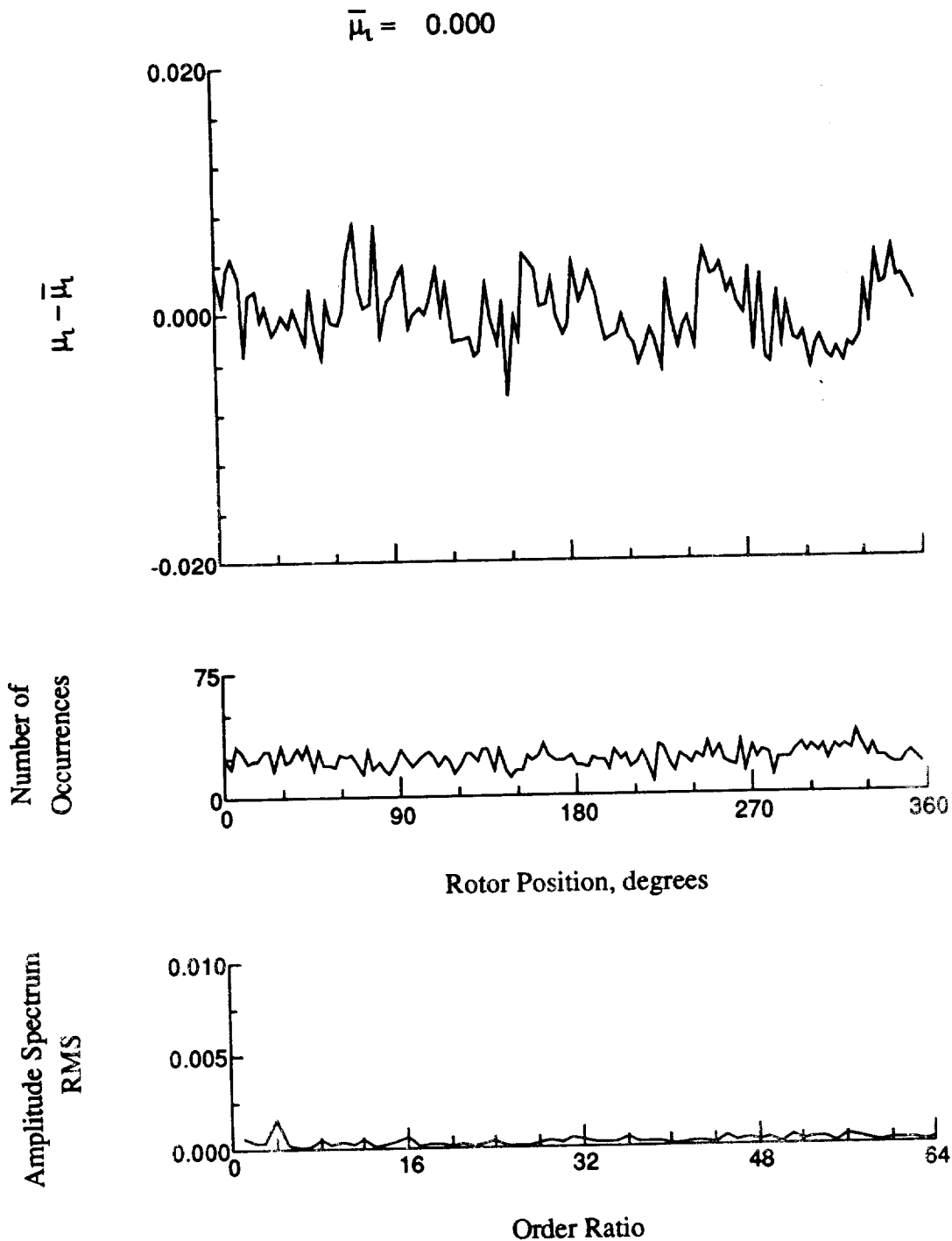


Figure 51.- Induced inflow velocity measured at 60 degrees and r/R of 0.58.

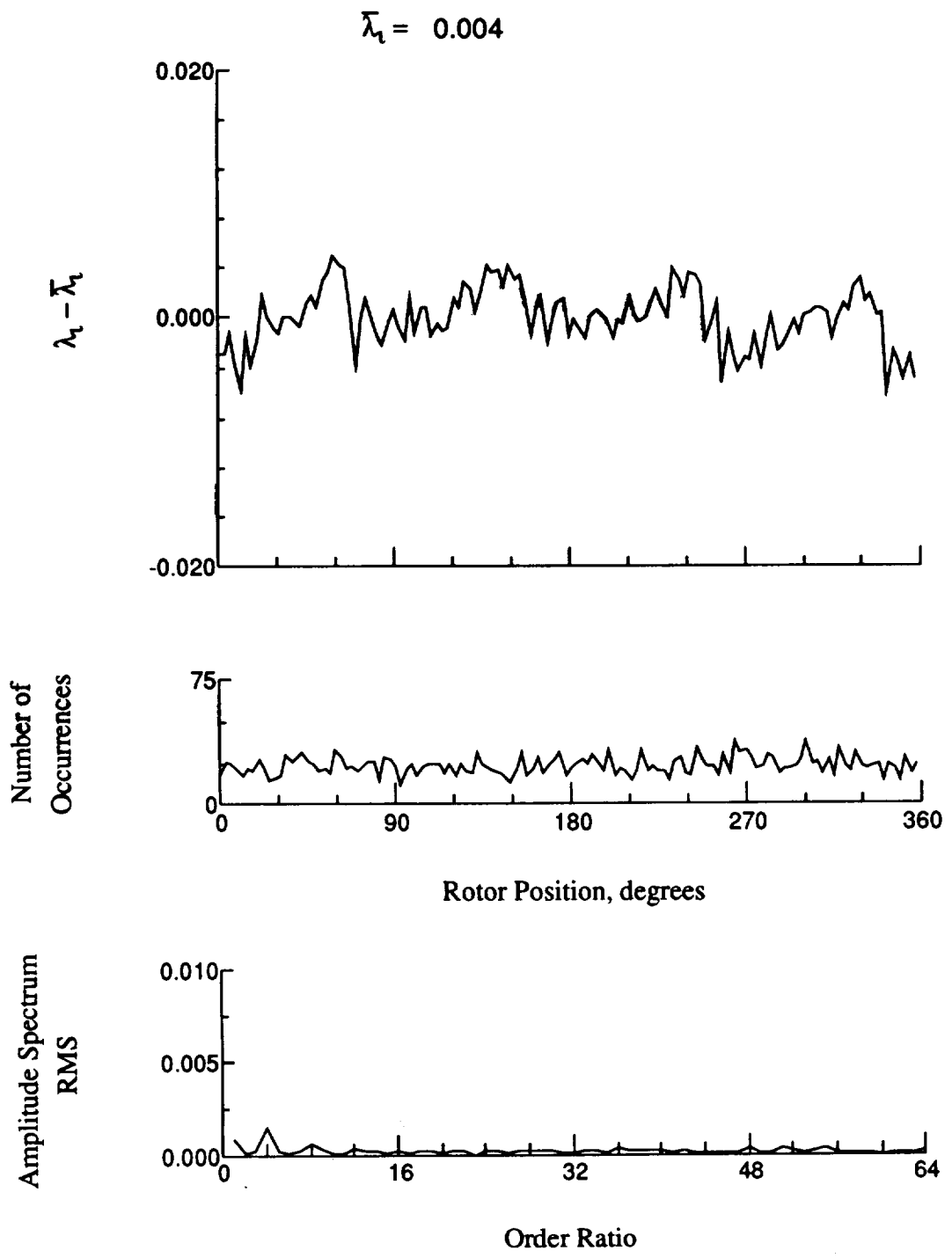


Figure 51.- Concluded.

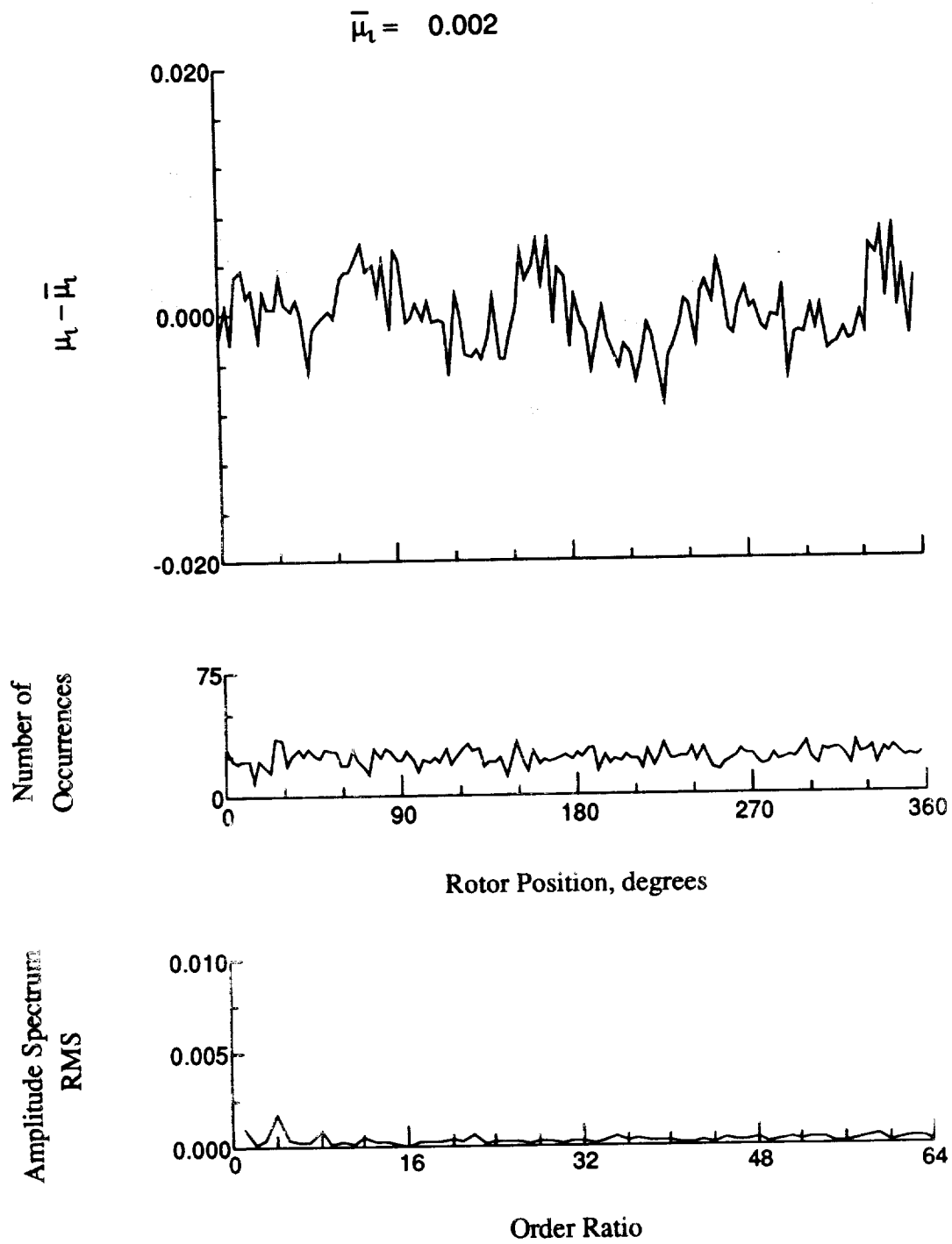


Figure 52.- Induced inflow velocity measured at 60 degrees and r/R of 0.69.

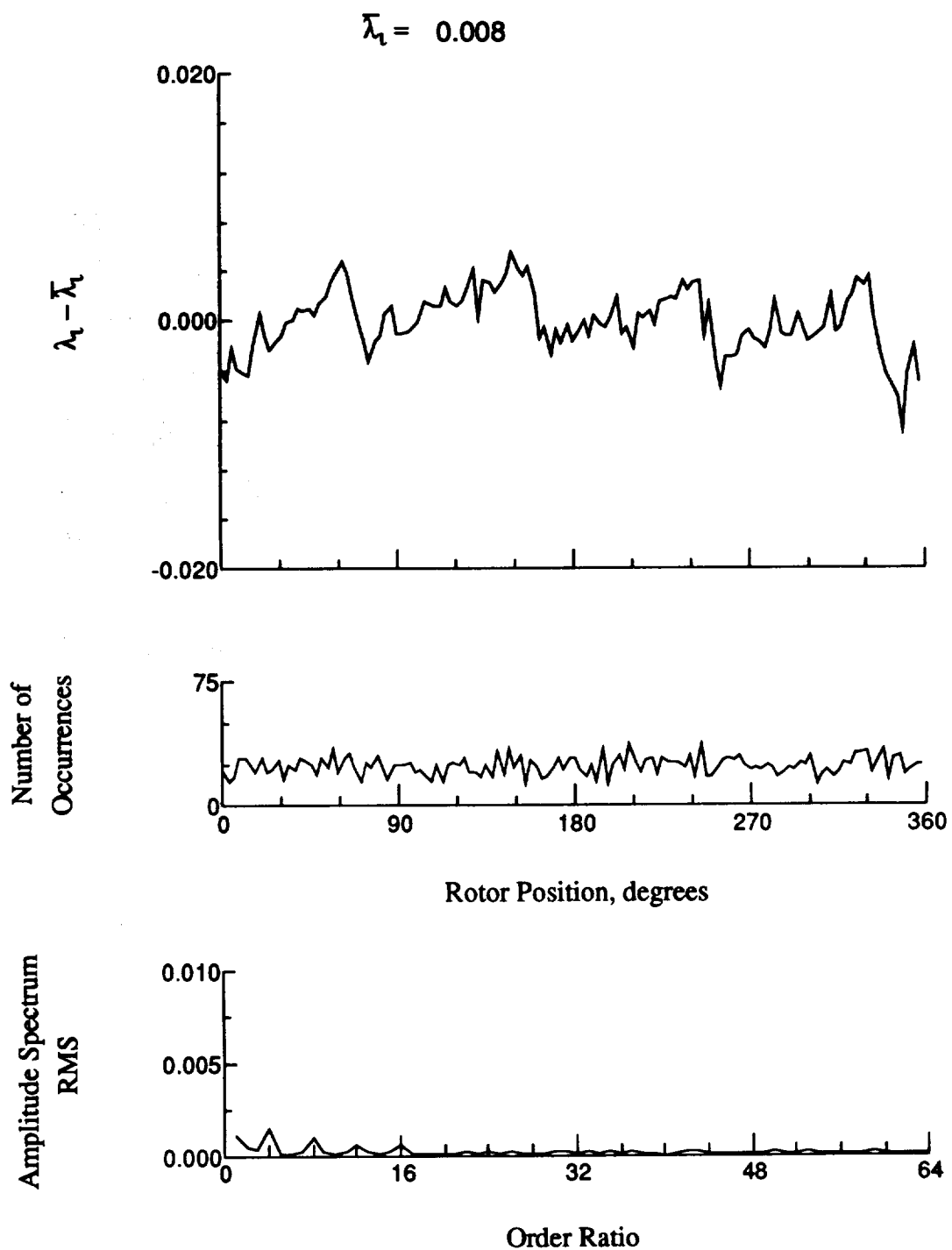


Figure 52.- Concluded.

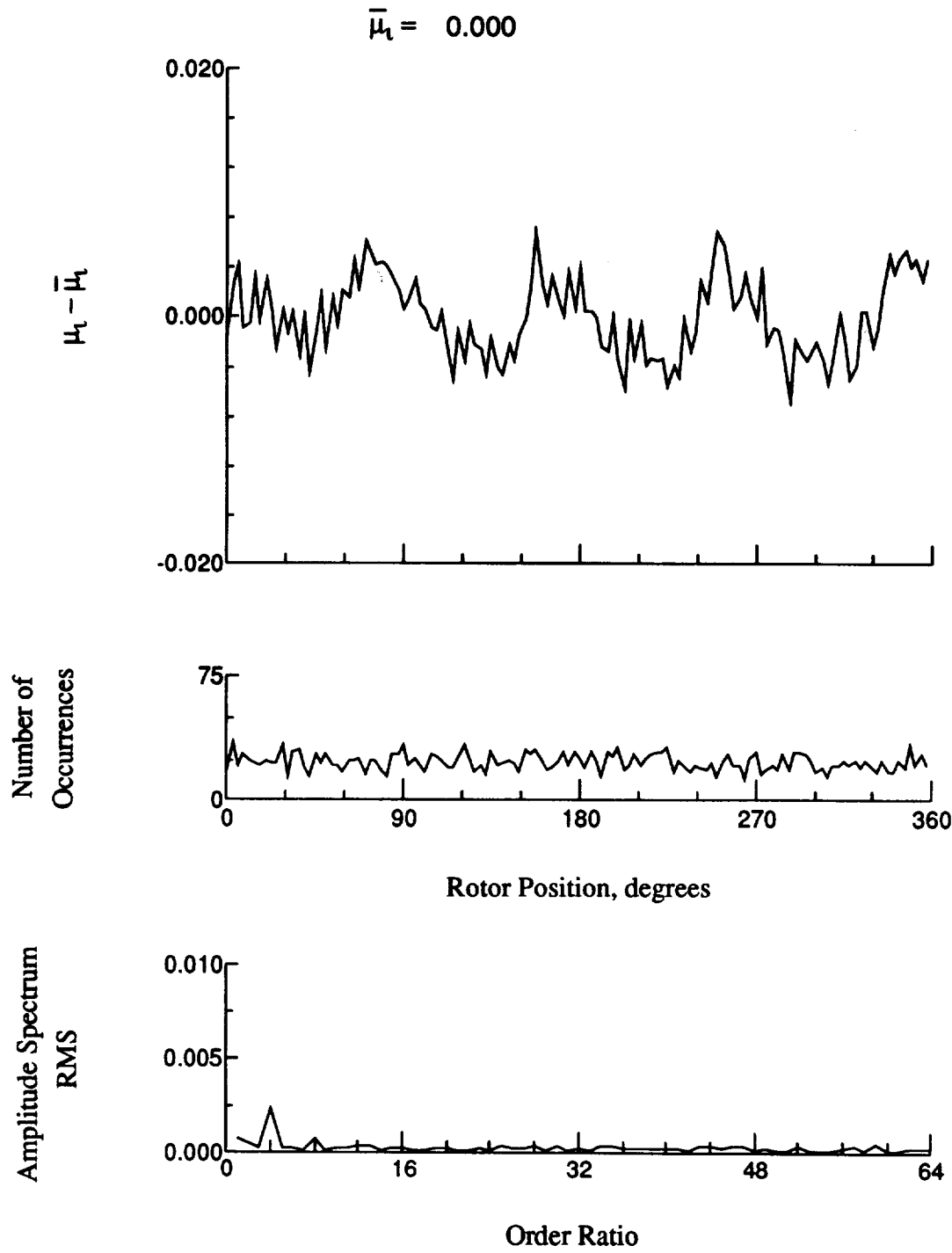


Figure 53.- Induced inflow velocity measured at 60 degrees and r/R of 0.73.

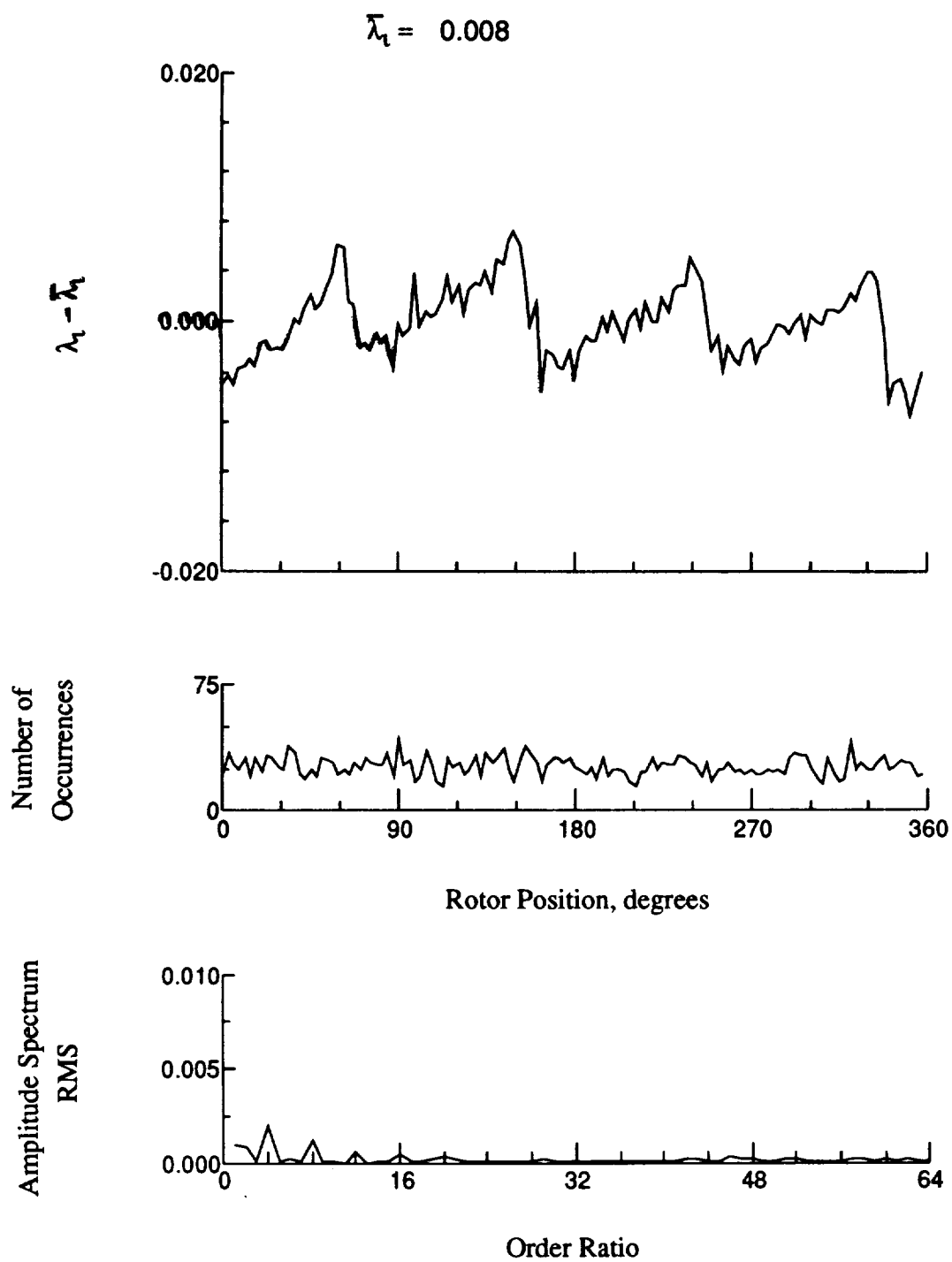


Figure 53.- Concluded.

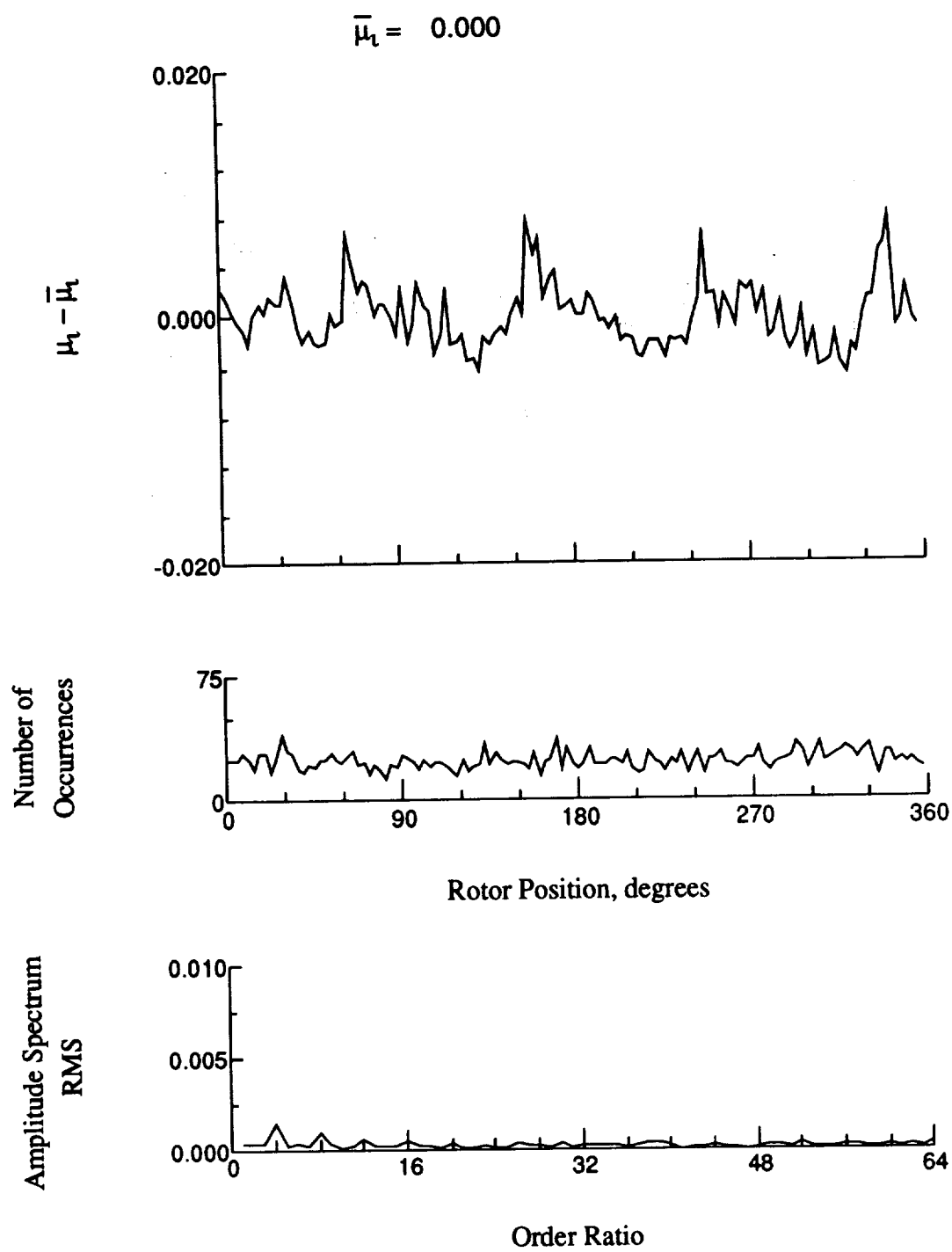


Figure 54.- Induced inflow velocity measured at 60 degrees and r/R of 0.75.

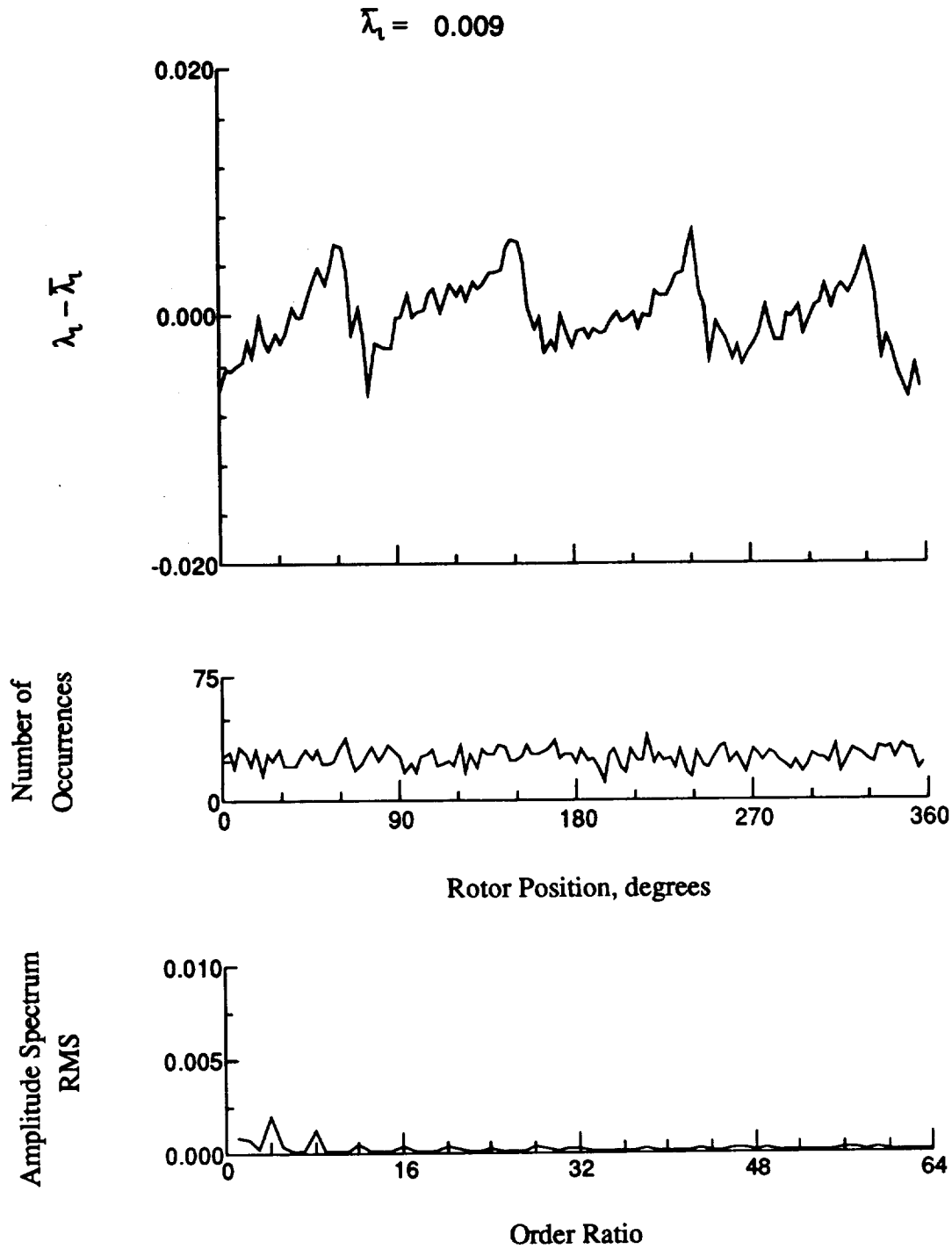


Figure 54.- Concluded.

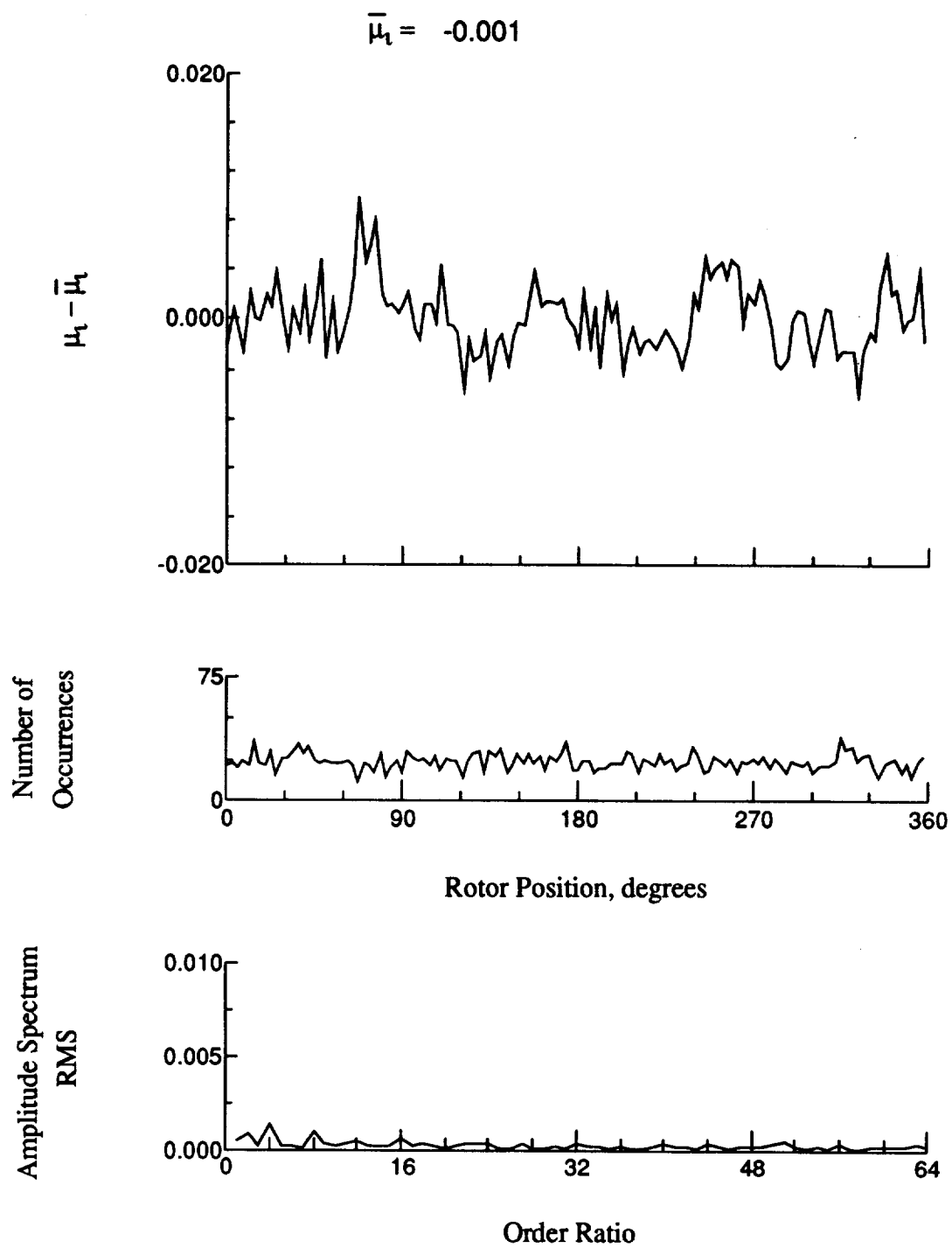


Figure 55.- Induced inflow velocity measured at 60 degrees and r/R of 0.81.

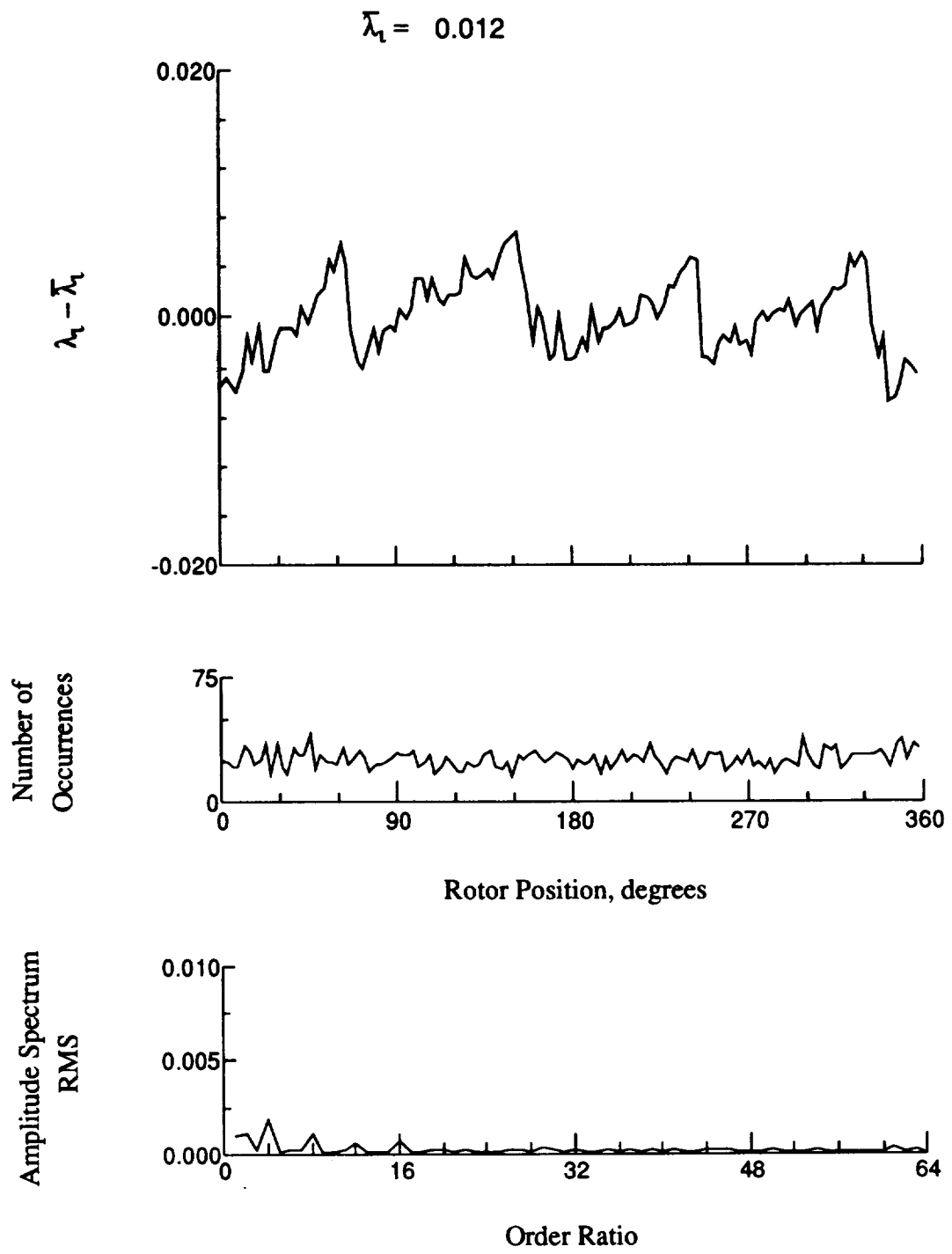


Figure 55.- Concluded.

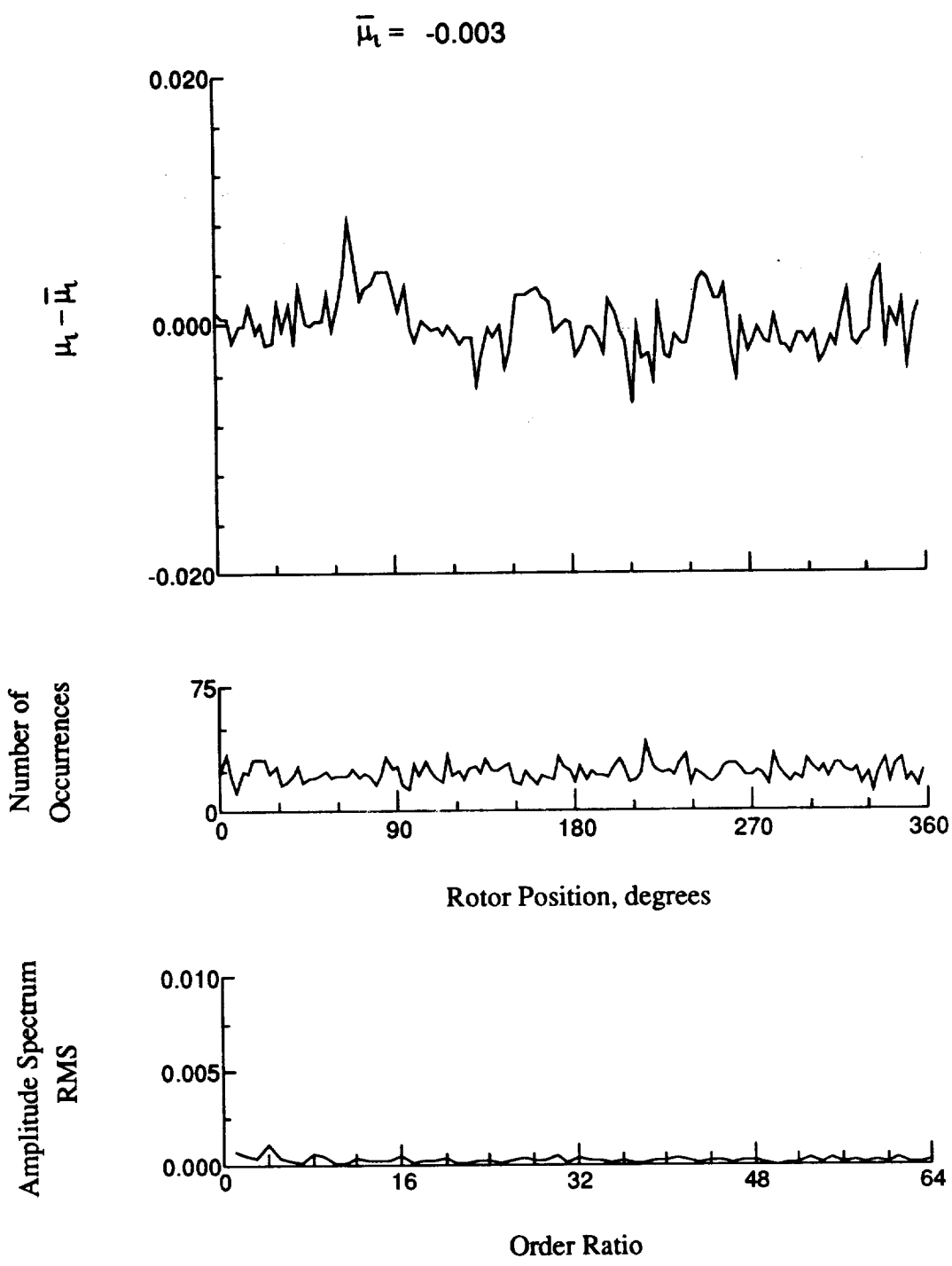


Figure 56.- Induced inflow velocity measured at 60 degrees and r/R of 0.86.

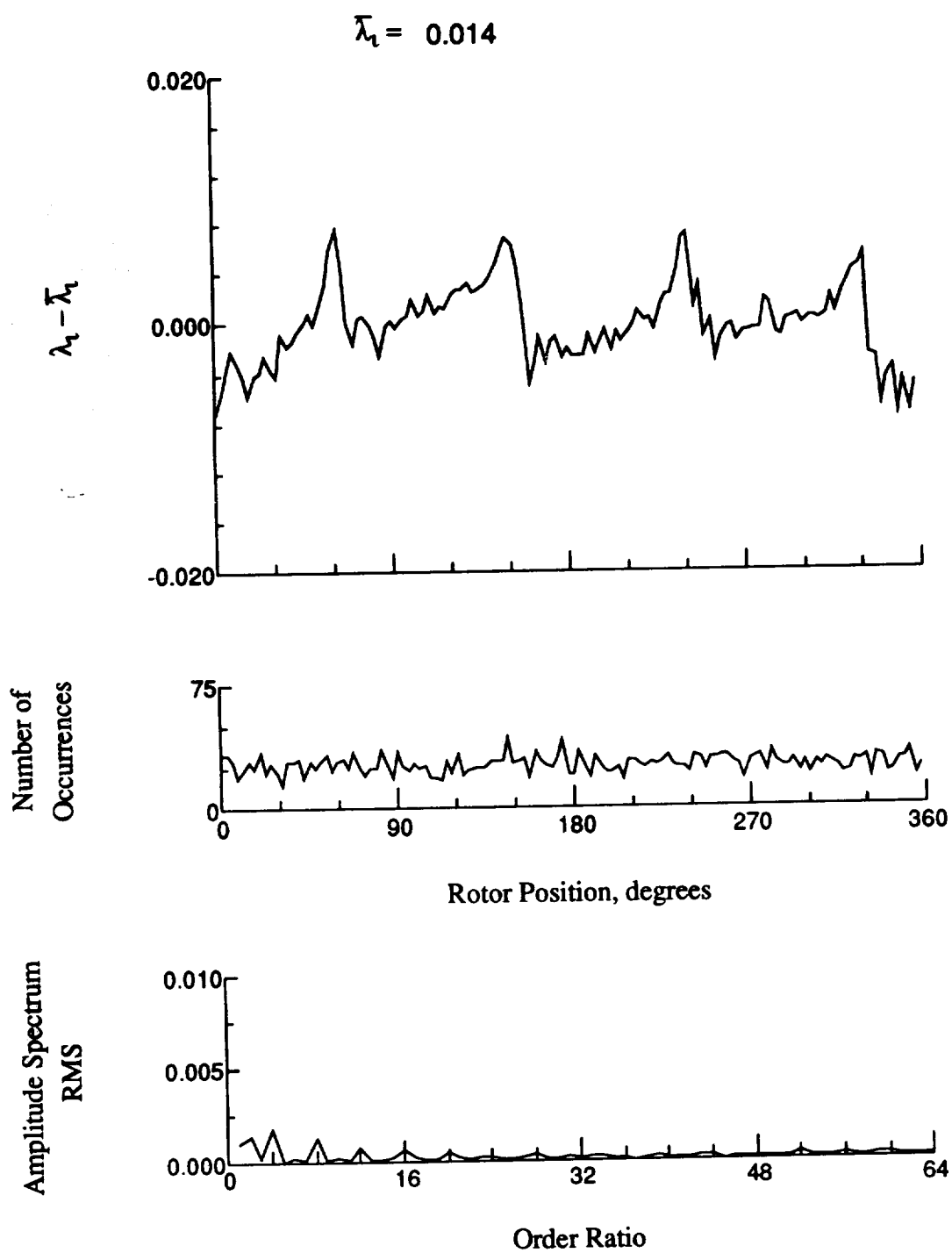


Figure 56.- Concluded.

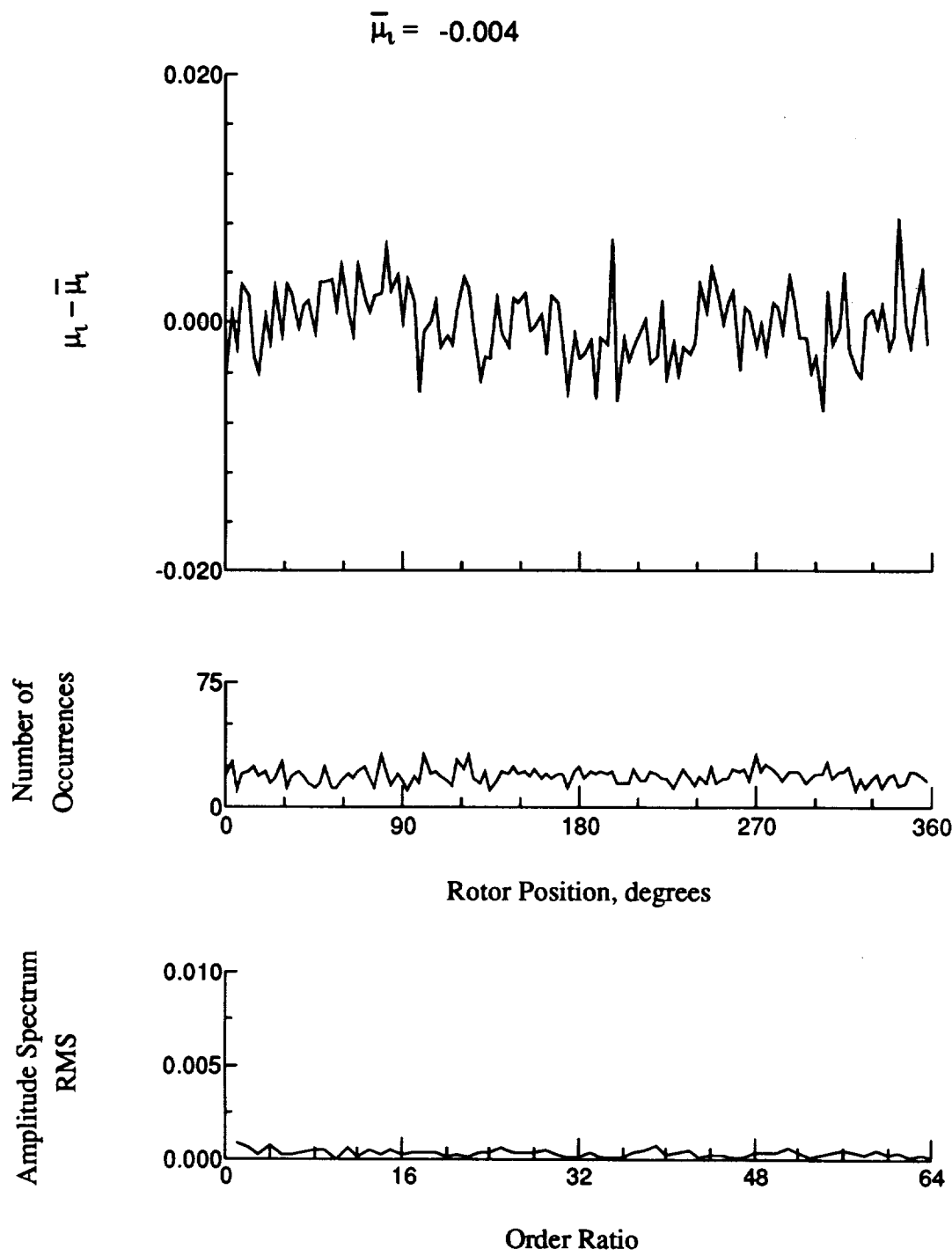


Figure 57.- Induced inflow velocity measured at 60 degrees and r/R of 0.90.

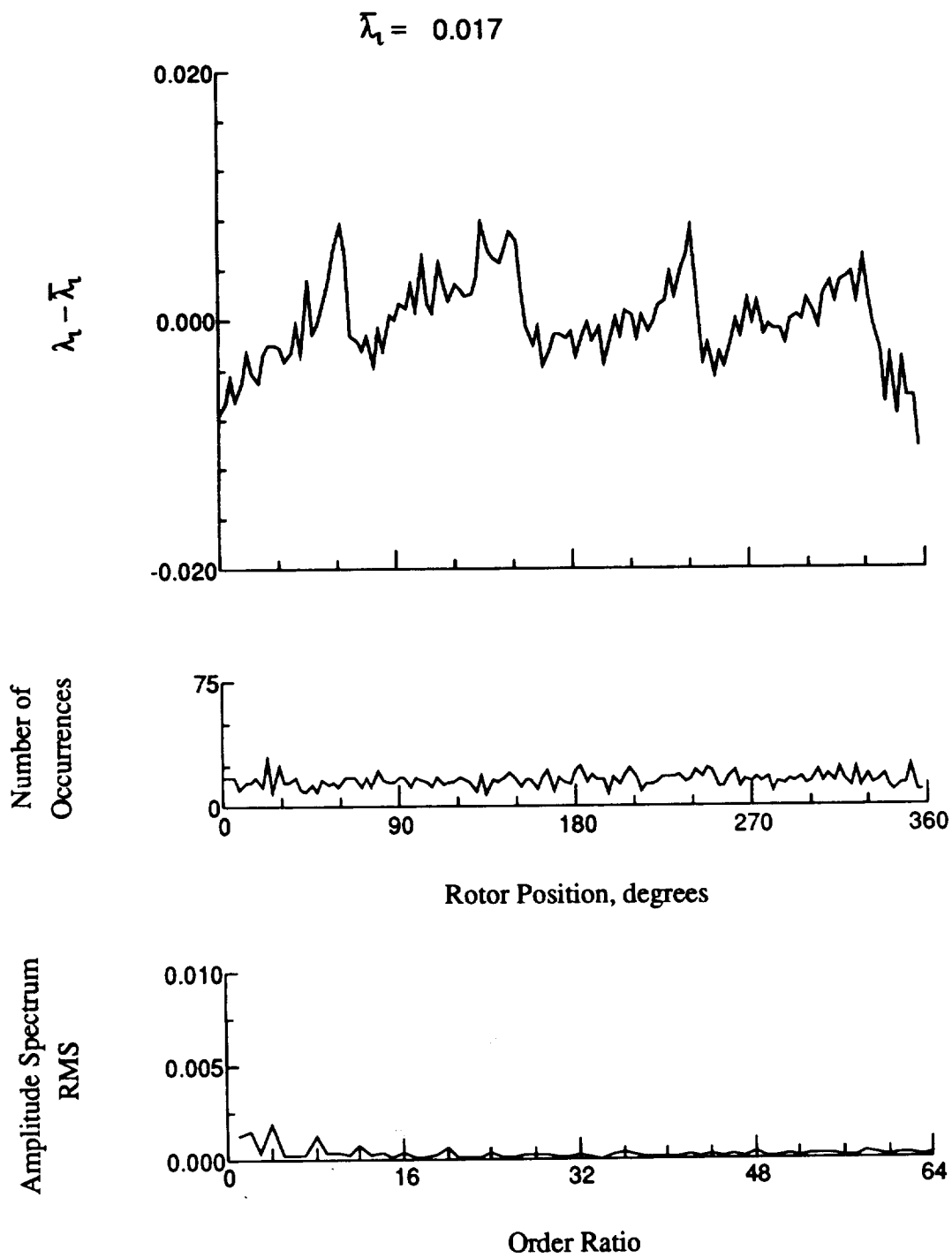


Figure 57.- Concluded.

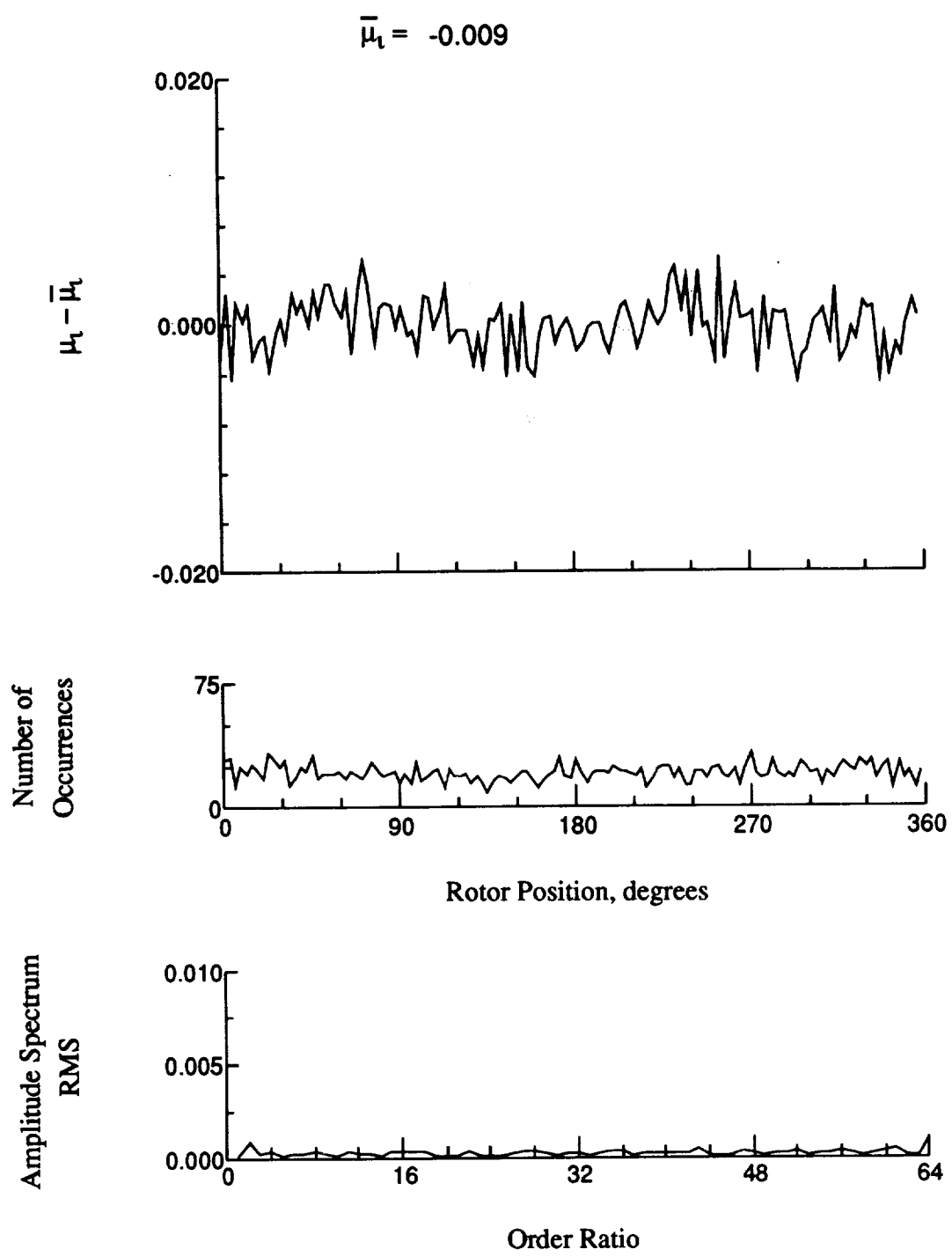


Figure 58.- Induced inflow velocity measured at 60 degrees and r/R of 0.94.

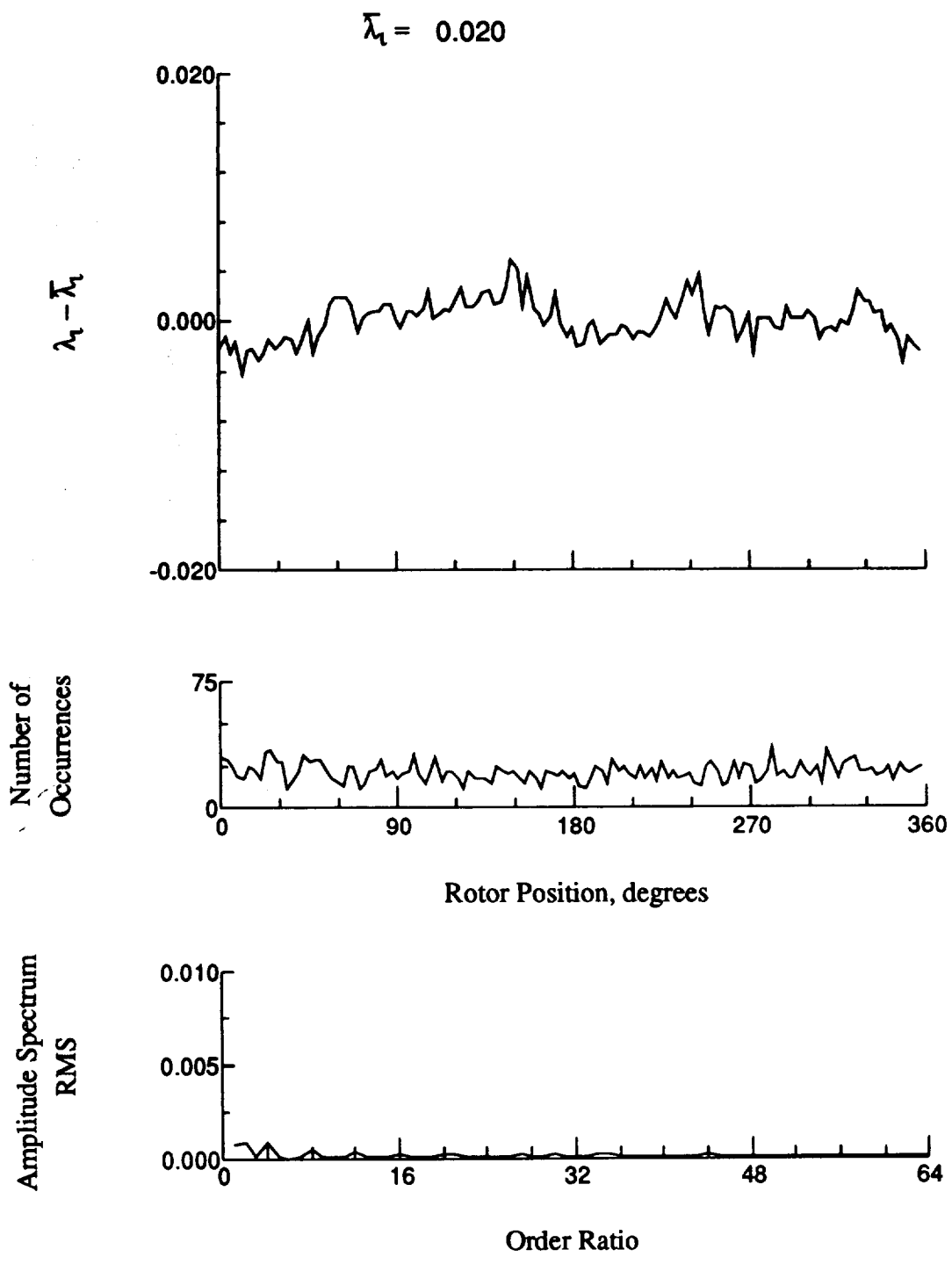


Figure 58.- Concluded.

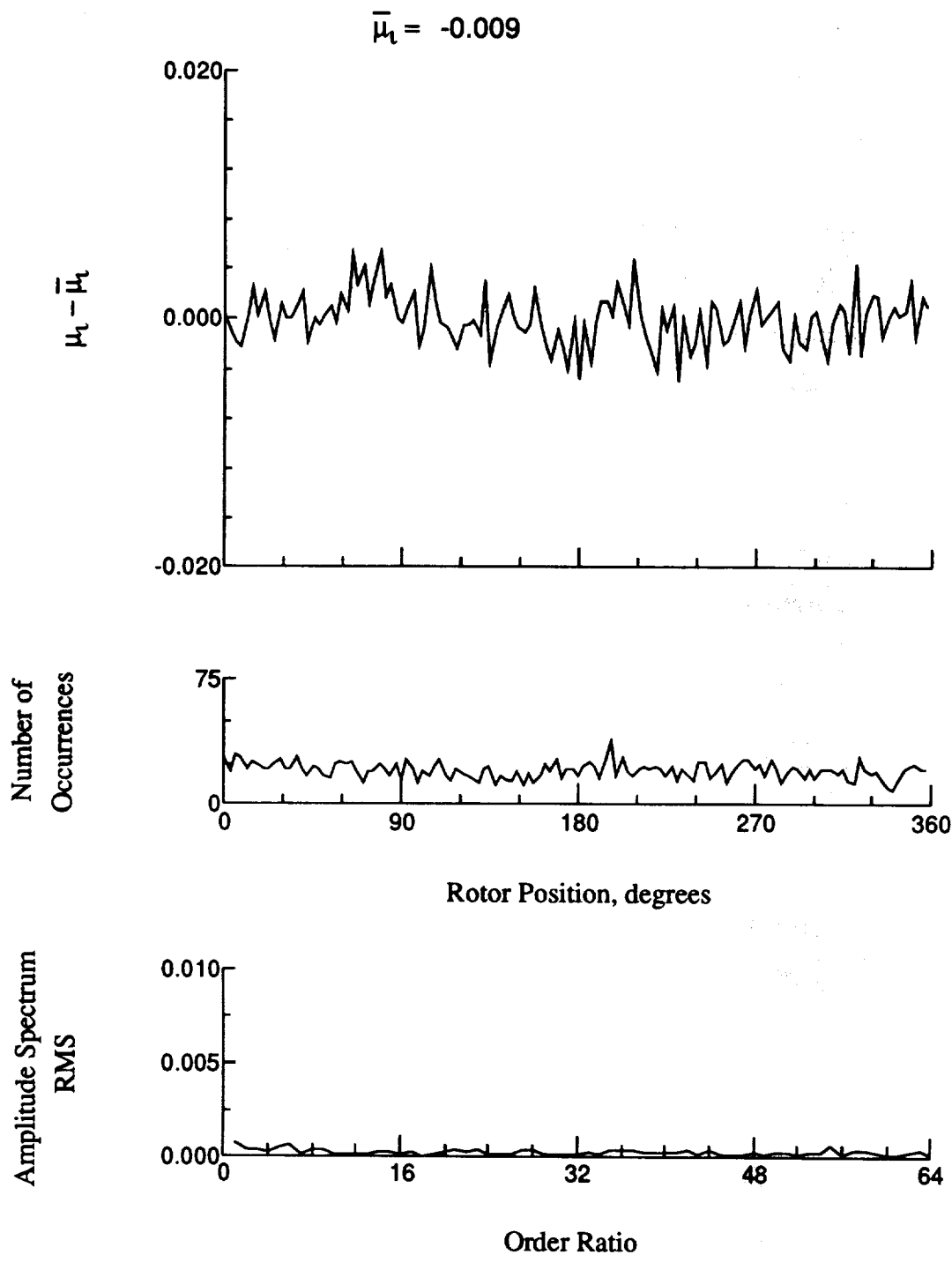


Figure 59.- Induced inflow velocity measured at 60 degrees and r/R of 0.96.

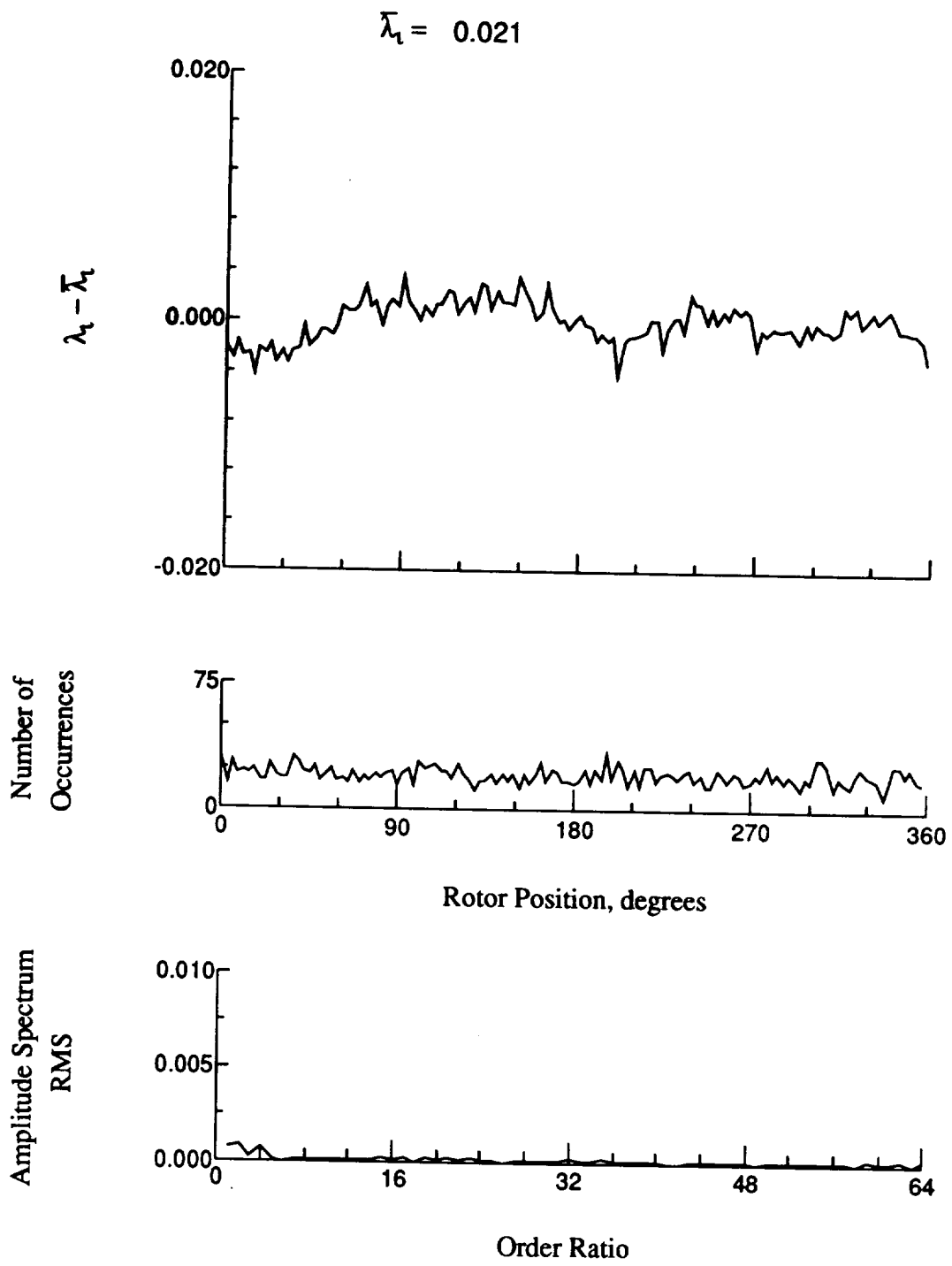


Figure 59.- Concluded.

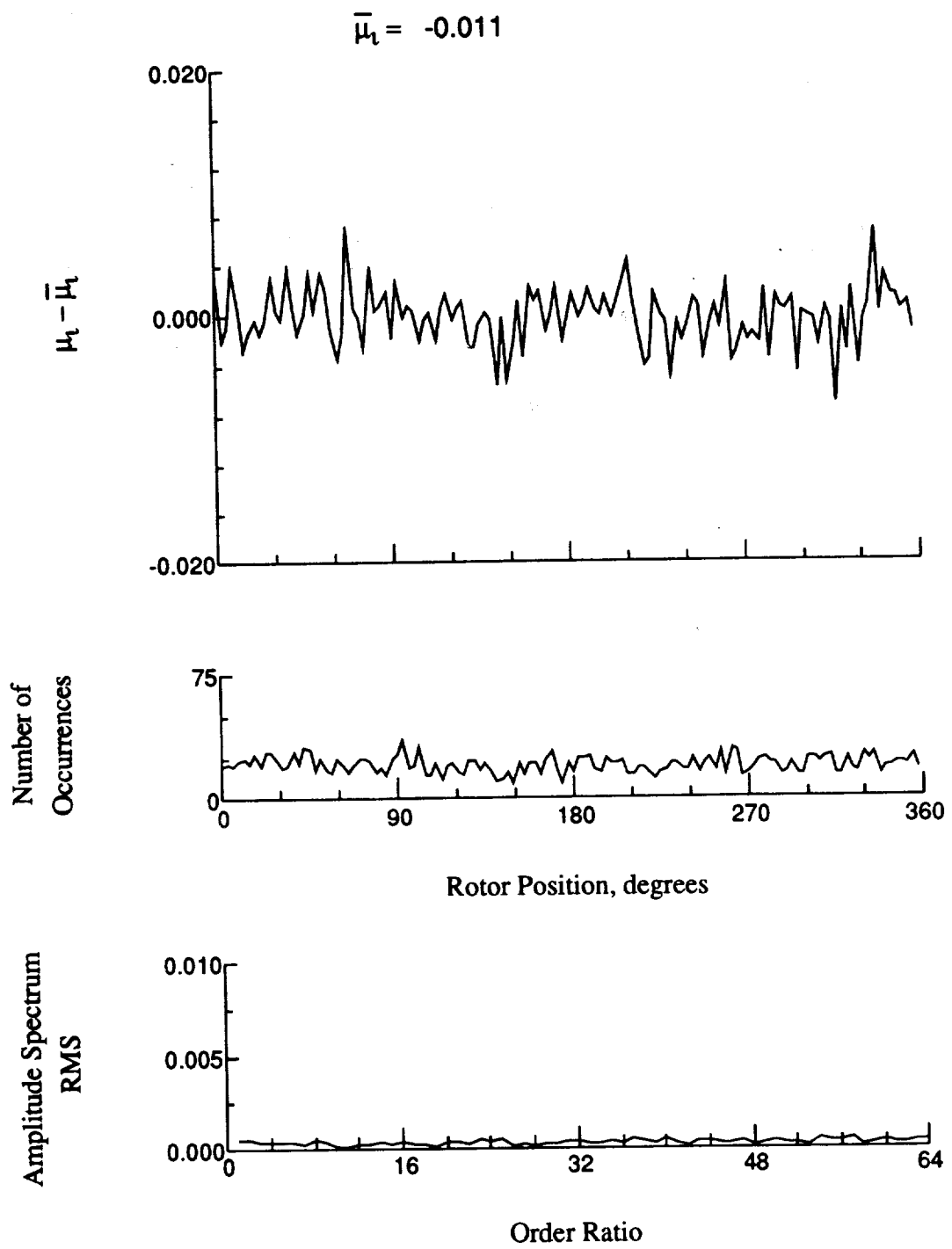


Figure 60.- Induced inflow velocity measured at 60 degrees and r/R of 1.00.

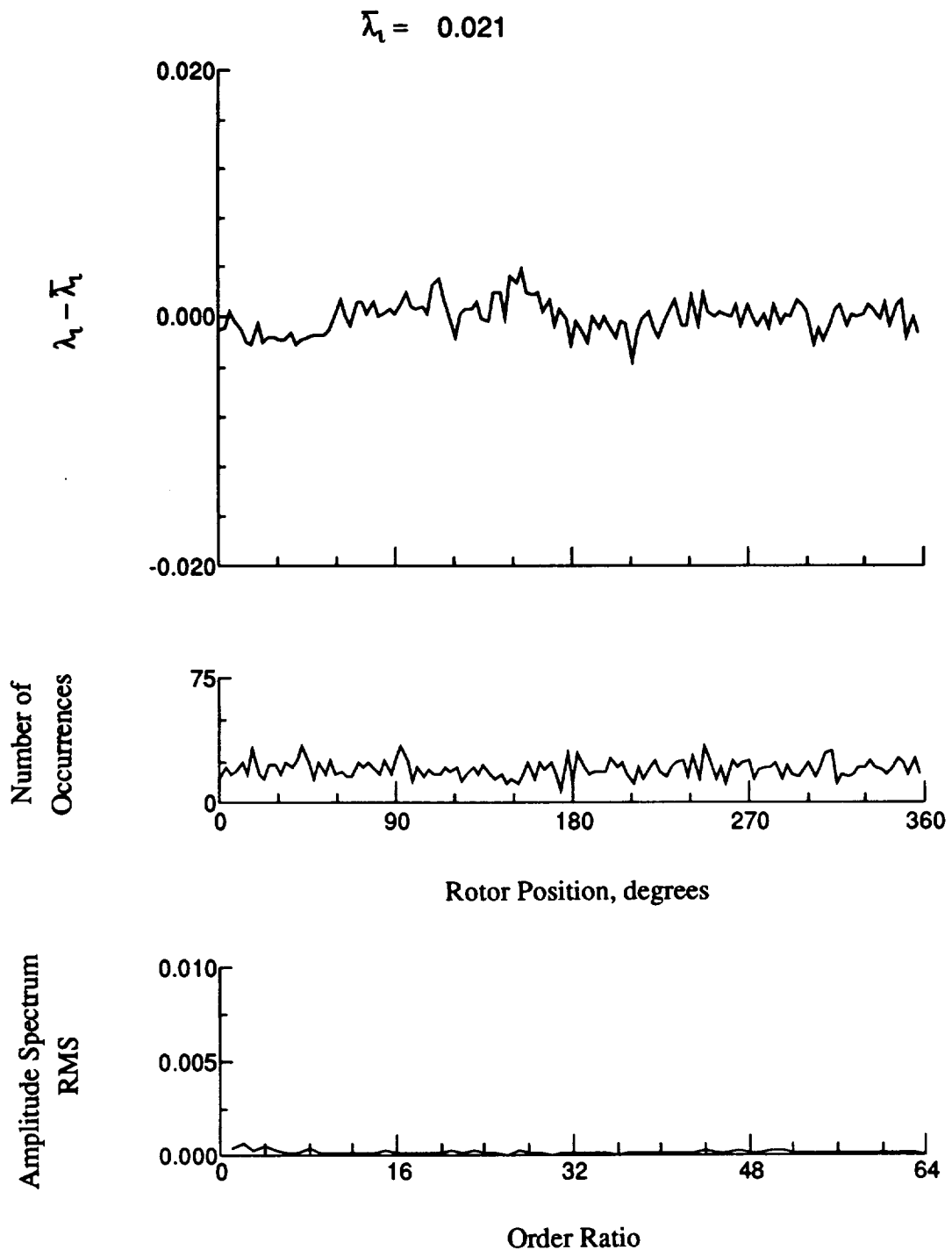


Figure 60.- Concluded.

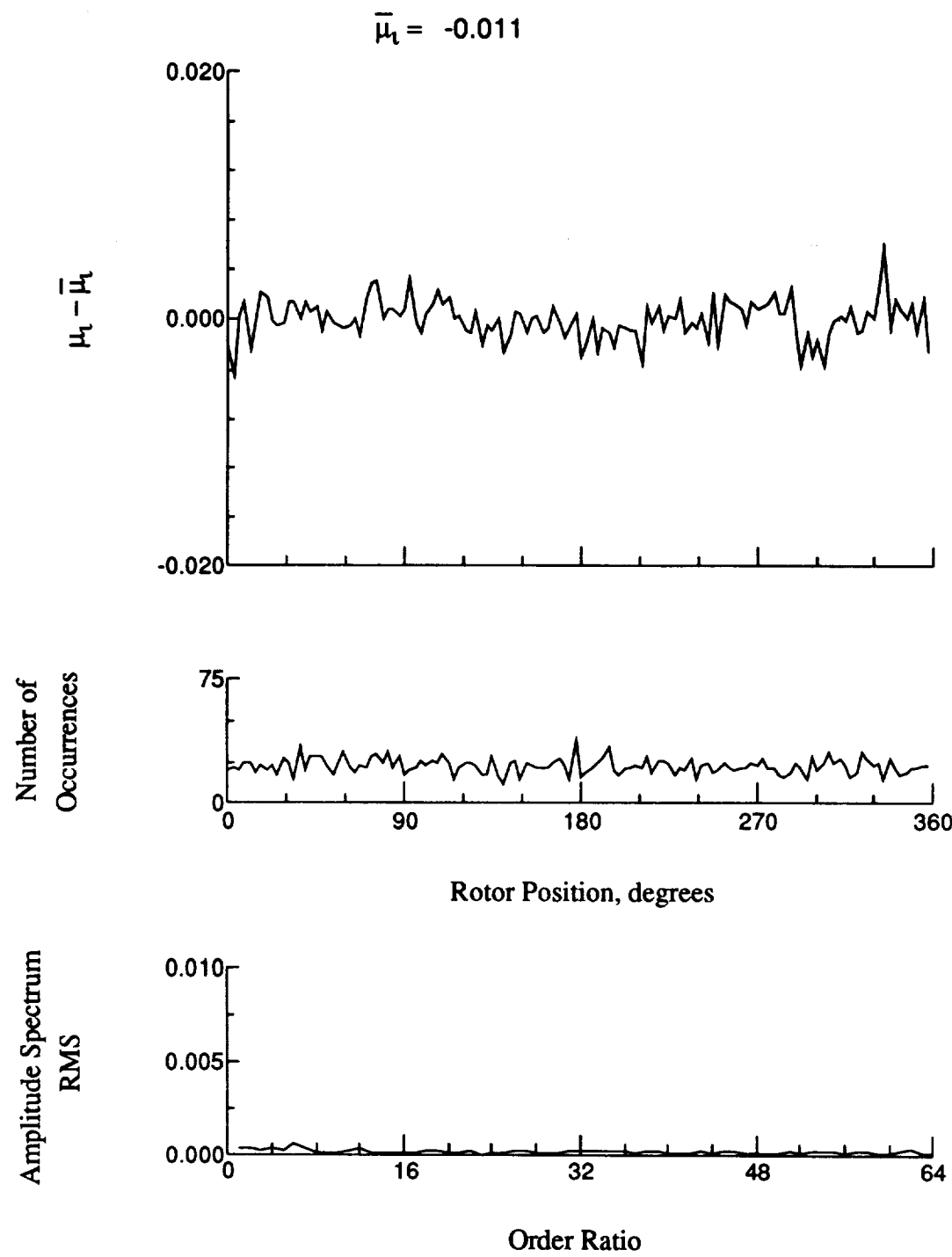


Figure 61.- Induced inflow velocity measured at 60 degrees and r/R of 1.10.

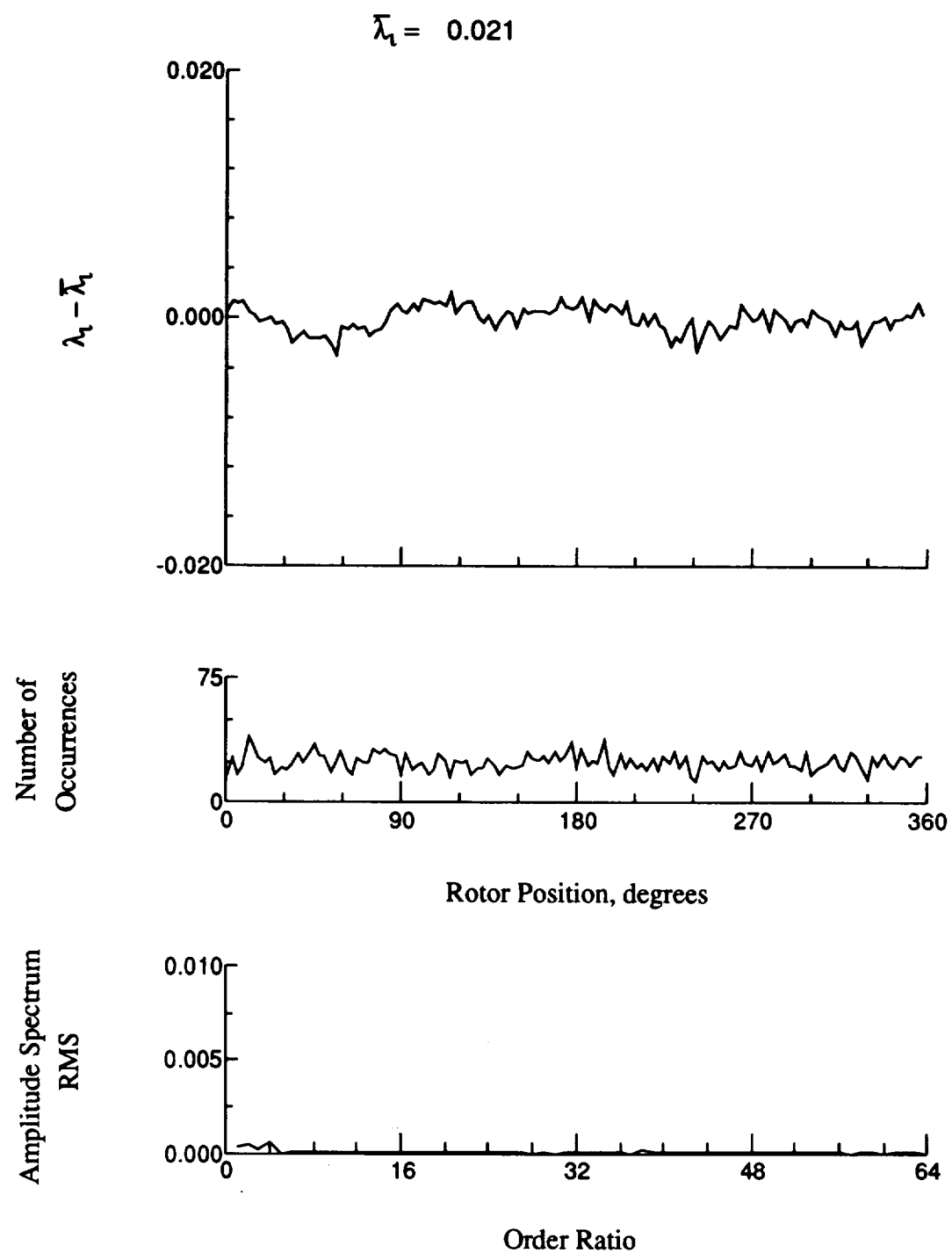


Figure 61.- Concluded.

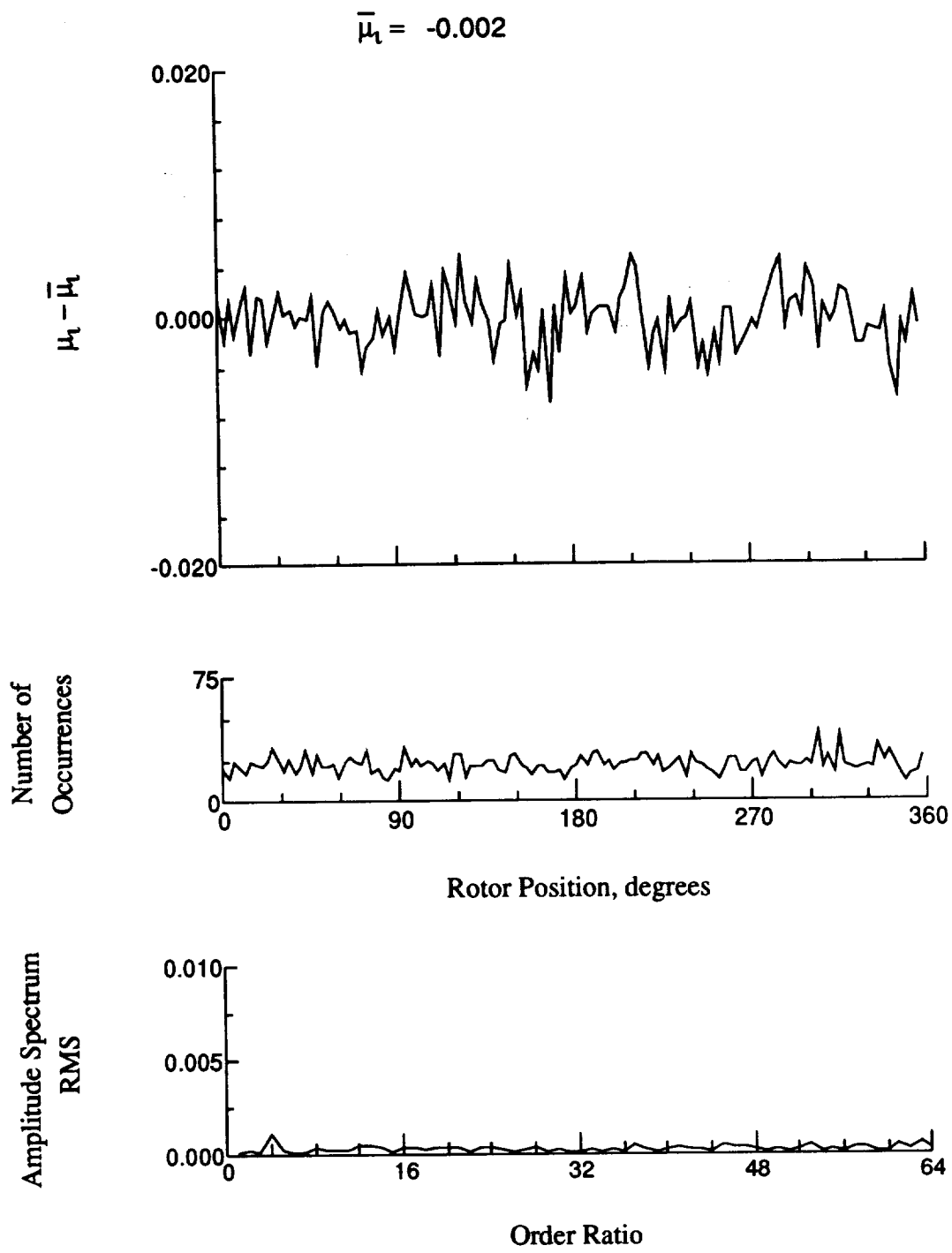


Figure 62.- Induced inflow velocity measured at 90 degrees and r/R of 0.20.

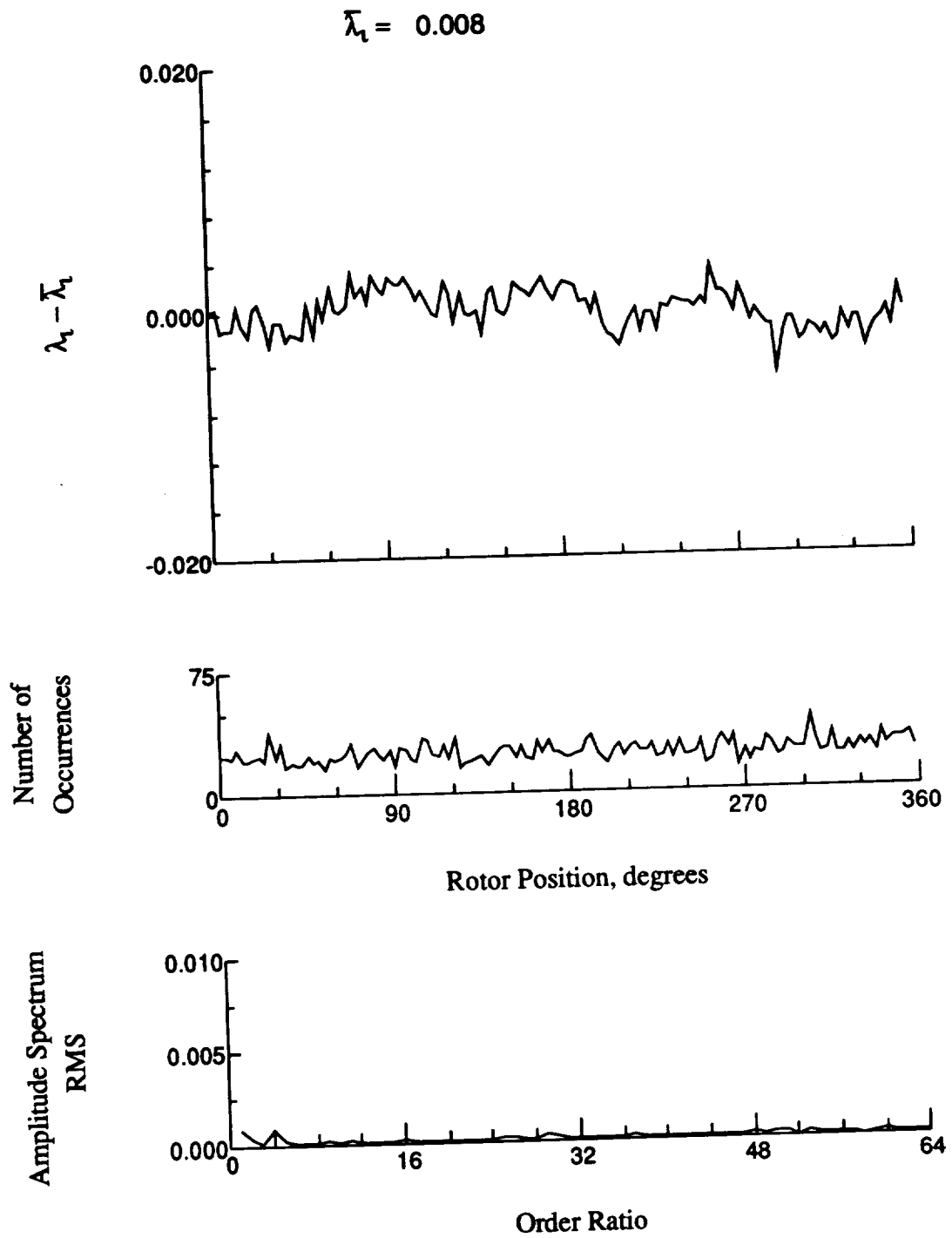


Figure 62.- Concluded.

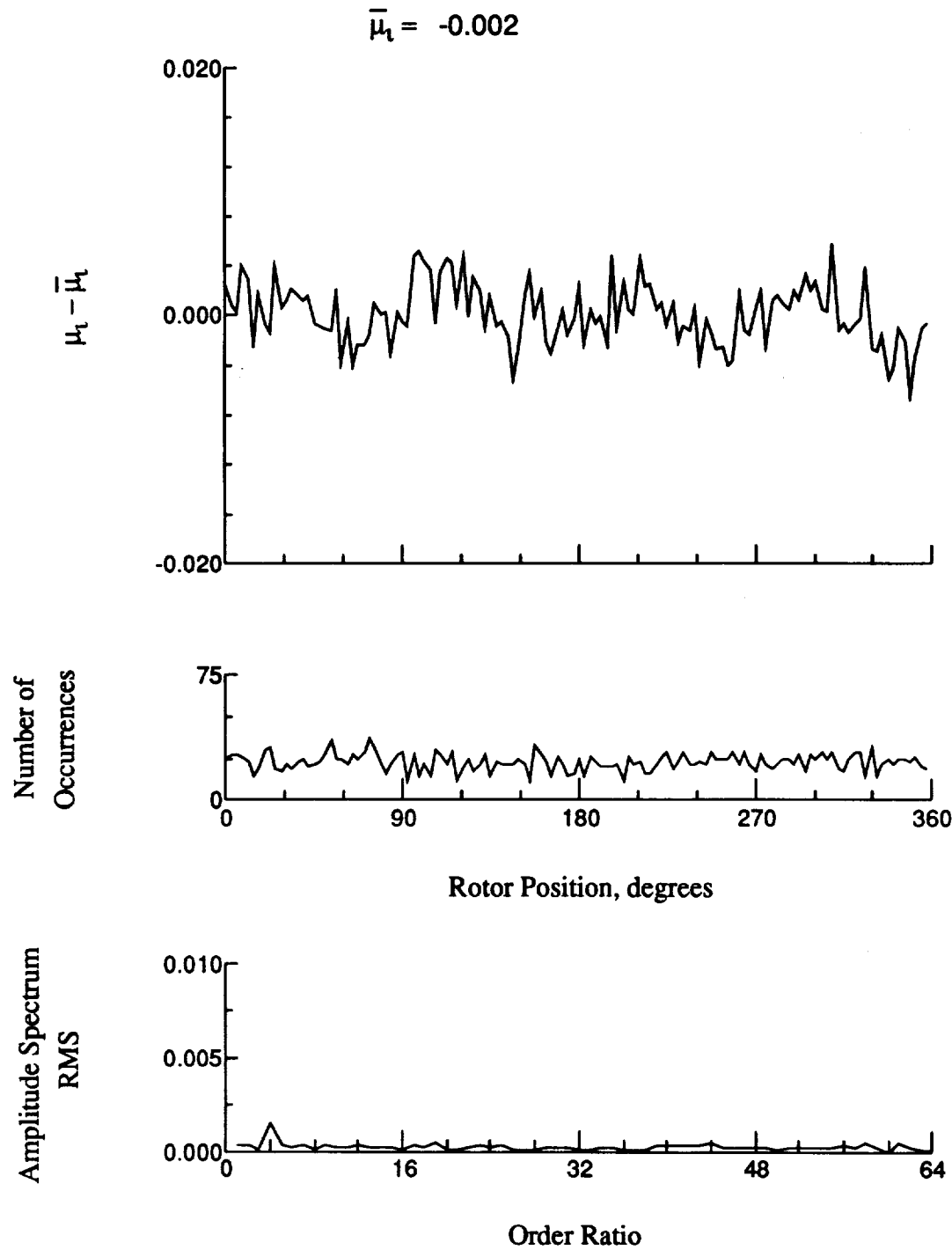


Figure 63.- Induced inflow velocity measured at 90 degrees and r/R of 0.32.

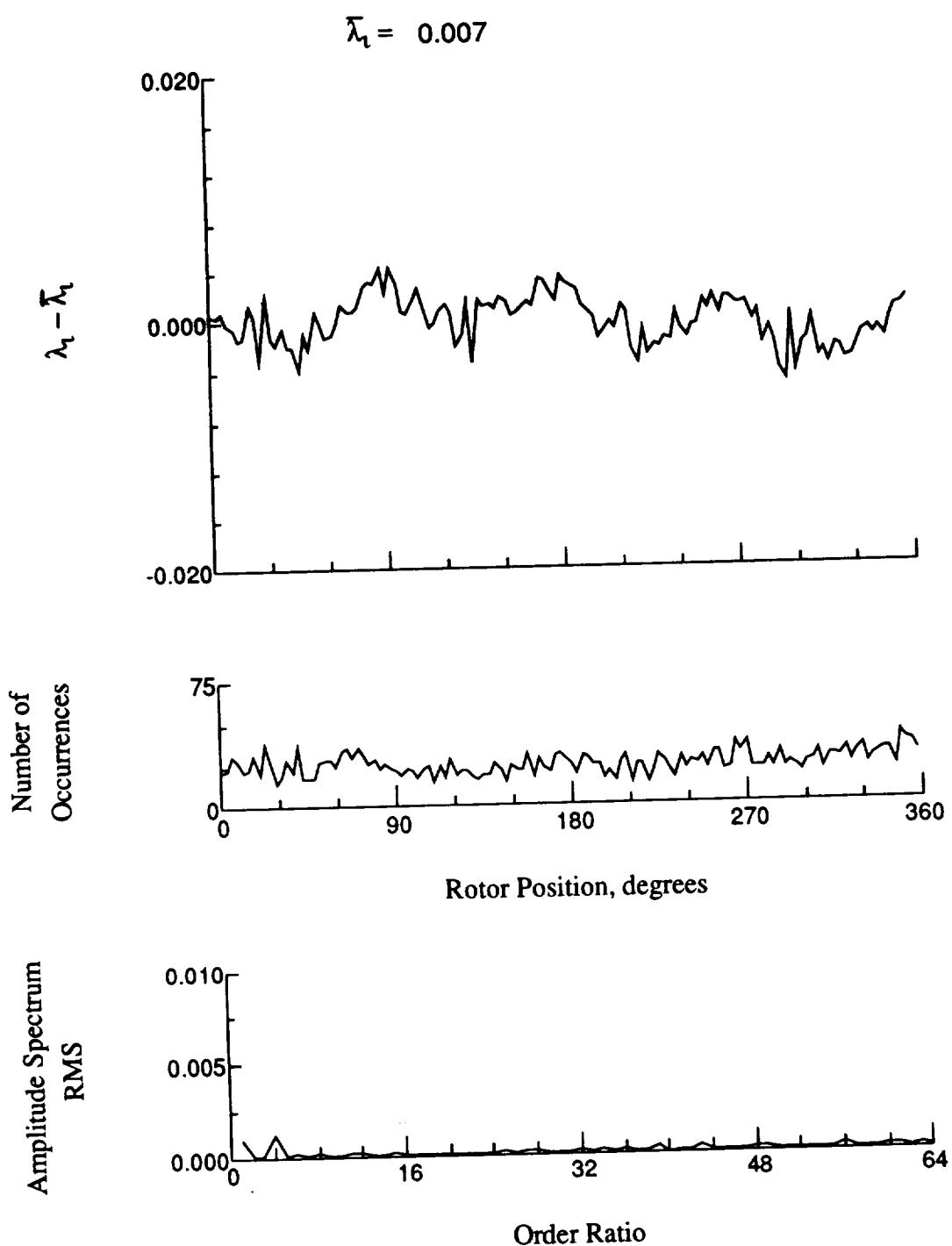


Figure 63.- Concluded.

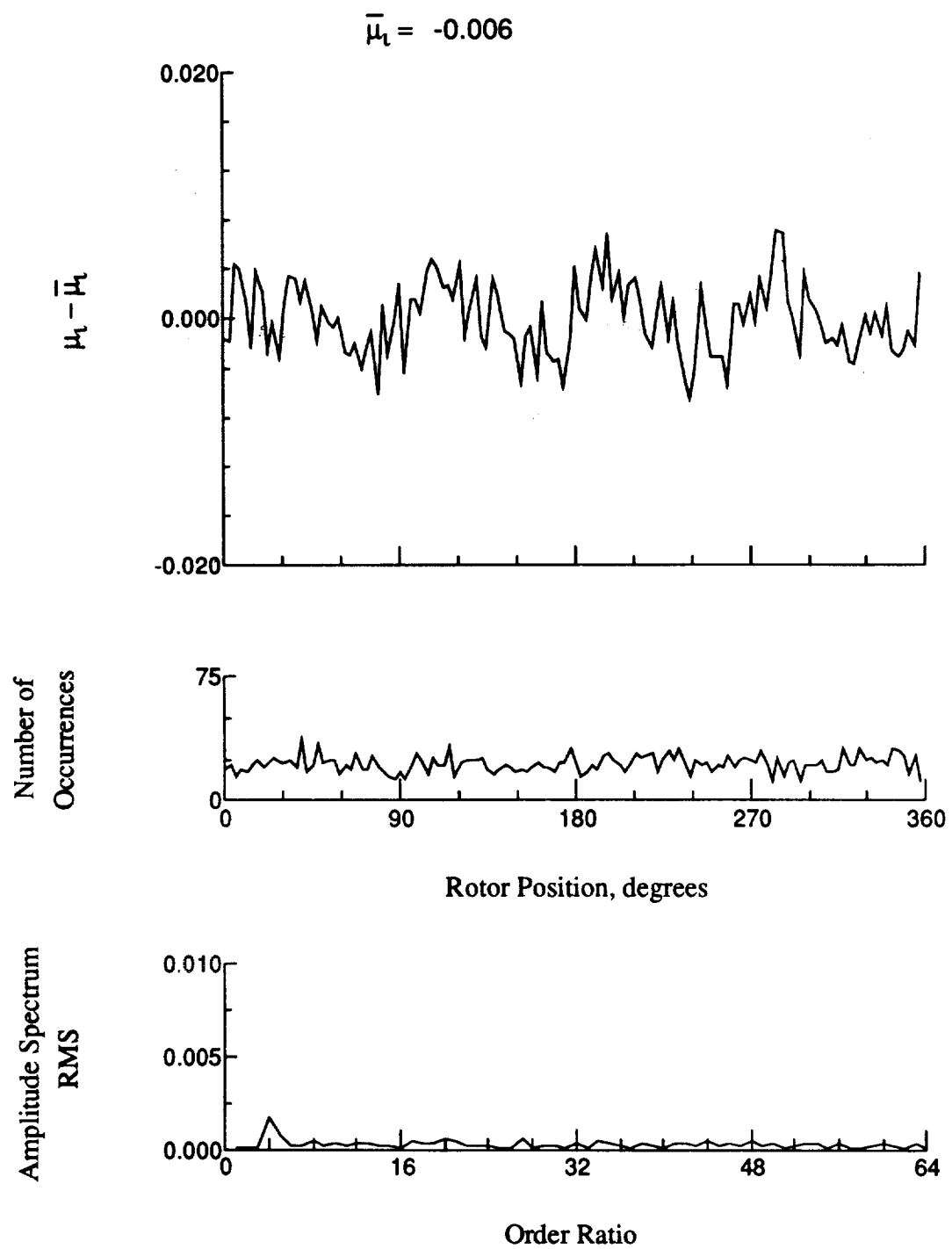


Figure 64.- Induced inflow velocity measured at 90 degrees and r/R of 0.50.

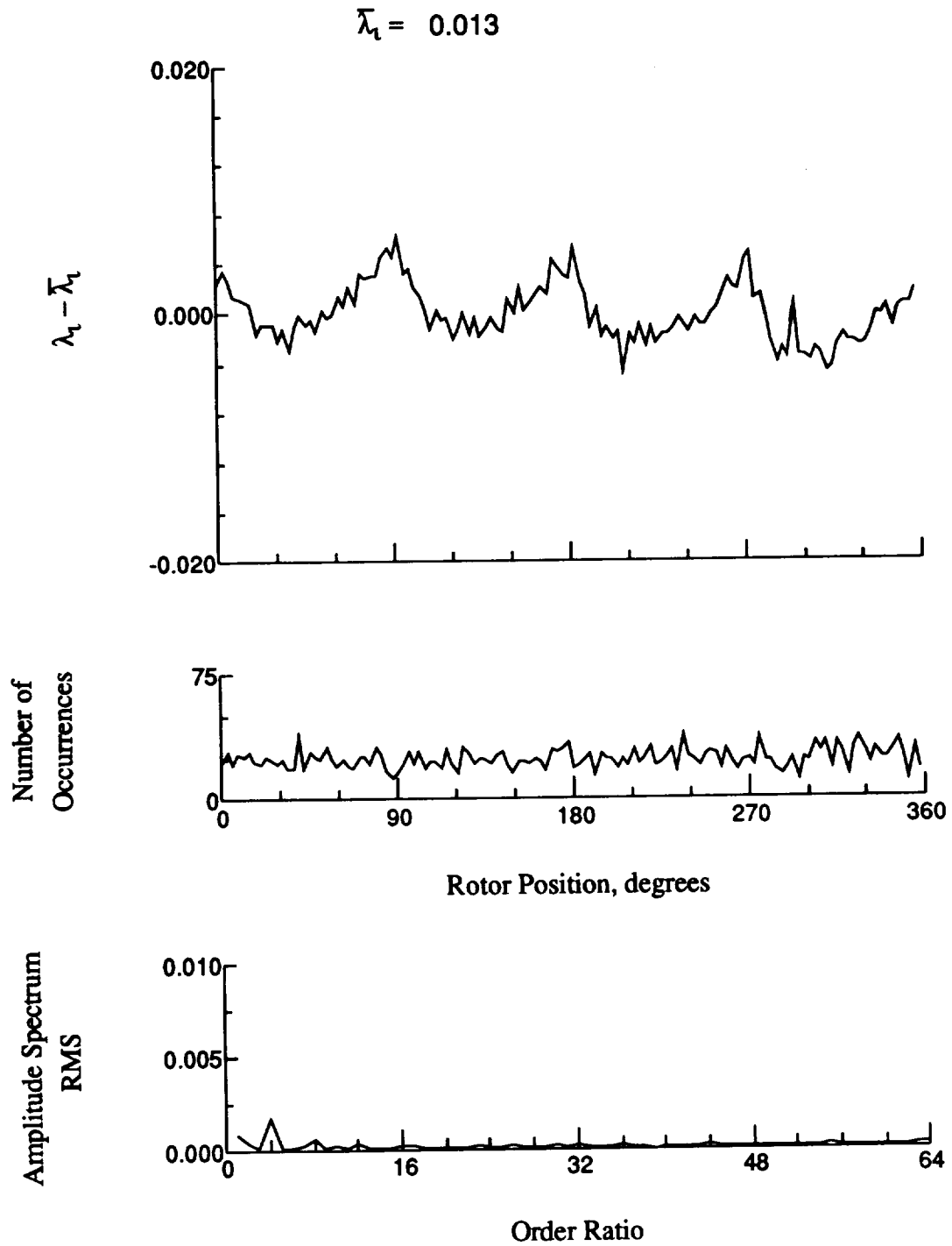


Figure 64.- Concluded.

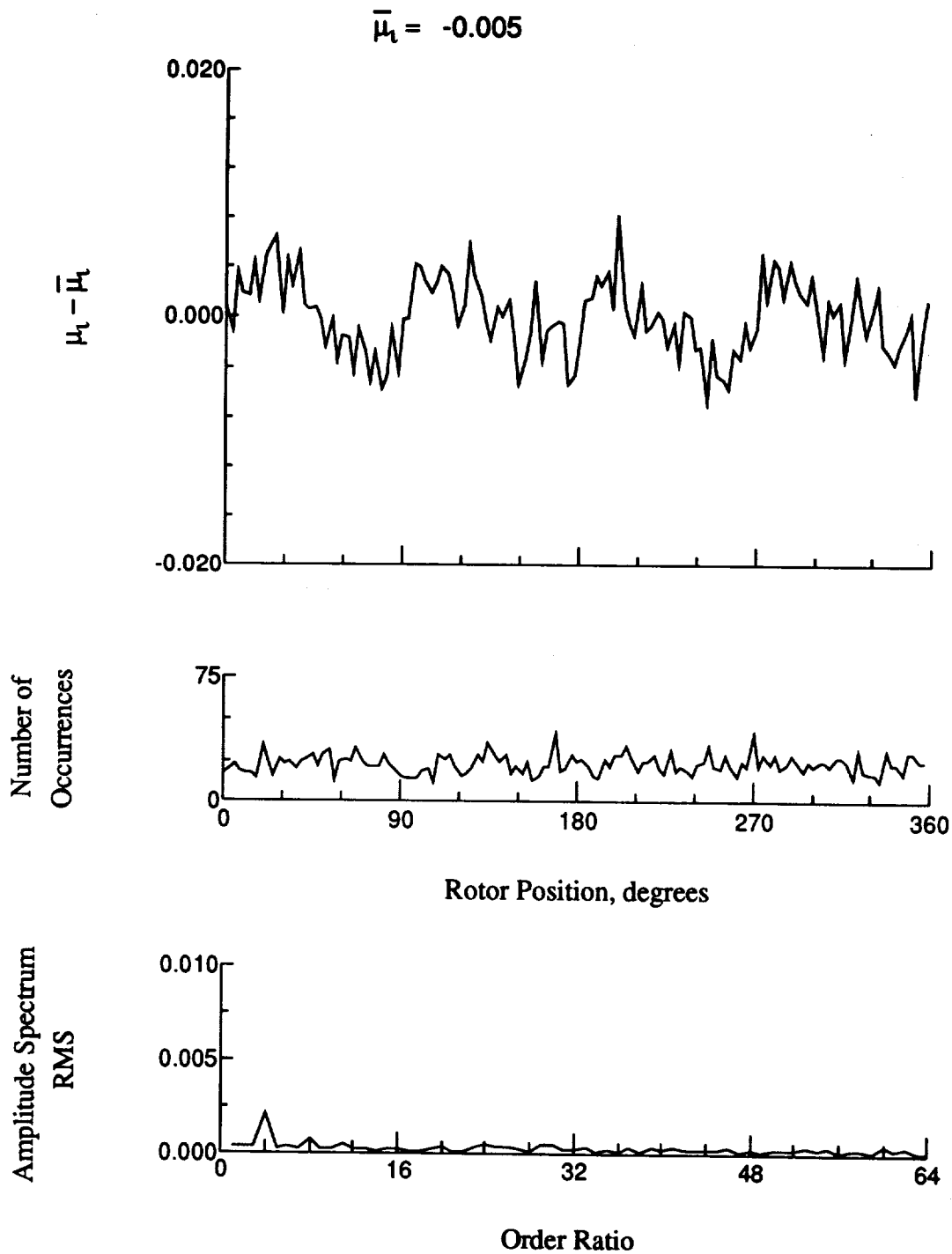


Figure 65.- Induced inflow velocity measured at 90 degrees and r/R of 0.58.

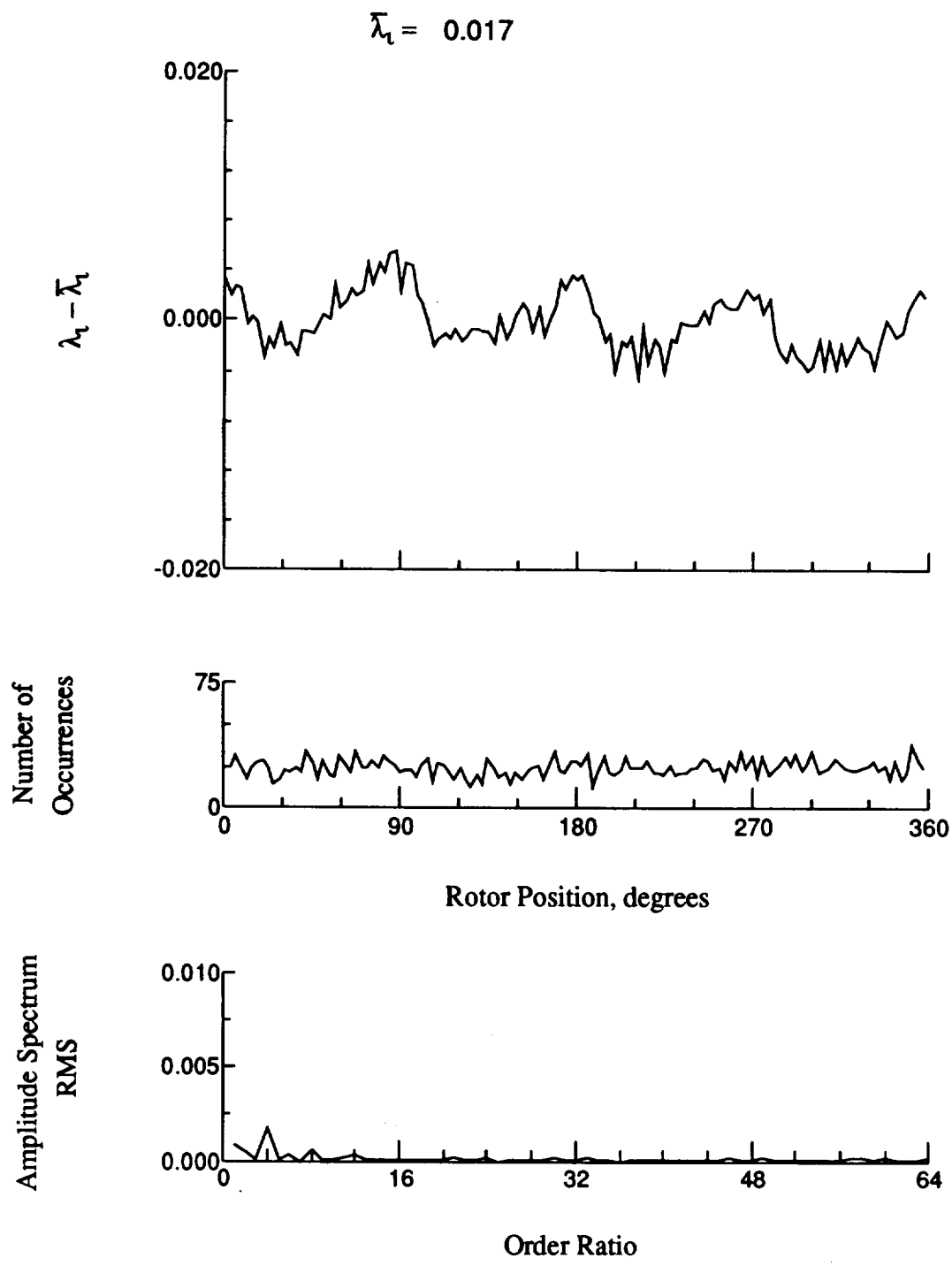


Figure 65.- Concluded.

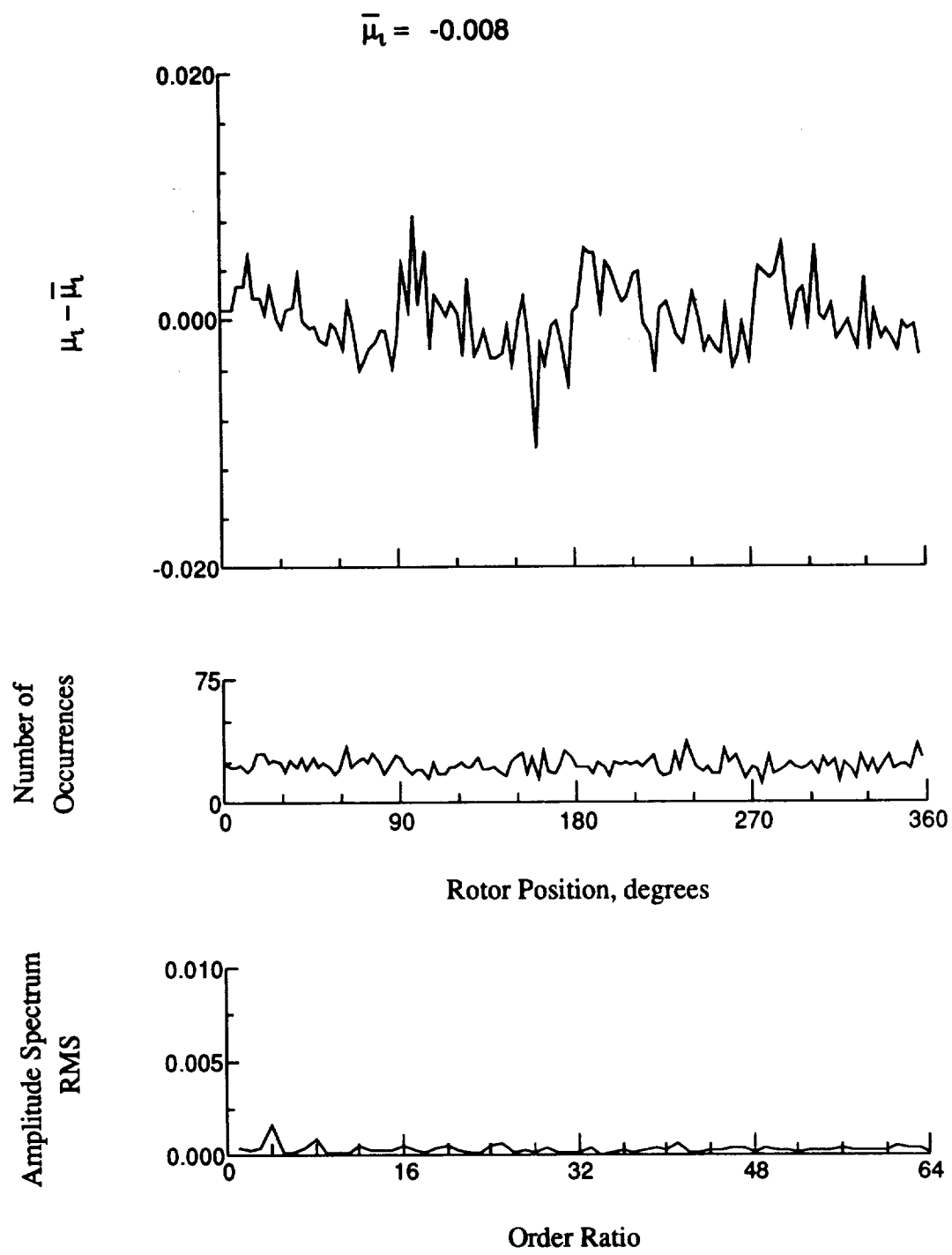


Figure 66.- Induced inflow velocity measured at 90 degrees and r/R of 0.69.

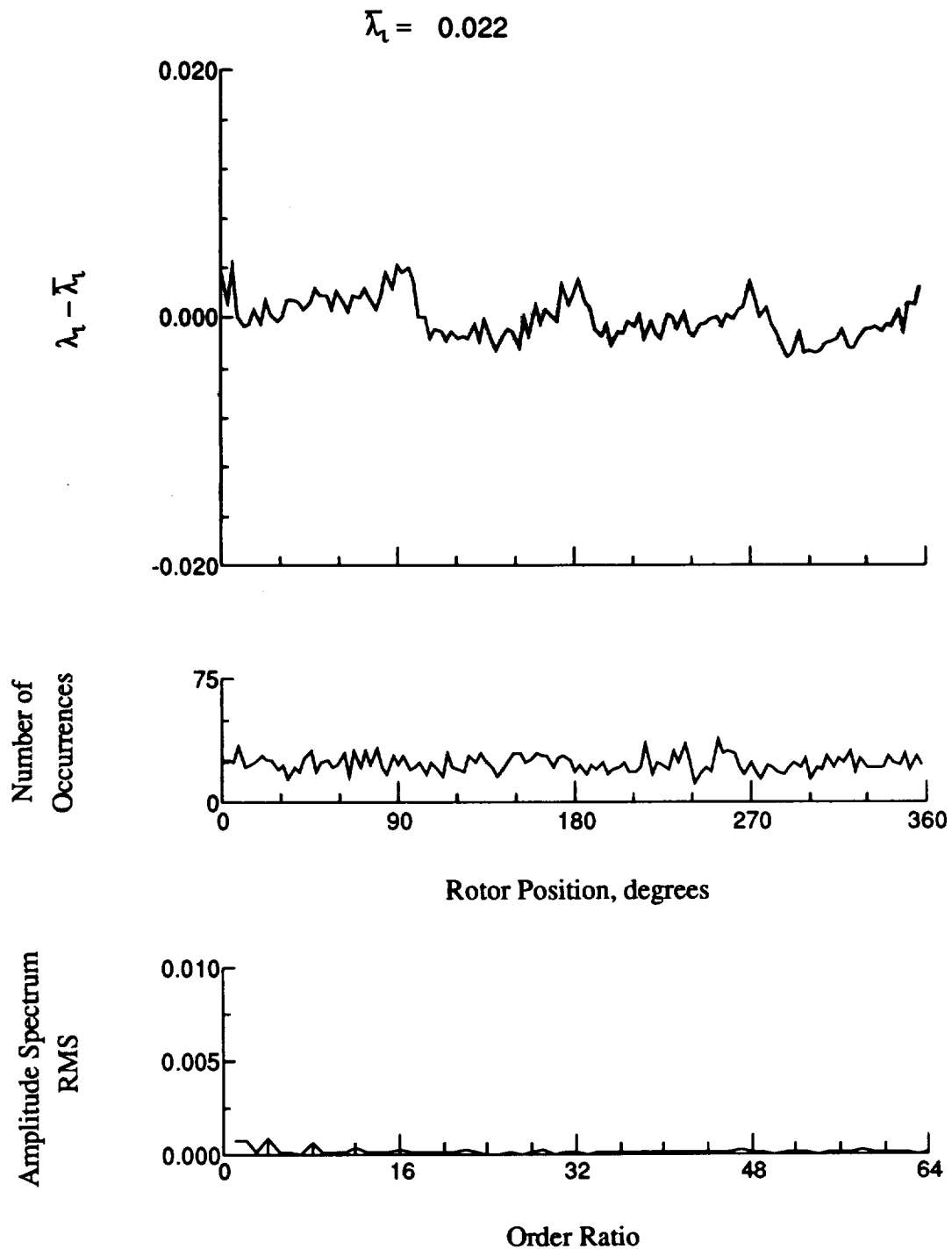


Figure 66.- Concluded.

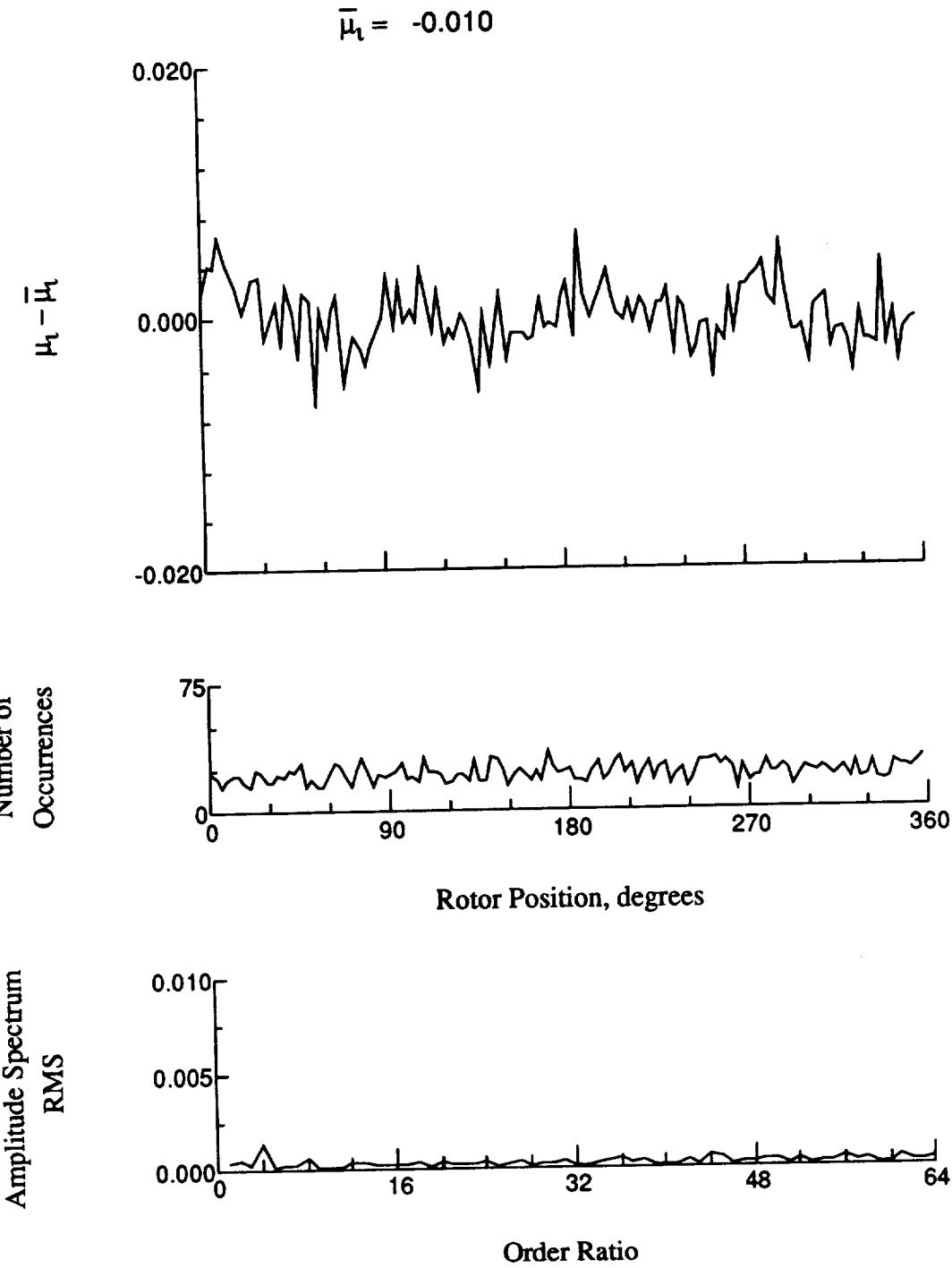


Figure 67.- Induced inflow velocity measured at 90 degrees and r/R of 0.73.

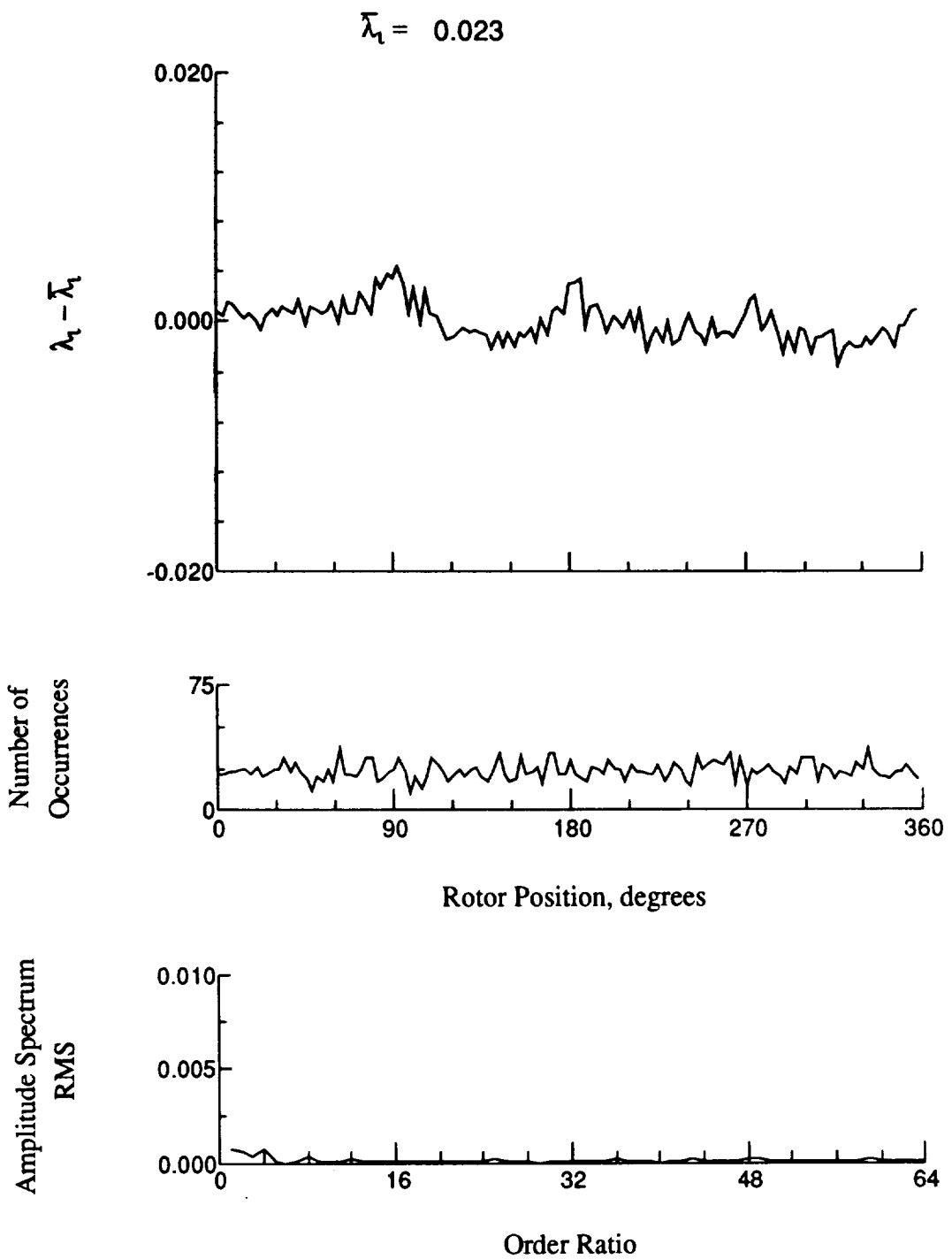


Figure 67.- Concluded.

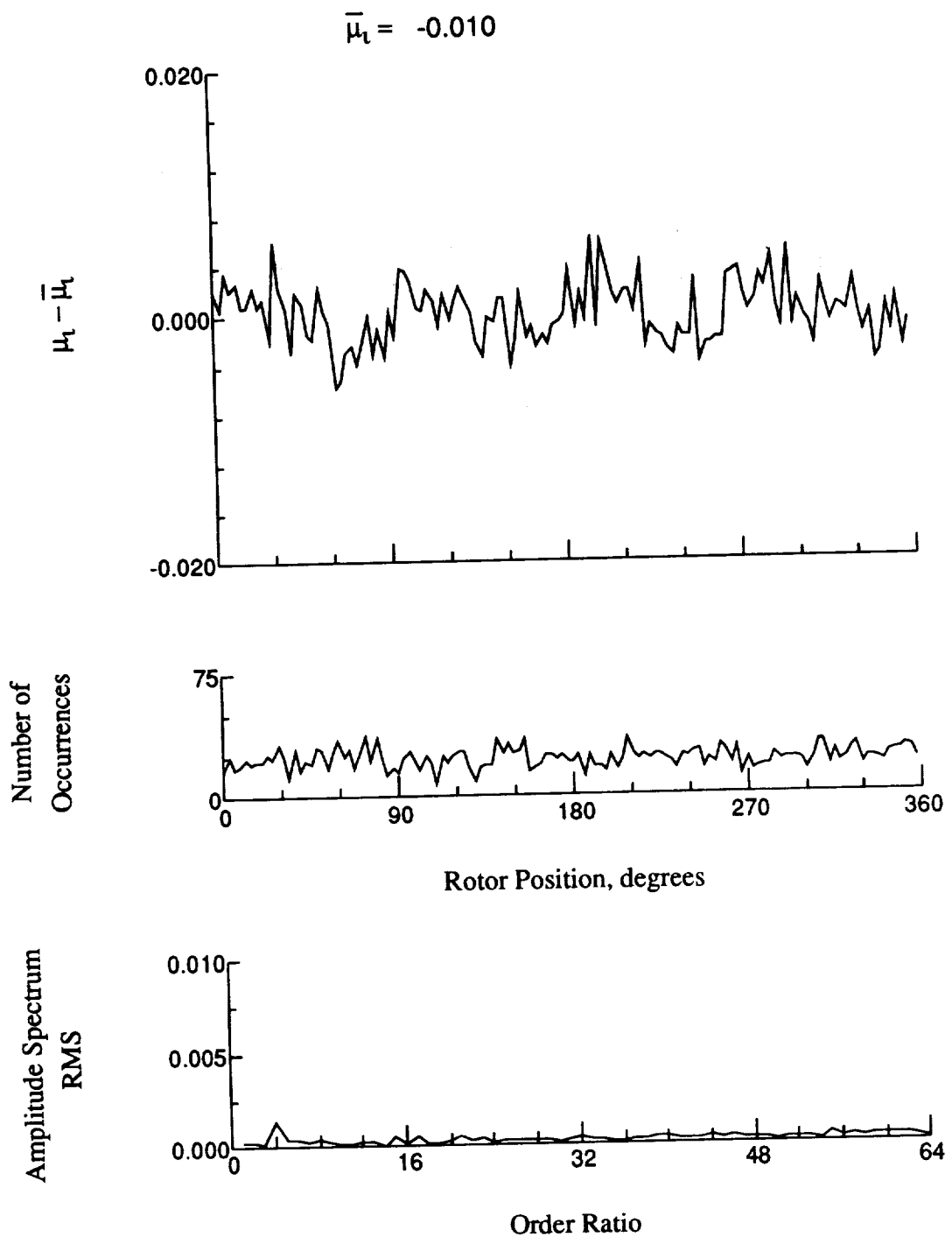


Figure 68.- Induced inflow velocity measured at 90 degrees and r/R of 0.75.

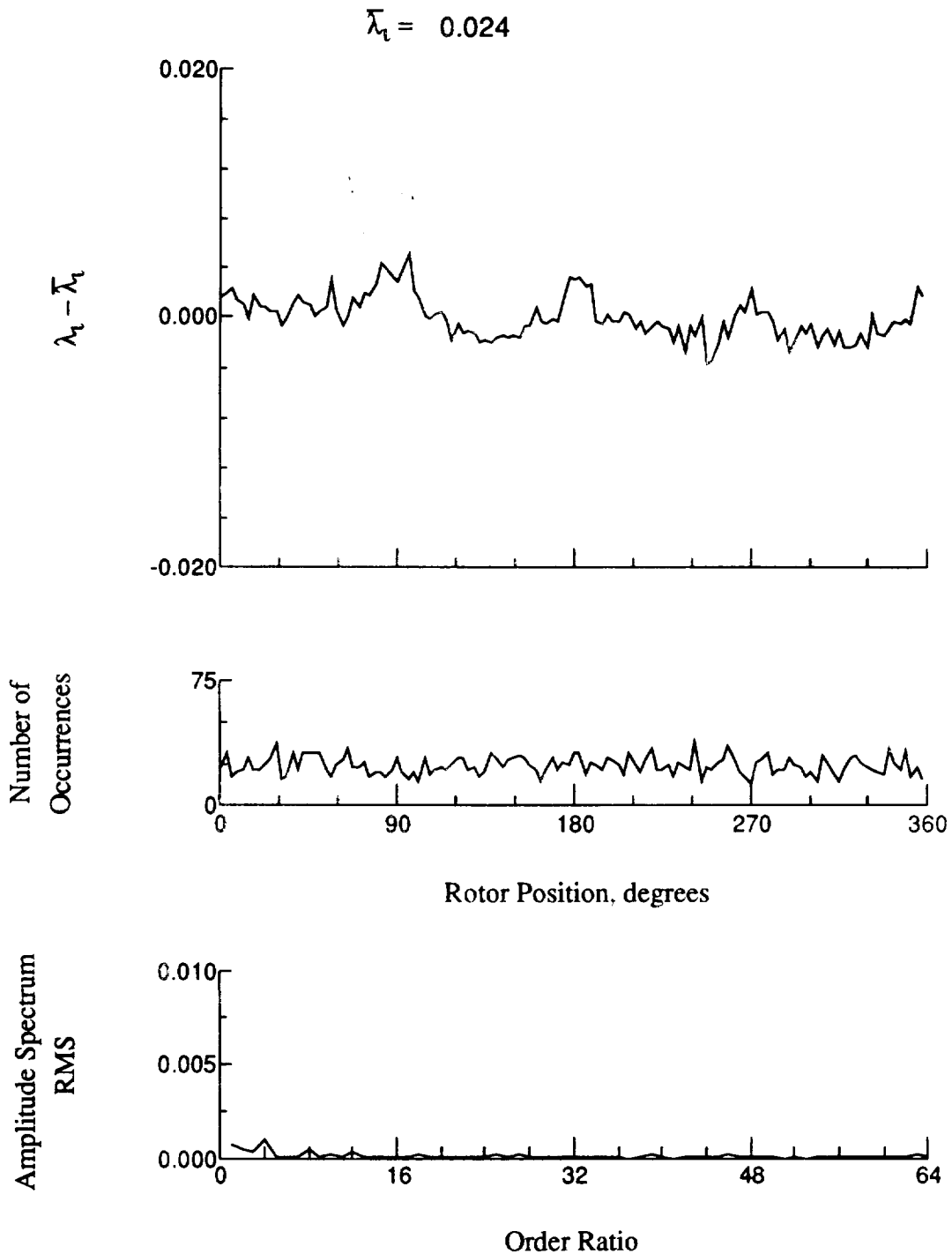


Figure 68.- Concluded.

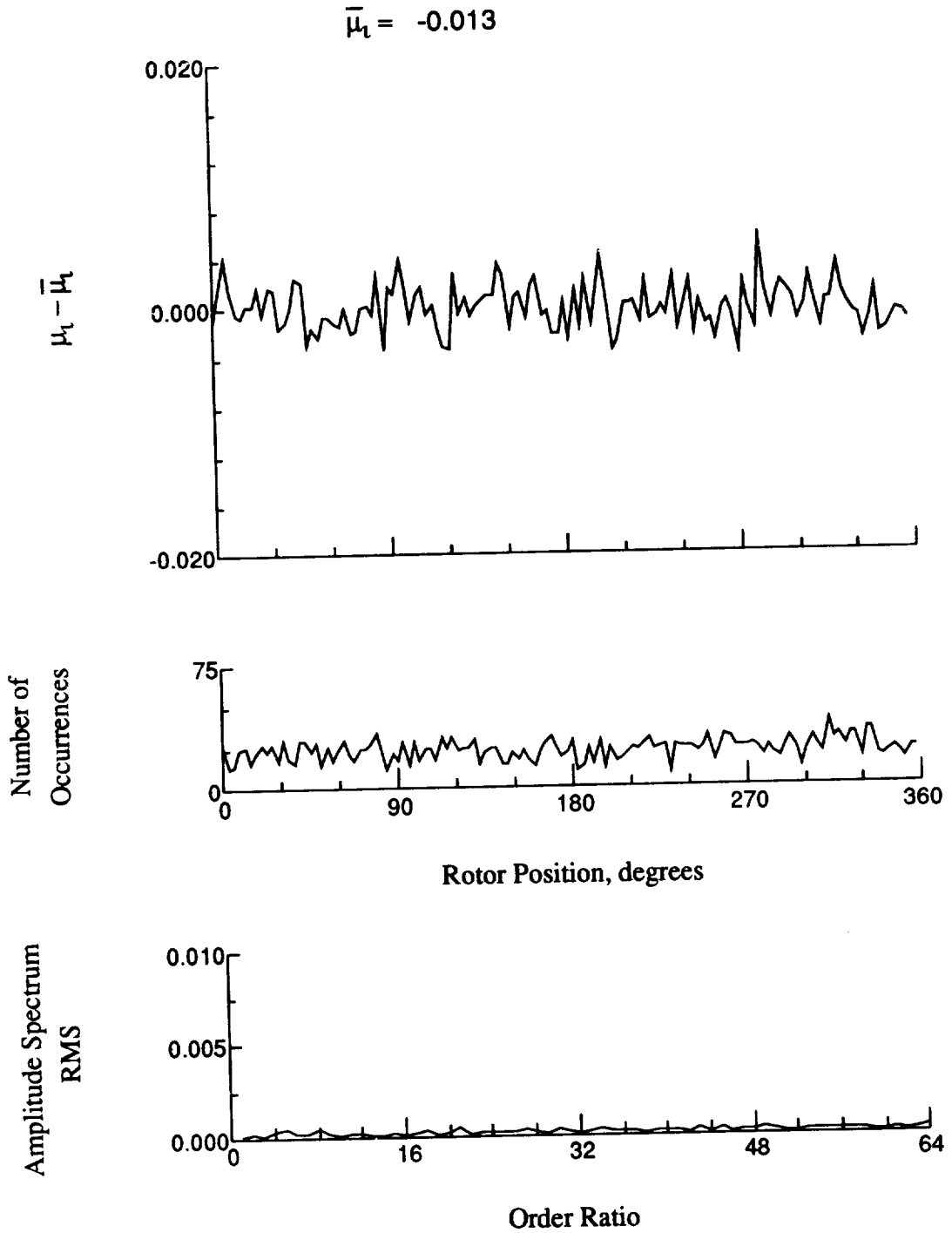


Figure 69.- Induced inflow velocity measured at 90 degrees and r/R of 0.81.

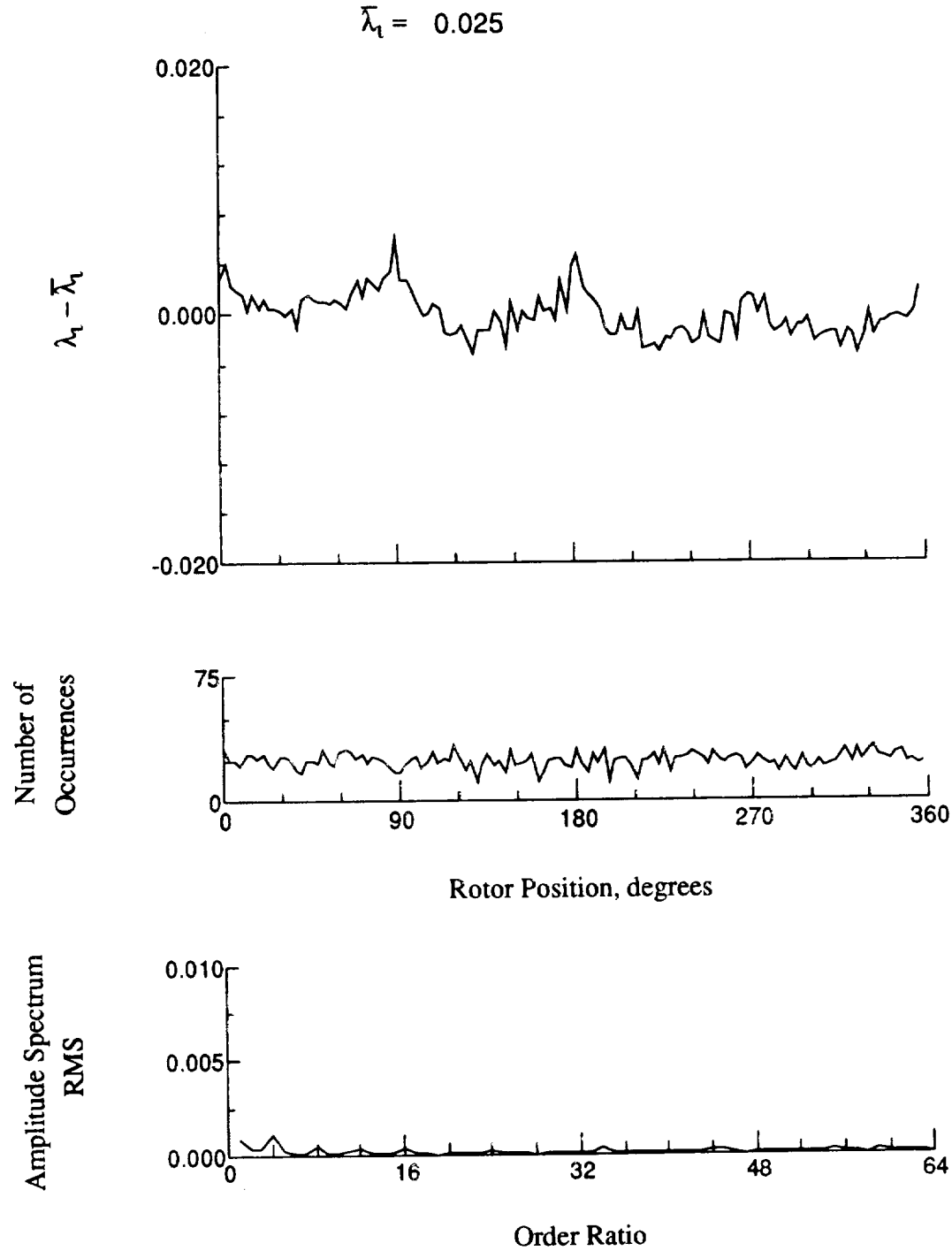


Figure 69.- Concluded.

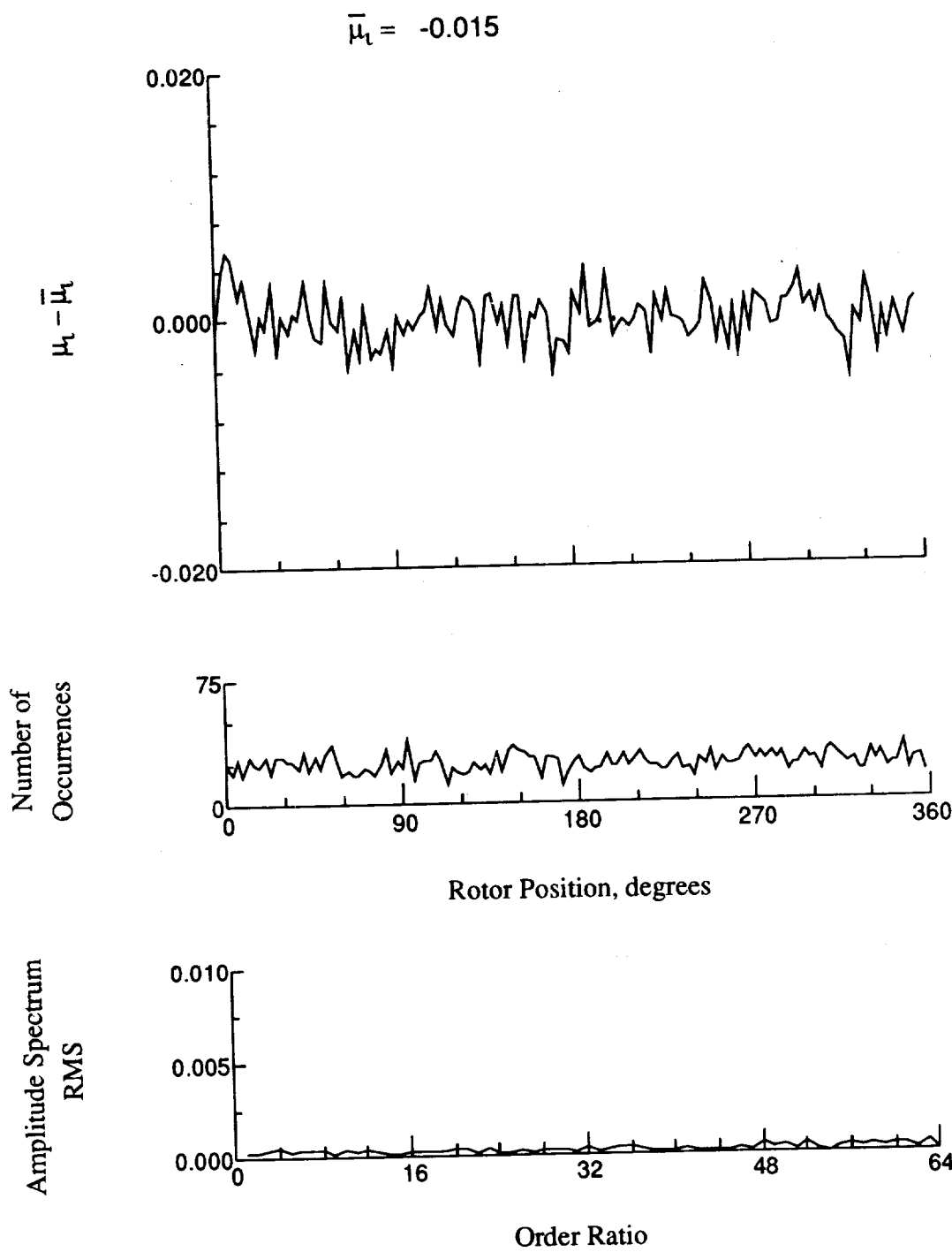


Figure 70.- Induced inflow velocity measured at 90 degrees and r/R of 0.86.

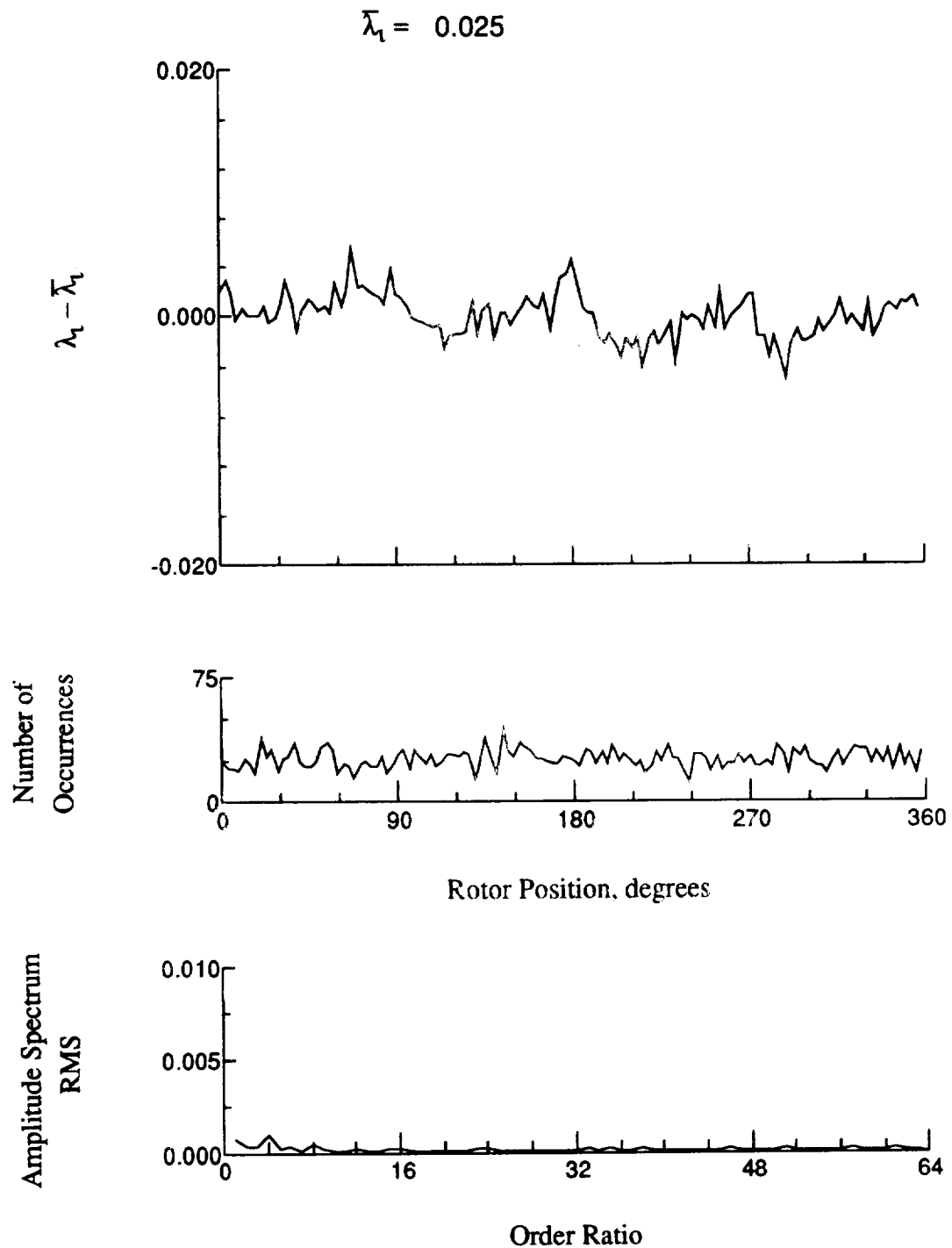


Figure 70.- Concluded.

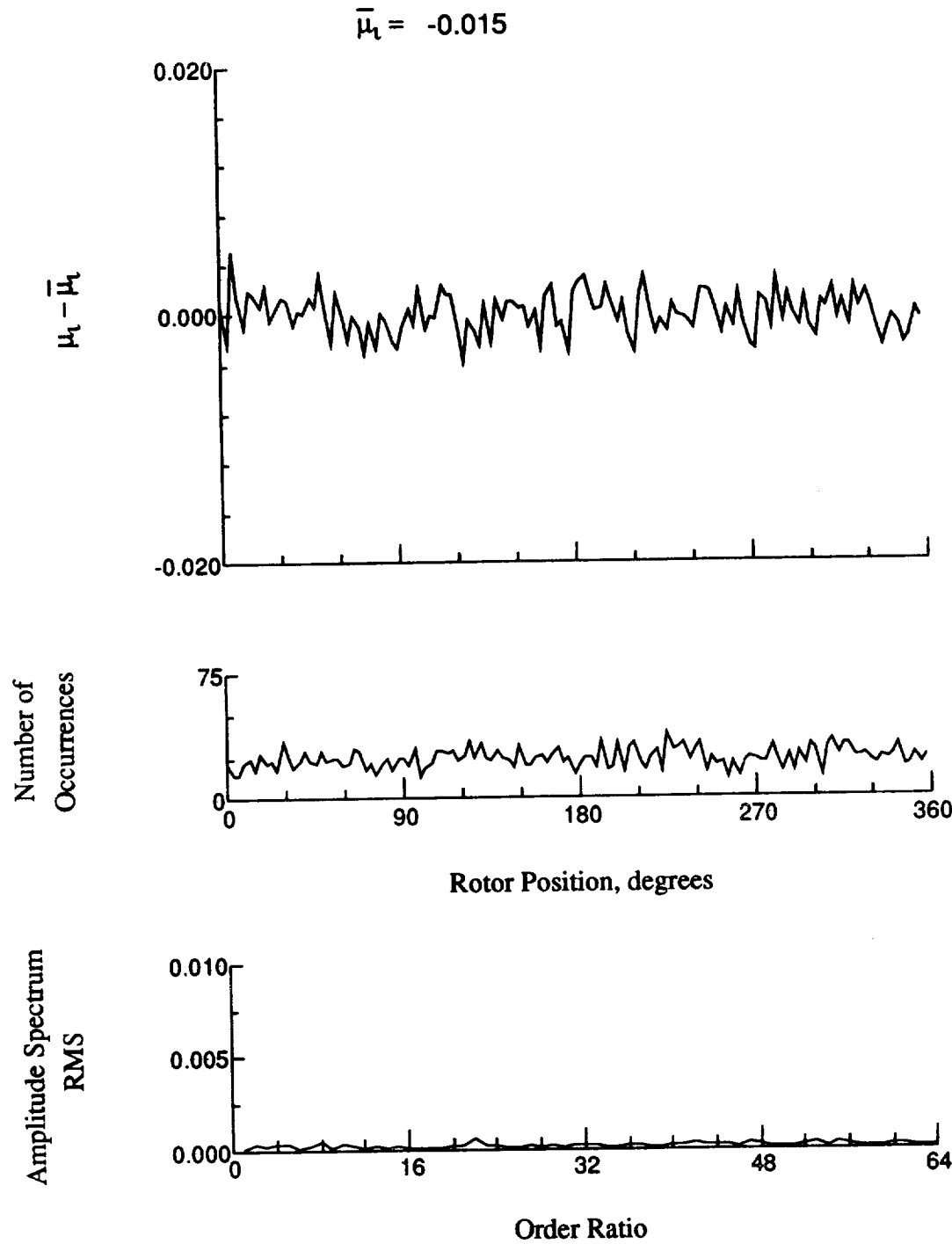


Figure 71.- Induced inflow velocity measured at 90 degrees and r/R of 0.90.

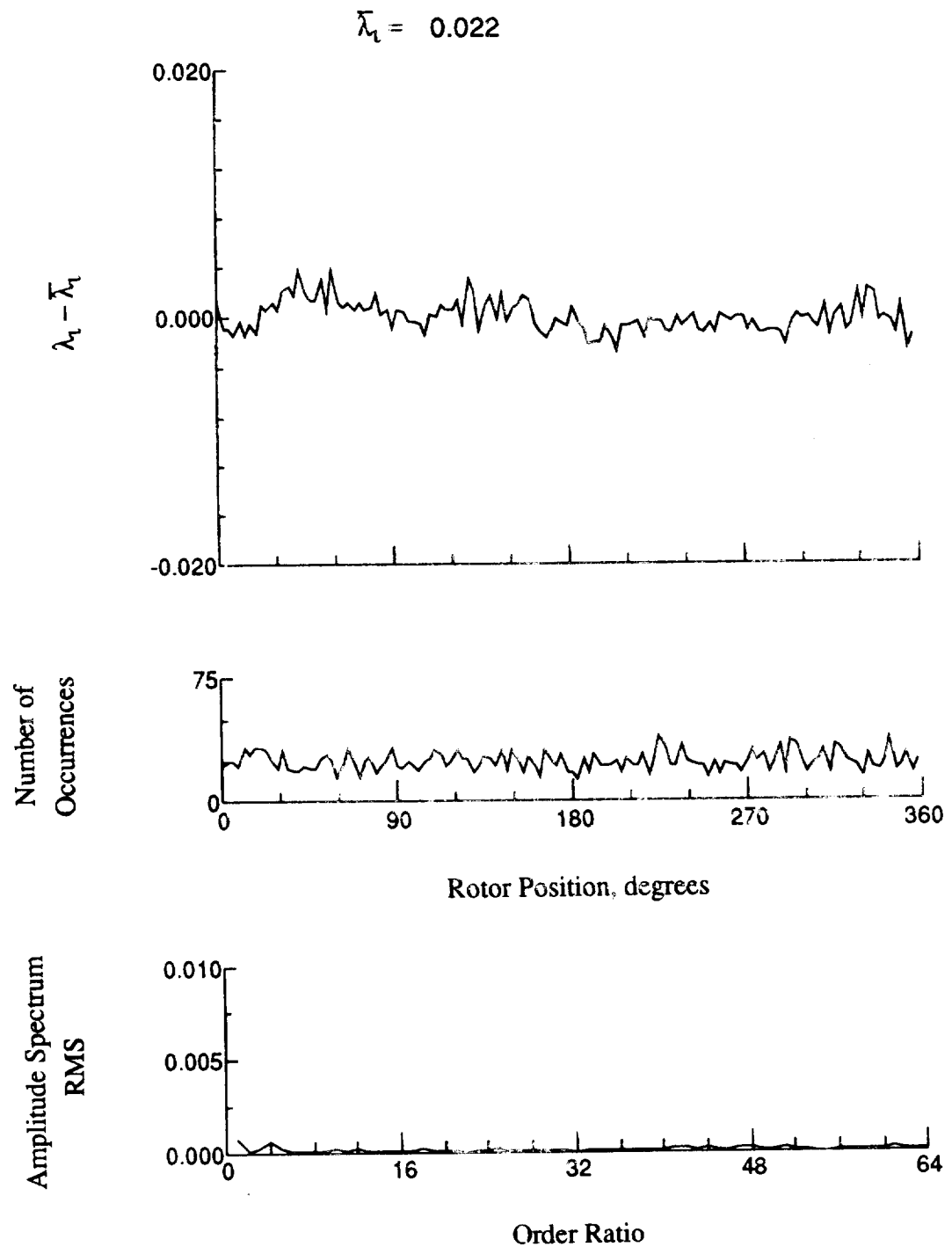


Figure 71.- Concluded.

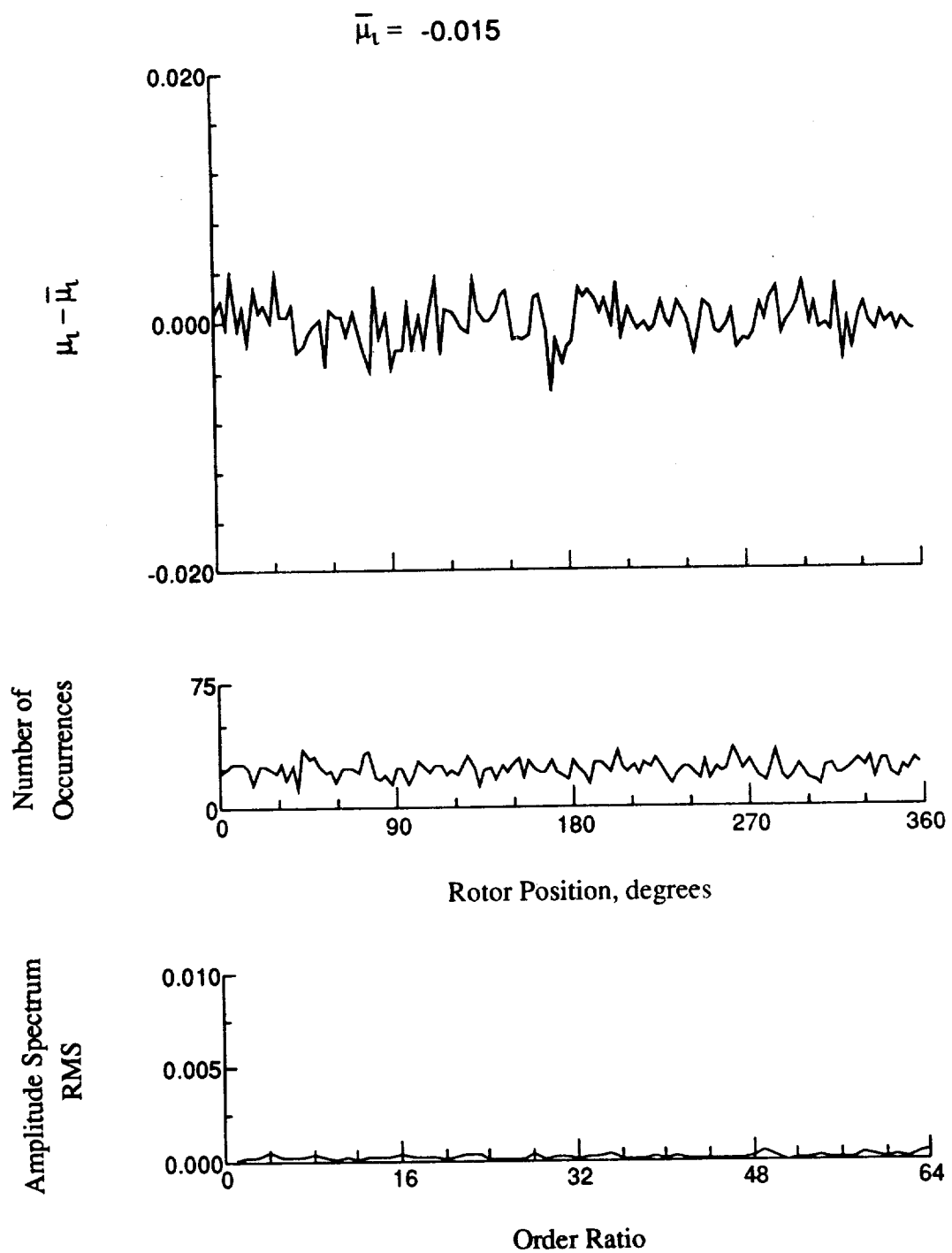


Figure 72.- Induced inflow velocity measured at 90 degrees and r/R of 0.94.

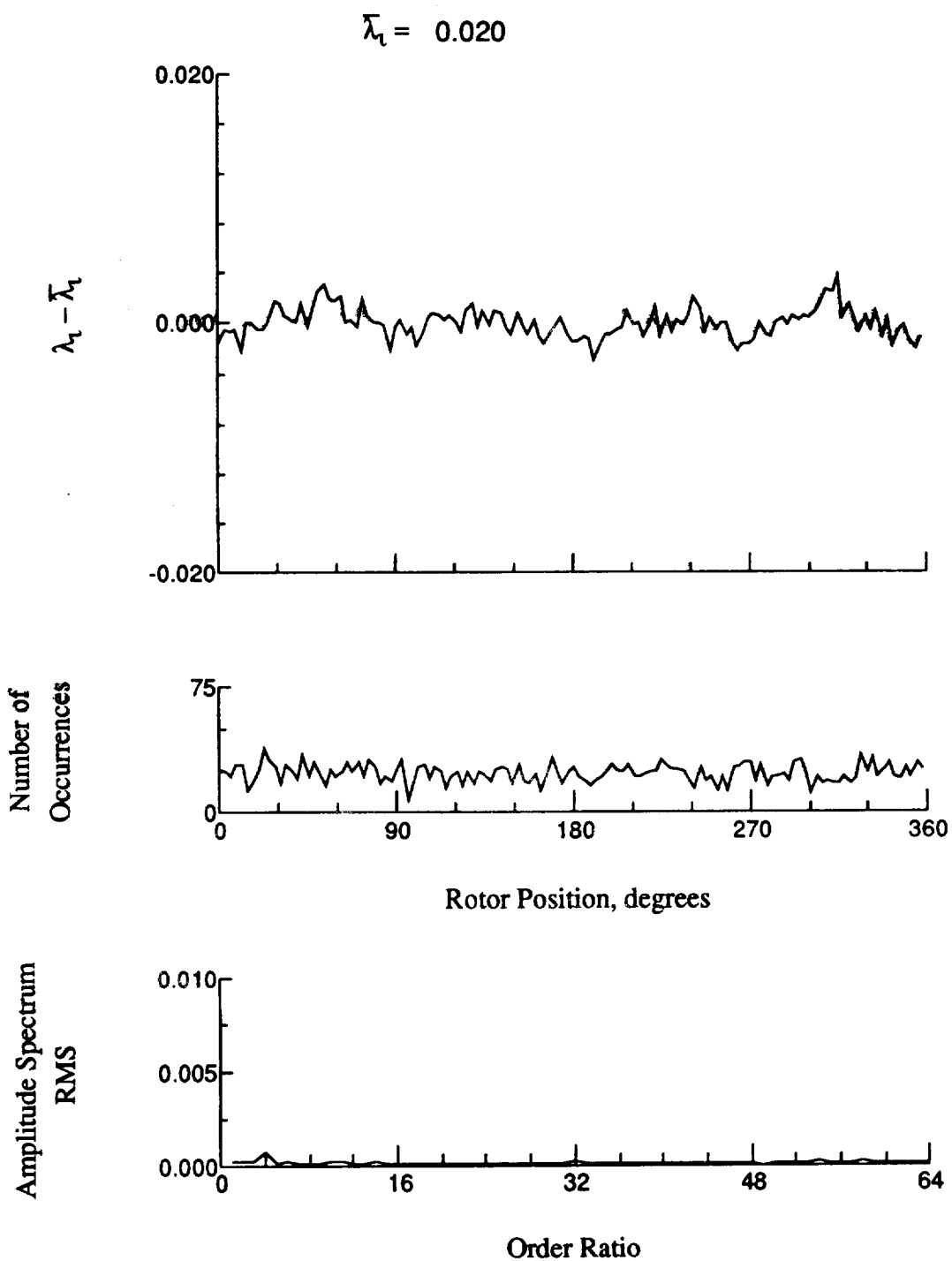


Figure 72.- Concluded.

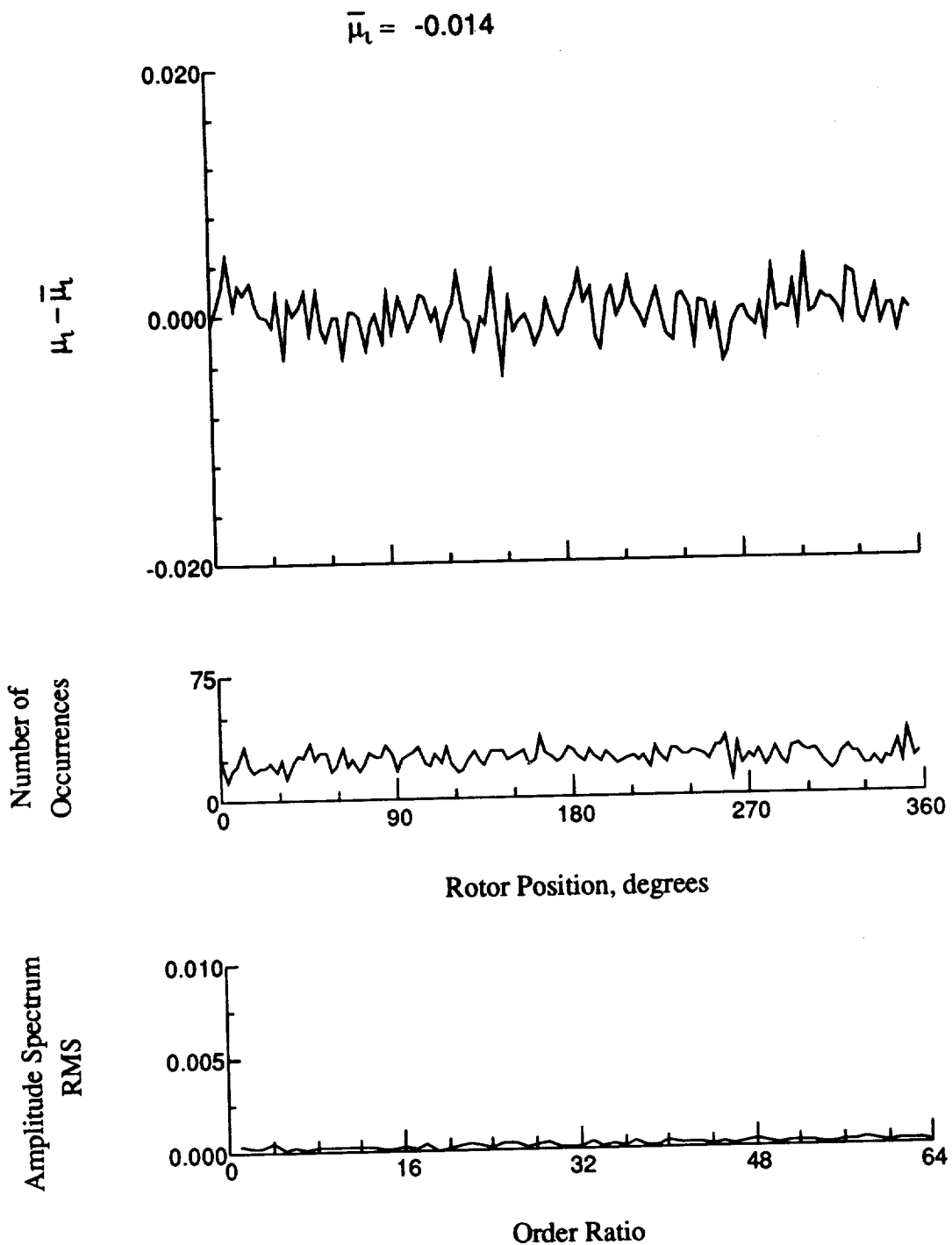


Figure 73.- Induced inflow velocity measured at 90 degrees and r/R of 0.96.

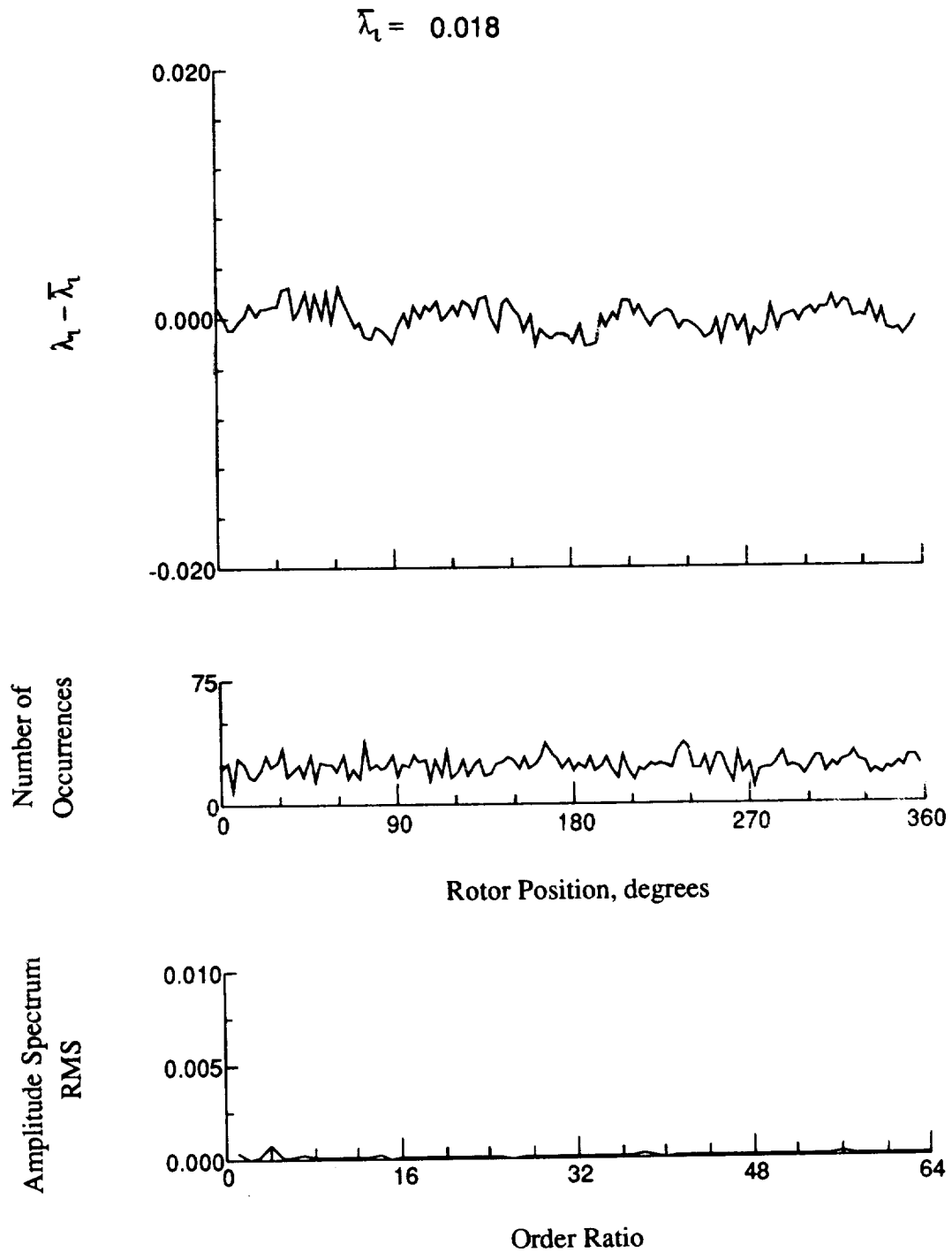


Figure 73.- Concluded.

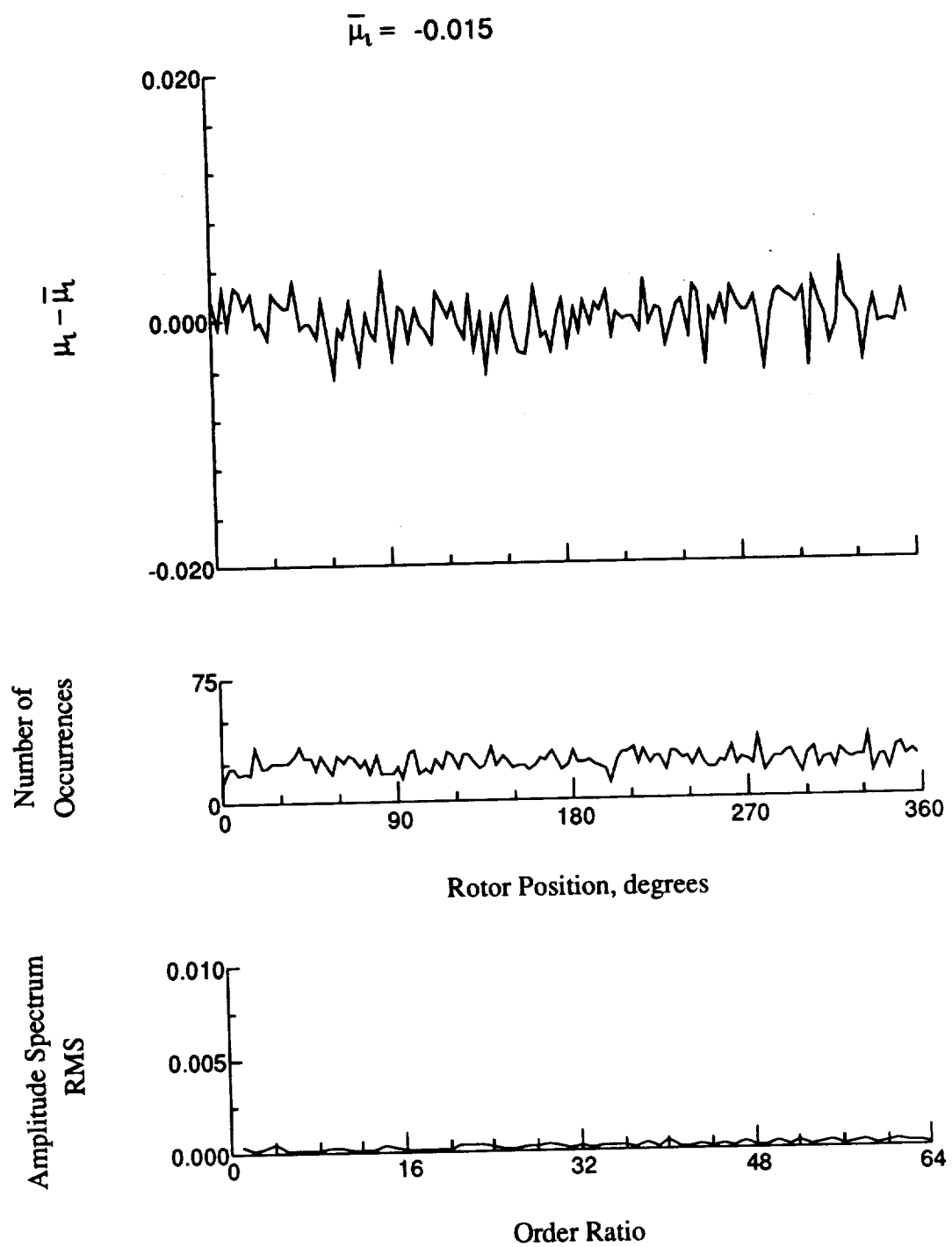


Figure 74.- Induced inflow velocity measured at 90 degrees and r/R of 1.00.

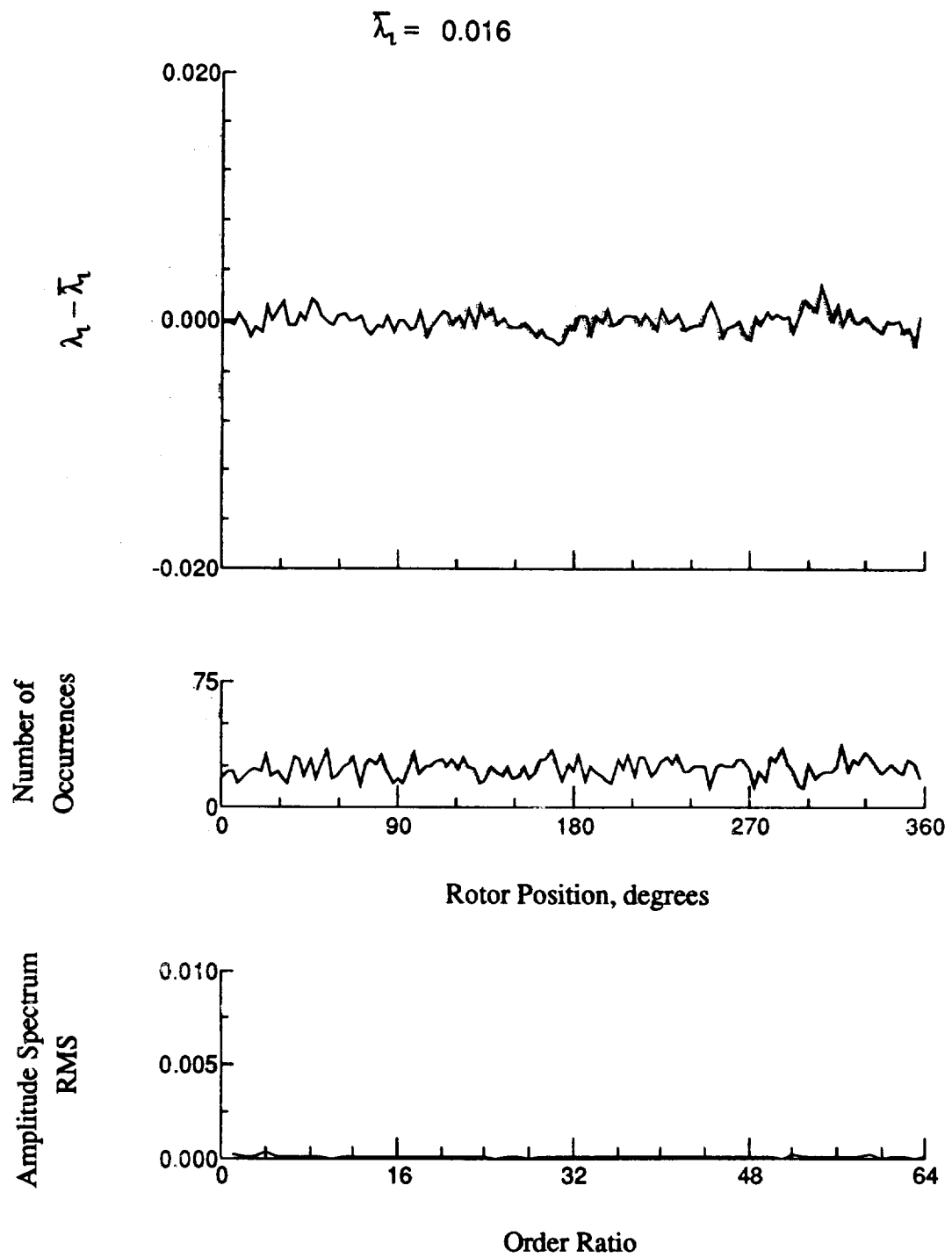


Figure 74.- Concluded.

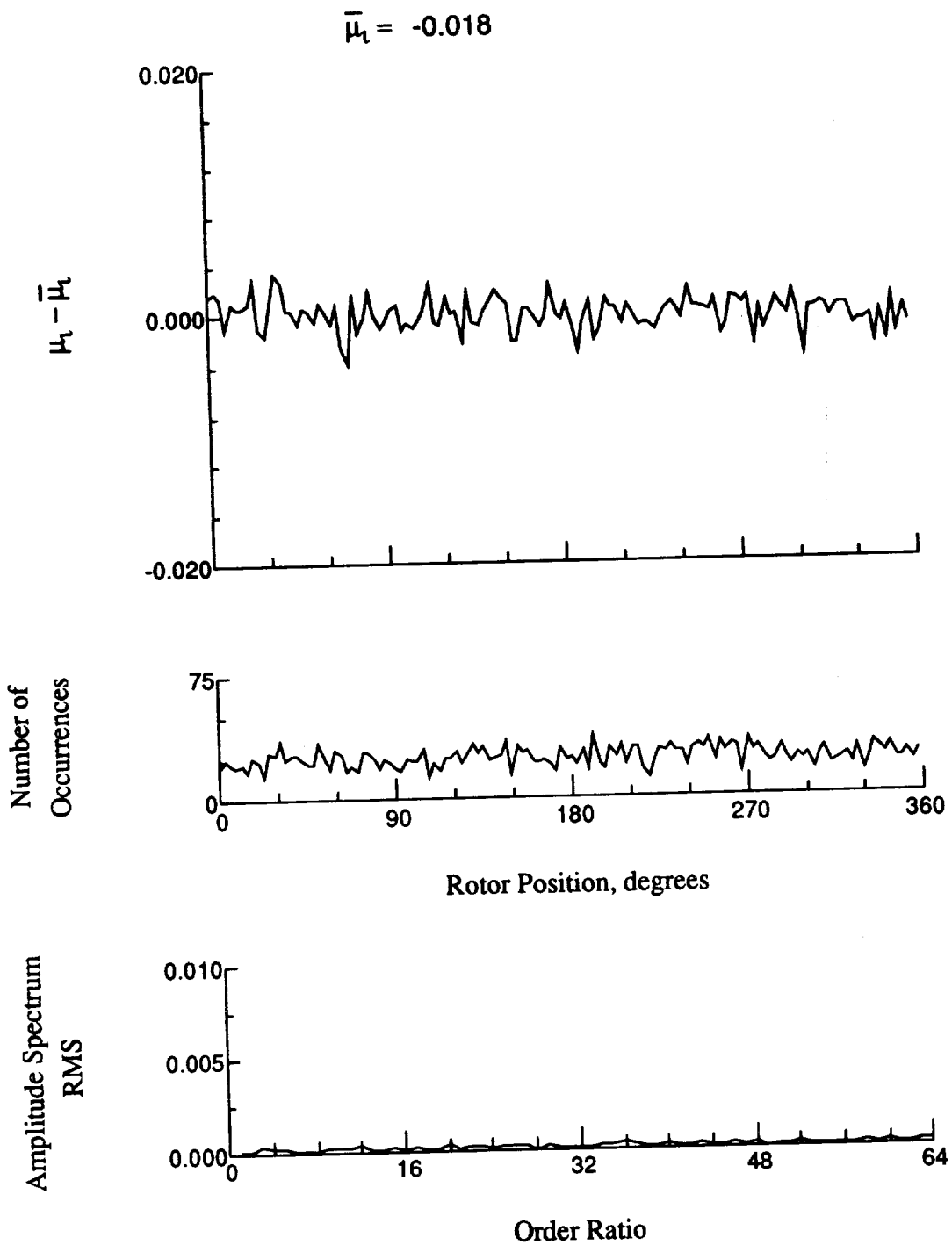


Figure 75.- Induced inflow velocity measured at 90 degrees and r/R of 1.10.

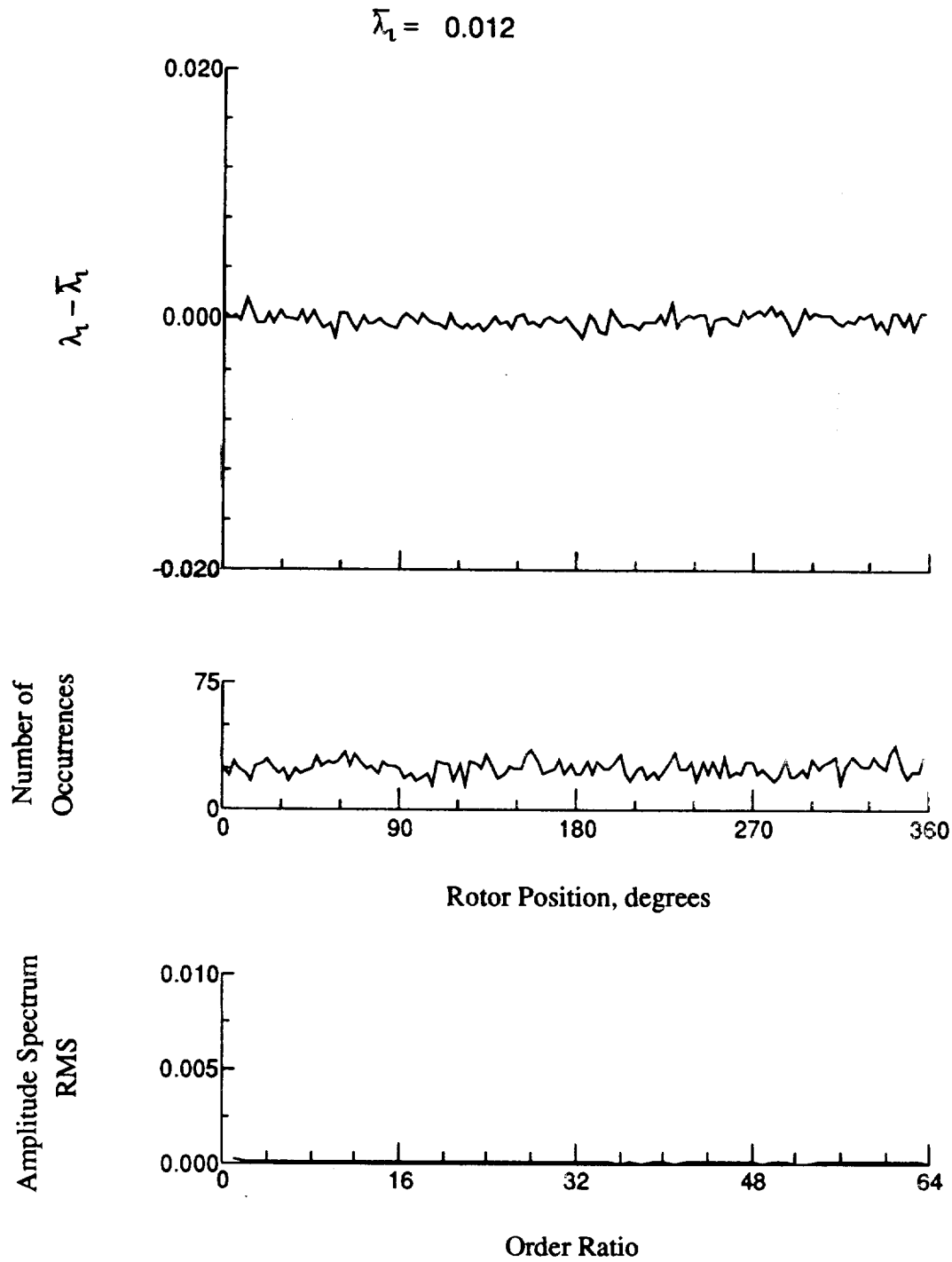


Figure 75.- Concluded.

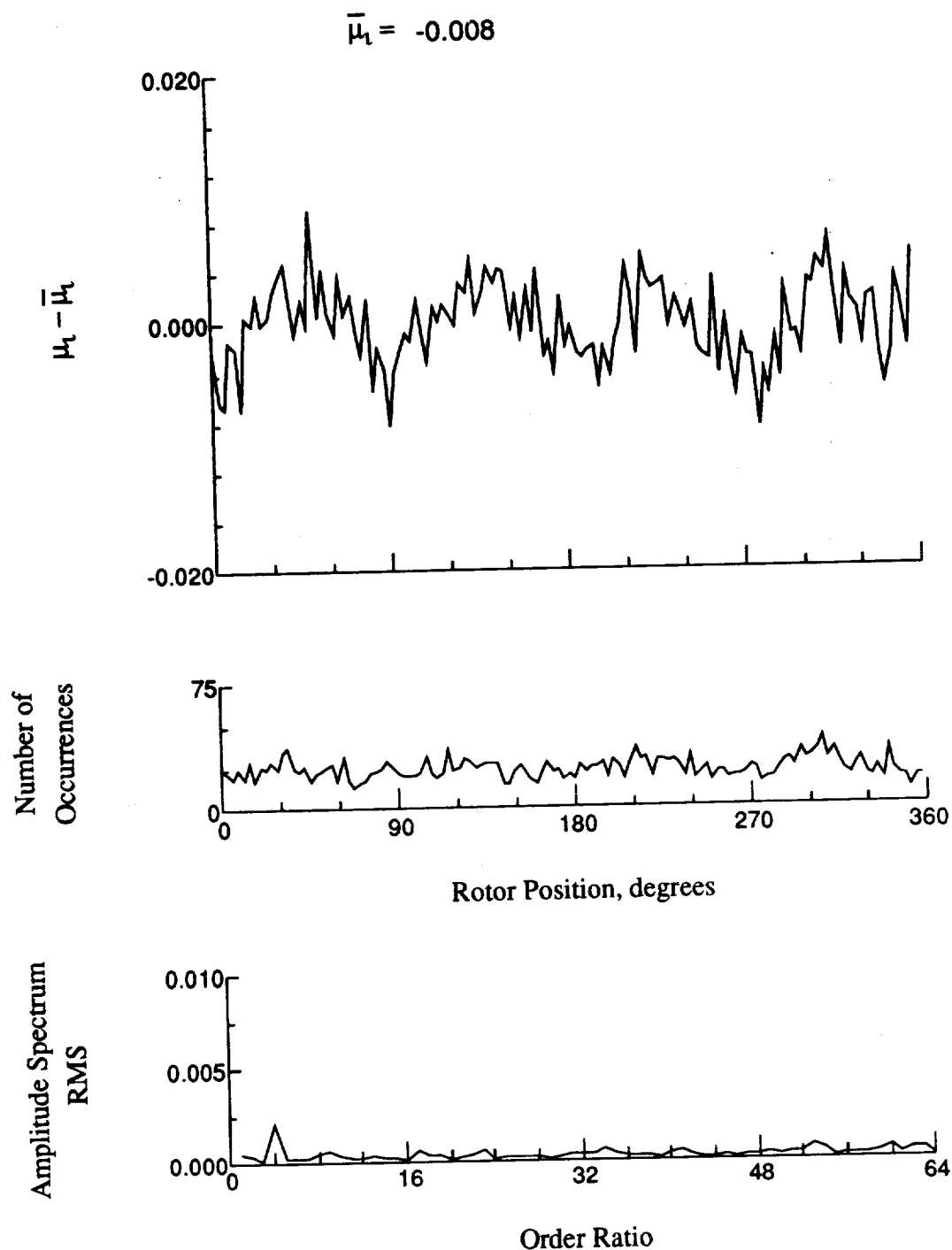


Figure 76.- Induced inflow velocity measured at 120 degrees and r/R of 0.20.

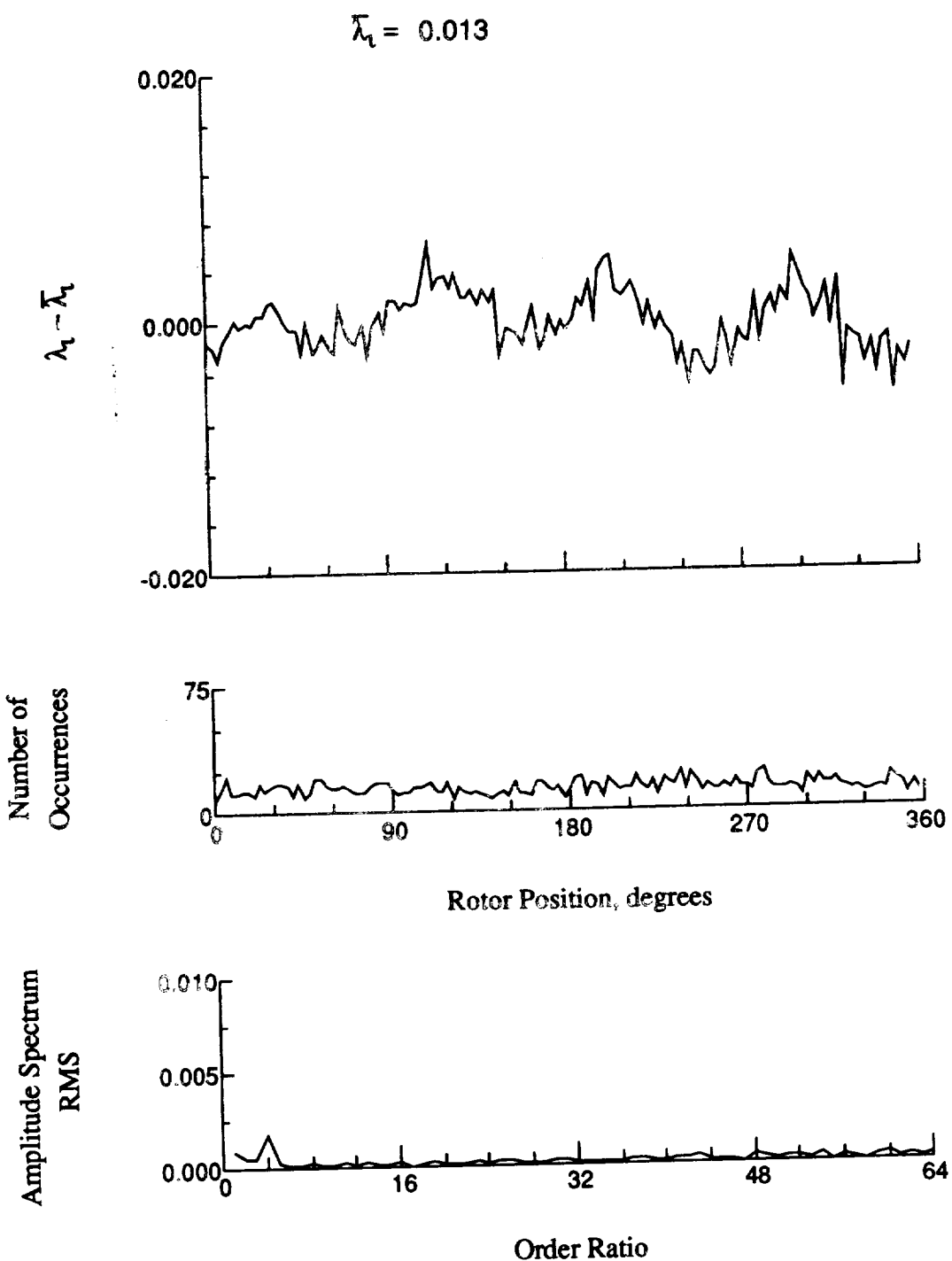


Figure 76.- Concluded.

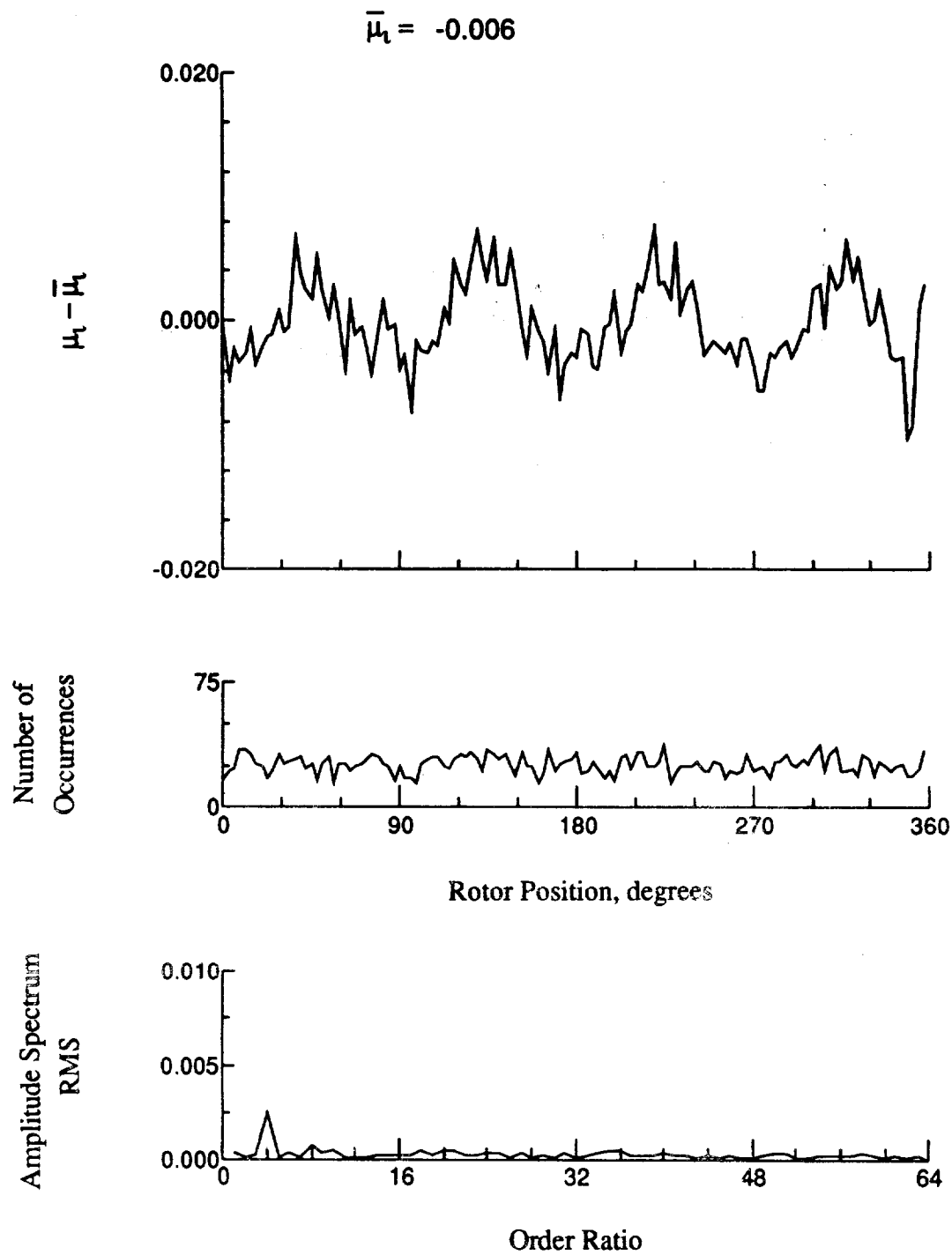


Figure 77.- Induced inflow velocity measured at 120 degrees and r/R of 0.32.

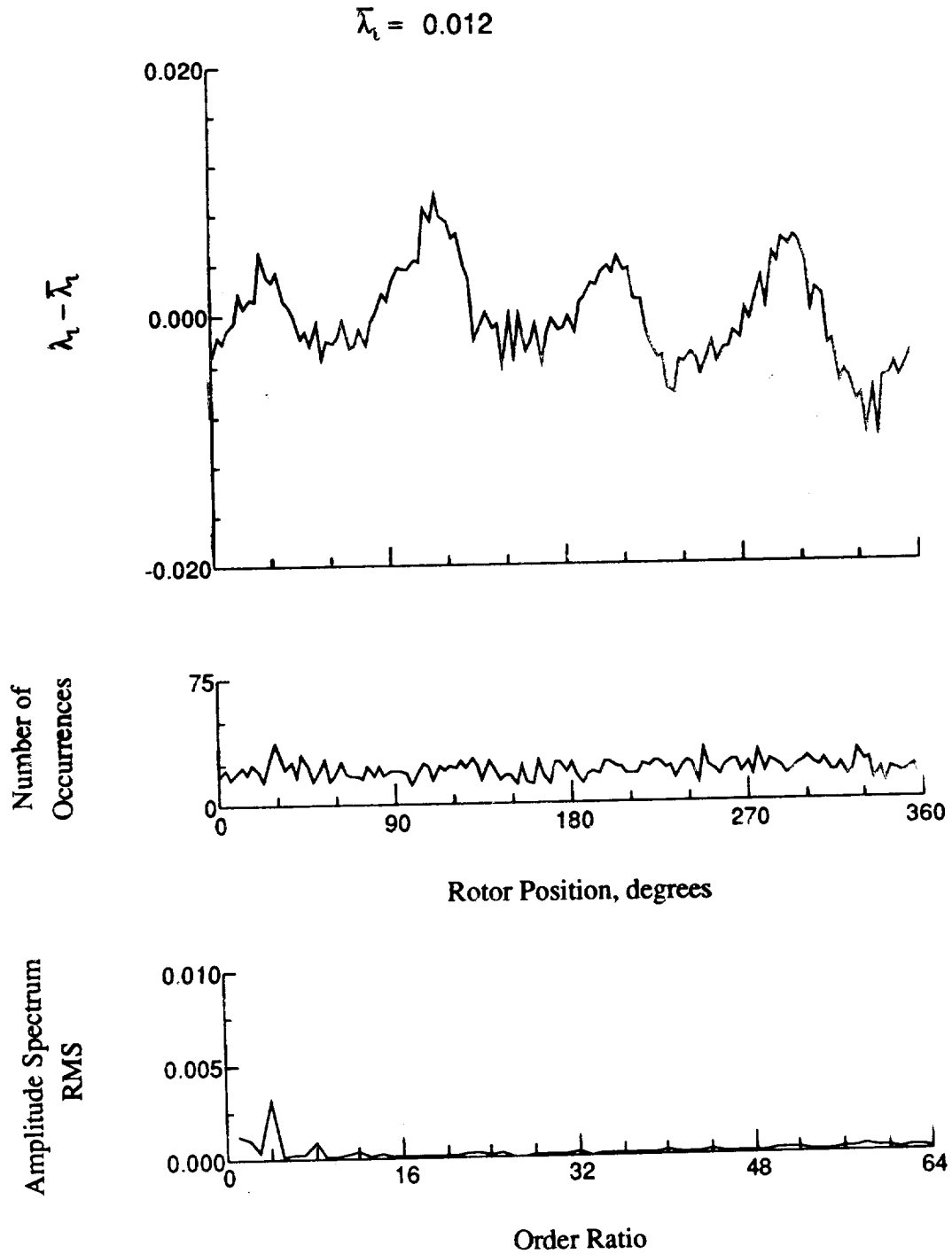


Figure 77.- Concluded.

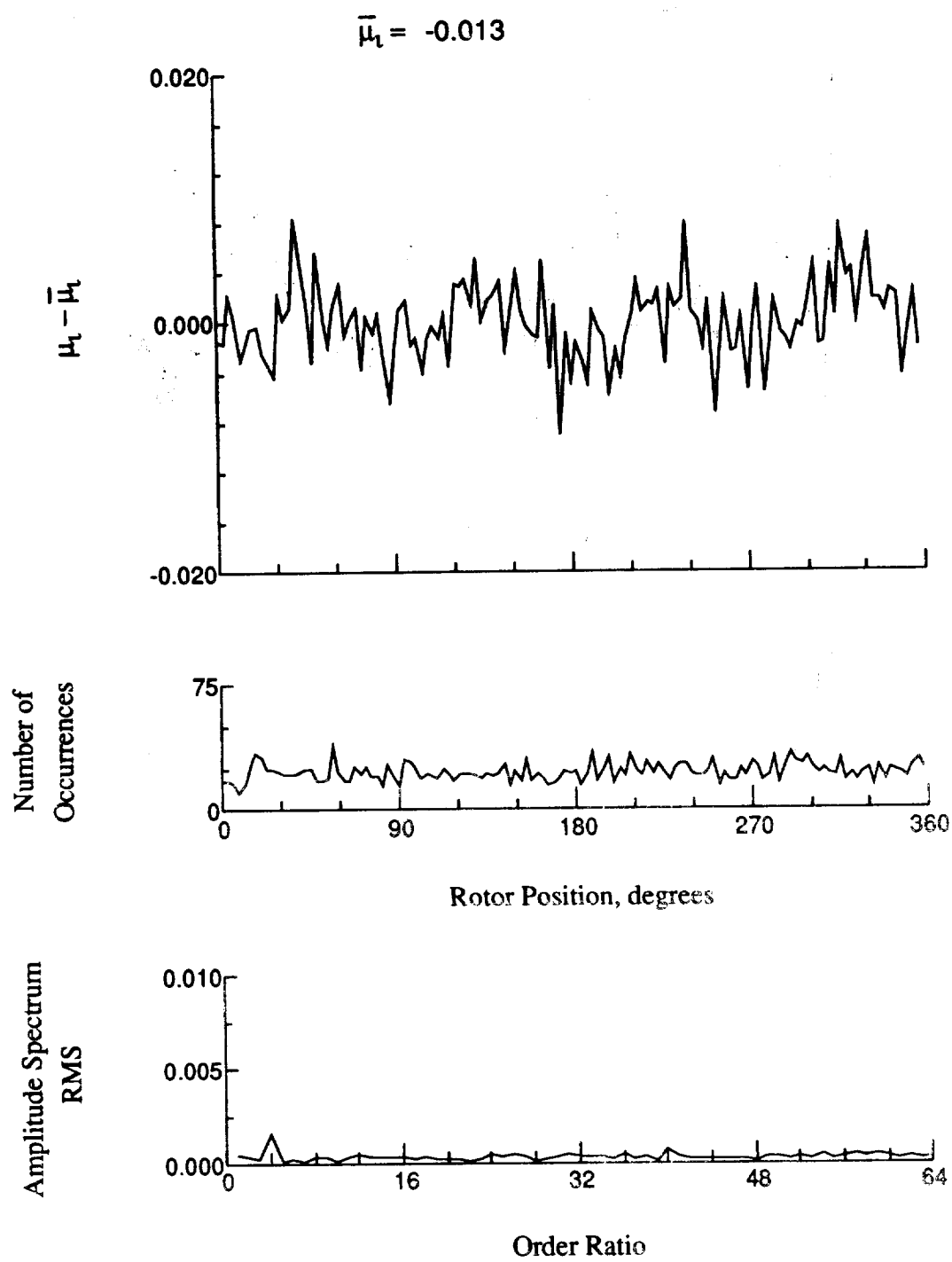


Figure 78.- Induced inflow velocity measured at 120 degrees and r/R of 0.50.

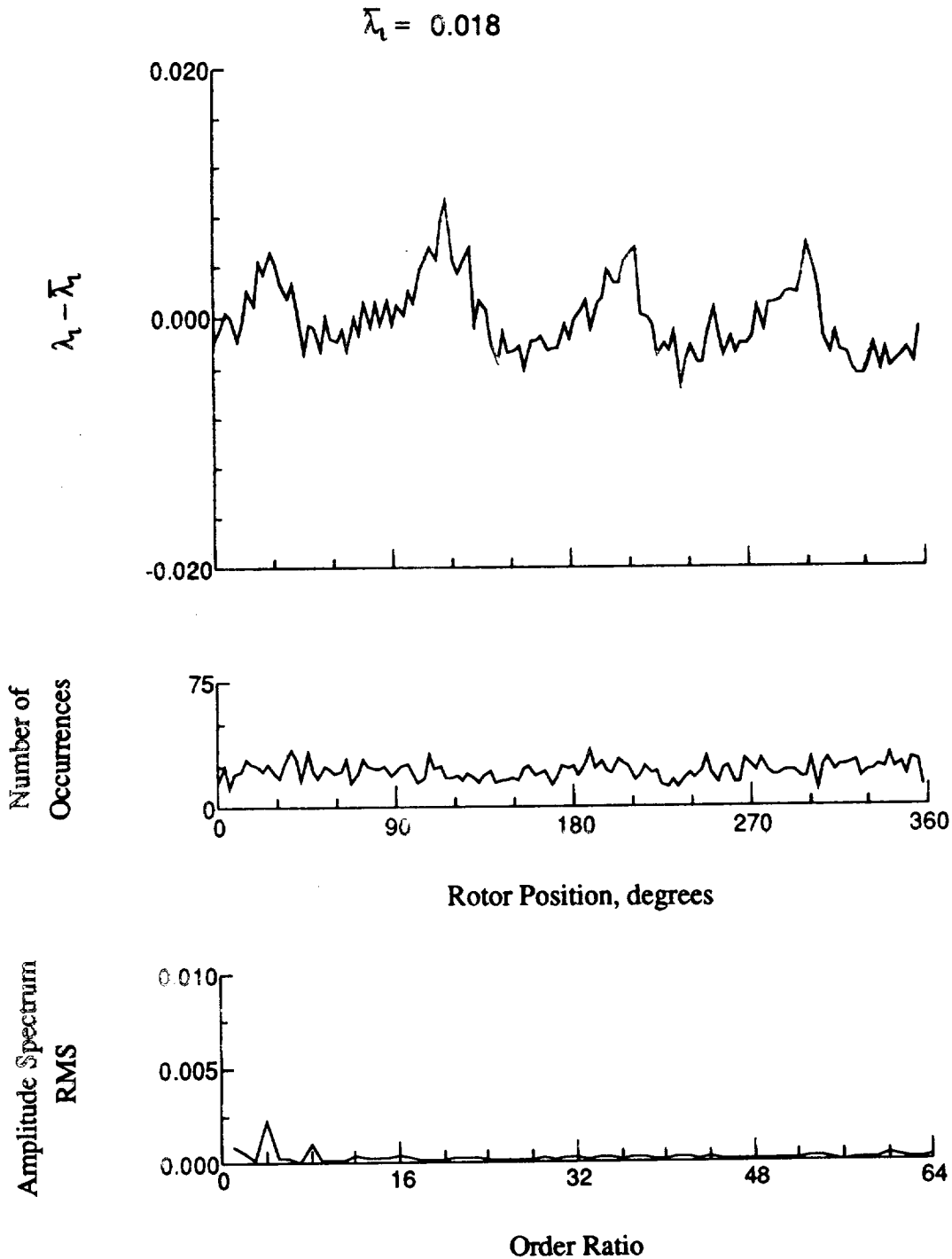


Figure 78.- Concluded.

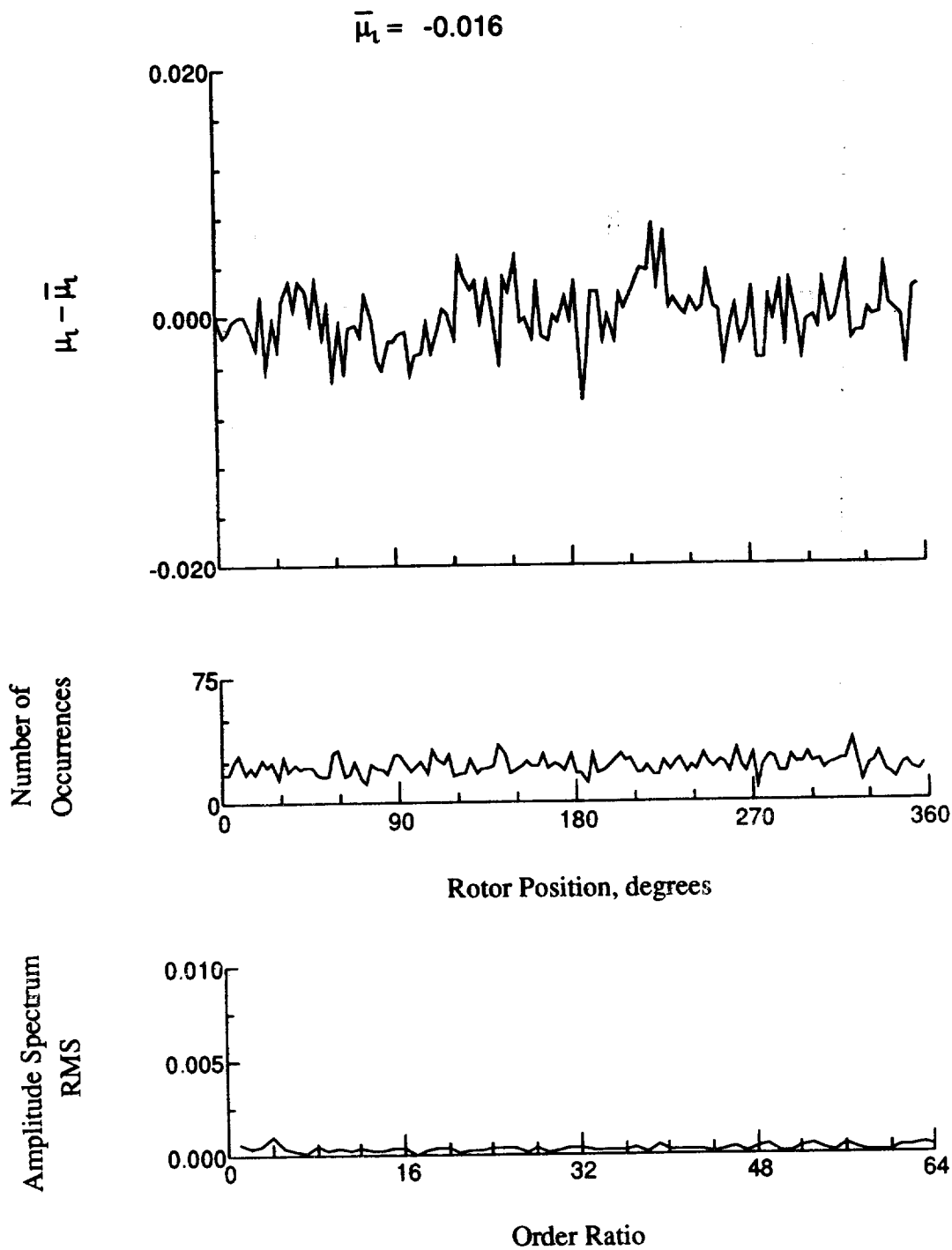


Figure 79.- Induced inflow velocity measured at 120 degrees and r/R of 0.58.

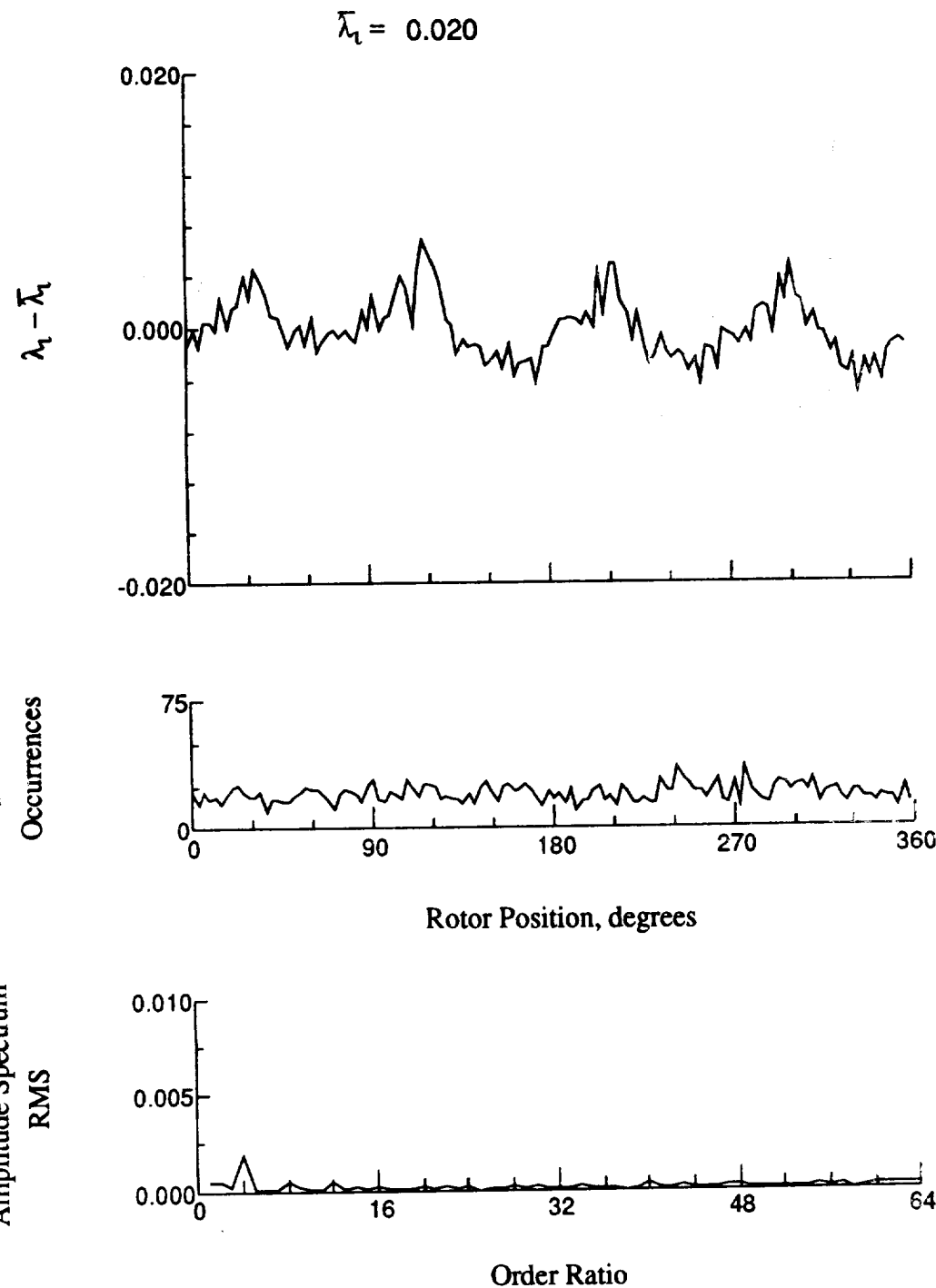


Figure 79.- Concluded.

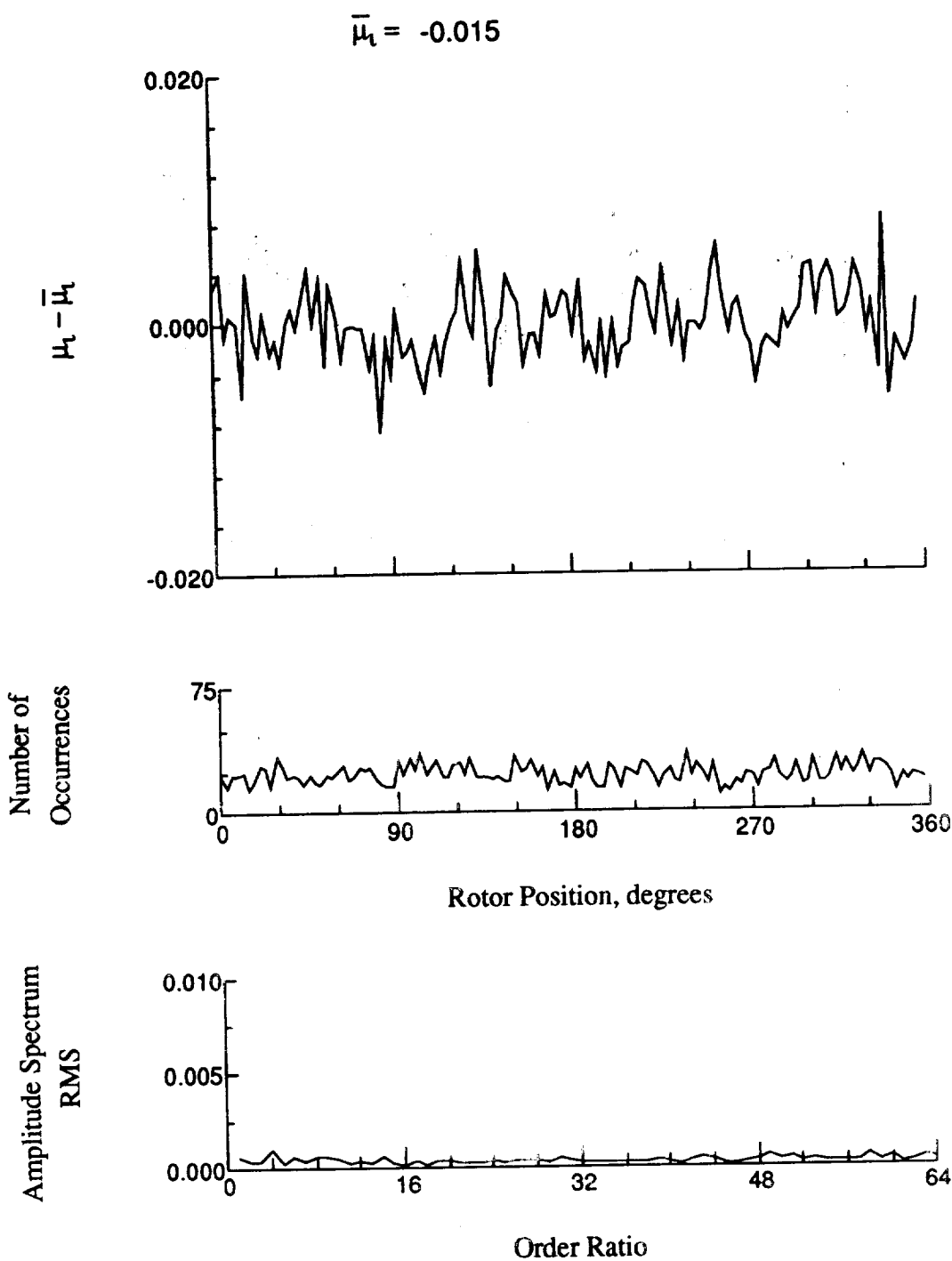


Figure 80.- Induced inflow velocity measured at 120 degrees and r/R of 0.69.

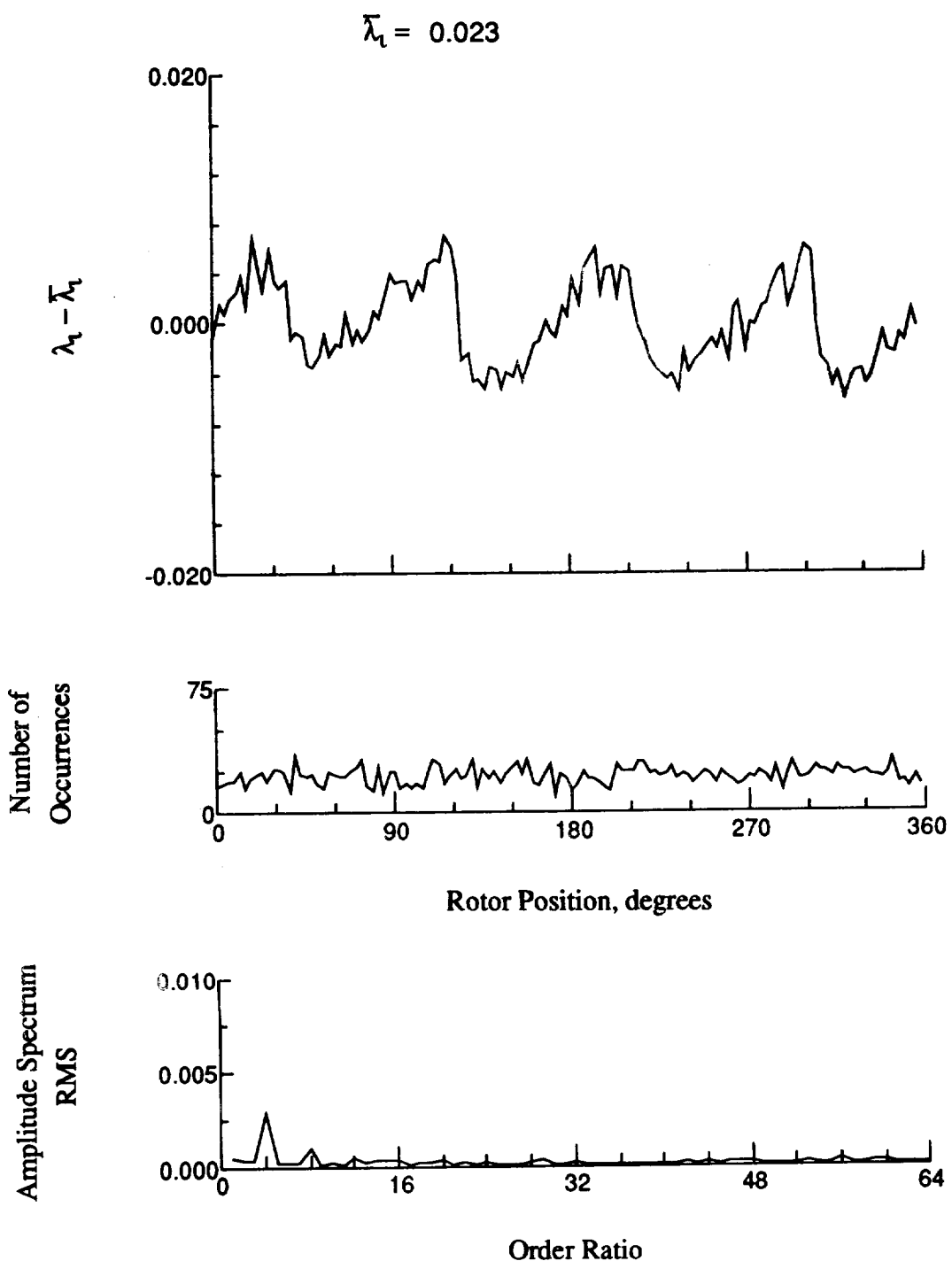


Figure 80.- Concluded.

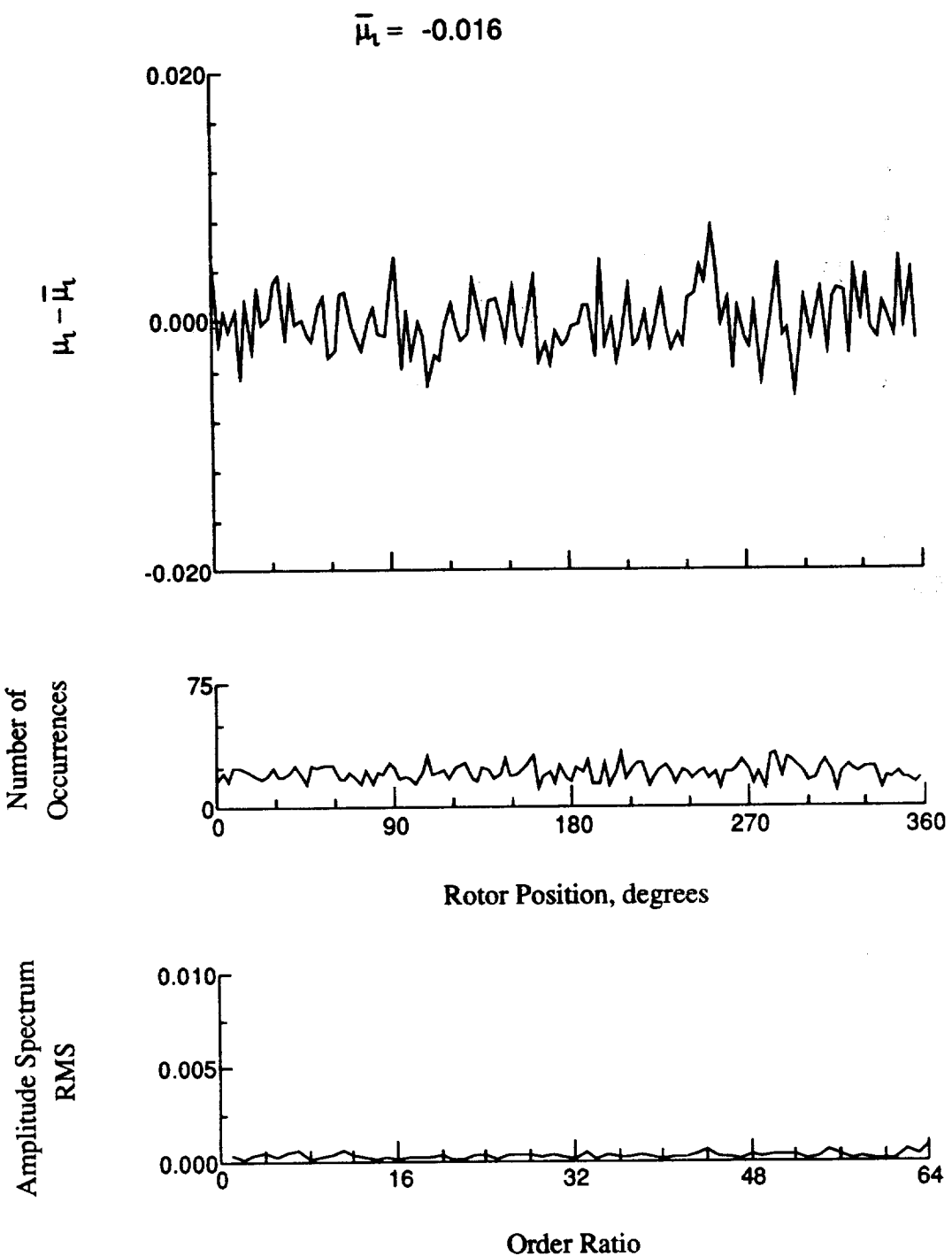


Figure 81.- Induced inflow velocity measured at 120 degrees and r/R of 0.73.

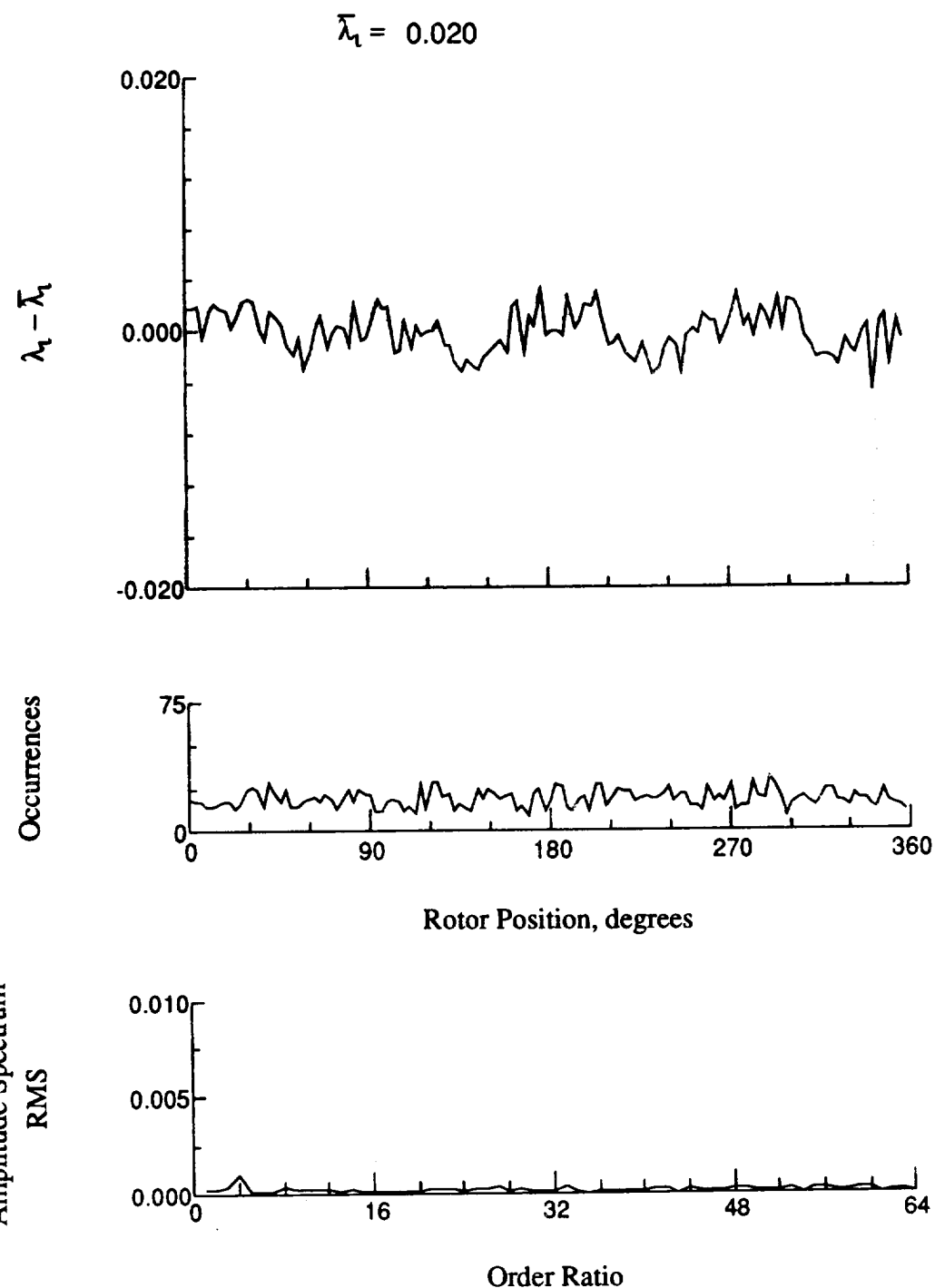


Figure 81.- Concluded.

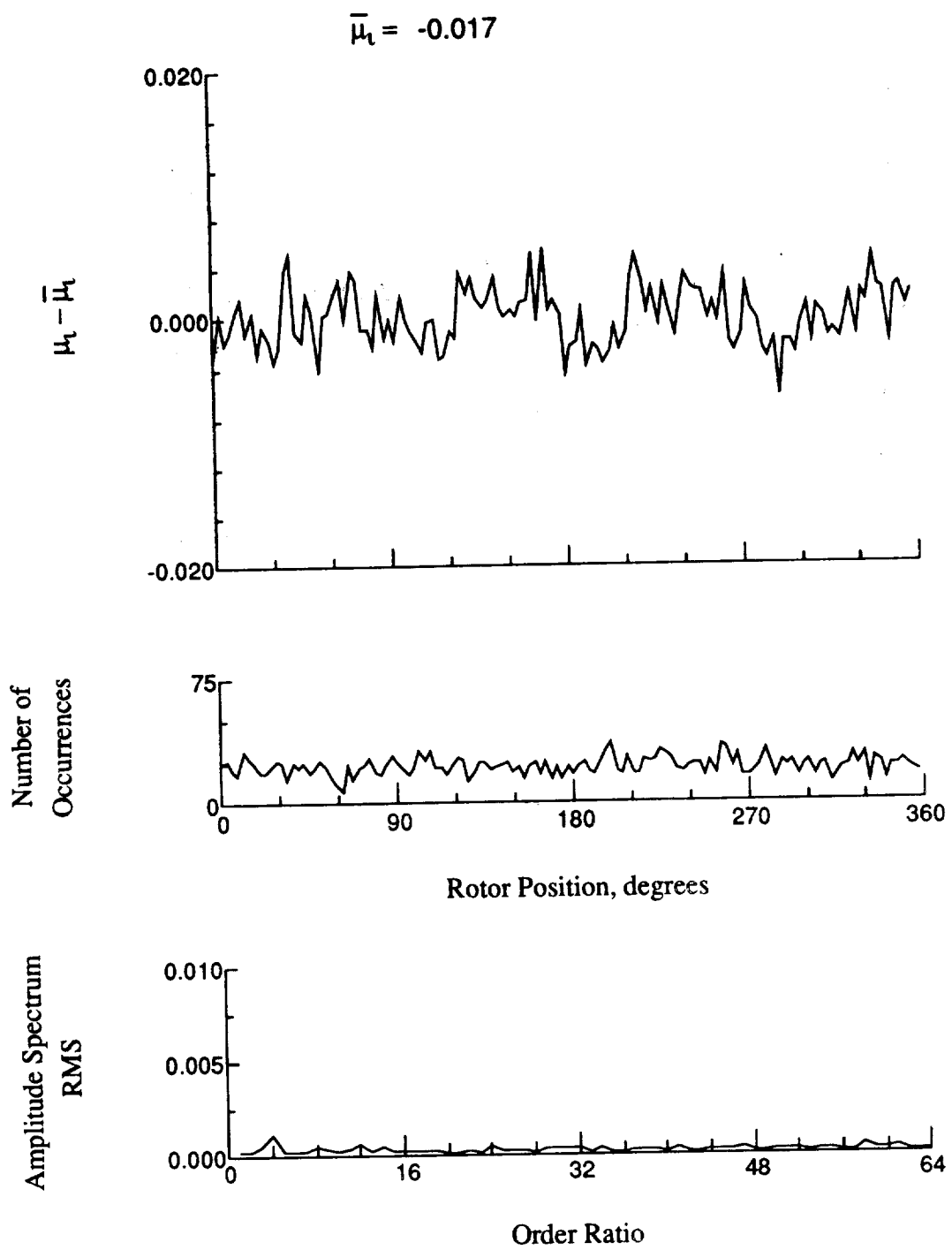


Figure 82.- Induced inflow velocity measured at 120 degrees and r/R of 0.75.

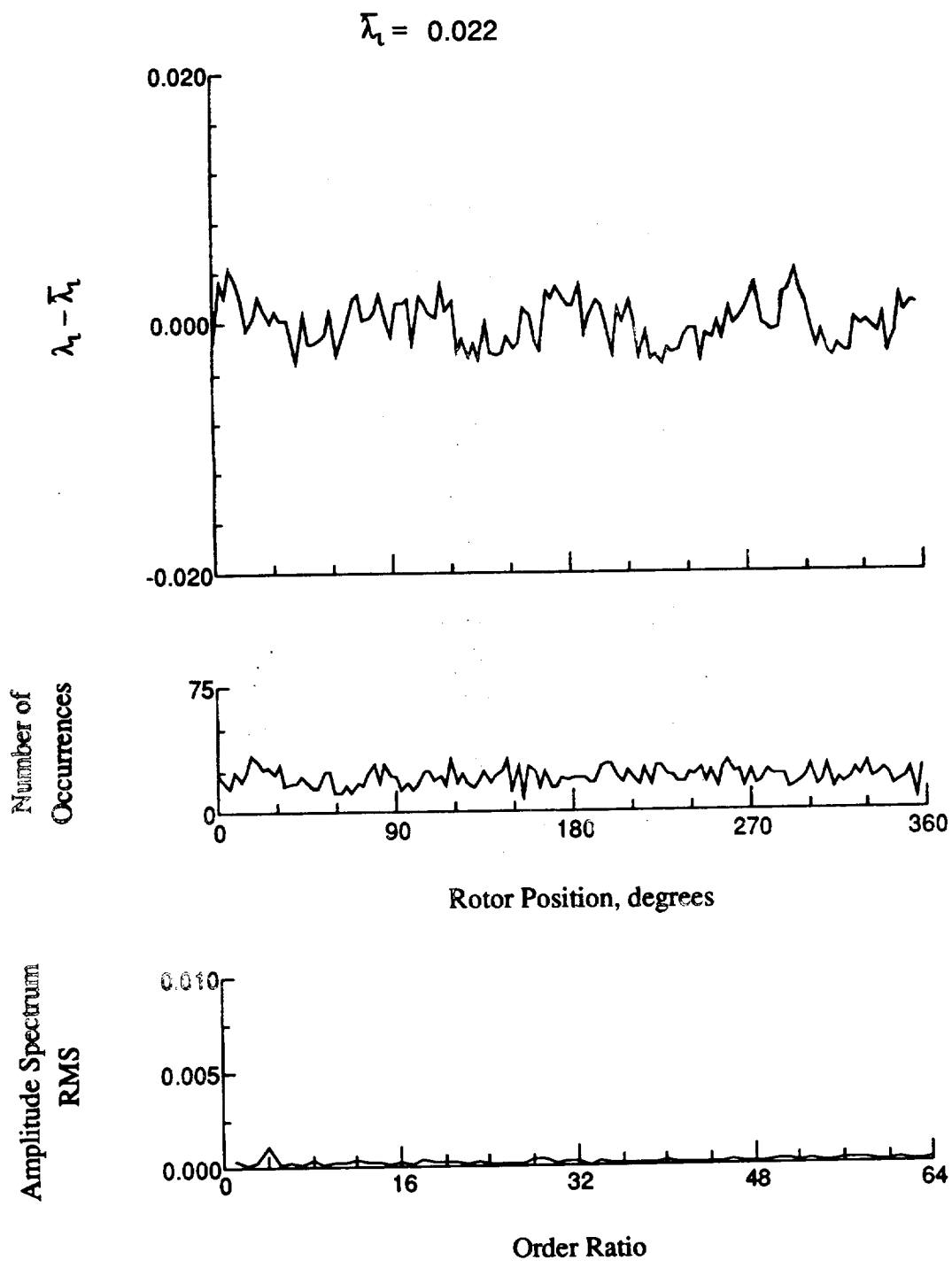


Figure 82.- Concluded.

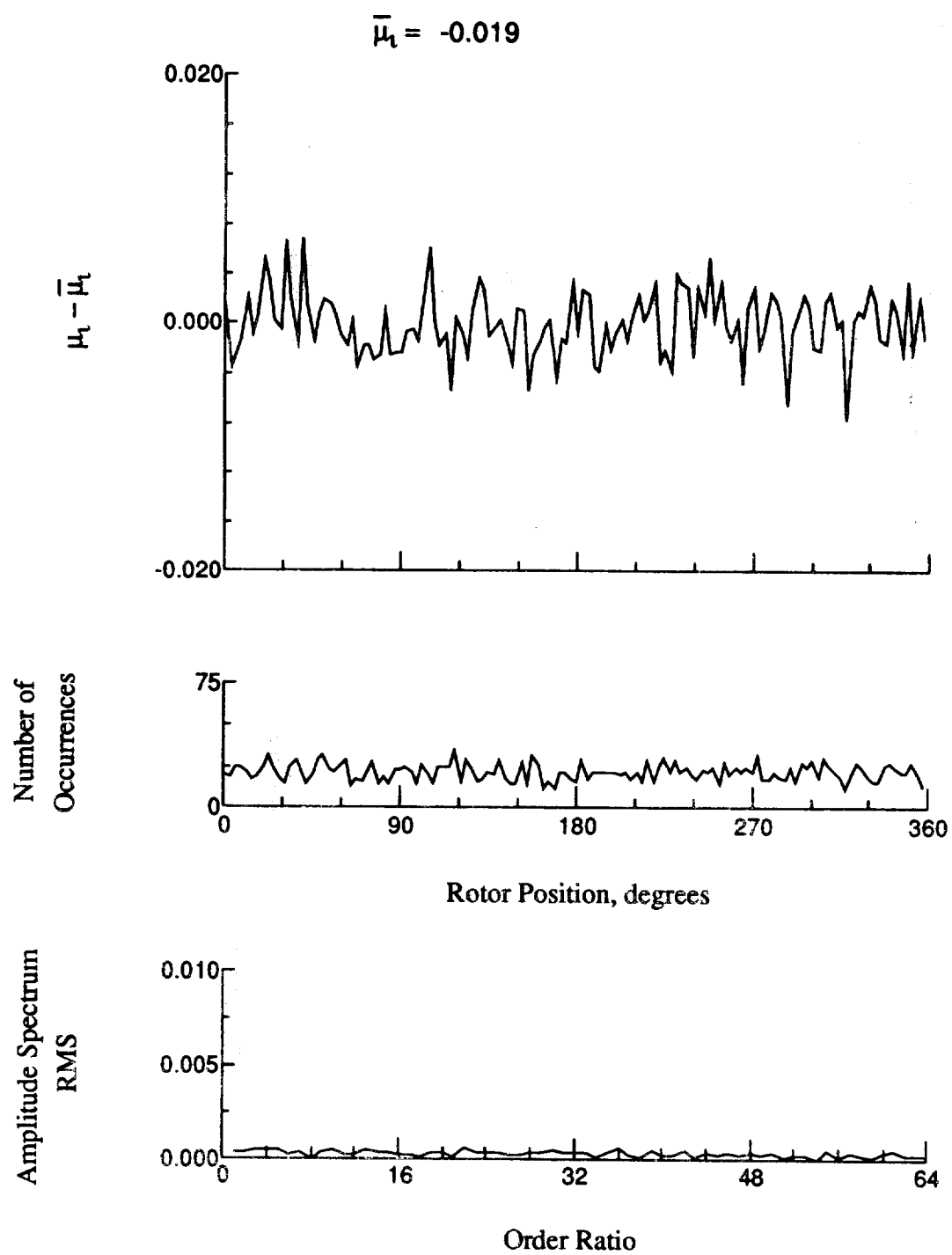


Figure 83.- Induced inflow velocity measured at 120 degrees and r/R of 0.86.

$$\bar{\lambda}_i = 0.019$$

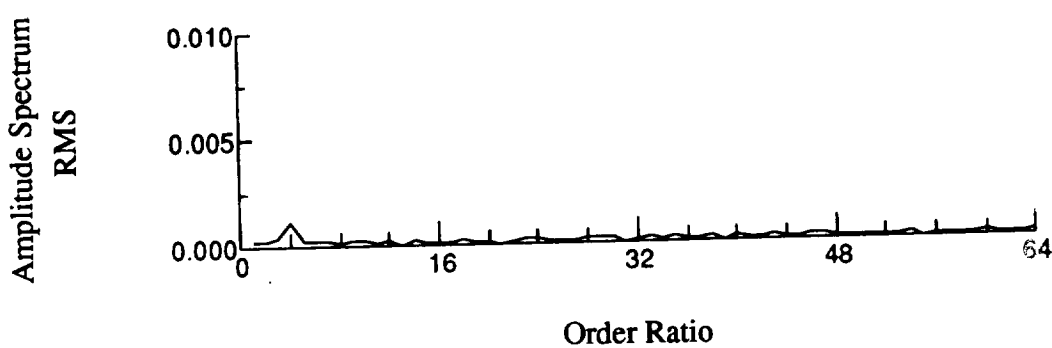
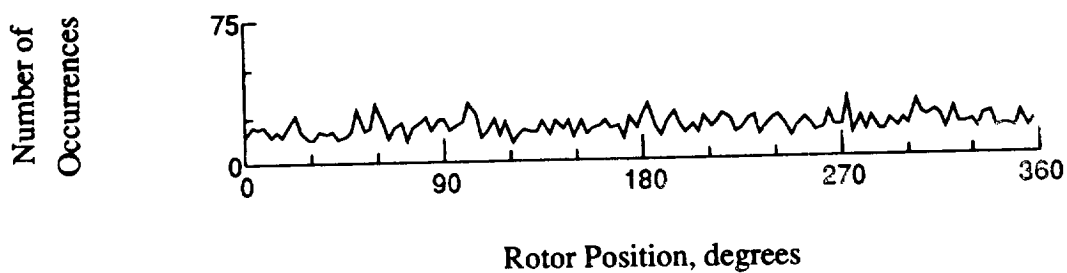
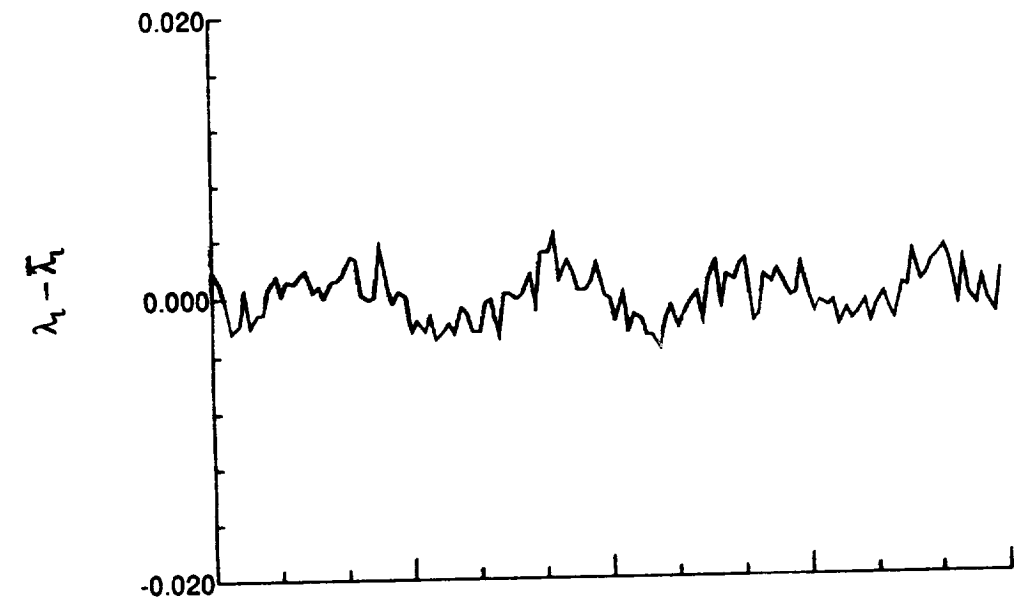


Figure 83.- Concluded.

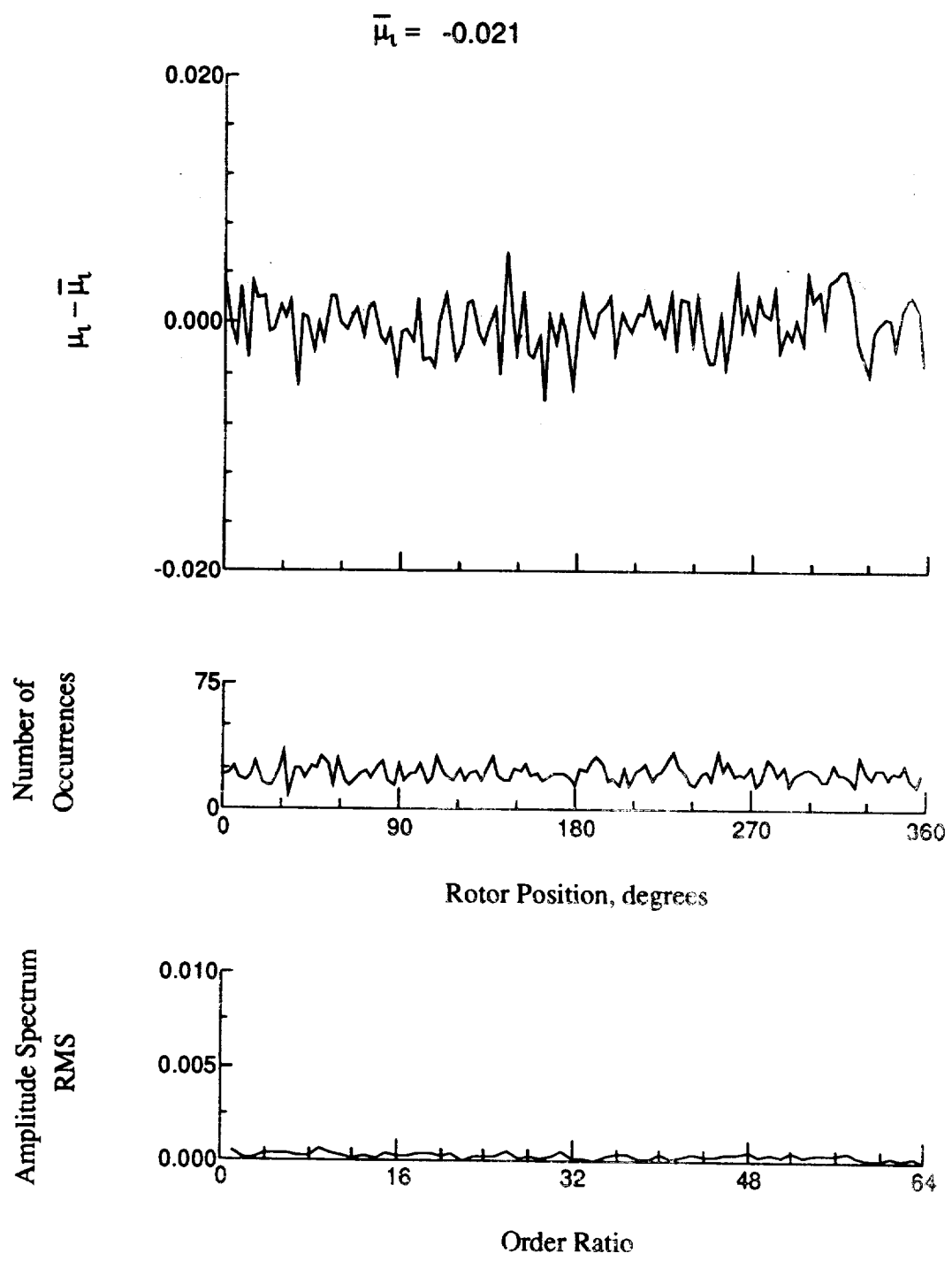


Figure 84.- Induced inflow velocity measured at 120 degrees and r/R of 0.90.

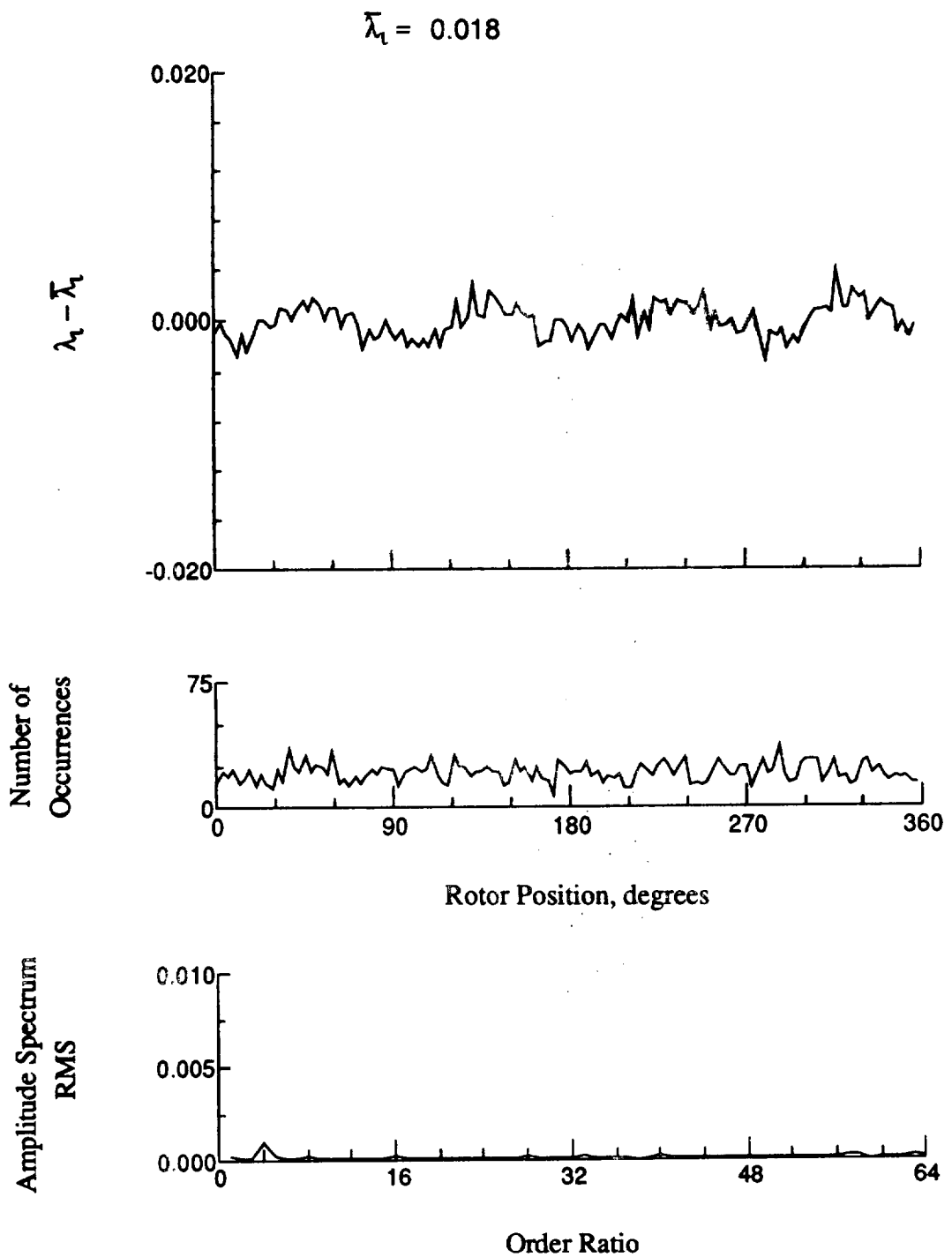


Figure 84.- Concluded.

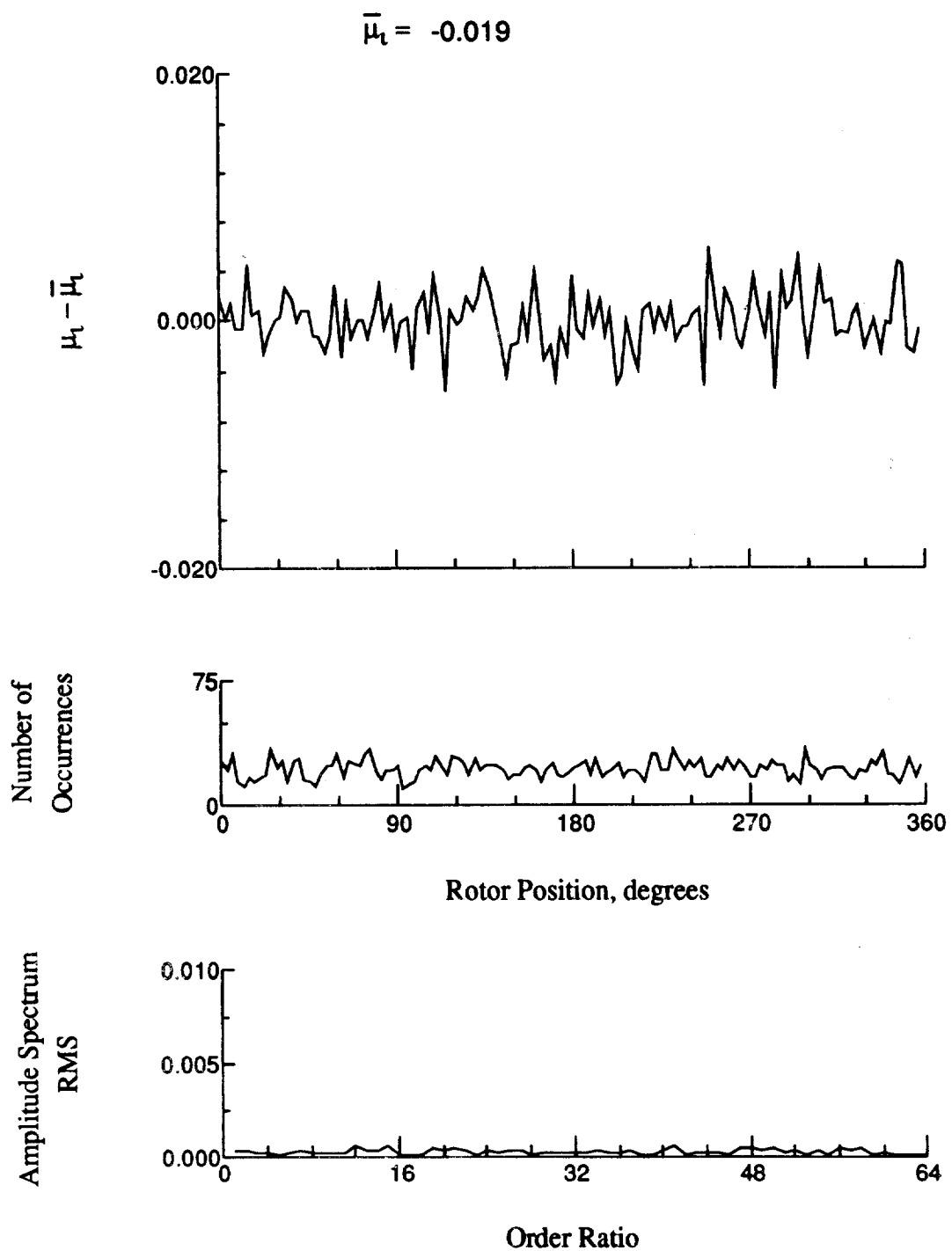


Figure 85.- Induced inflow velocity measured at 120 degrees and r/R of 0.94.

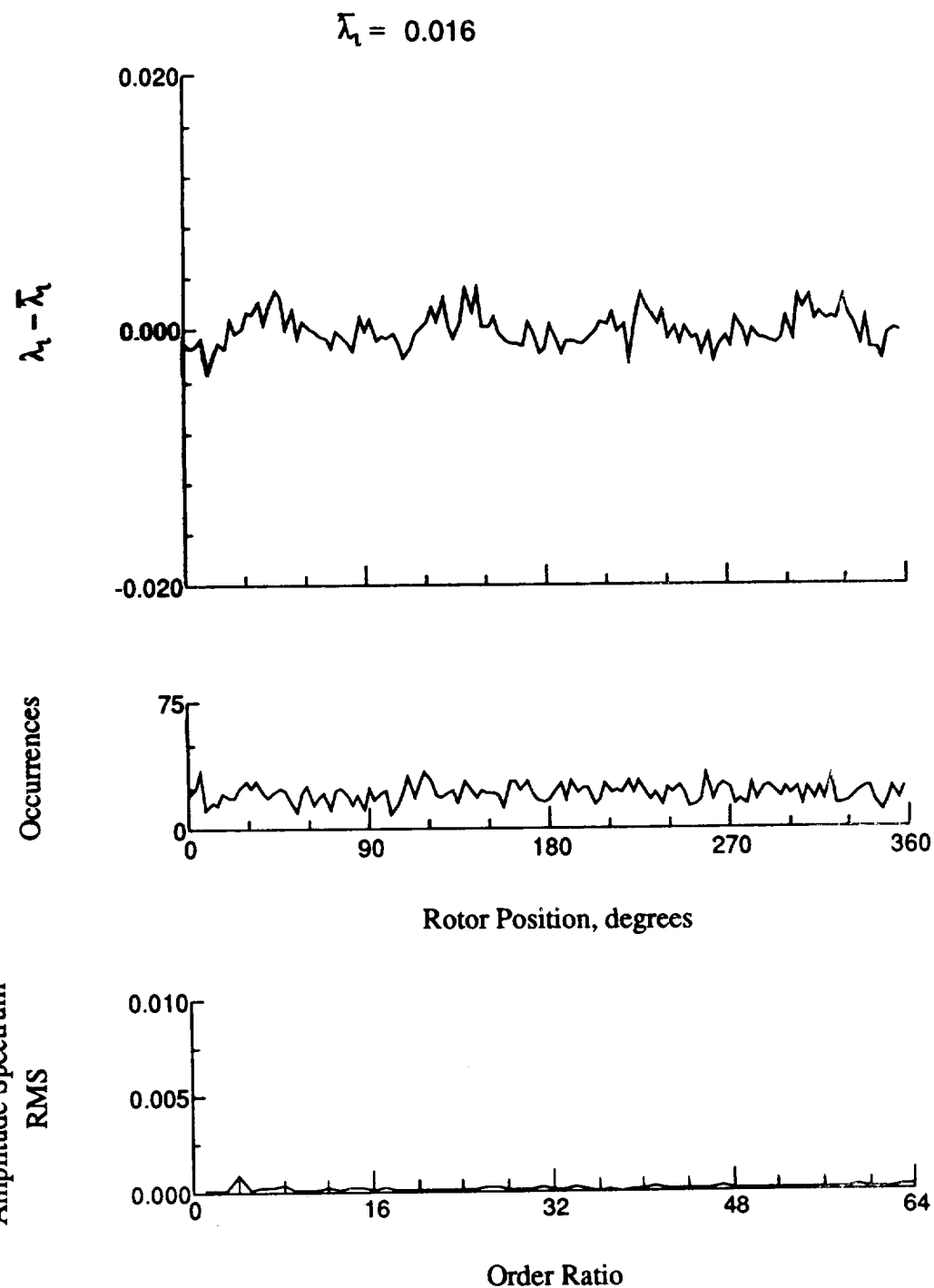


Figure 85.- Concluded.

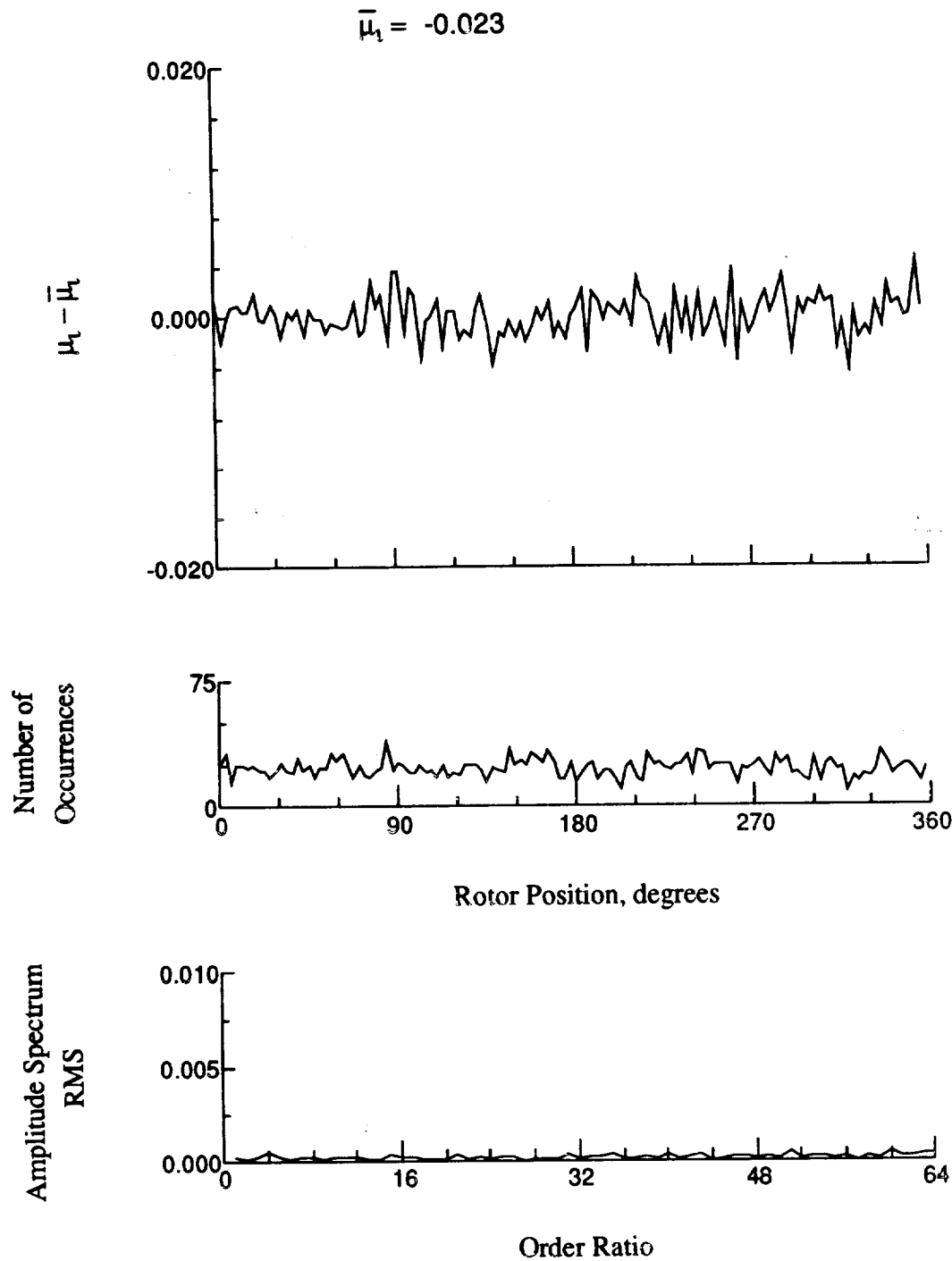


Figure 86.- Induced inflow velocity measured at 120 degrees and r/R of 0.96.

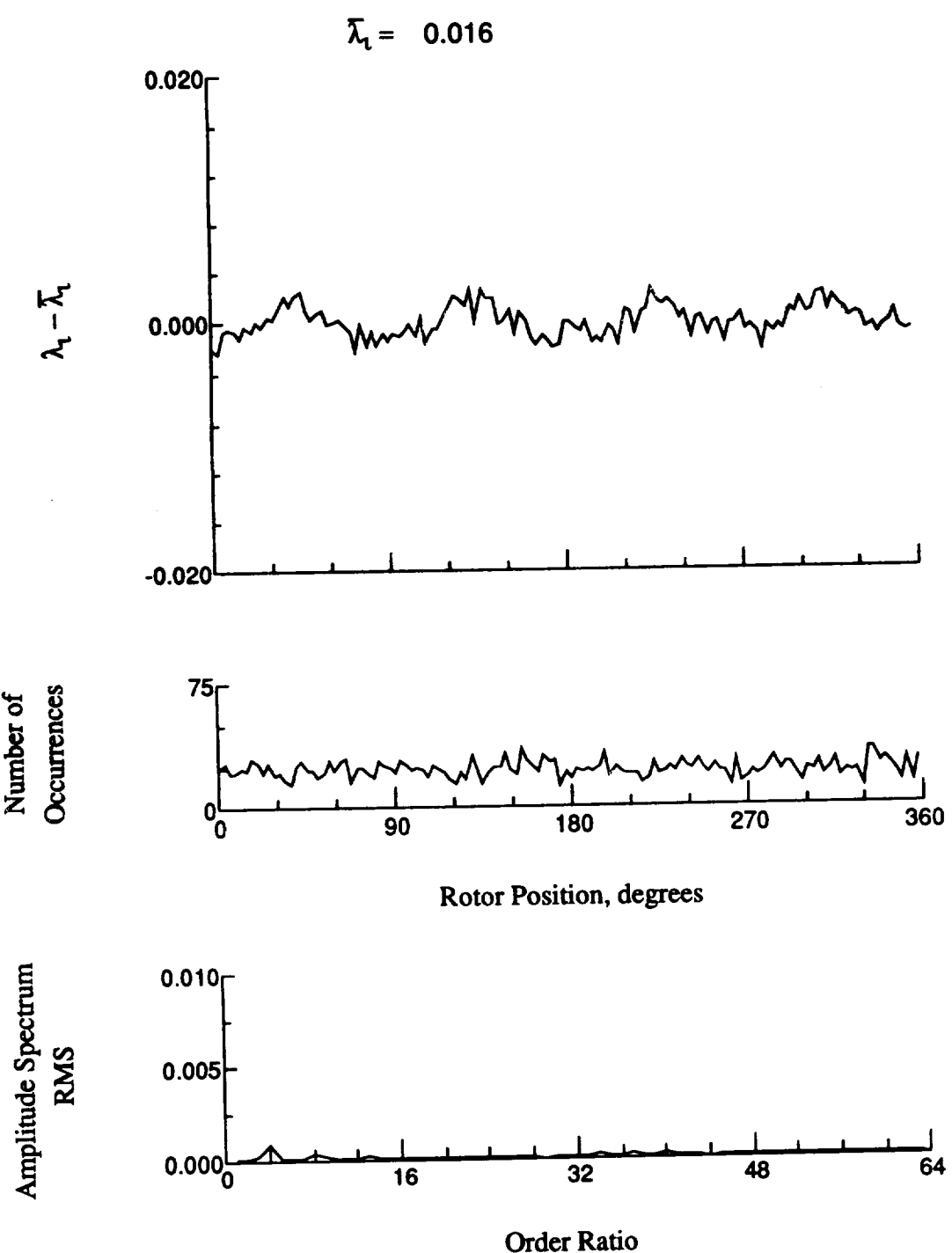


Figure 86.- Concluded.

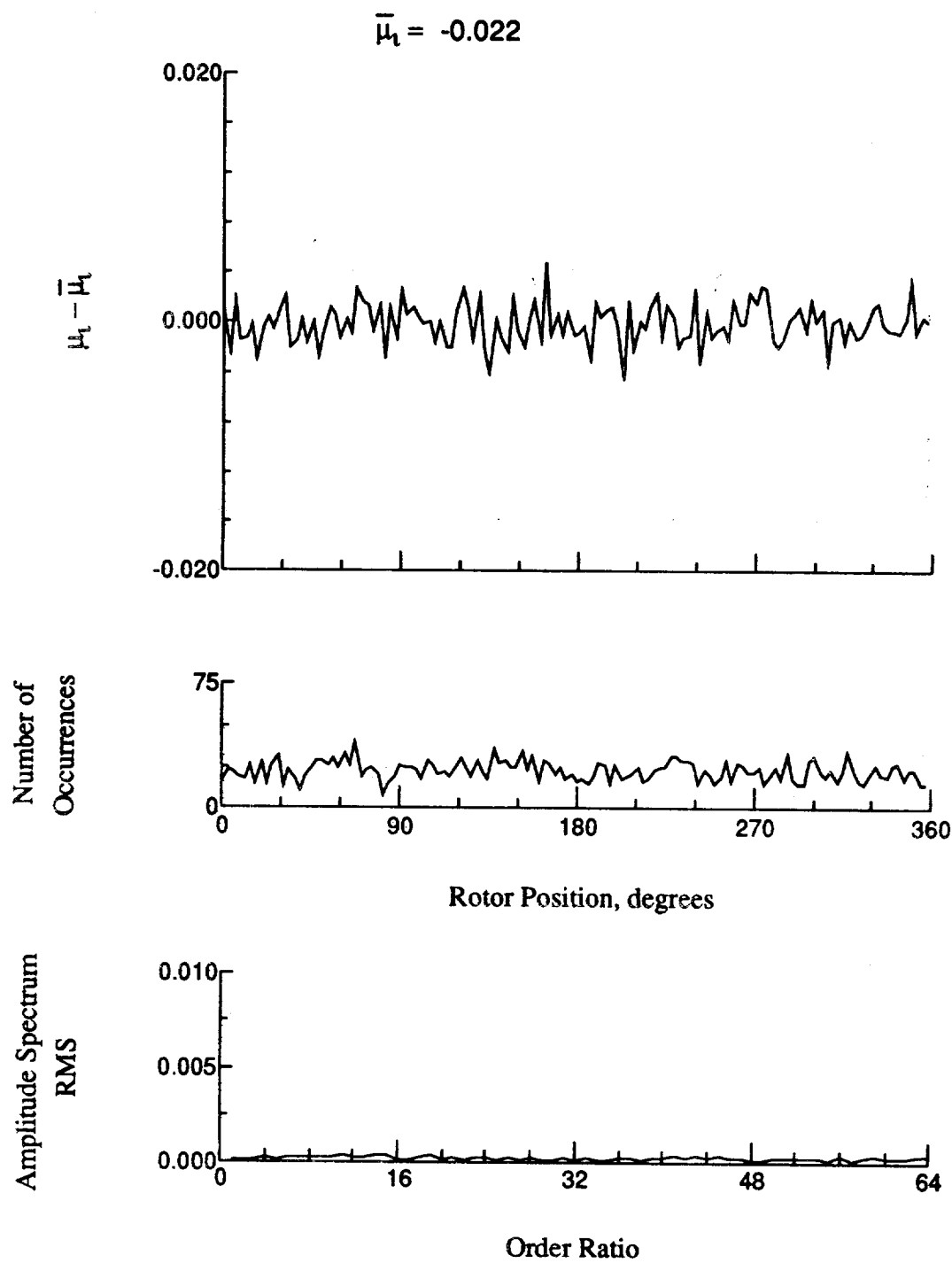


Figure 87.- Induced inflow velocity measured at 120 degrees and r/R of 1.00.

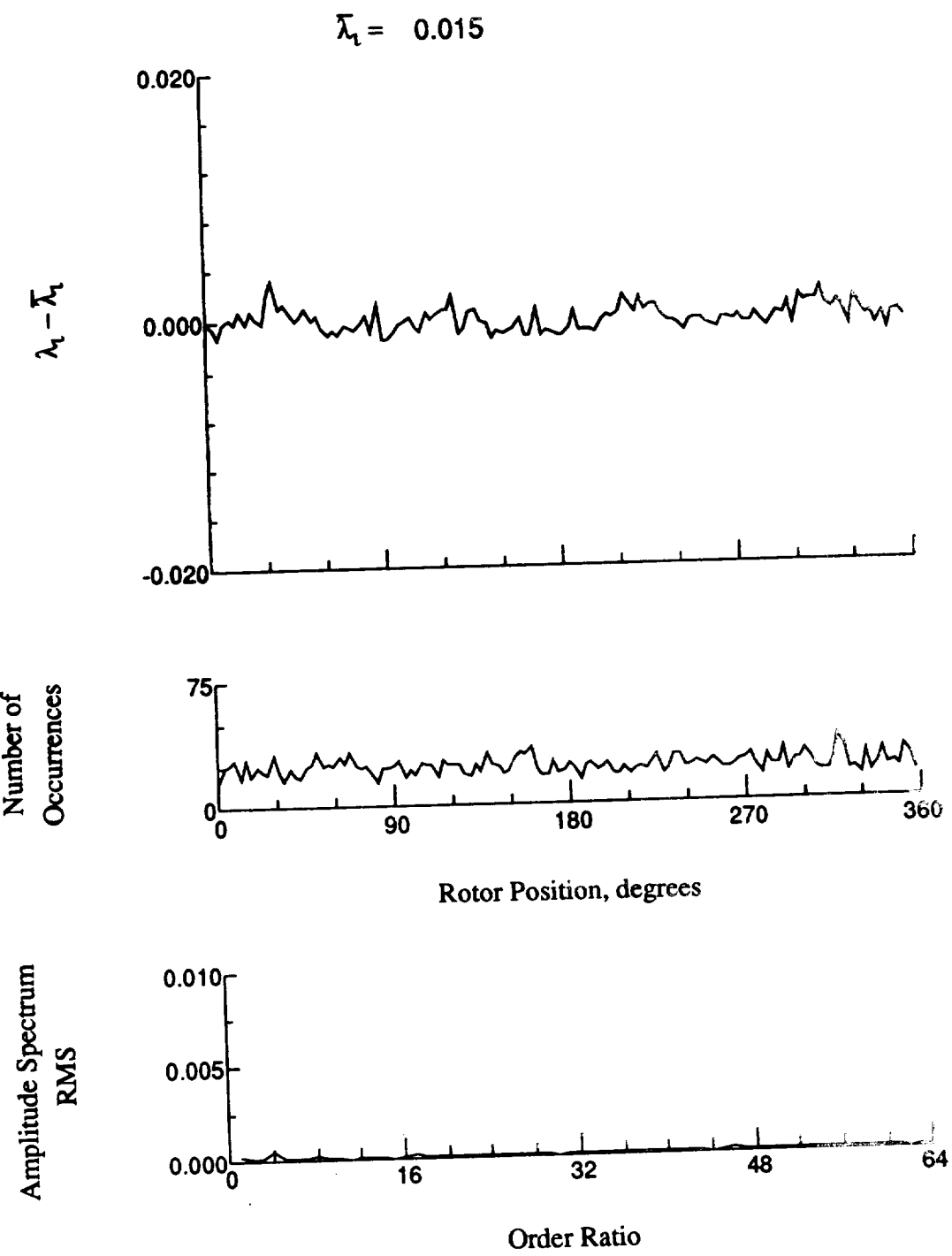


Figure 87.- Concluded.

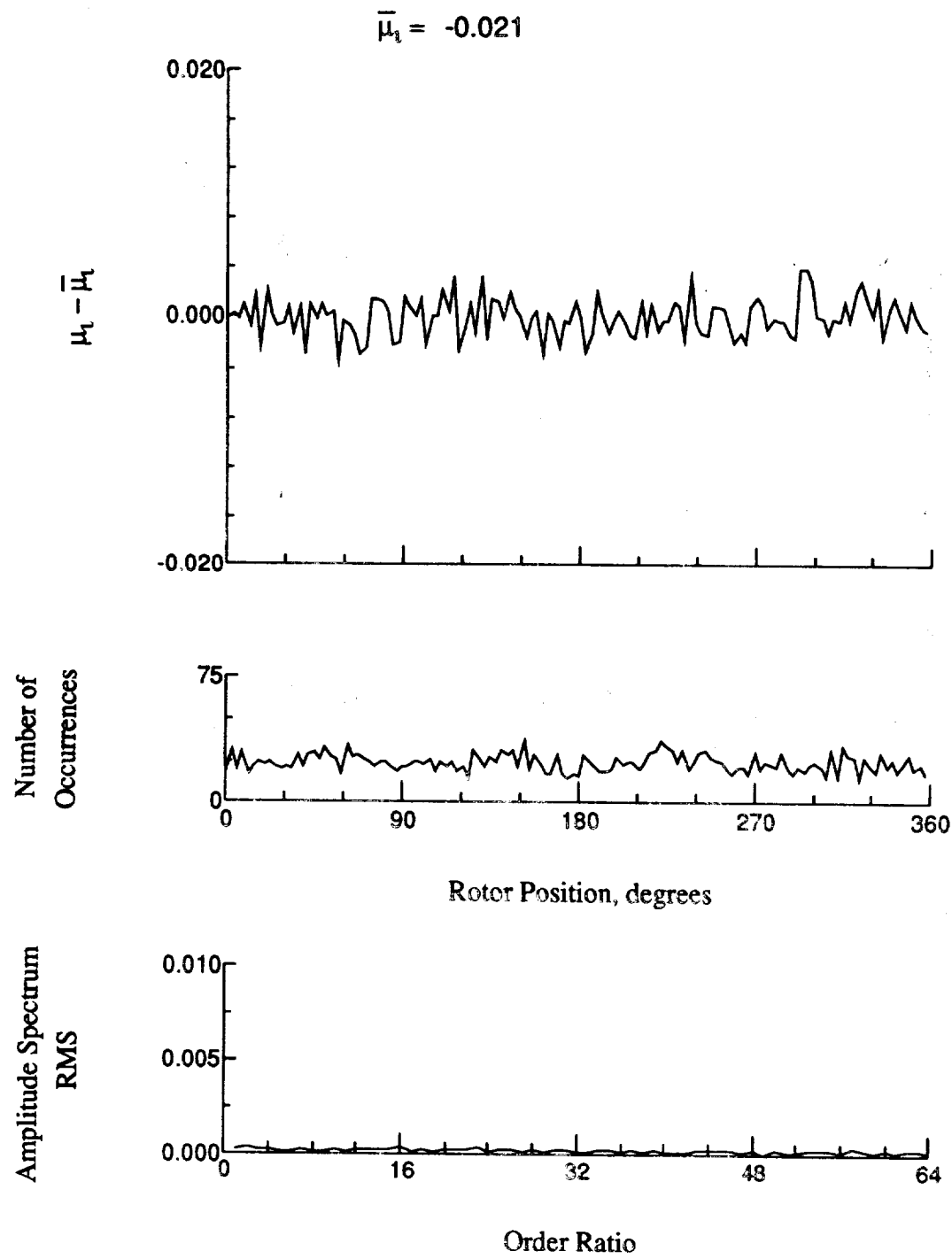


Figure 88.- Induced inflow velocity measured at 120 degrees and r/R of 1.10.

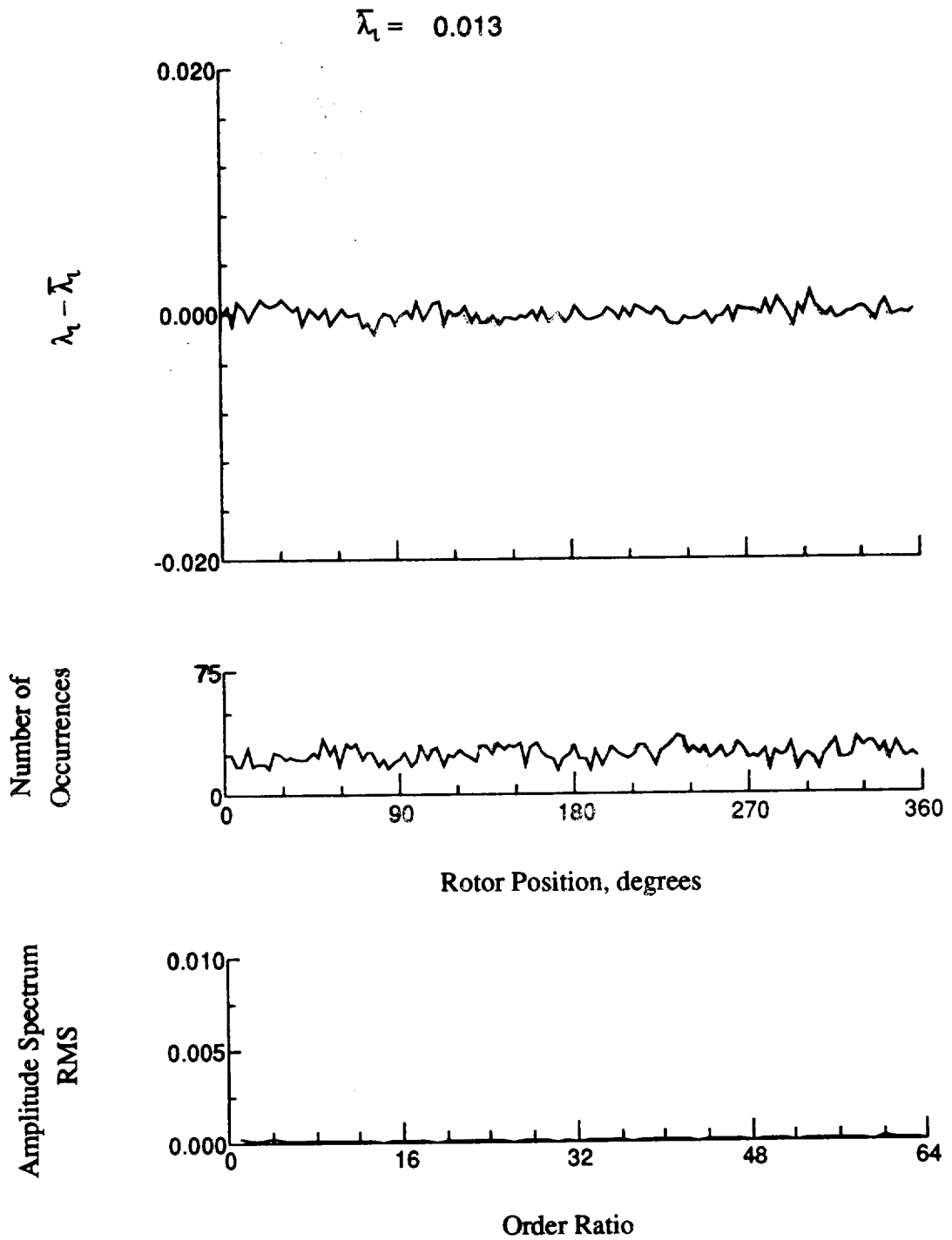


Figure 88.- Concluded.

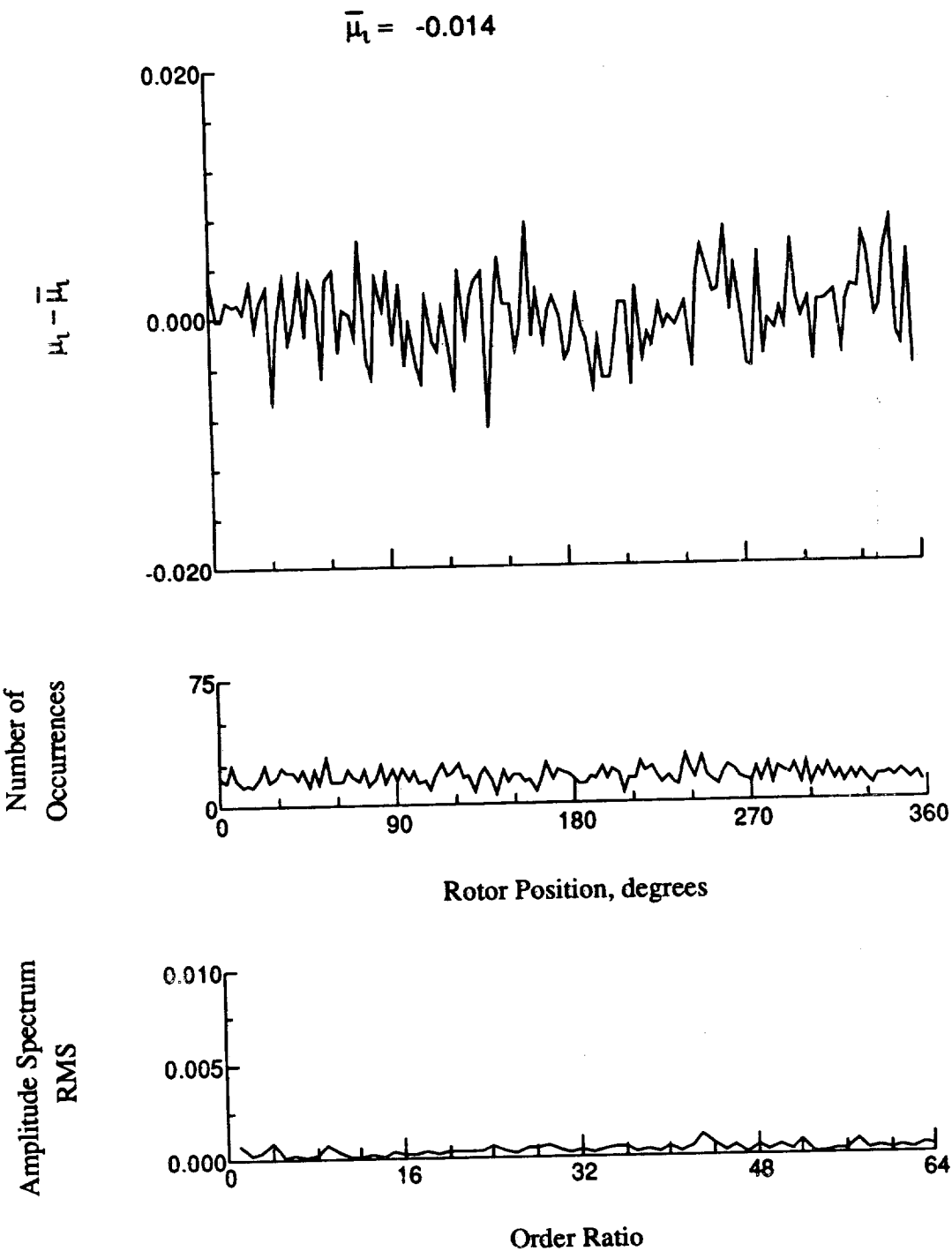


Figure 89.- Induced inflow velocity measured at 150 degrees and r/R of 0.20.

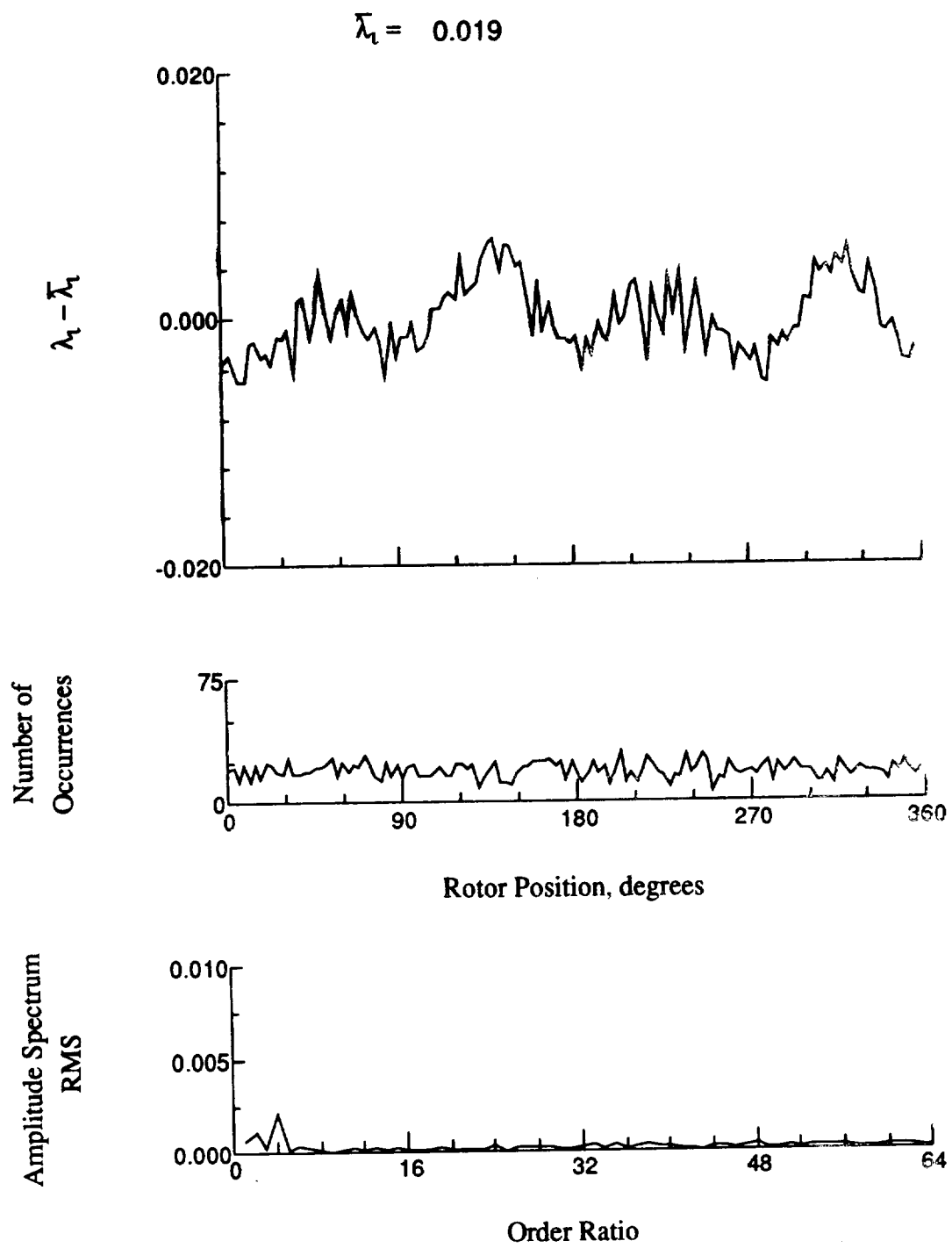


Figure 89.- Concluded.

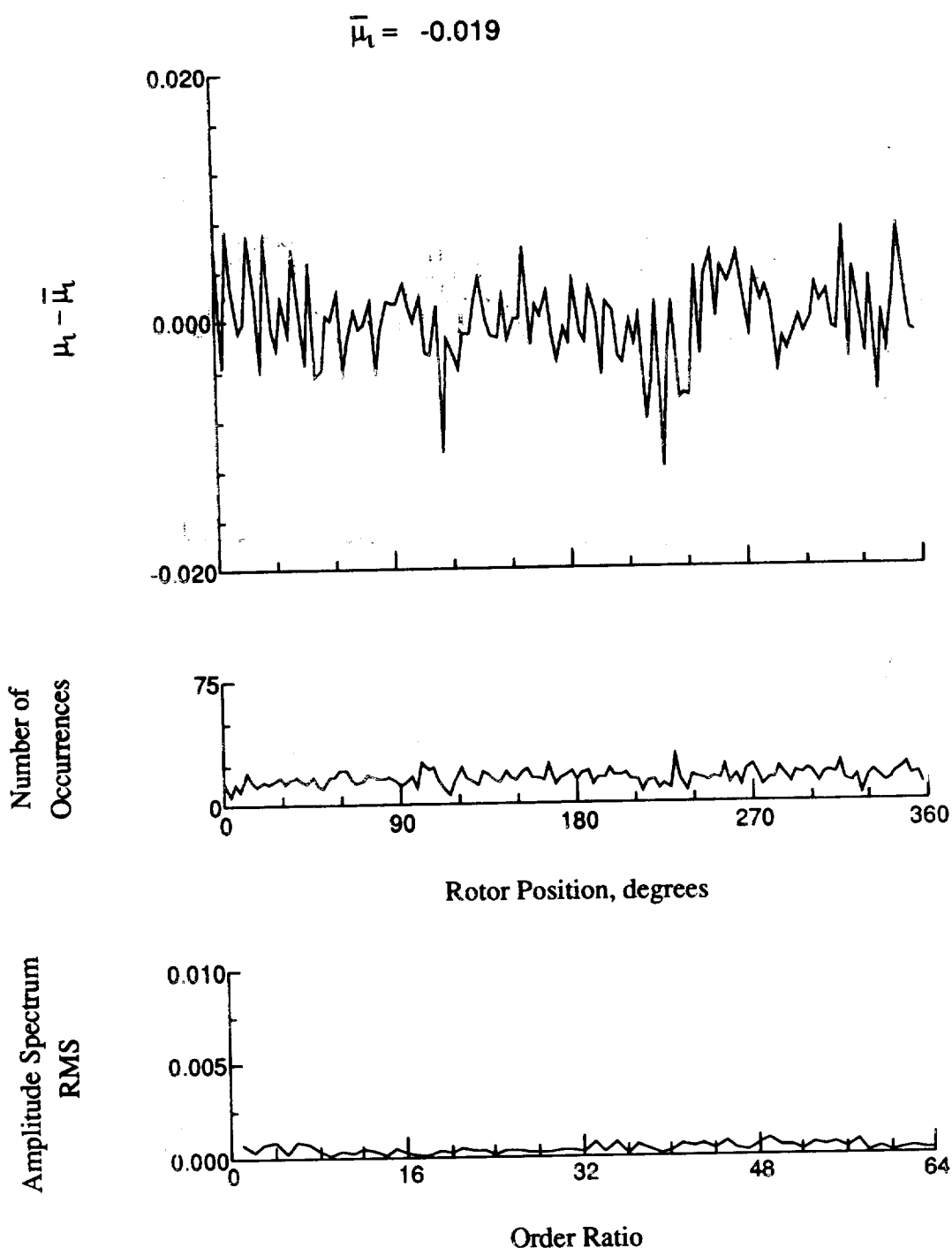


Figure 90.- Induced inflow velocity measured at 150 degrees and r/R of 0.32.

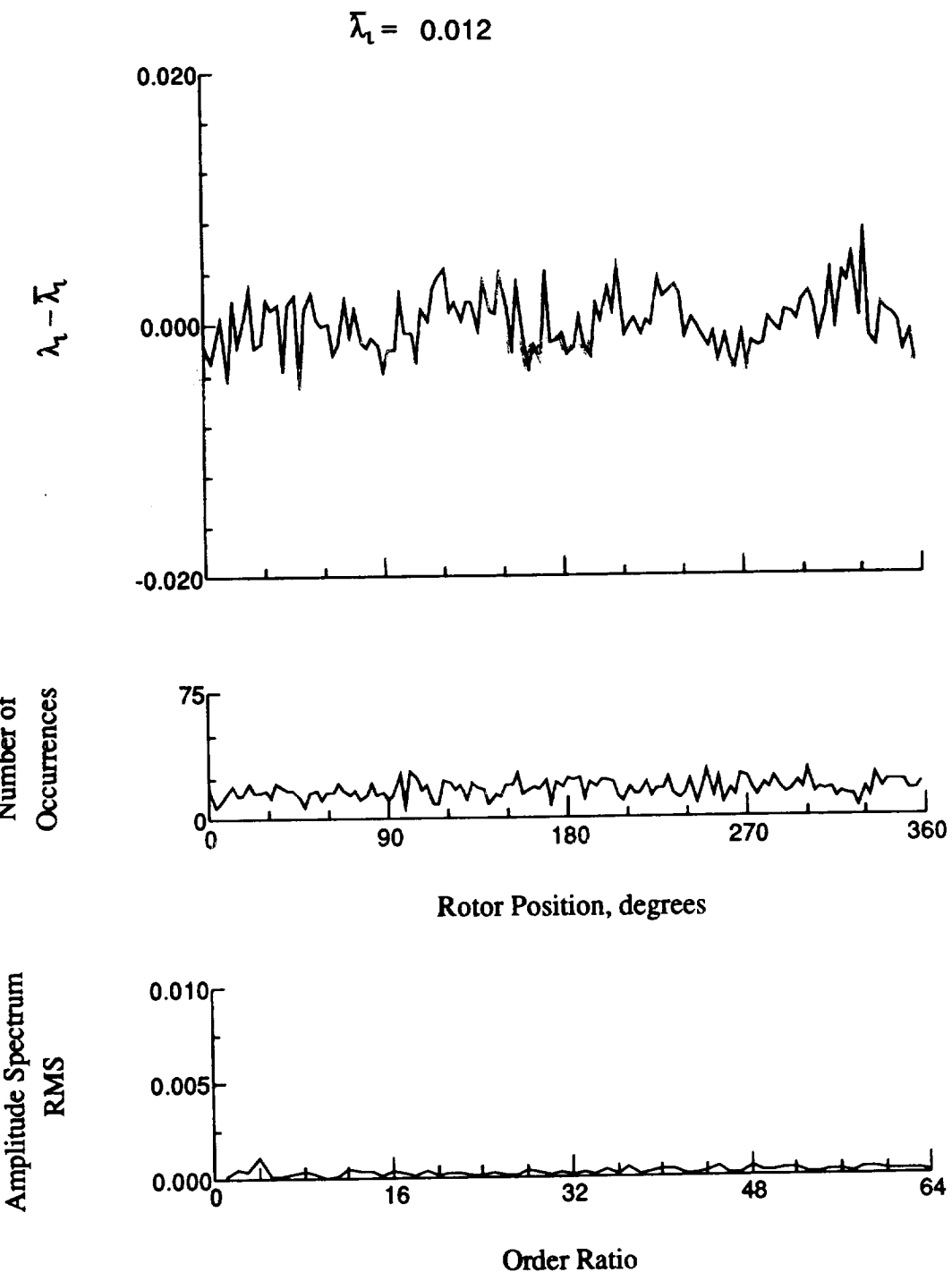


Figure 90.- Concluded.

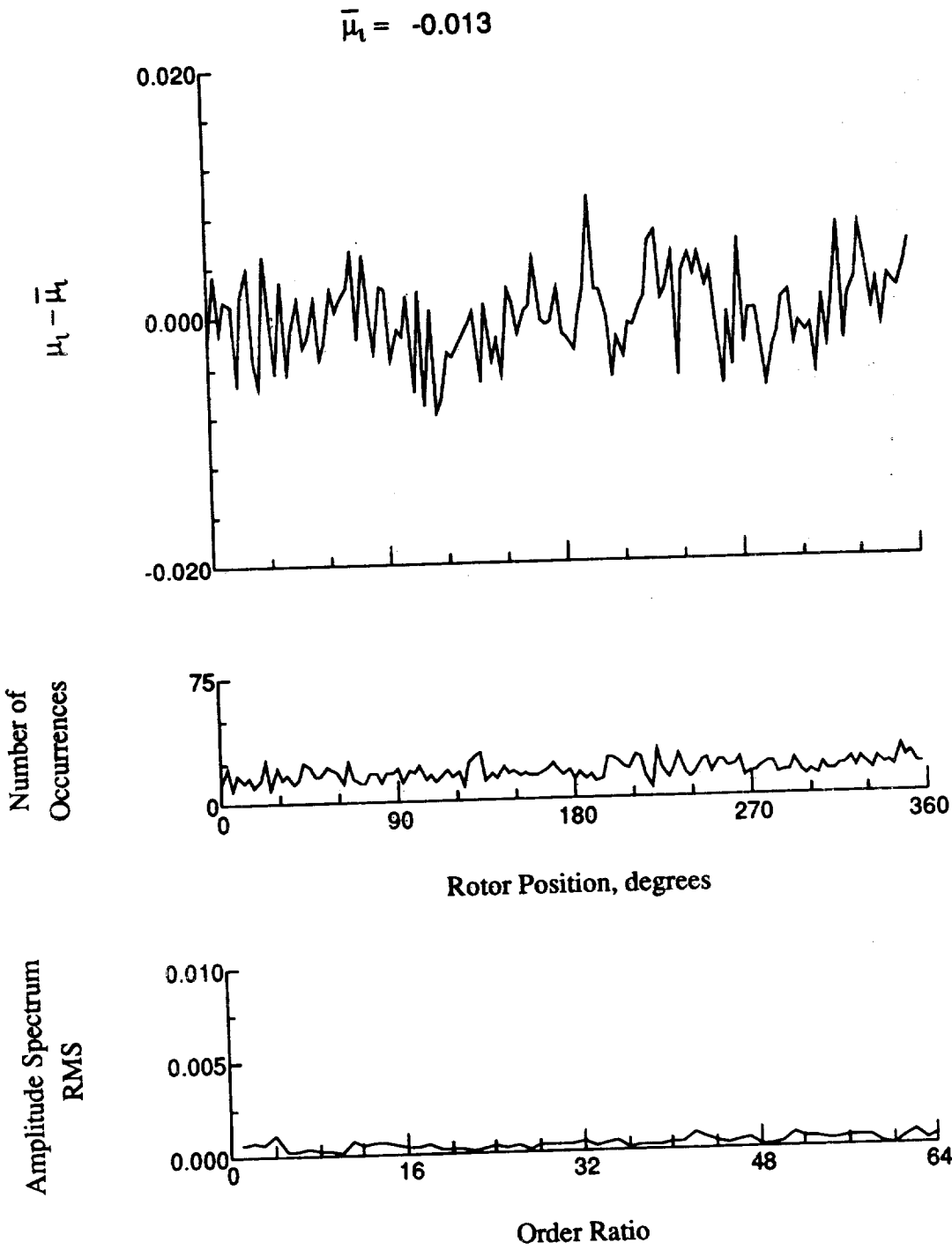


Figure 91.- Induced inflow velocity measured at 150 degrees and r/R of 0.50.

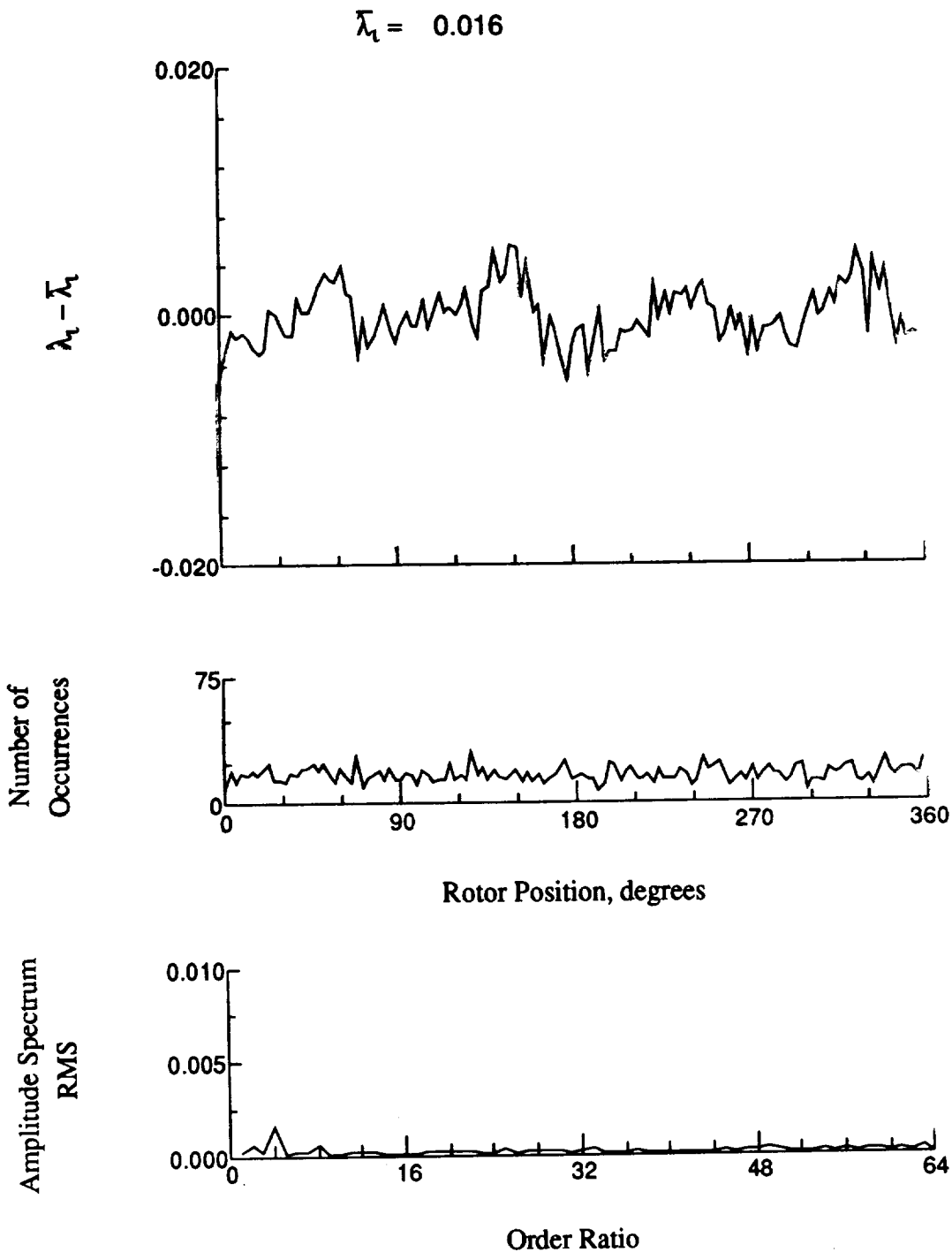


Figure 91.- Concluded.

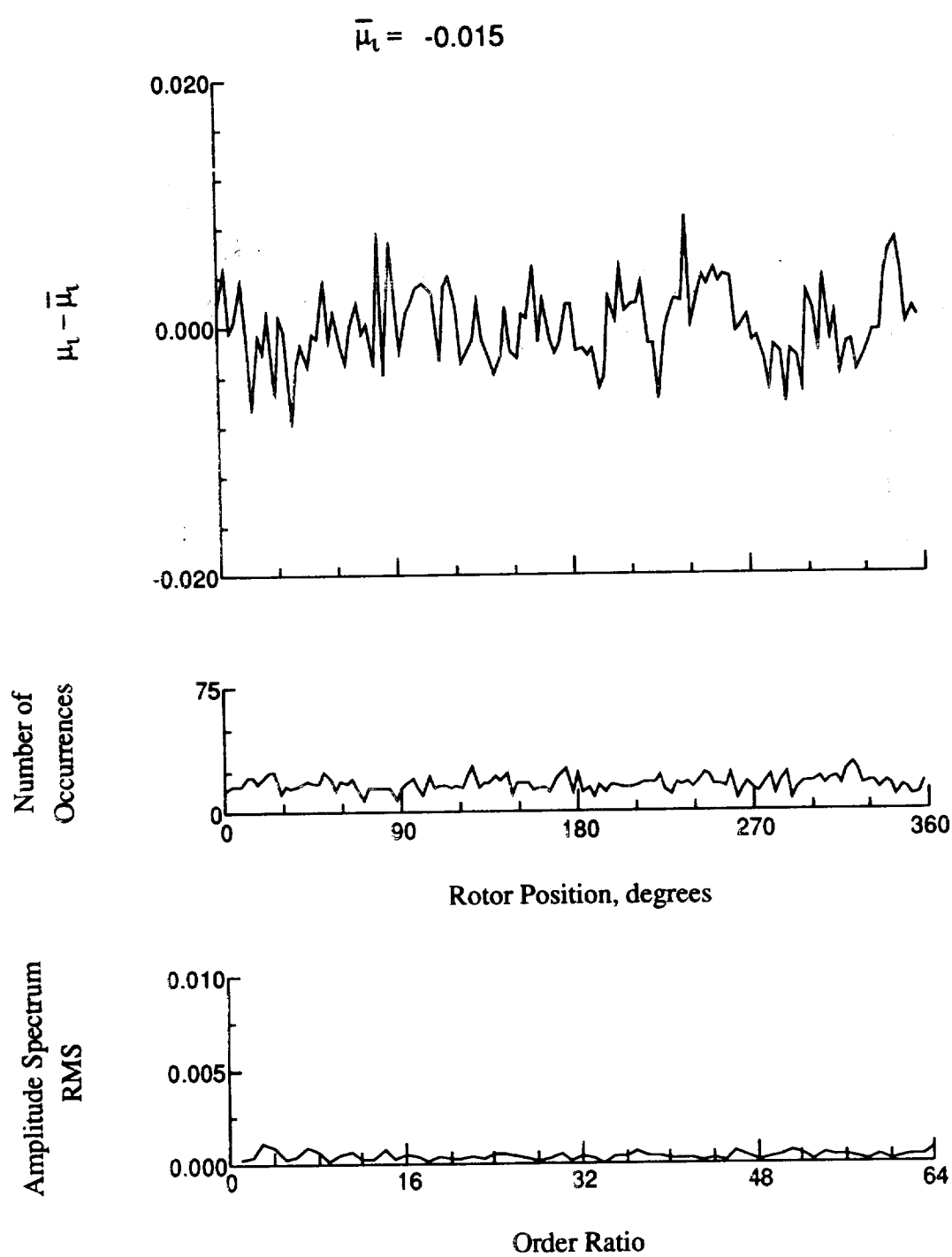


Figure 92.- Induced inflow velocity measured at 150 degrees and r/R of 0.58.

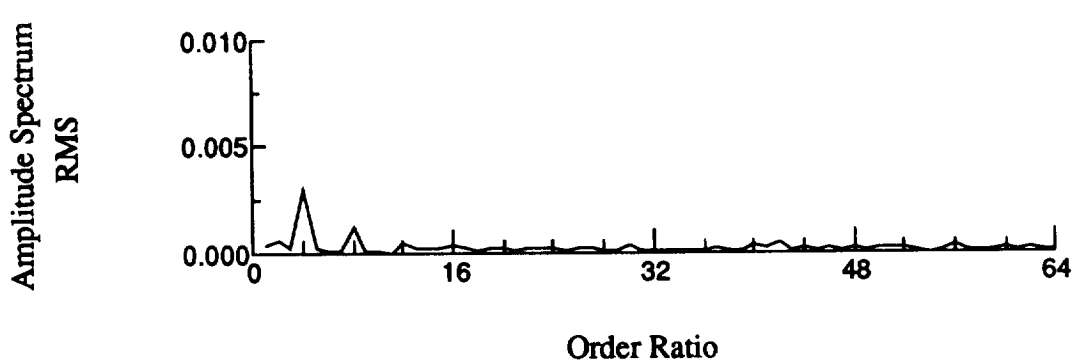
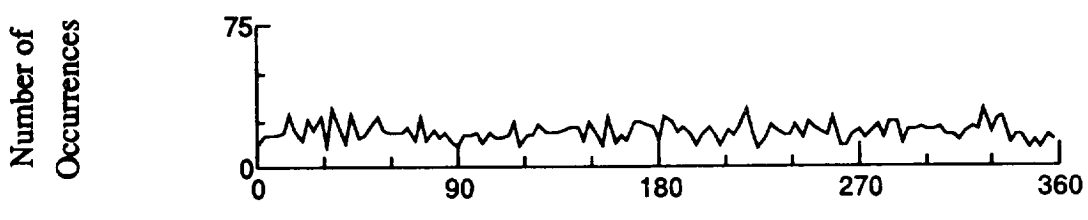
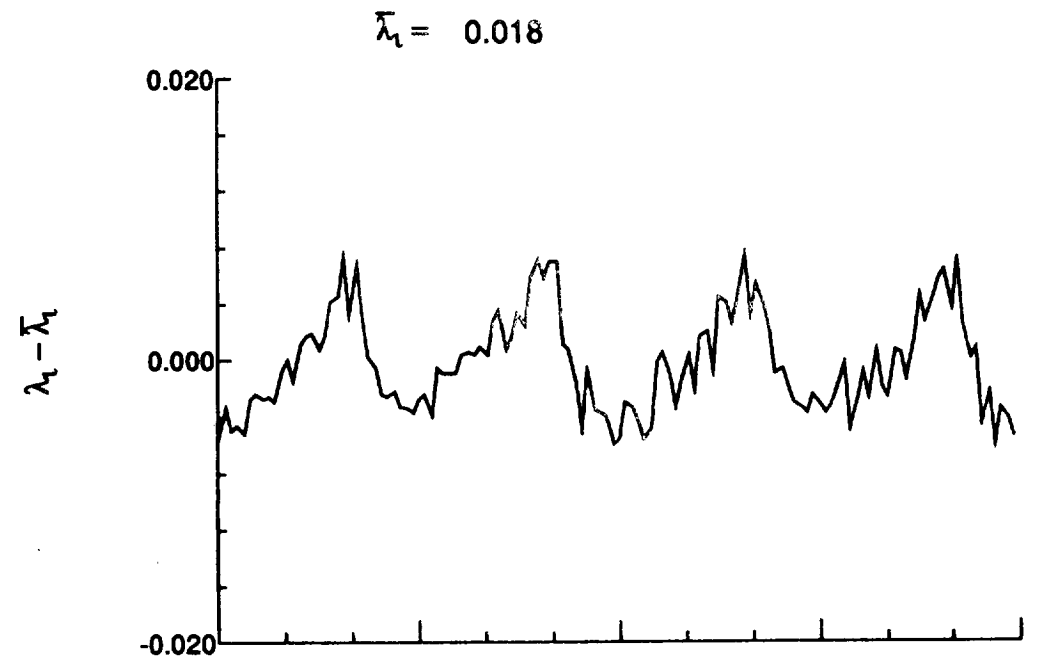


Figure 92.- Concluded.

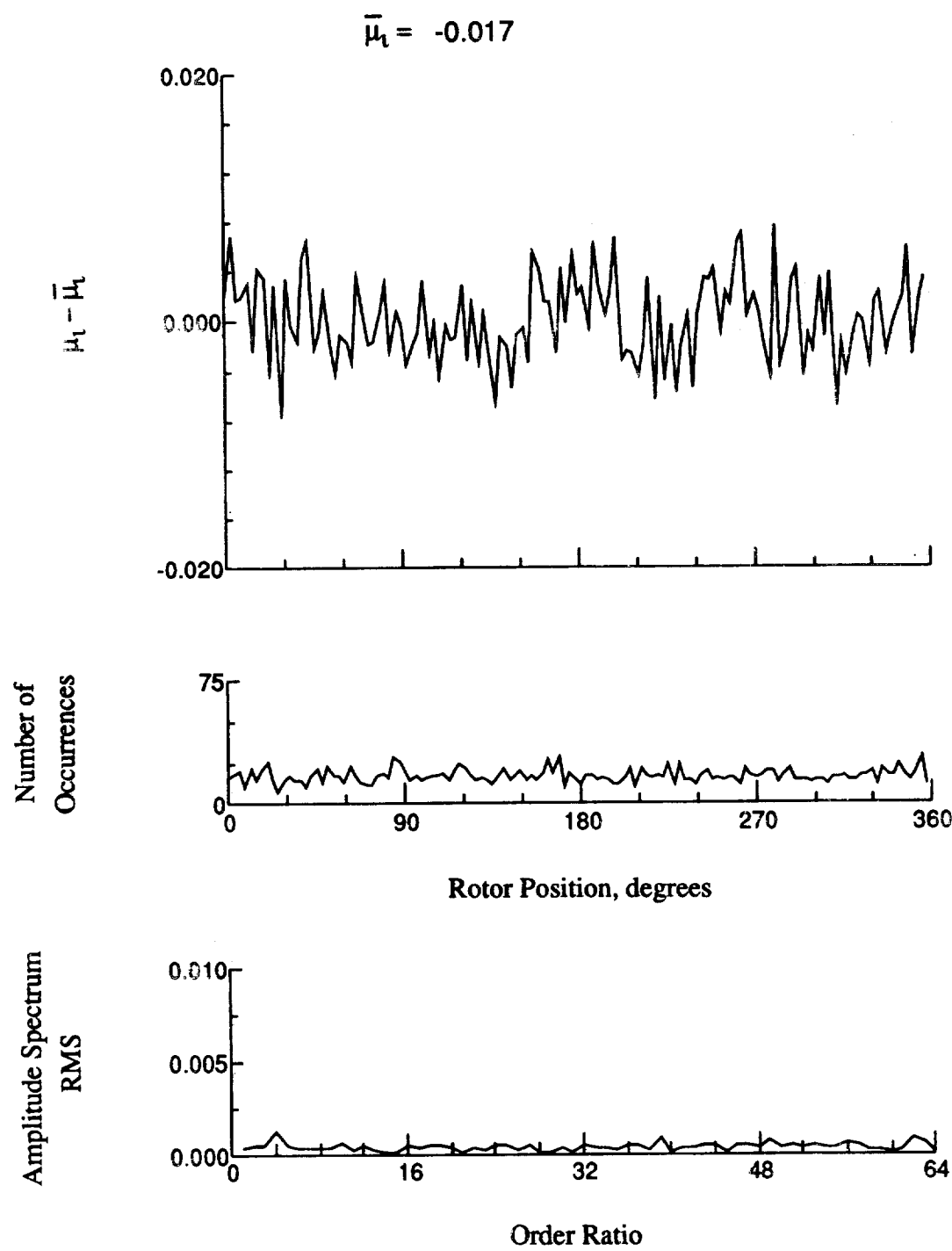


Figure 93.- Induced inflow velocity measured at 150 degrees and r/R of 0.69.

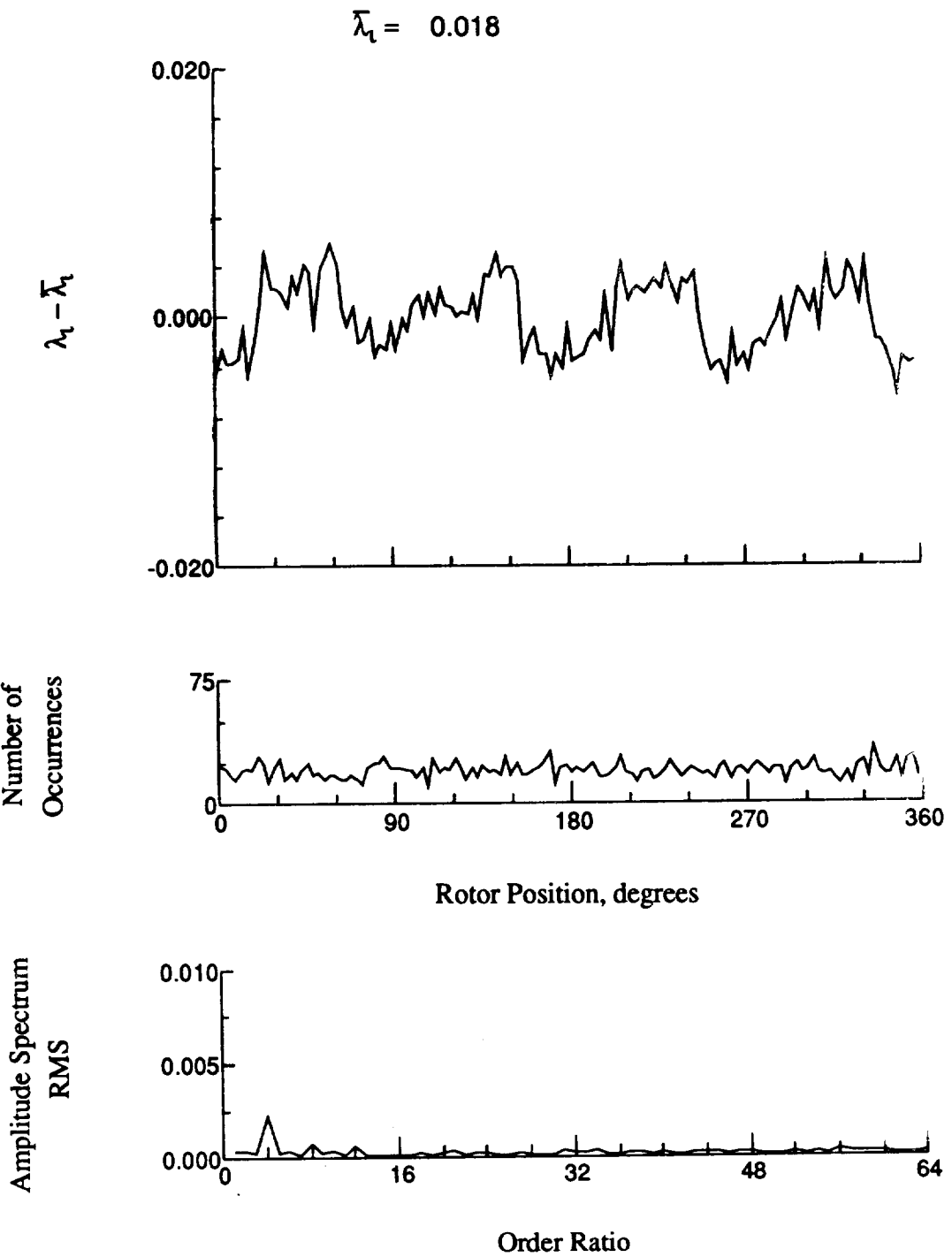


Figure 93.- Concluded.

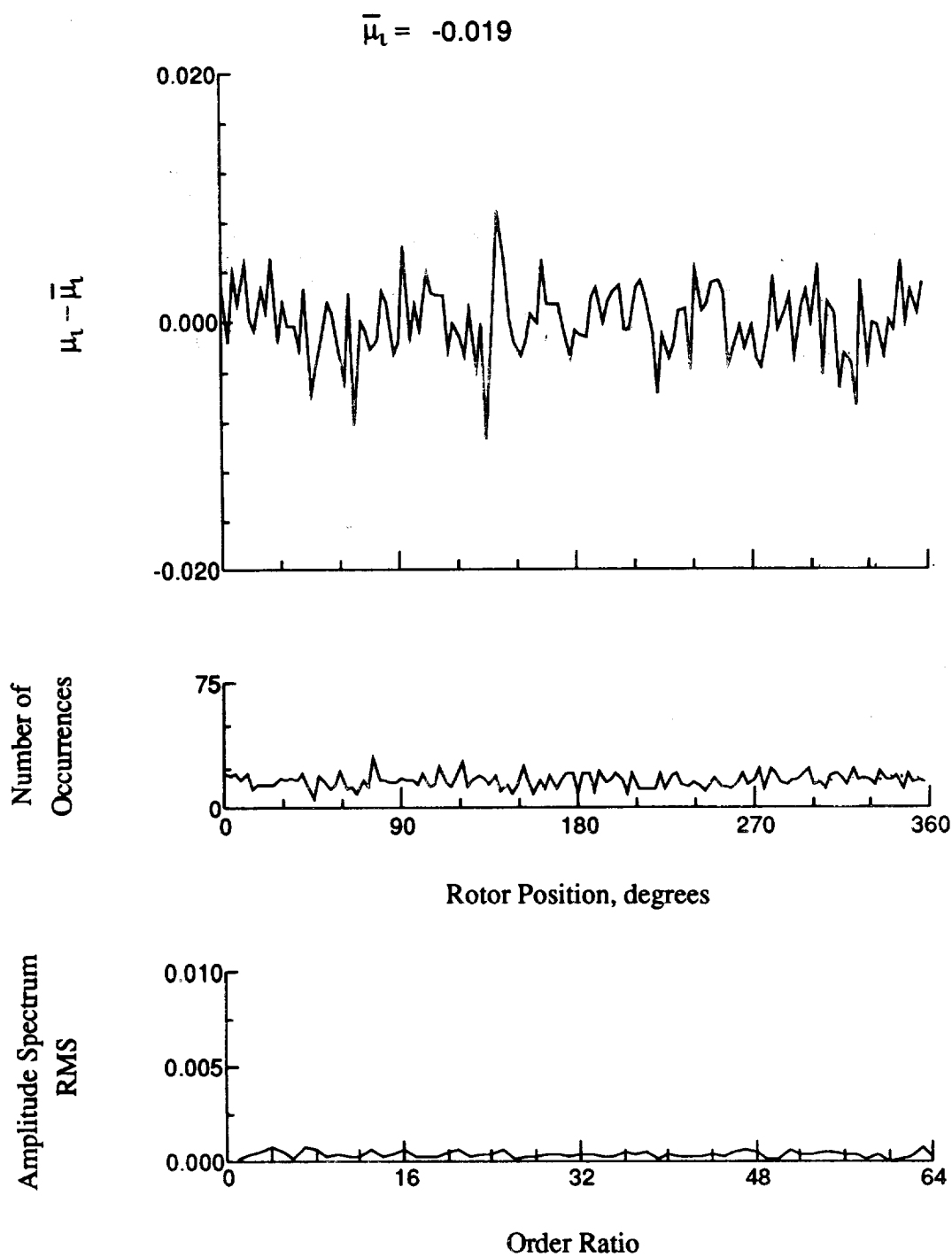


Figure 94.- Induced inflow velocity measured at 150 degrees and r/R of 0.73.

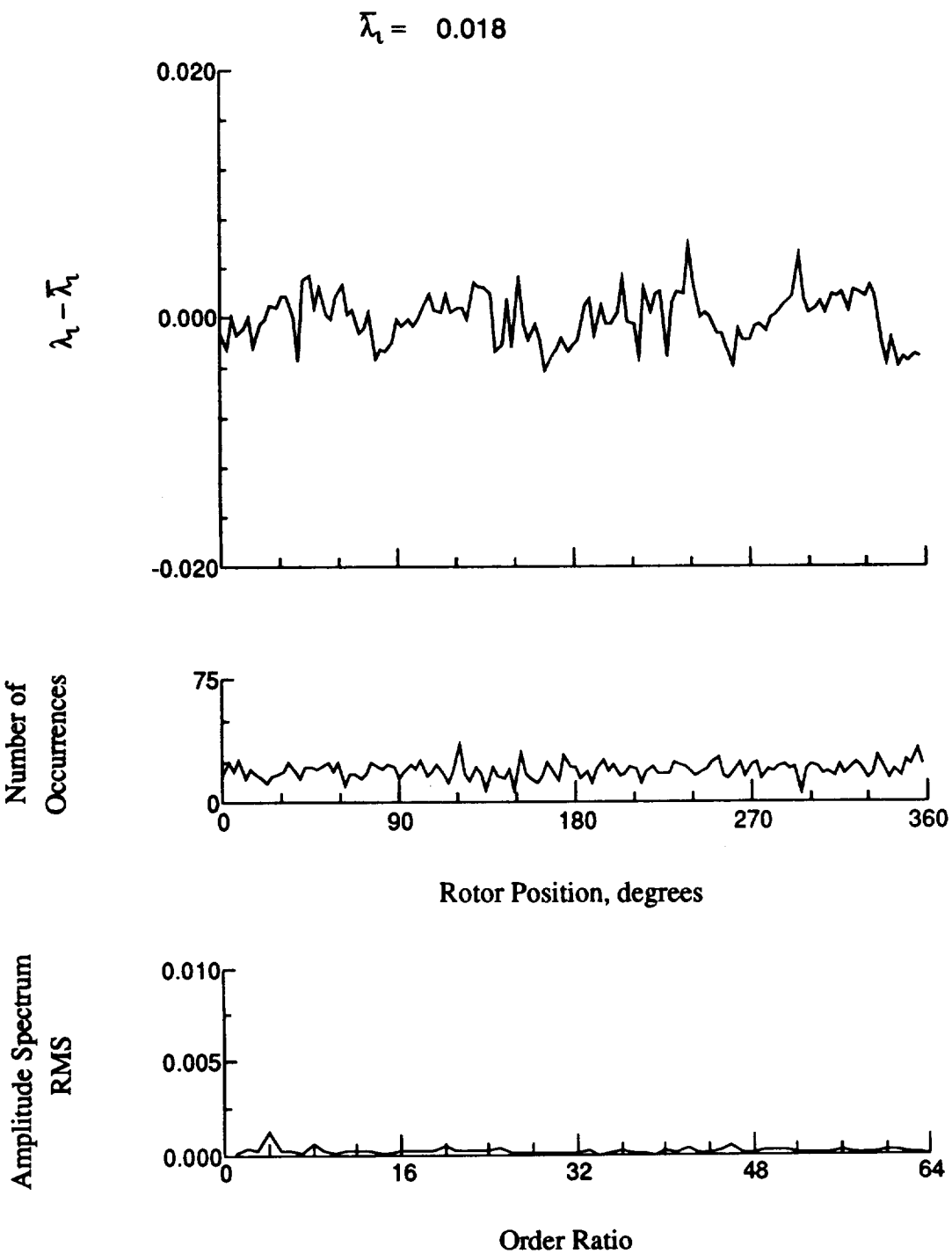


Figure 94.- Concluded.

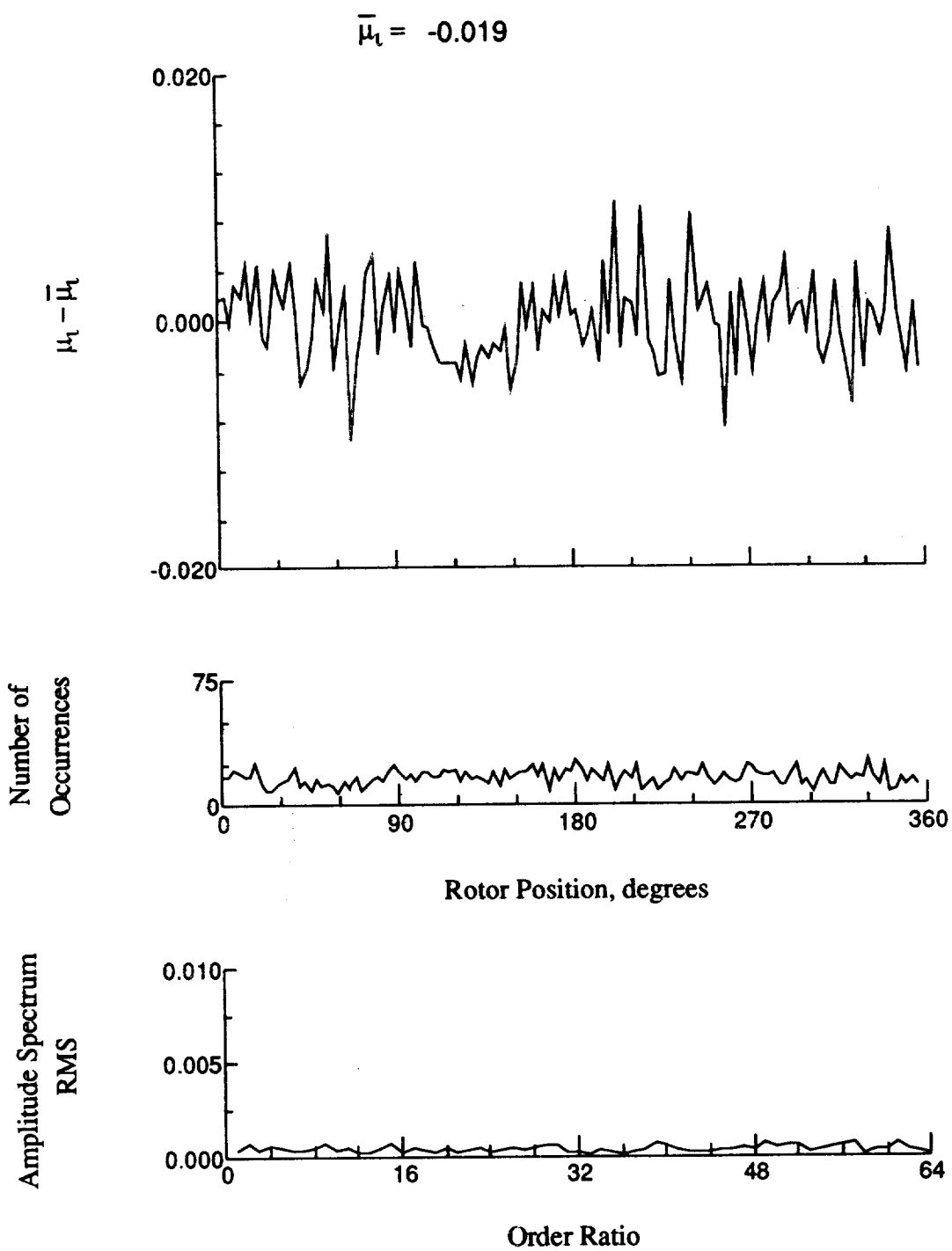


Figure 95.- Induced inflow velocity measured at 150 degrees and r/R of 0.75.

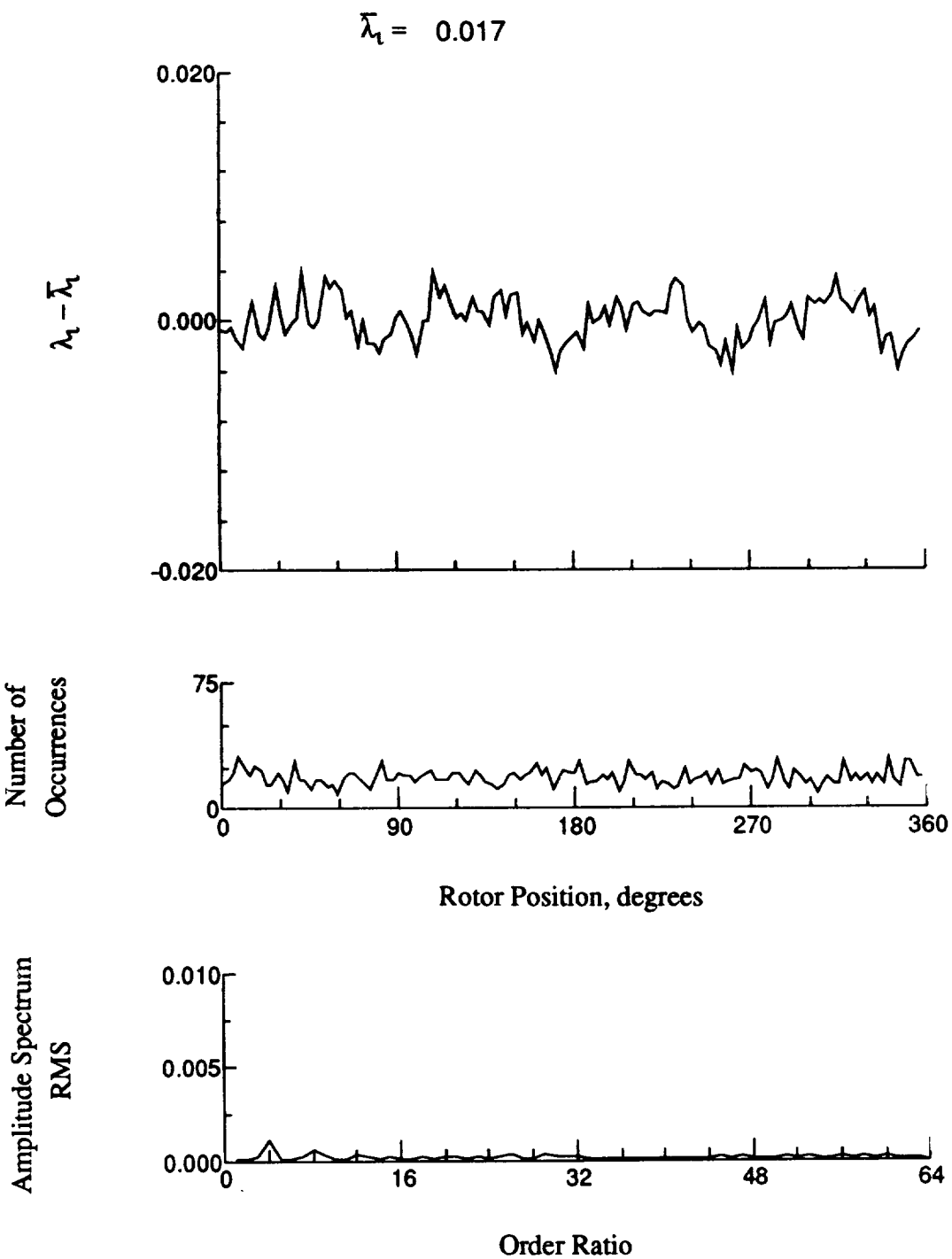


Figure 95.- Concluded.

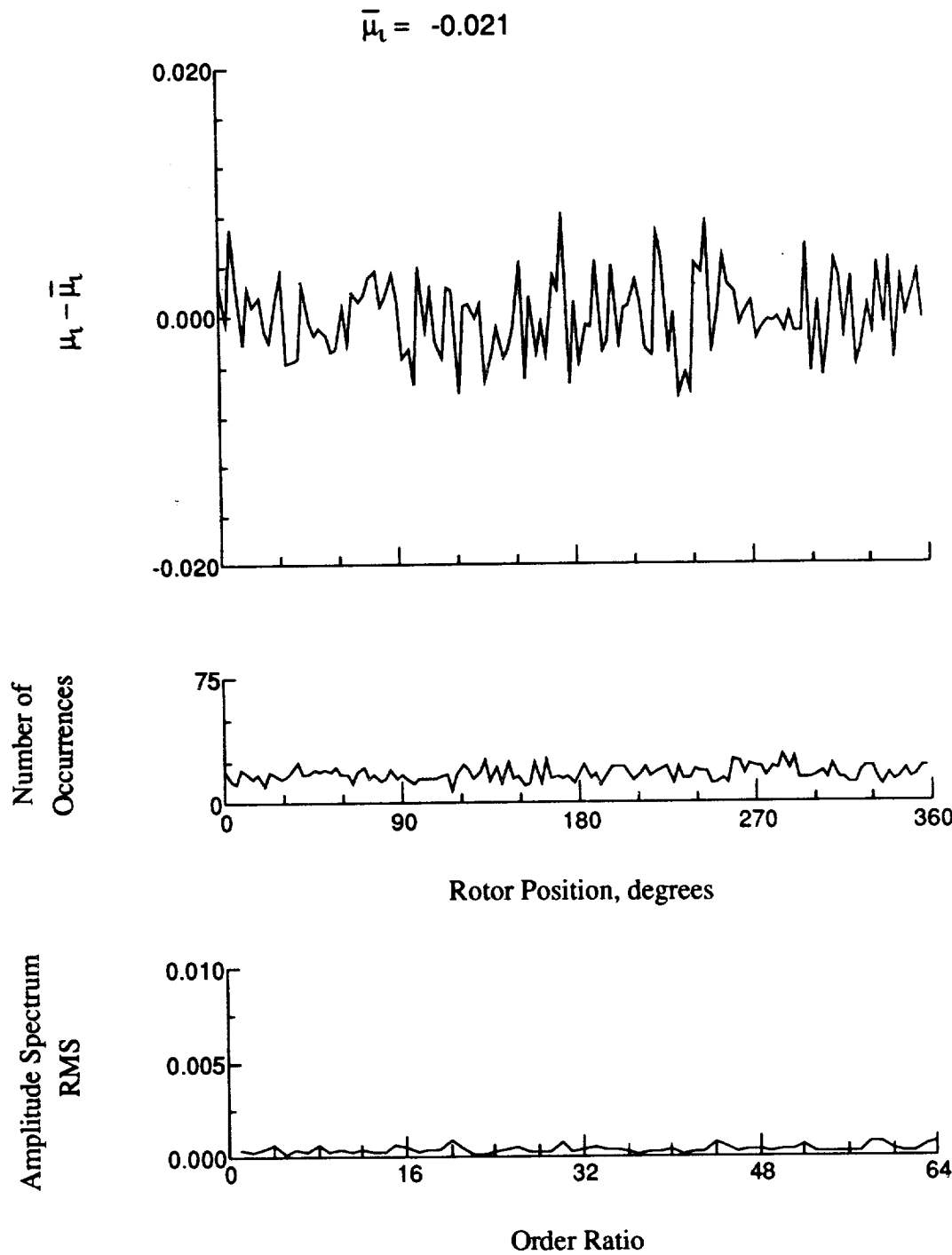


Figure 96.- Induced inflow velocity measured at 150 degrees and r/R of 0.81.

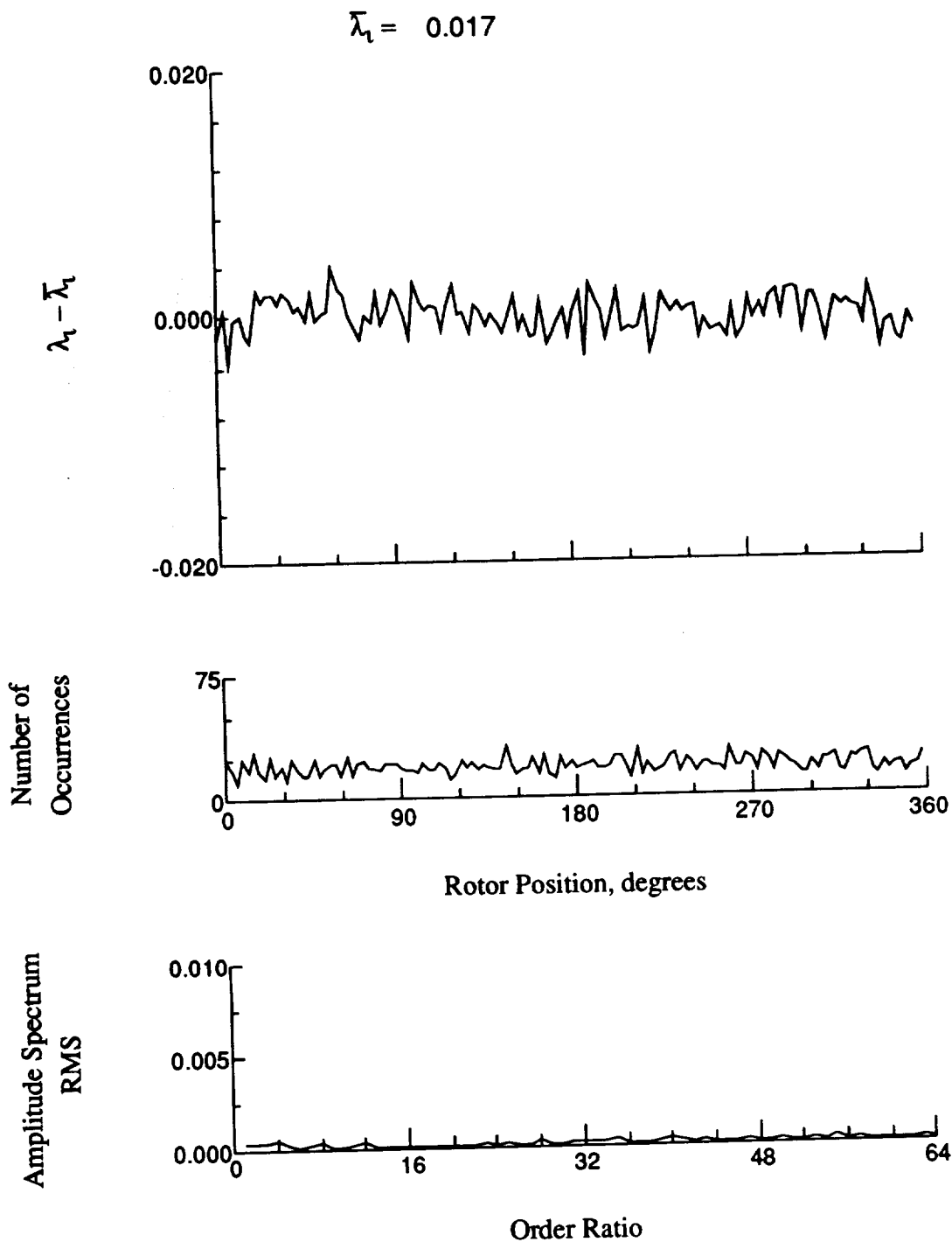


Figure 96.- Concluded.

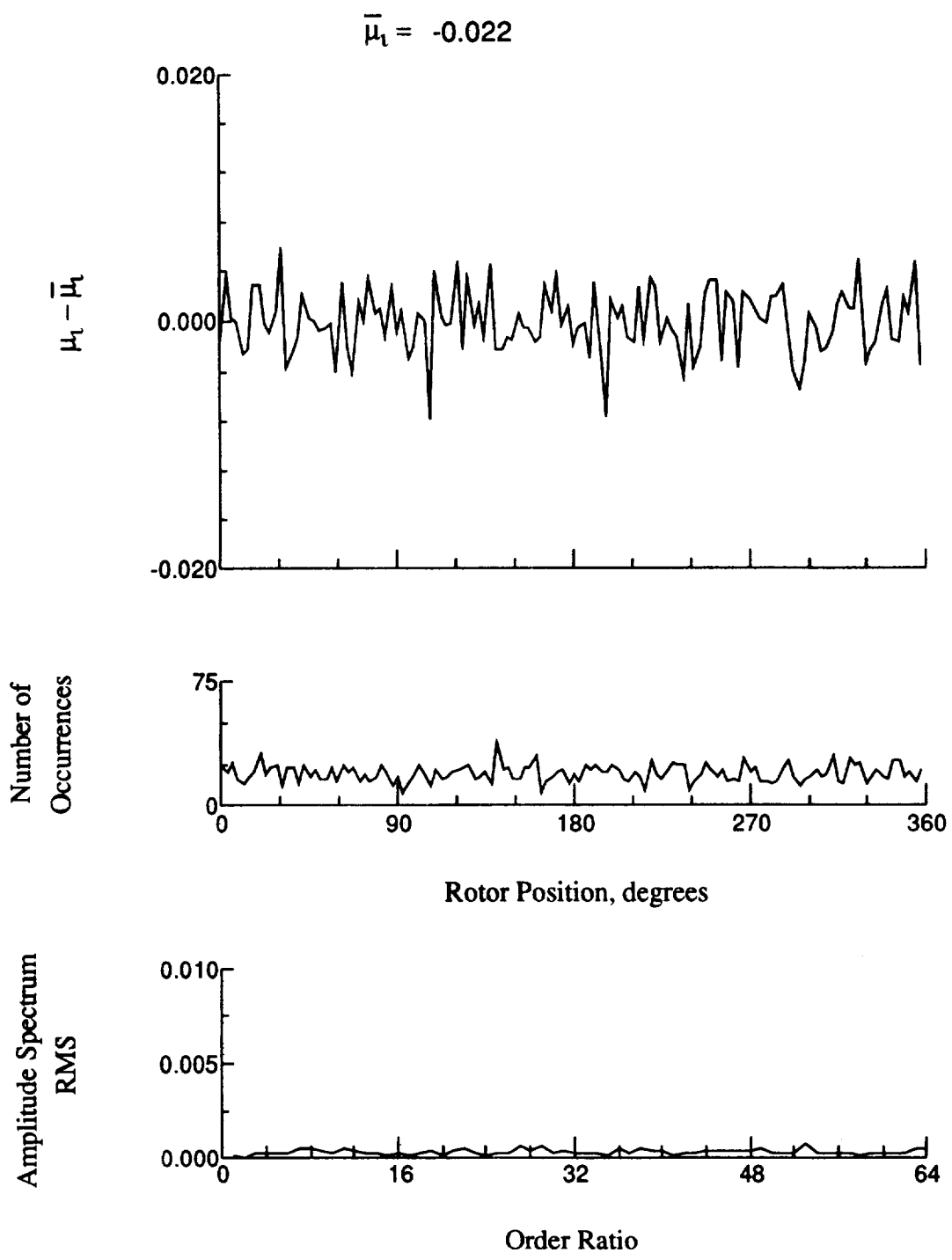


Figure 97.- Induced inflow velocity measured at 150 degrees and r/R of 0.86.

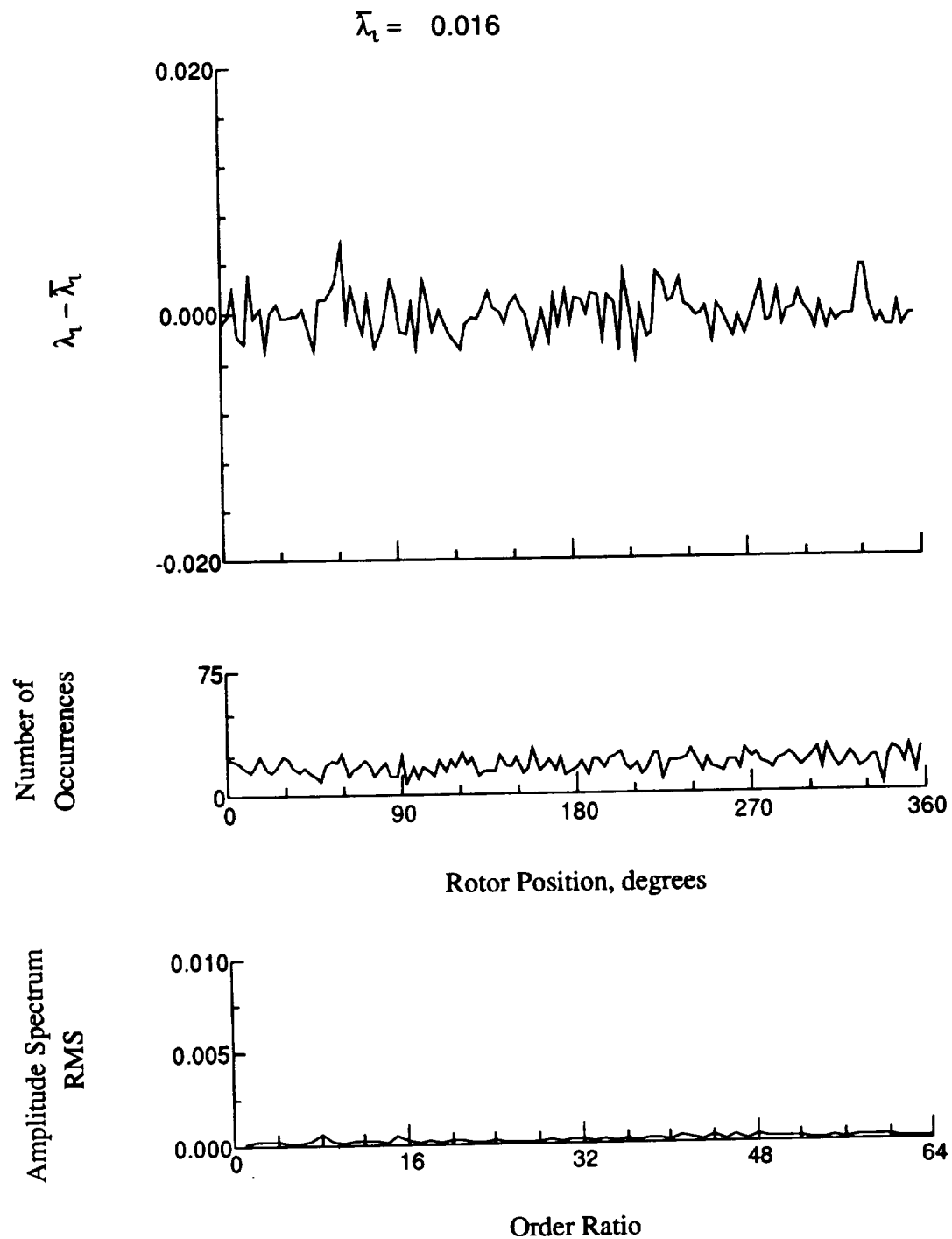


Figure 97.- Concluded.

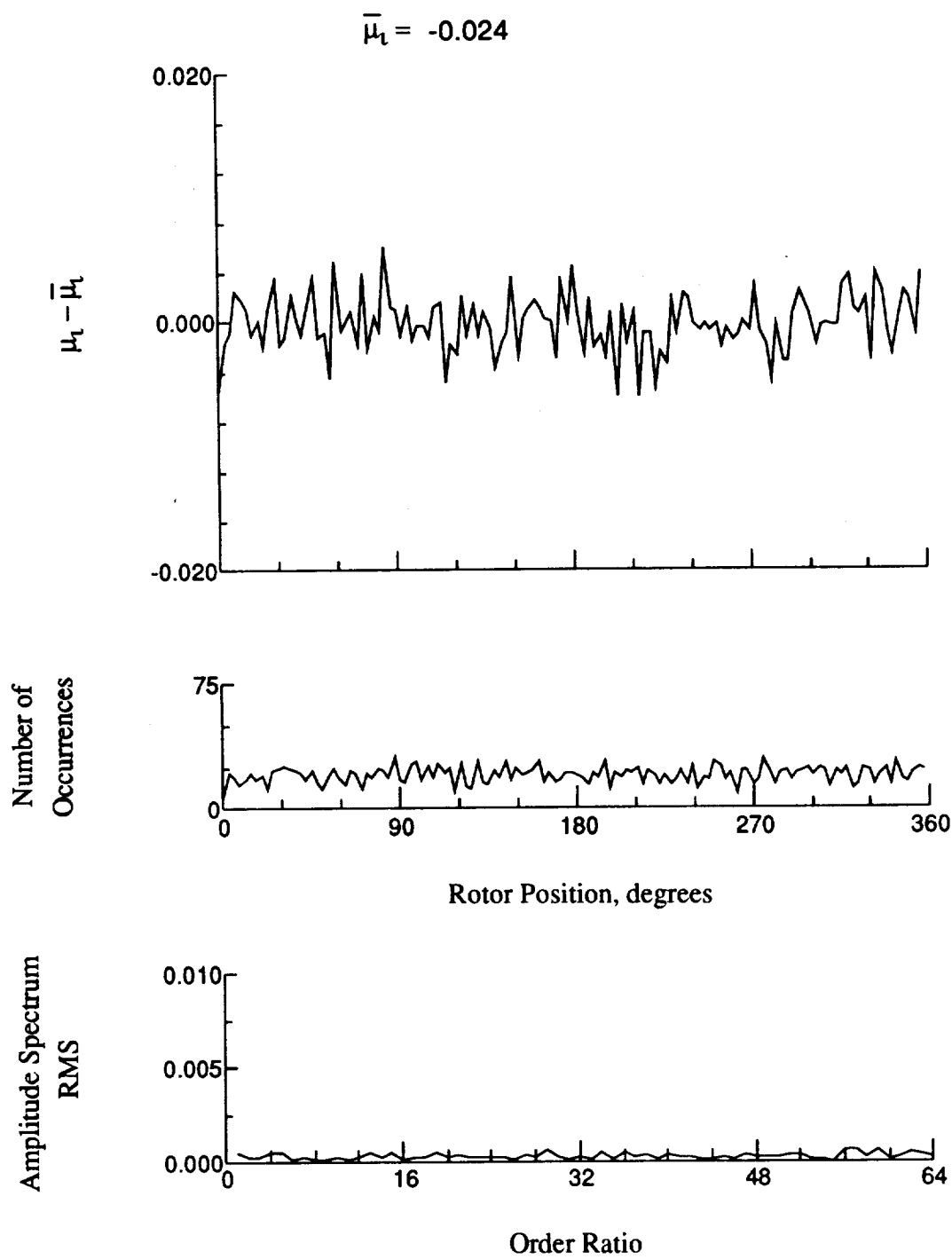


Figure 98.- Induced inflow velocity measured at 150 degrees and r/R of 0.90.

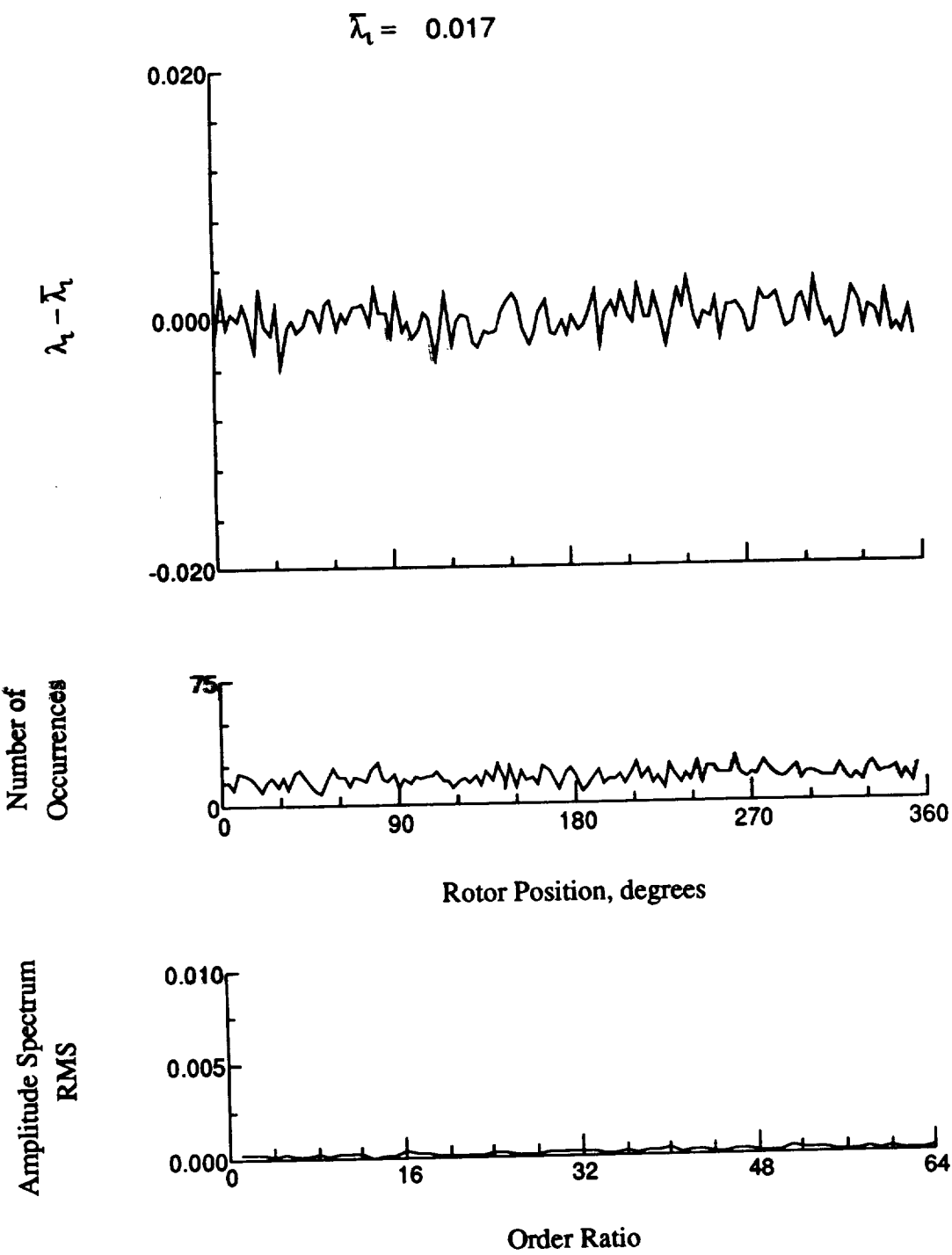


Figure 98.- Concluded.

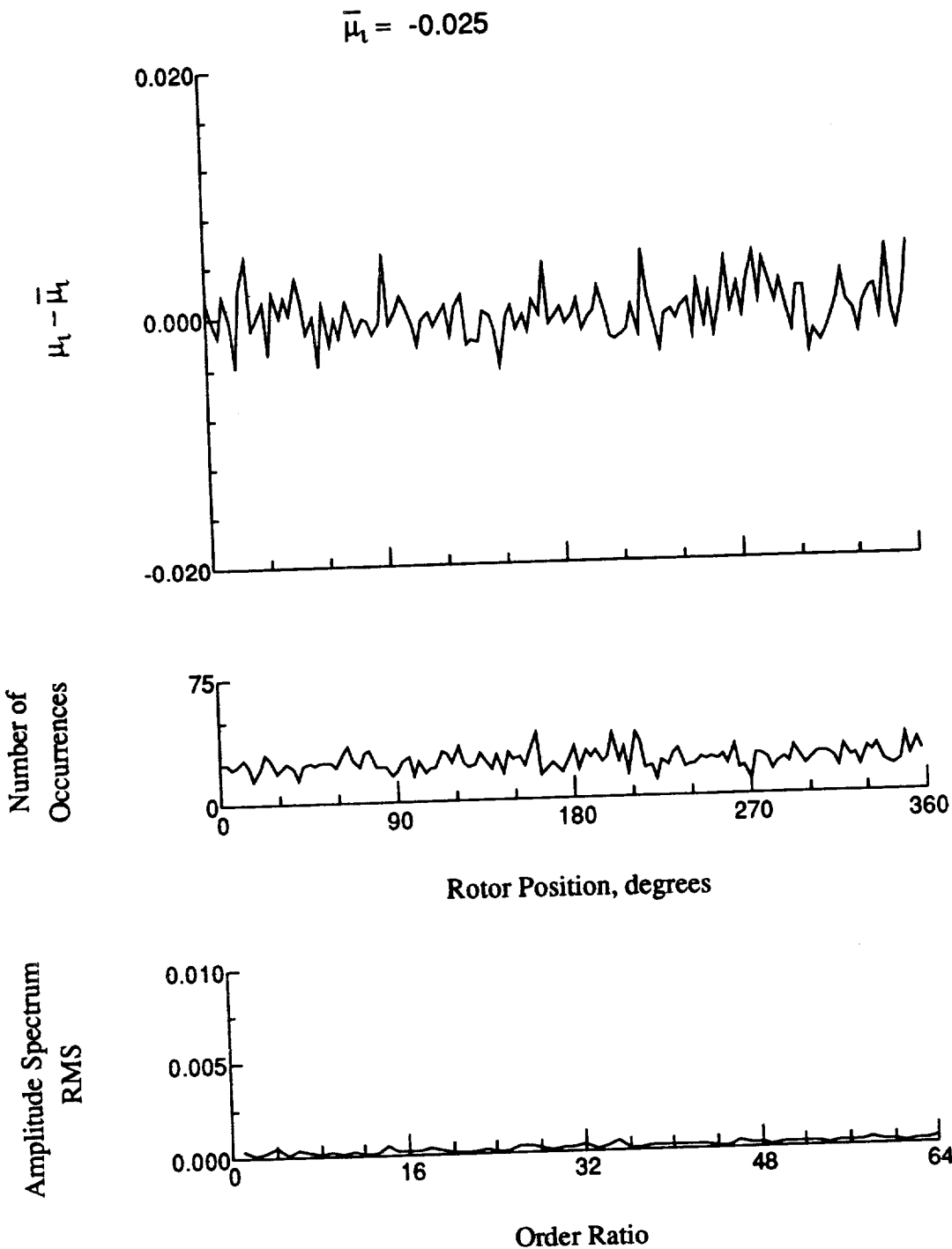


Figure 99.- Induced inflow velocity measured at 150 degrees and r/R of 0.94.

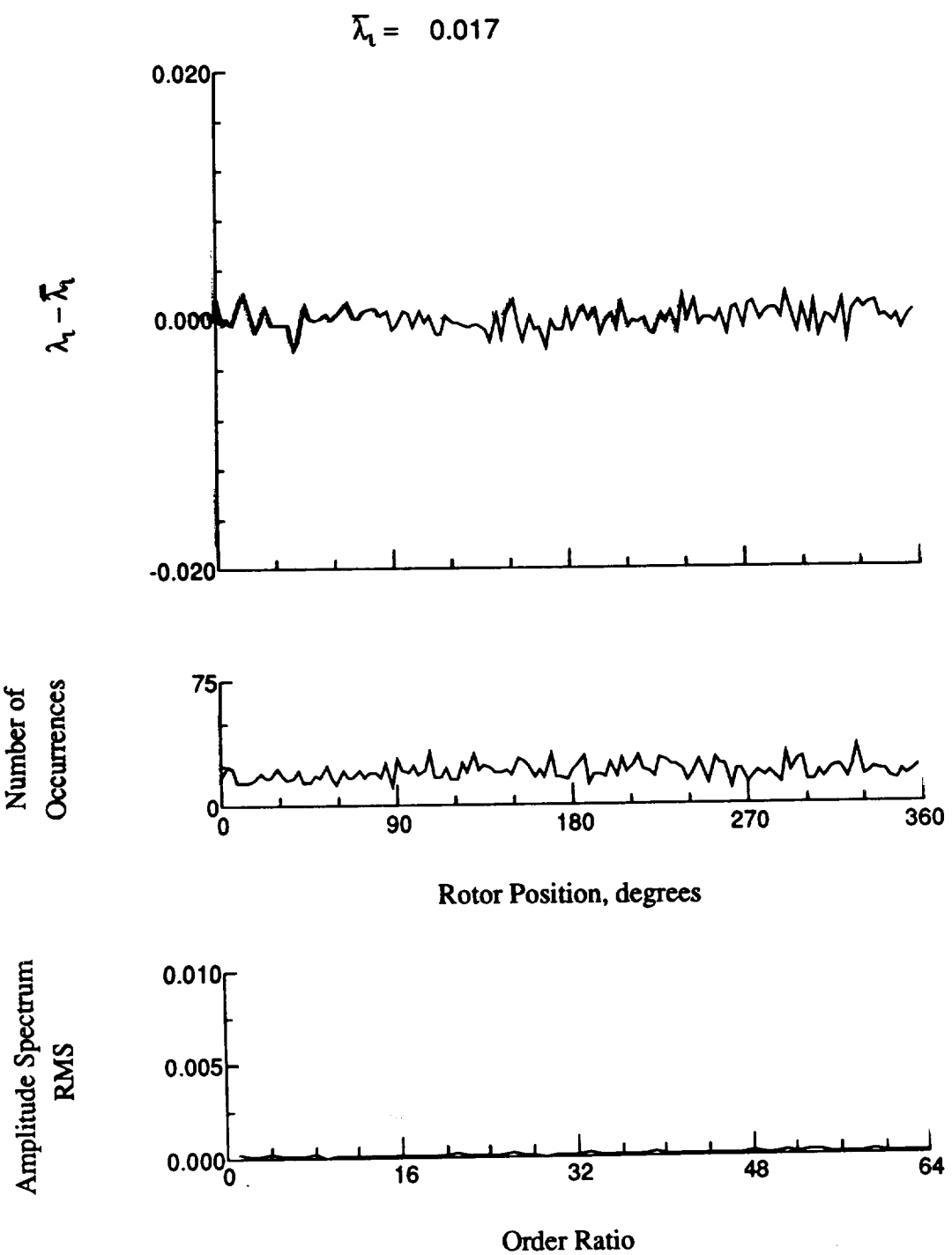


Figure 99.- Concluded.

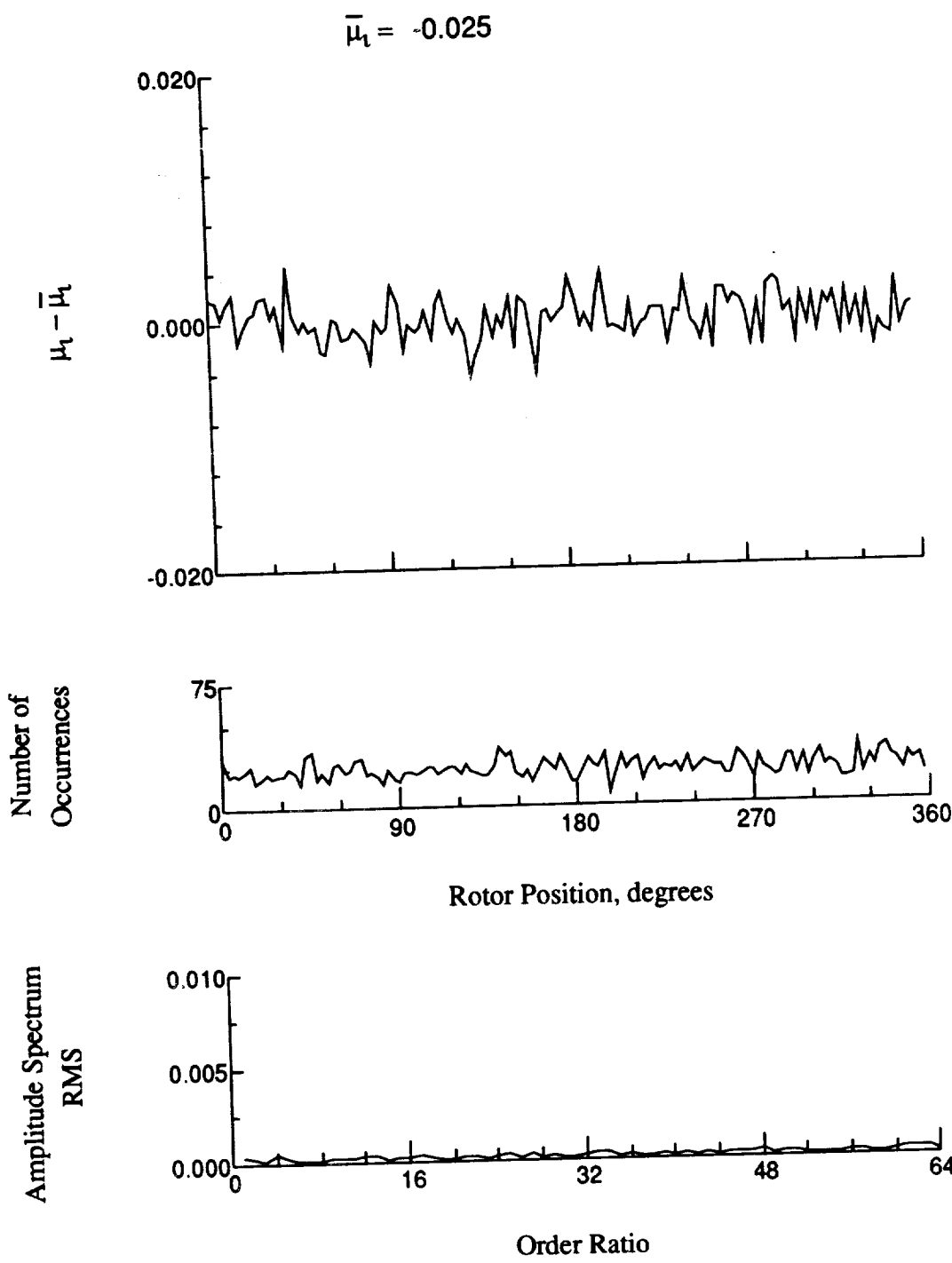


Figure 100.- Induced inflow velocity measured at 150 degrees and r/R of 0.96.

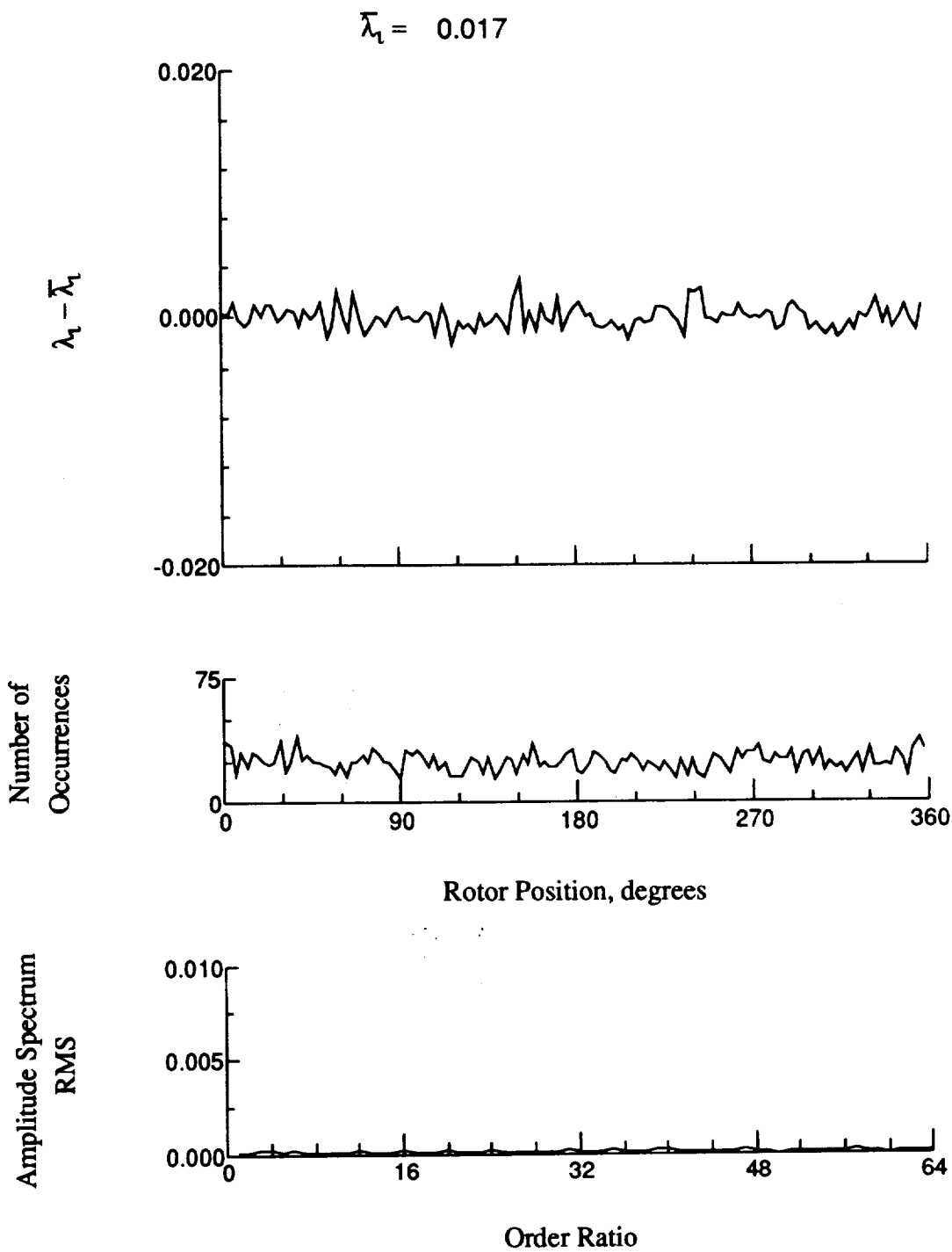


Figure 100.- Concluded.

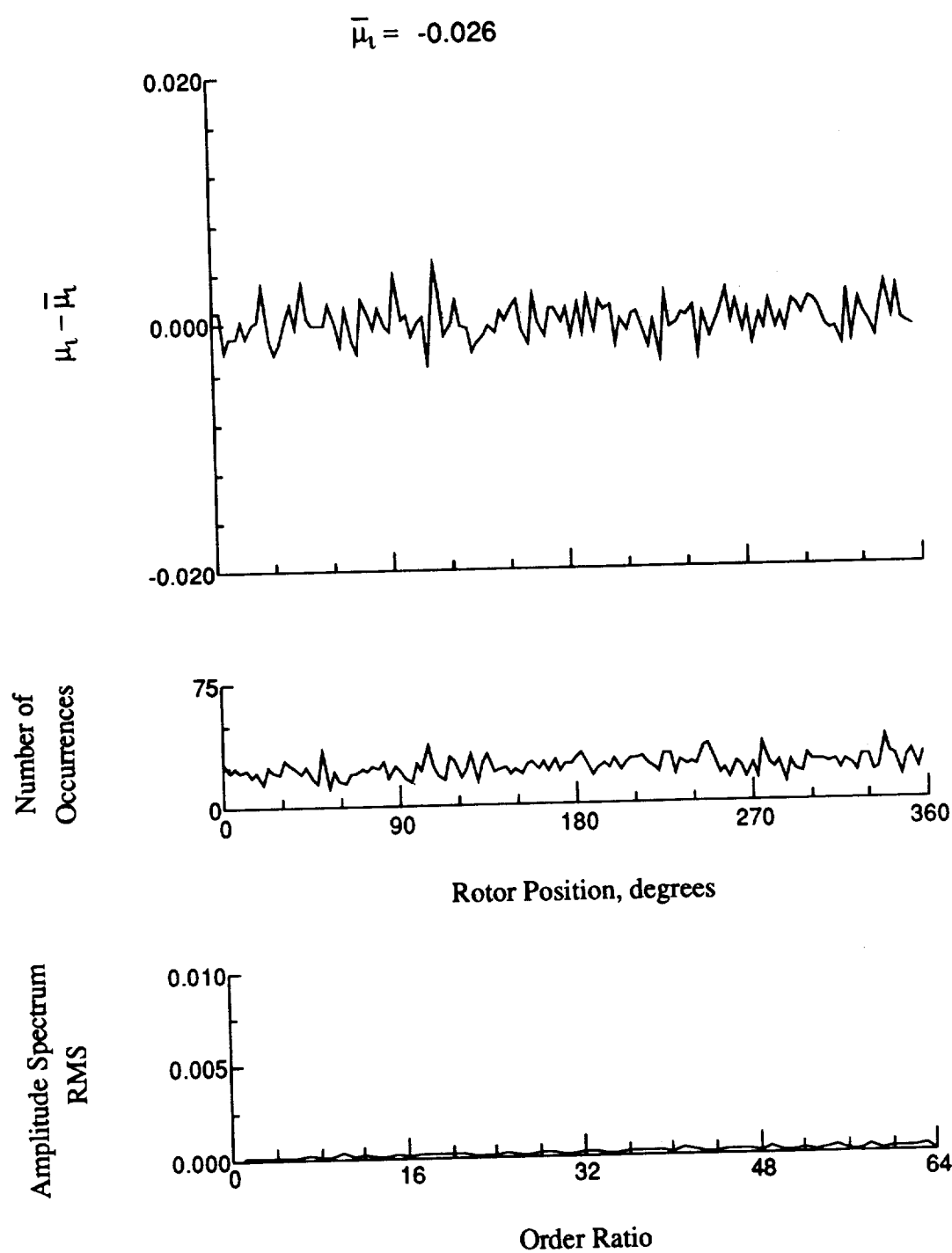


Figure 101.- Induced inflow velocity measured at 150 degrees and r/R of 1.00.

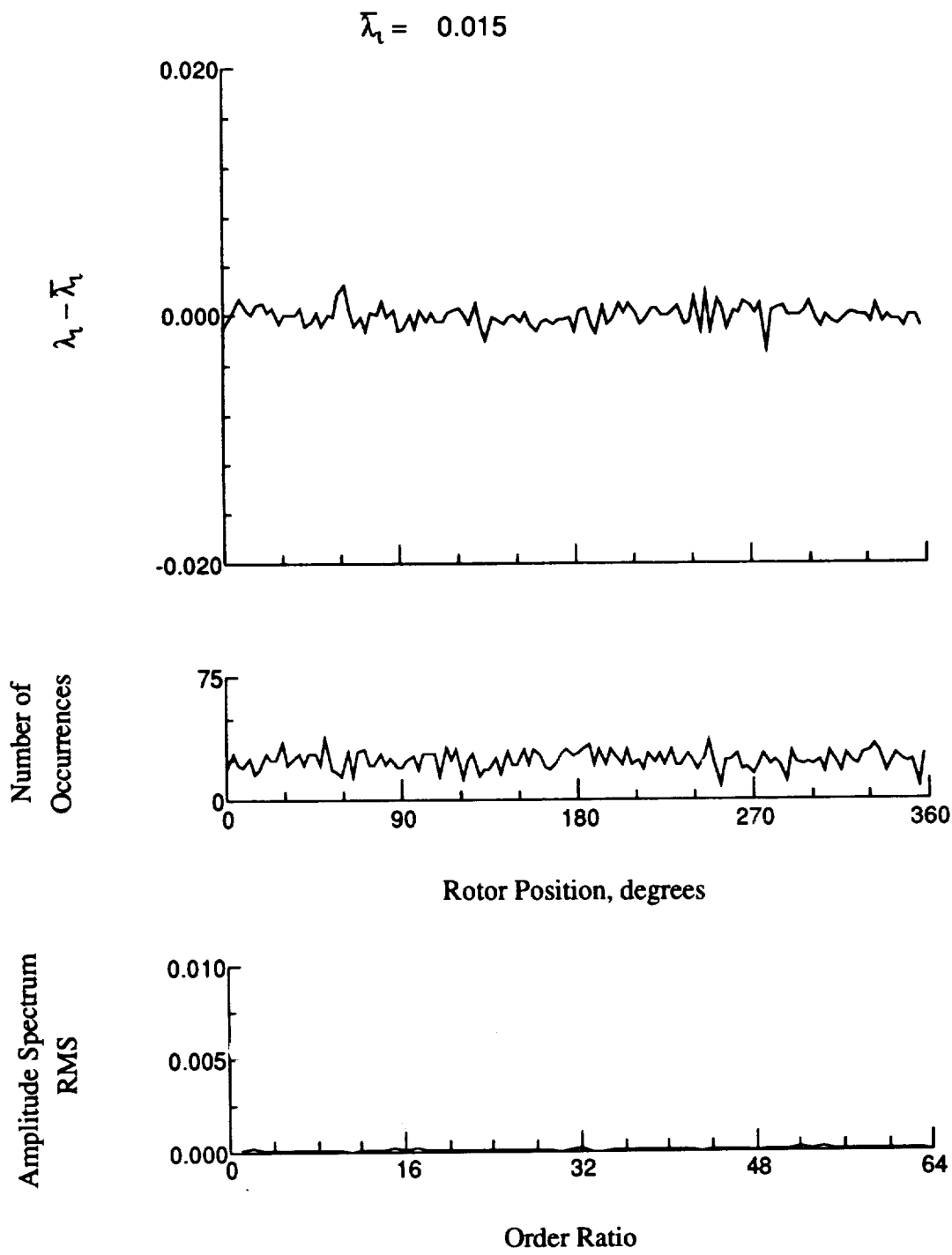


Figure 101.- Concluded.

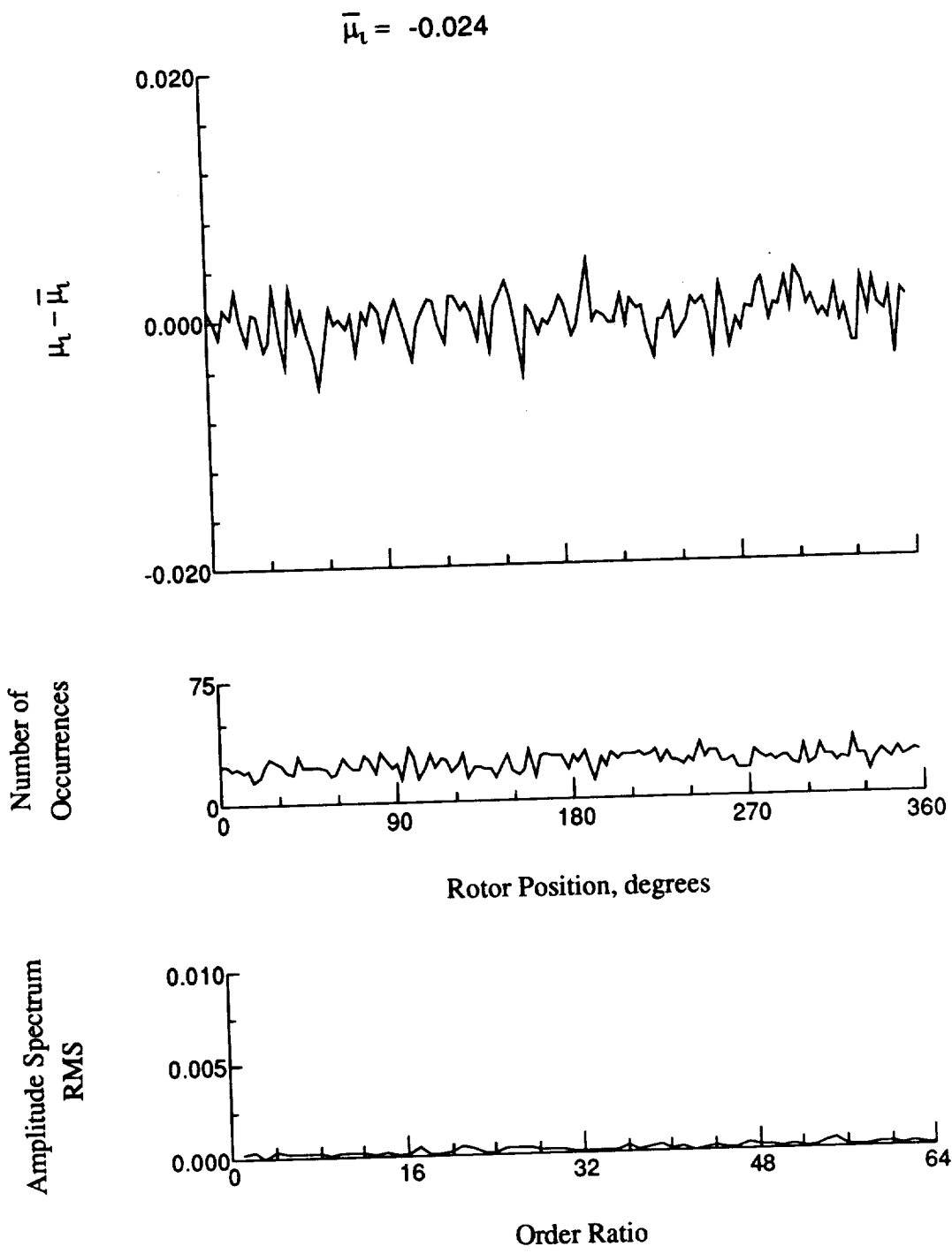


Figure 102.- Induced inflow velocity measured at 150 degrees and r/R of 1.10.

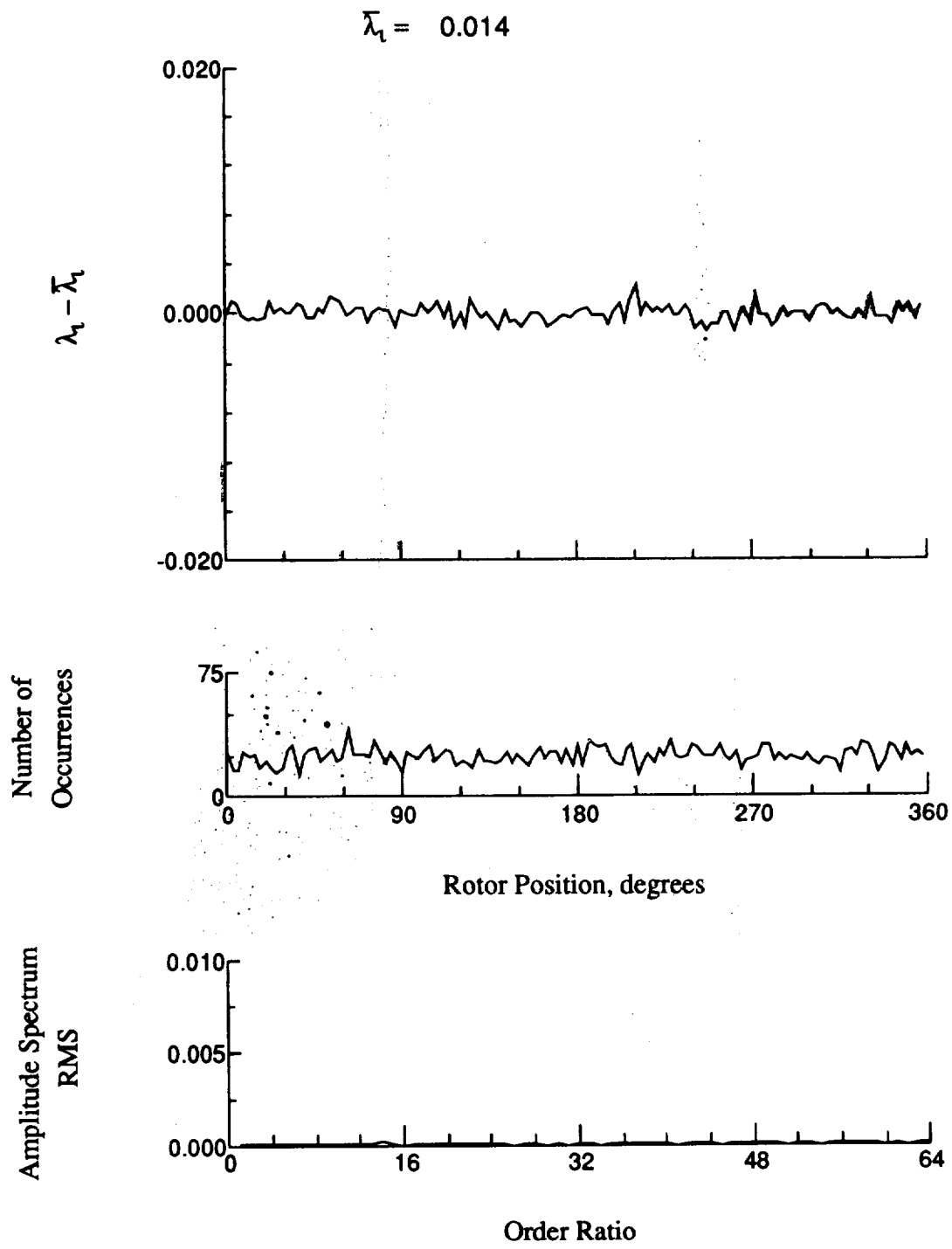


Figure 102.- Concluded.

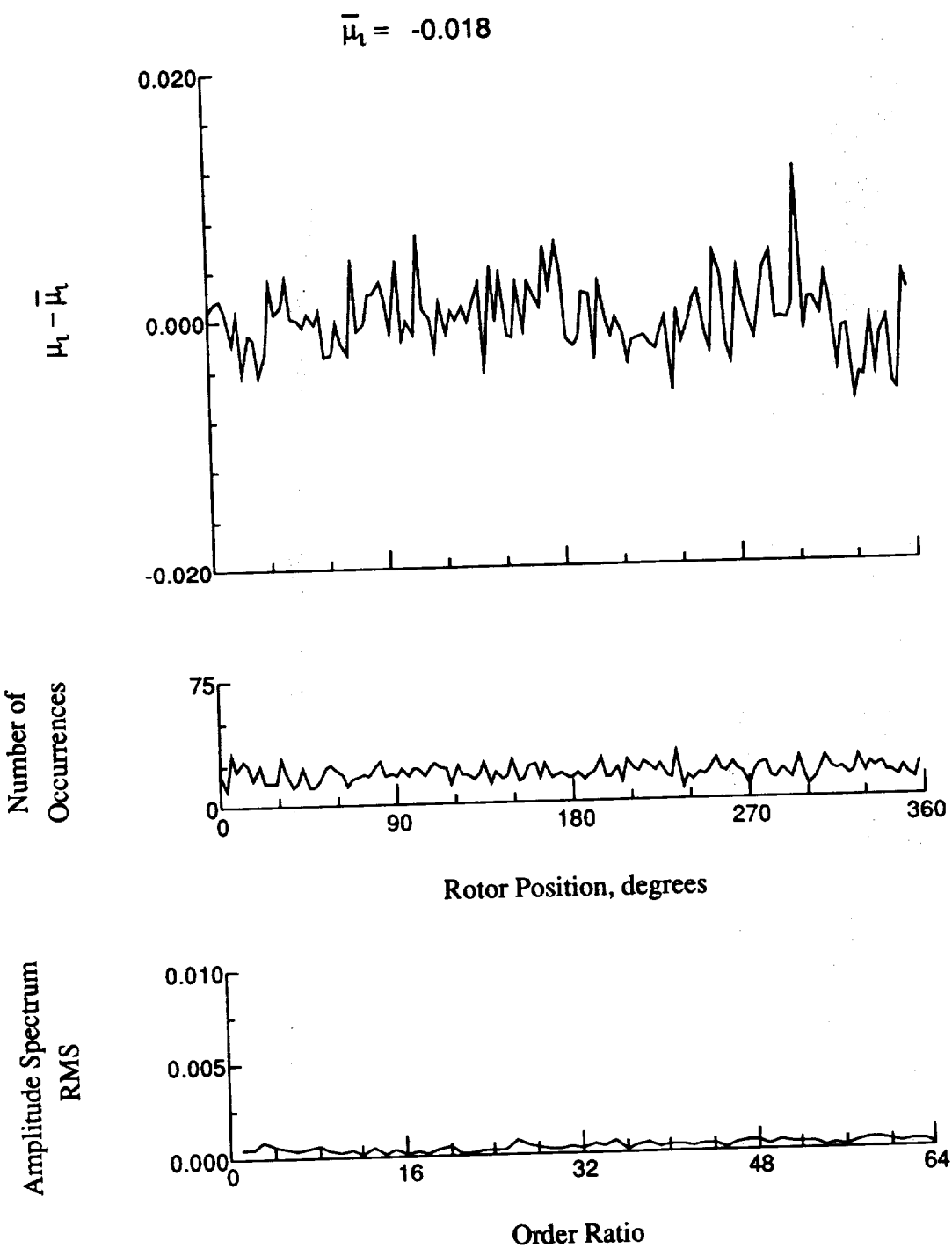


Figure 103.- Induced inflow velocity measured at 180 degrees and r/R of 0.20.

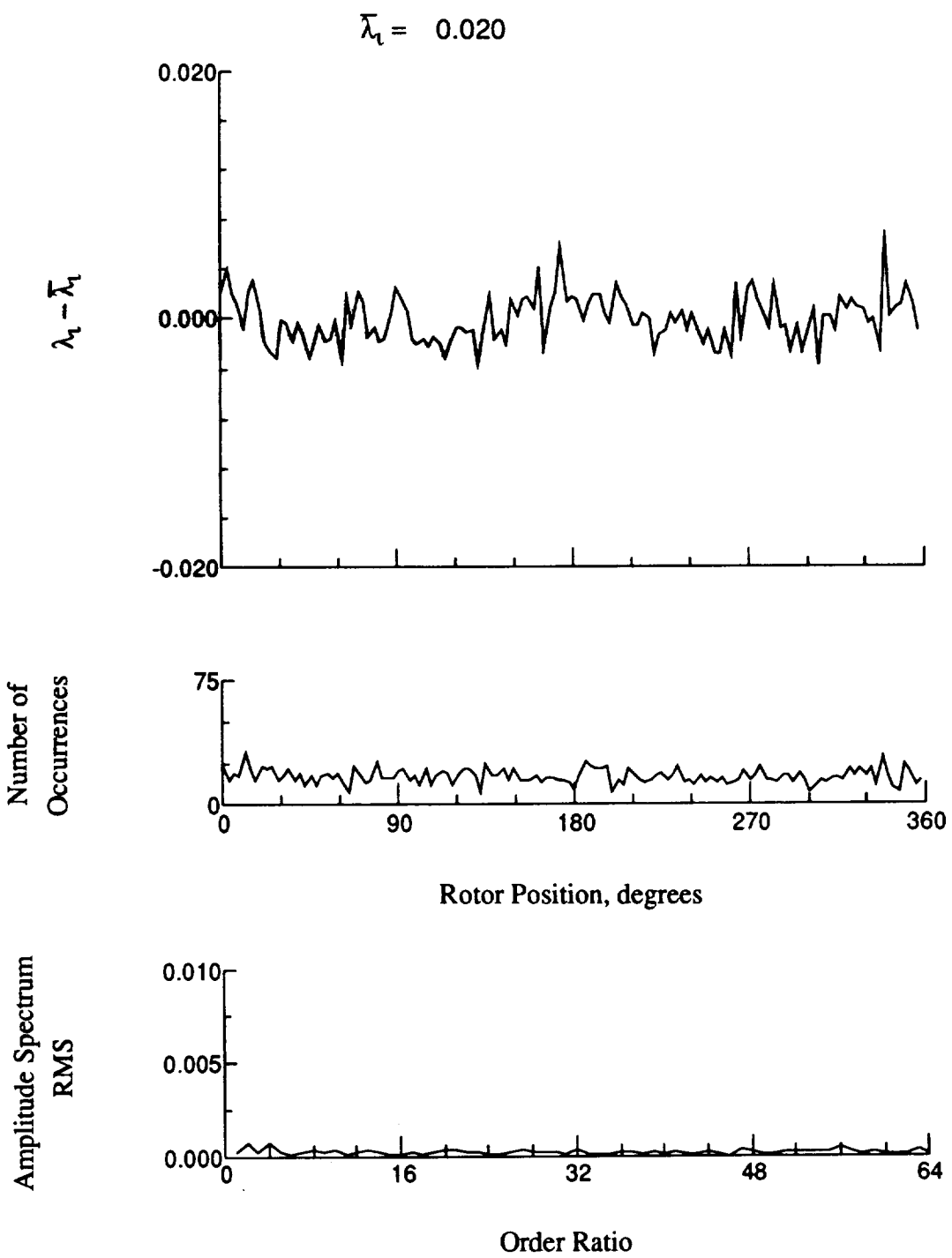


Figure 103.- Concluded.

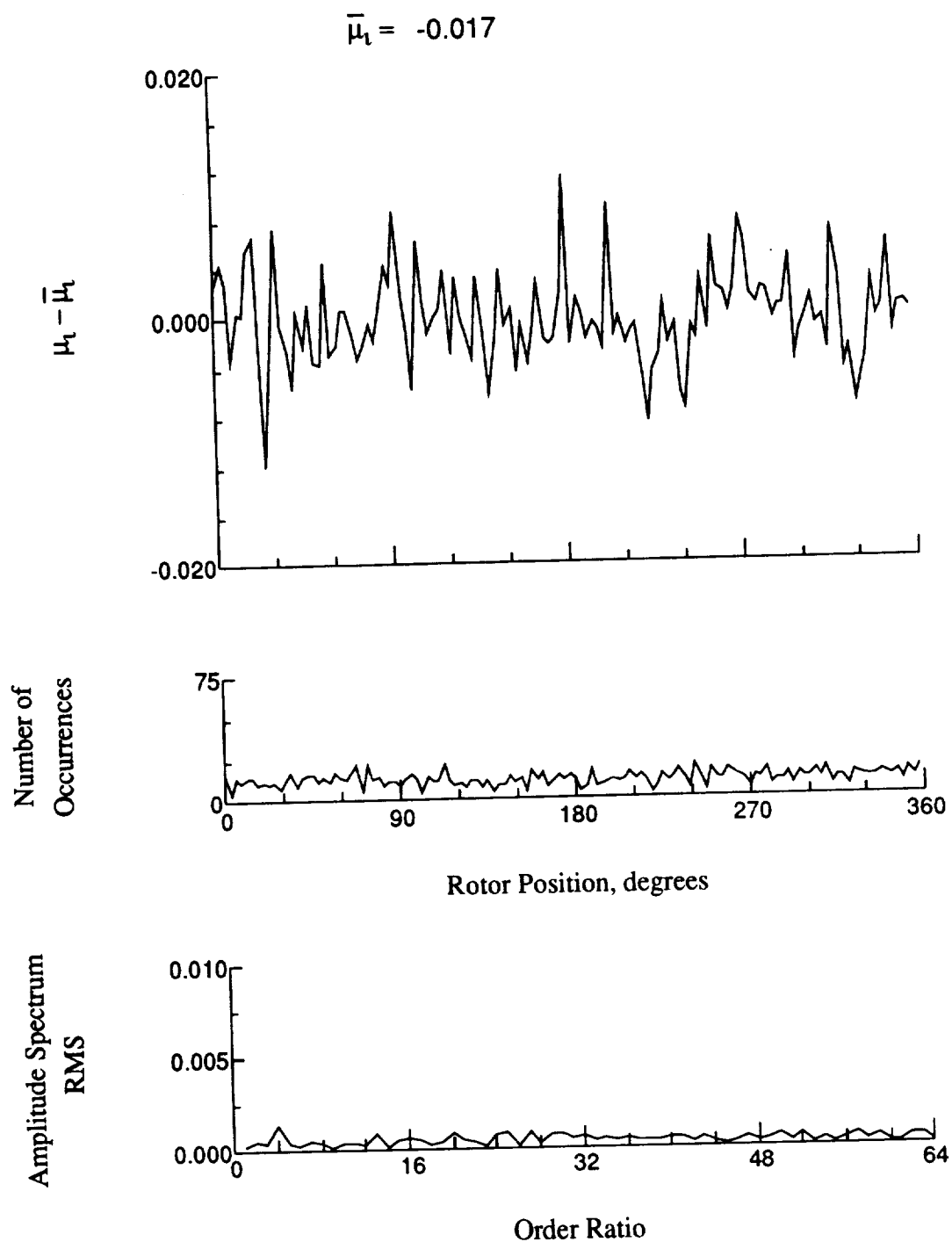


Figure 104.- Induced inflow velocity measured at 180 degrees and r/R of 0.32.

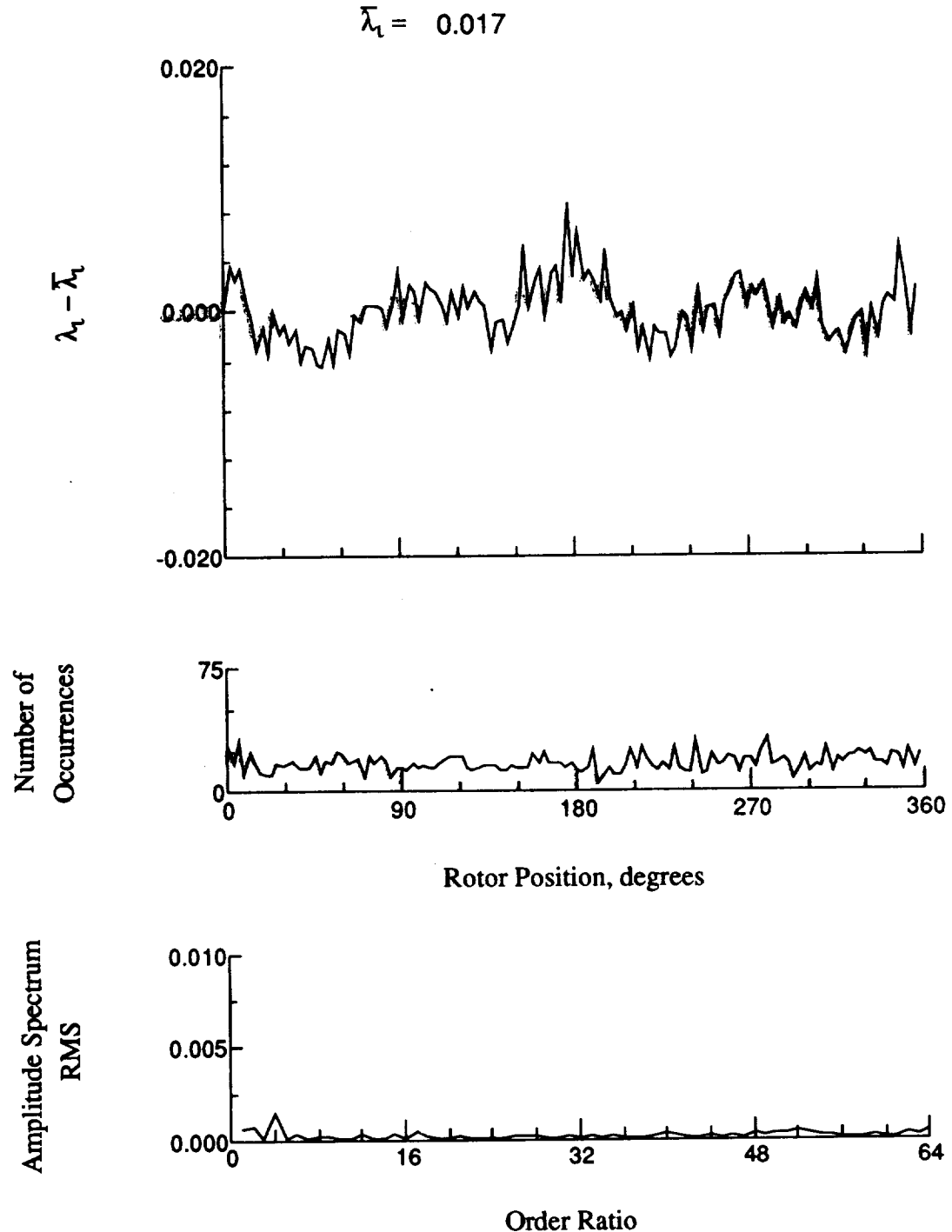


Figure 104.- Concluded.

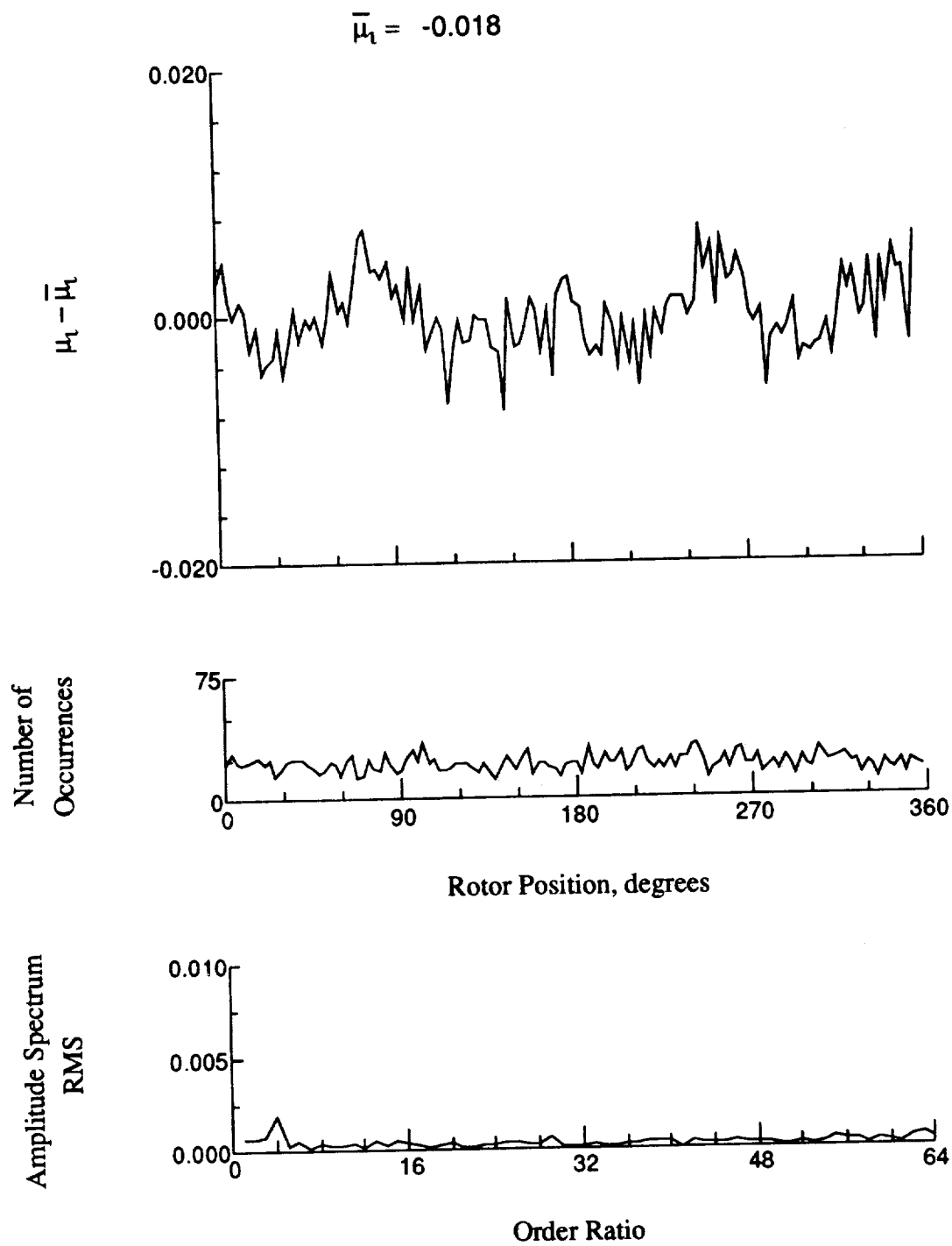


Figure 105.- Induced inflow velocity measured at 180 degrees and r/R of 0.50.

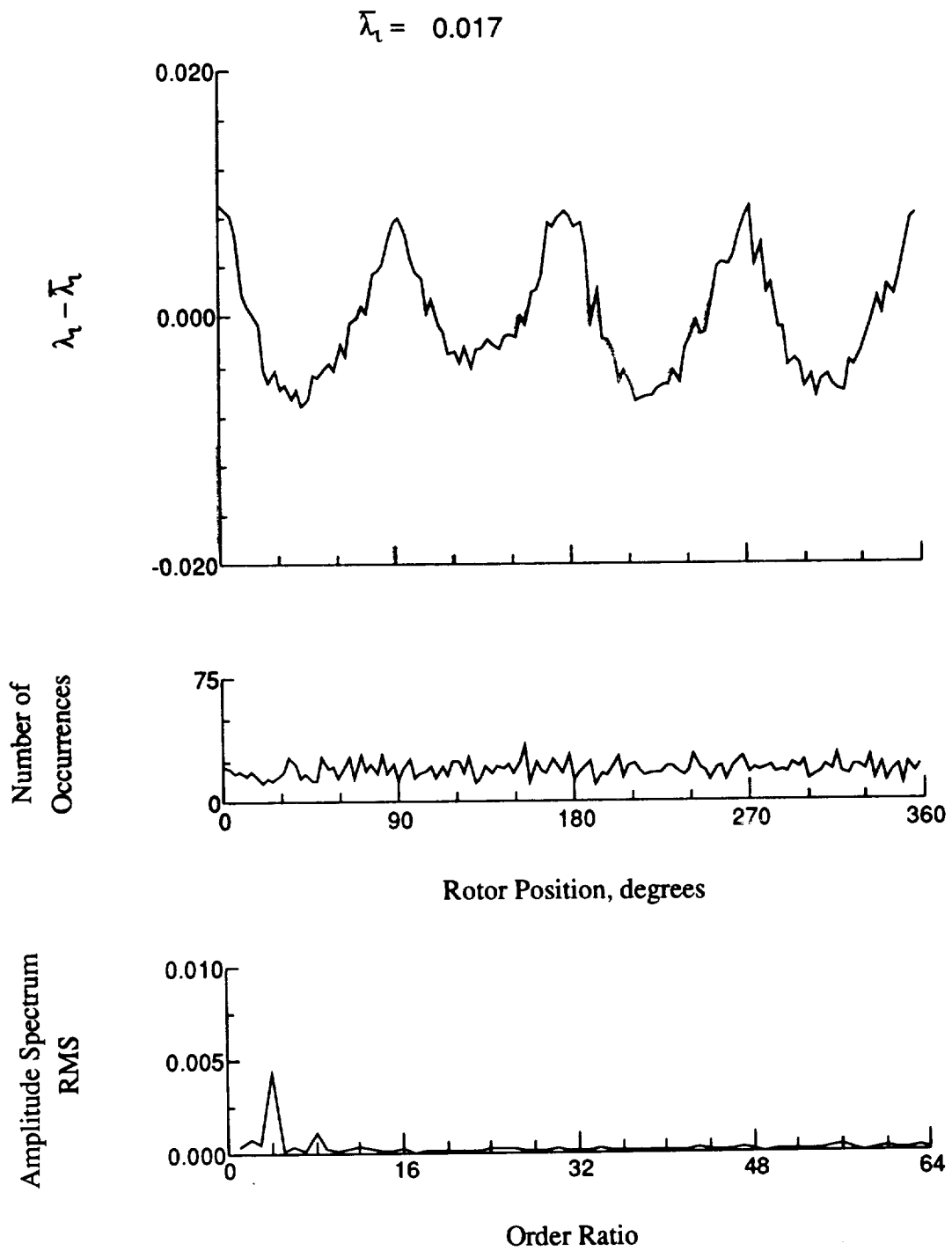


Figure 105.- Concluded.

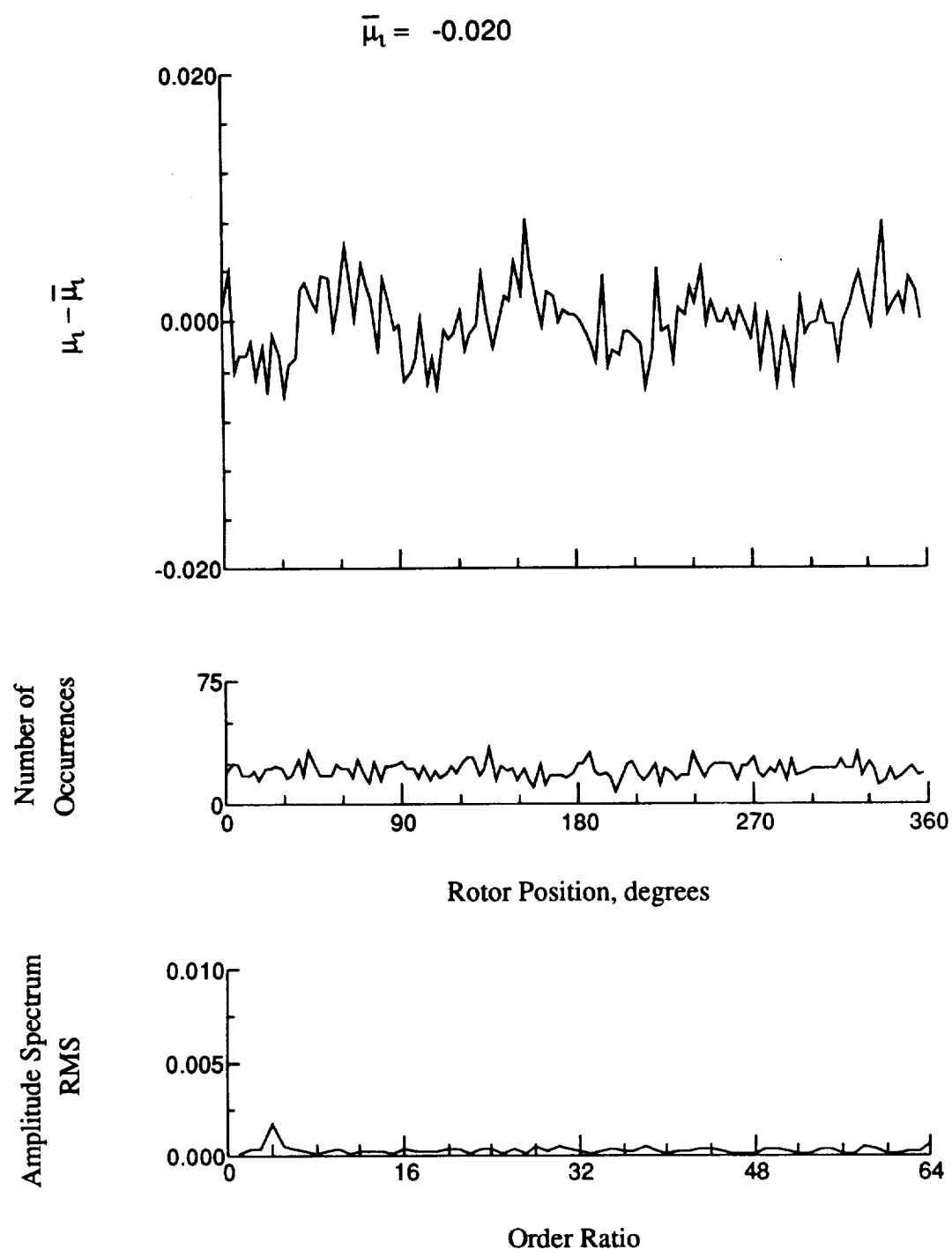


Figure 106.- Induced inflow velocity measured at 180 degrees and r/R of 0.58.

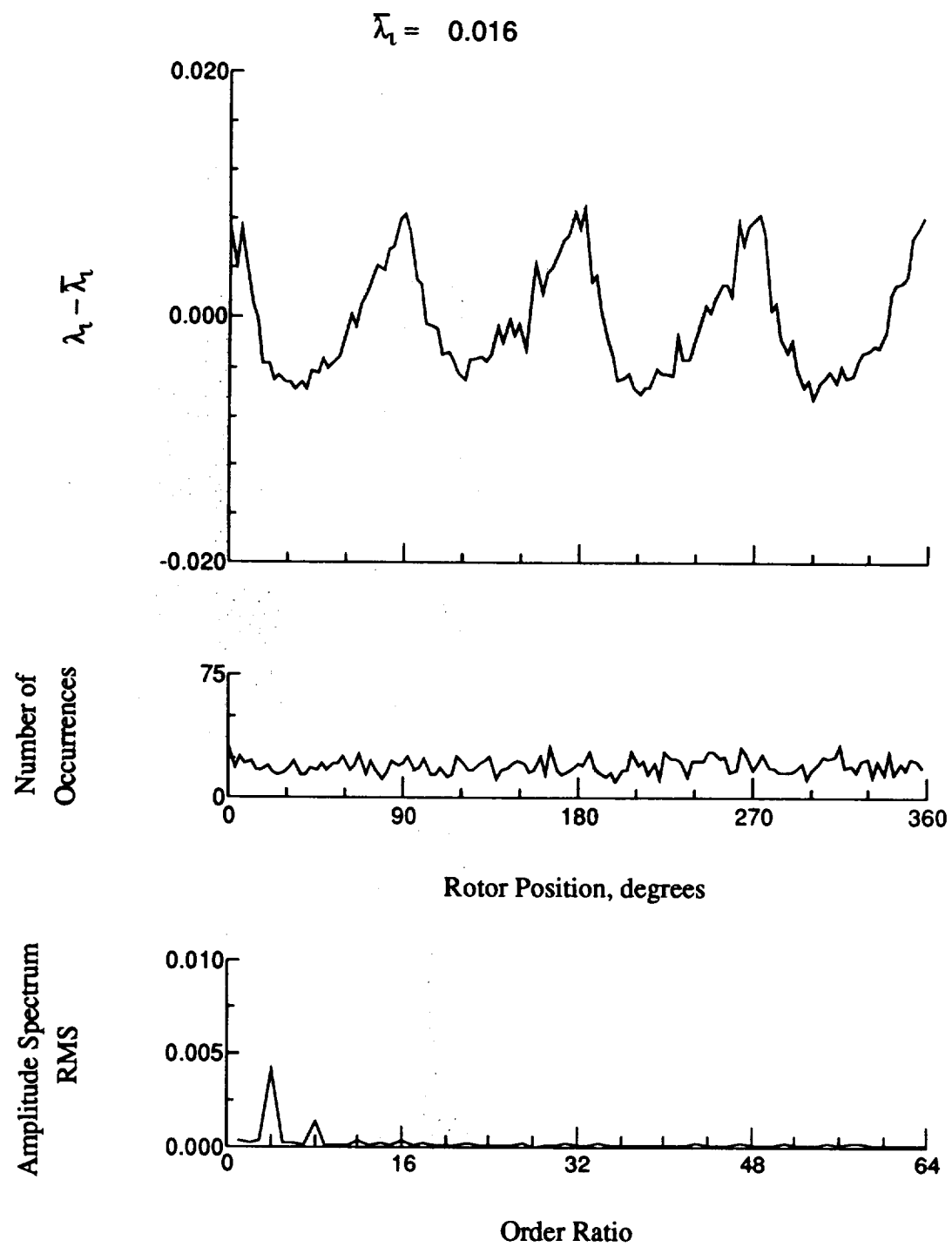


Figure 106.- Concluded.

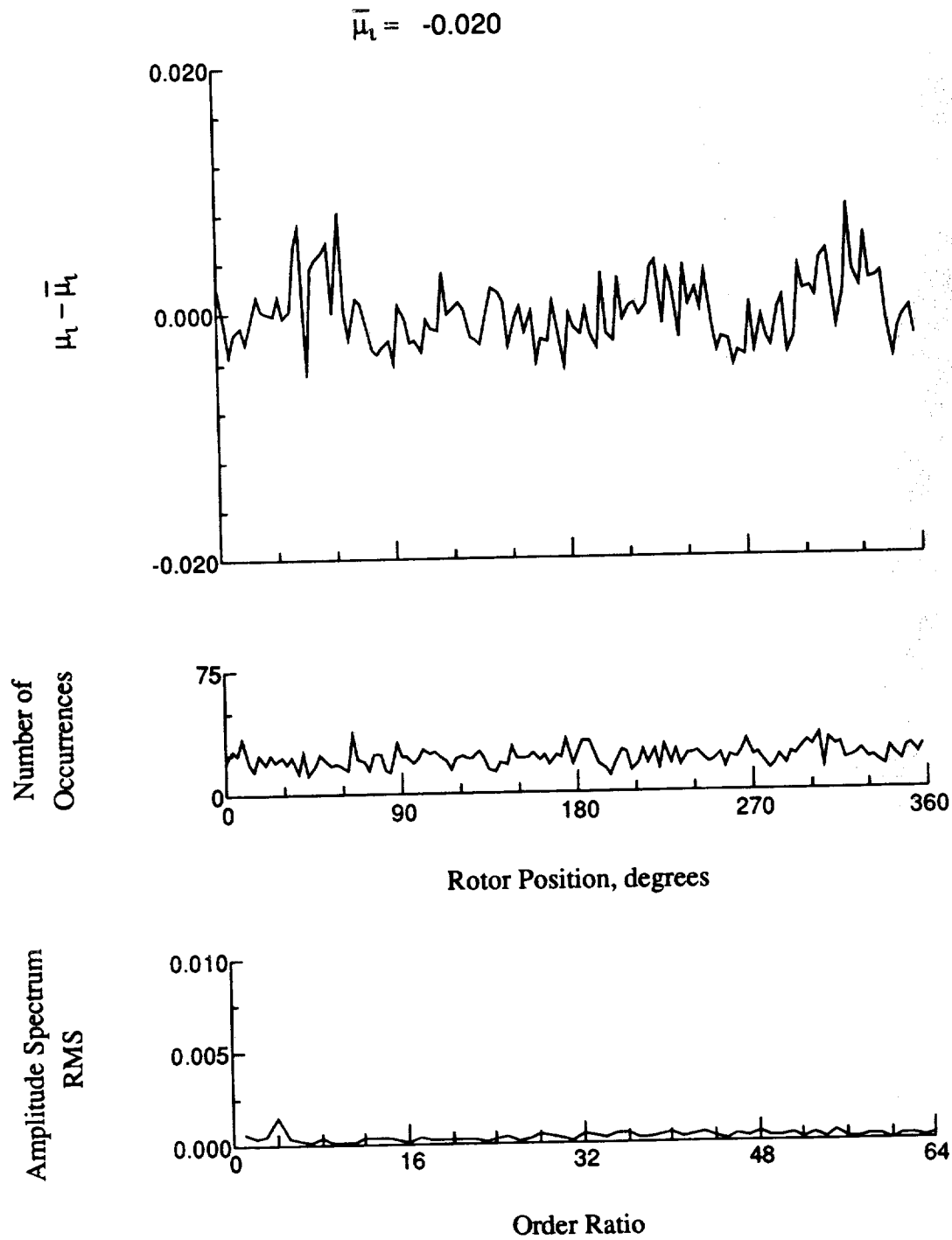


Figure 107.- Induced inflow velocity measured at 180 degrees and r/R of 0.69.

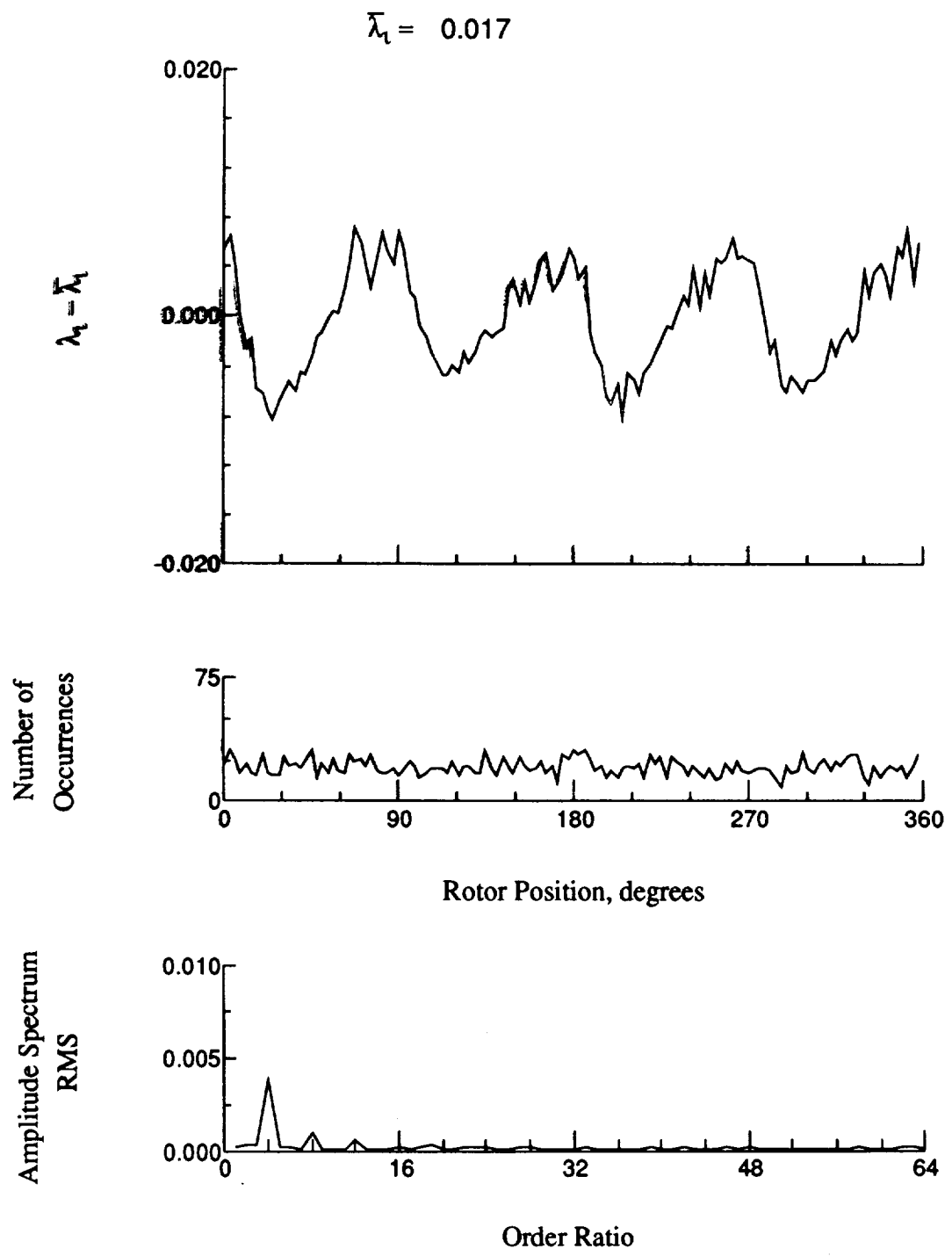


Figure 107.- Concluded.

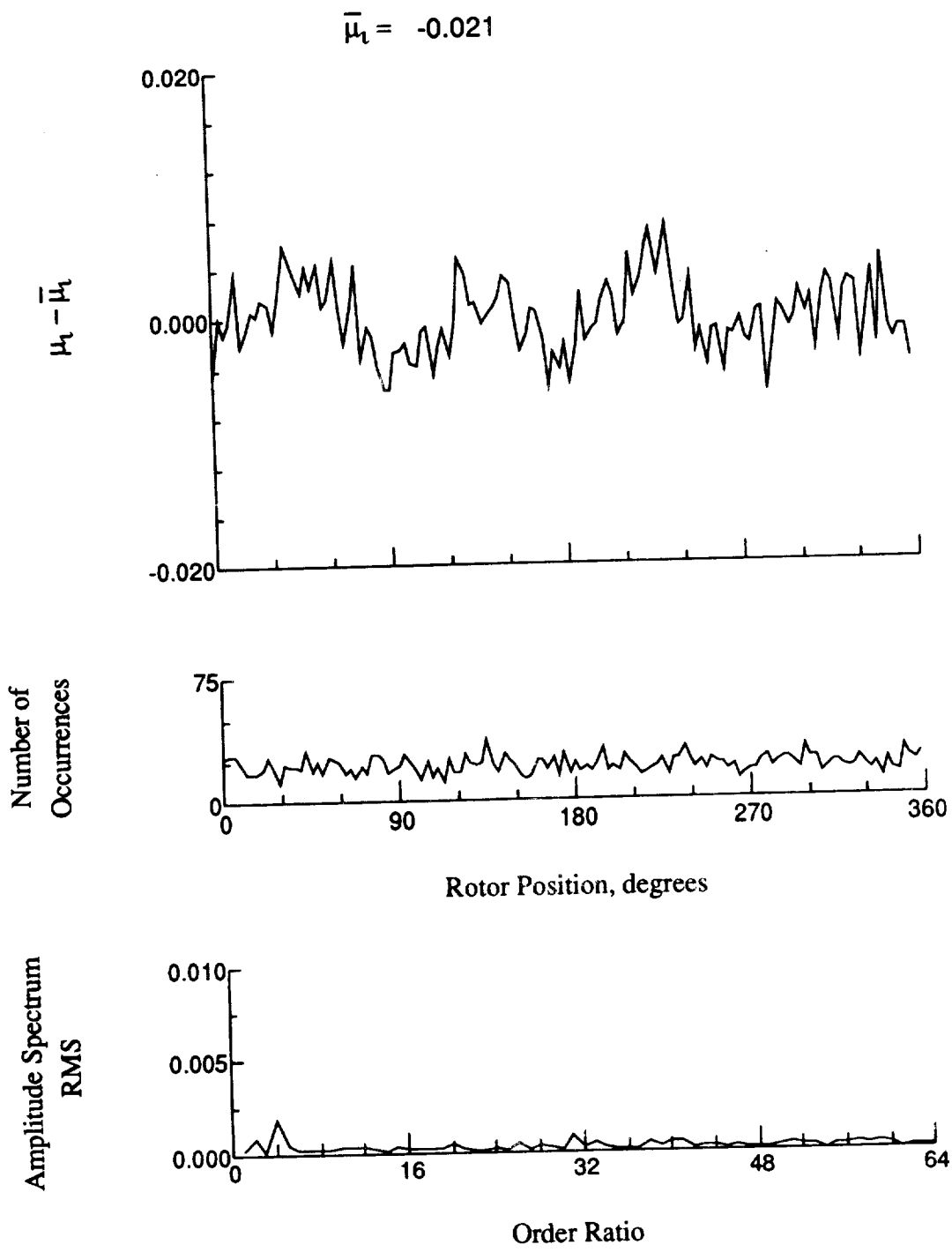


Figure 108.- Induced inflow velocity measured at 180 degrees and r/R of 0.73.

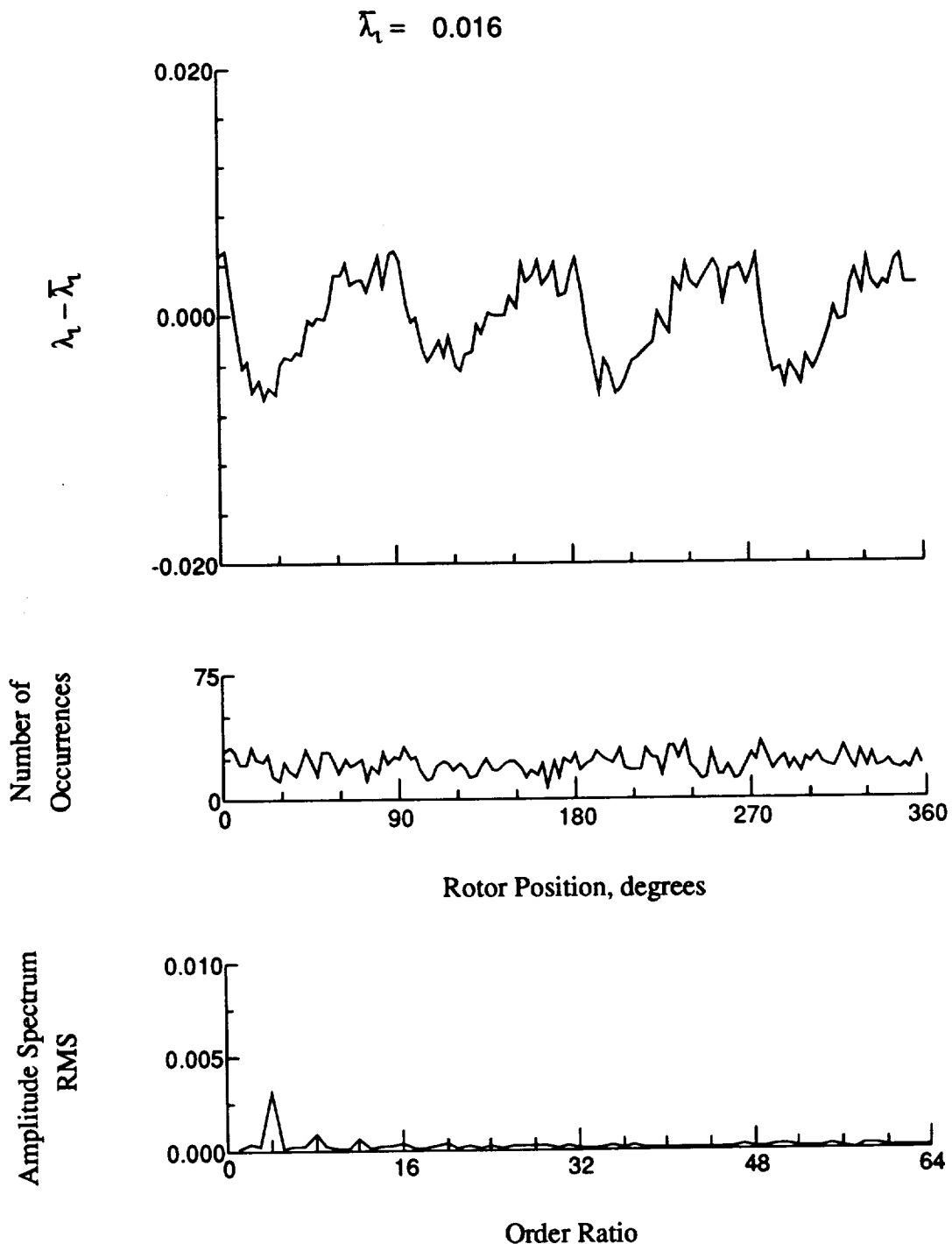


Figure 108.- Concluded.

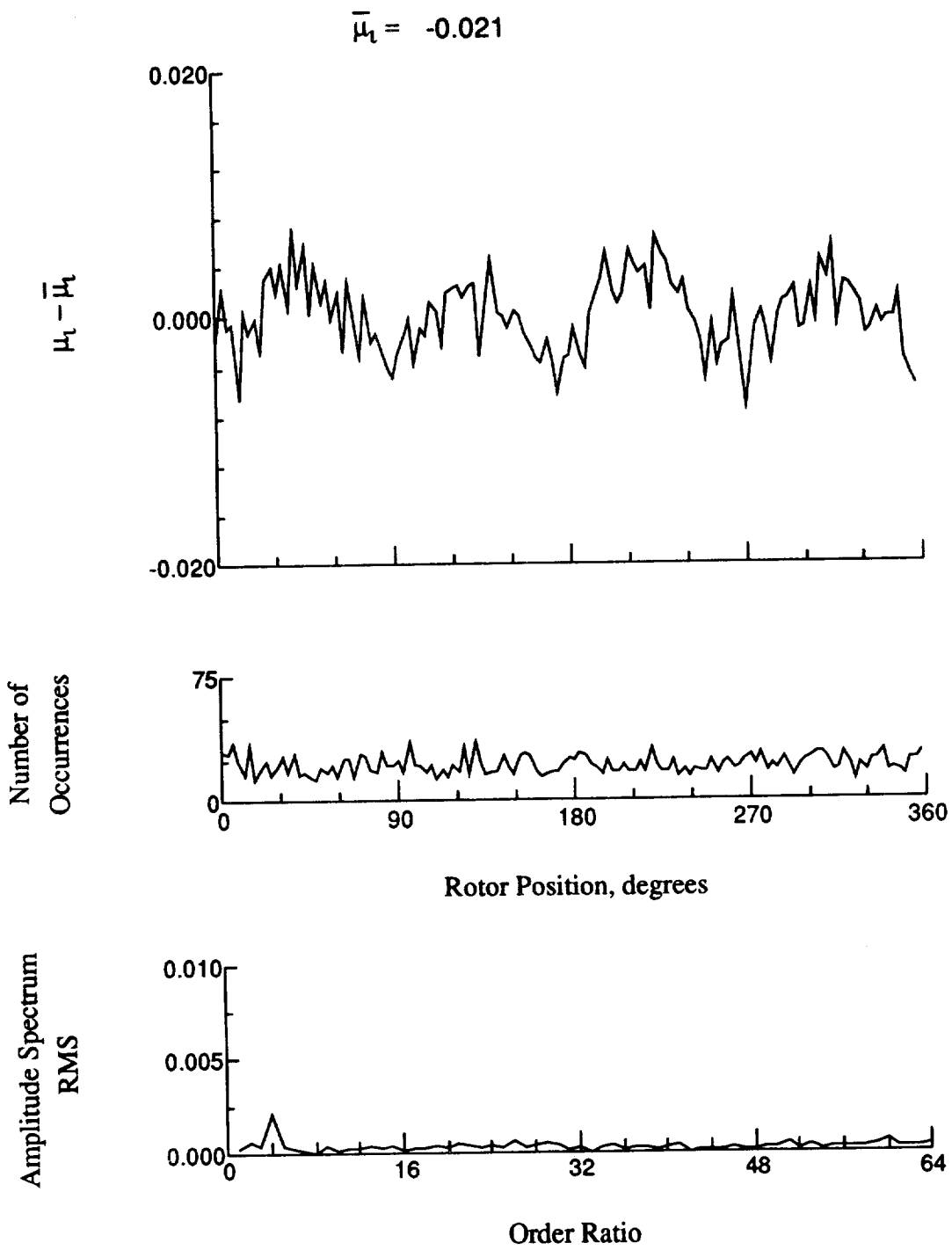


Figure 109.- Induced inflow velocity measured at 180 degrees and r/R of 0.75.

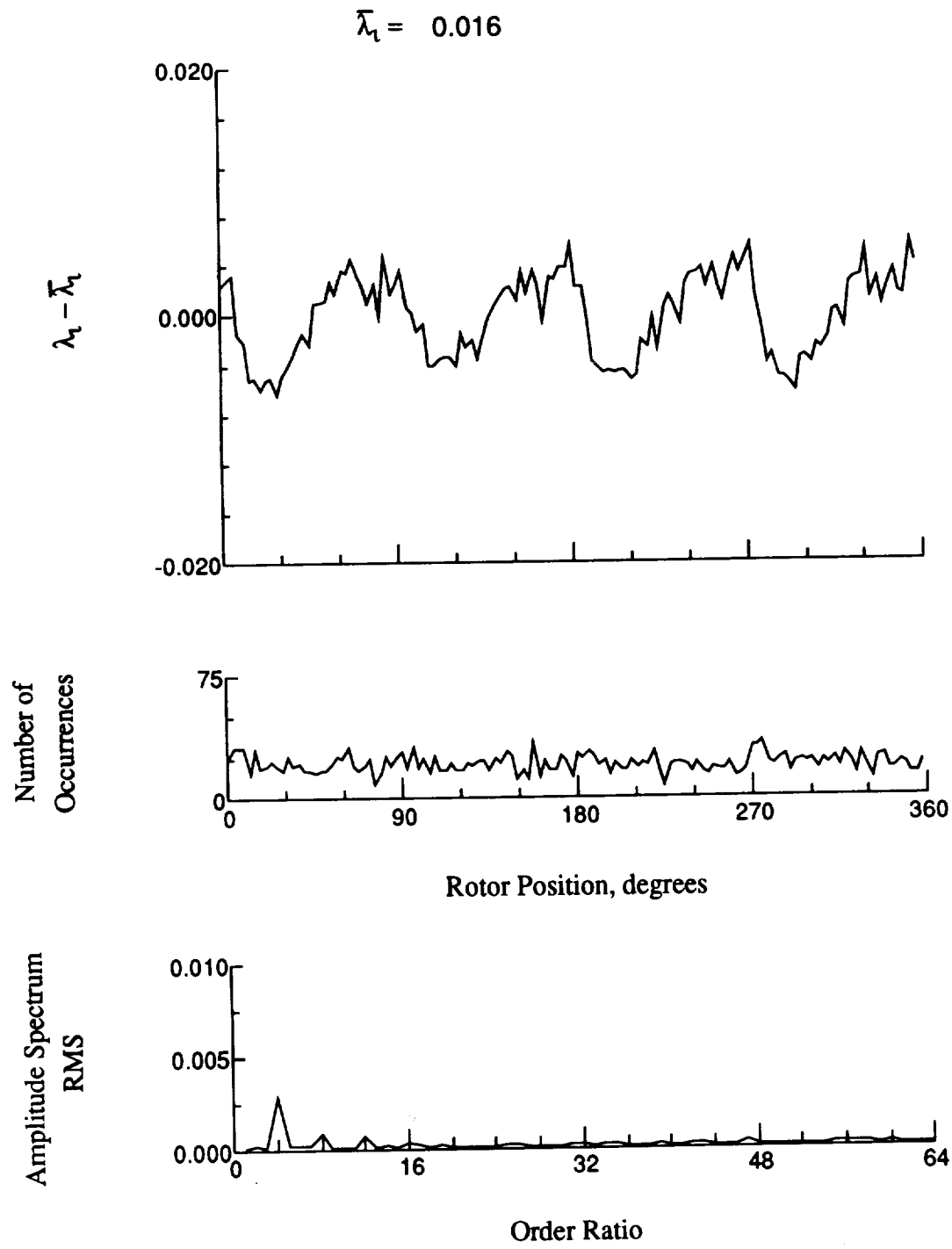


Figure 109.- Concluded.

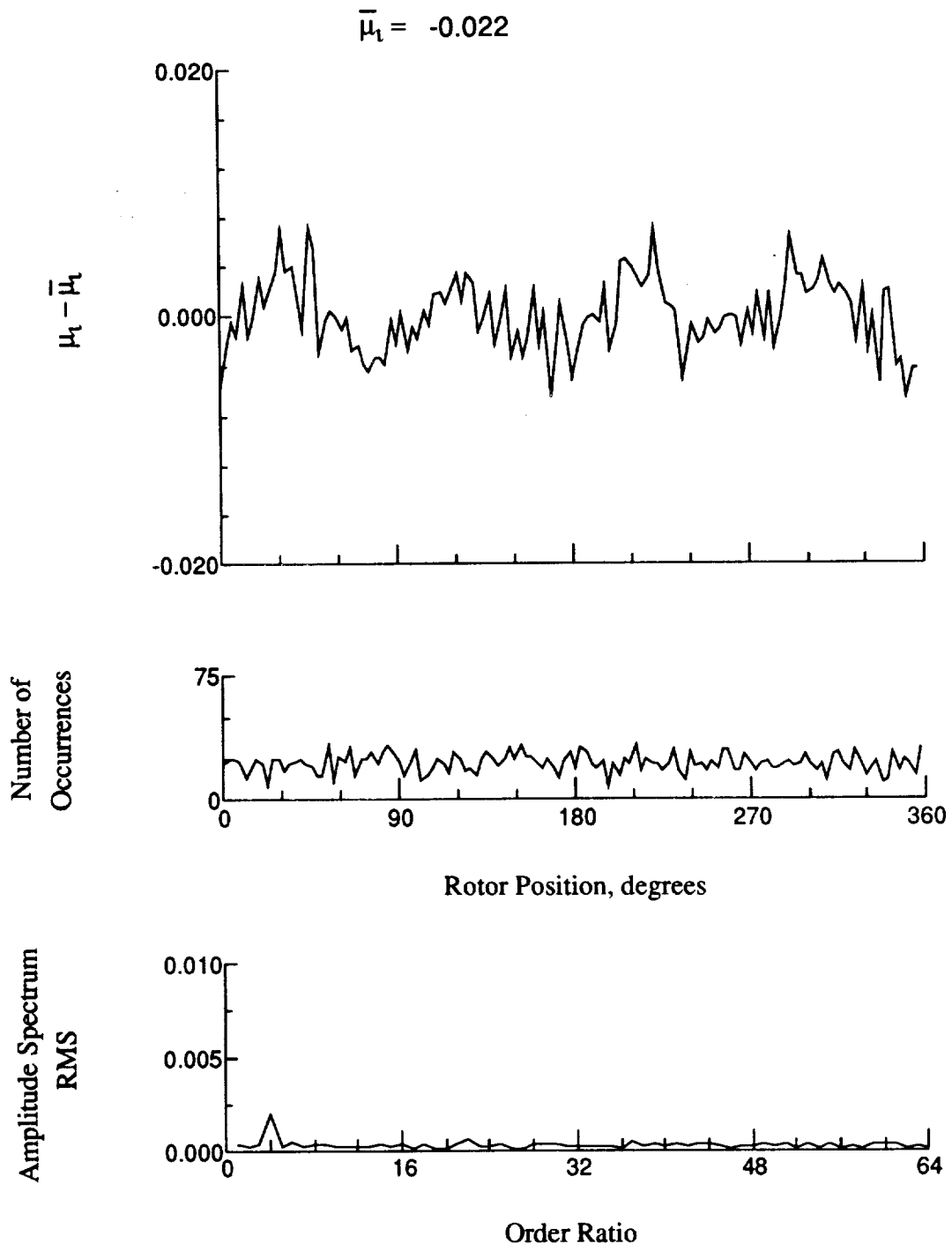


Figure 110.- Induced inflow velocity measured at 180 degrees and r/R of 0.81.

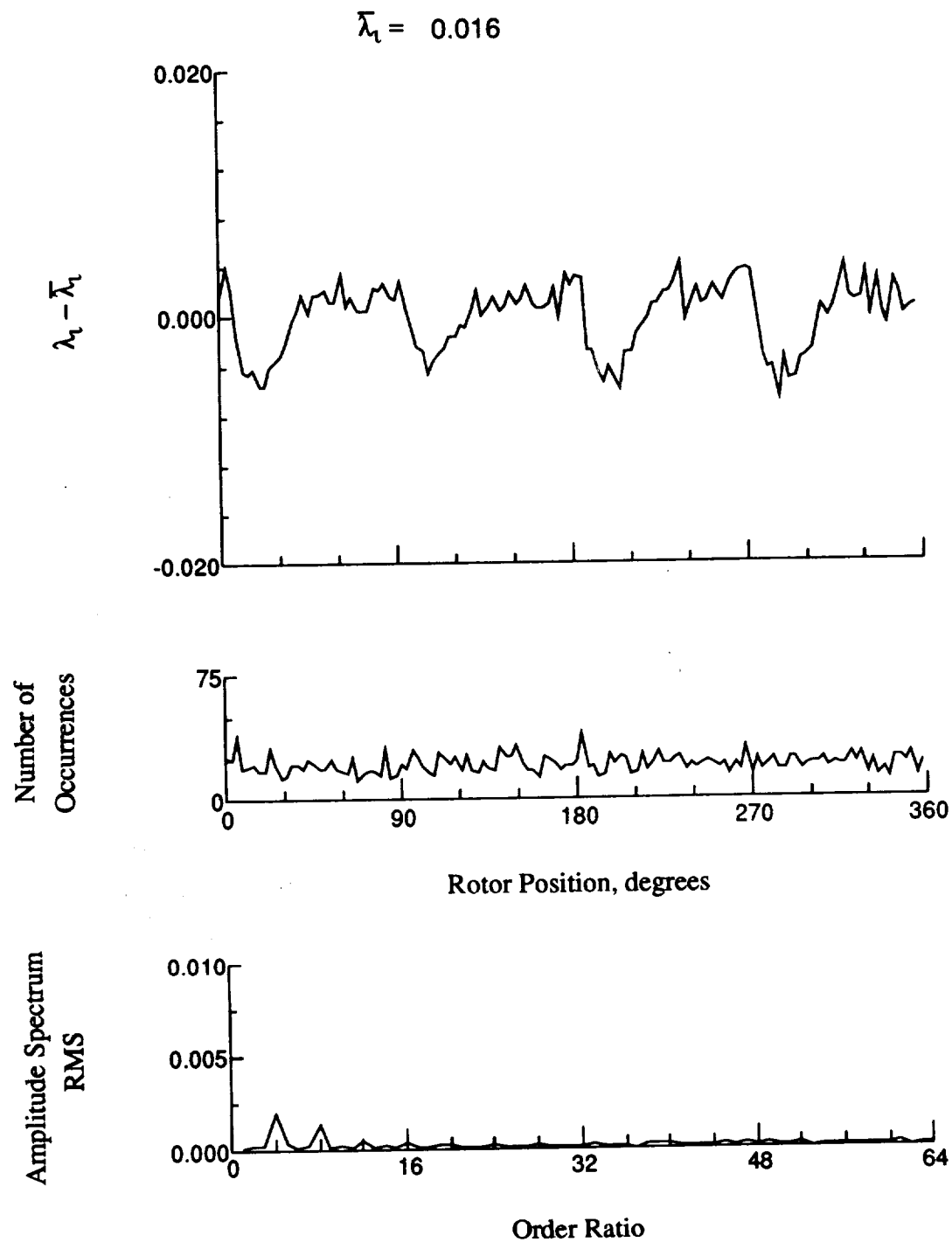


Figure 110.- Concluded.

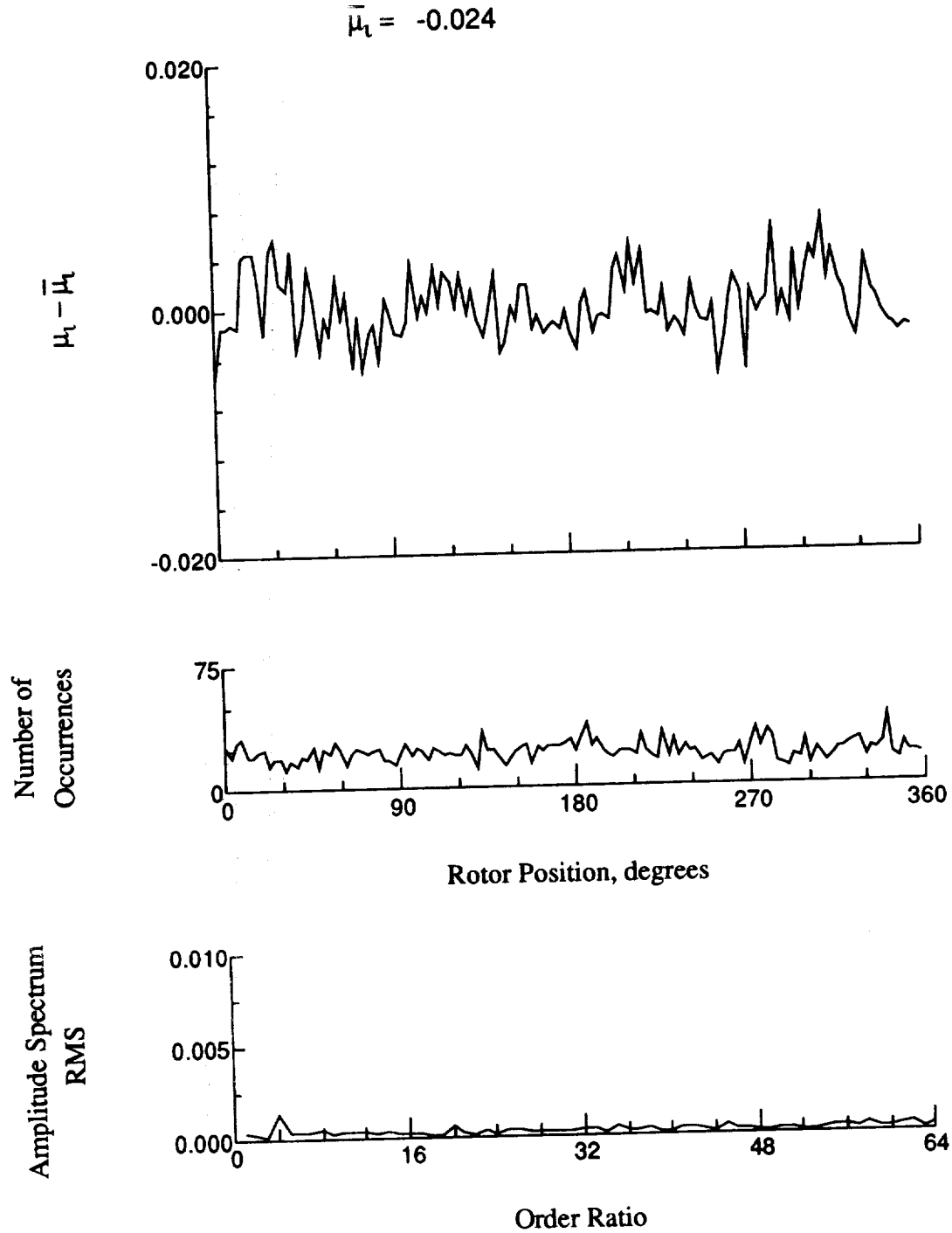


Figure 111.- Induced inflow velocity measured at 180 degrees and r/R of 0.86.

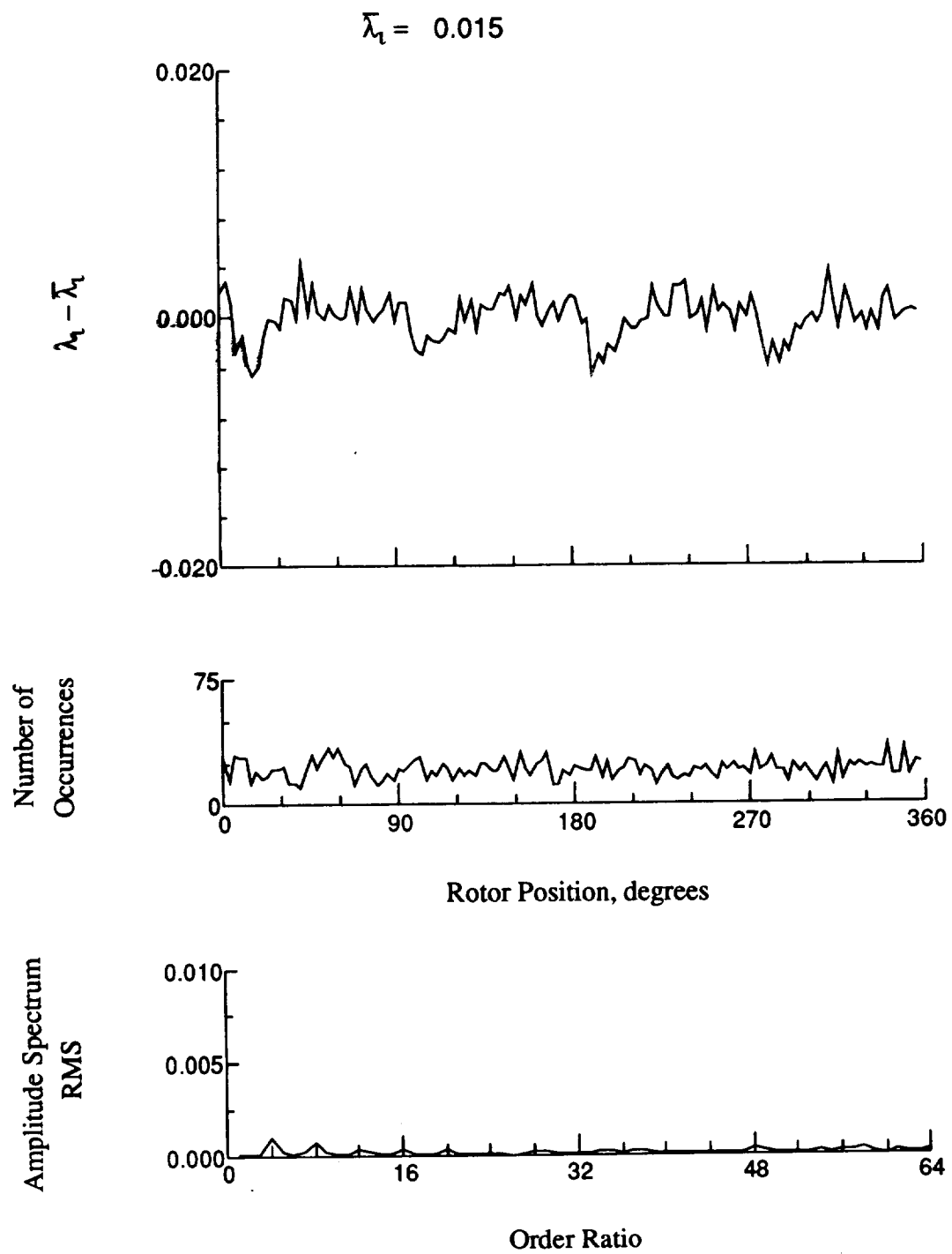


Figure 111.- Concluded.

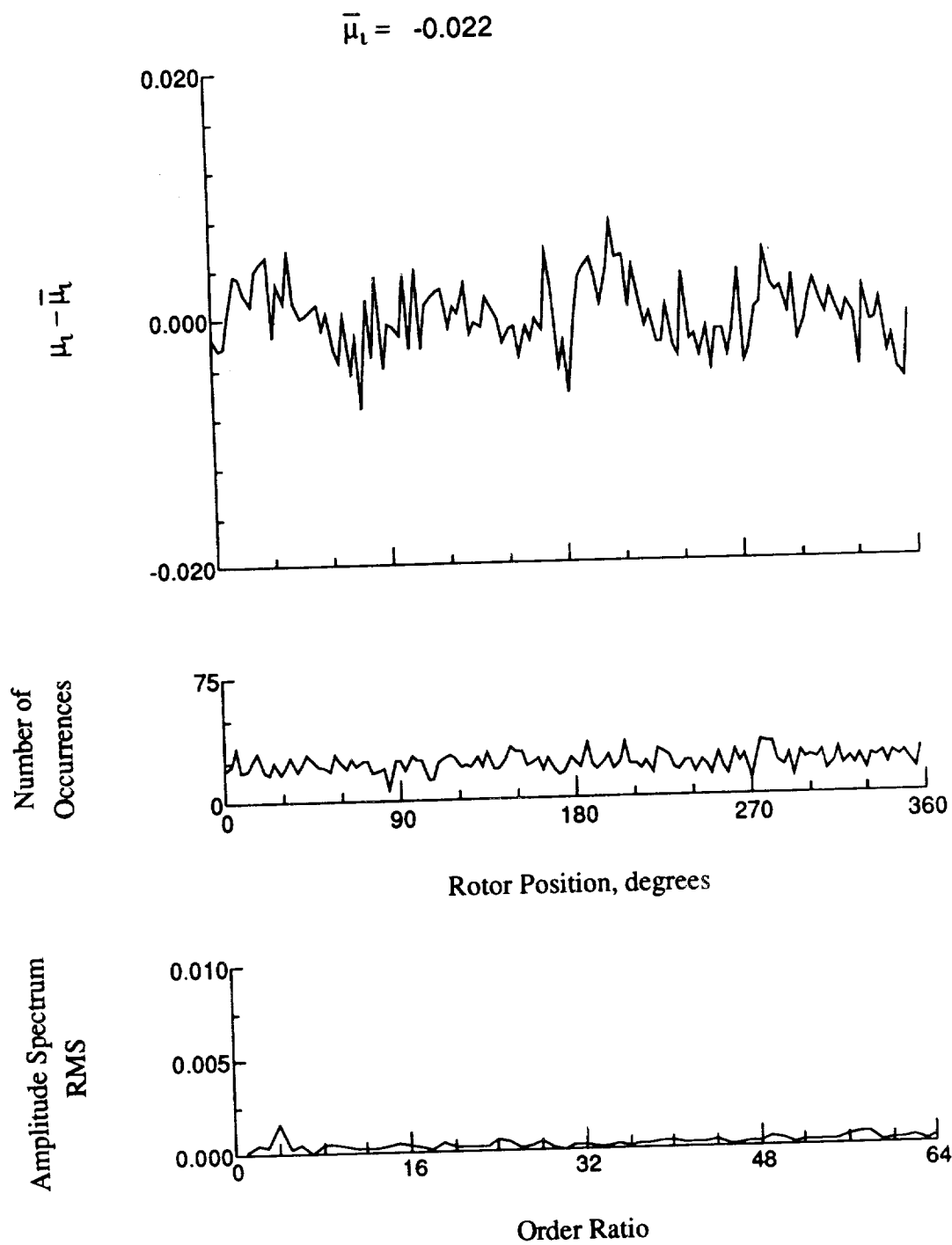


Figure 112.- Induced inflow velocity measured at 180 degrees and r/R of 0.90.

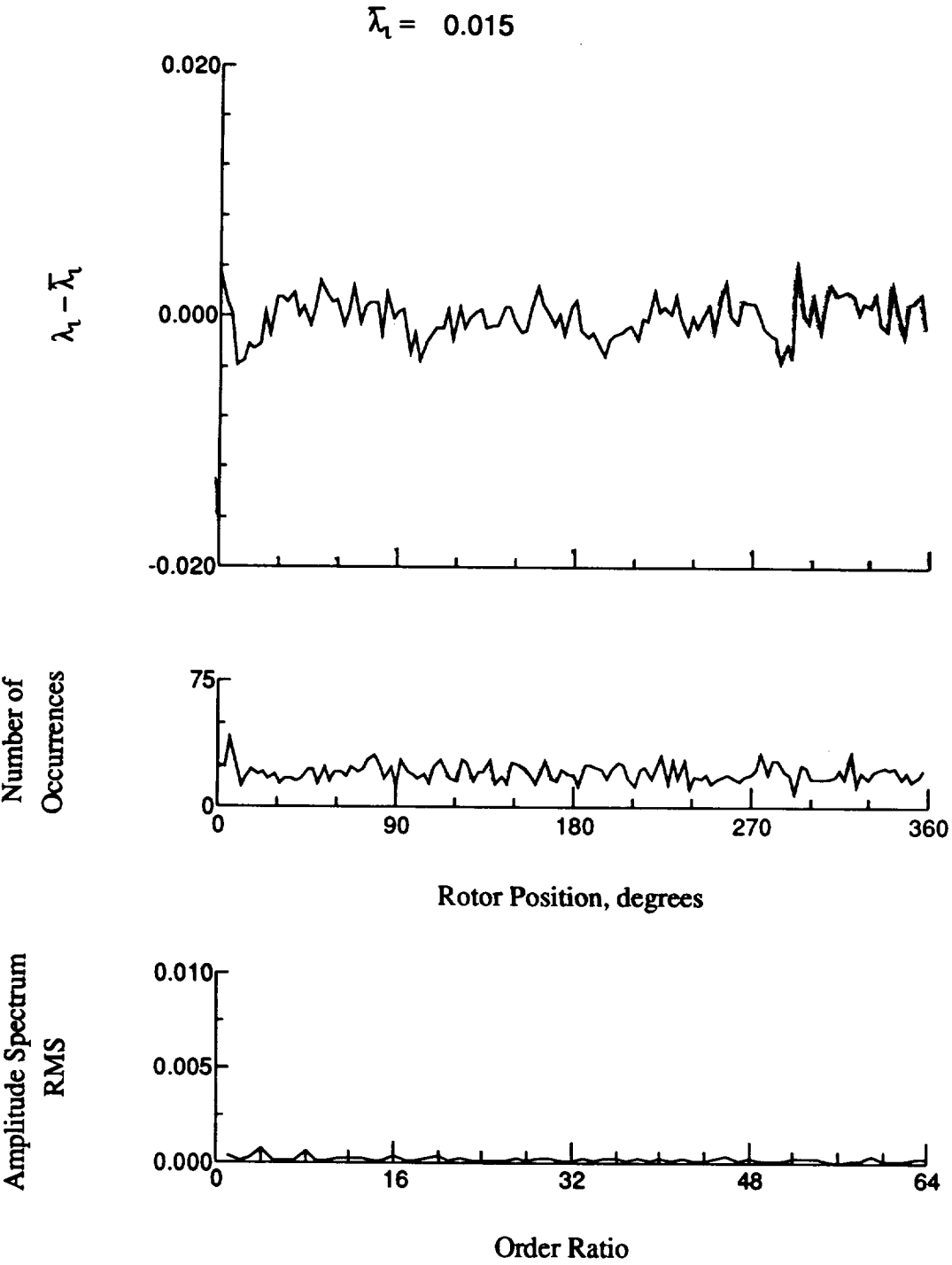


Figure 112.- Concluded.

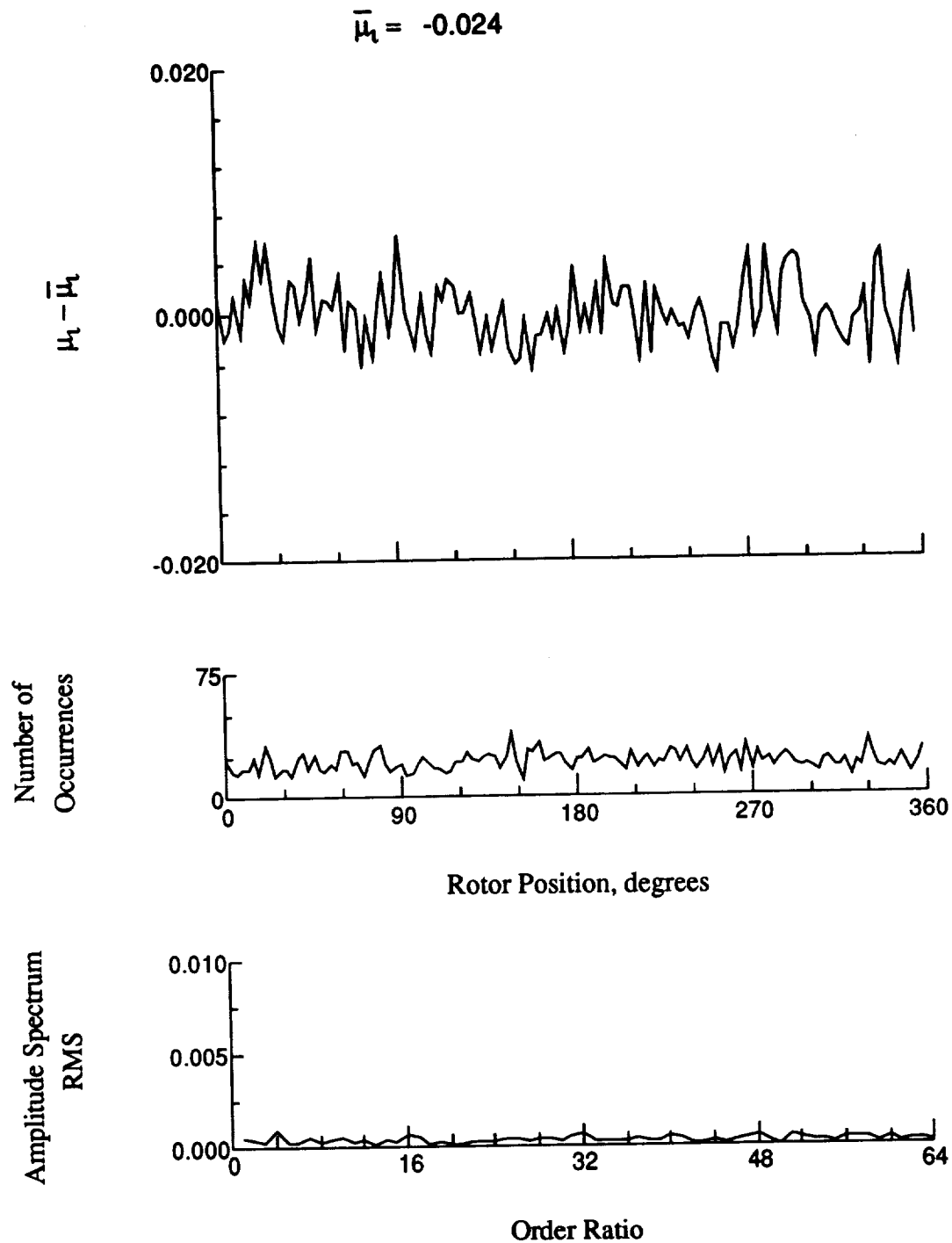


Figure 113.- Induced inflow velocity measured at 180 degrees and r/R of 0.94.

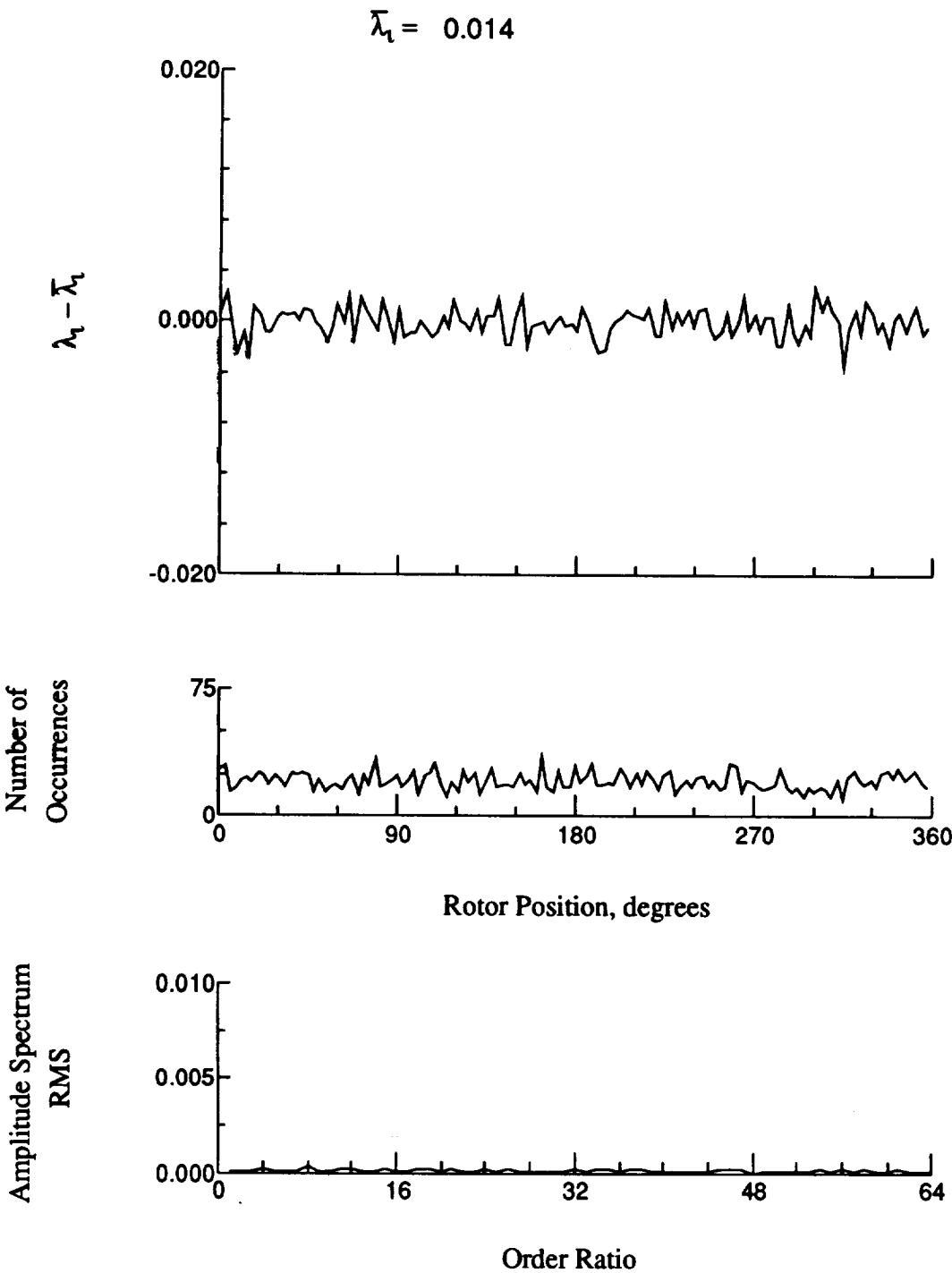


Figure 113.- Concluded.

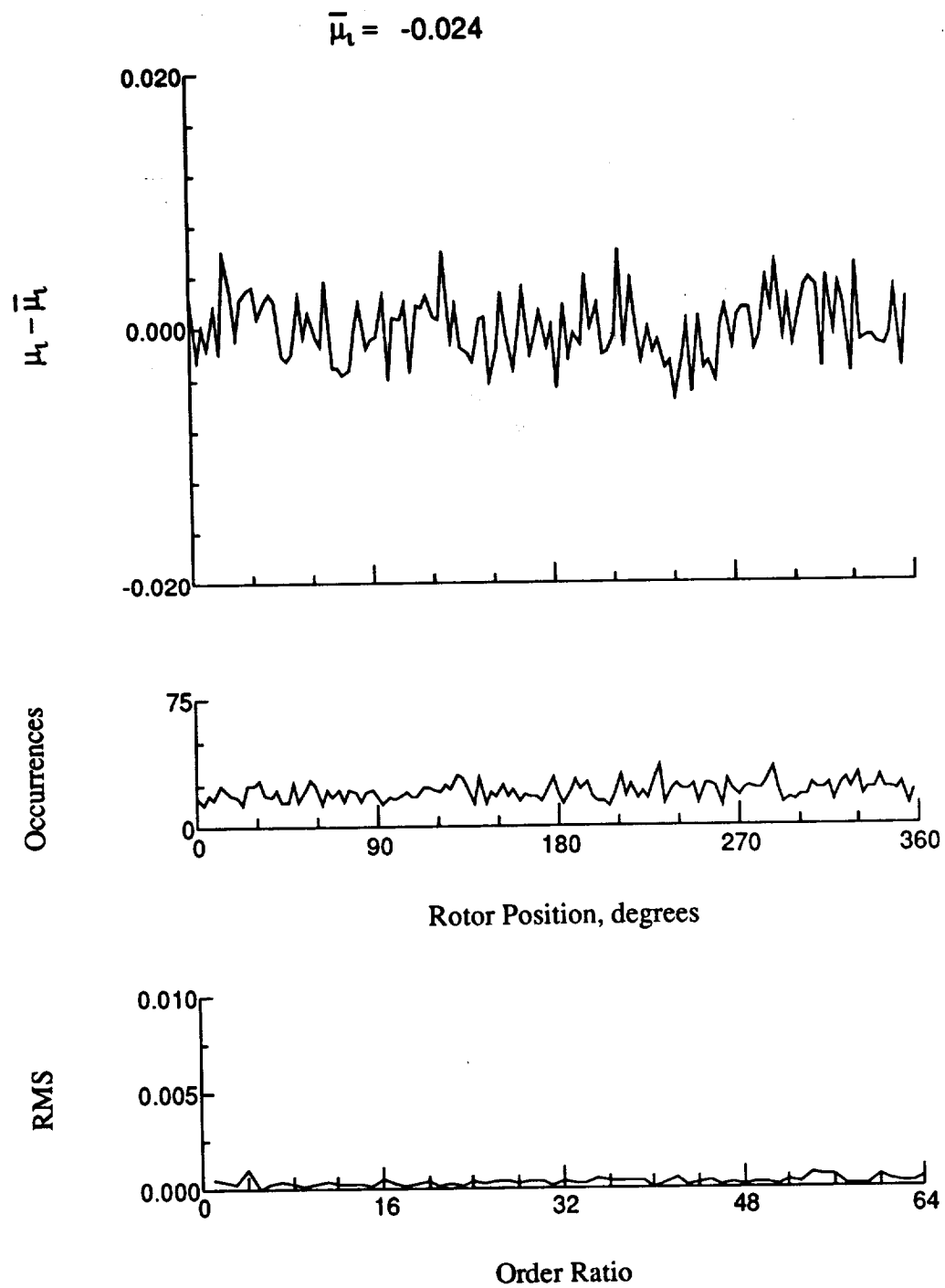


Figure 114.- Induced inflow velocity measured at 180 degrees and r/R of 0.96.

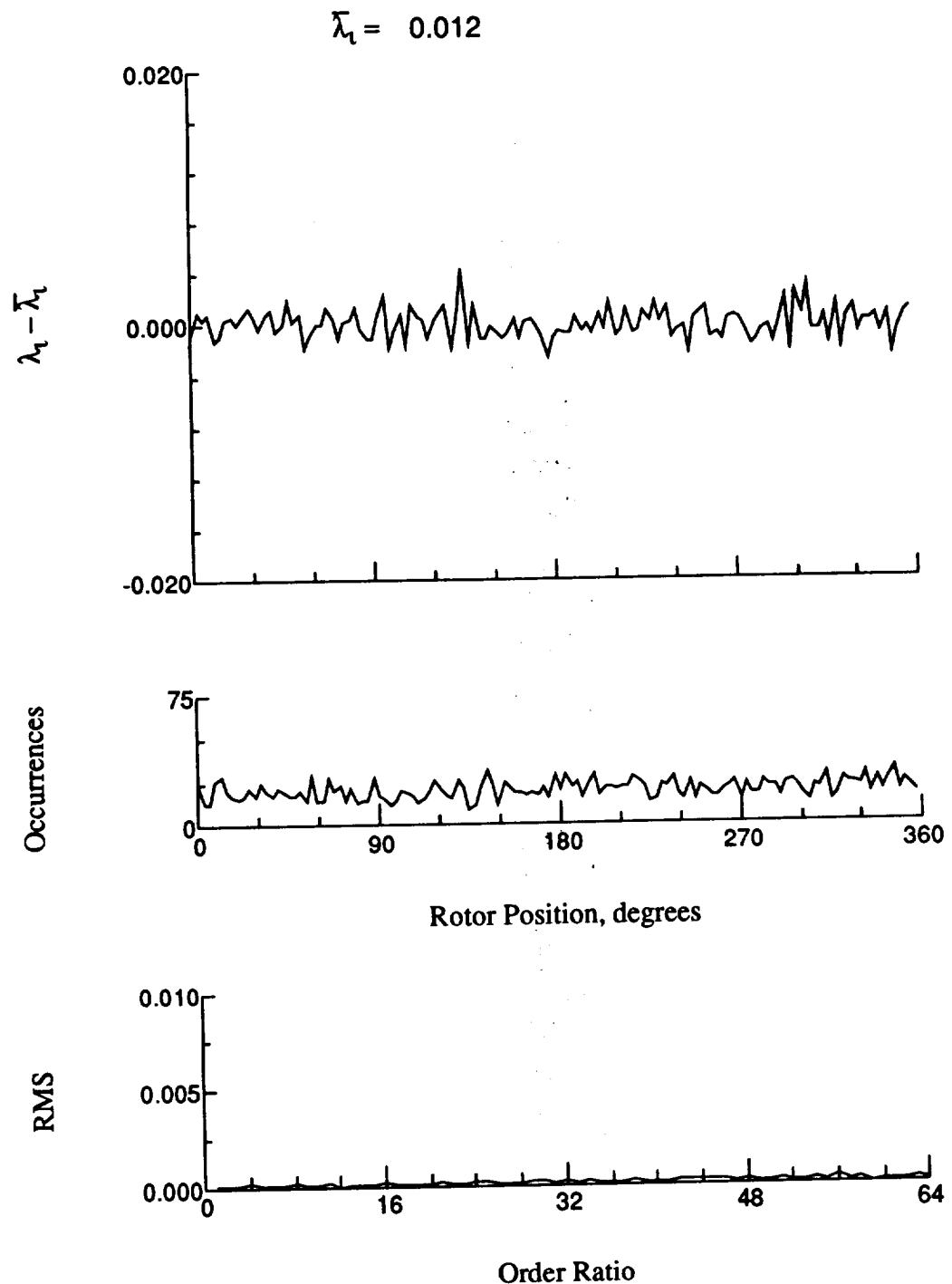


Figure 114.- Concluded.

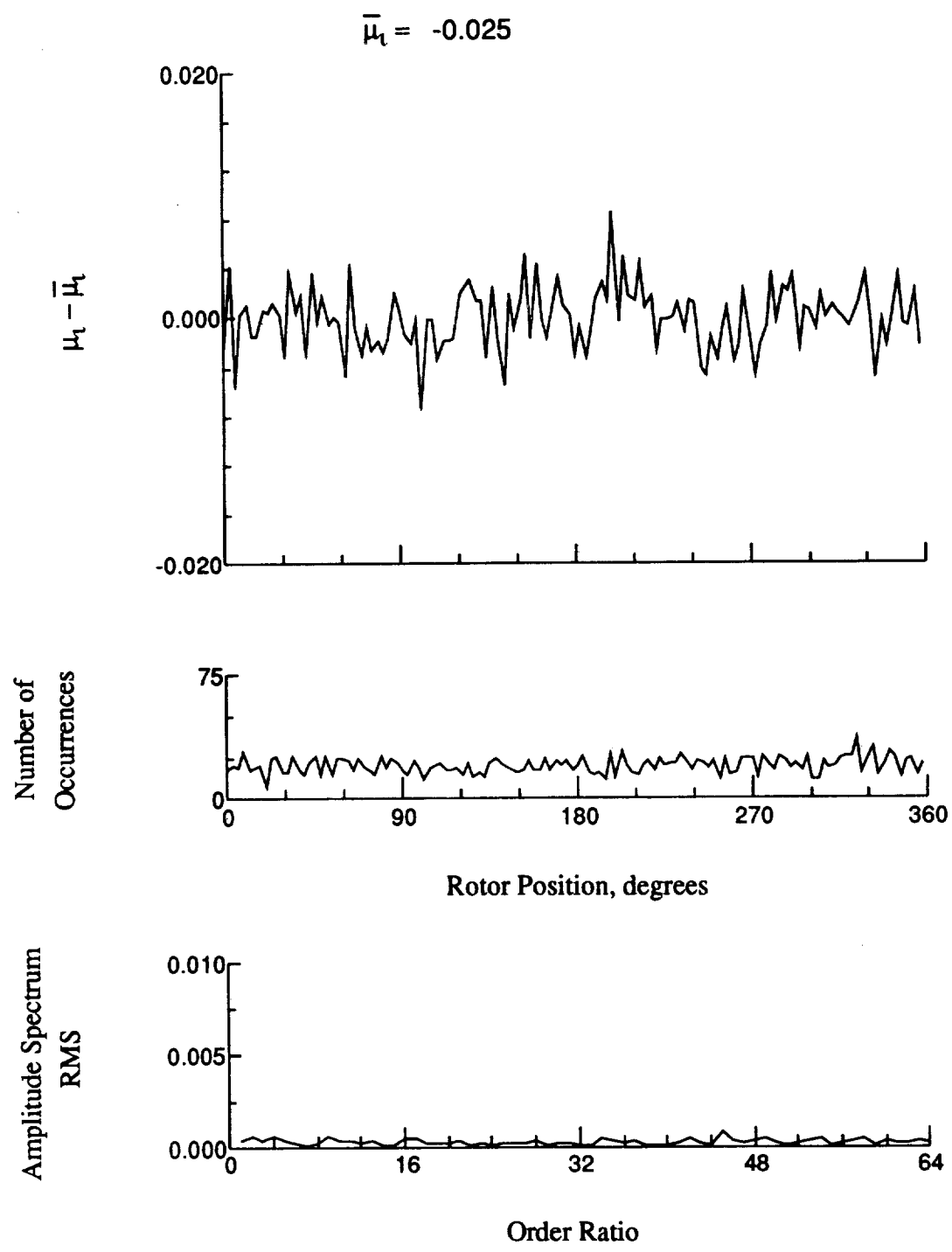


Figure 115.- Induced inflow velocity measured at 180 degrees and r/R of 1.00.

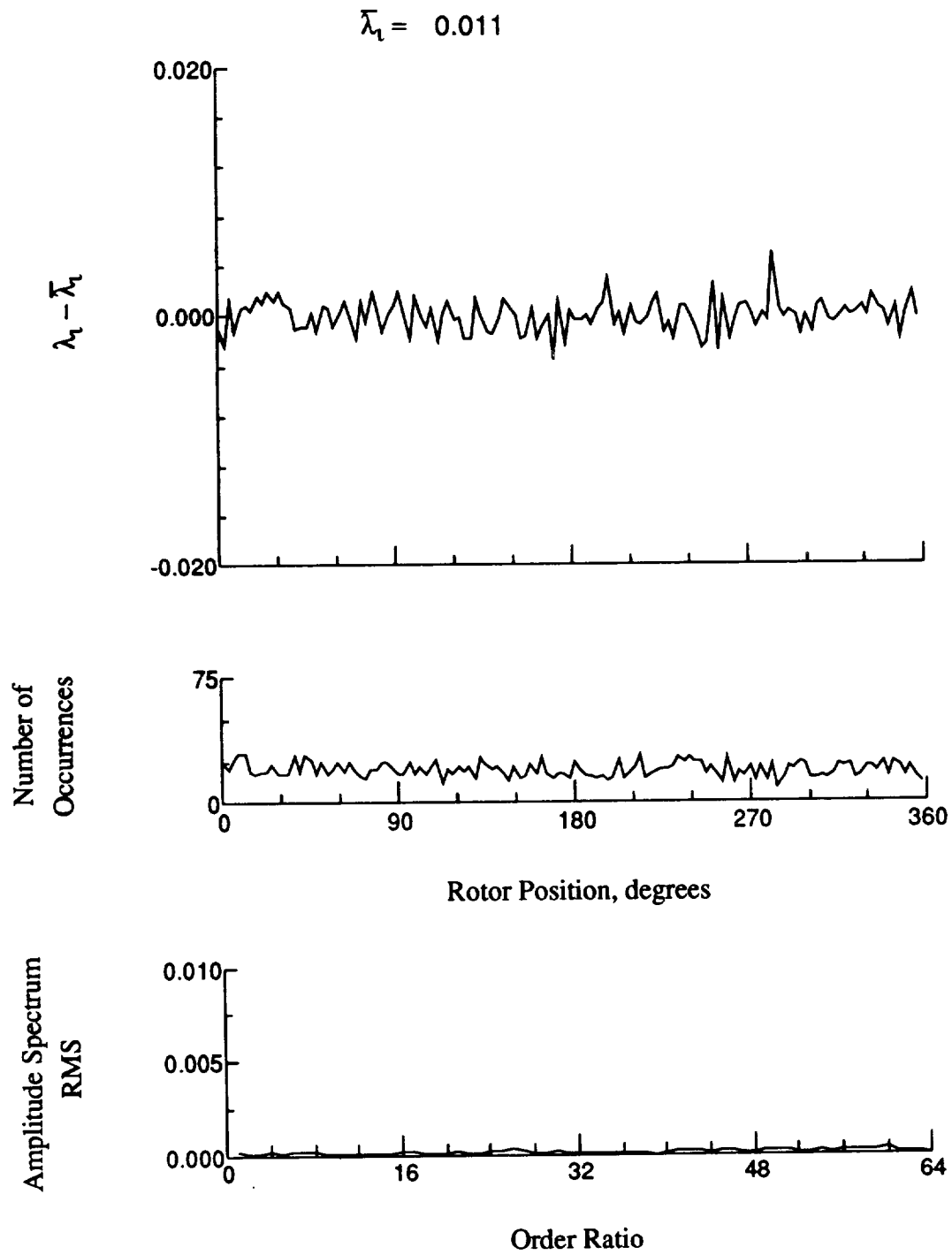


Figure 115.- Concluded.

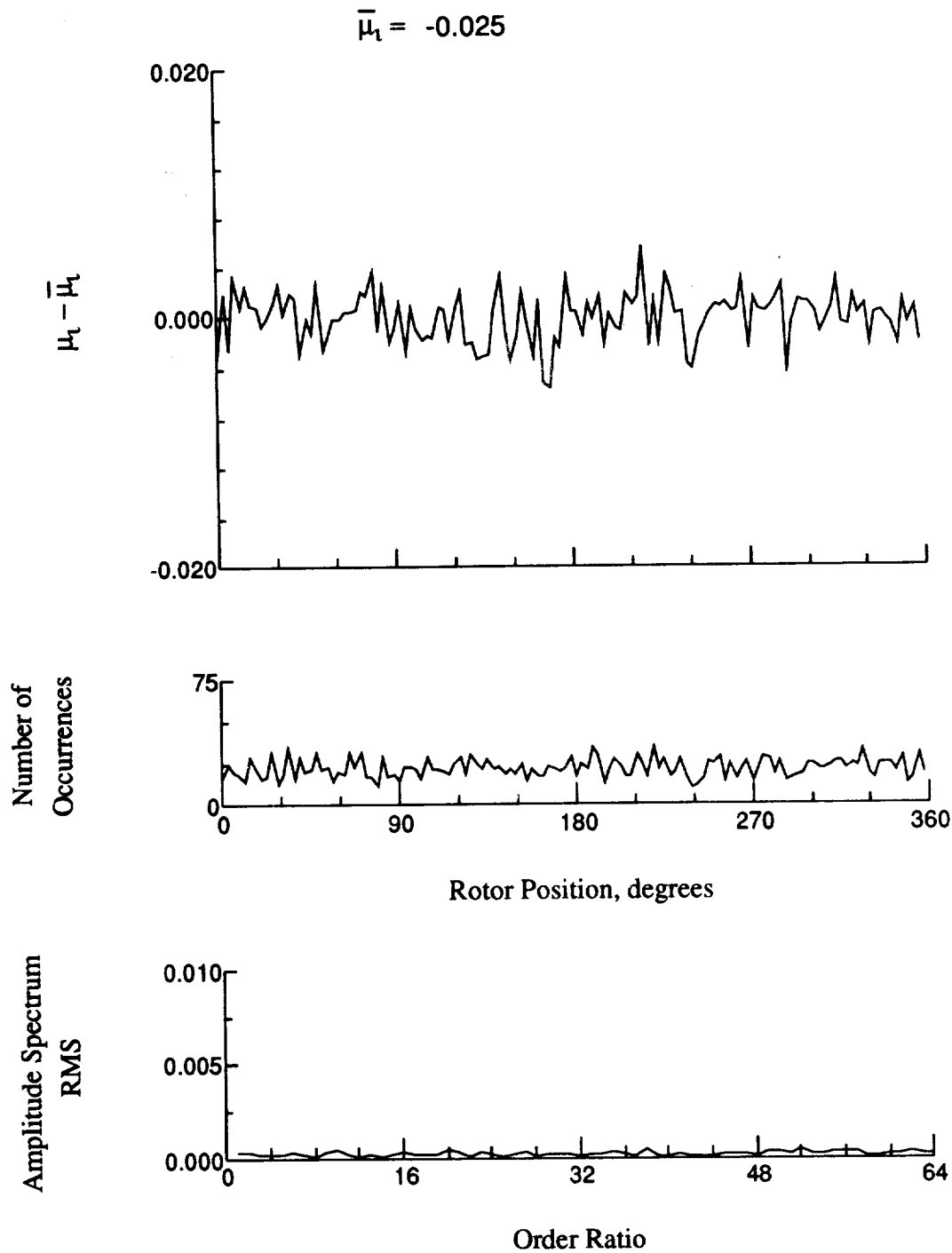


Figure 116.- Induced inflow velocity measured at 180 degrees and r/R of 1.10.

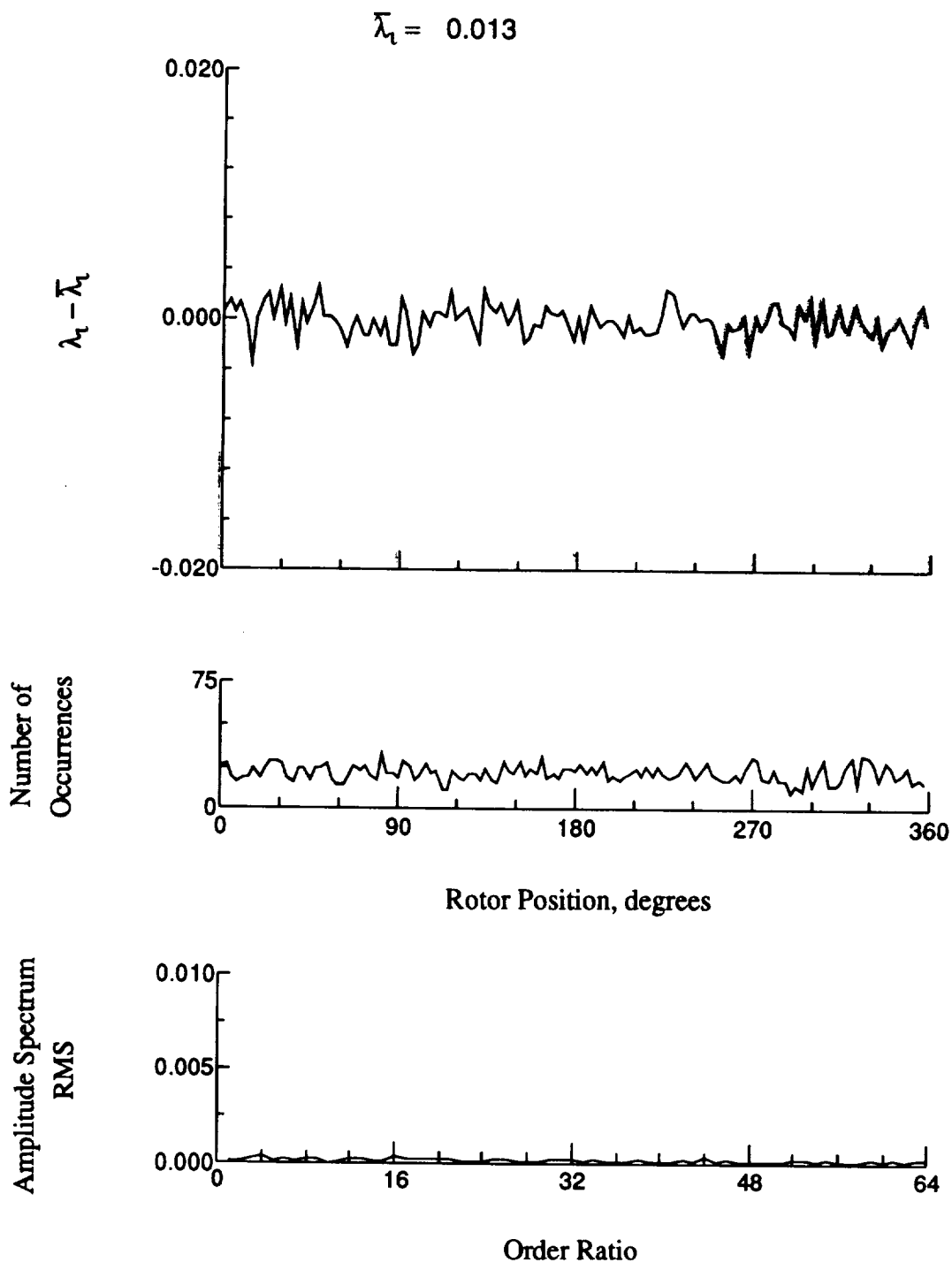


Figure 116.- Concluded.

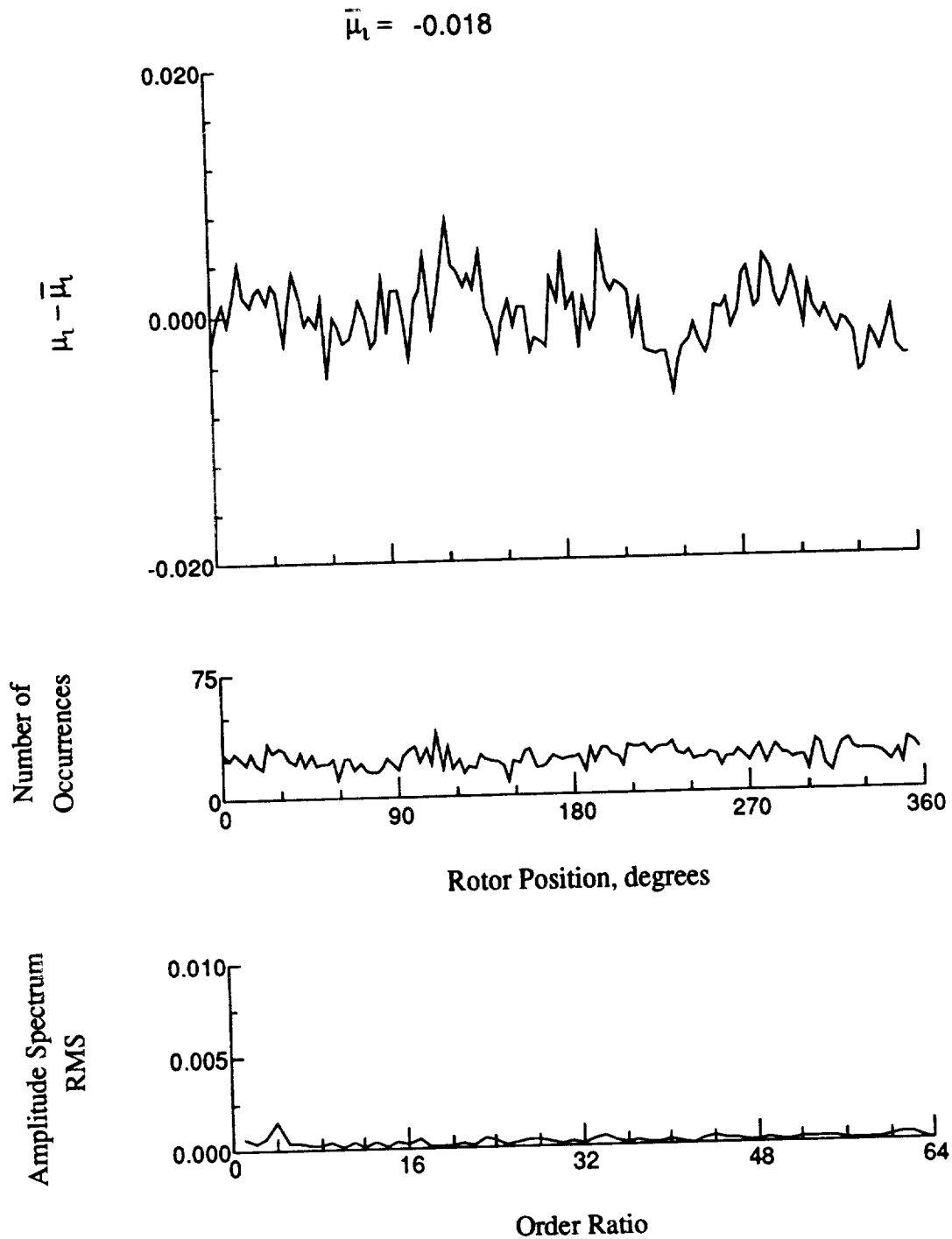


Figure 117.- Induced inflow velocity measured at 210 degrees and r/R of 0.20.

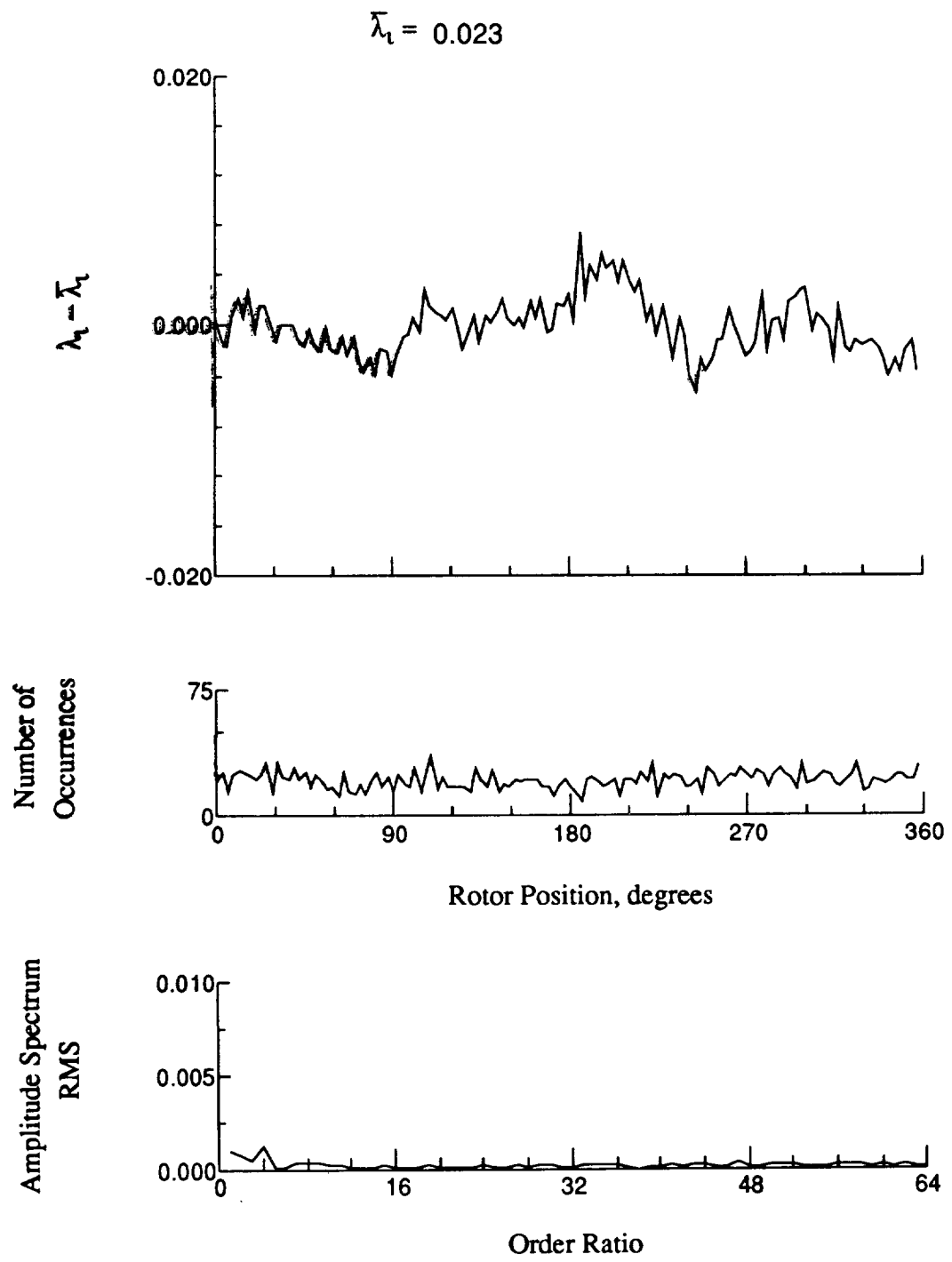


Figure 117.- Concluded.

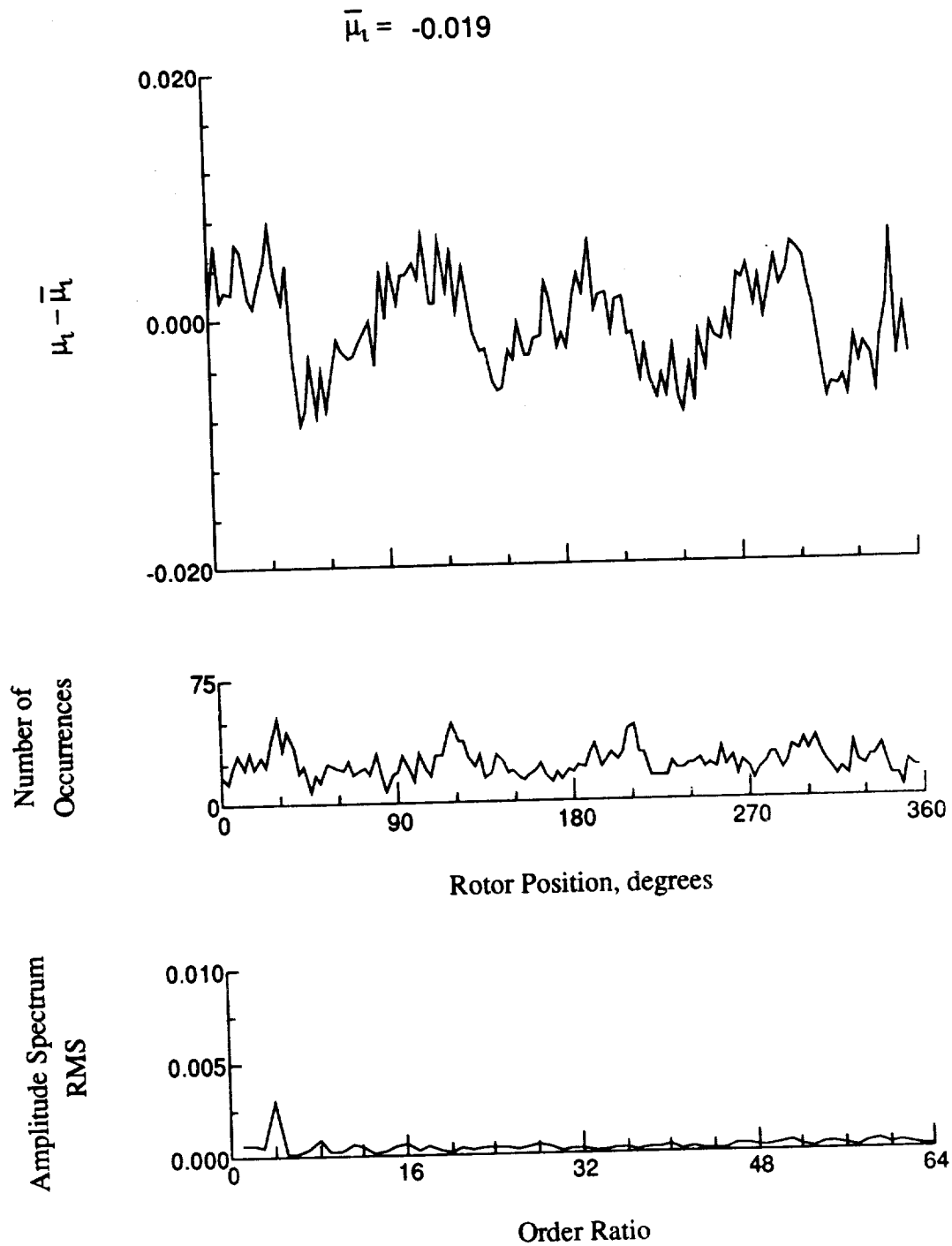


Figure 118.- Induced inflow velocity measured at 210 degrees and r/R of 0.32.

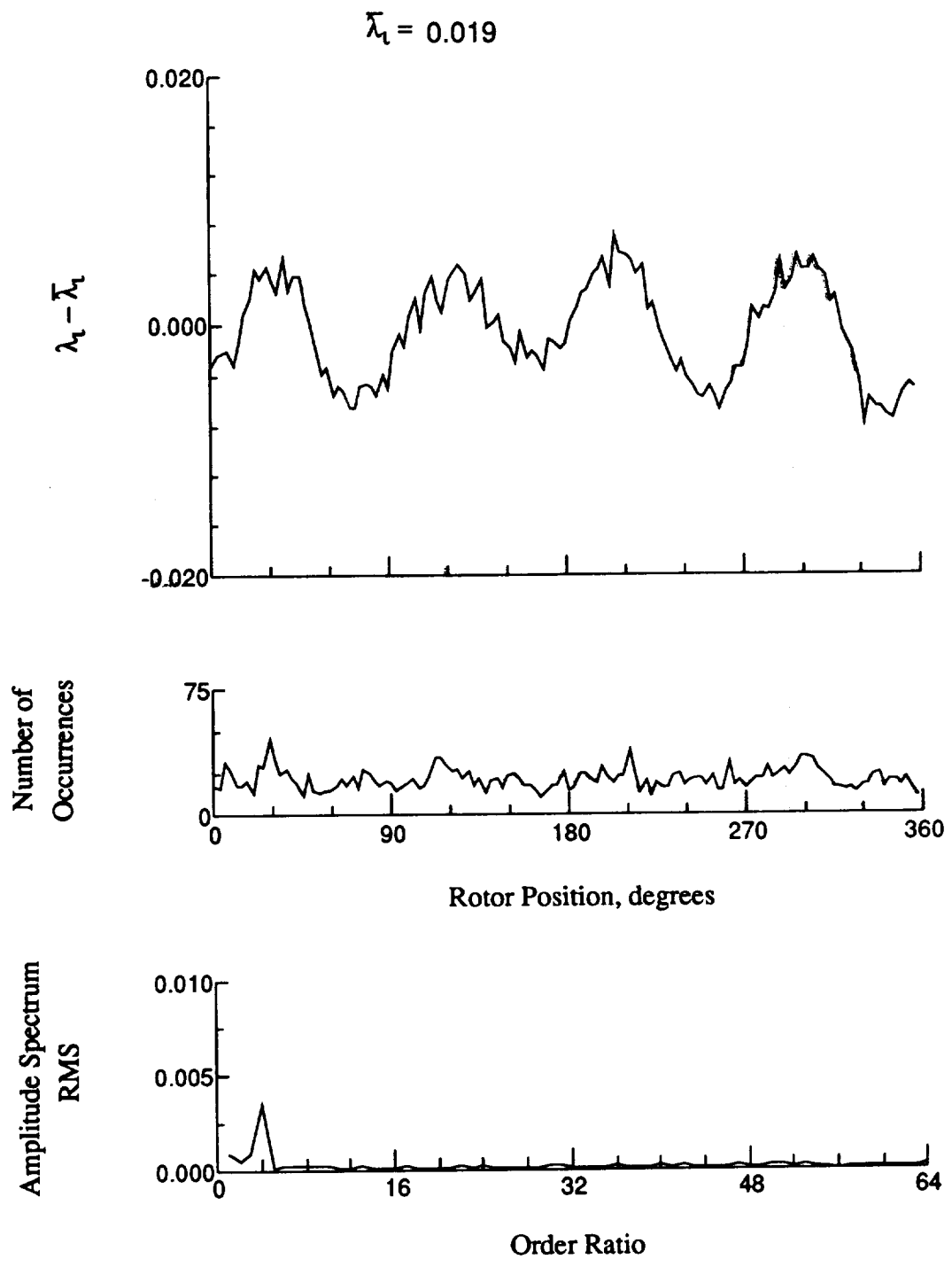


Figure 118.- Concluded.

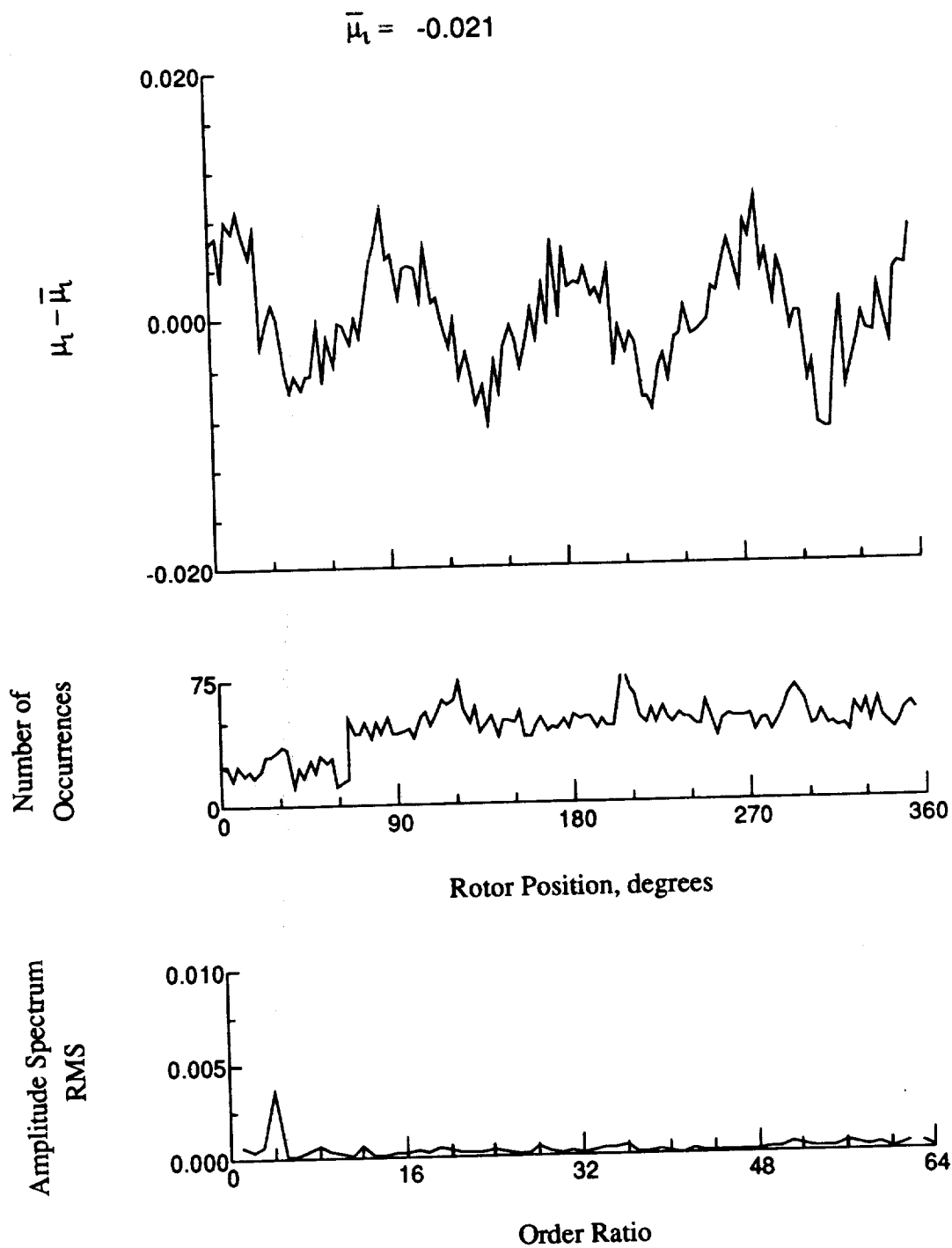


Figure 119.- Induced inflow velocity measured at 210 degrees and r/R of 0.50.

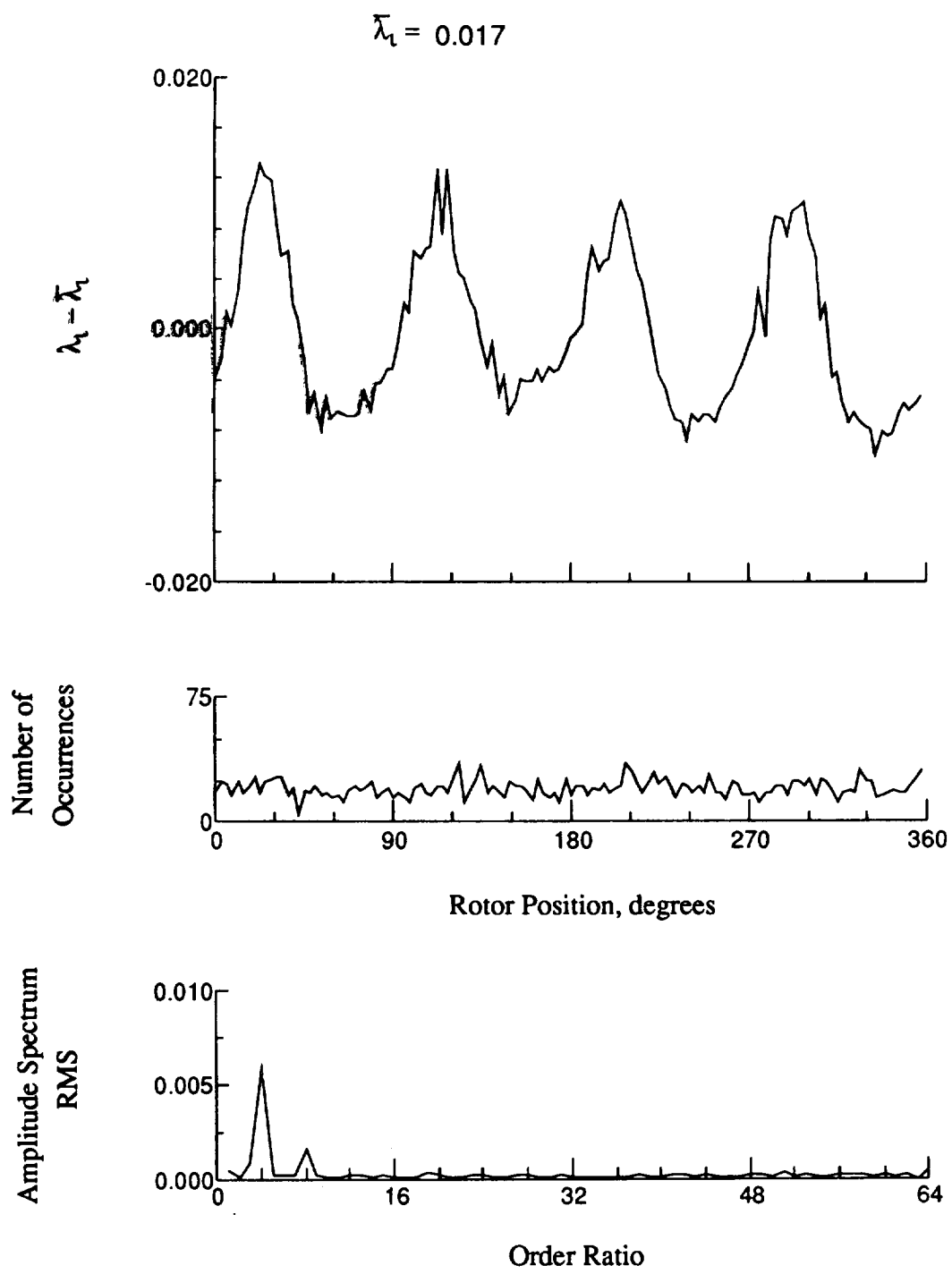


Figure 119.- Concluded.

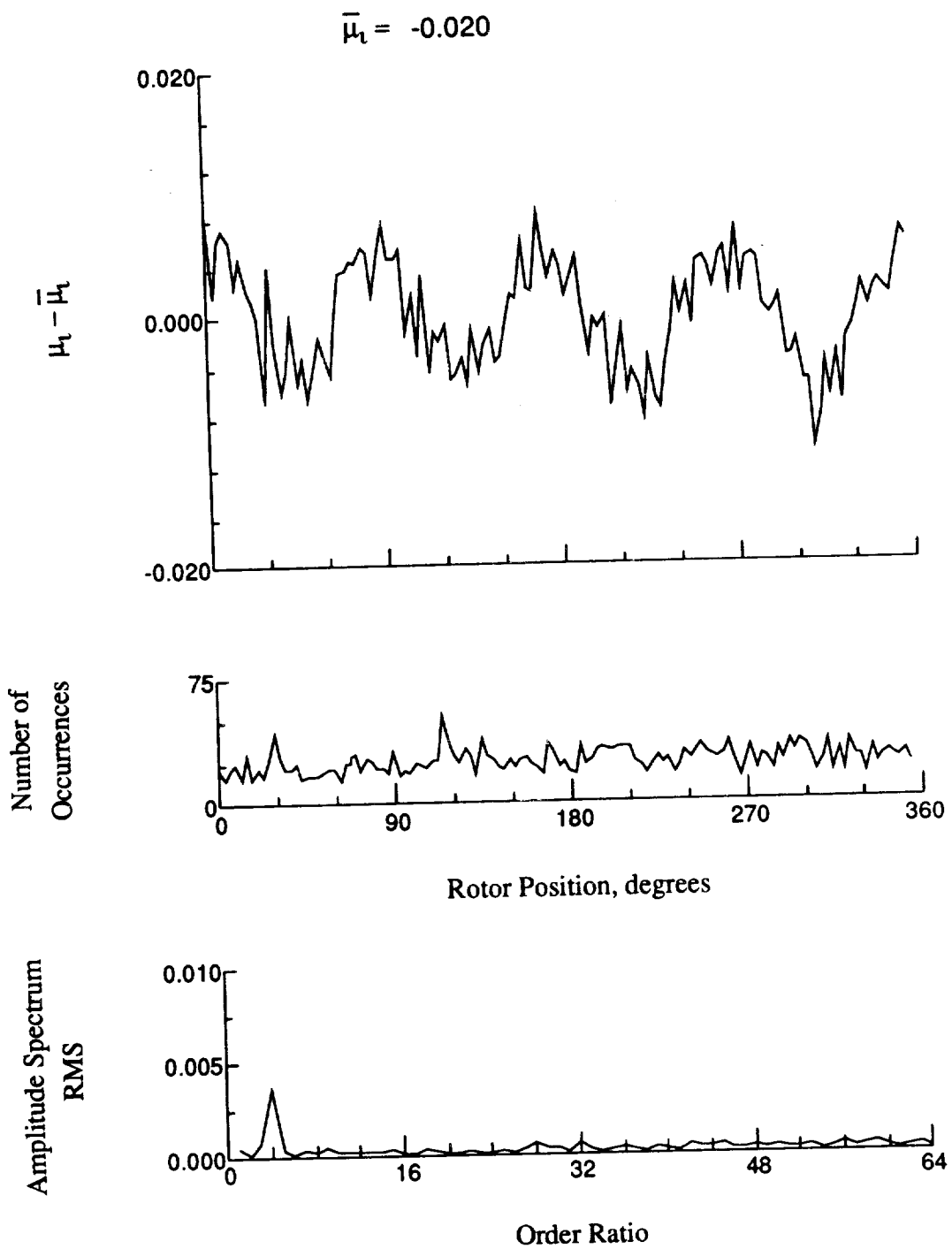


Figure 120.- Induced inflow velocity measured at 210 degrees and r/R of 0.58.

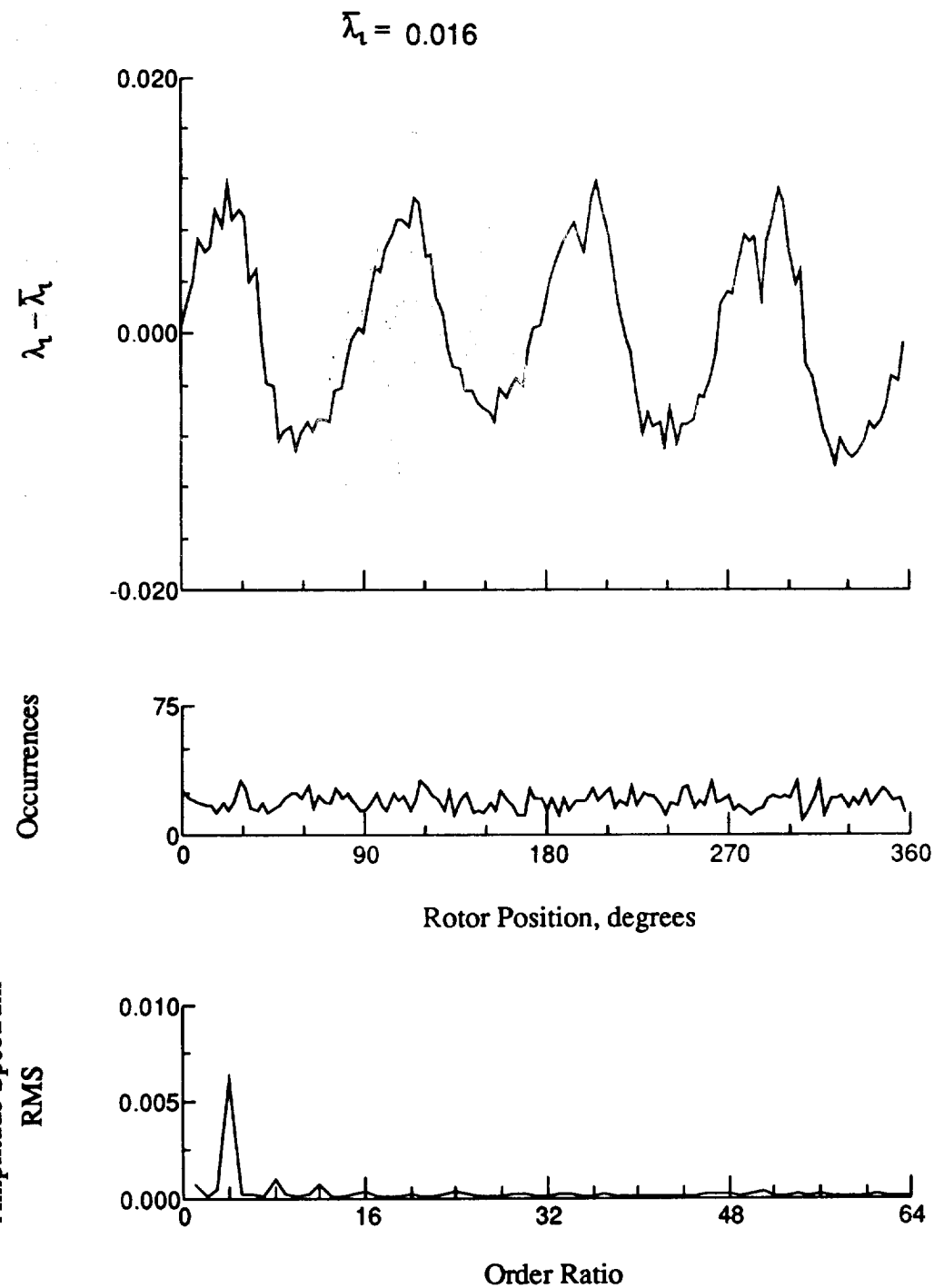


Figure 120.- Concluded.

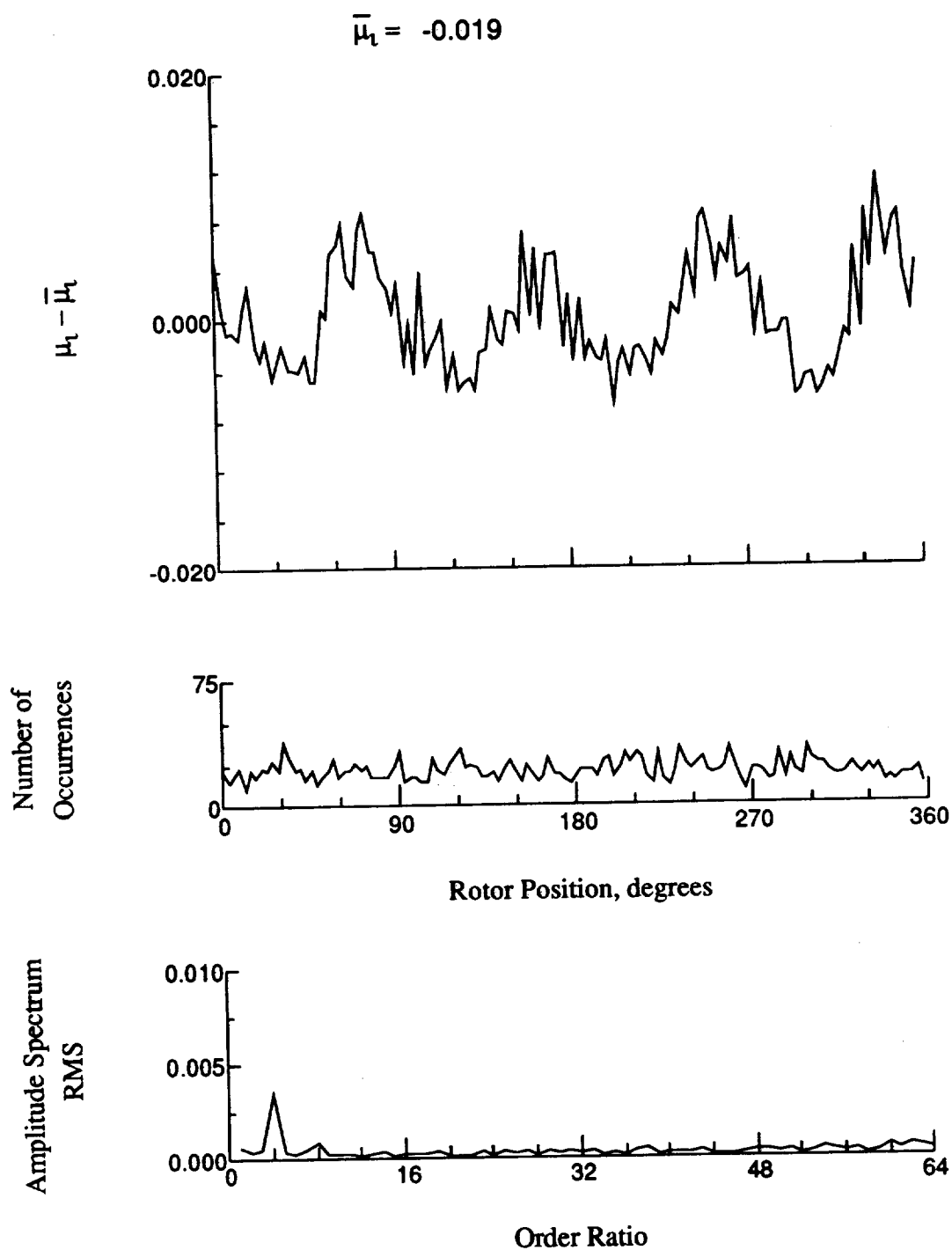


Figure 121.- Induced inflow velocity measured at 210 degrees and r/R of 0.69.

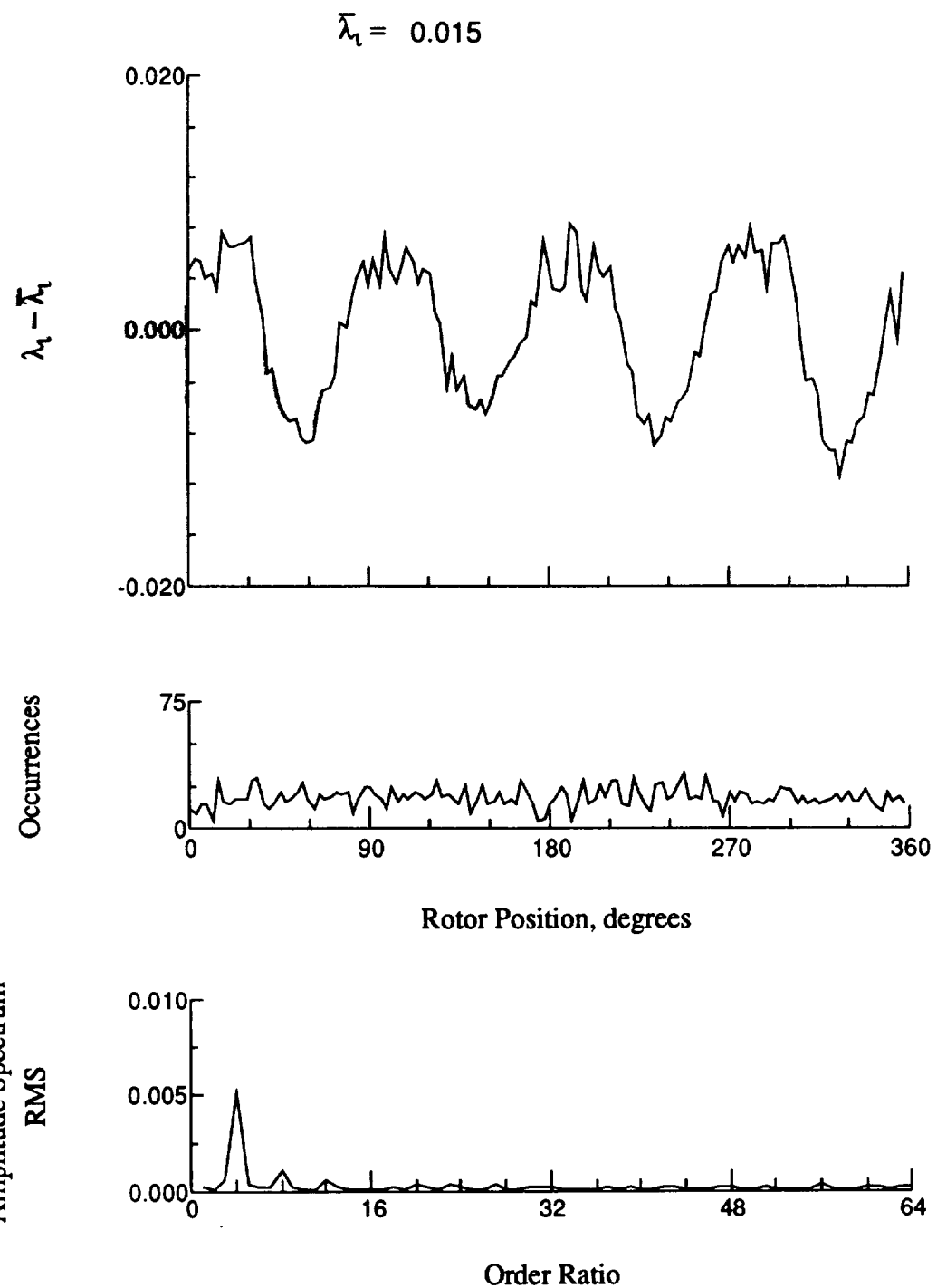


Figure 121.- Concluded.

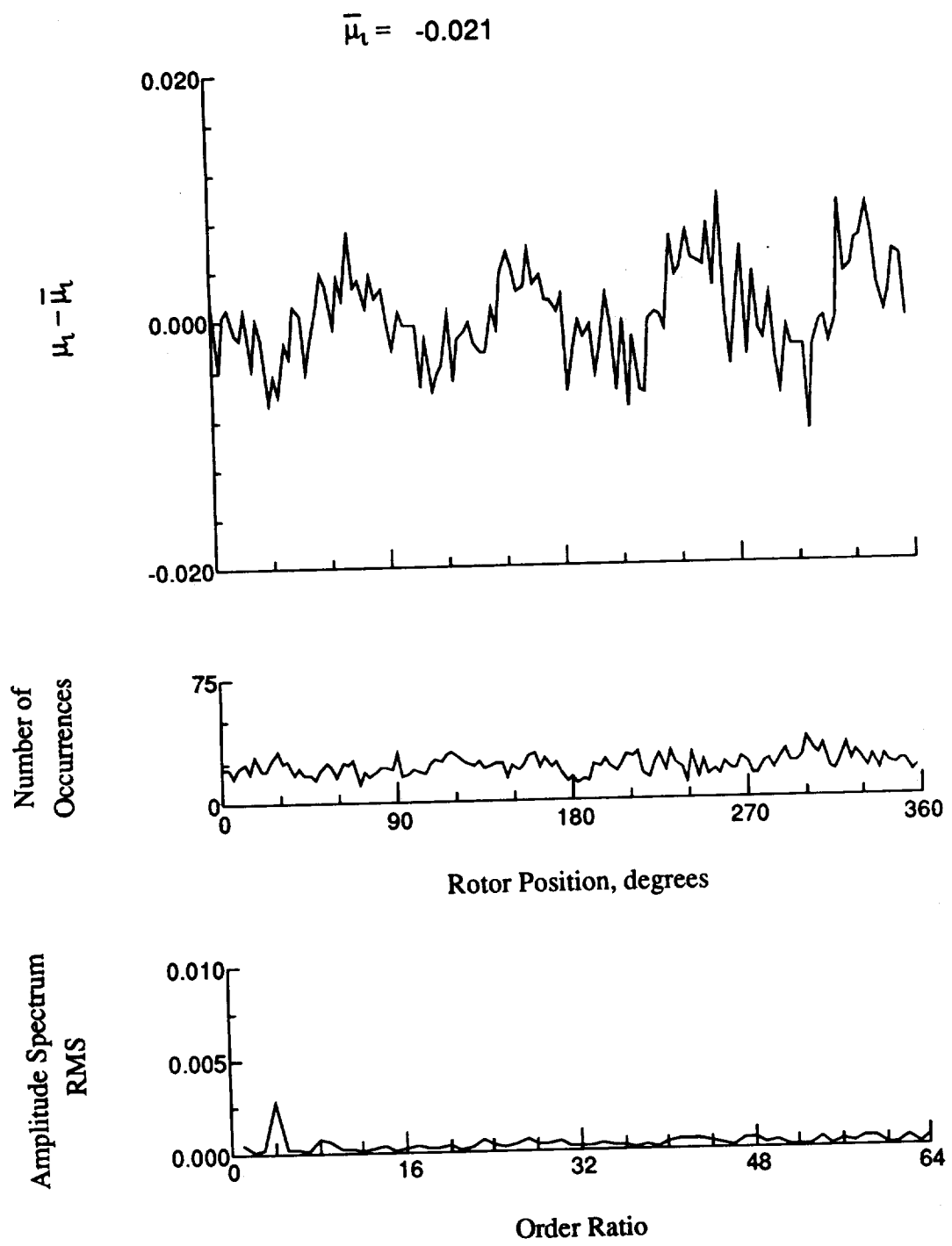


Figure 122.- Induced inflow velocity measured at 210 degrees and r/R of 0.73.

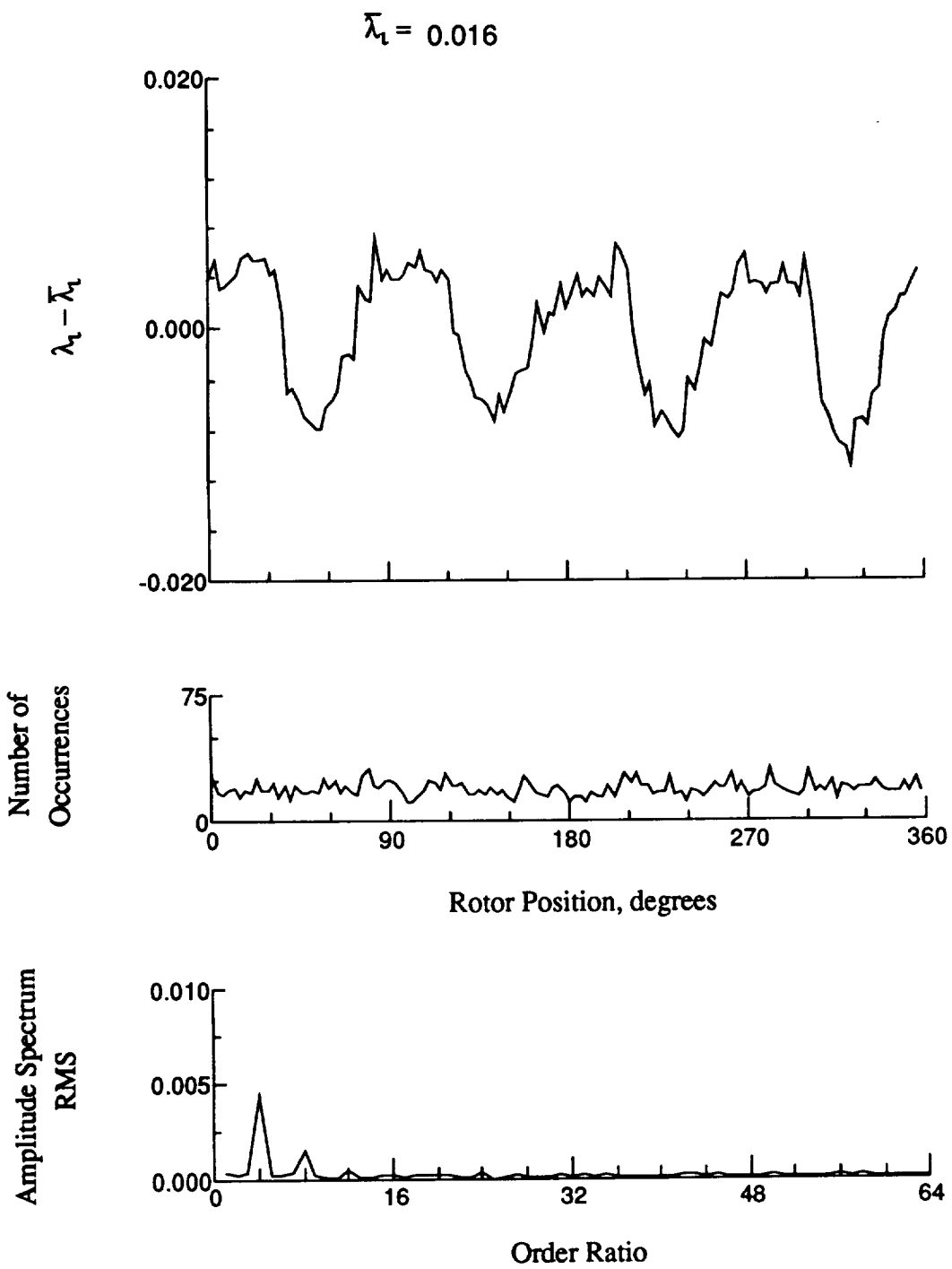


Figure 122.- Concluded.

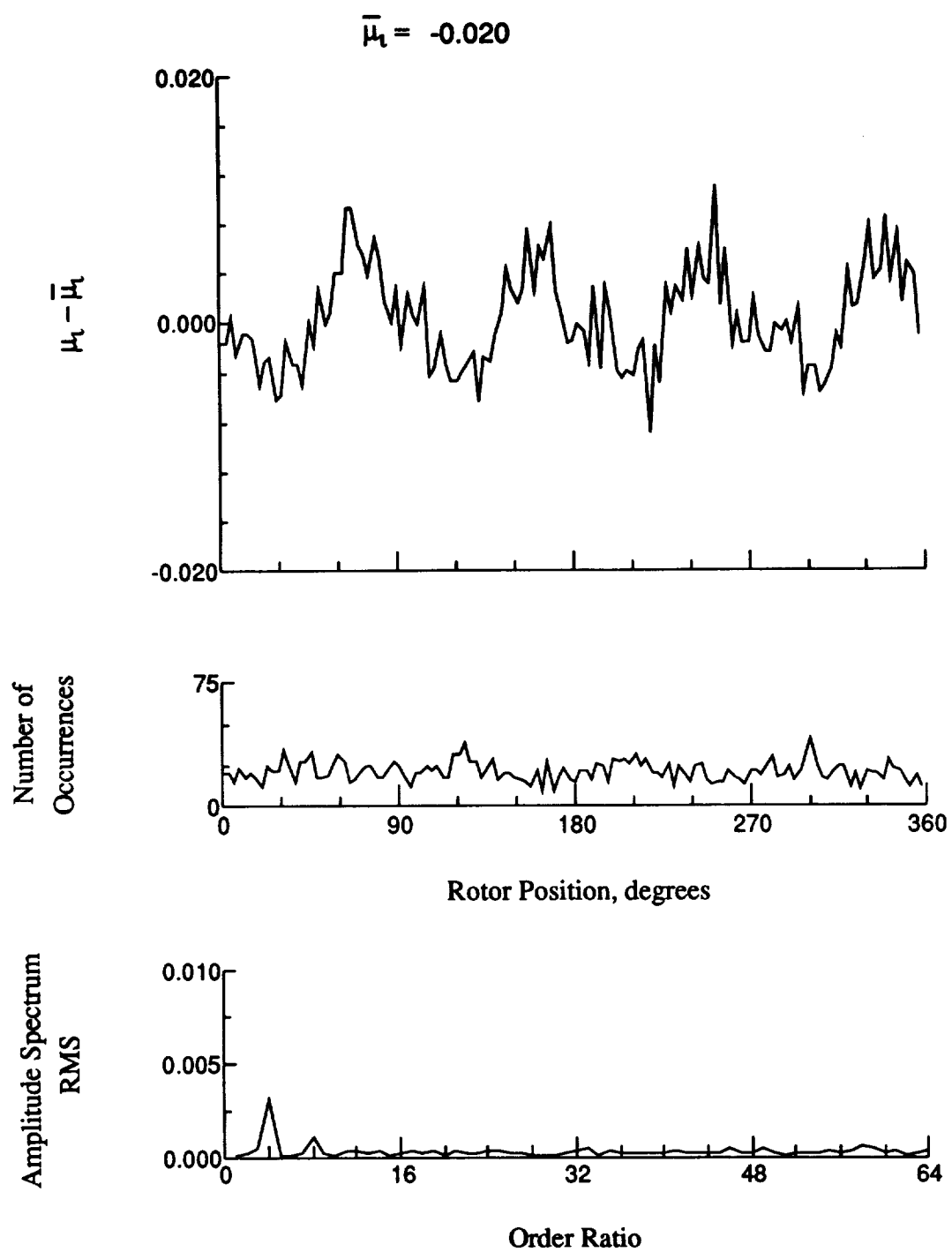


Figure 123.- Induced inflow velocity measured at 210 degrees and r/R of 0.75.

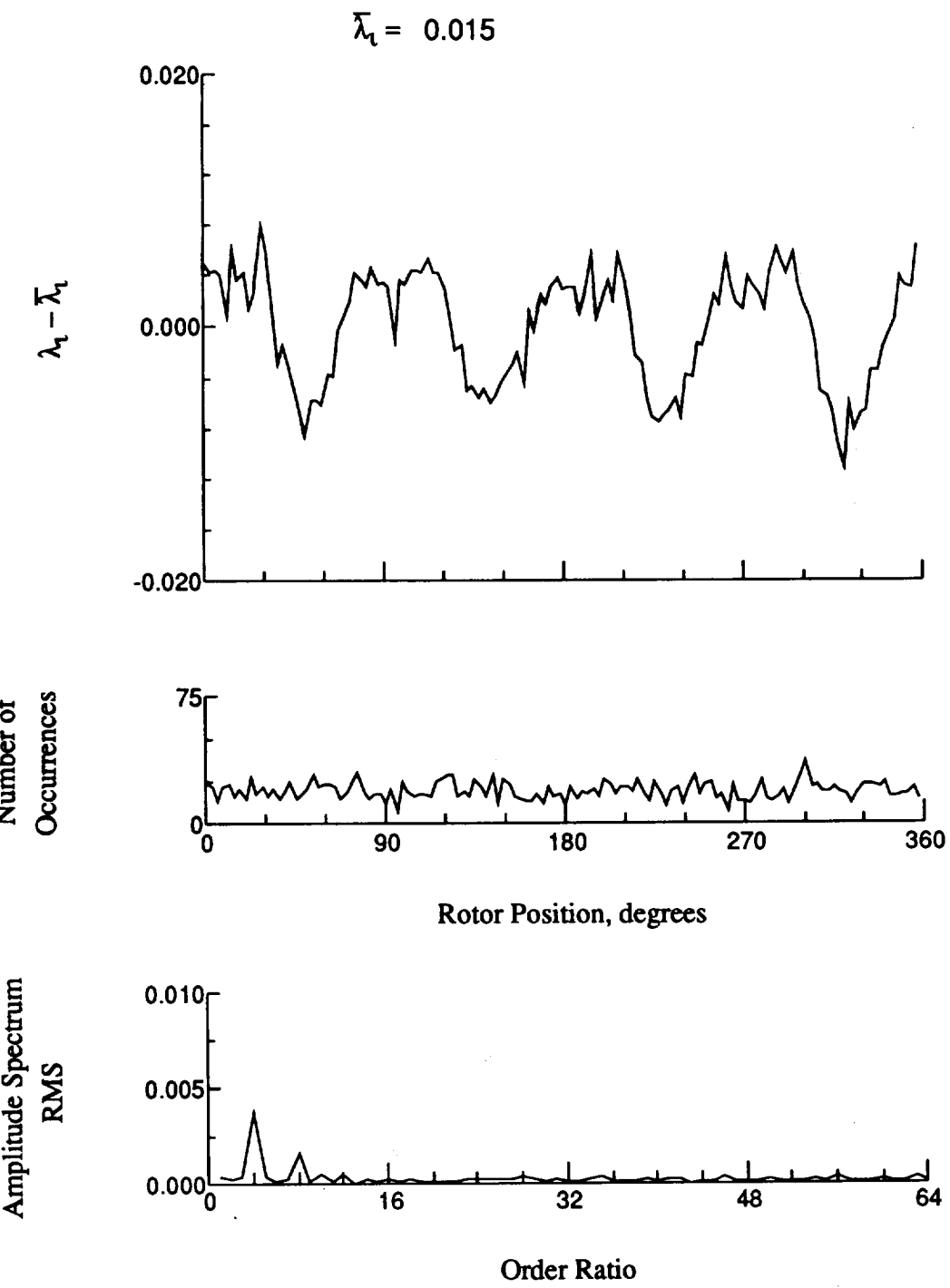


Figure 123.- Concluded.

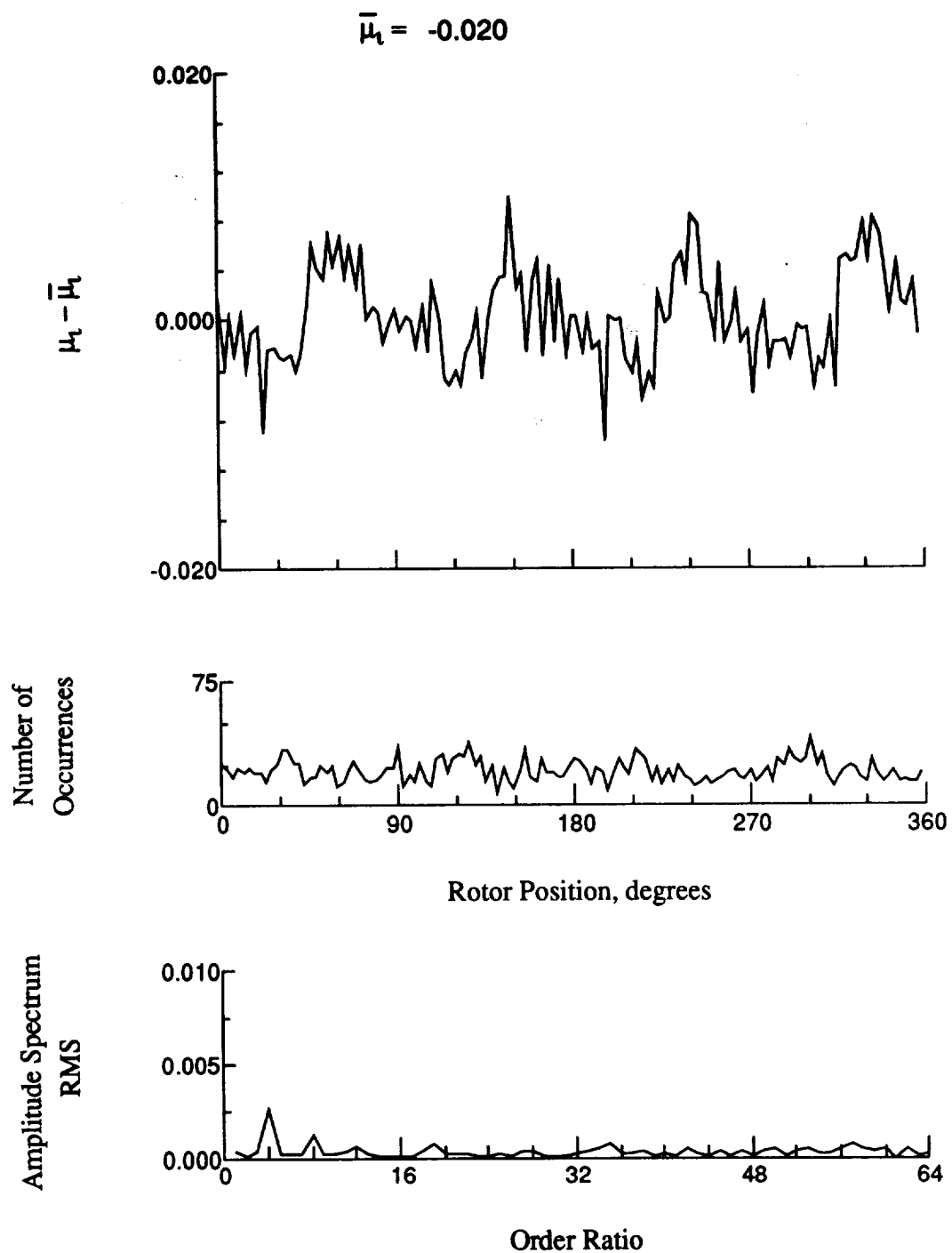


Figure 124.- Induced inflow velocity measured at 210 degrees and r/R of 0.81.

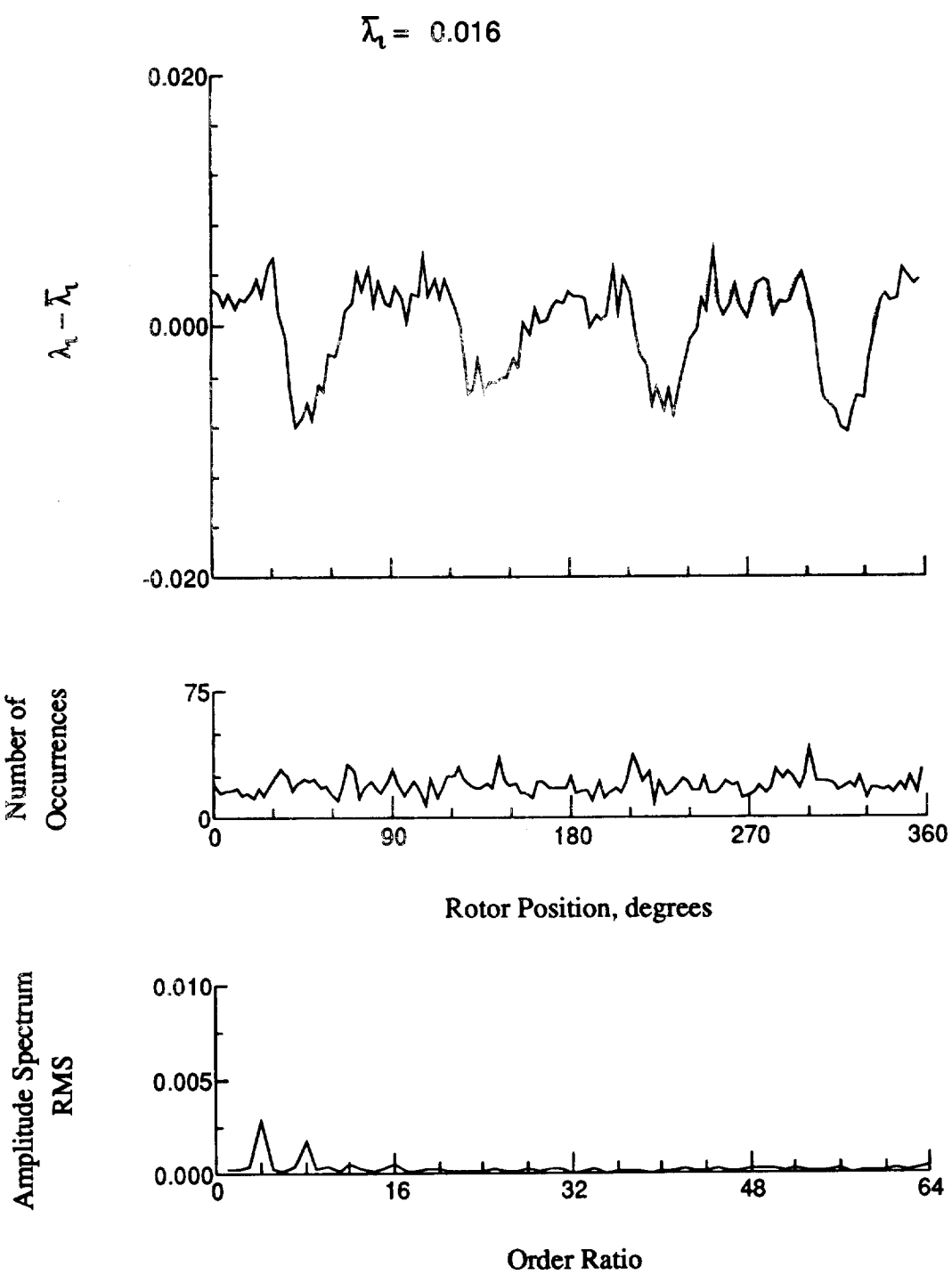


Figure 124.- Concluded.

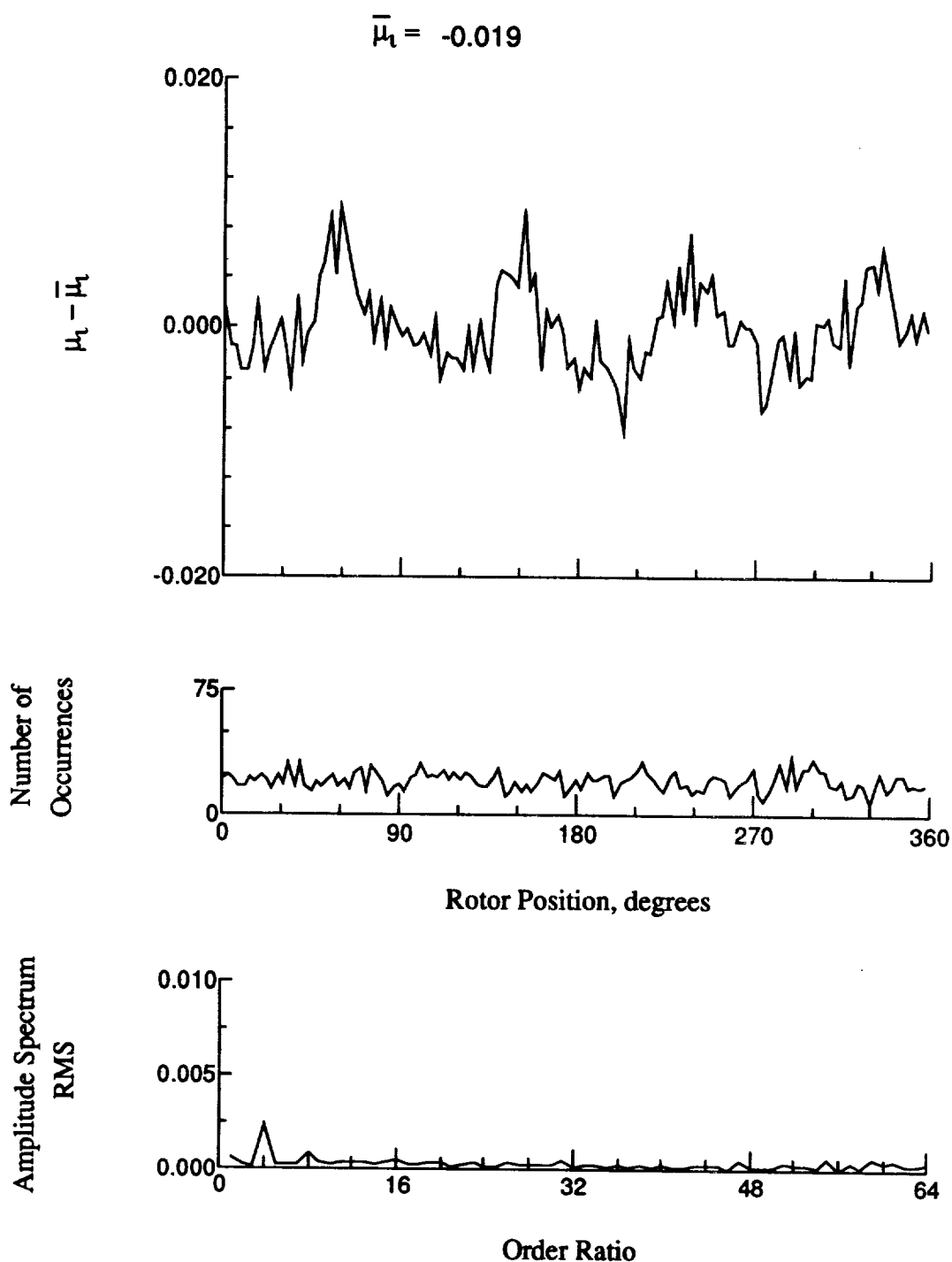


Figure 125.- Induced inflow velocity measured at 210 degrees and r/R of 0.86.

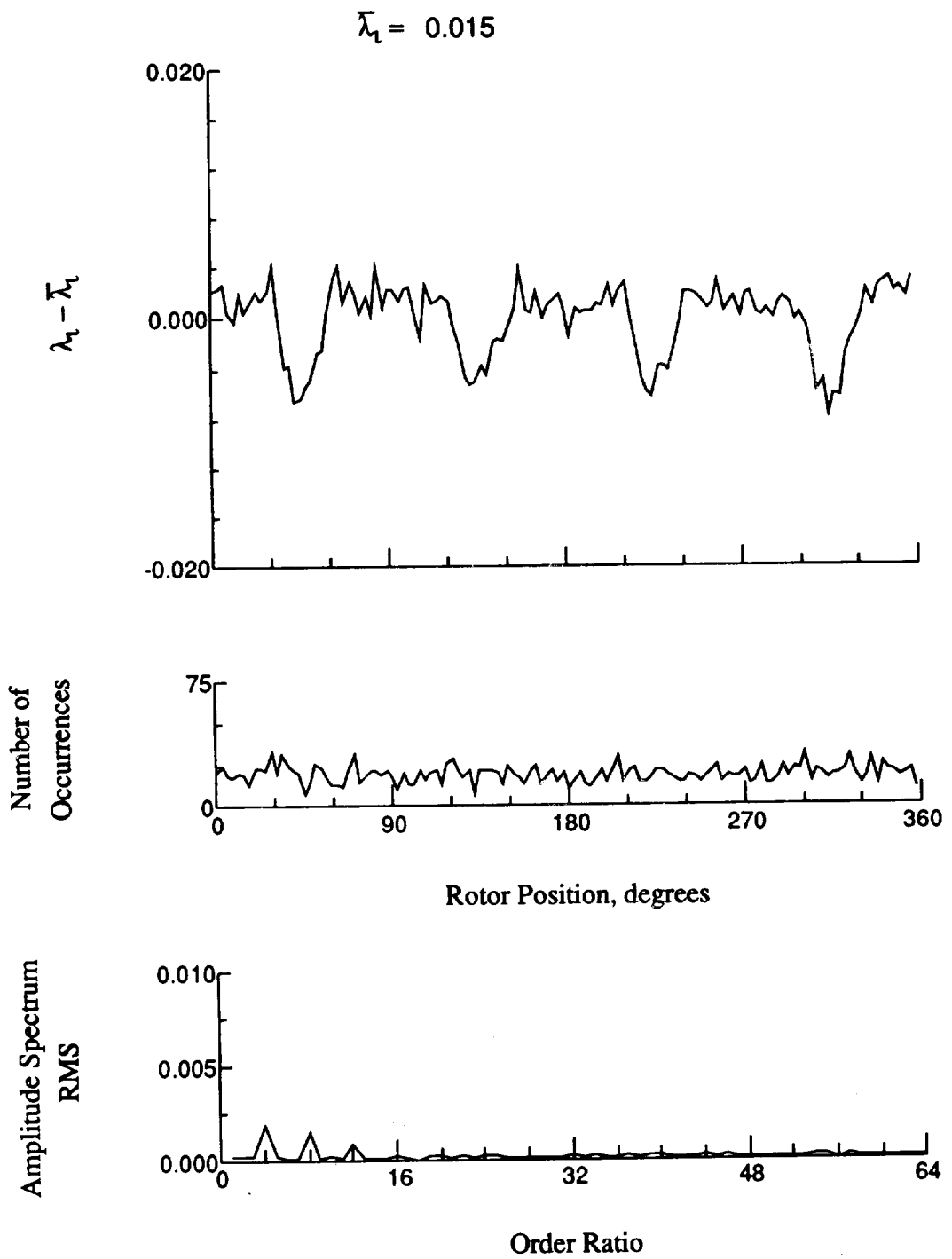


Figure 125.- Concluded.

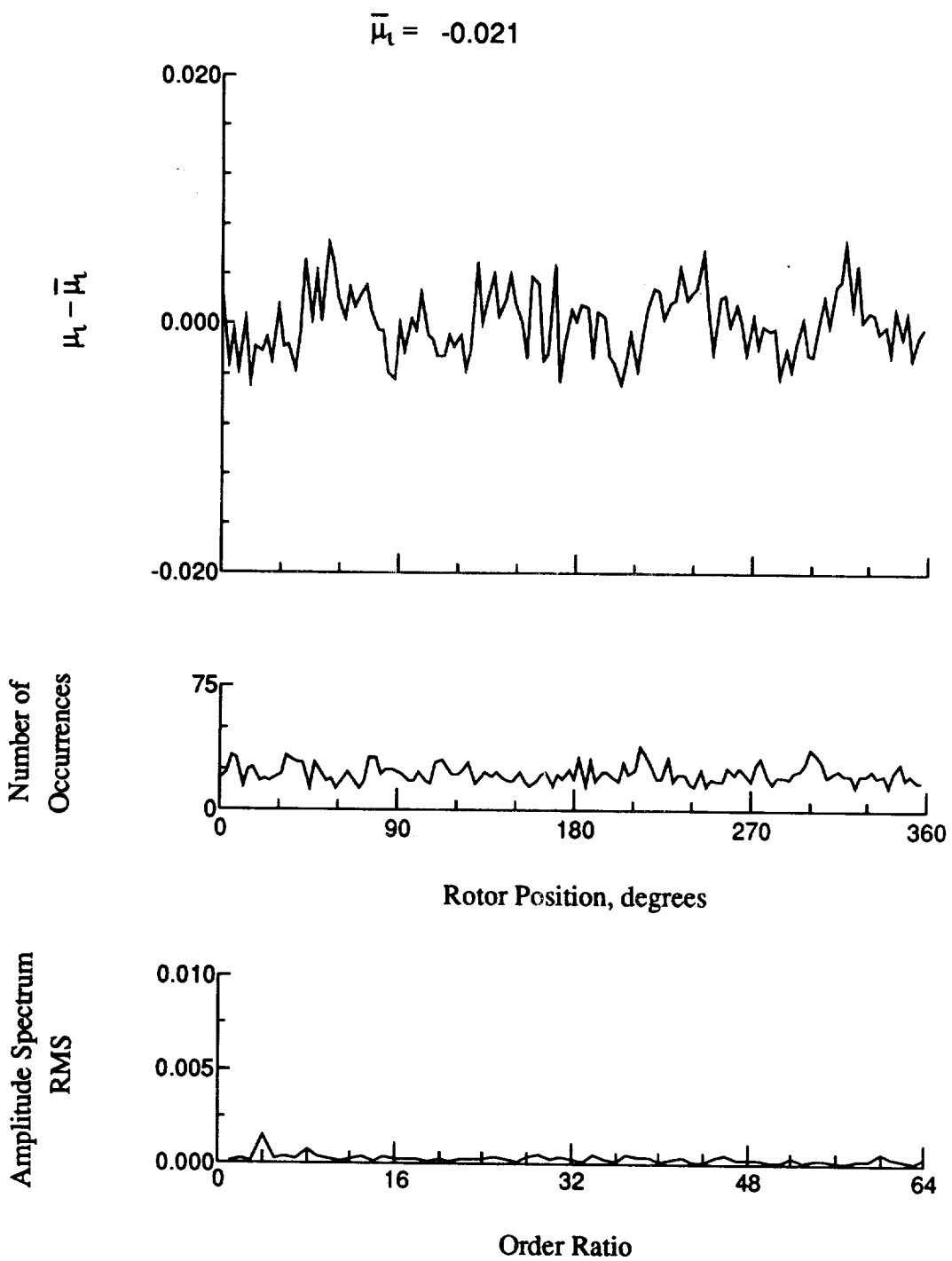


Figure 126.- Induced inflow velocity measured at 210 degrees and r/R of 0.90.

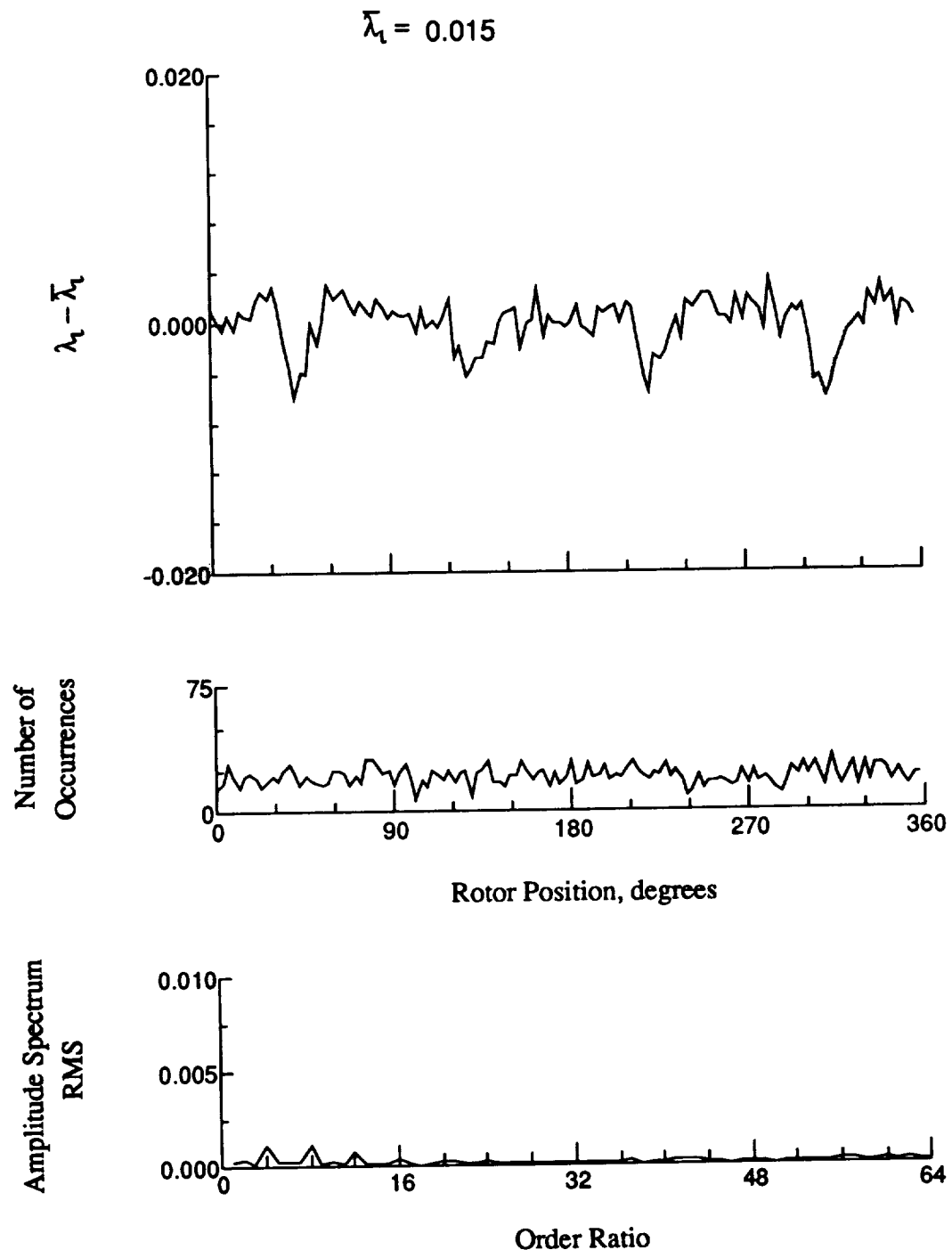


Figure 126.- Concluded.

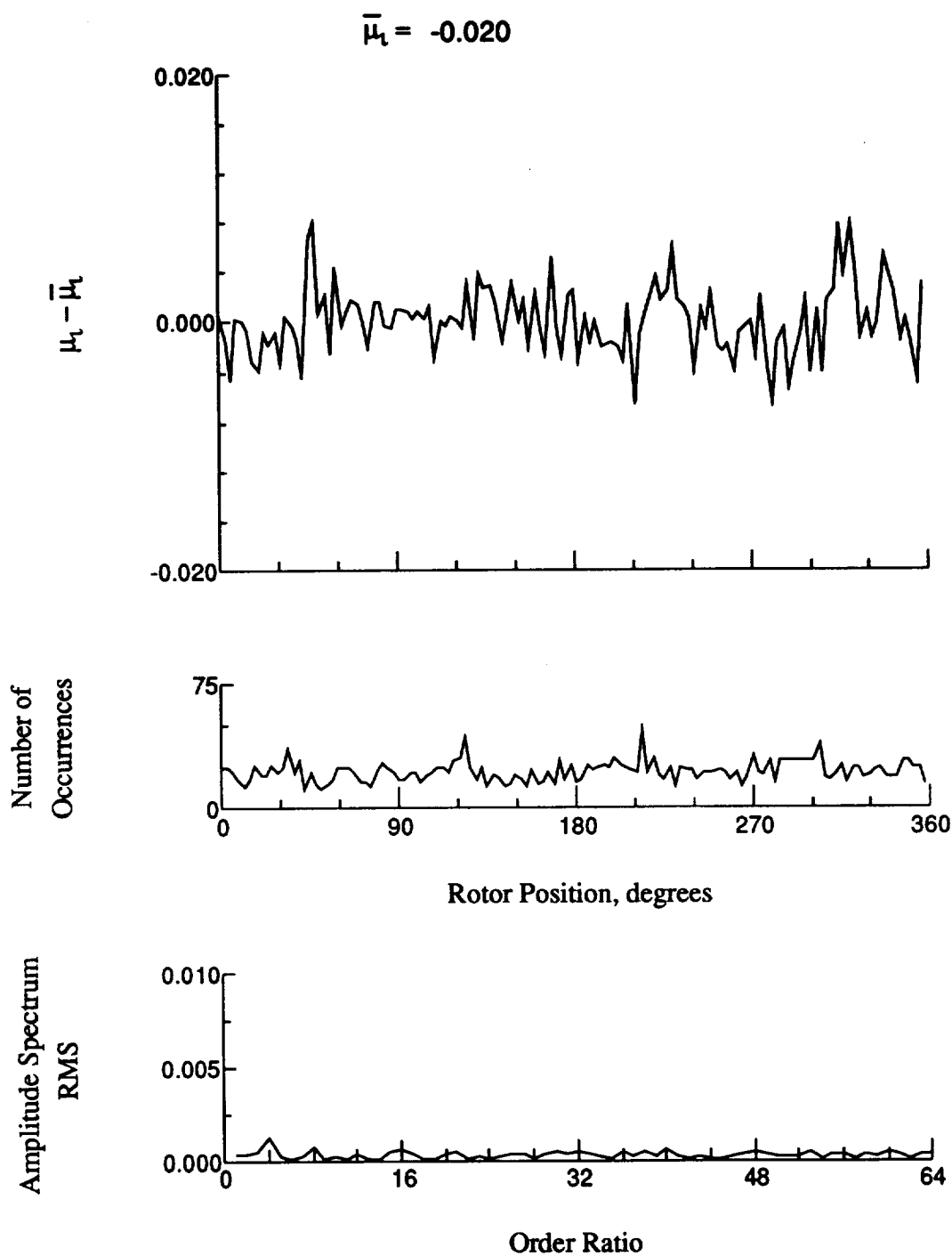


Figure 127.- Induced inflow velocity measured at 210 degrees and r/R of 0.94.

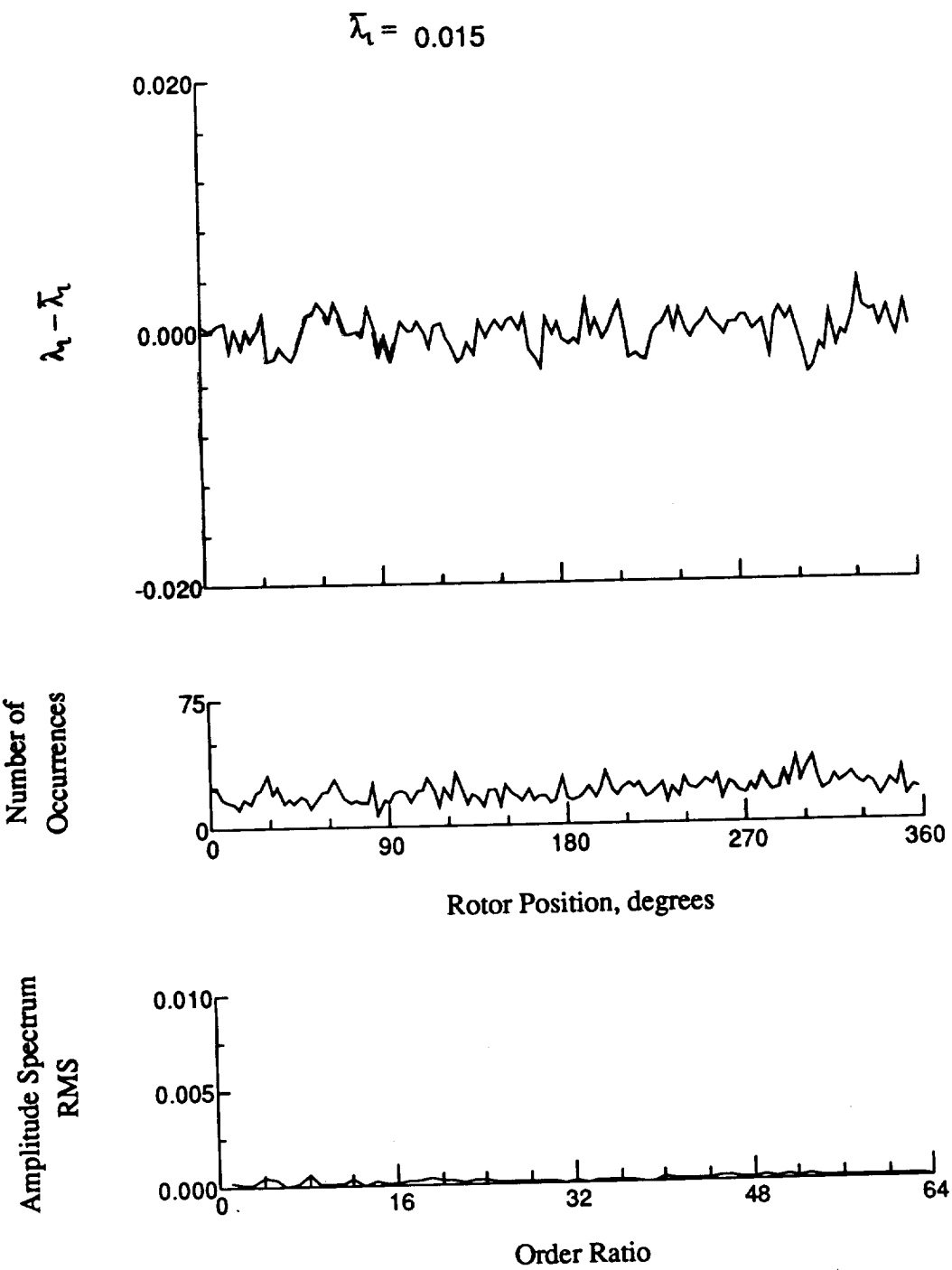


Figure 127.- Concluded.

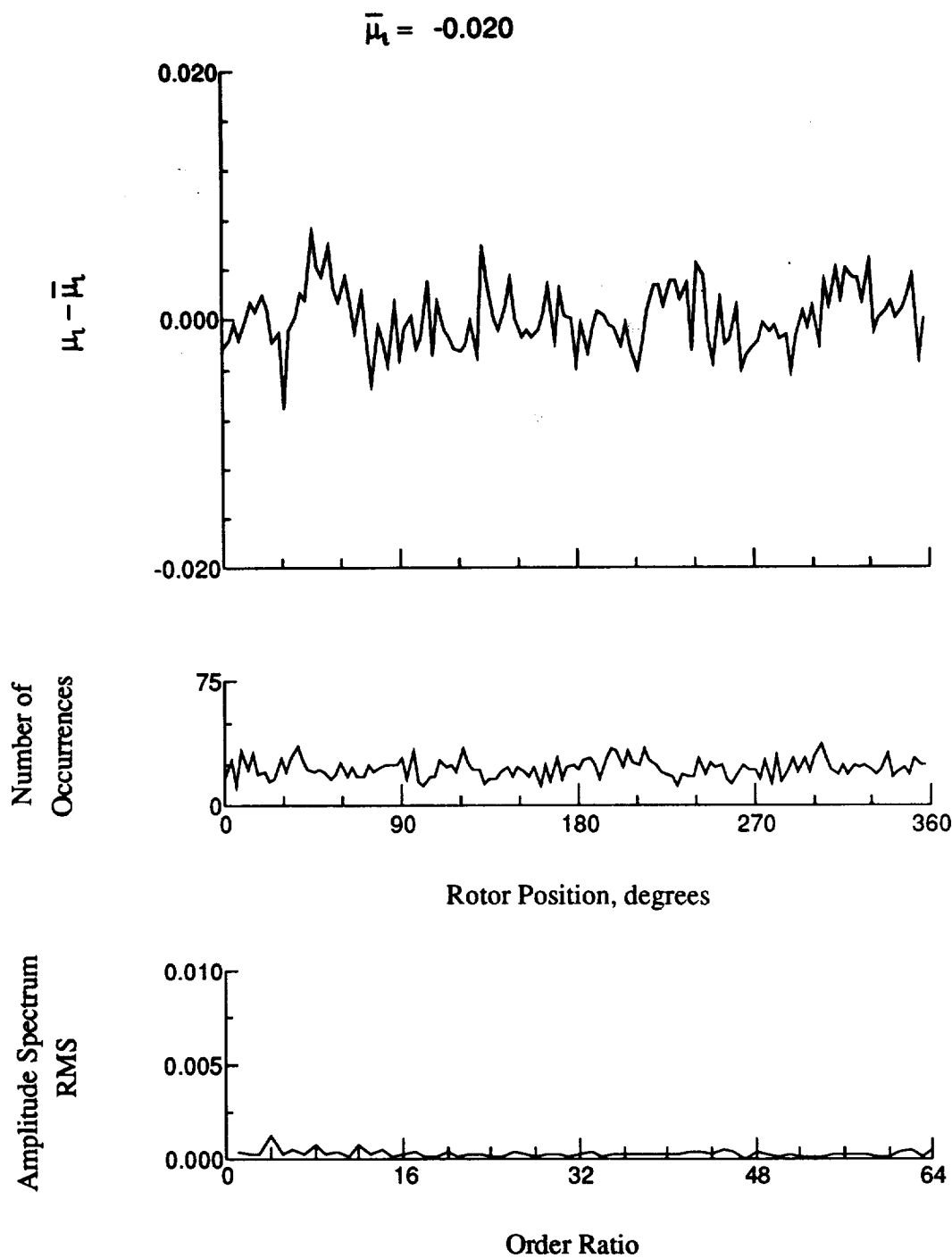


Figure 128.- Induced inflow velocity measured at 210 degrees and r/R of 0.96.

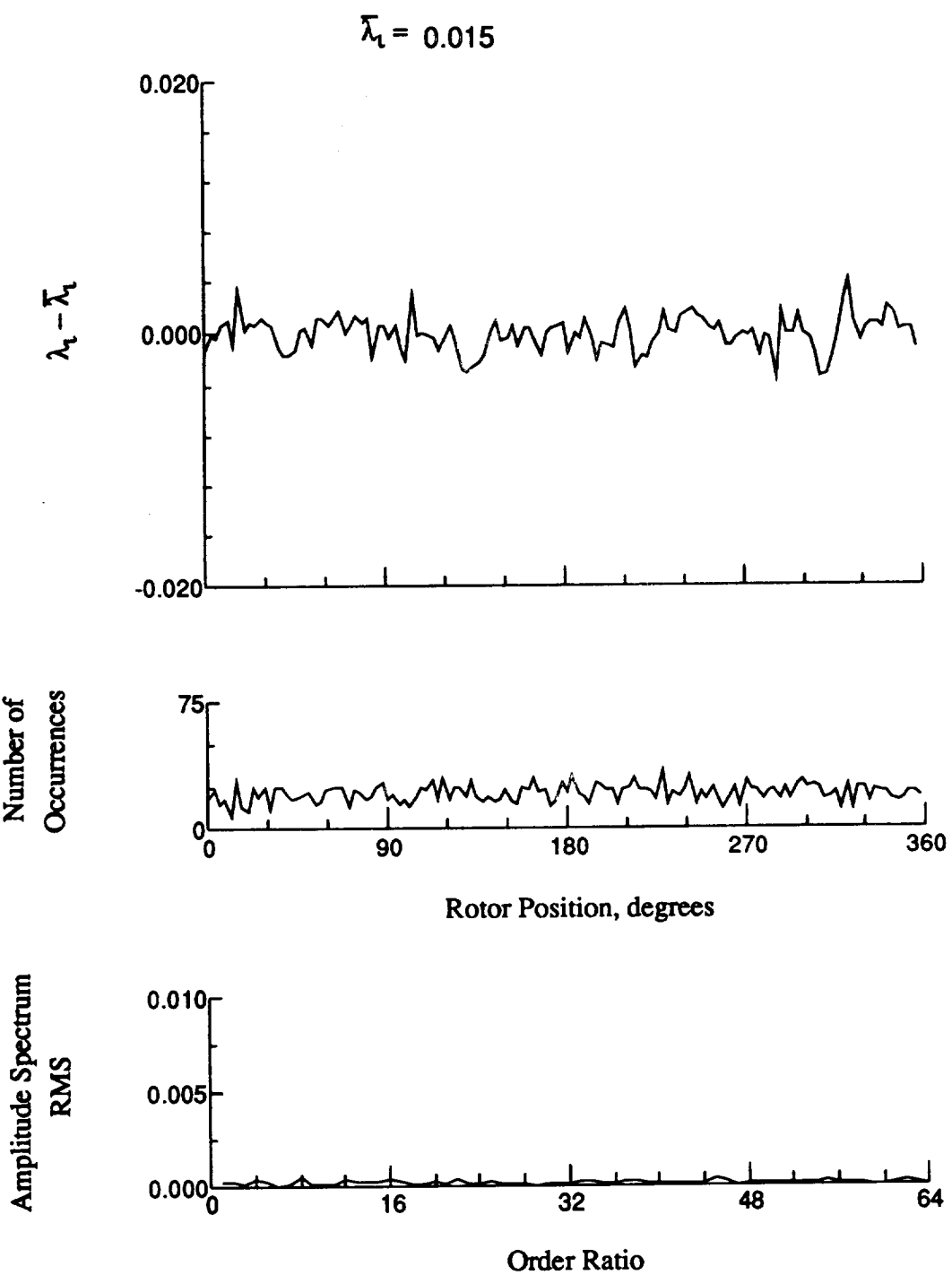


Figure 128.- Concluded.

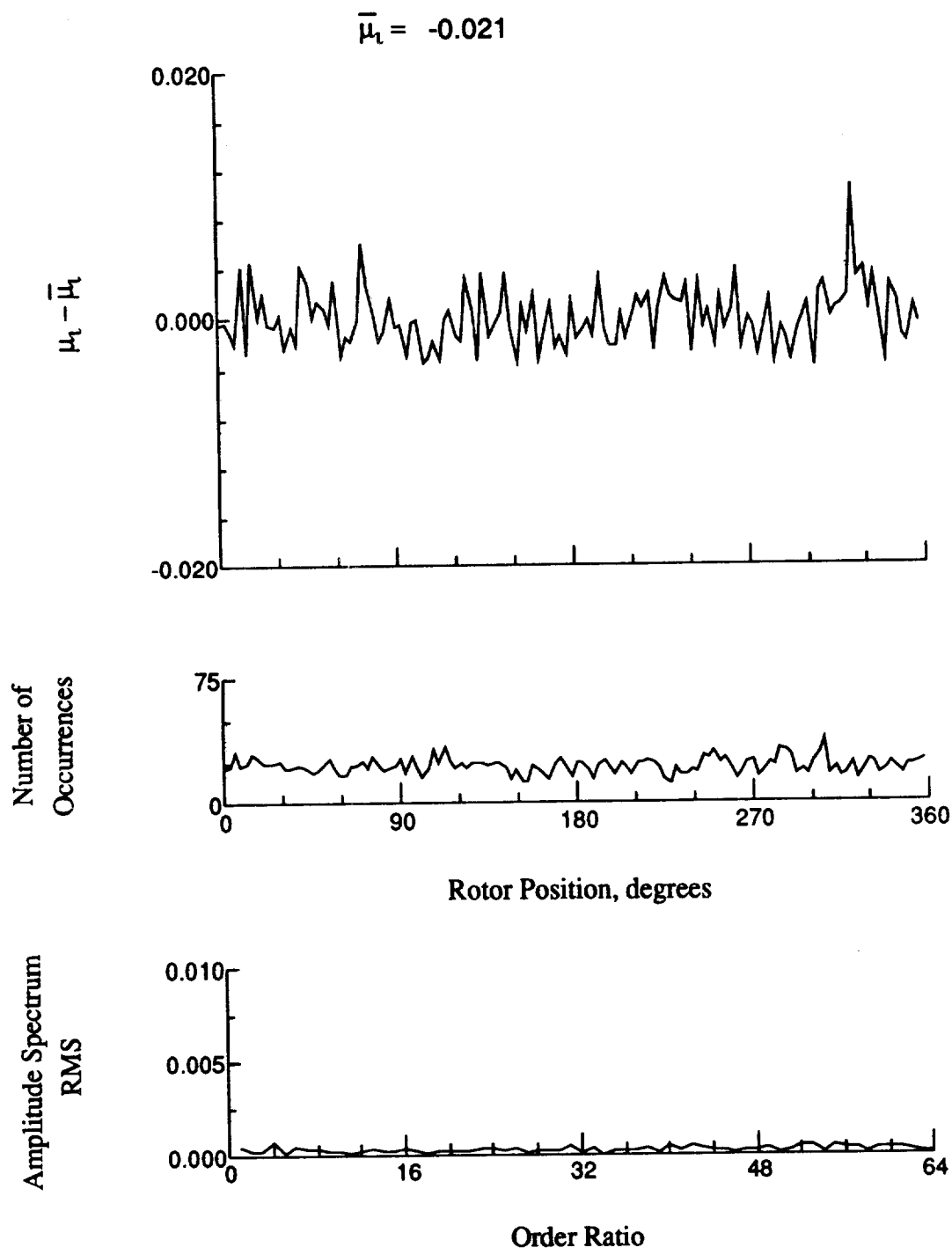


Figure 129.- Induced inflow velocity measured at 210 degrees and r/R of 1.00.

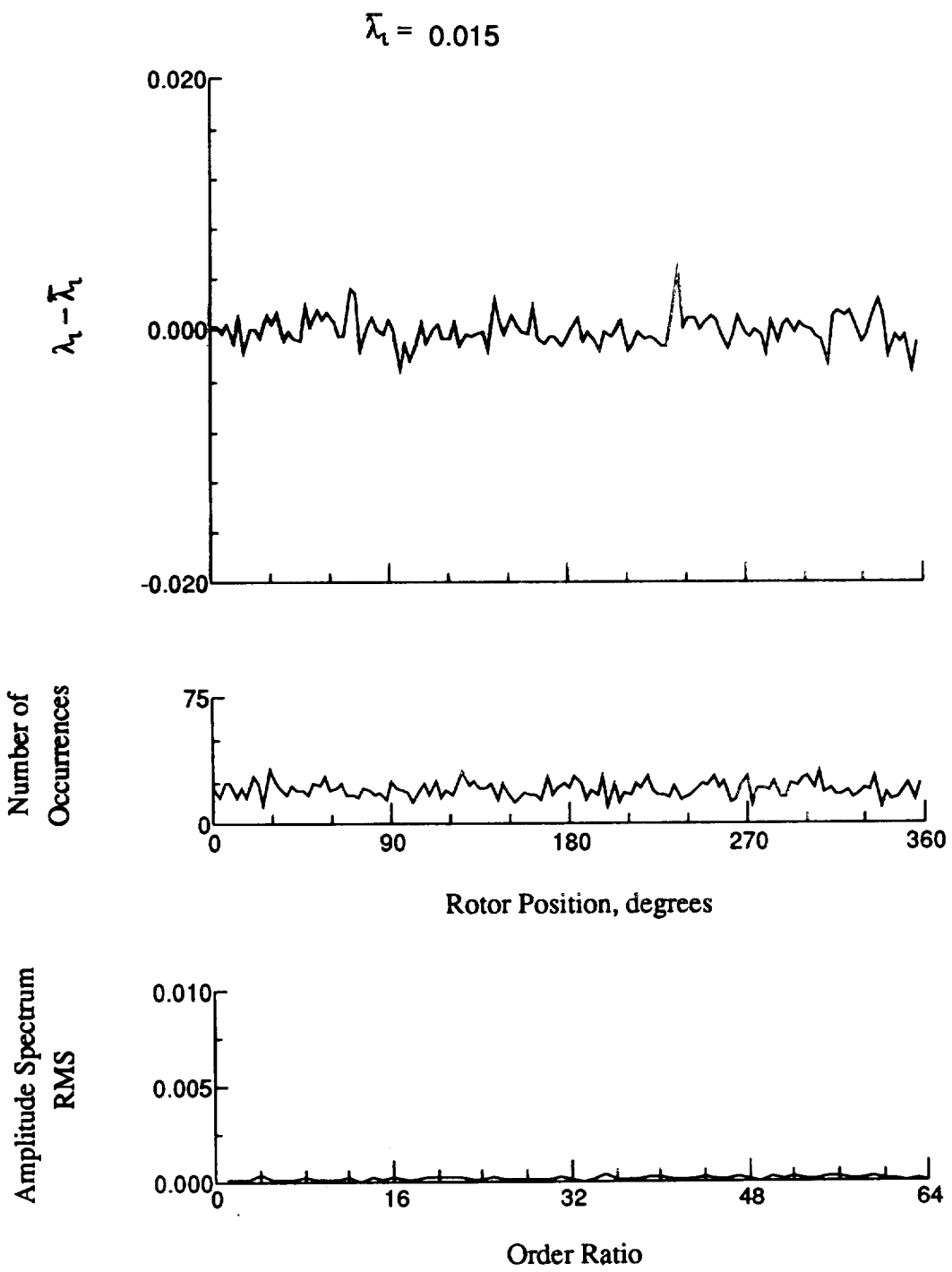


Figure 129.- Concluded.

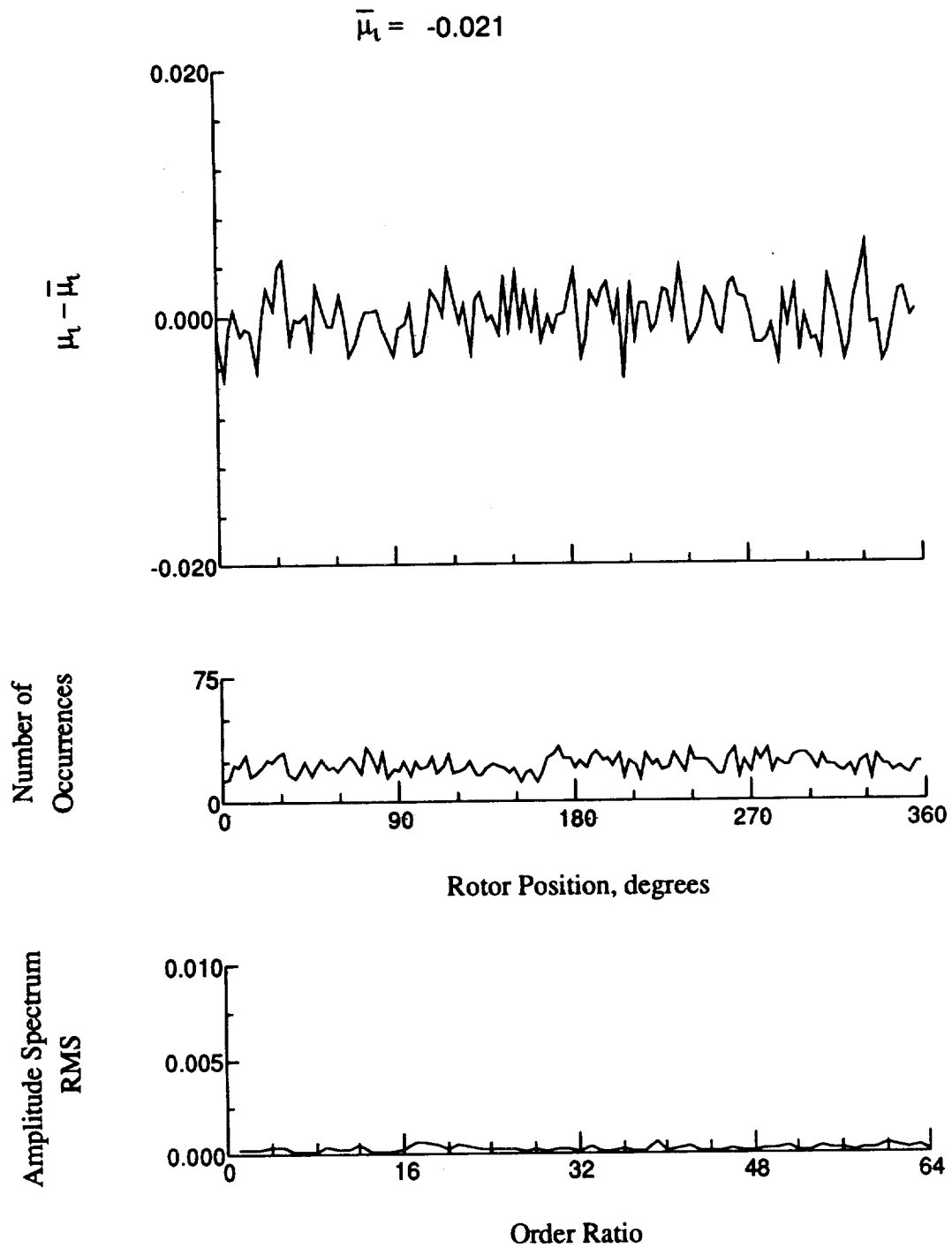


Figure 130.- Induced inflow velocity measured at 210 degrees and r/R of 1.10.

$$\bar{\lambda}_l = 0.012$$

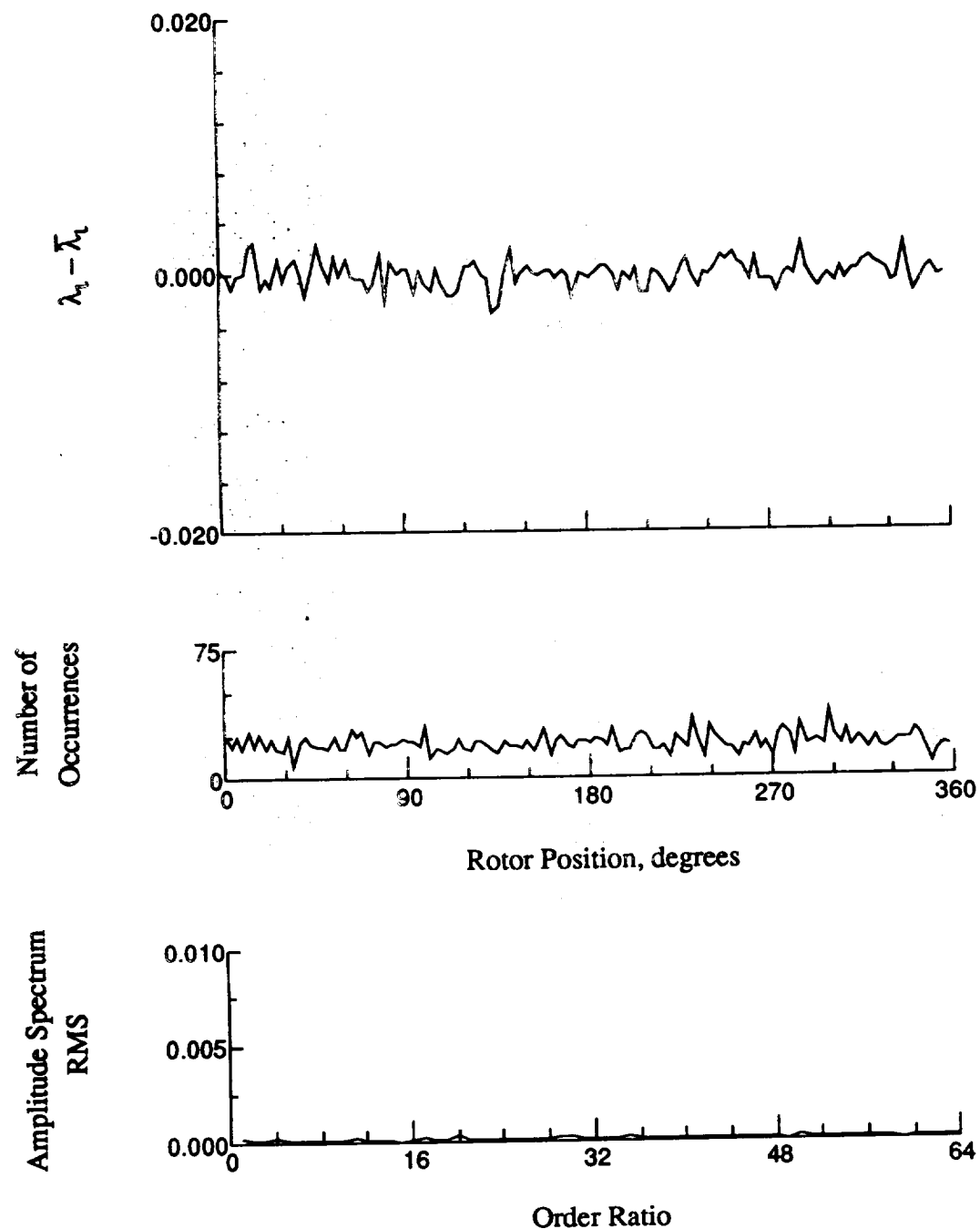


Figure 130.- Concluded.

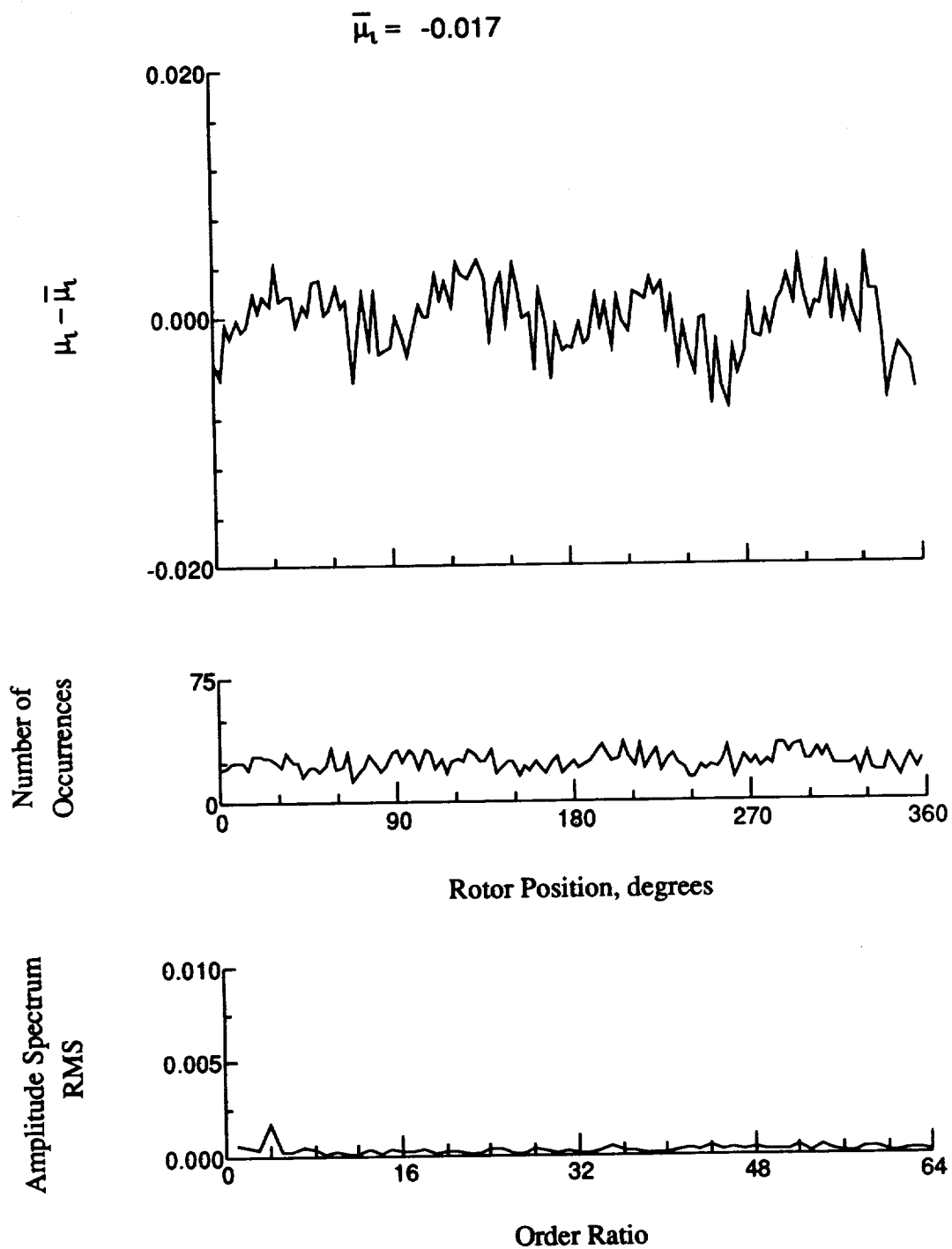


Figure 131.- Induced inflow velocity measured at 240 degrees and r/R of 0.20.

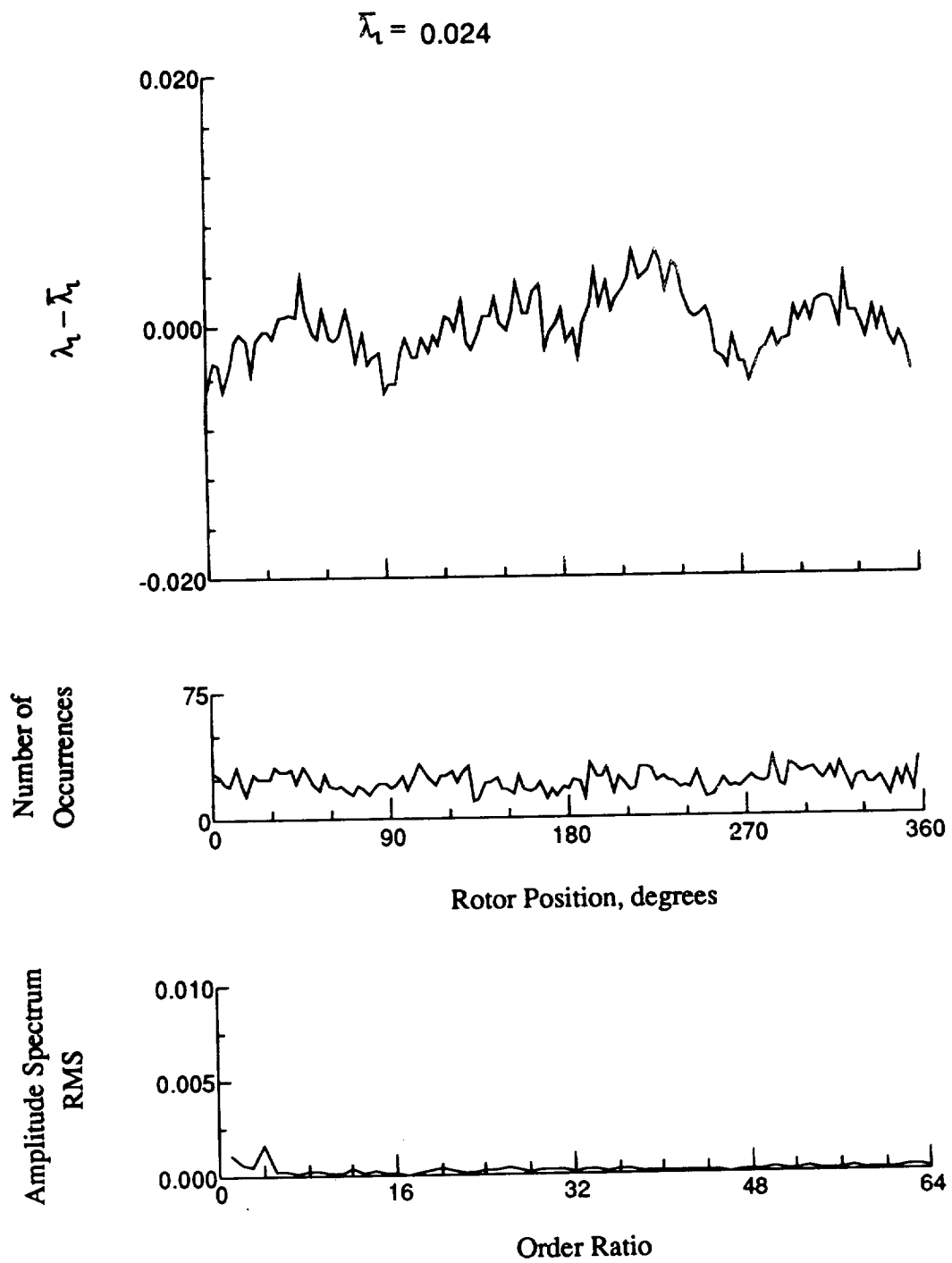


Figure 131.- Concluded.

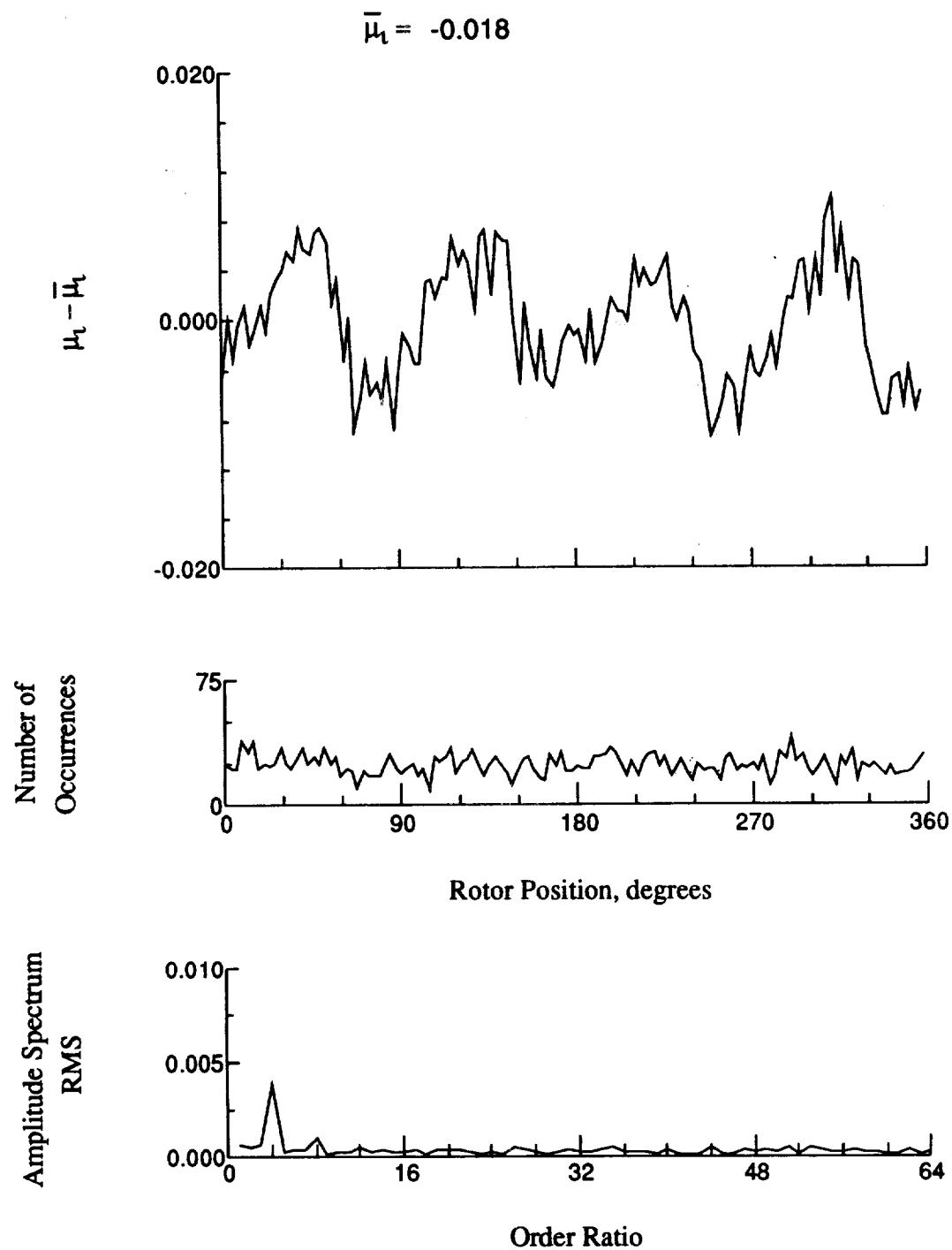


Figure 132.- Induced inflow velocity measured at 240 degrees and r/R of 0.32.

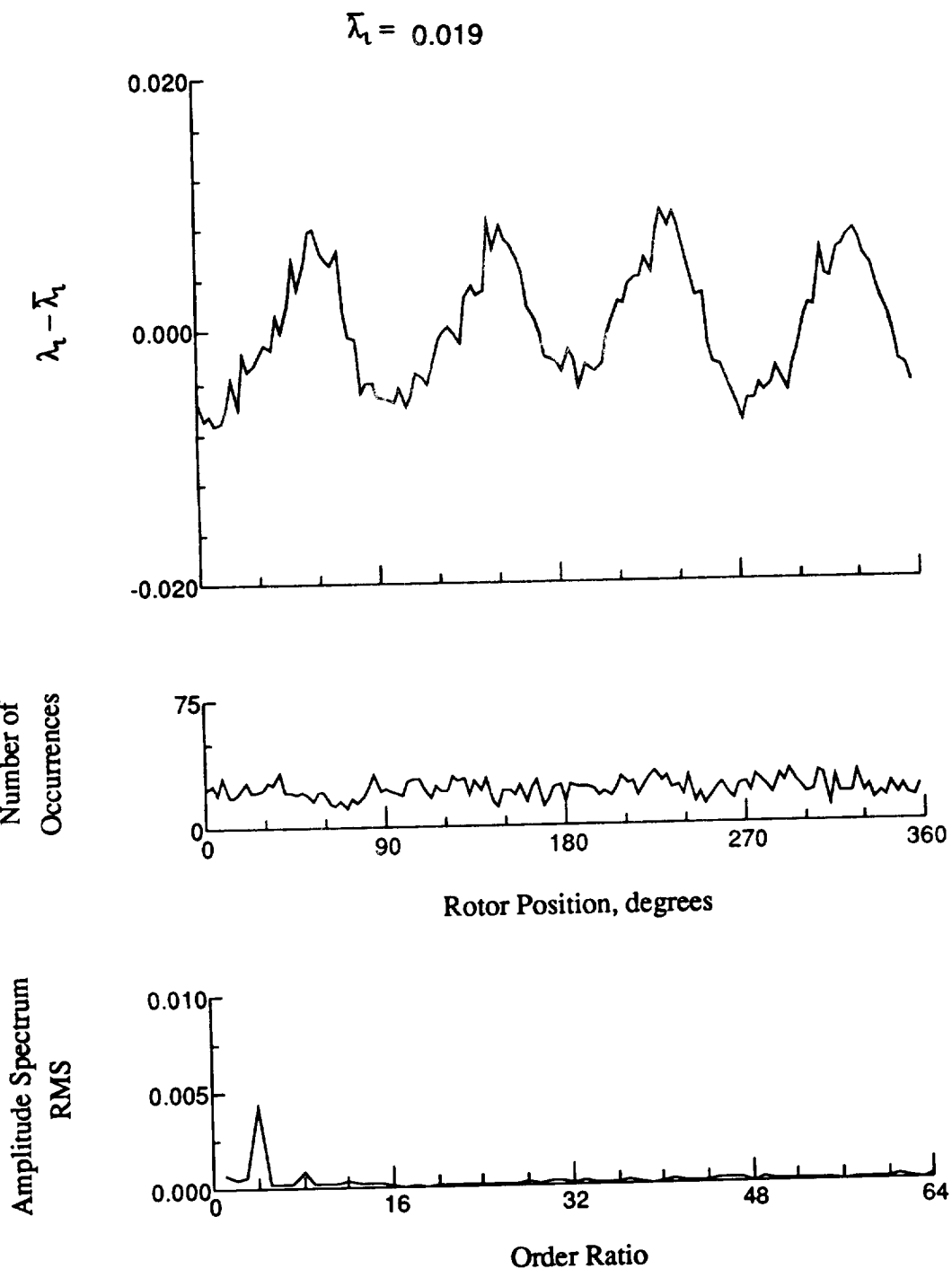


Figure 132.- Concluded.

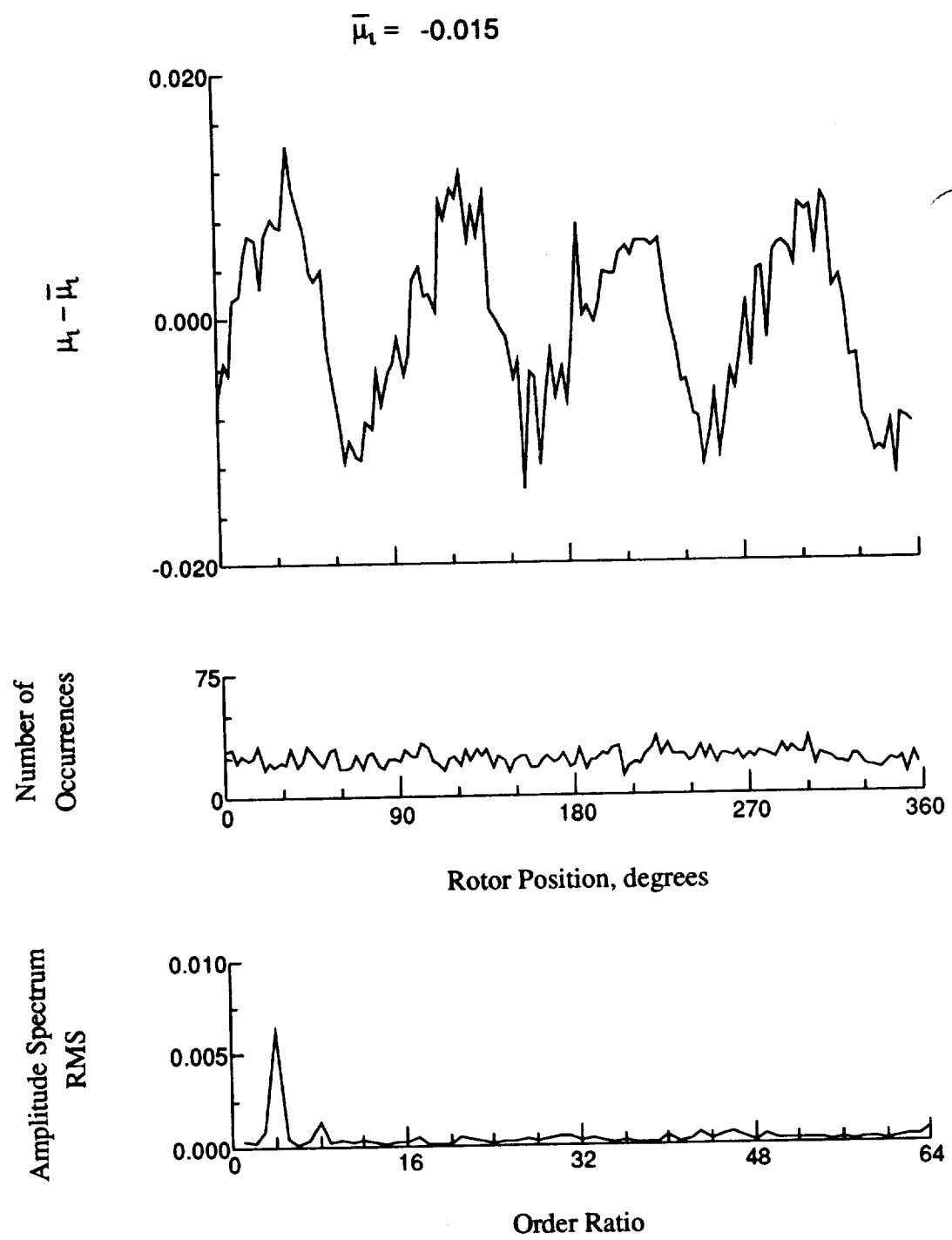


Figure 133.- Induced inflow velocity measured at 240 degrees and r/R of 0.50.

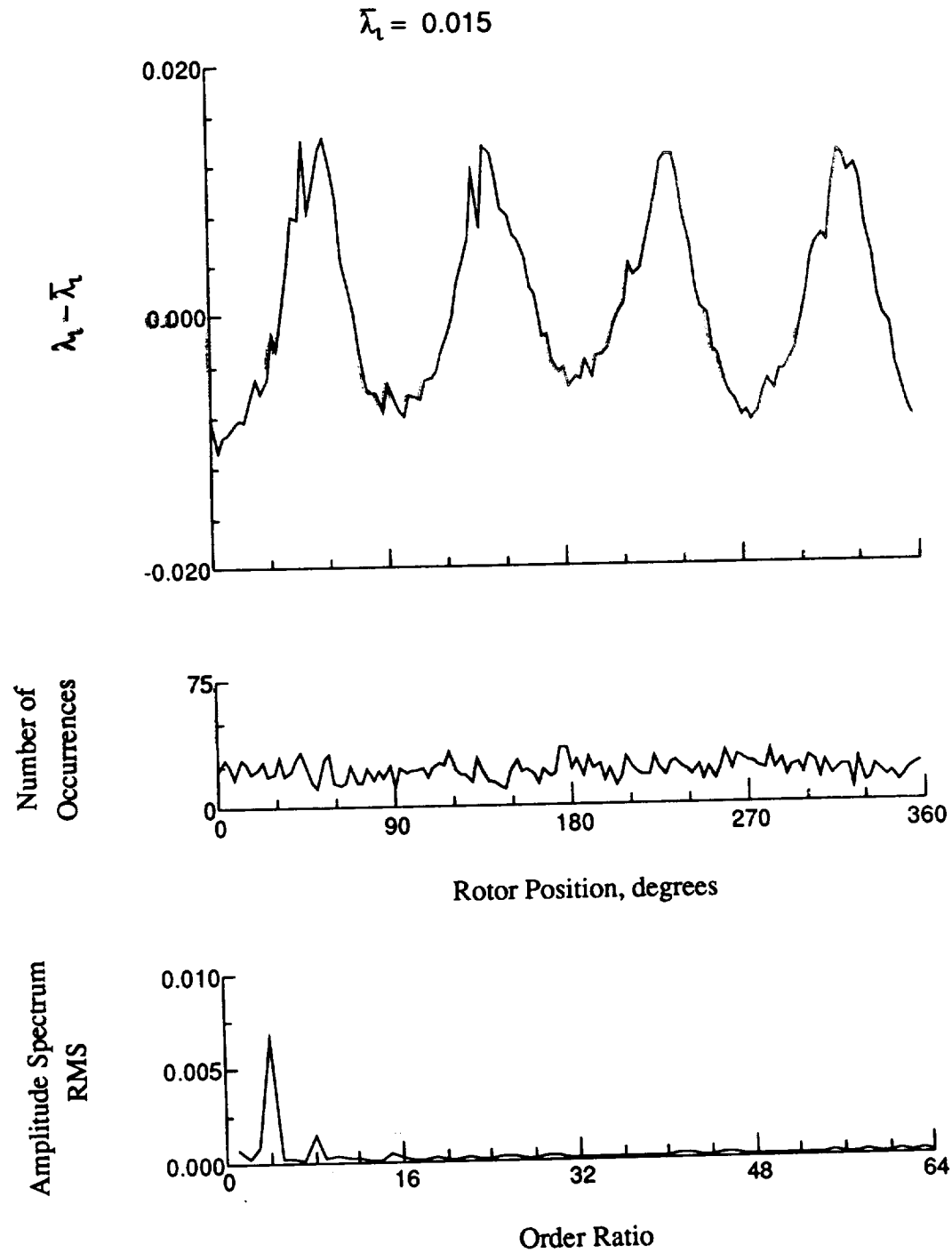


Figure 133.- Concluded.

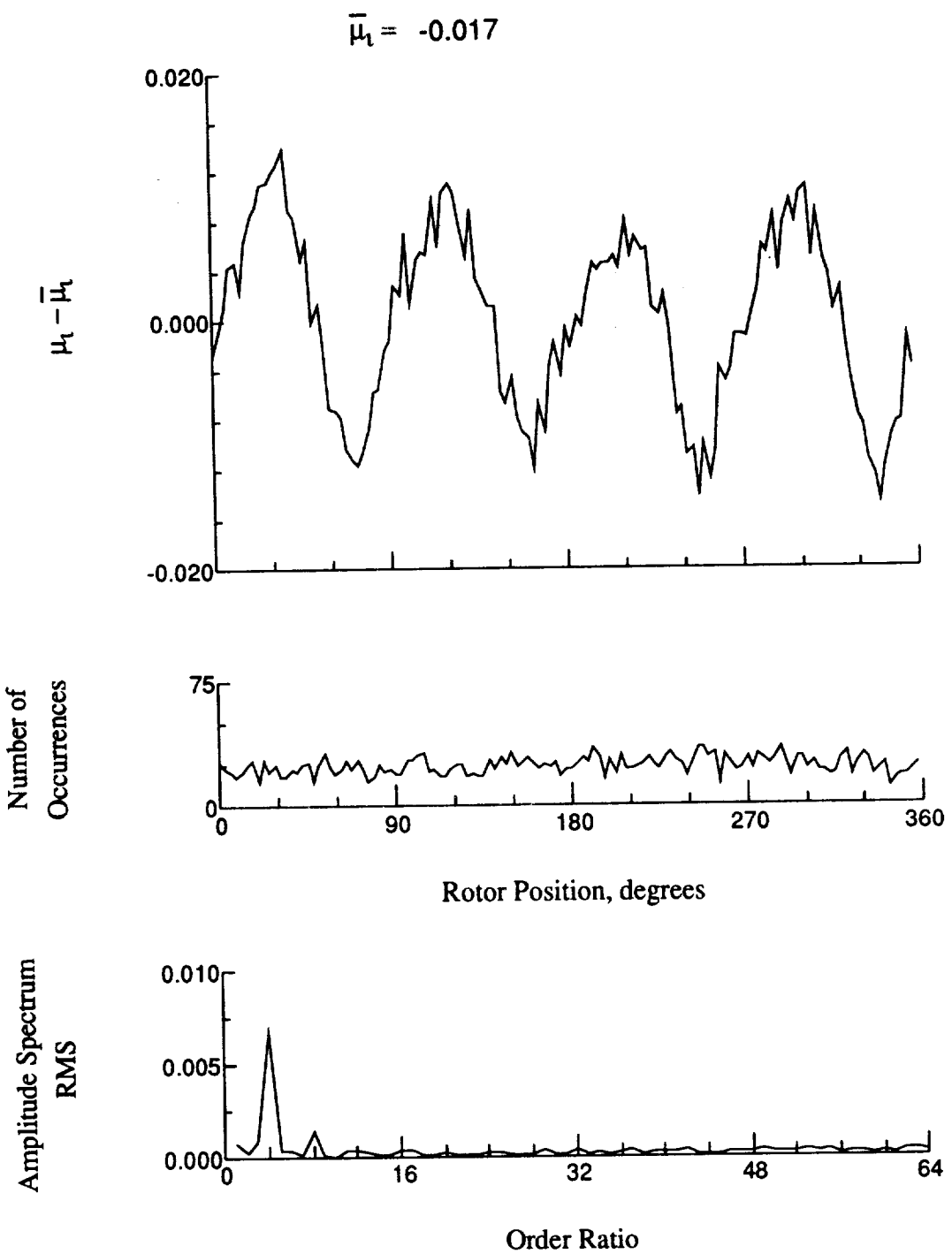


Figure 134.- Induced inflow velocity measured at 240 degrees and r/R of 0.58.

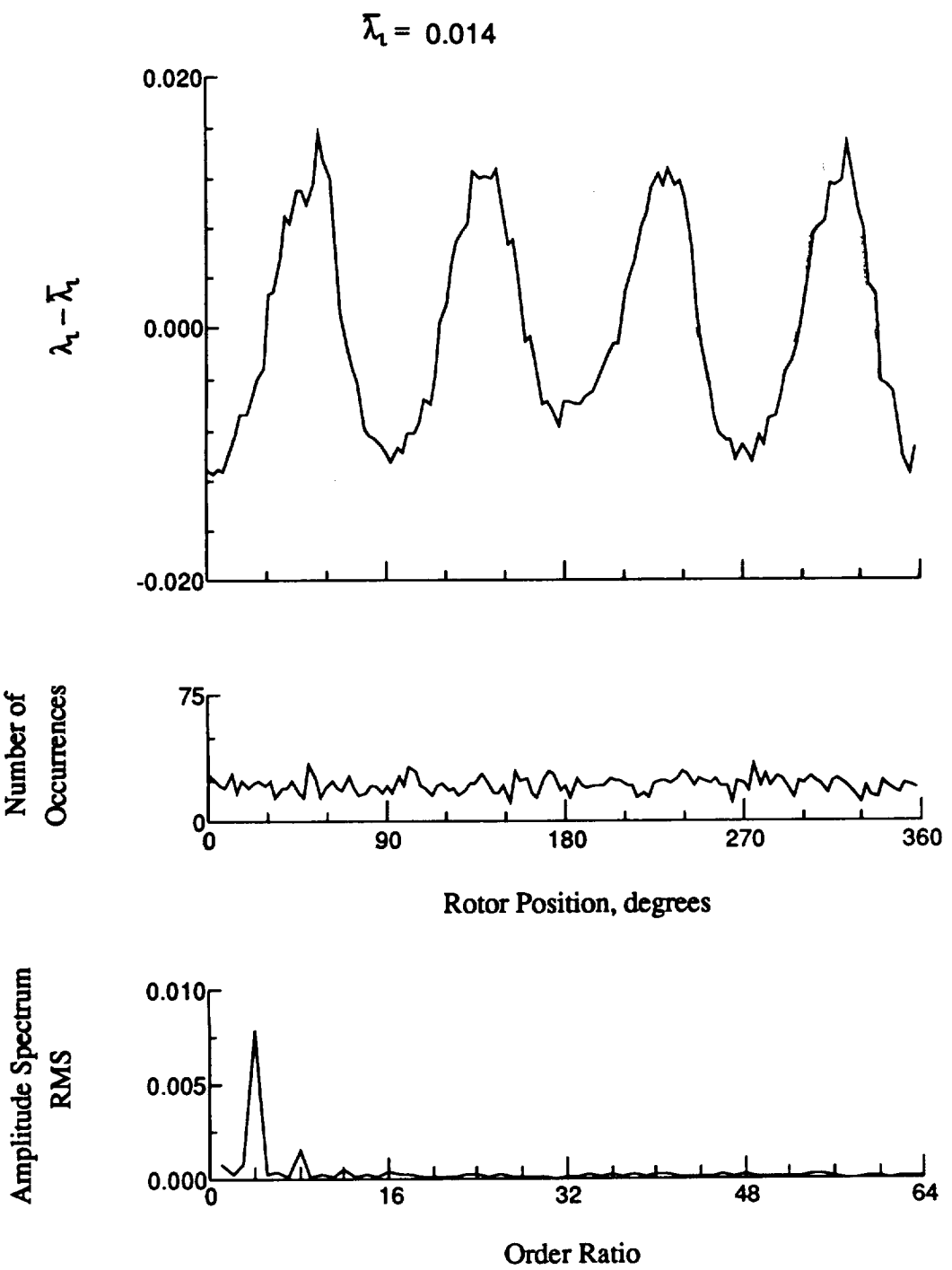


Figure 134.- Concluded.

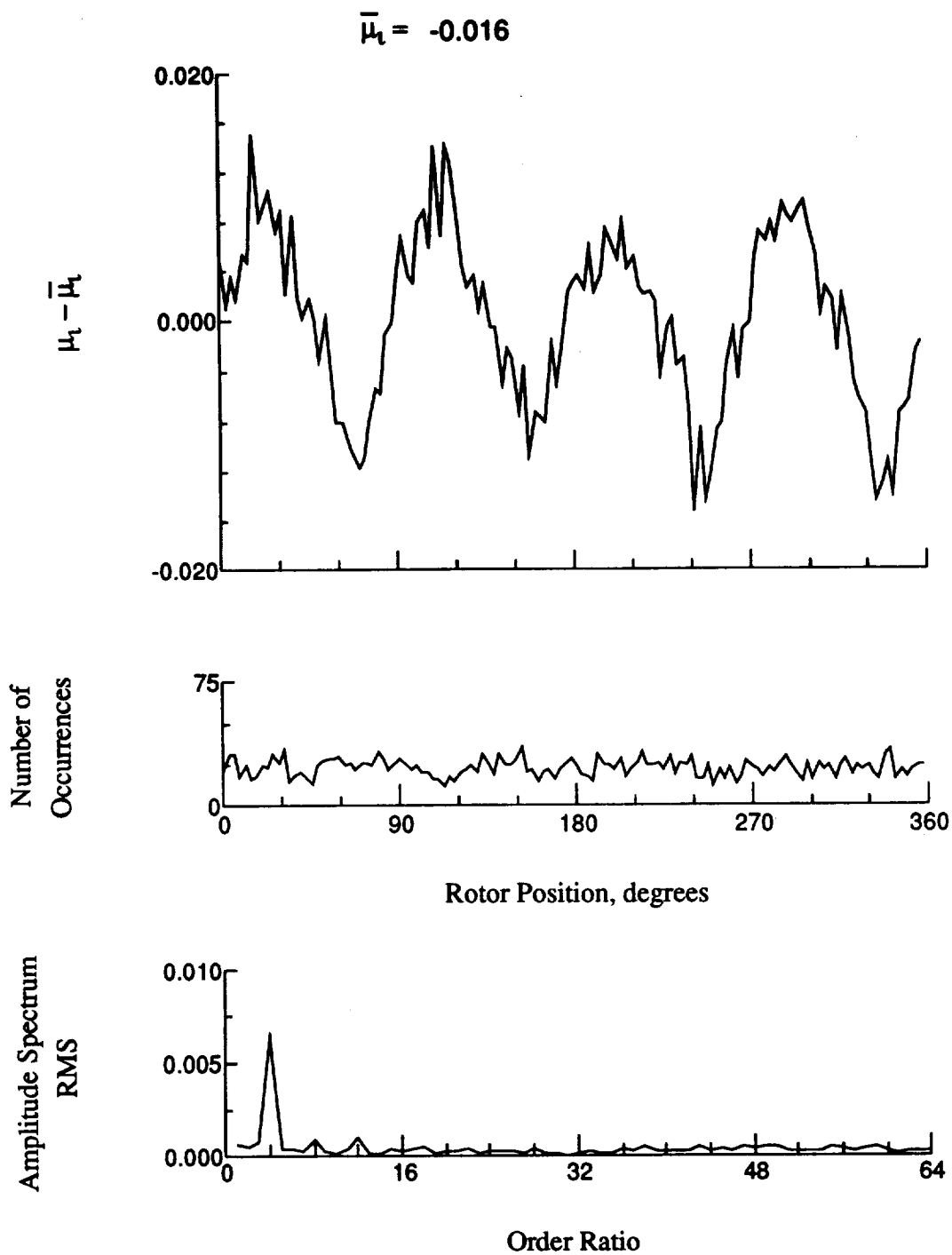


Figure 135.- Induced inflow velocity measured at 240 degrees and r/R of 0.69.

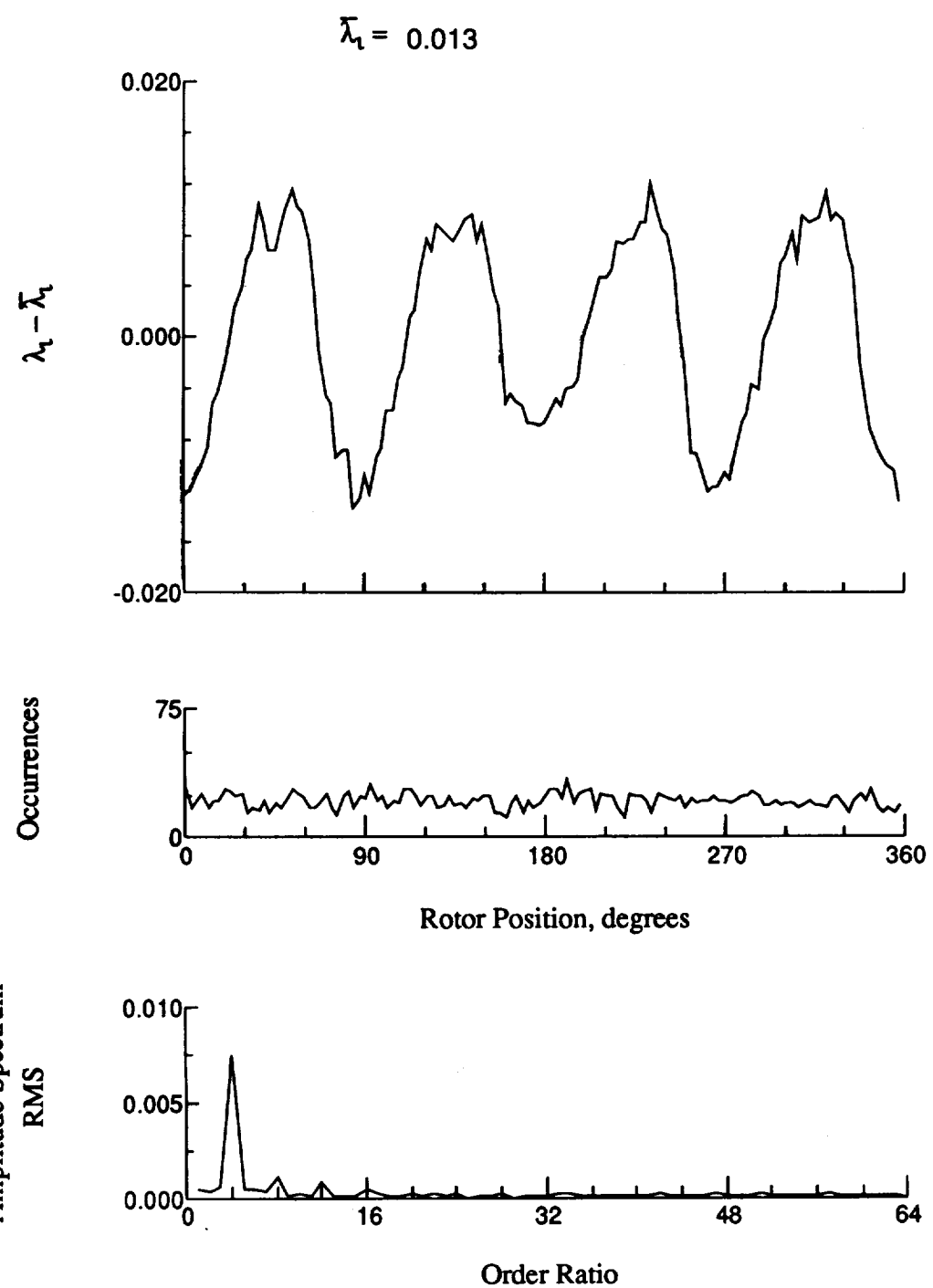


Figure 135.- Concluded.

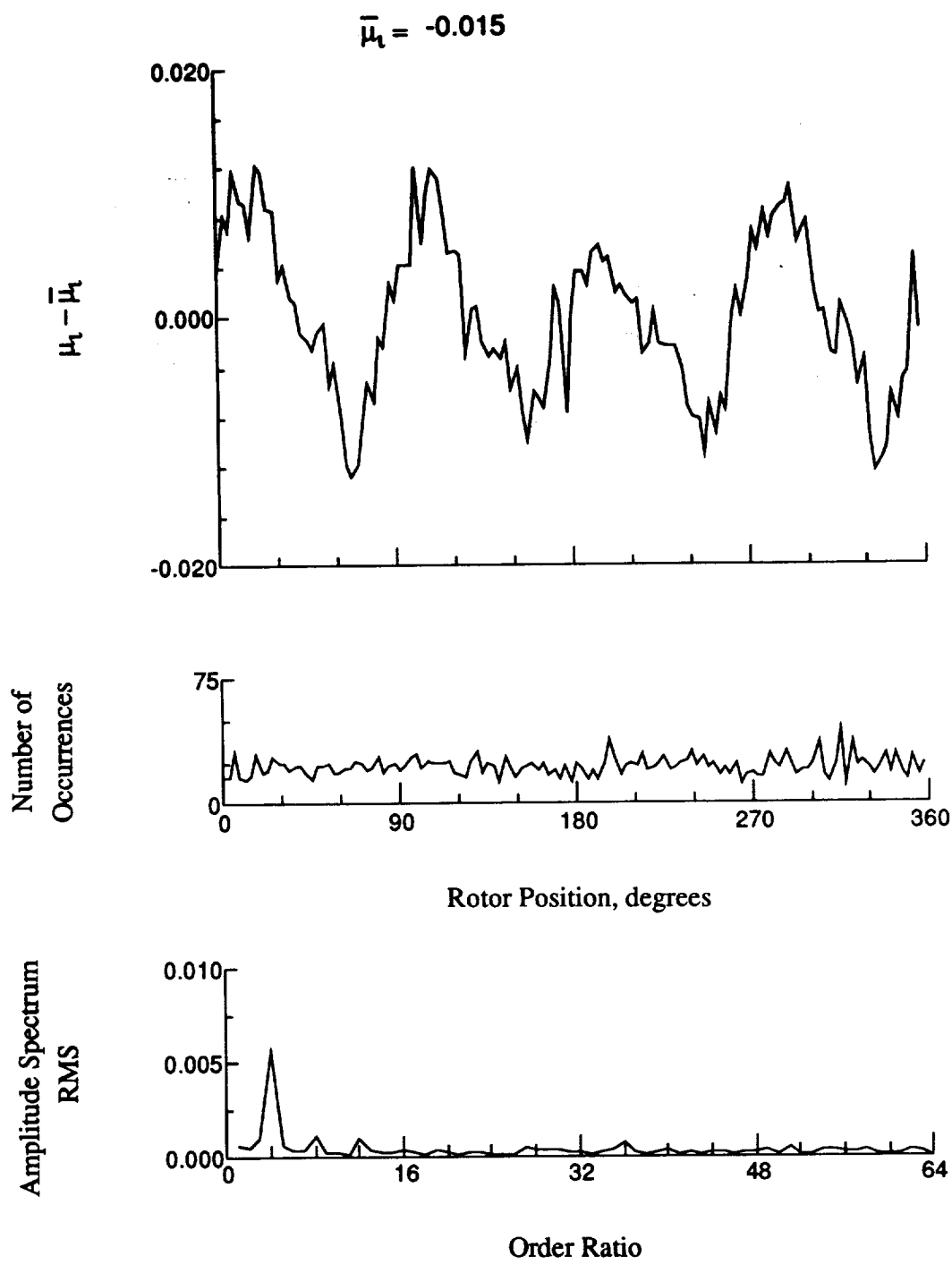


Figure 136.- Induced inflow velocity measured at 240 degrees and r/R of 0.73.

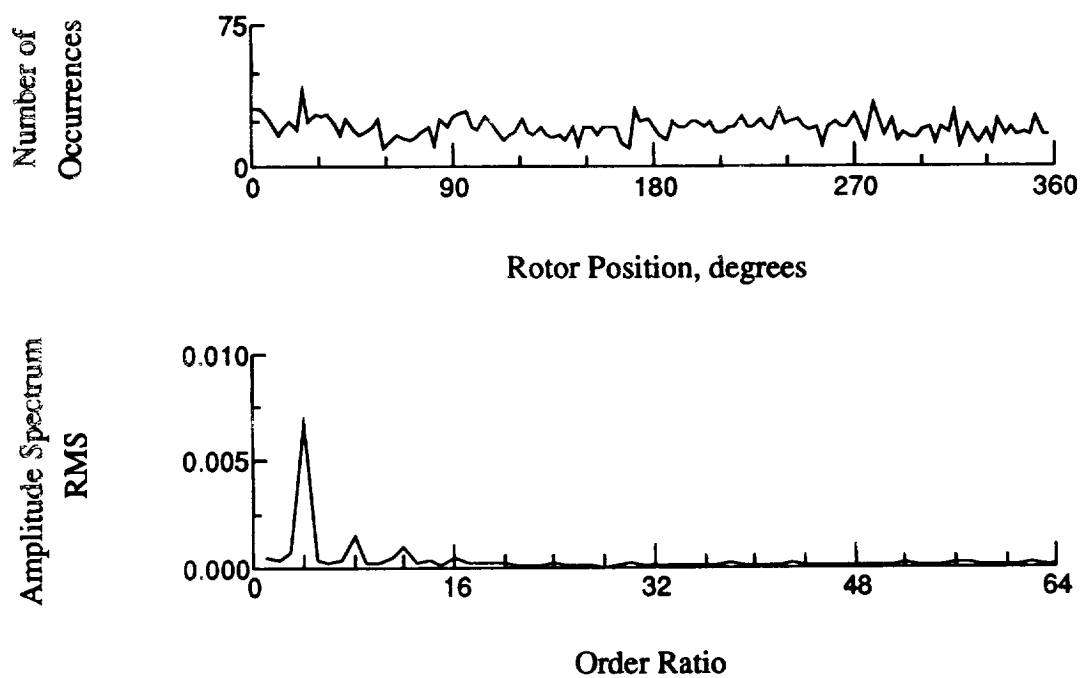
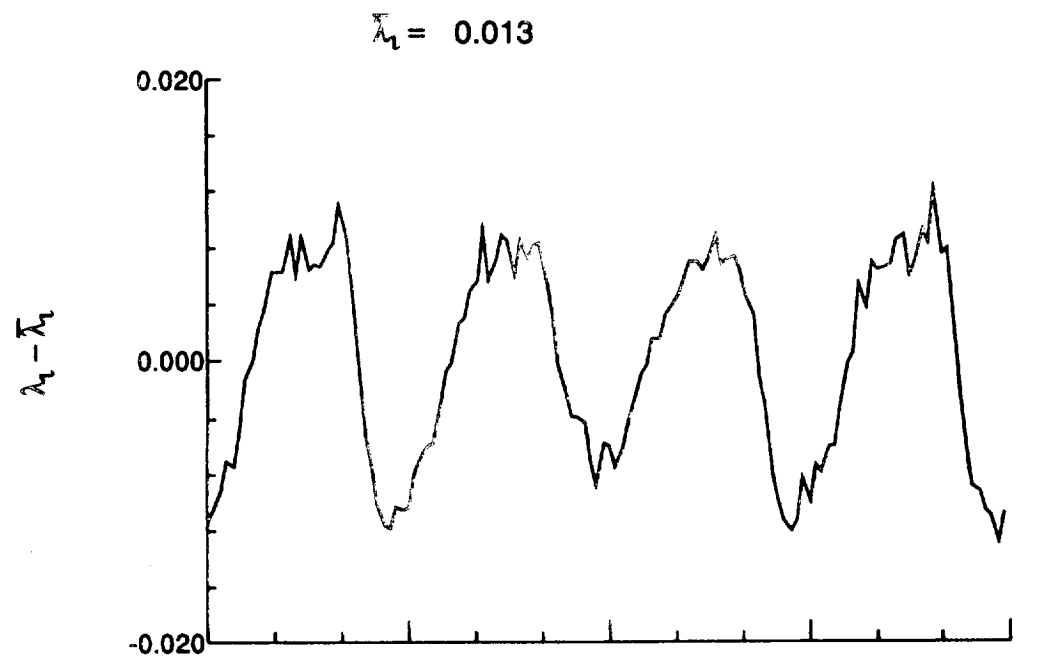


Figure 136.- Concluded.

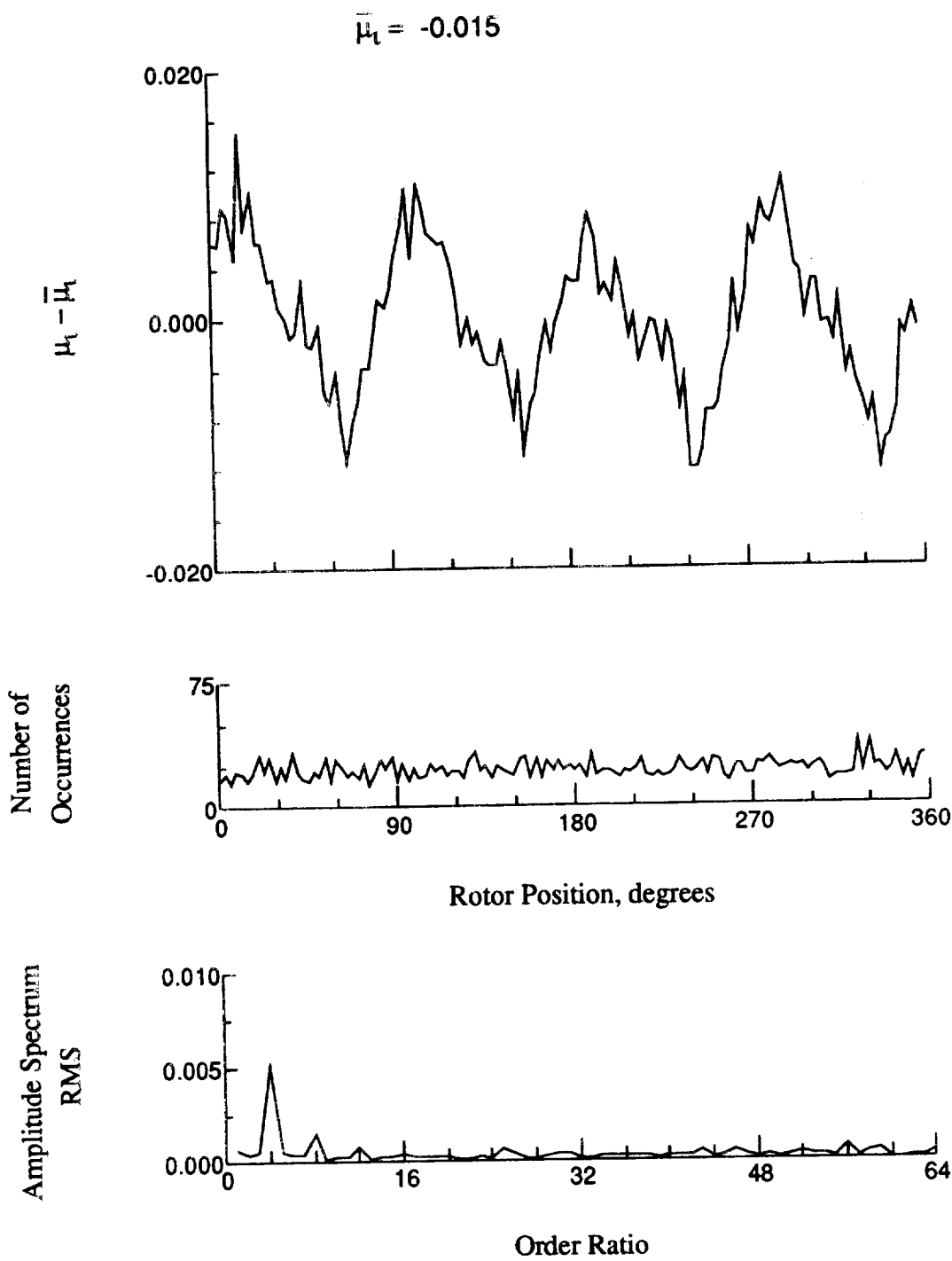


Figure 137.- Induced inflow velocity measured at 240 degrees and r/R of 0.75.

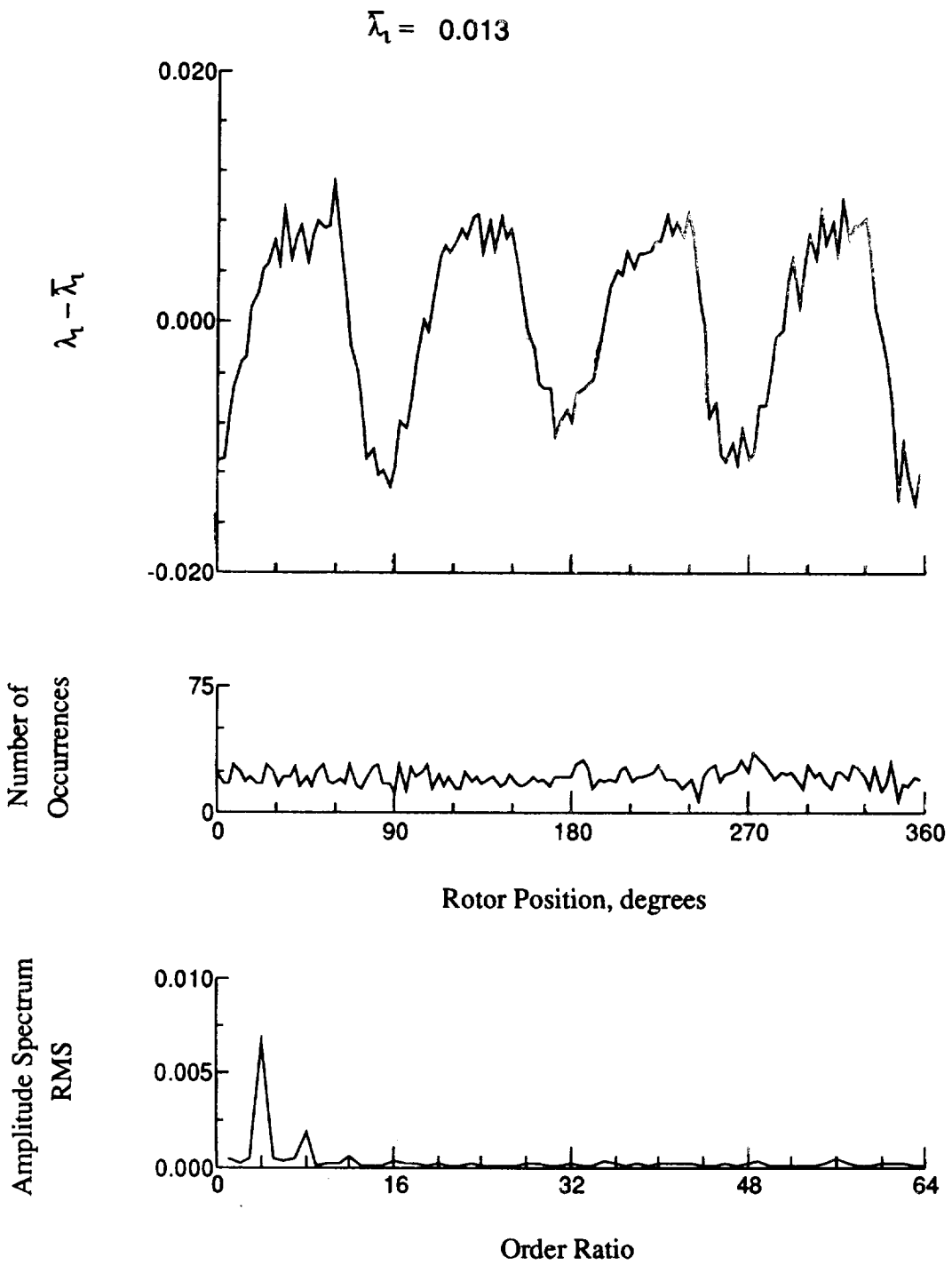


Figure 137.- Concluded.

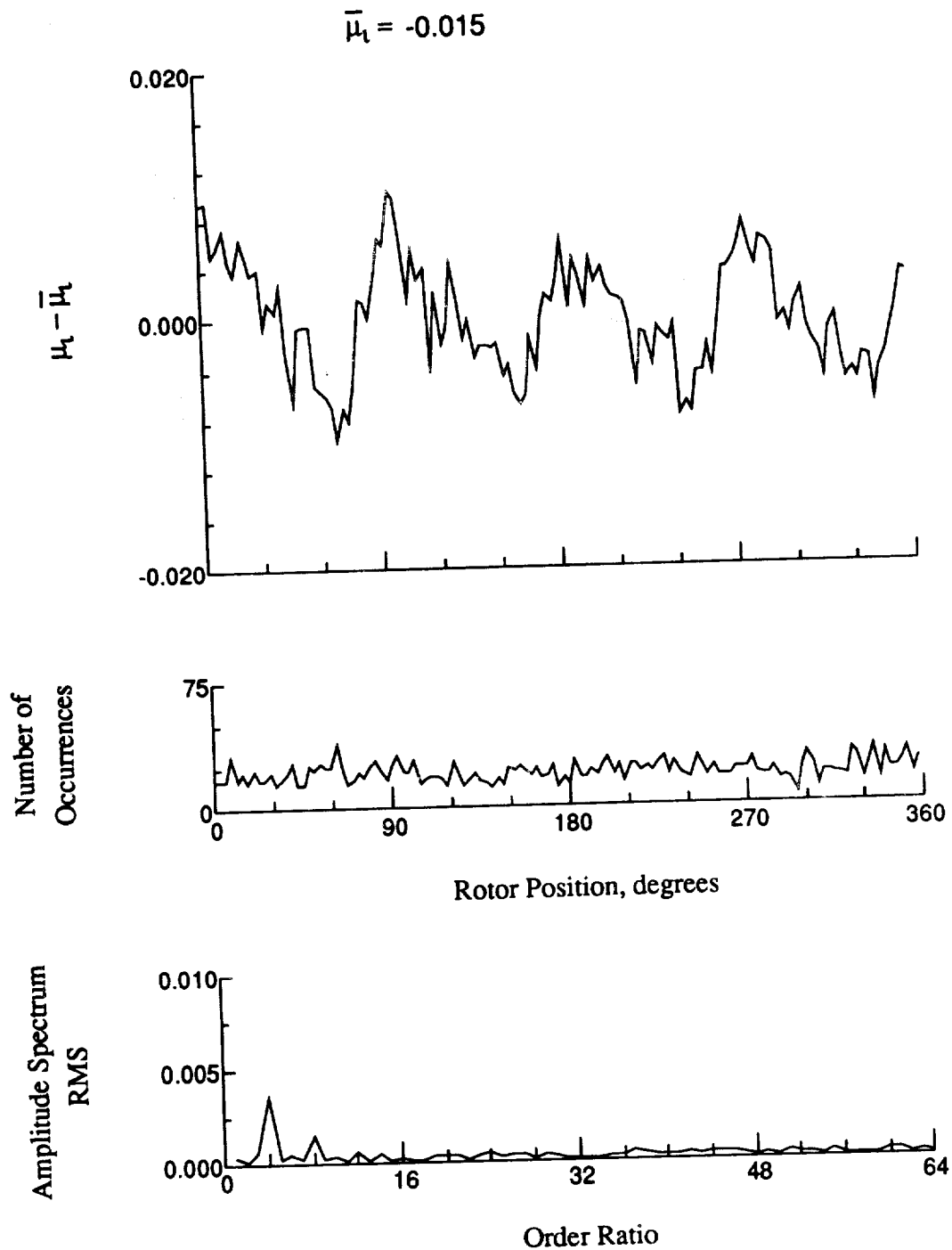


Figure 138.- Induced inflow velocity measured at 240 degrees and r/R of 0.81.

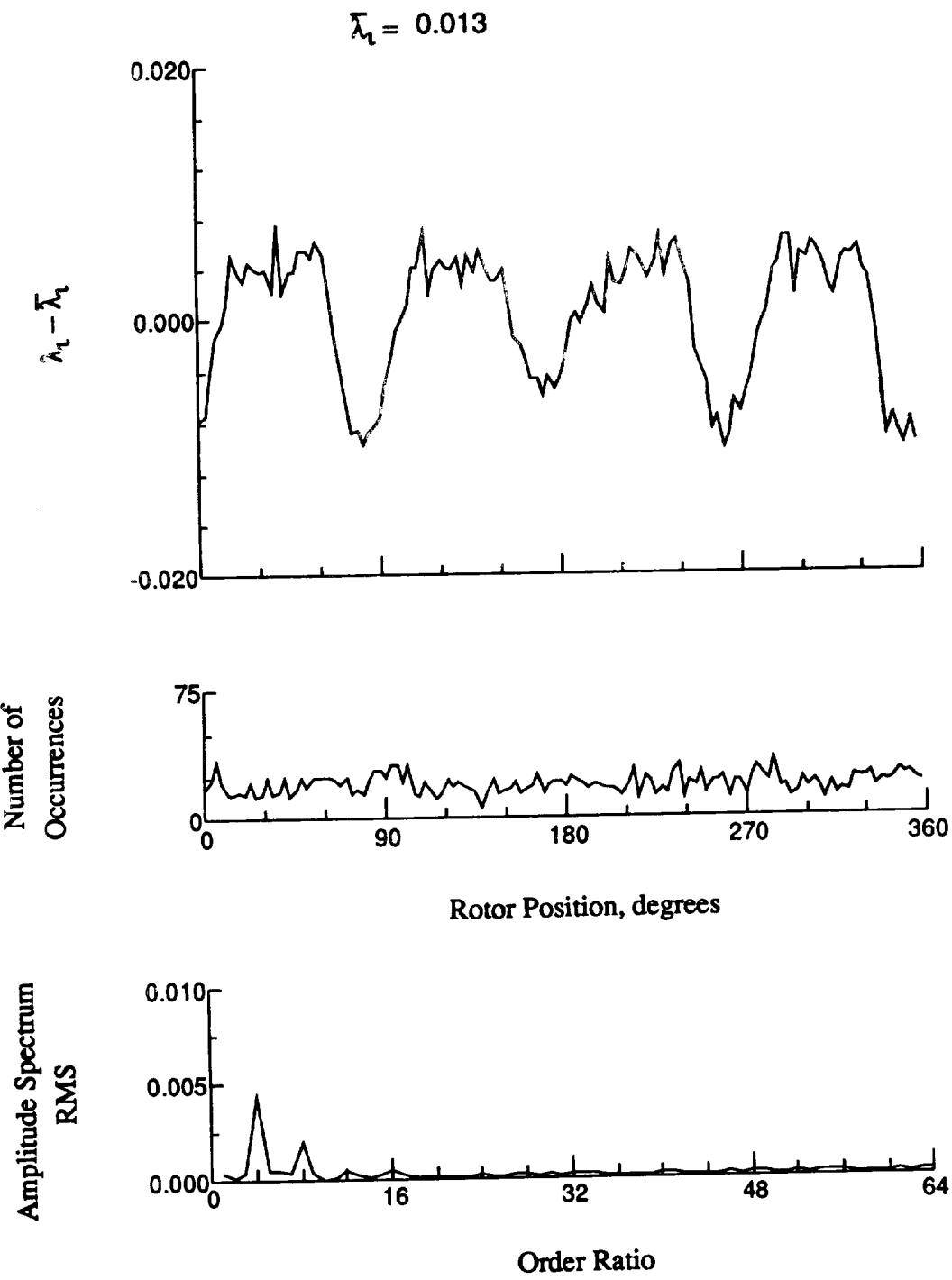


Figure 138.- Concluded.

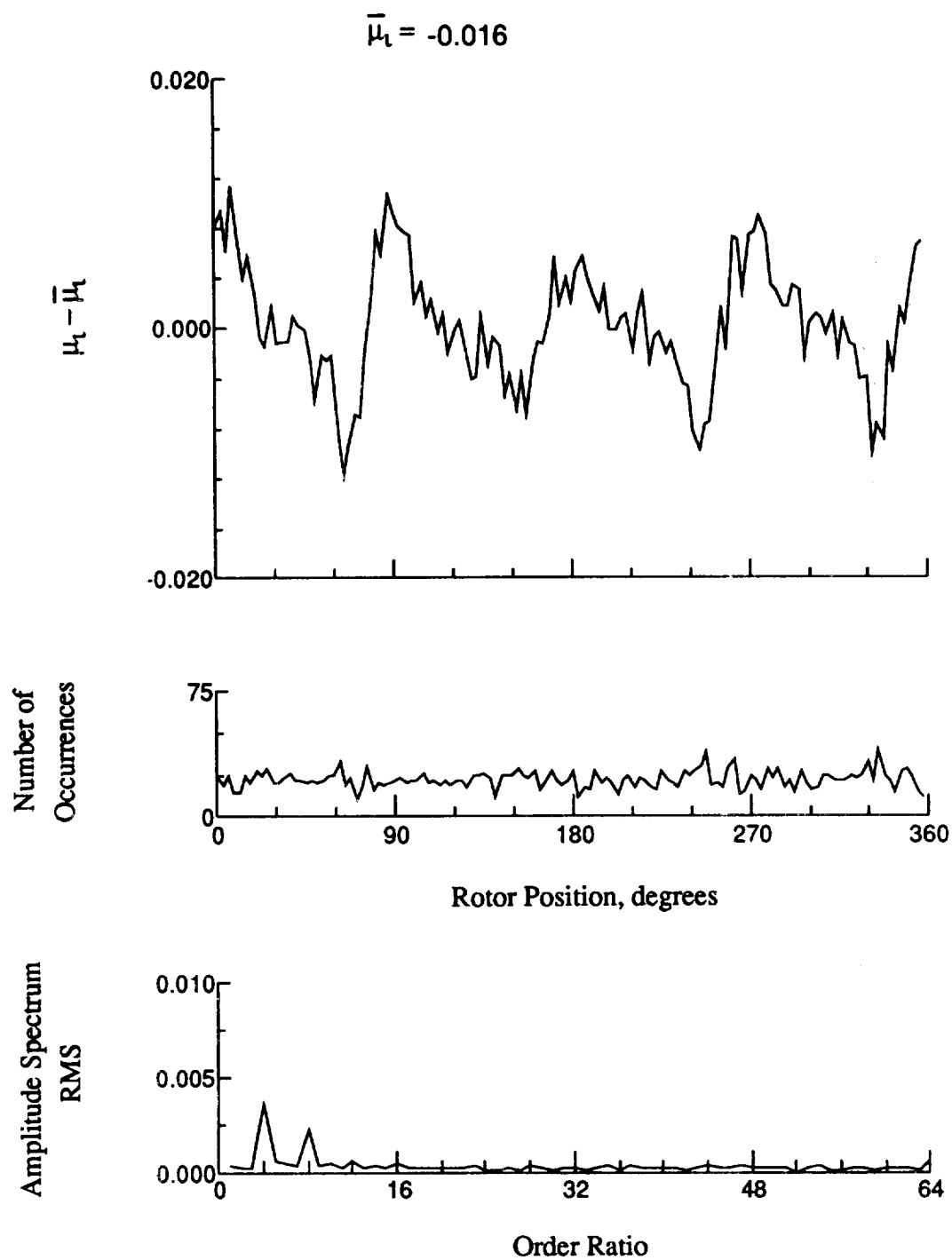


Figure 139. - Induced inflow velocity measured at 240 degrees and r/R of 0.86.

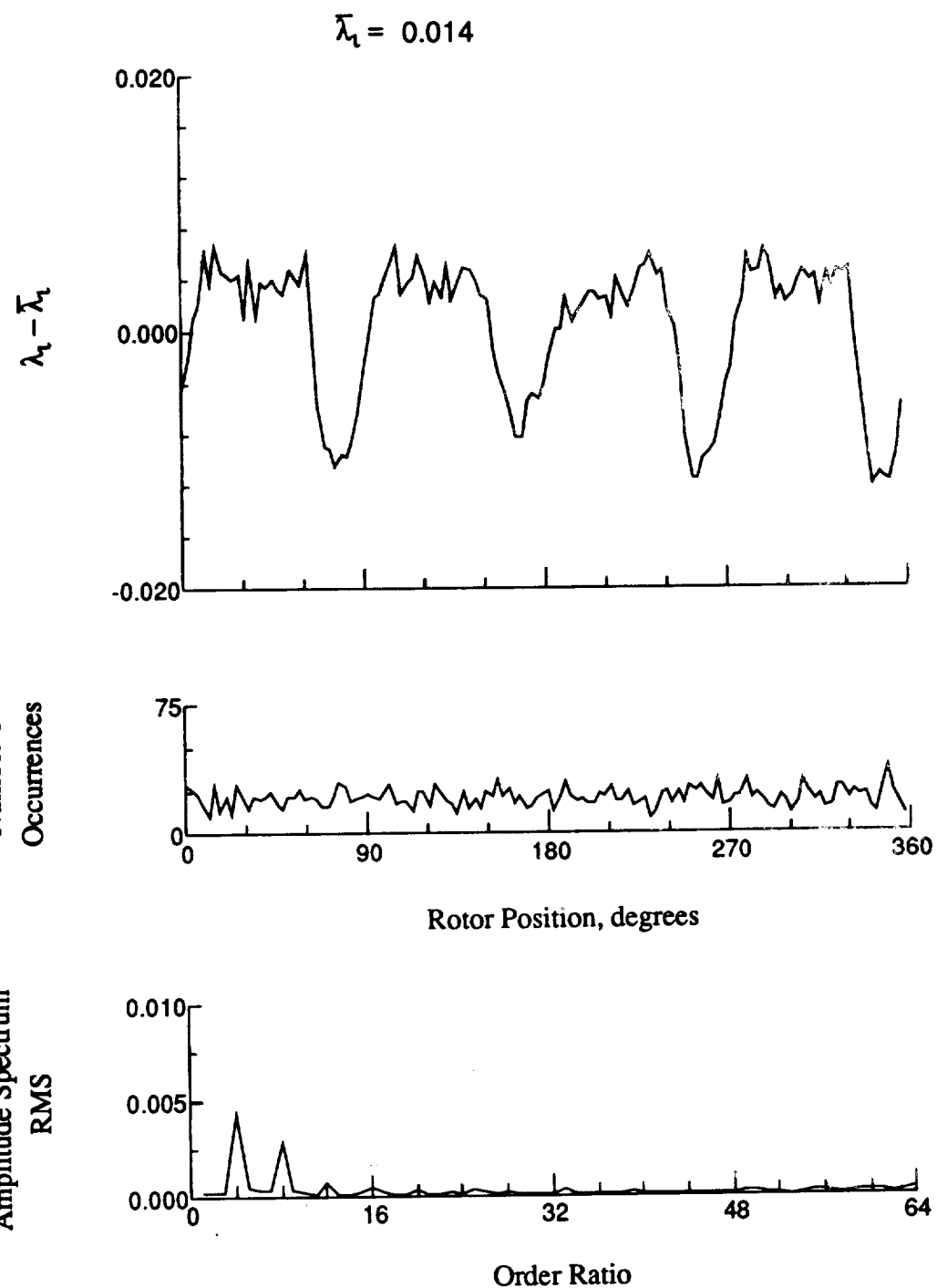


Figure 139.- Concluded.

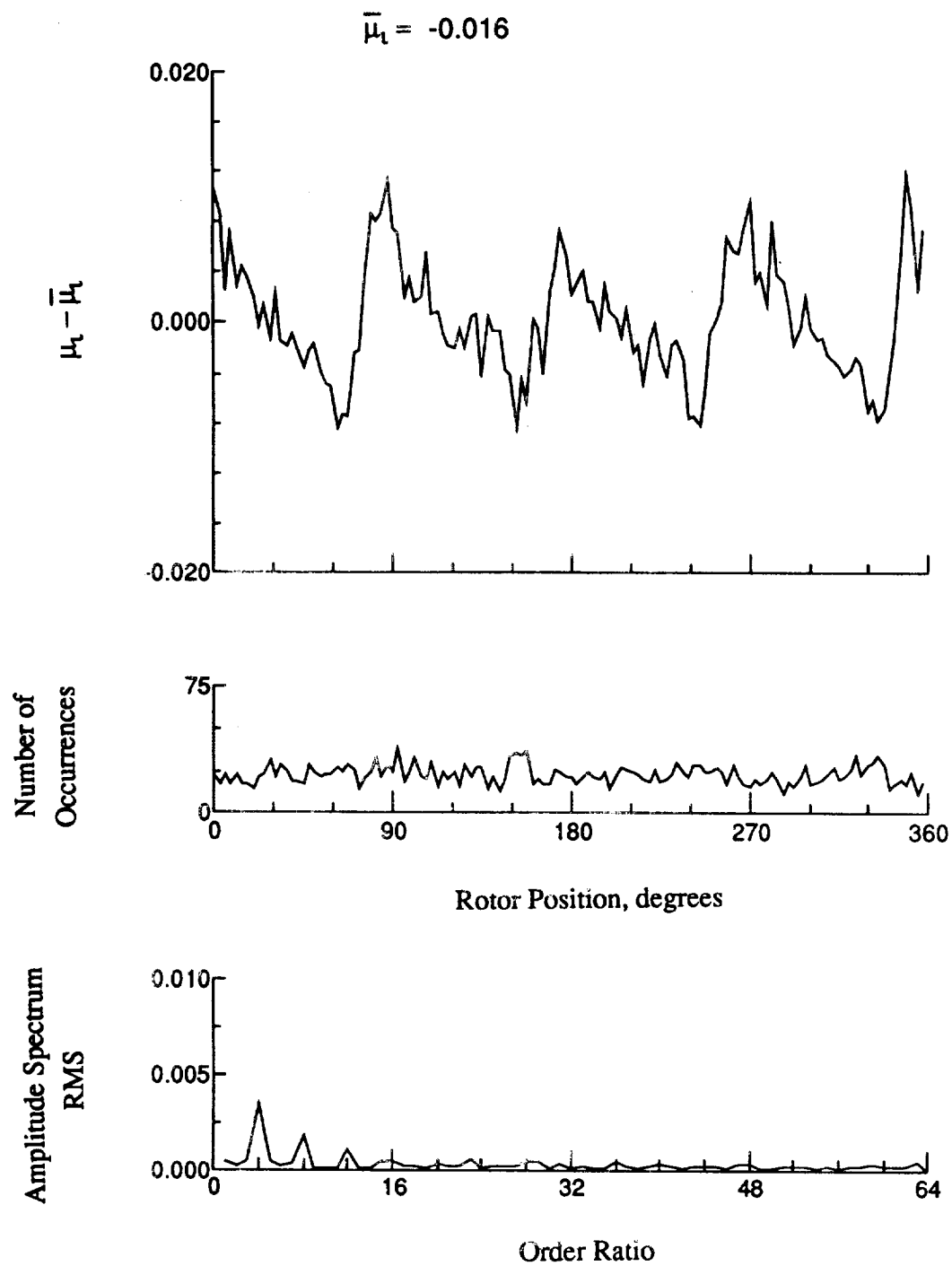


Figure 140.- Induced inflow velocity measured at 240 degrees and r/R of 0.90.

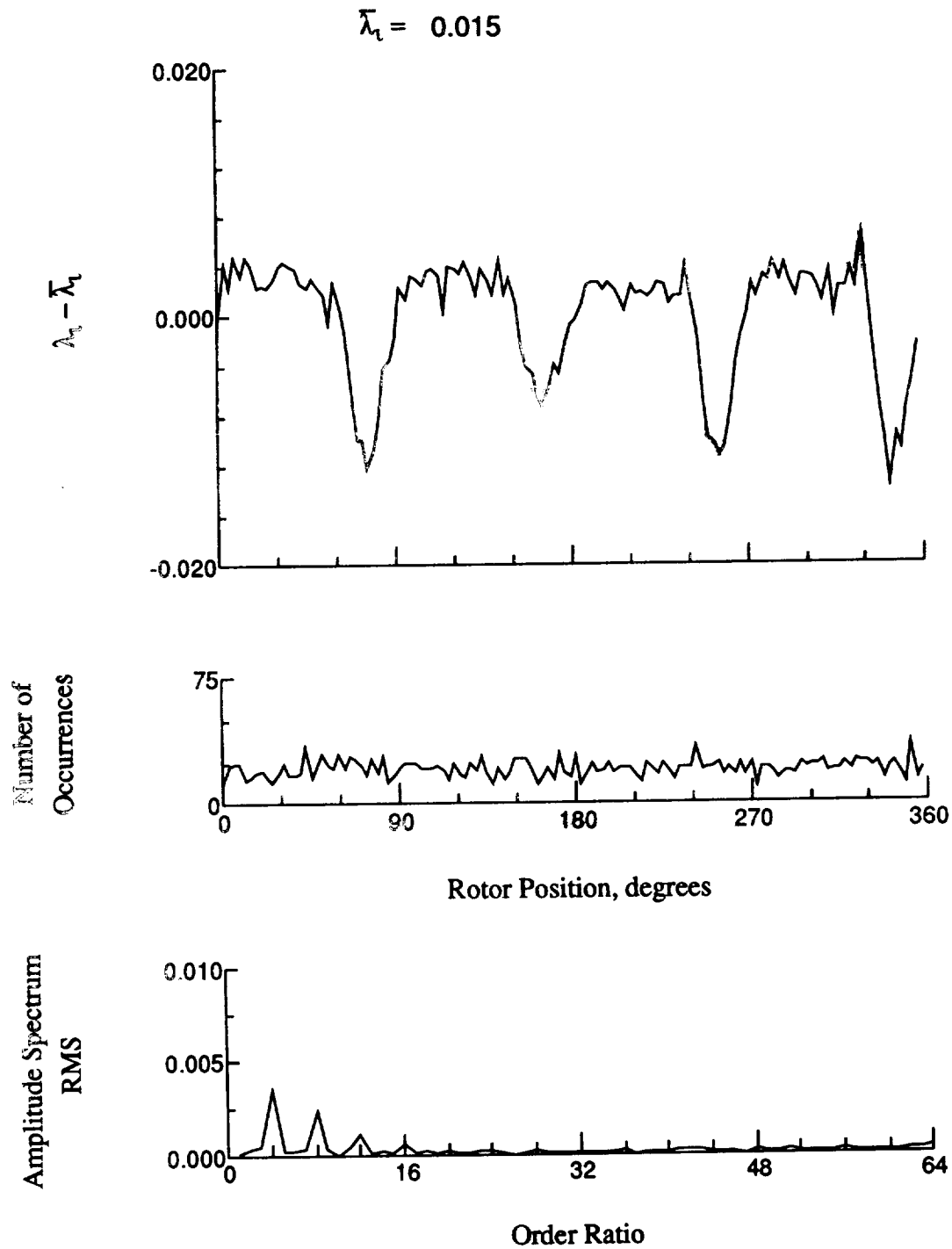


Figure 140.- Concluded.

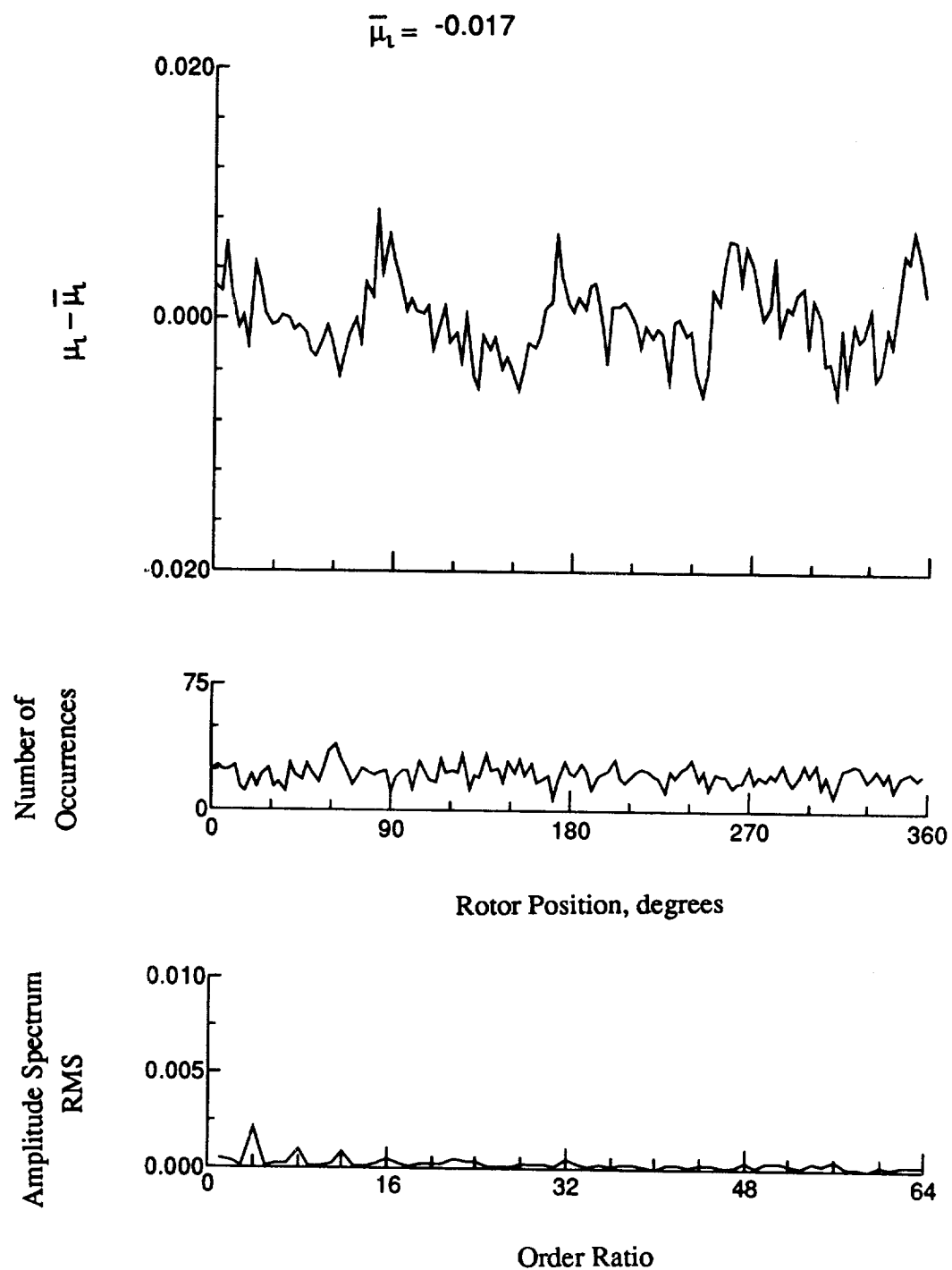


Figure 141.- Induced inflow velocity measured at 240 degrees and r/R of 0.94.

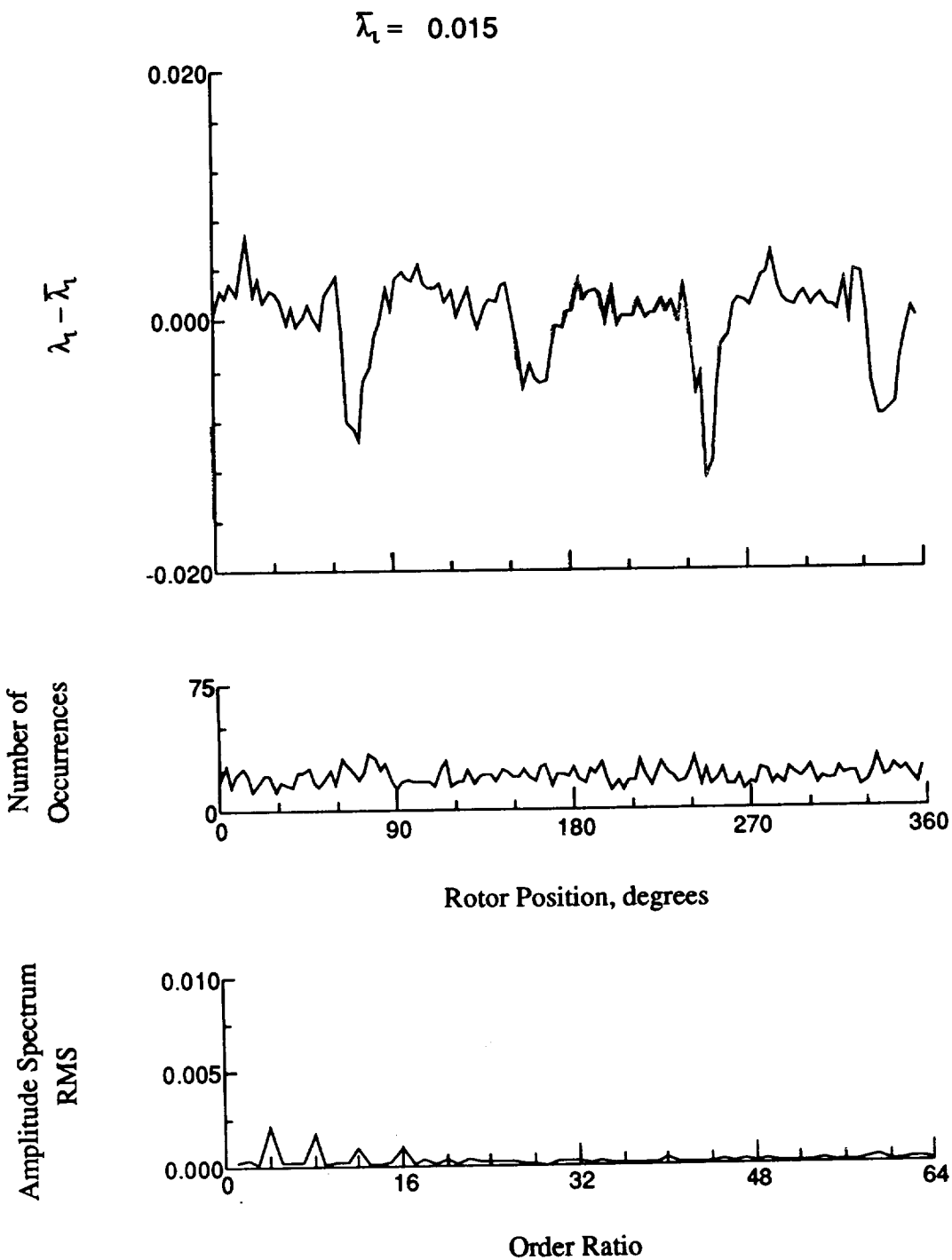


Figure 141.- Concluded.

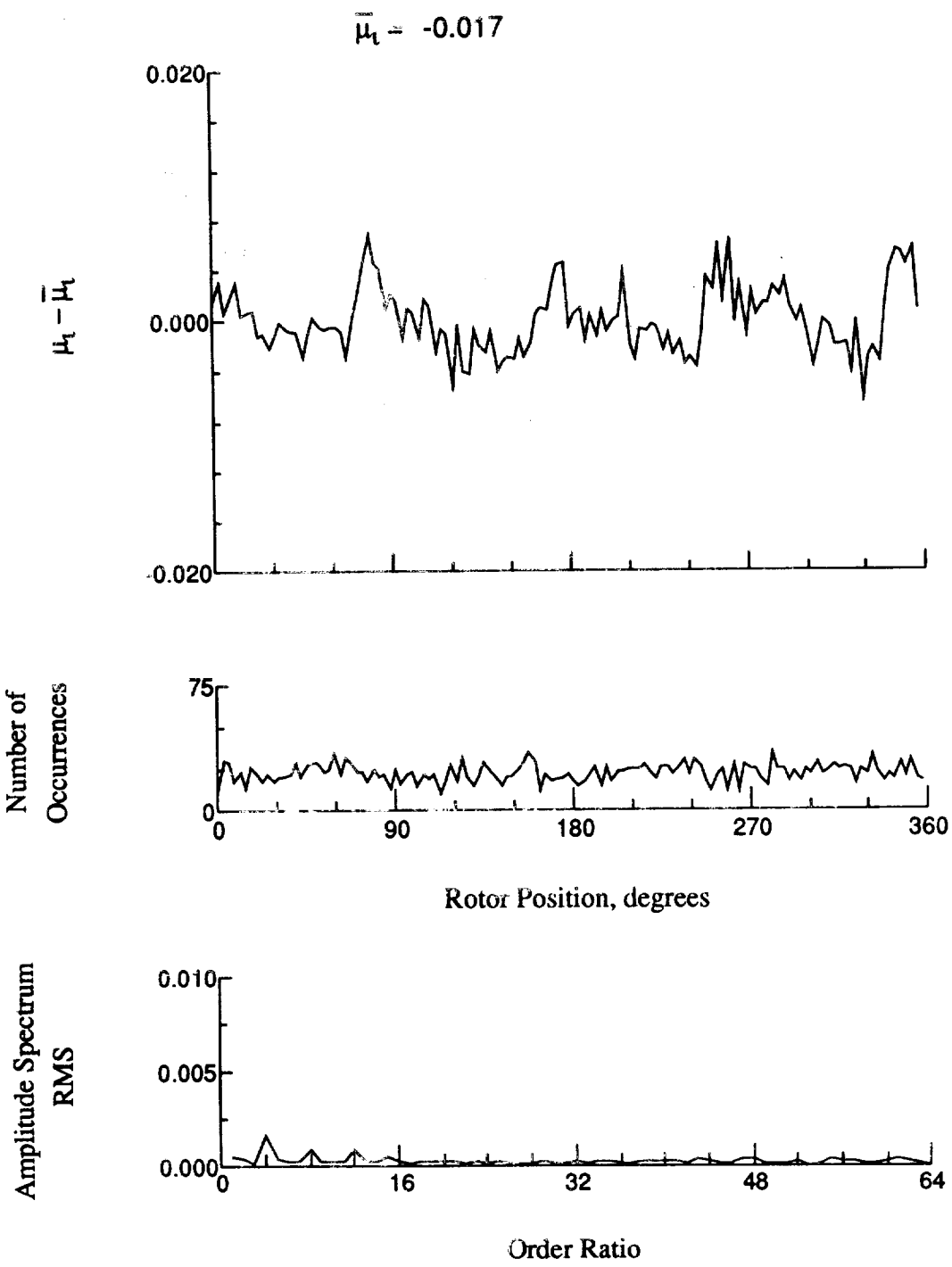


Figure 142.- Induced inflow velocity measured at 240 degrees and r/R of 0.96.

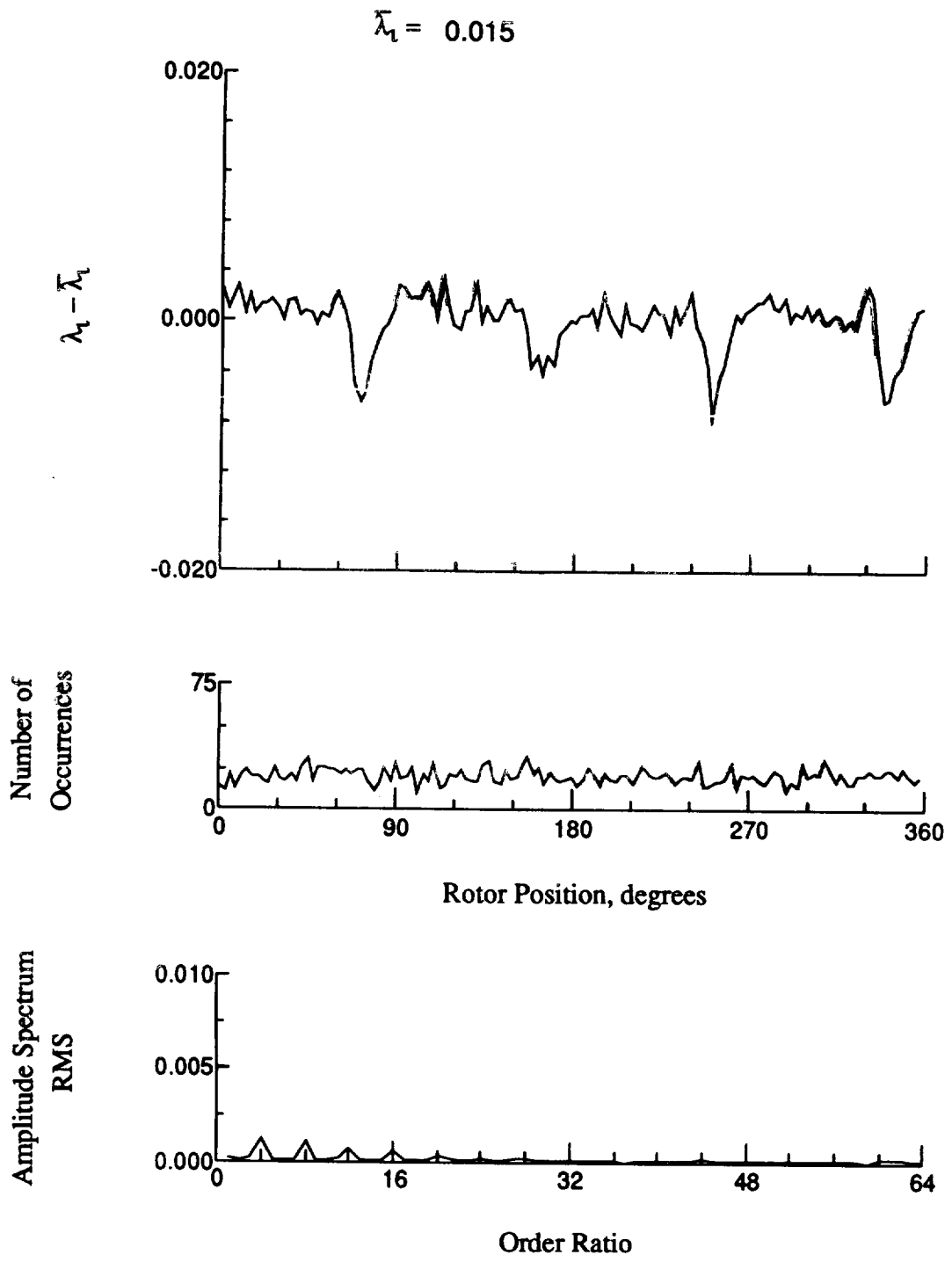


Figure 142.- Concluded.

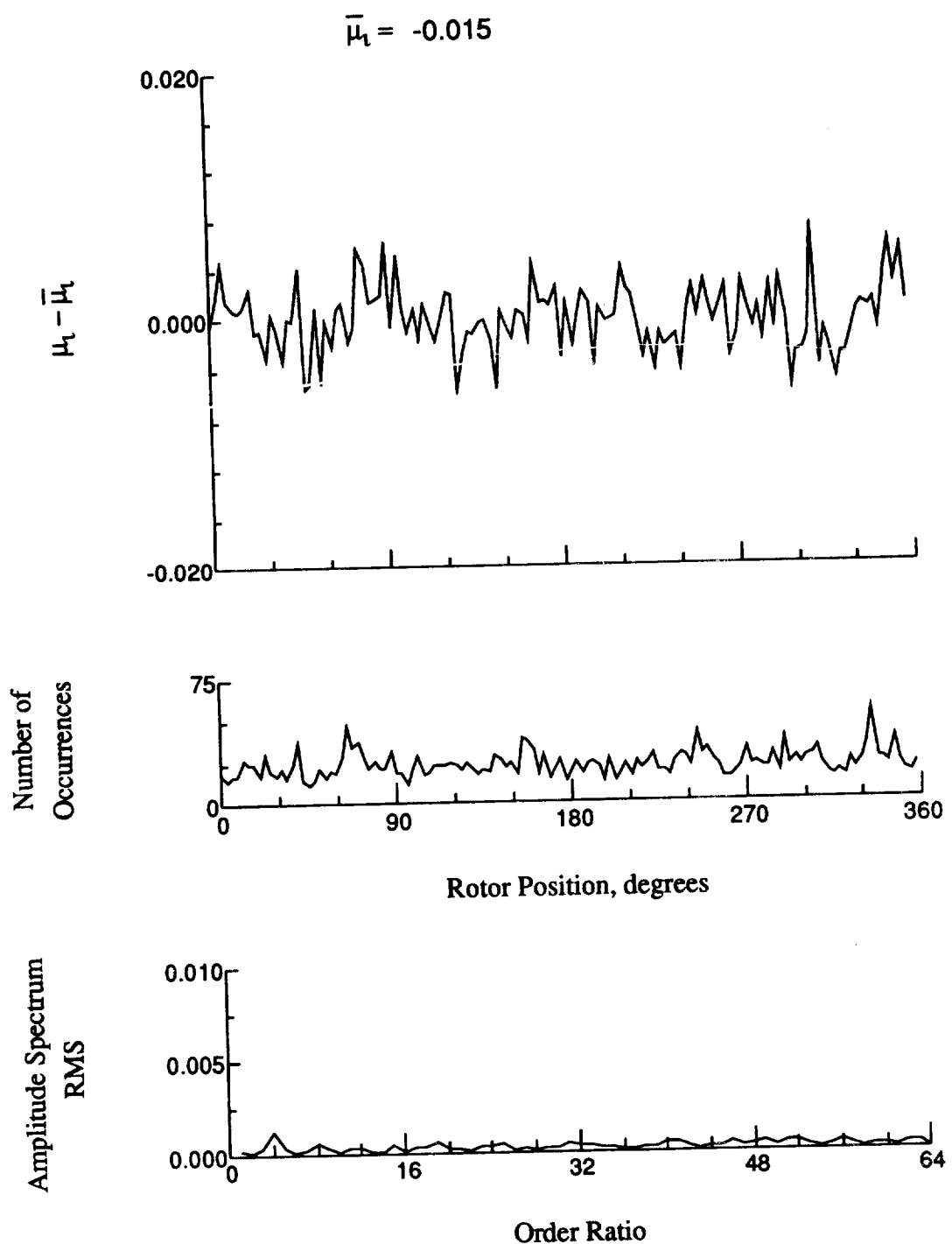


Figure 143.- Induced inflow velocity measured at 240 degrees and r/R of 1.00.

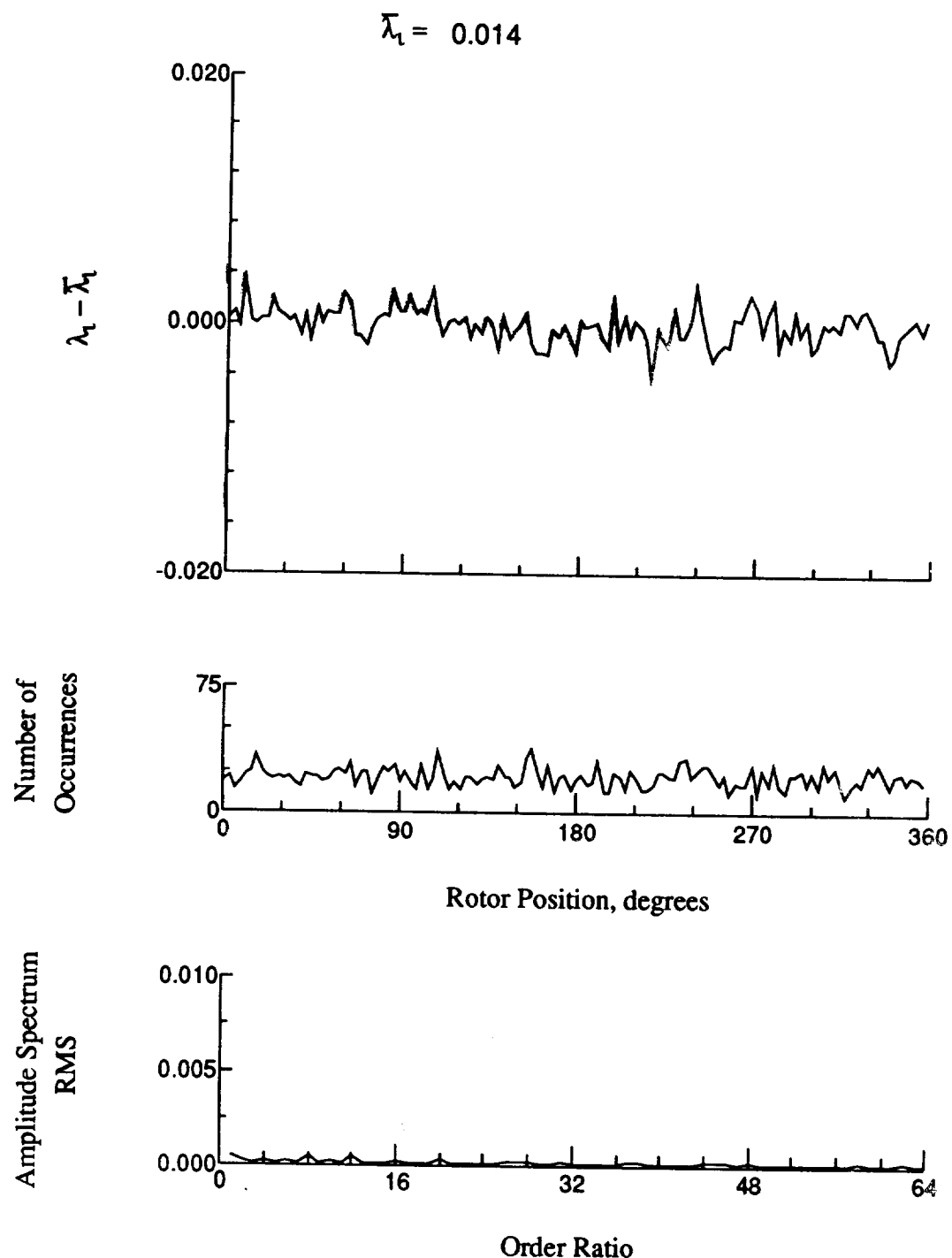


Figure 143.- Concluded.

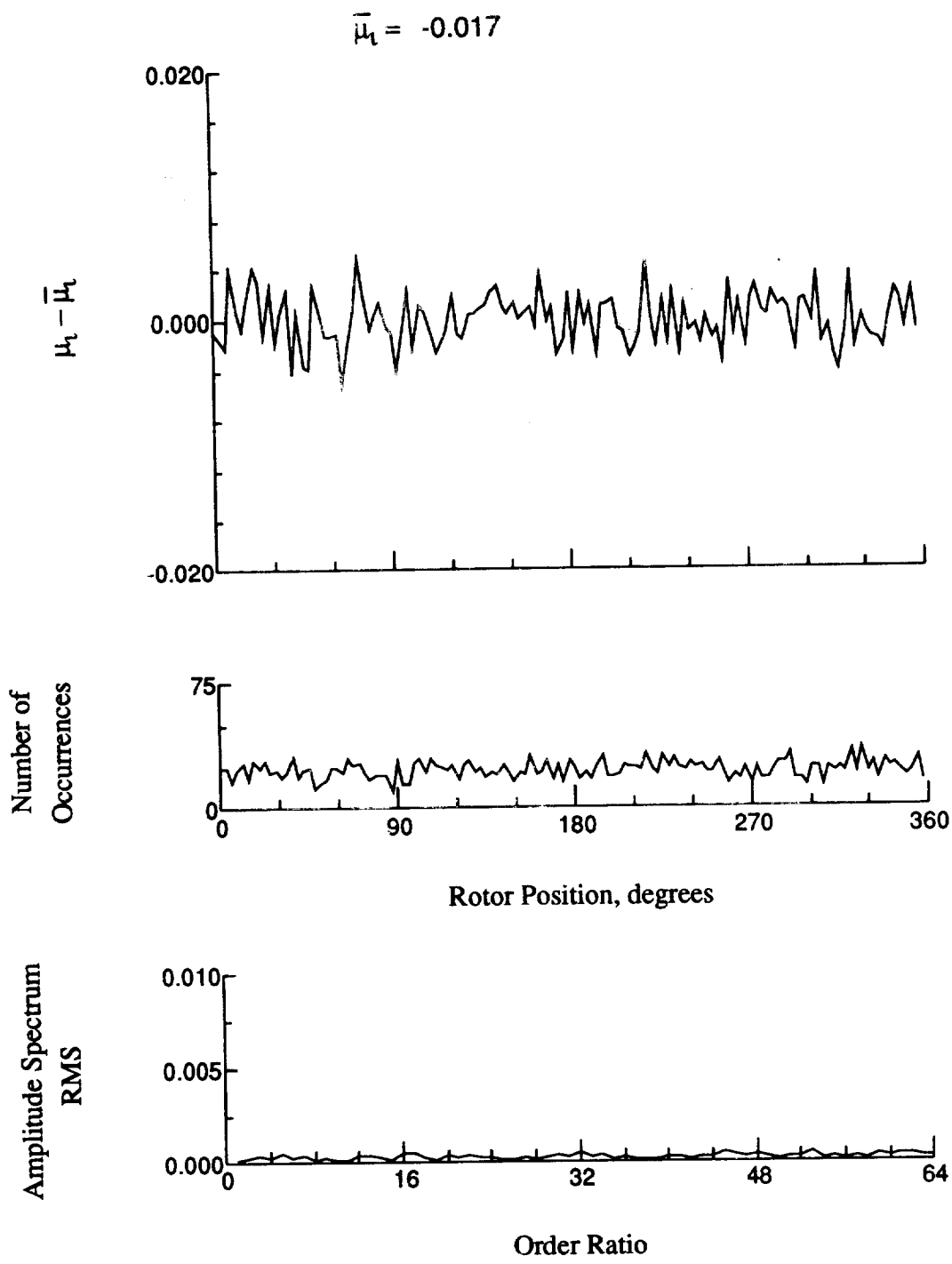


Figure 144.- Induced inflow velocity measured at 240 degrees and r/R of 1.10.

$$\bar{\lambda}_1 = 0.014$$

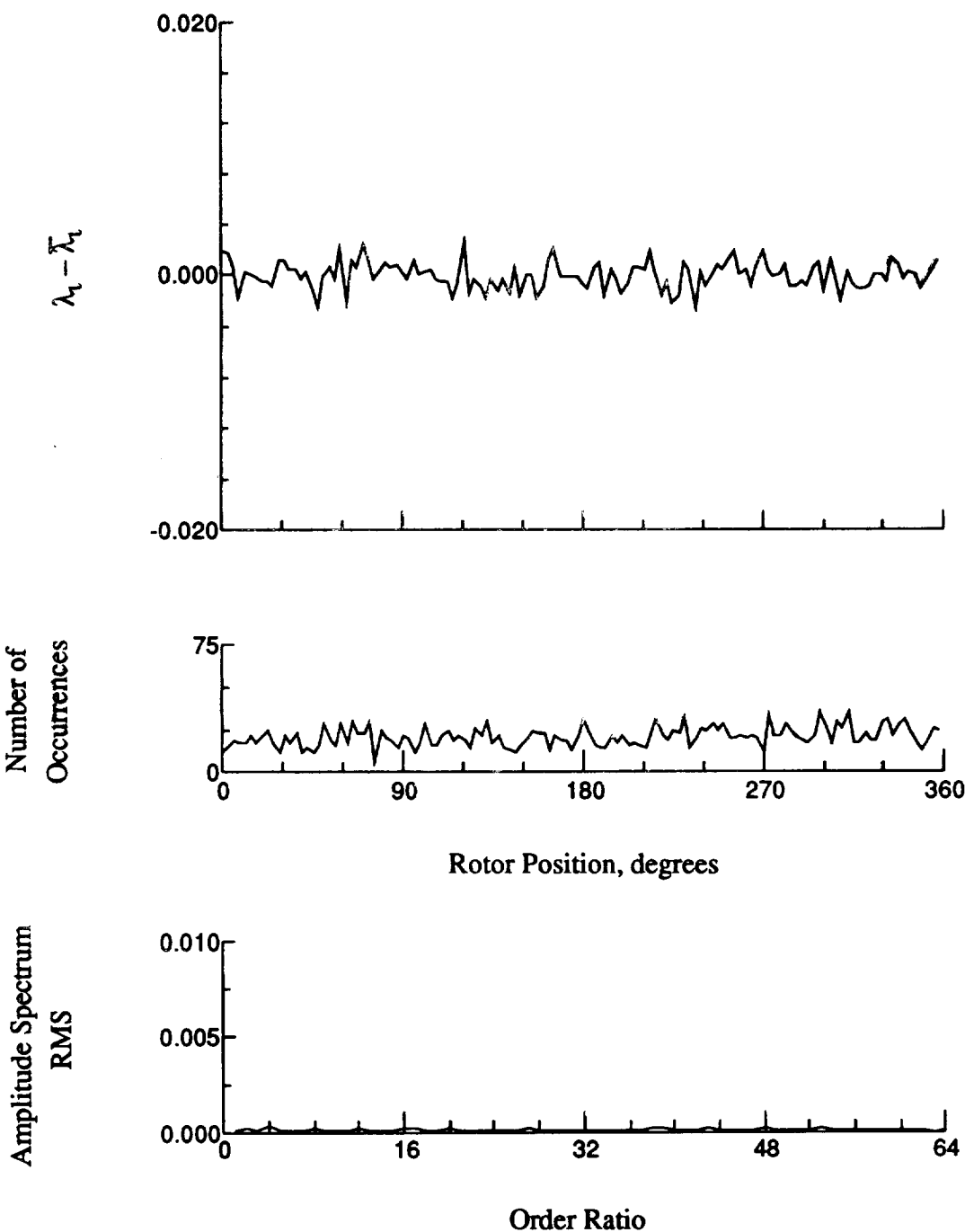


Figure 144.- Concluded.

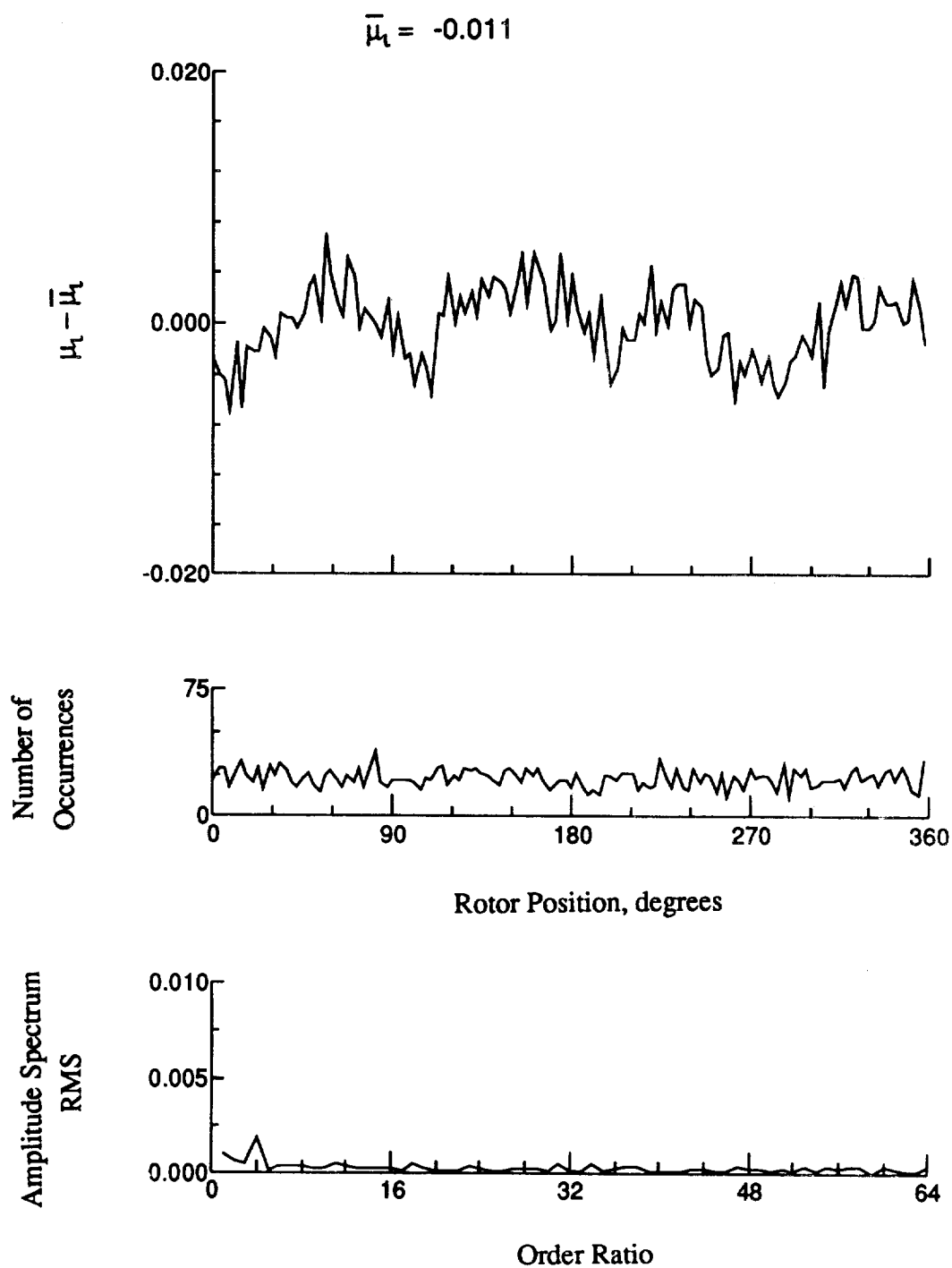


Figure 145.- Induced inflow velocity measured at 270 degrees and r/R of 0.20.

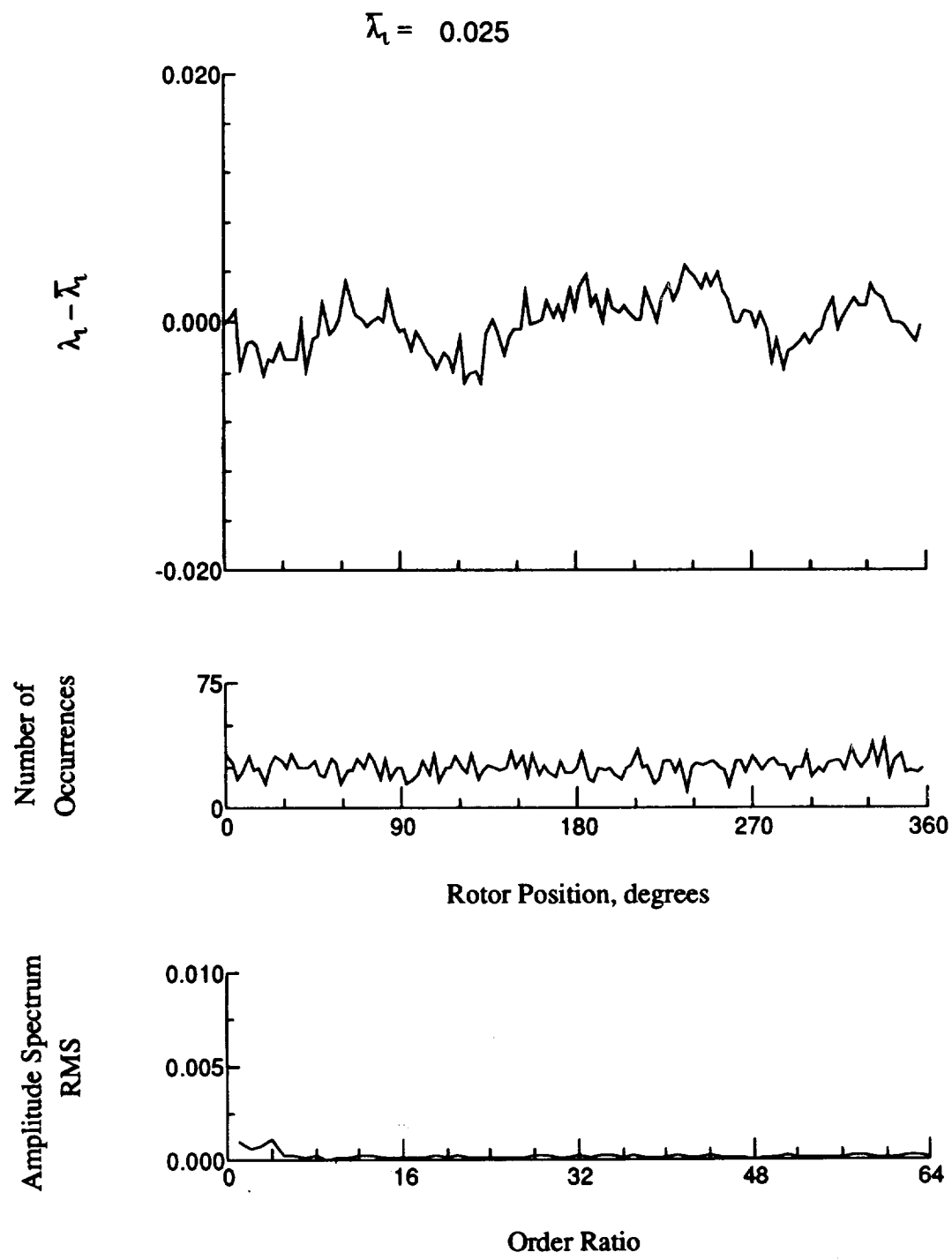


Figure 145.- Concluded.

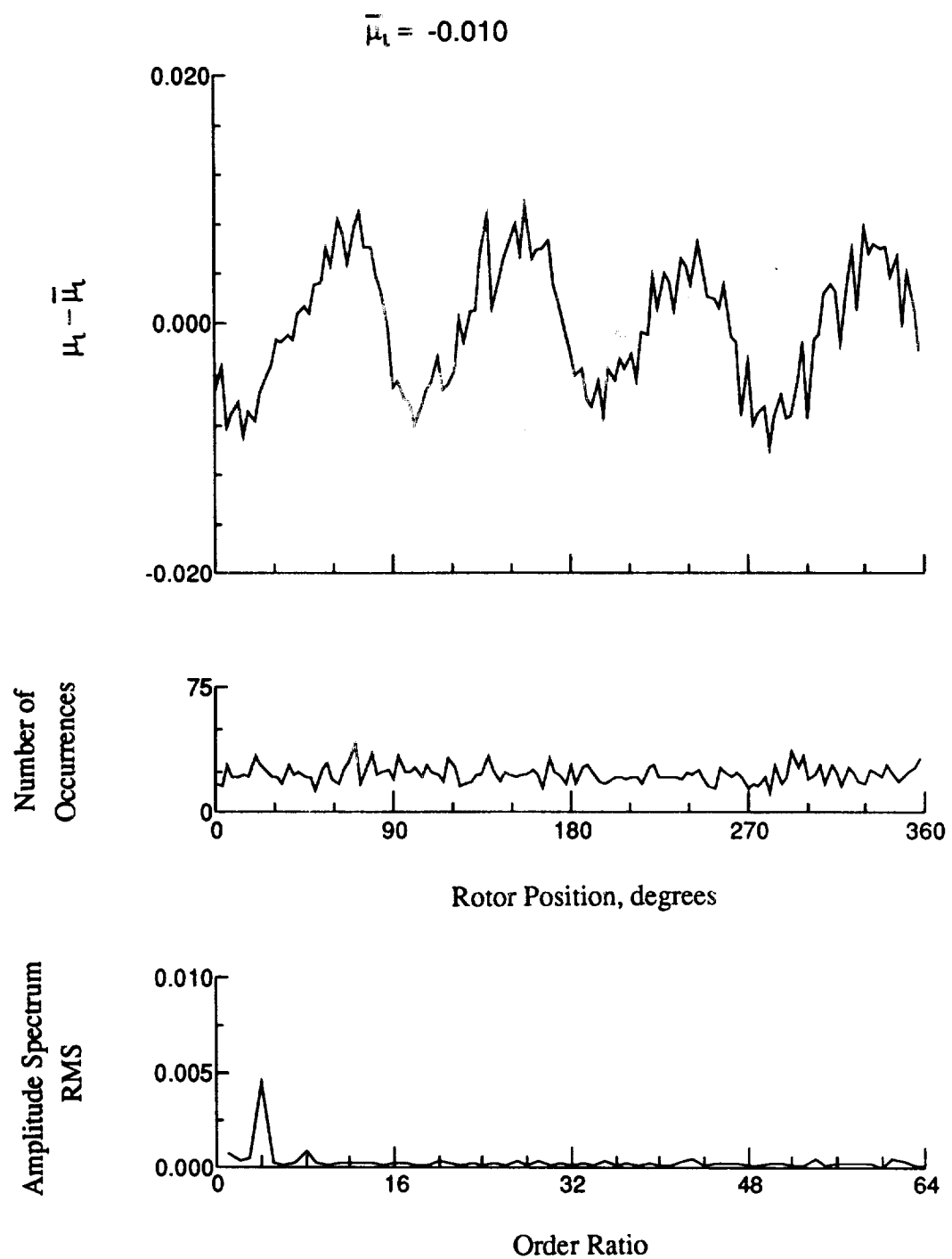


Figure 146.- Induced inflow velocity measured at 270 degrees and r/R of 0.32.

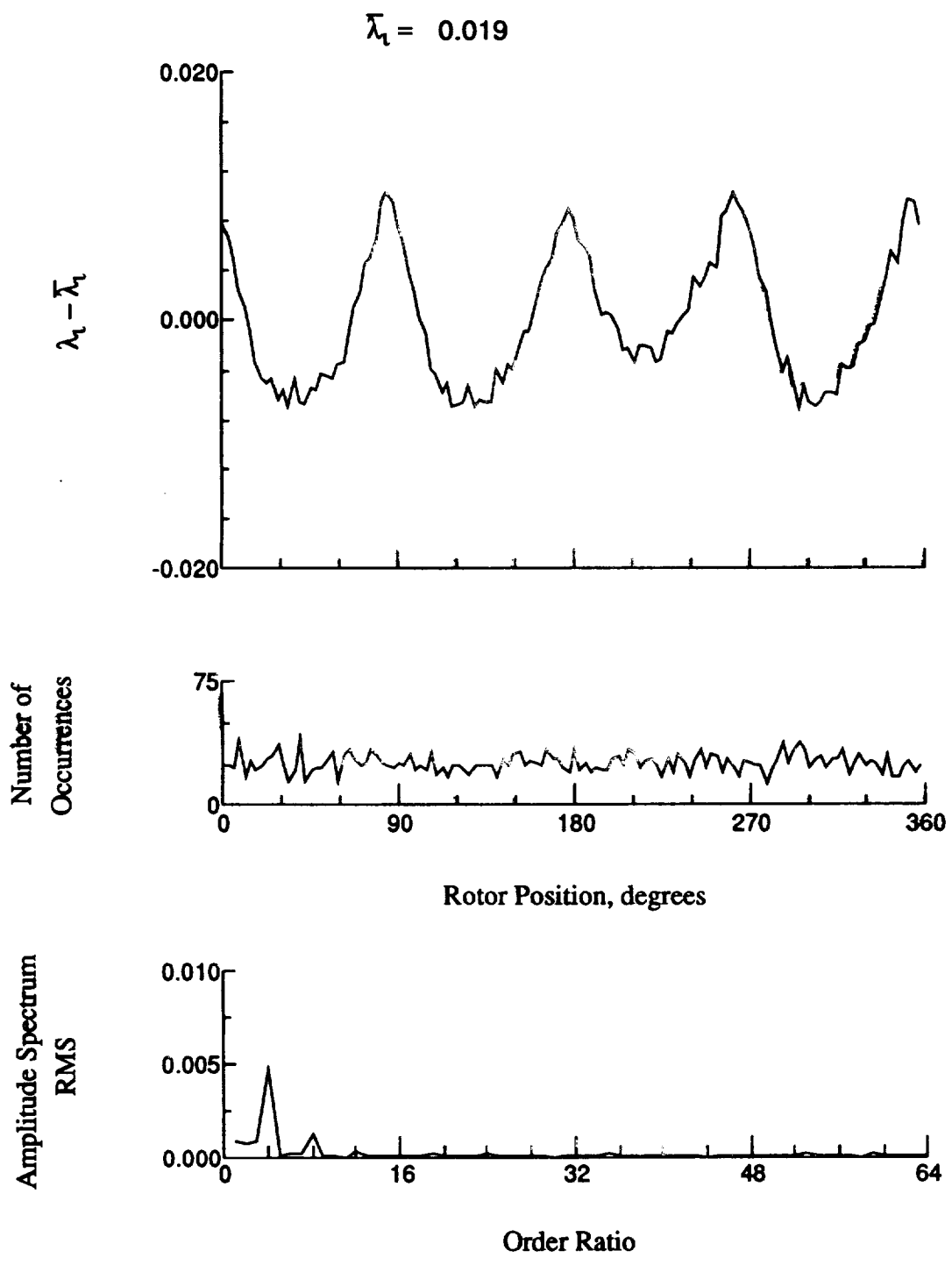


Figure 146.- Concluded.

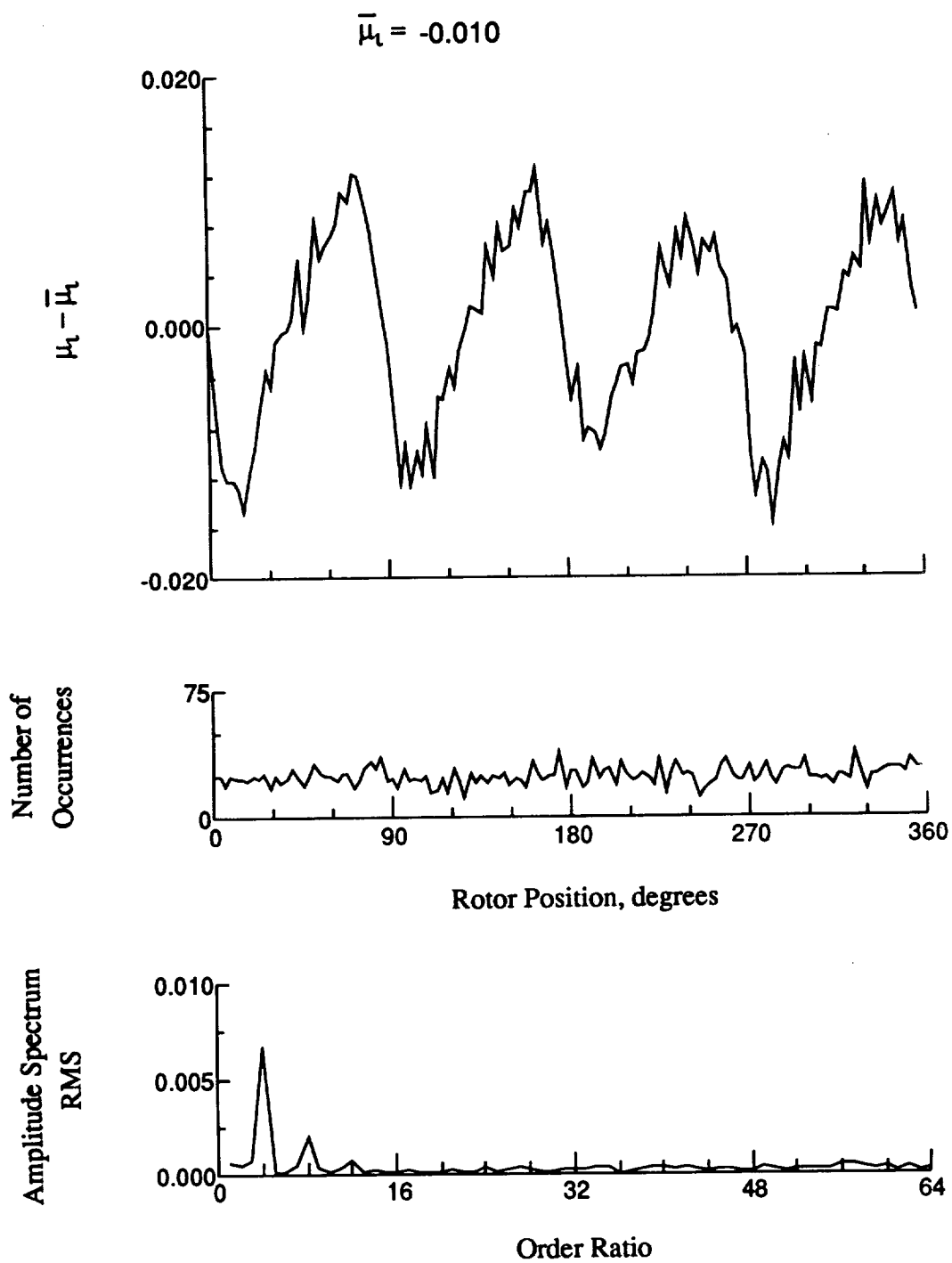


Figure 147.- Induced inflow velocity measured at 270 degrees and r/R of 0.50.

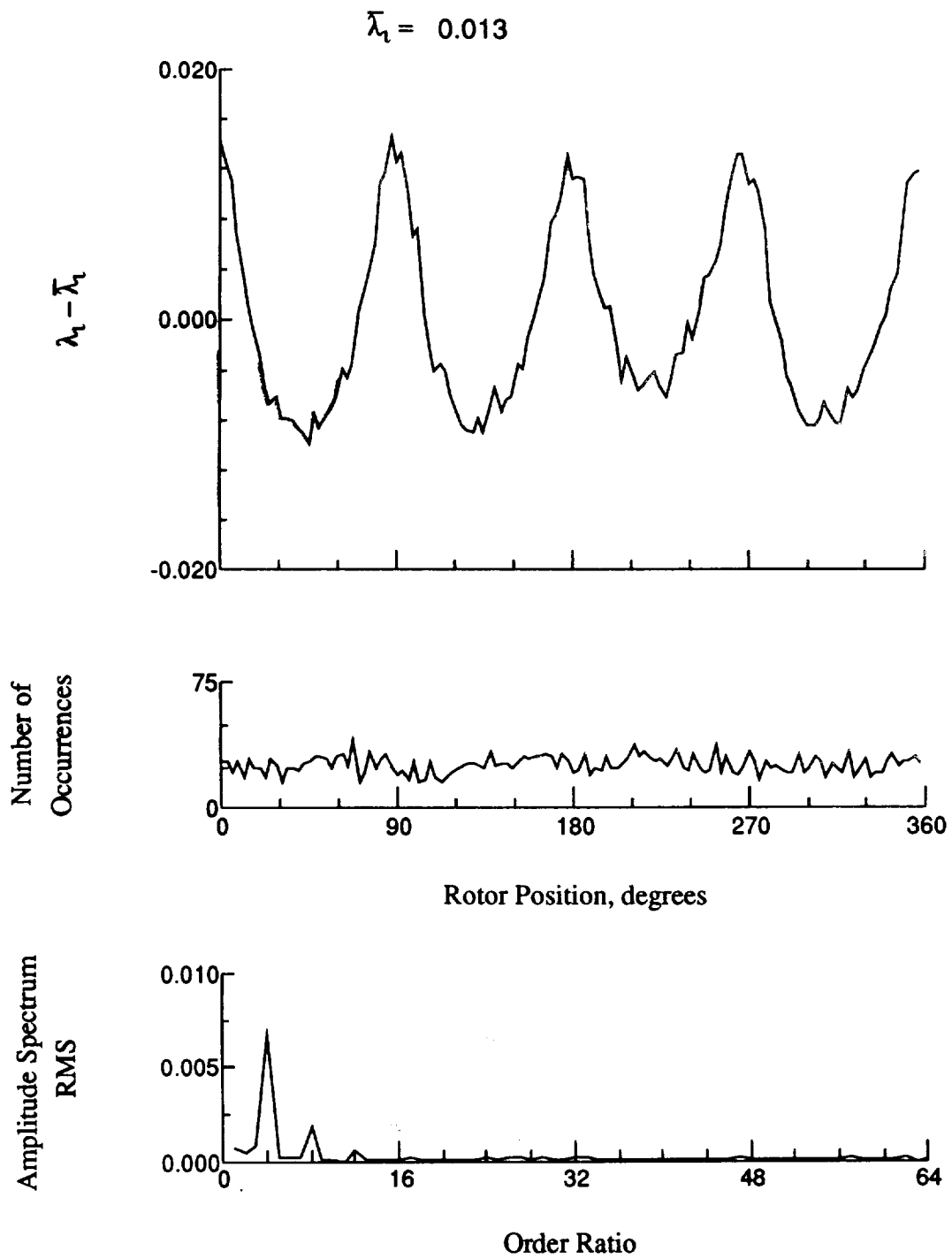


Figure 147.- Concluded.

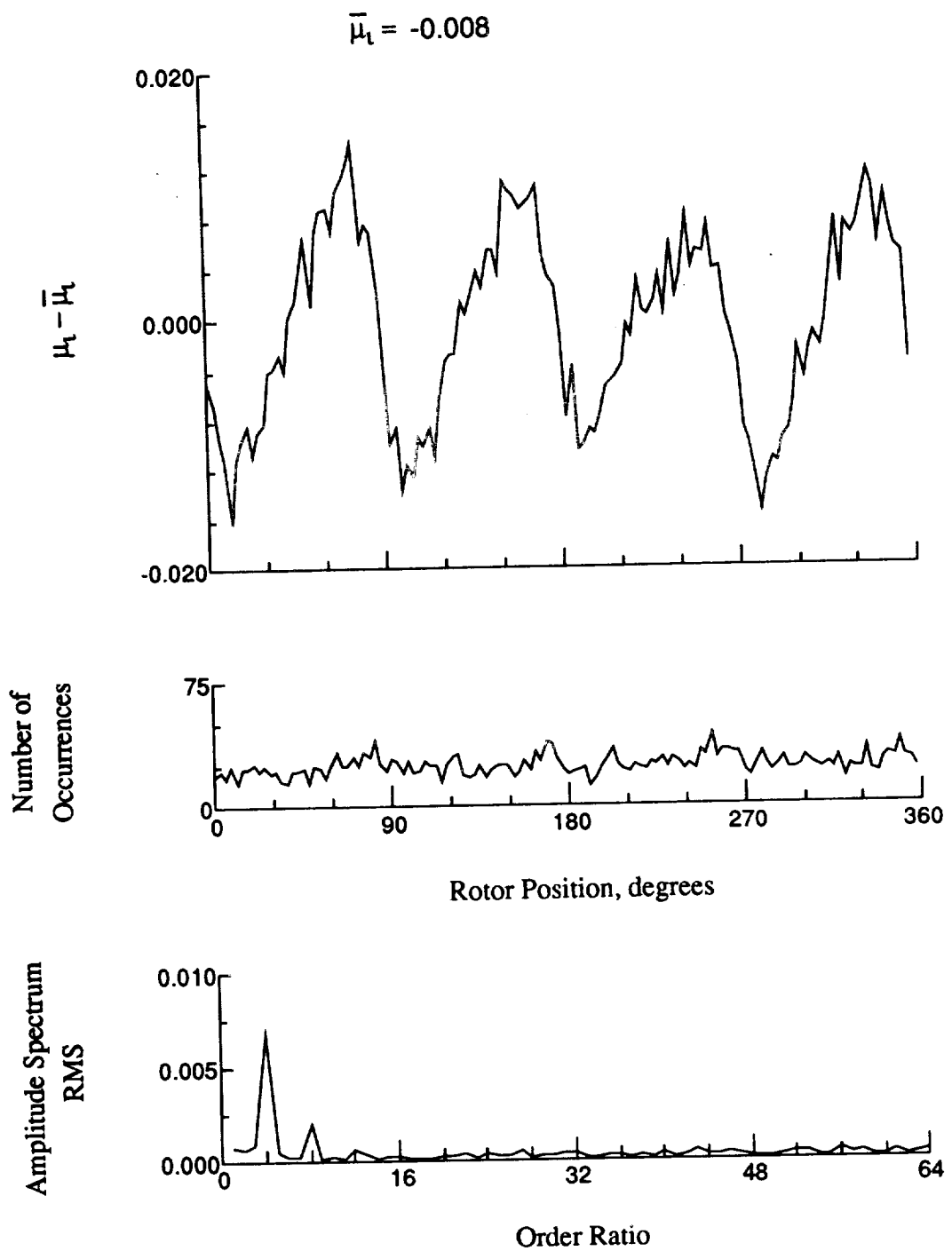


Figure 148.- Induced inflow velocity measured at 270 degrees and r/R of 0.58.

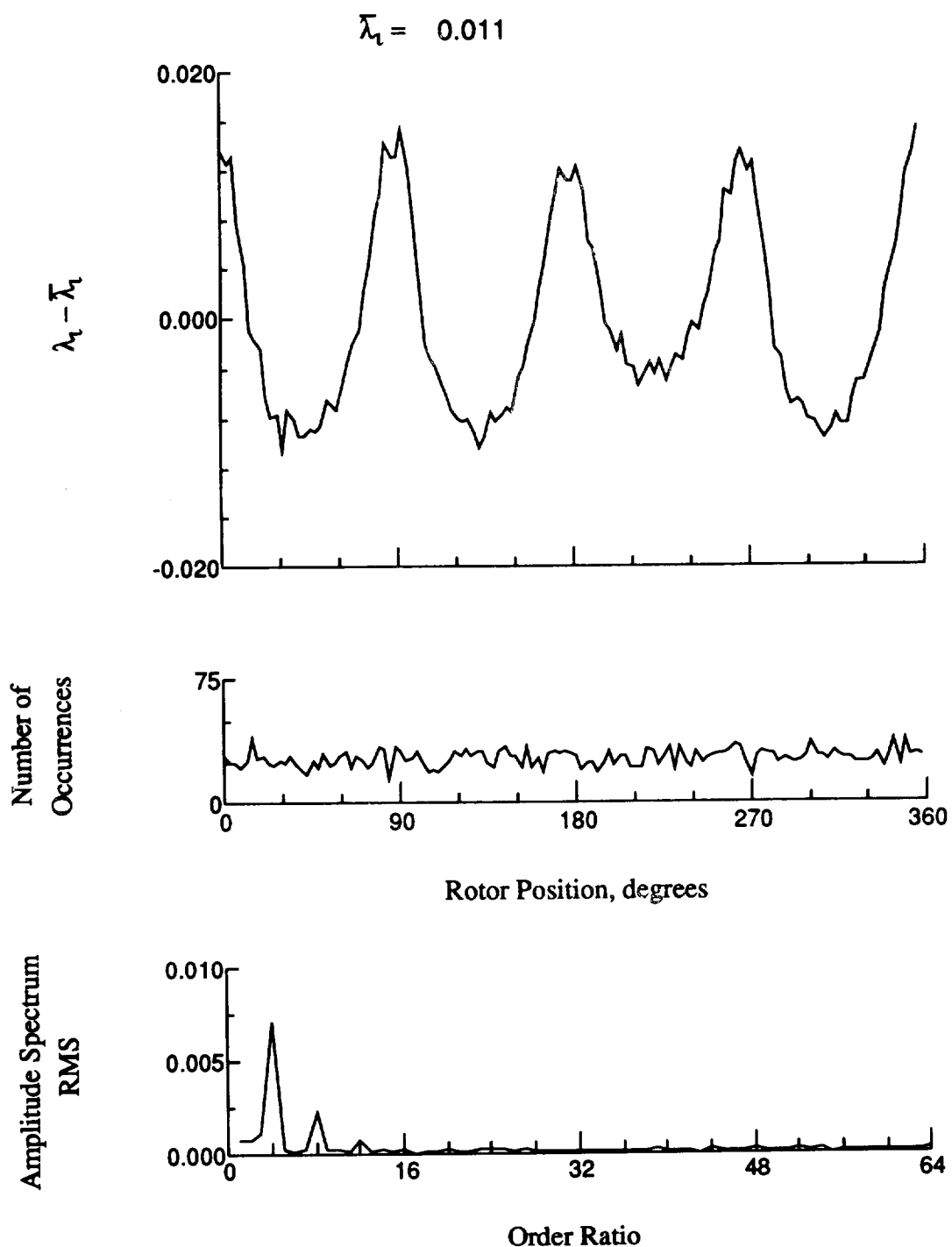


Figure 148.- Concluded.

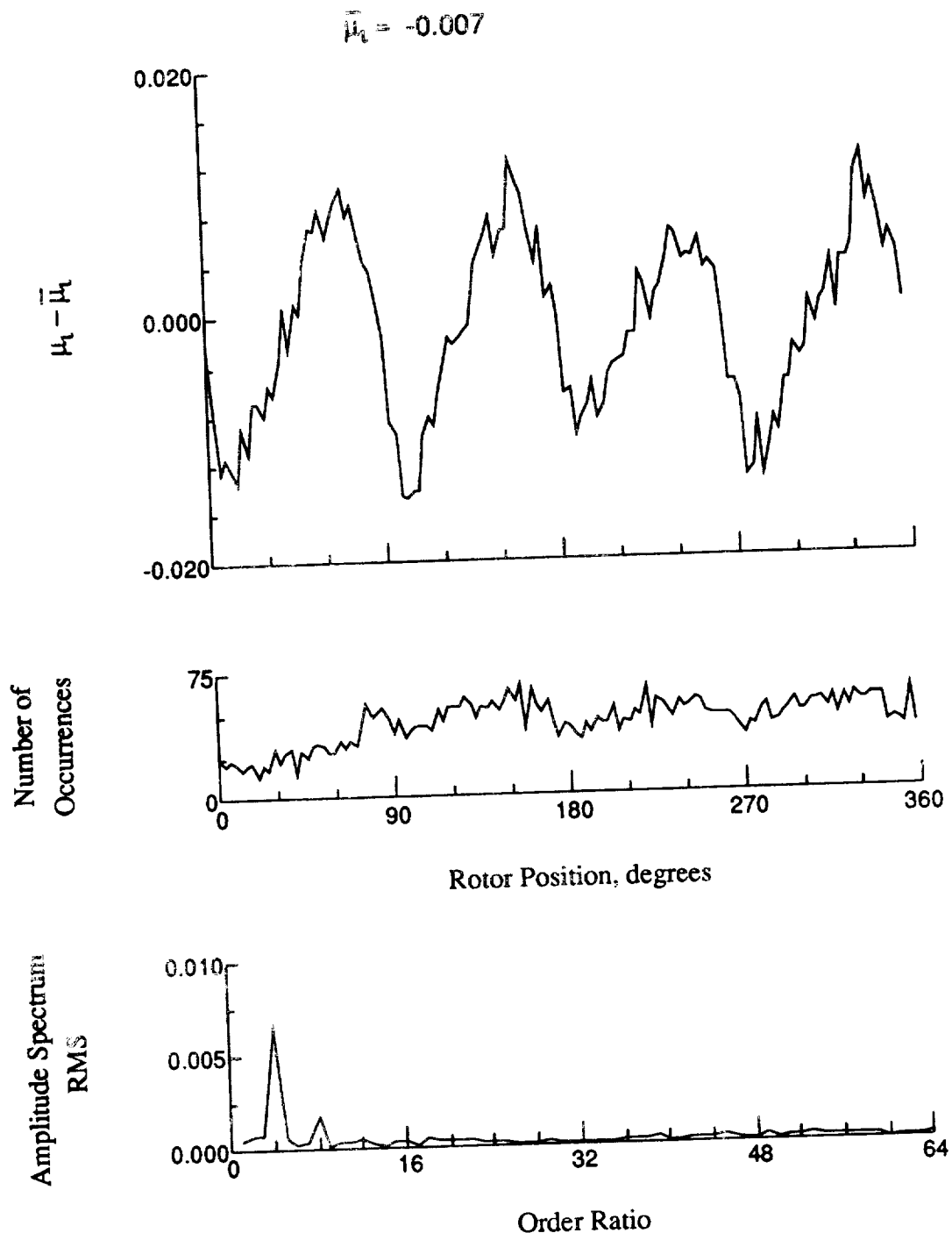


Figure 149.- Induced inflow velocity measured at 270 degrees and r/R of 0.69.

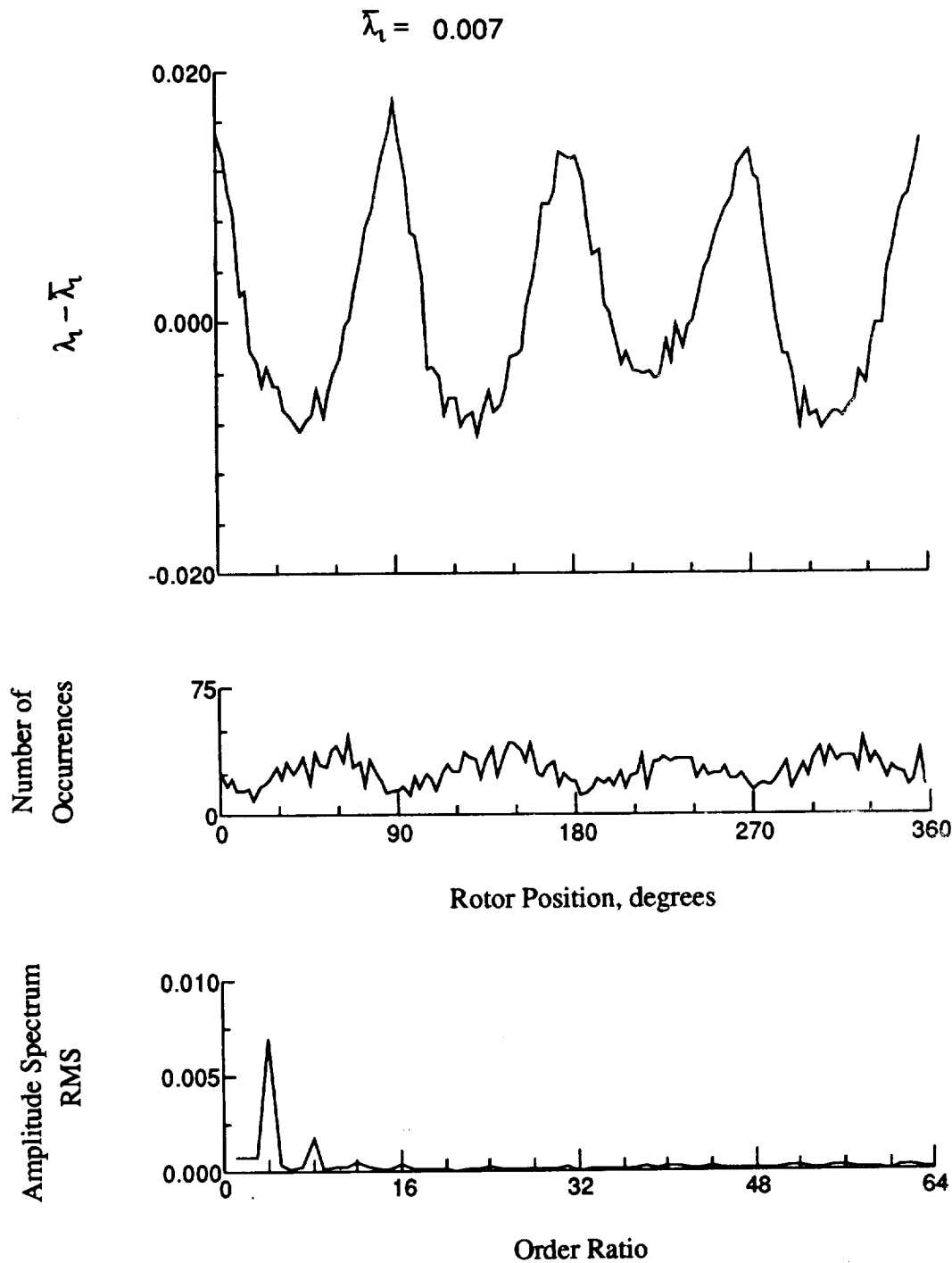


Figure 149.- Concluded.

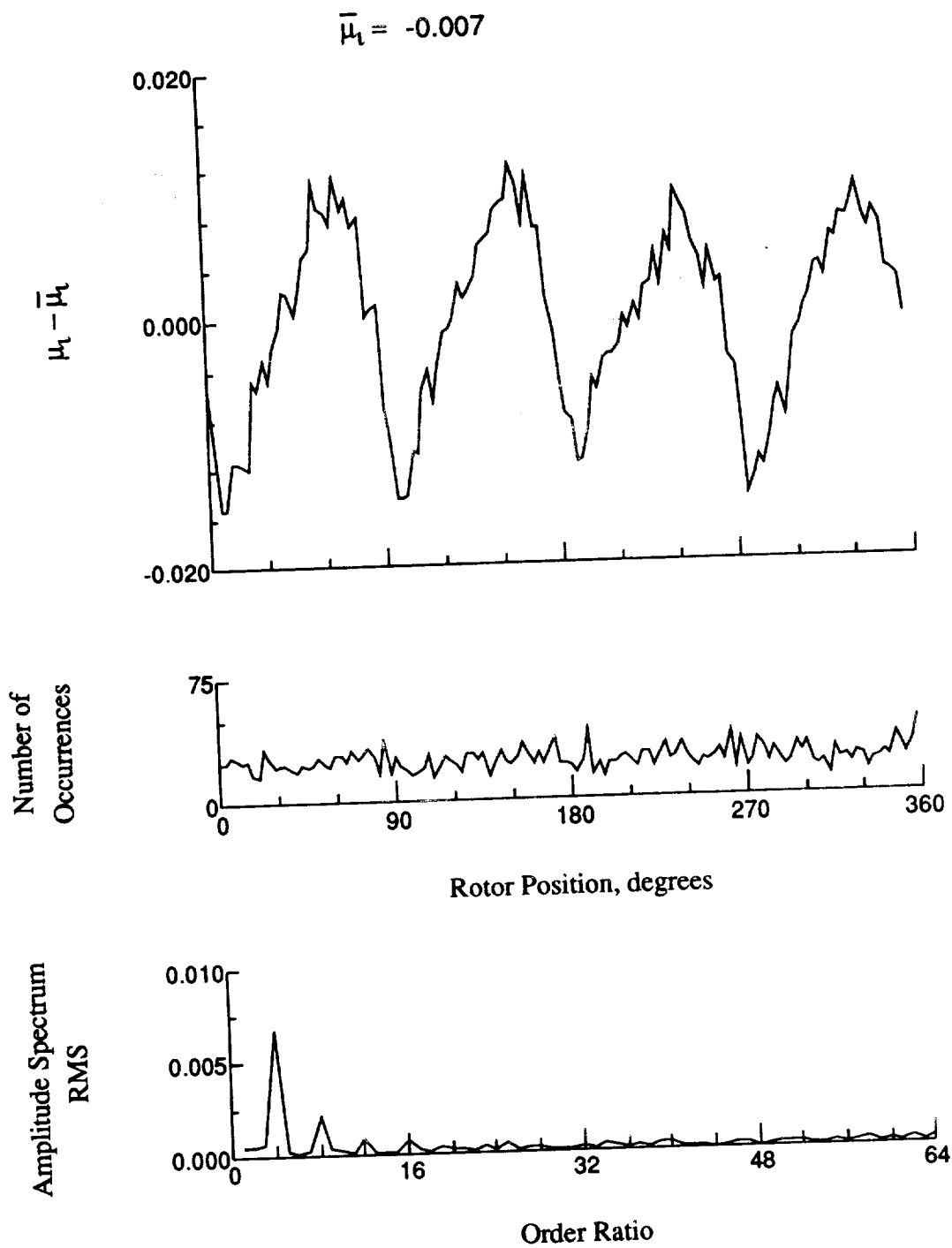


Figure 150.- Induced inflow velocity measured at 270 degrees and r/R of 0.73.

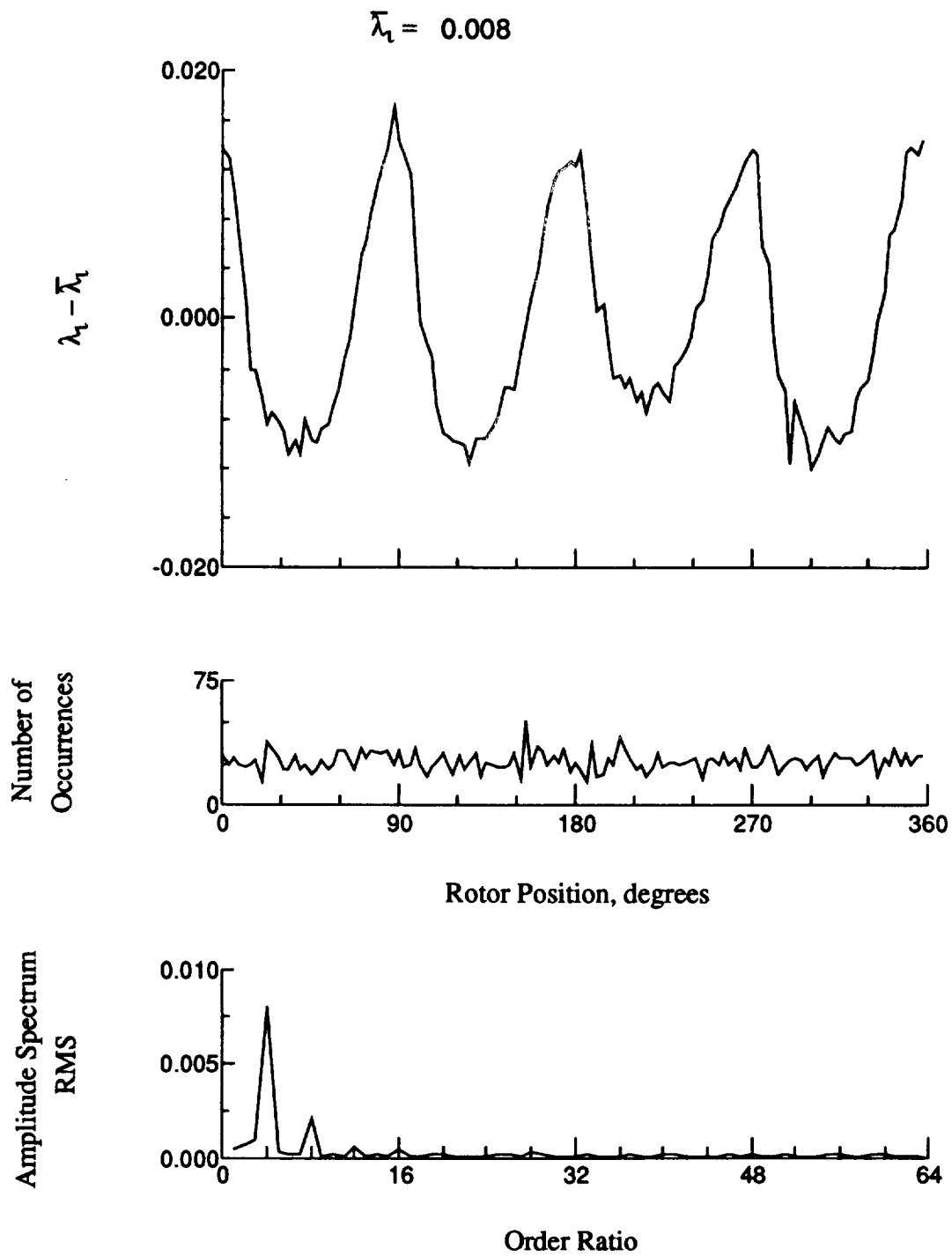


Figure 150.- Concluded.

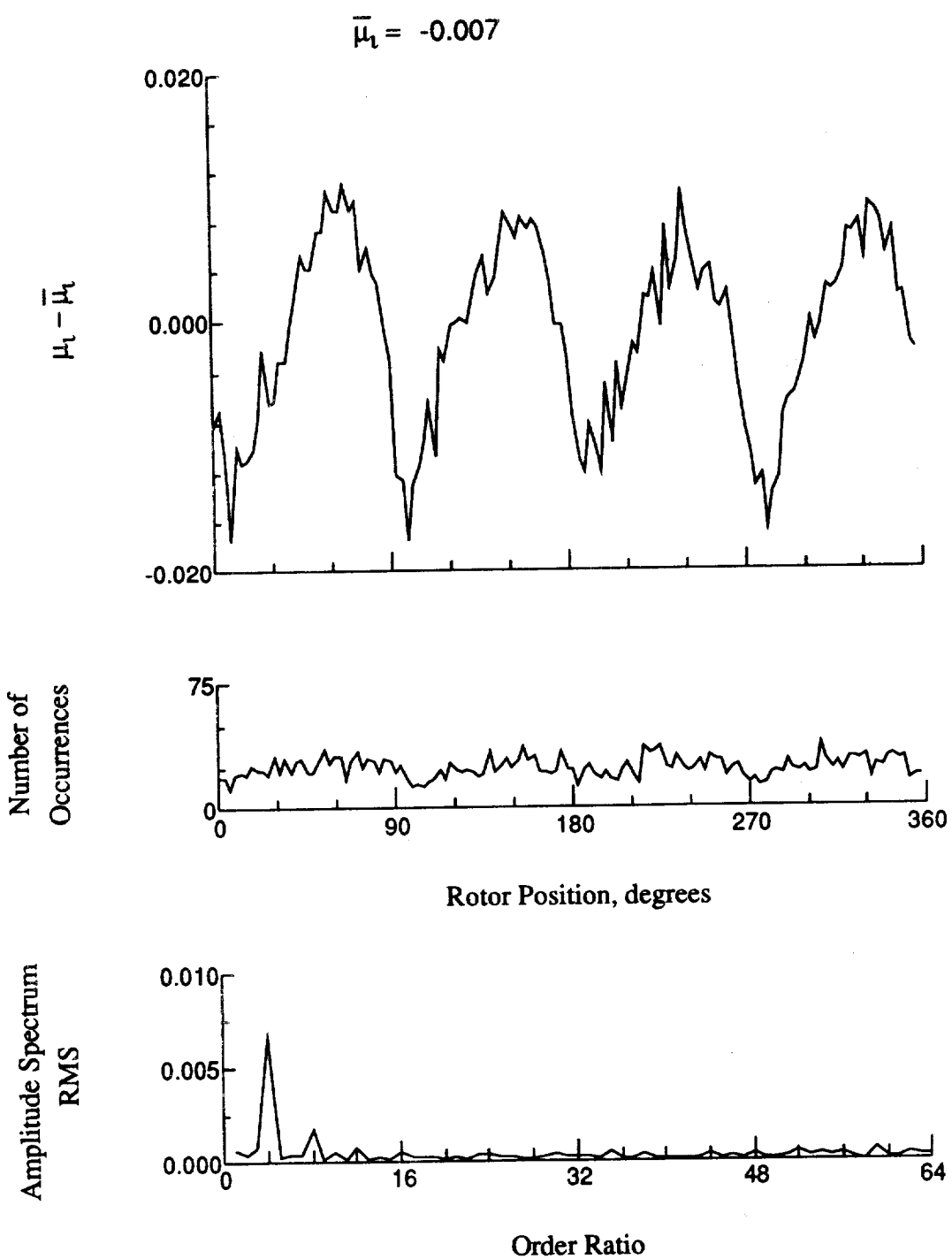


Figure 151.- Induced inflow velocity measured at 270 degrees and r/R of 0.75.

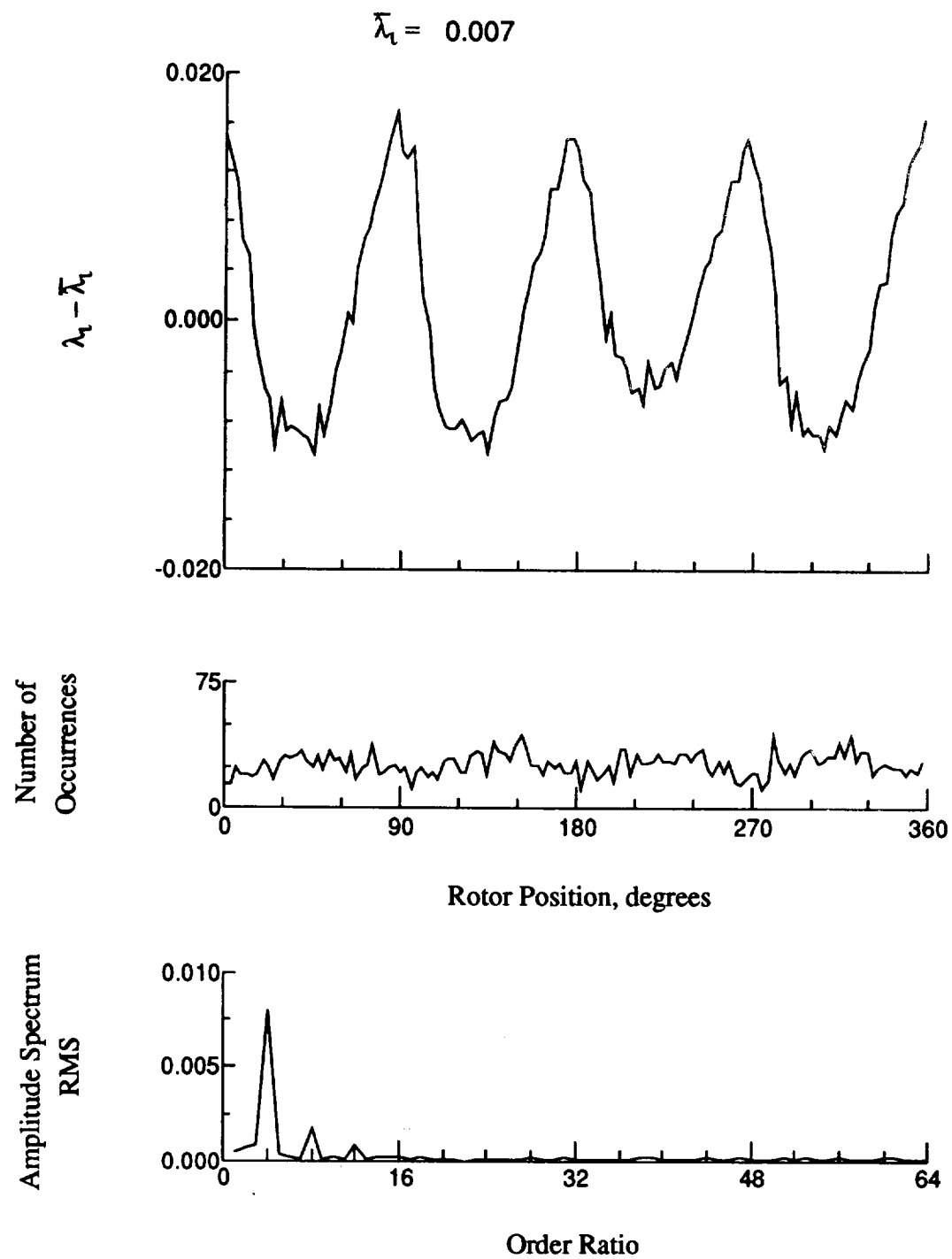


Figure 151.- Concluded.

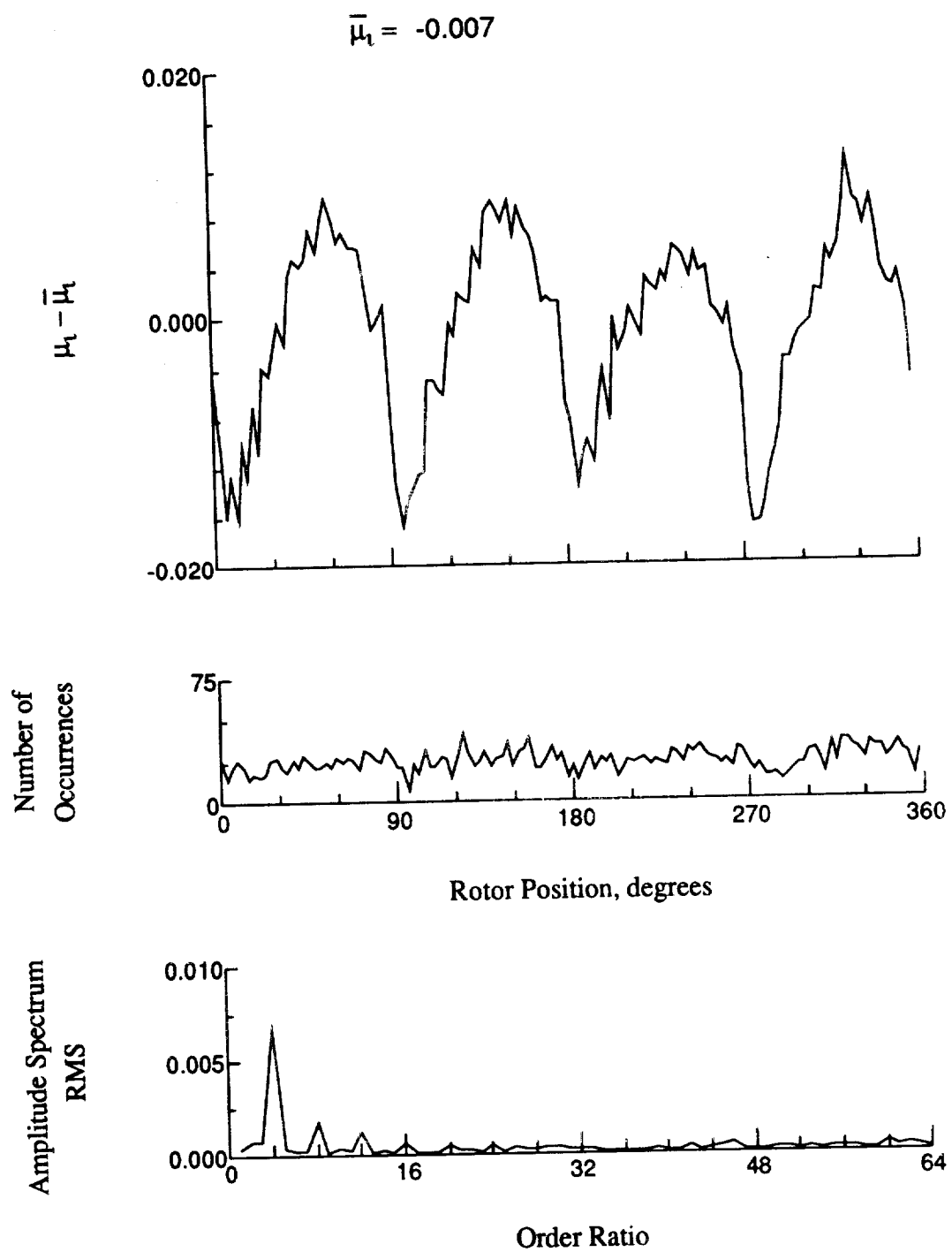


Figure 152.- Induced inflow velocity measured at 270 degrees and r/R of 0.81.

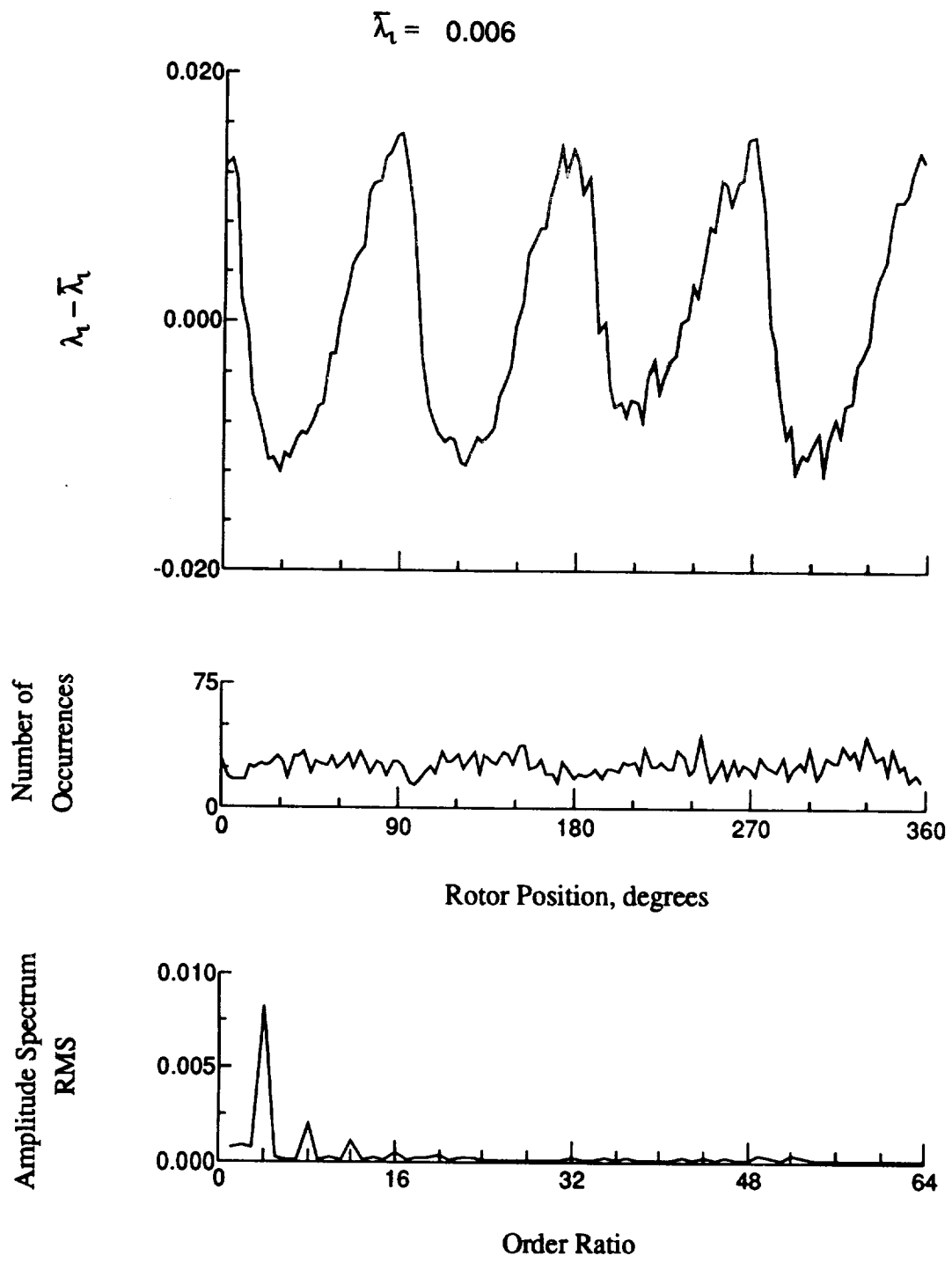


Figure 152.- Concluded.

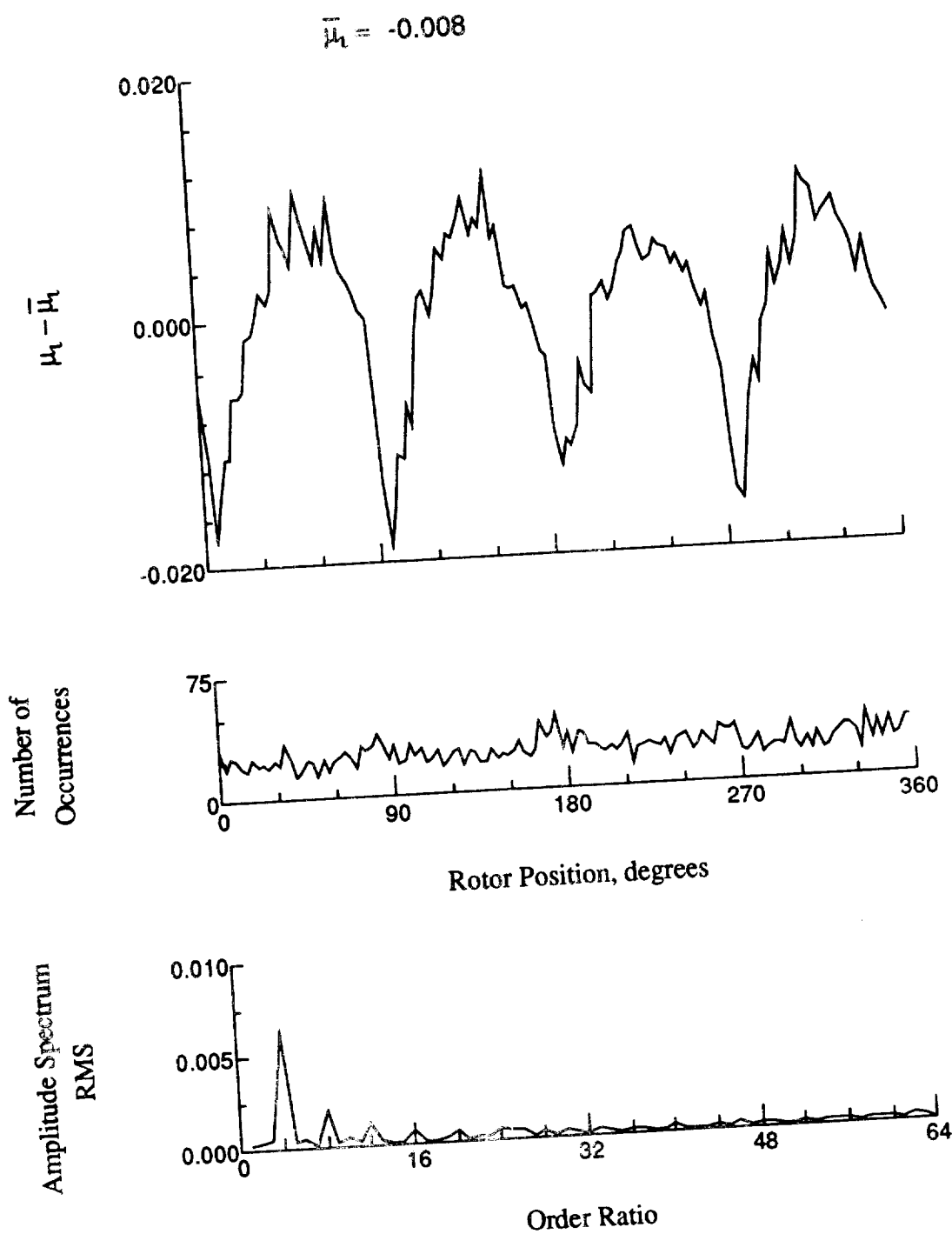


Figure 153.- Induced inflow velocity measured at 270 degrees and r/R of 0.86.

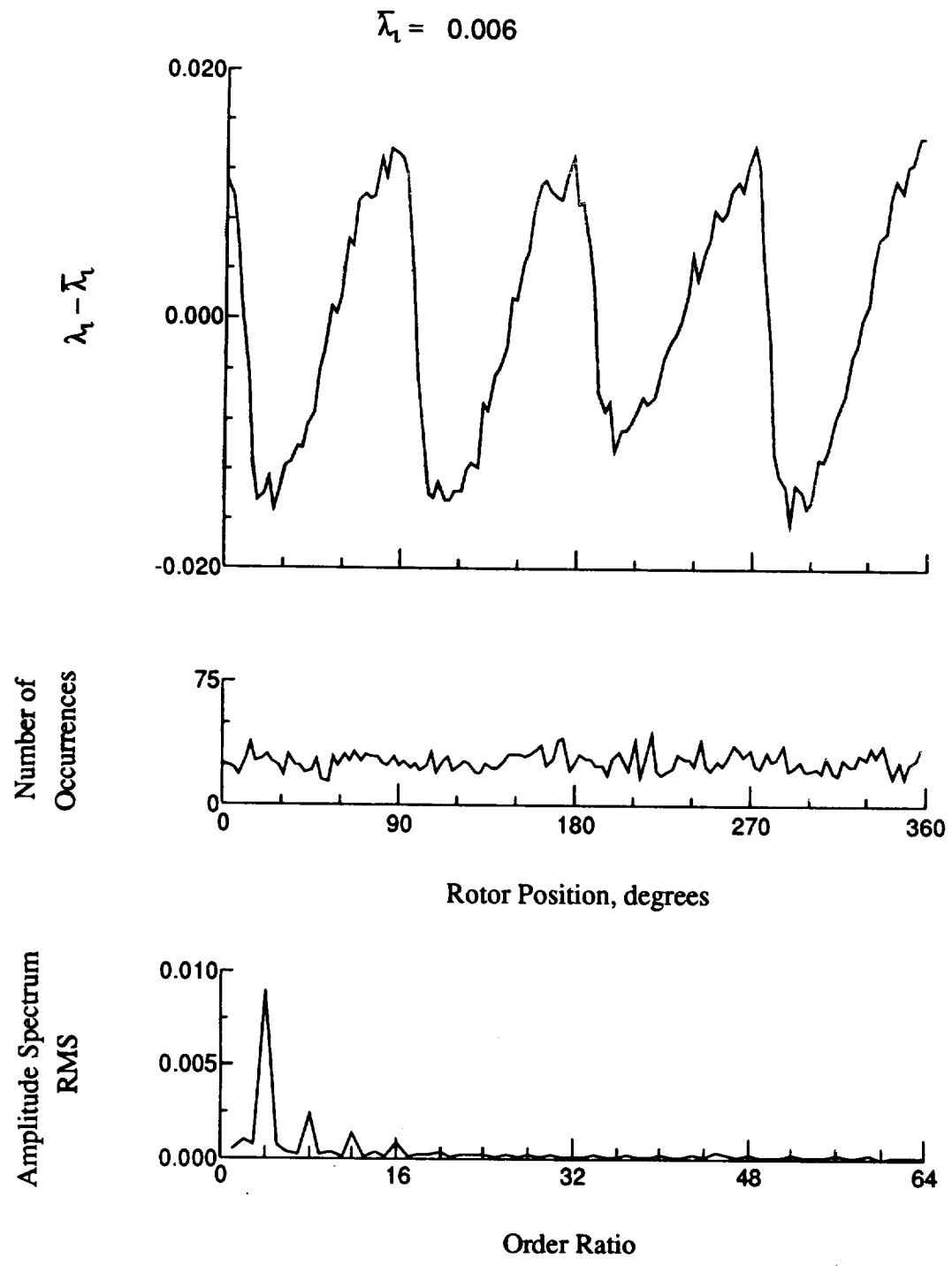


Figure 153.- Concluded.

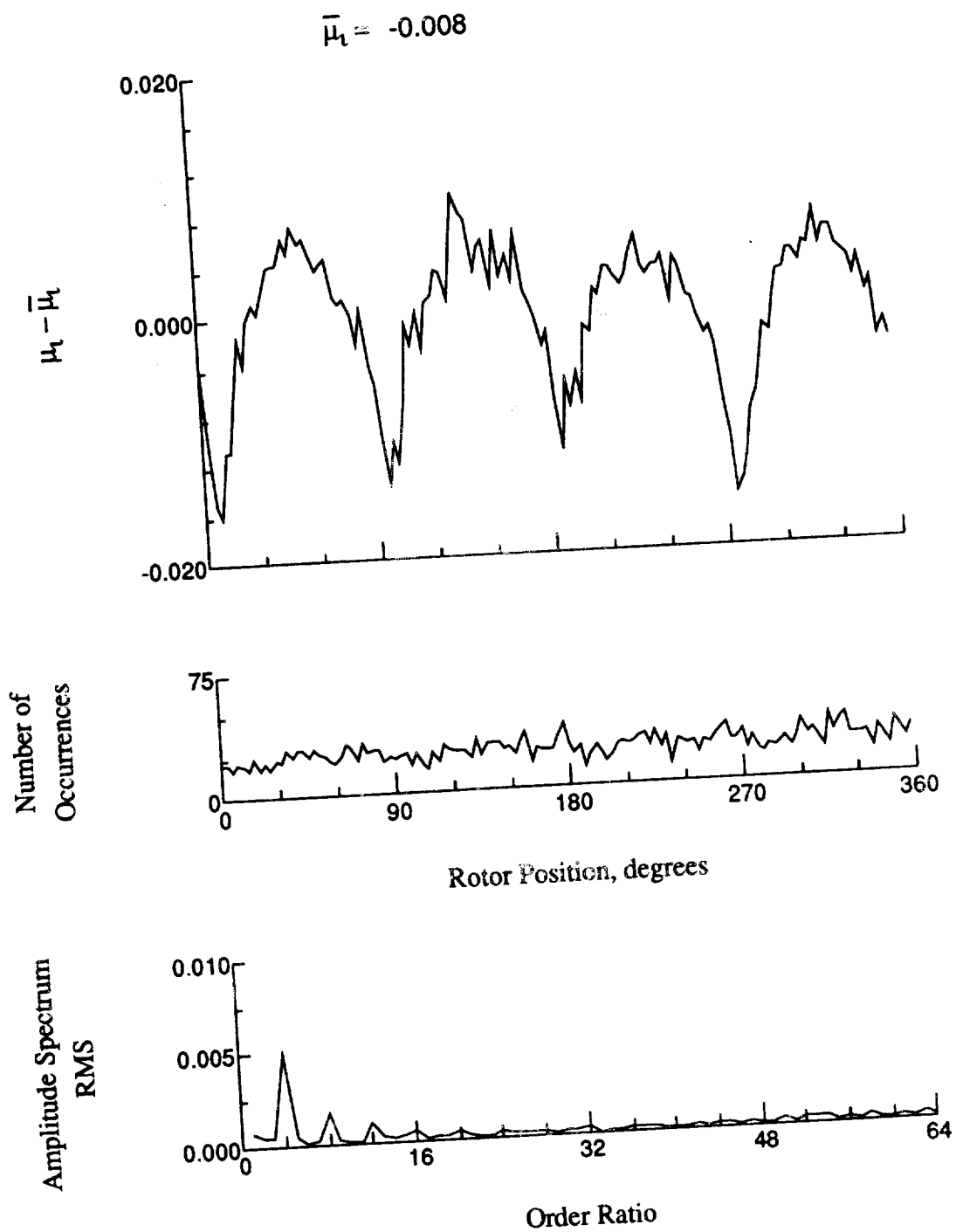


Figure 154.- Induced inflow velocity measured at 270 degrees and r/R of 0.90.

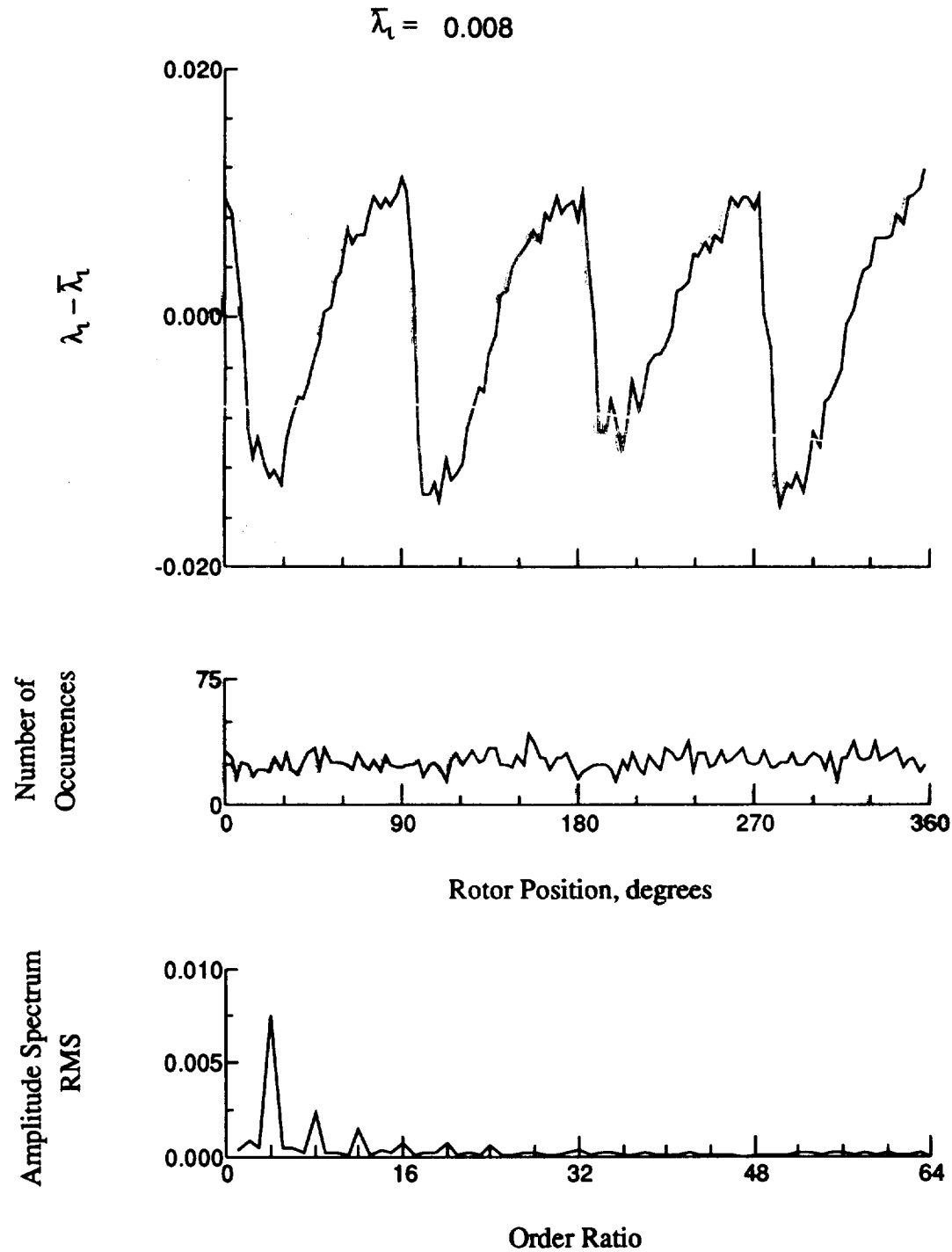


Figure 154.- Concluded.

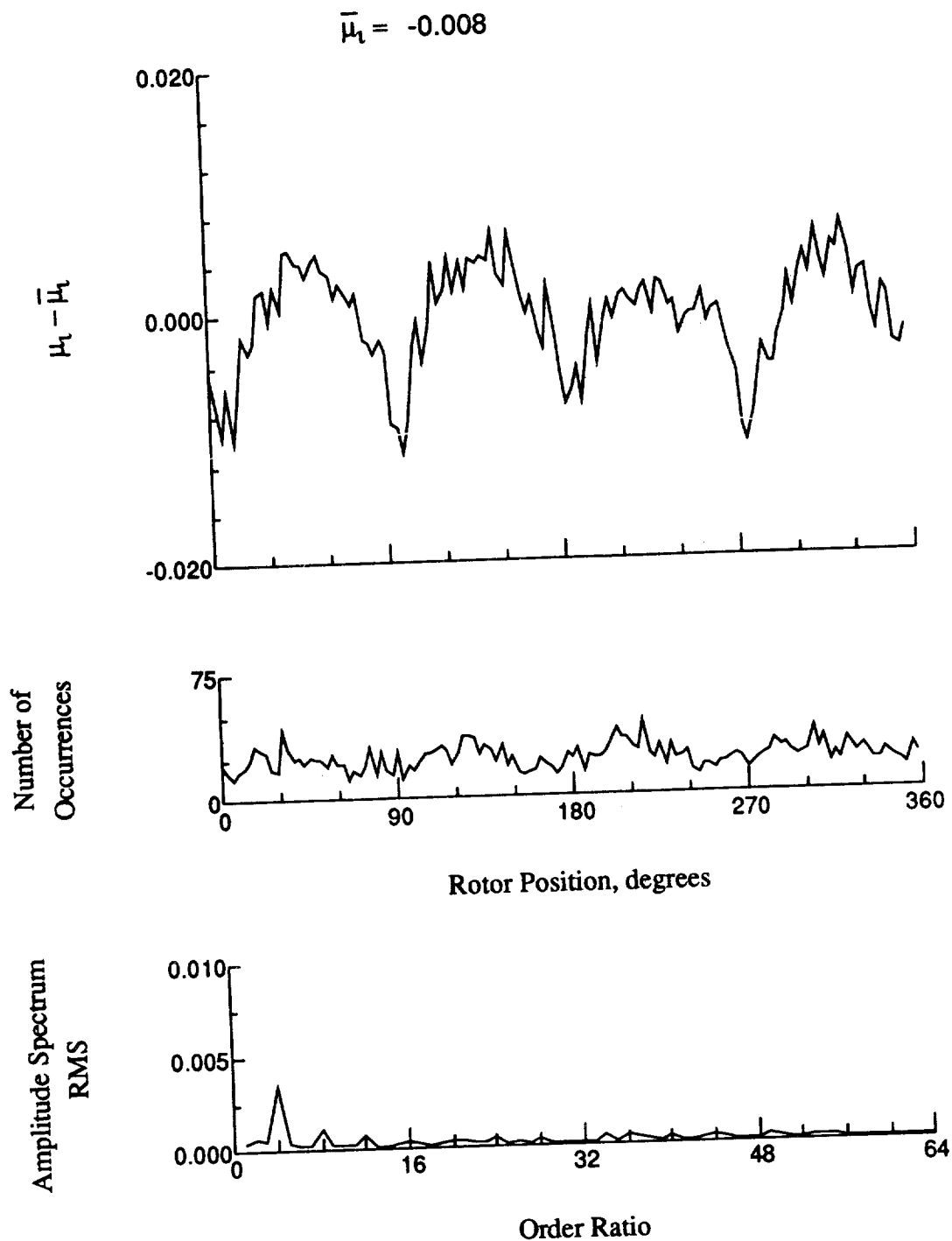


Figure 155.- Induced inflow velocity measured at 270 degrees and r/R of 0.94.

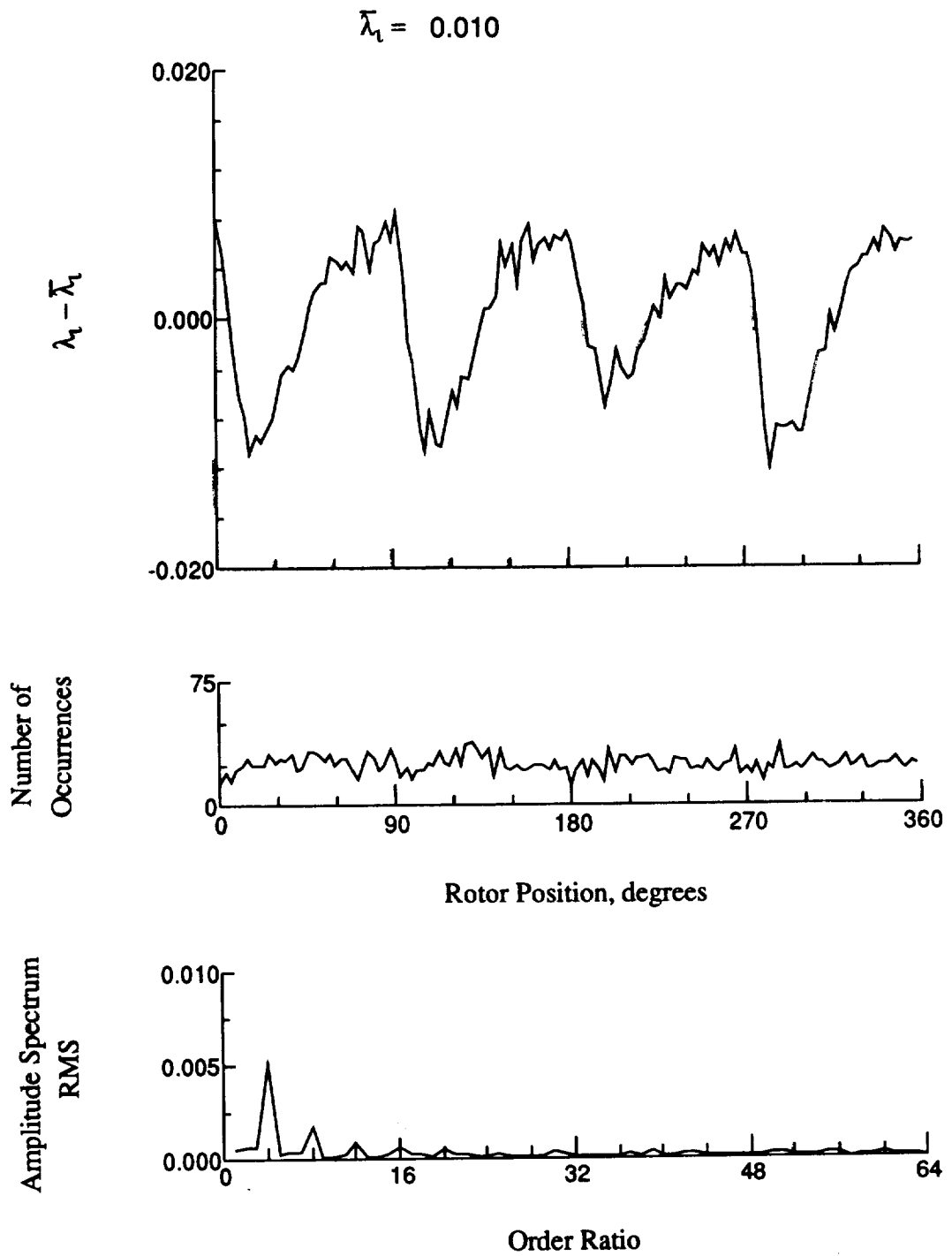


Figure 155.- Concluded.

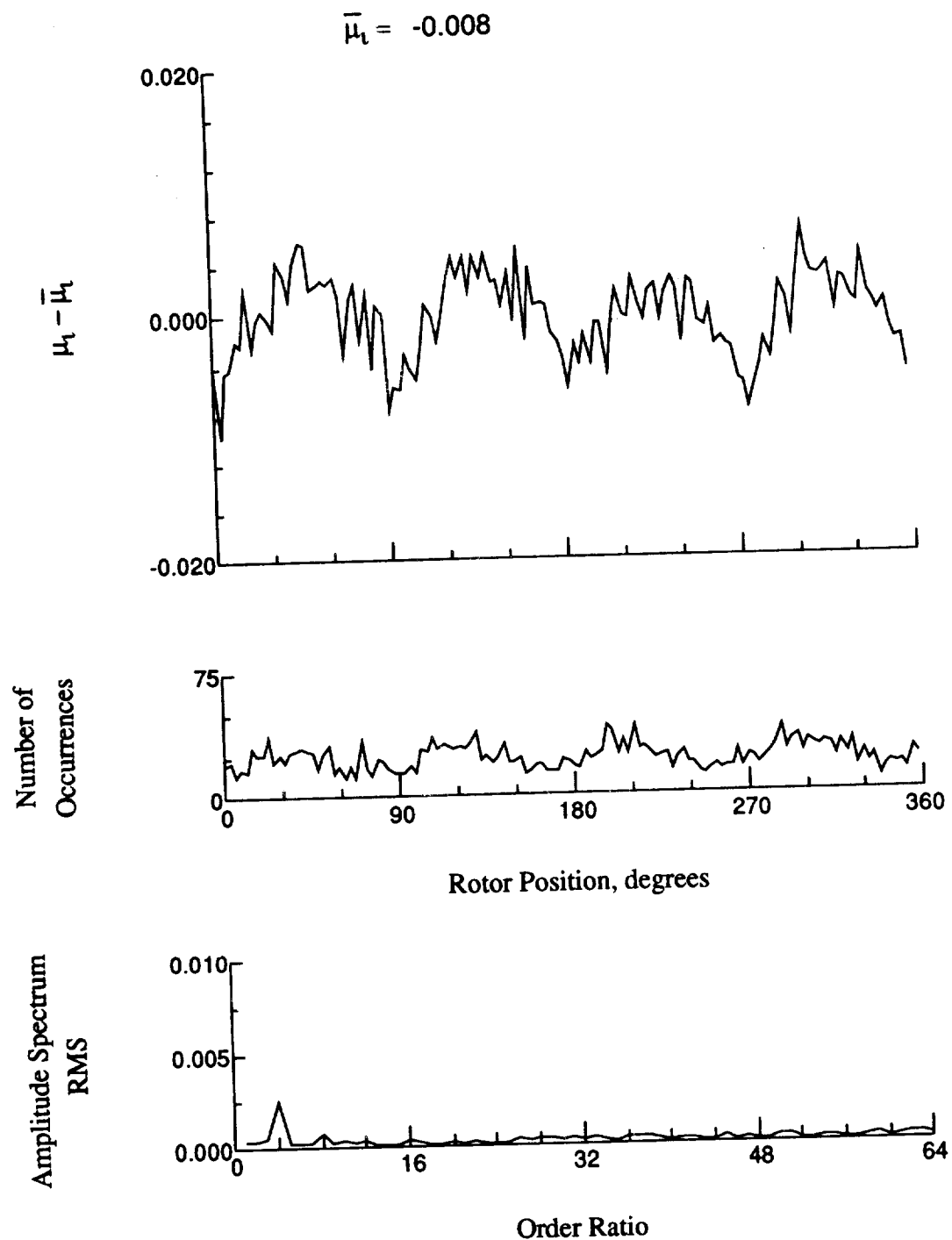


Figure 156.- Induced inflow velocity measured at 270 degrees and r/R of 0.96.

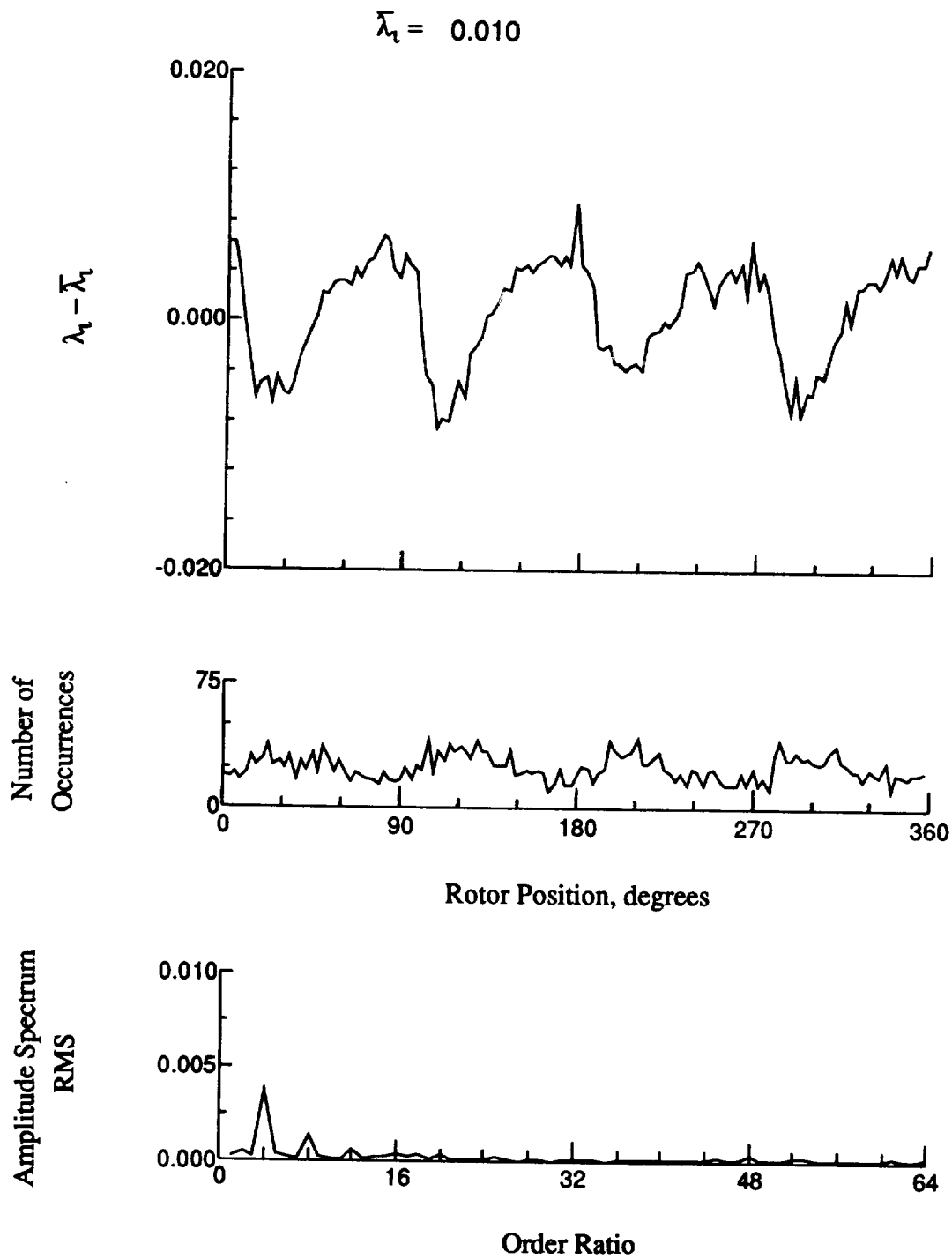


Figure 156.- Concluded.

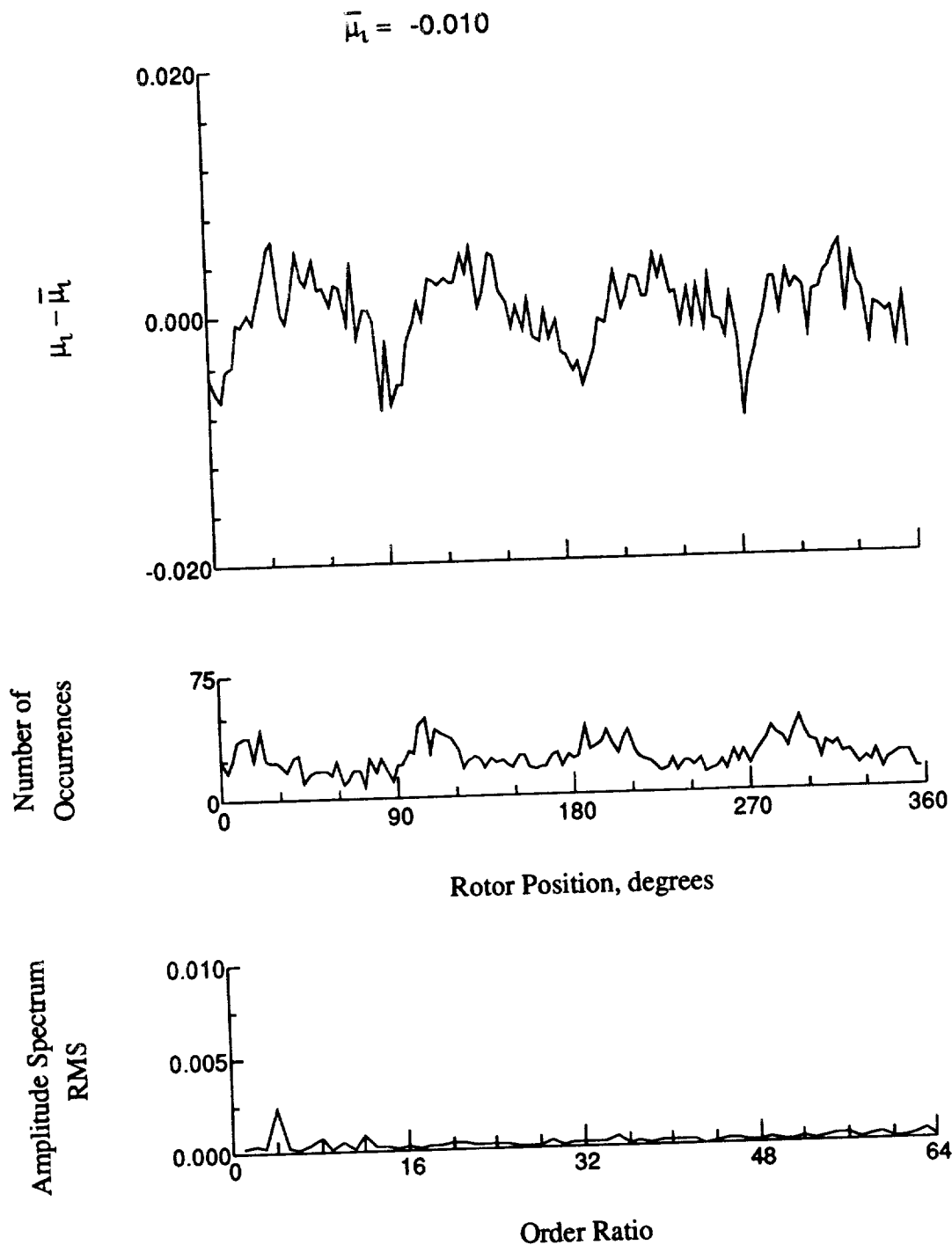


Figure 157.- Induced inflow velocity measured at 270 degrees and r/R of 1.00.

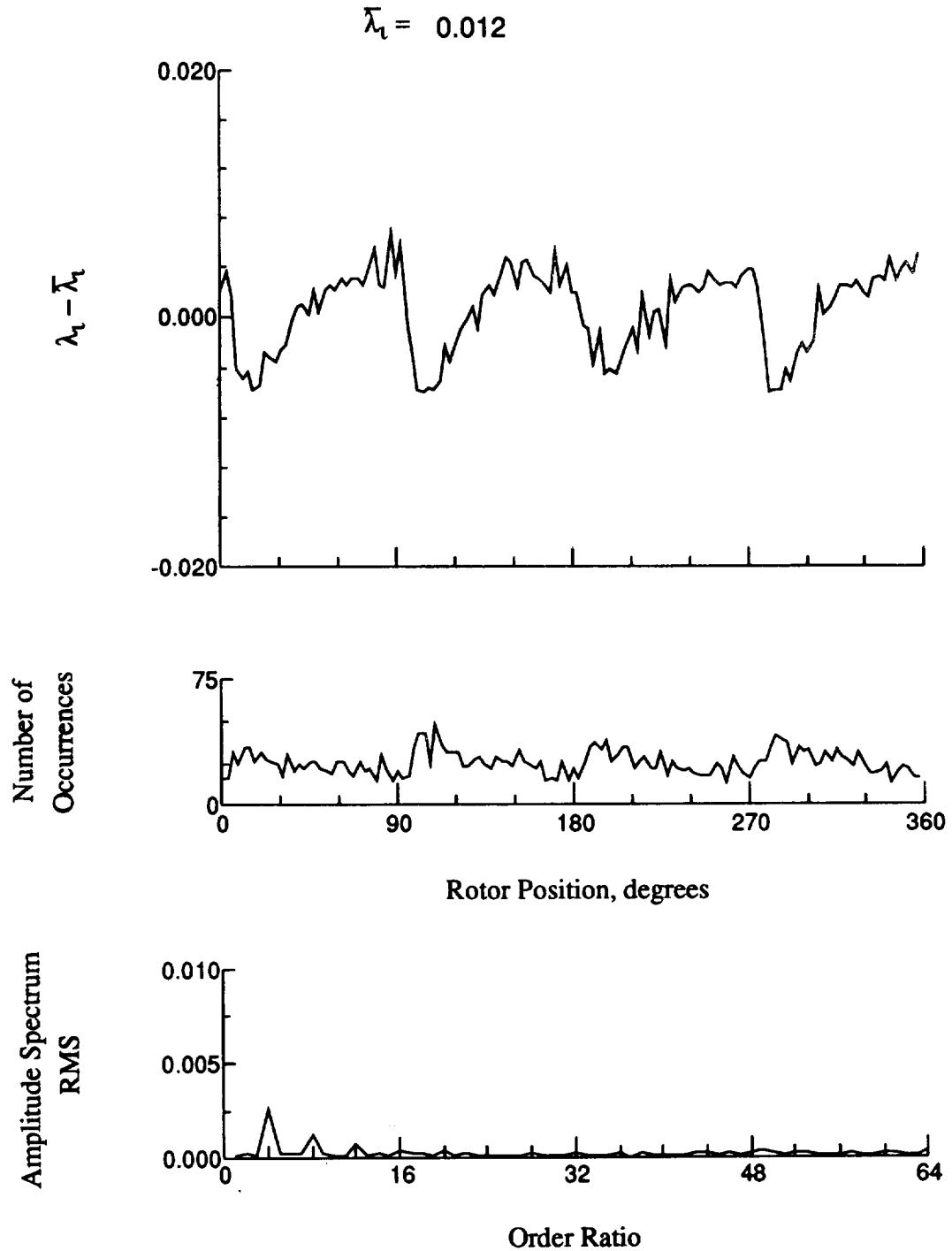


Figure 157.- Concluded.

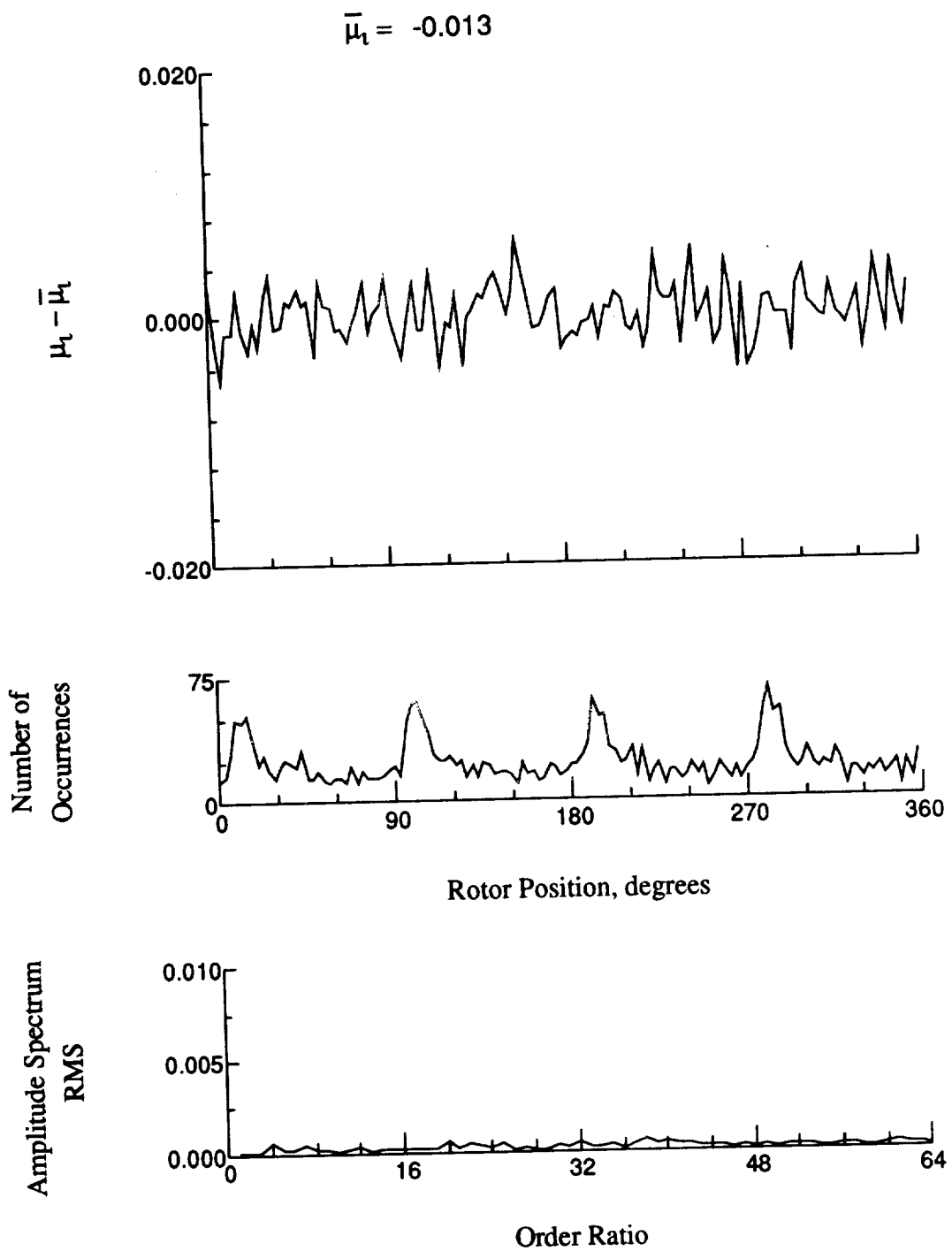


Figure 158.- Induced inflow velocity measured at 270 degrees and r/R of 1.10.

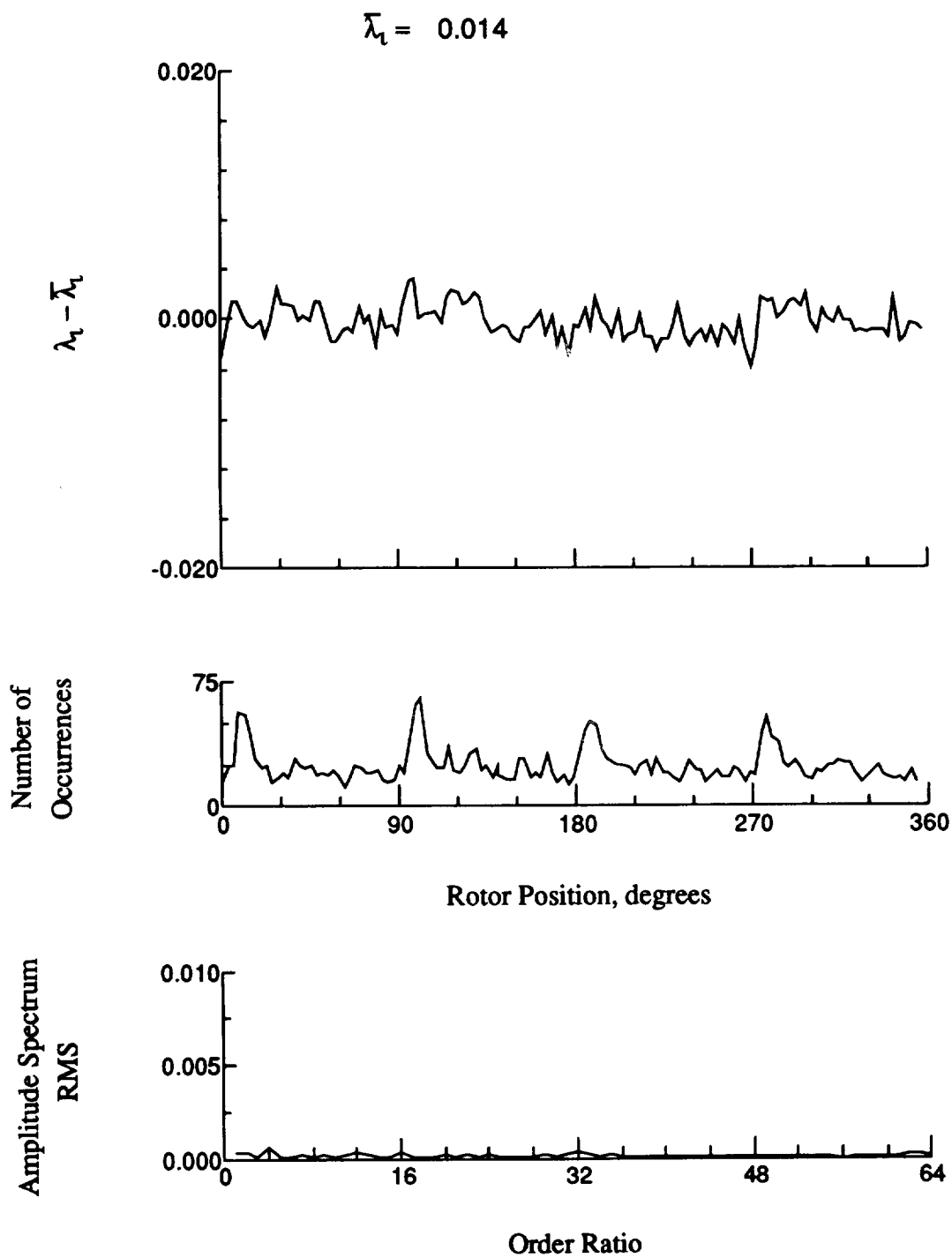


Figure 158.- Concluded.

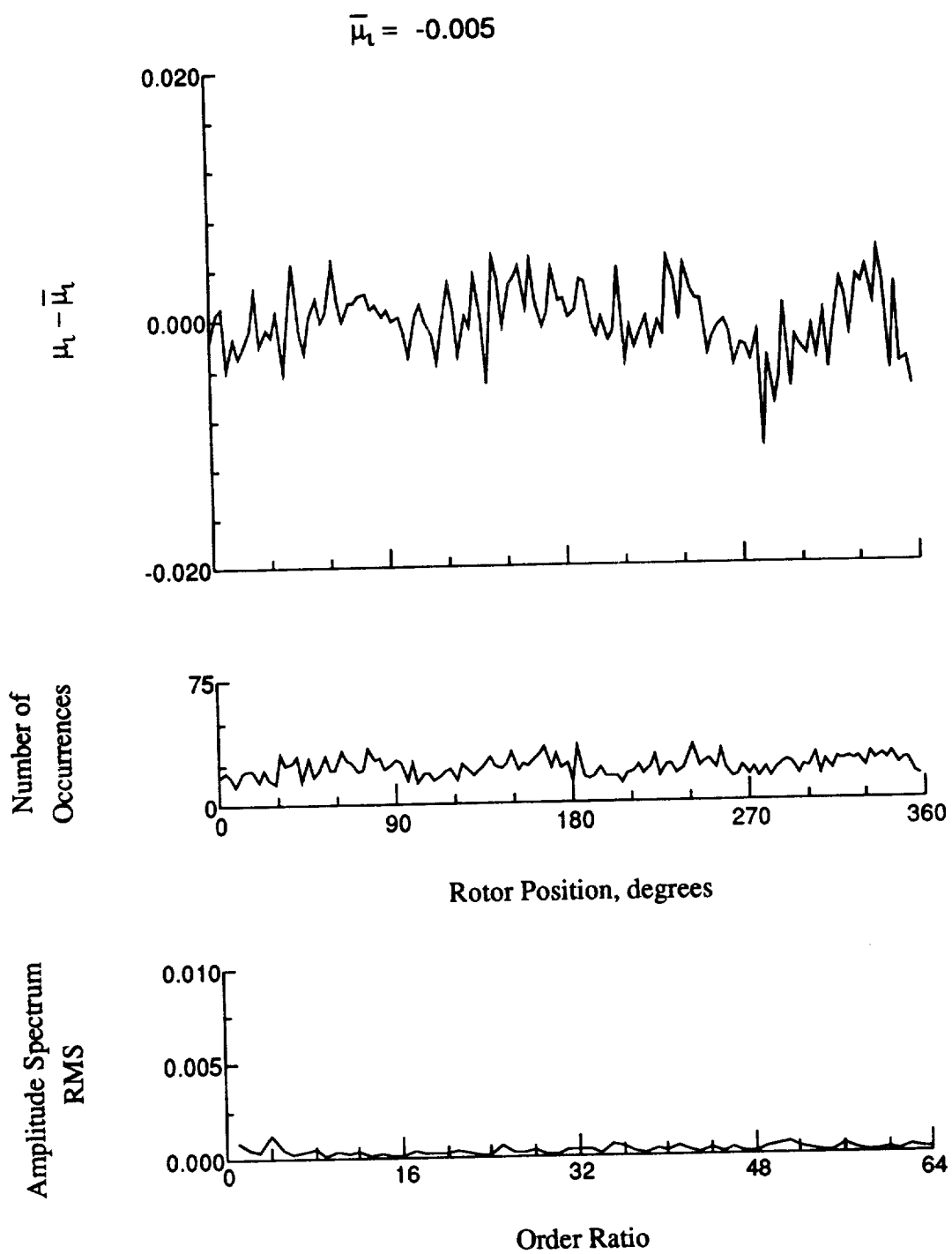


Figure 159.- Induced inflow velocity measured at 300 degrees and r/R of 0.20.

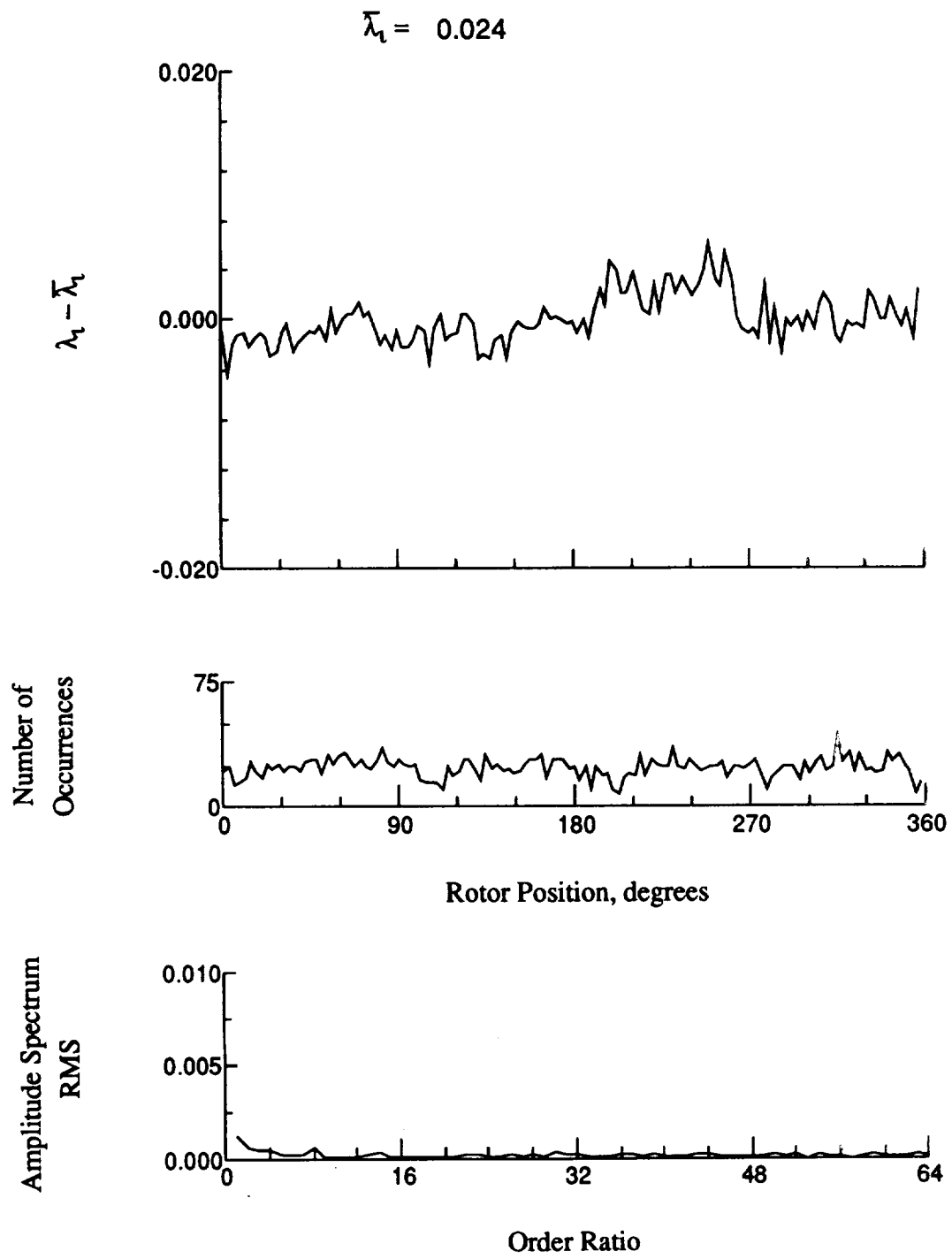


Figure 159.- Concluded.

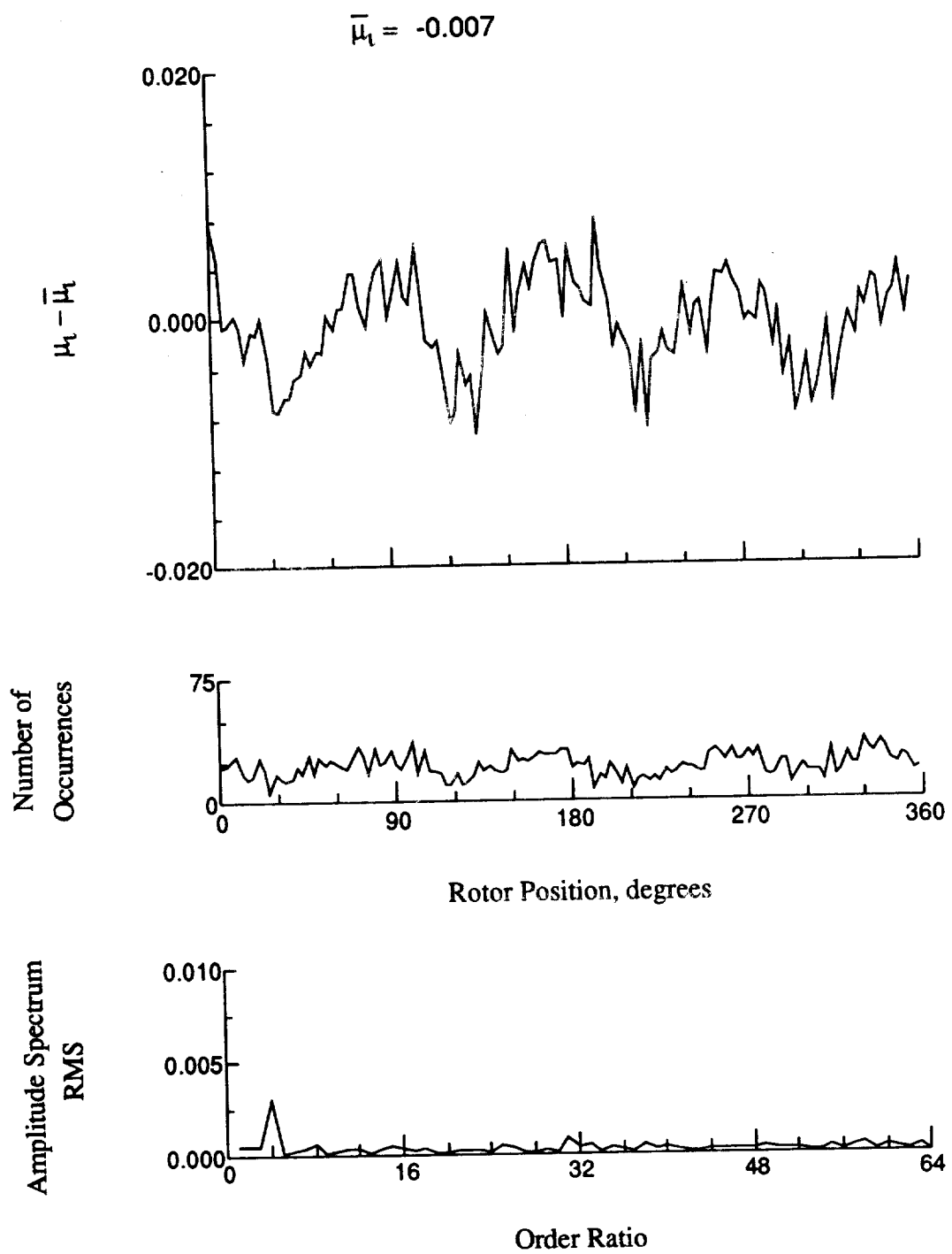


Figure 160.- Induced inflow velocity measured at 300 degrees and r/R of 0.32.

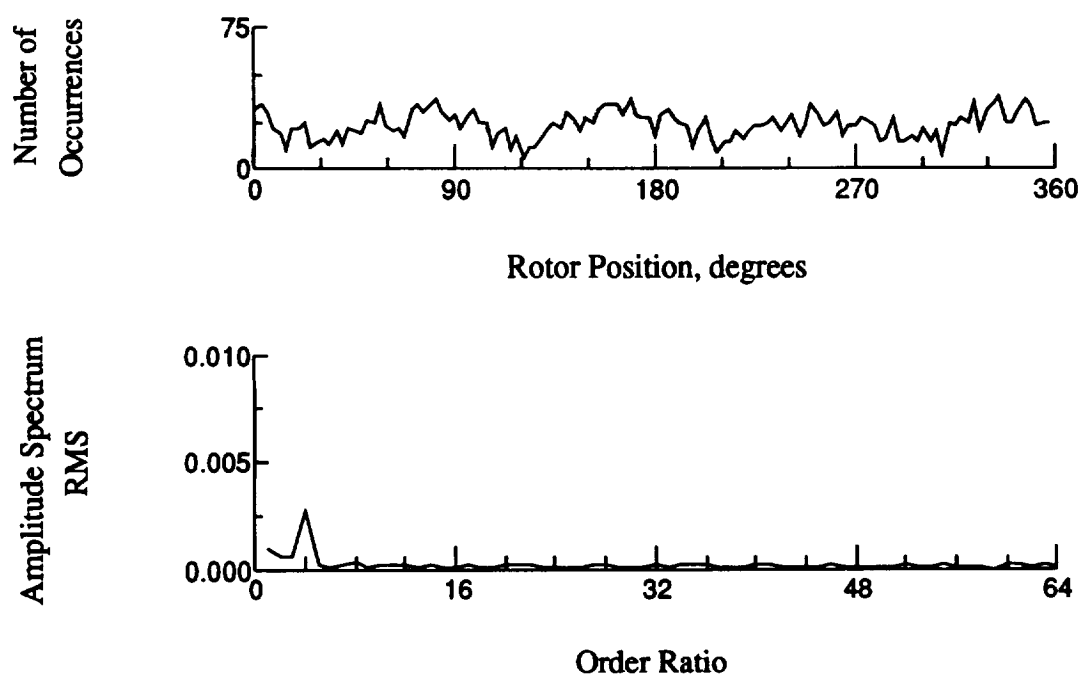
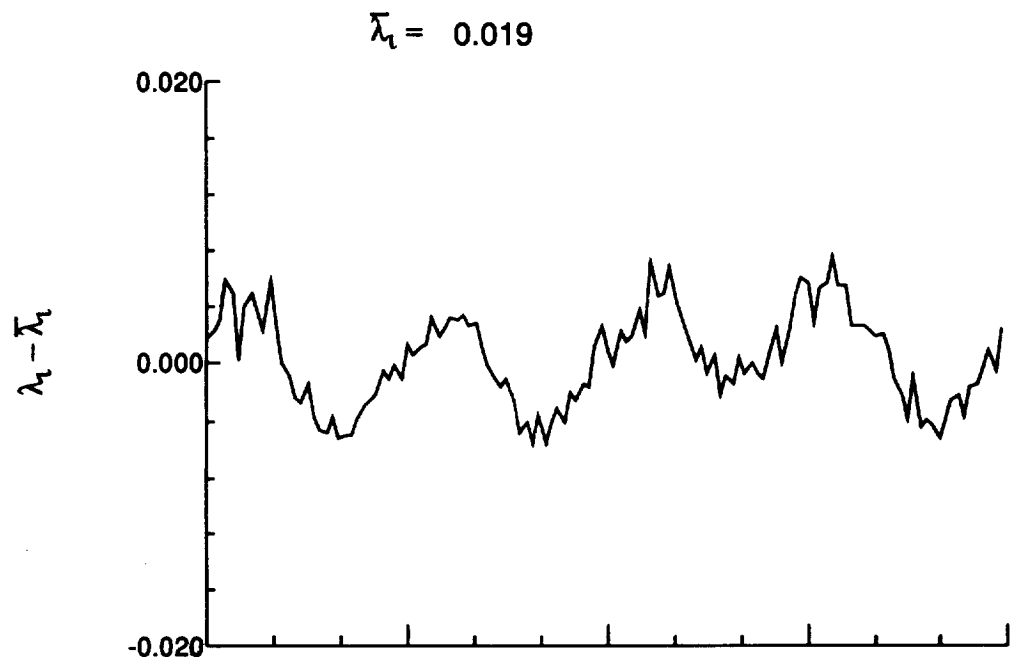


Figure 160.- Concluded.

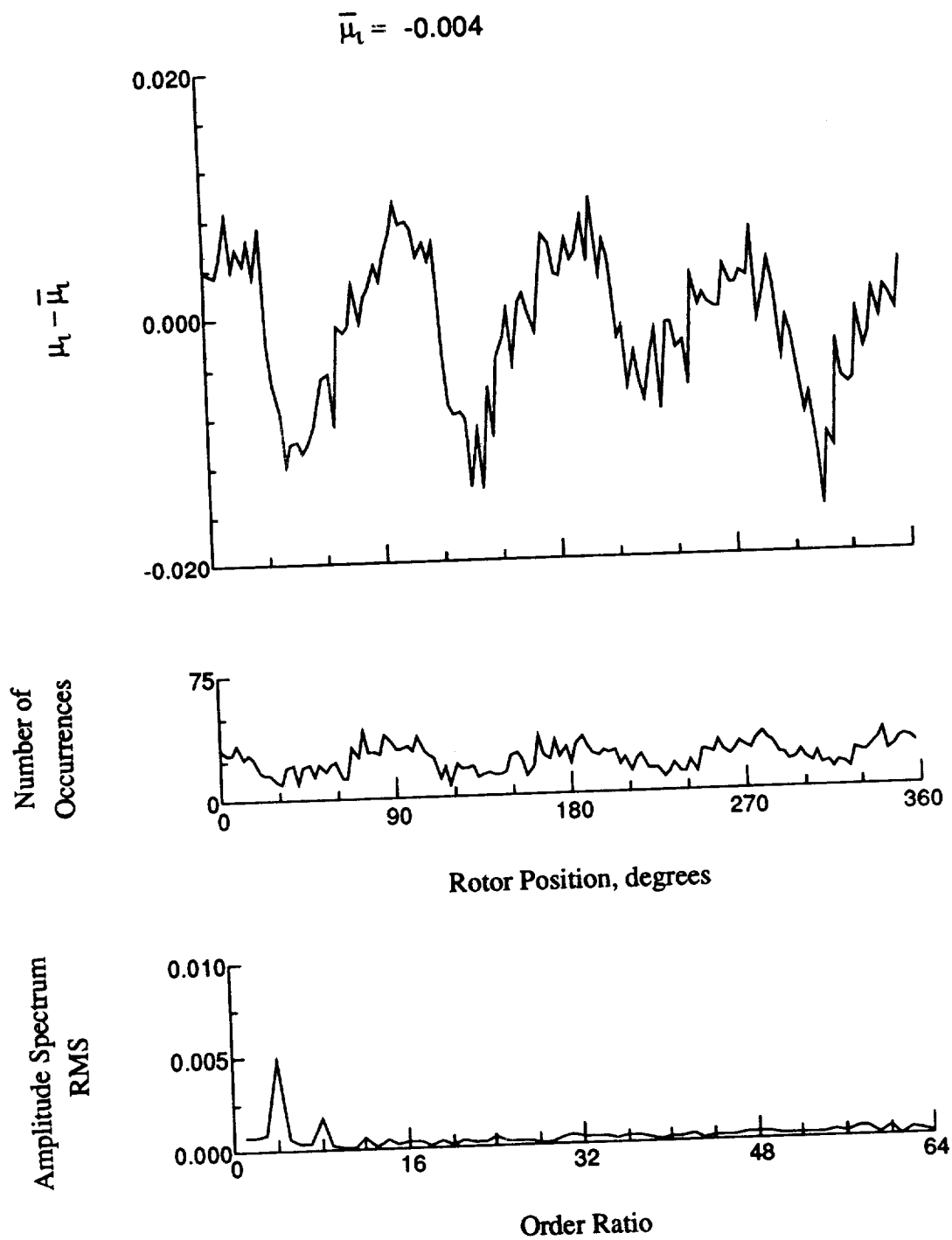


Figure 161.- Induced inflow velocity measured at 300 degrees and r/R of 0.50.

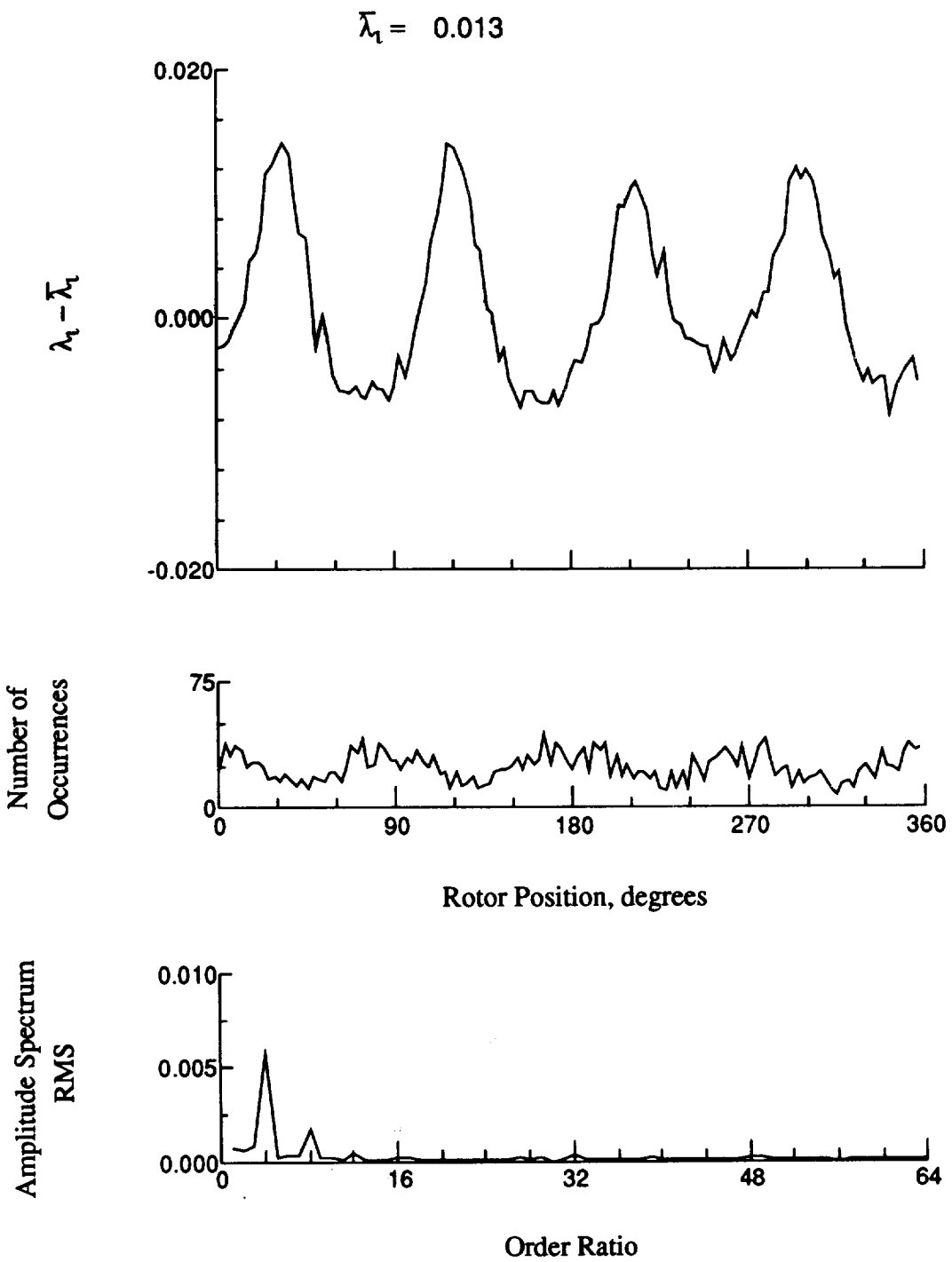


Figure 161.- Concluded.

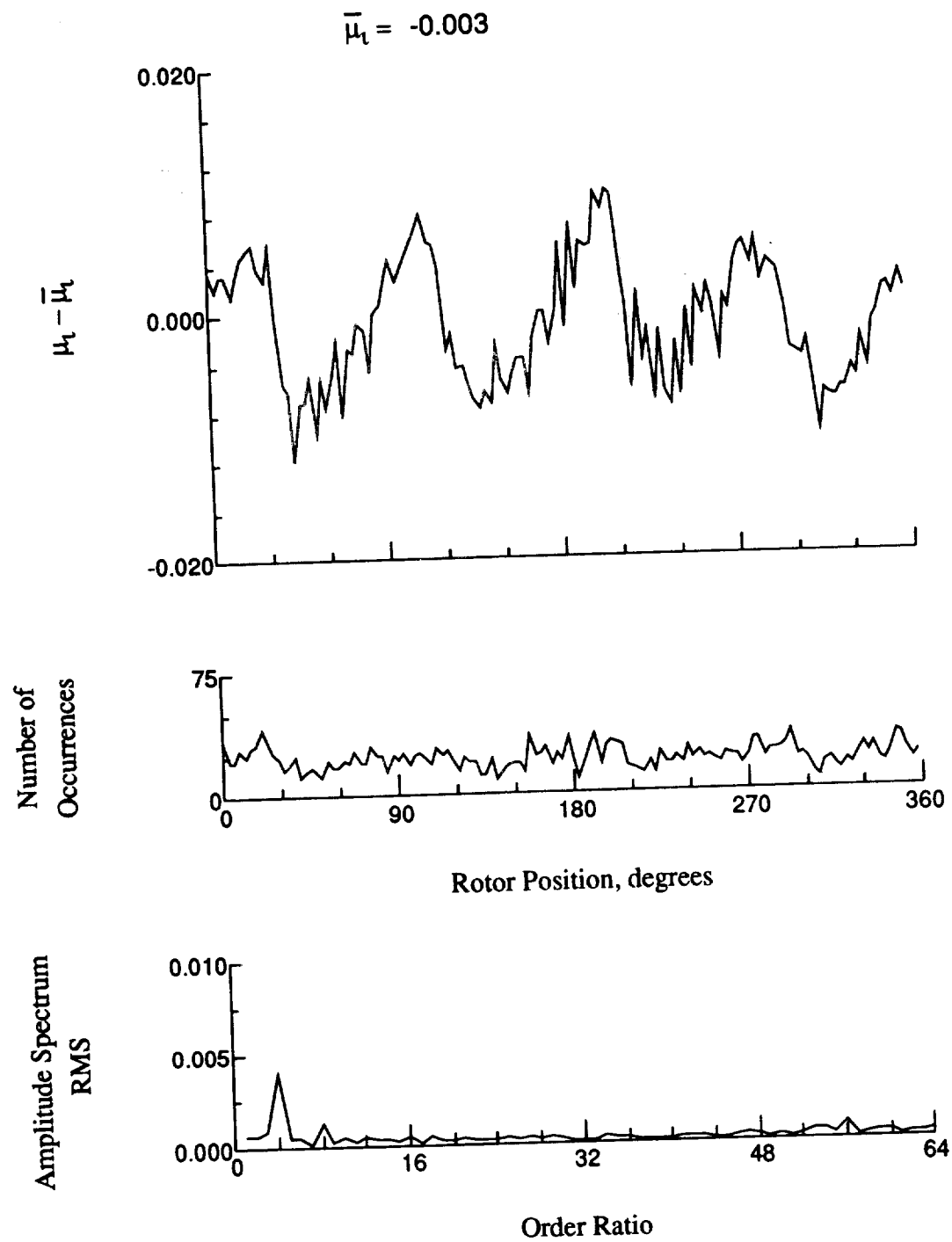


Figure 162.- Induced inflow velocity measured at 300 degrees and r/R of 0.58.

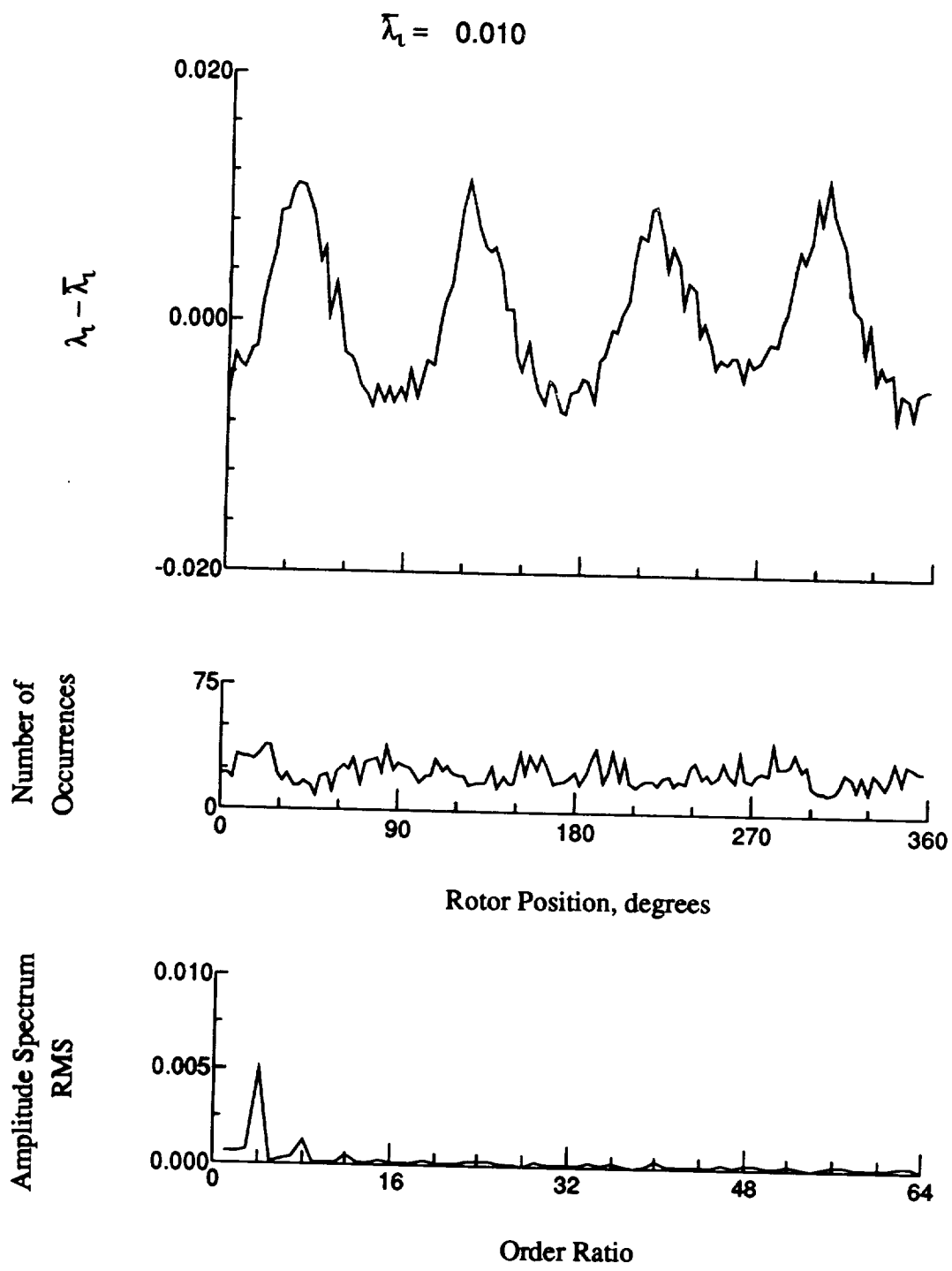


Figure 162.- Concluded.

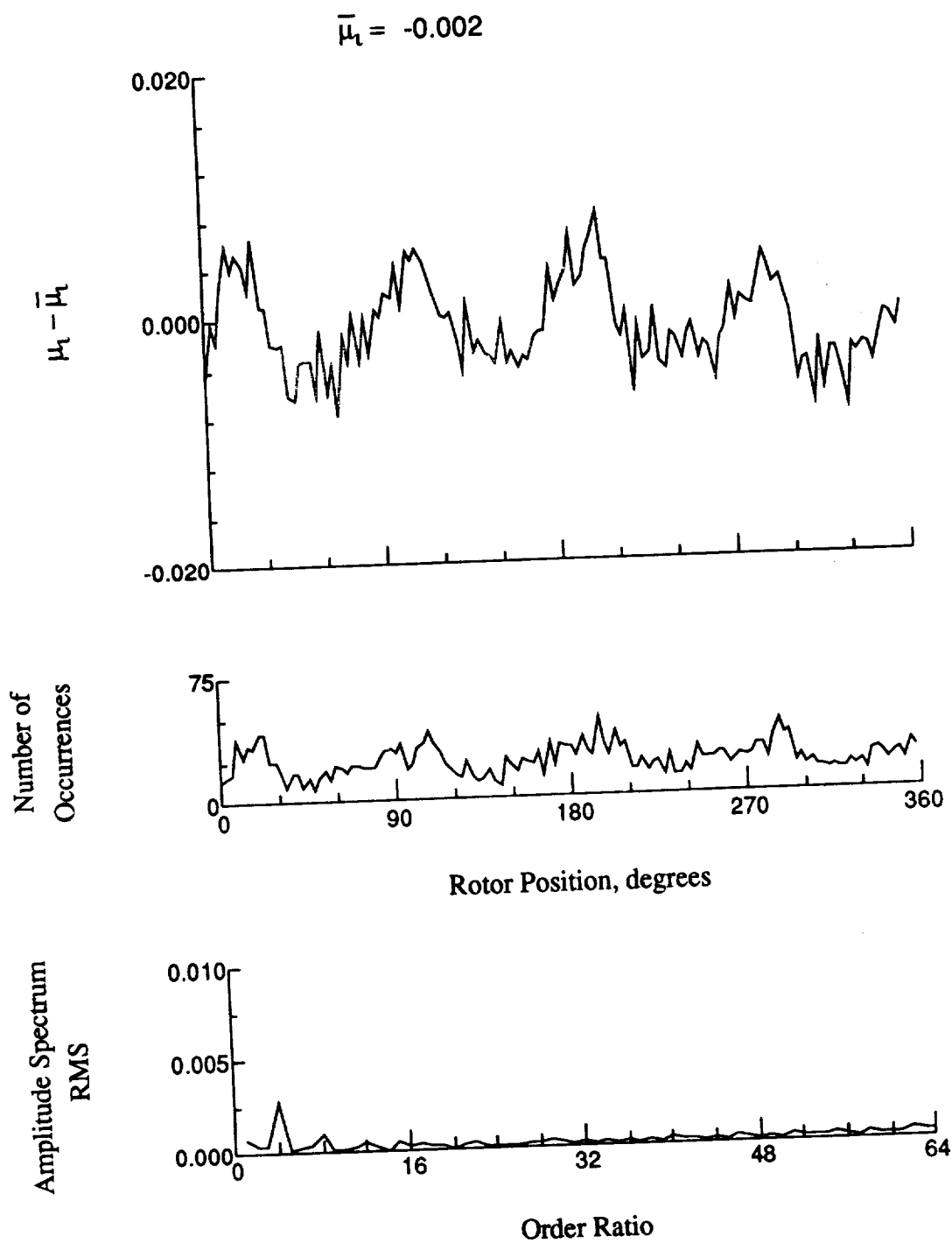


Figure 163.- Induced inflow velocity measured at 300 degrees and r/R of 0.69.

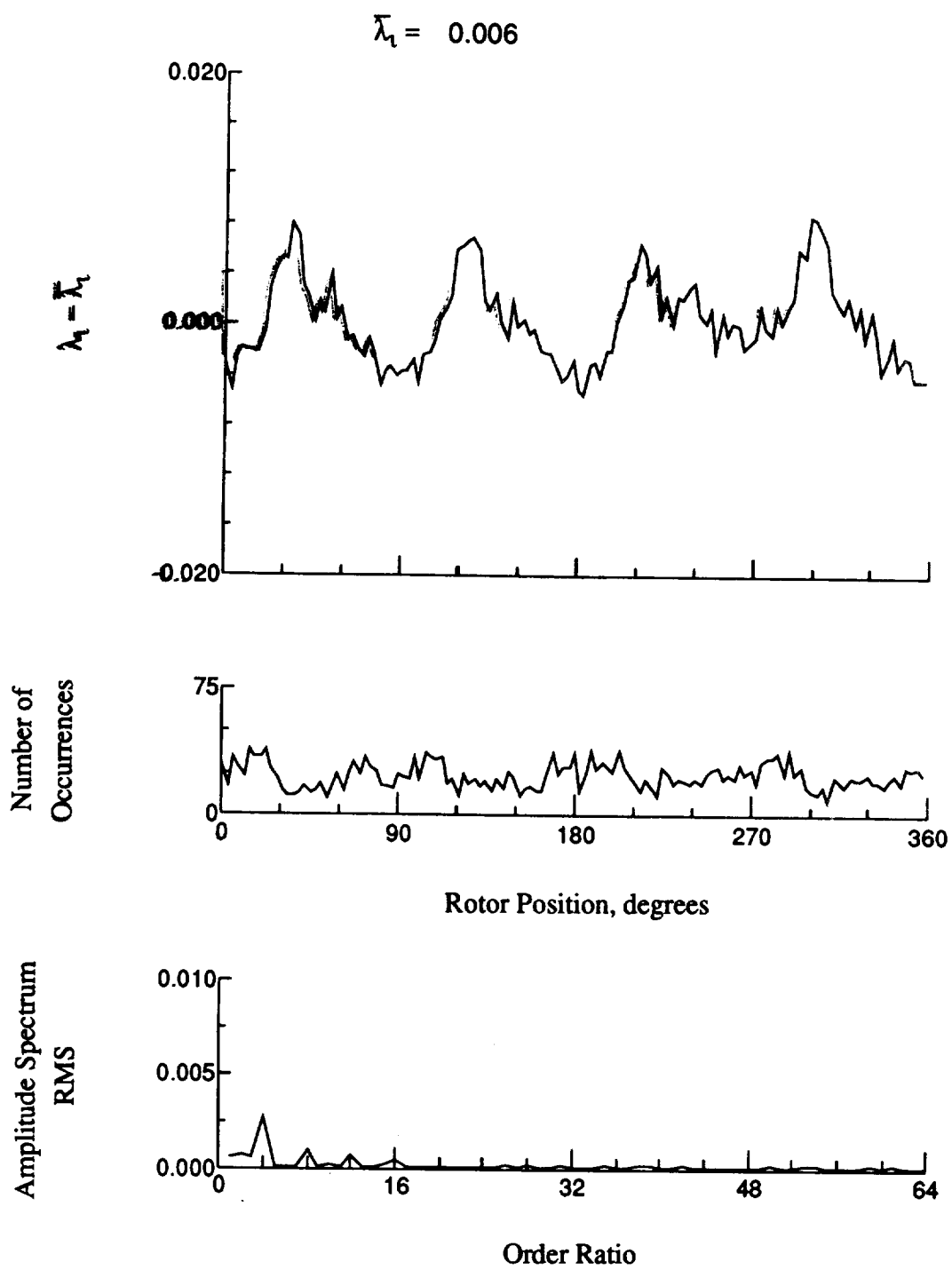


Figure 163.- Concluded.

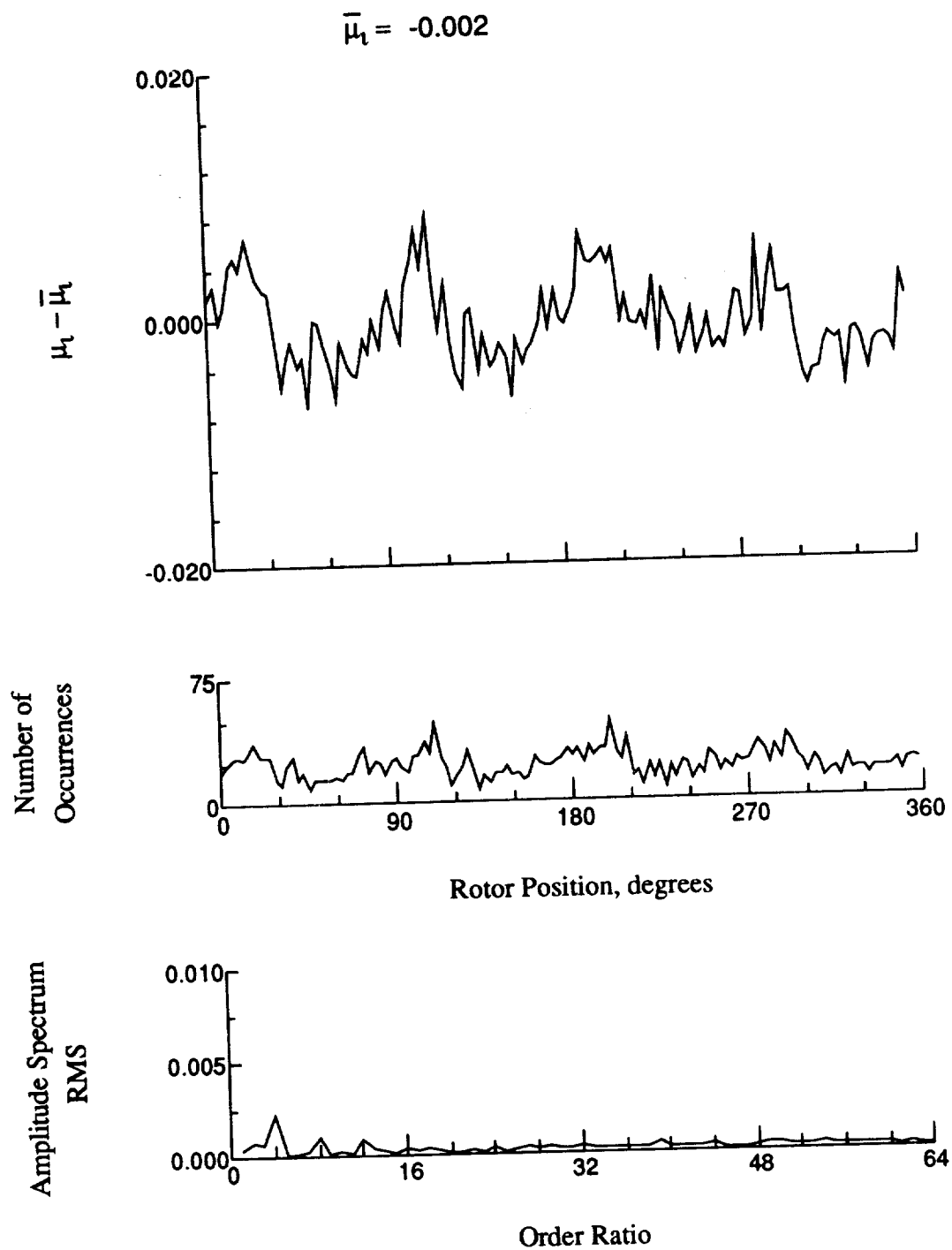


Figure 164.- Induced inflow velocity measured at 300 degrees and r/R of 0.73.

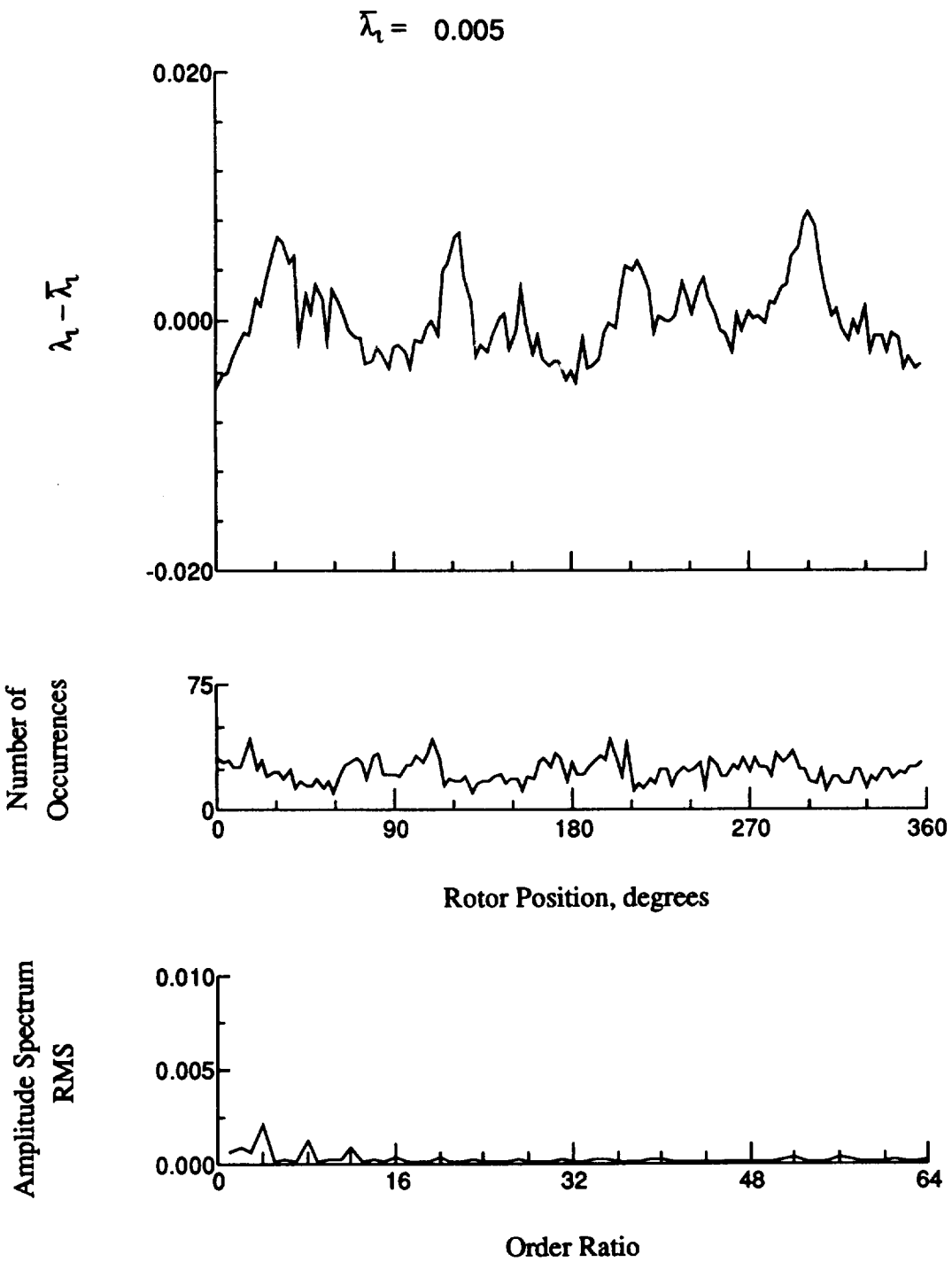


Figure 164.- Concluded.

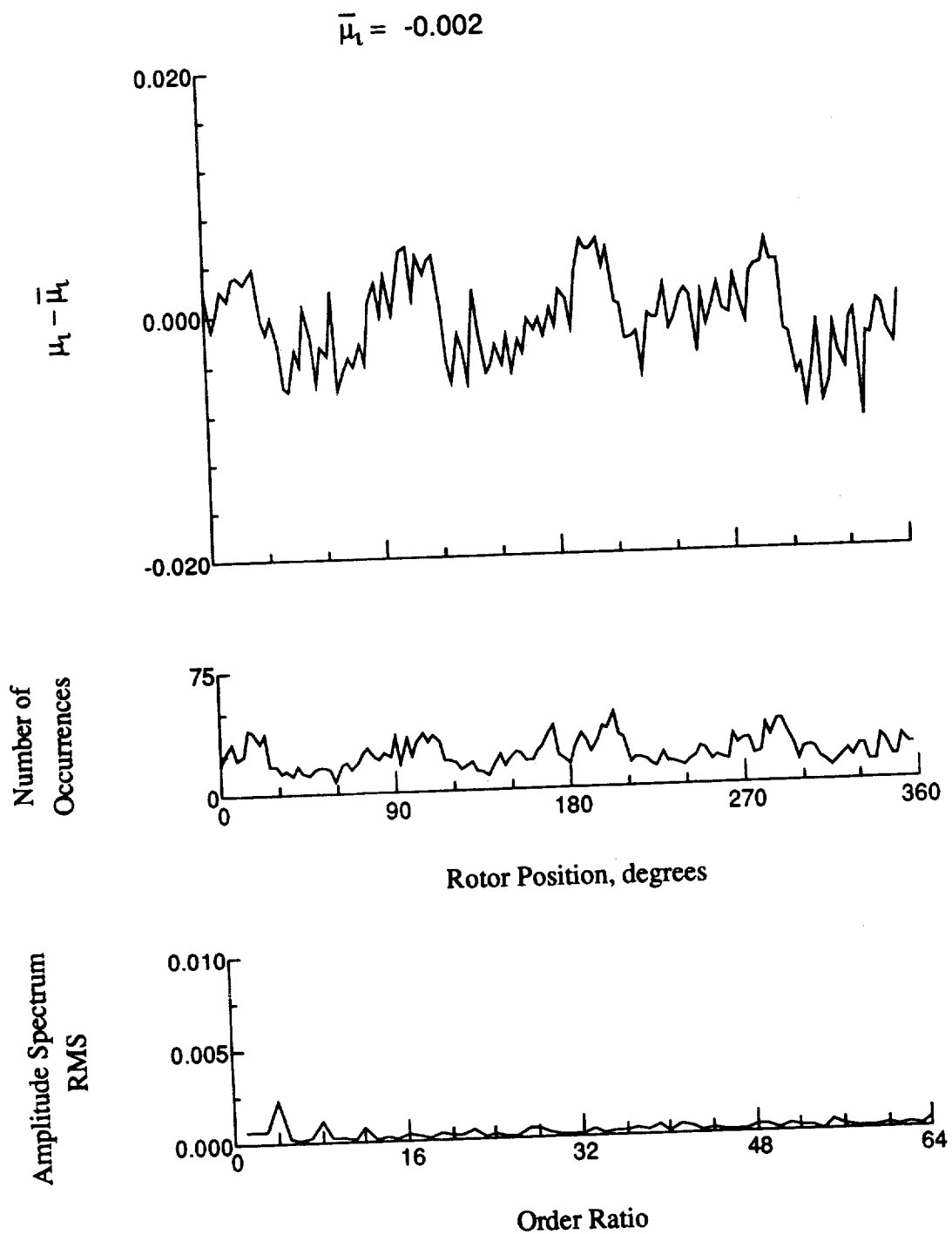


Figure 165.- Induced inflow velocity measured at 300 degrees and r/R of 0.75.

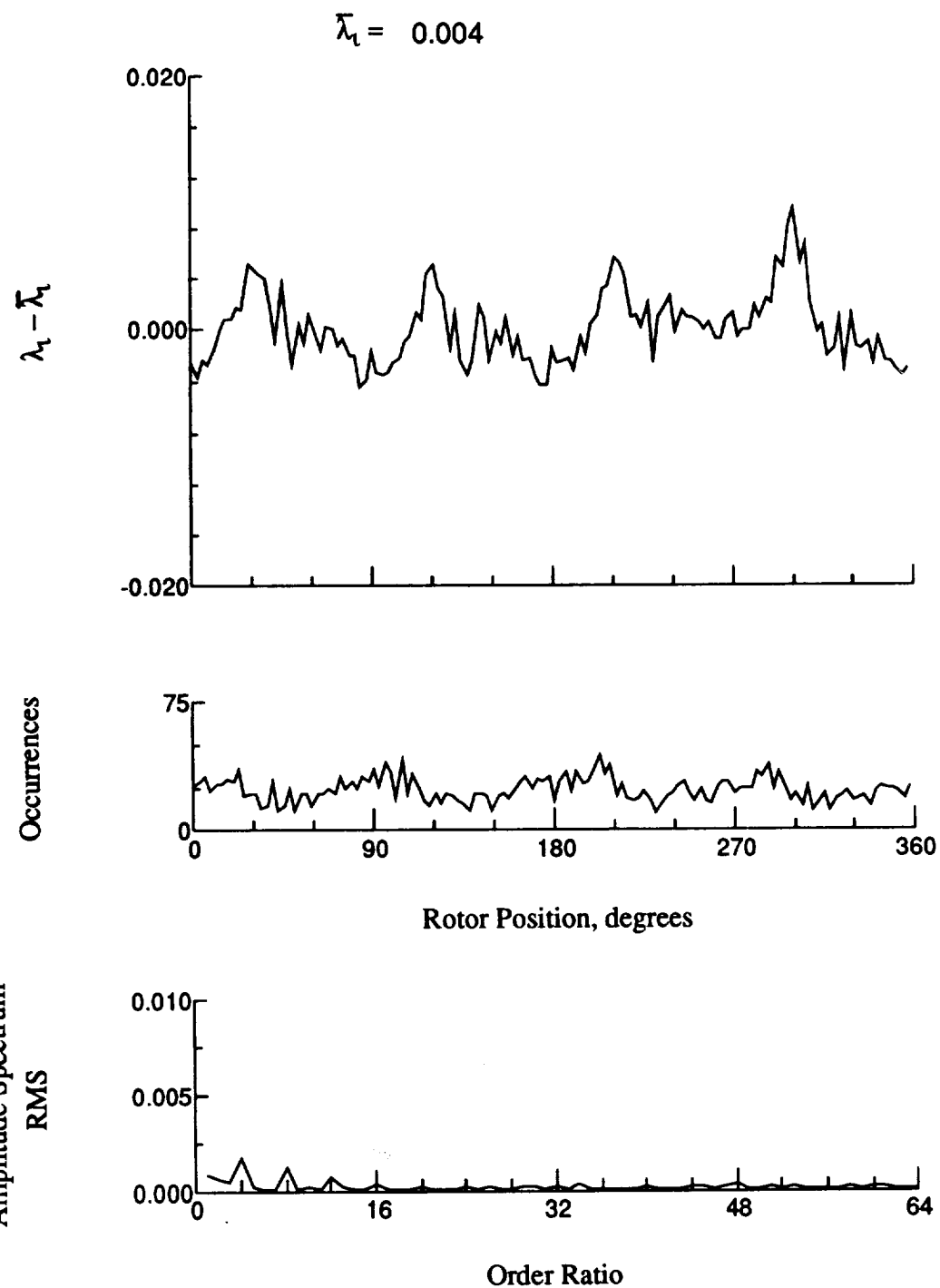


Figure 165.- Concluded.

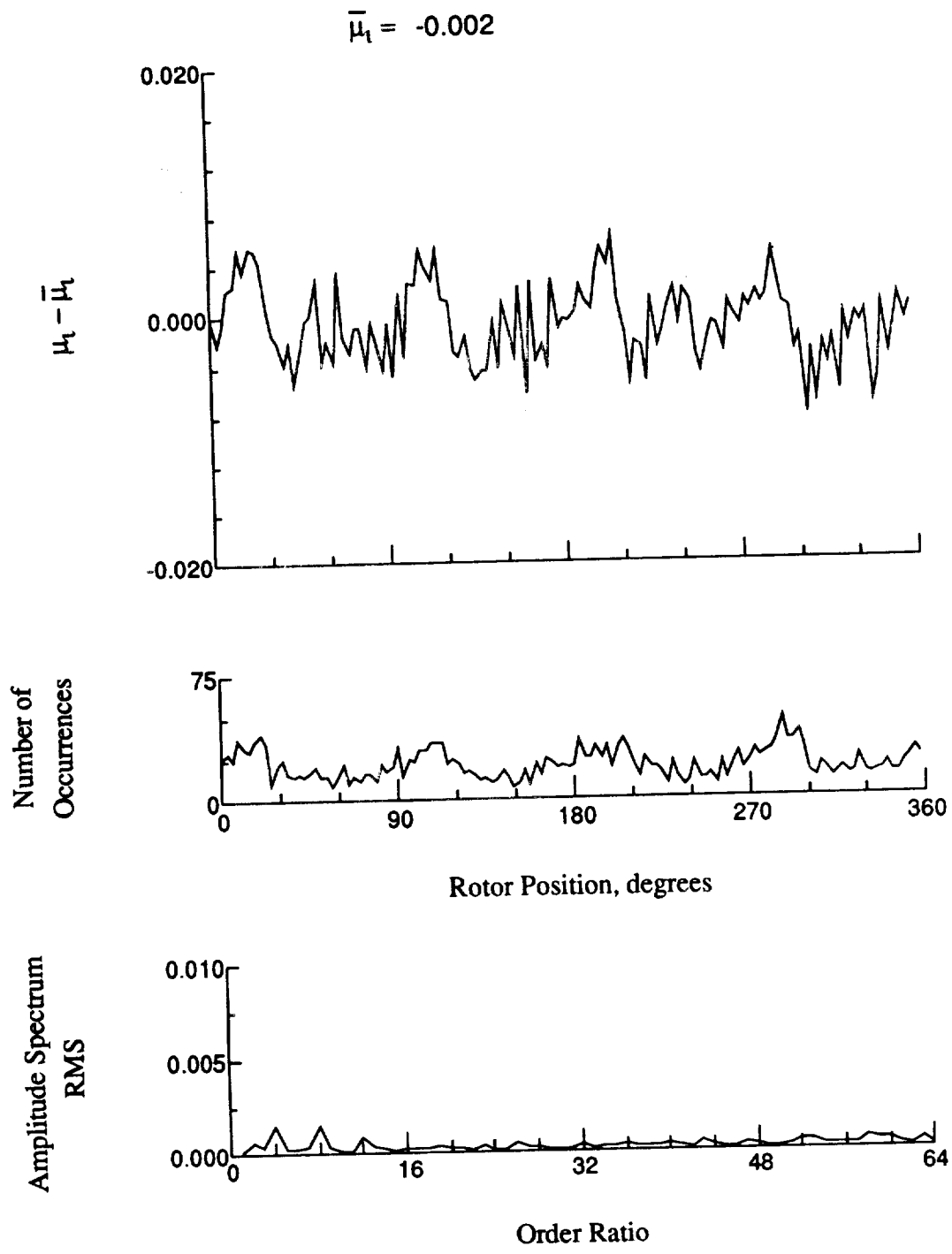


Figure 166.- Induced inflow velocity measured at 300 degrees and r/R of 0.81.

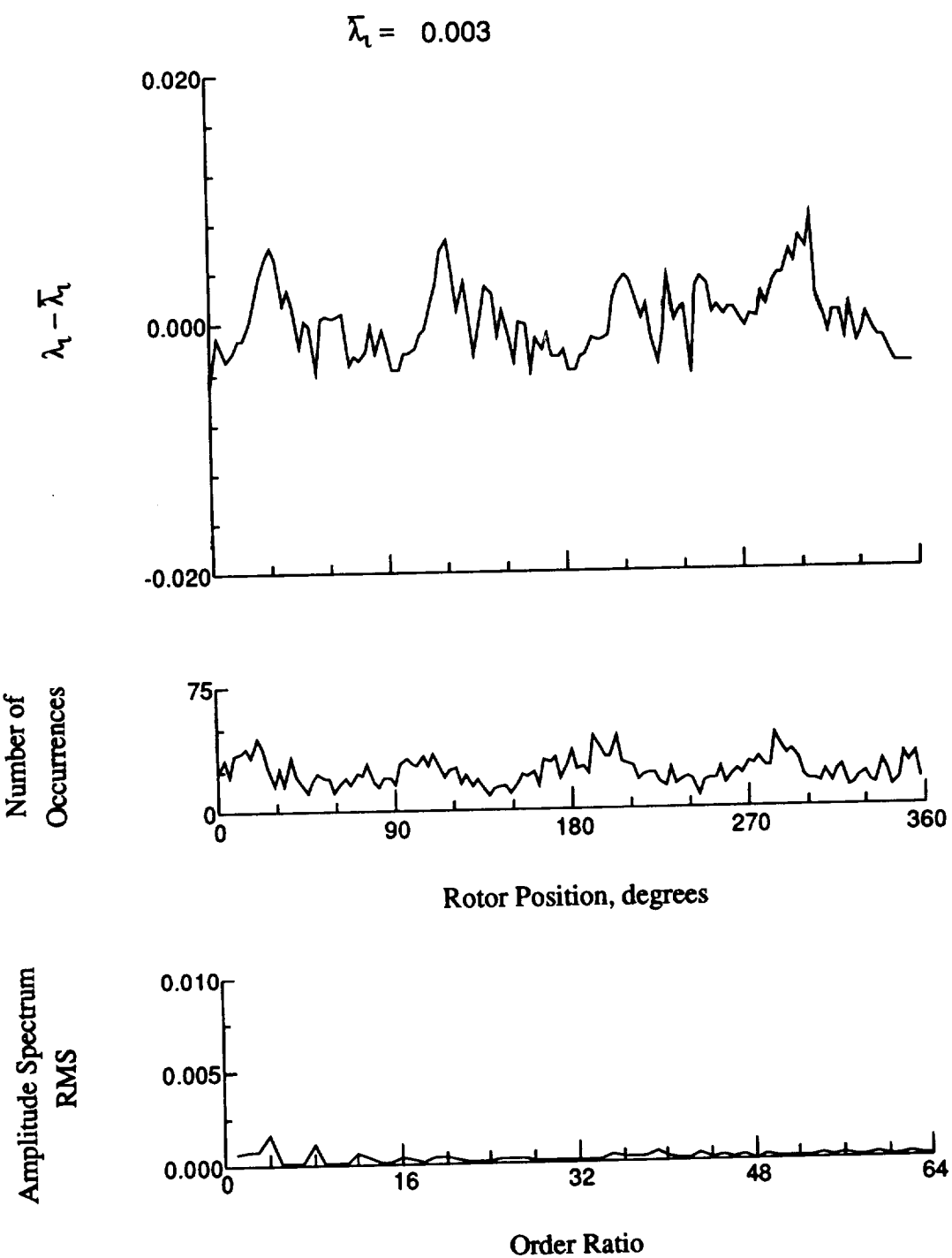


Figure 166.- Concluded.

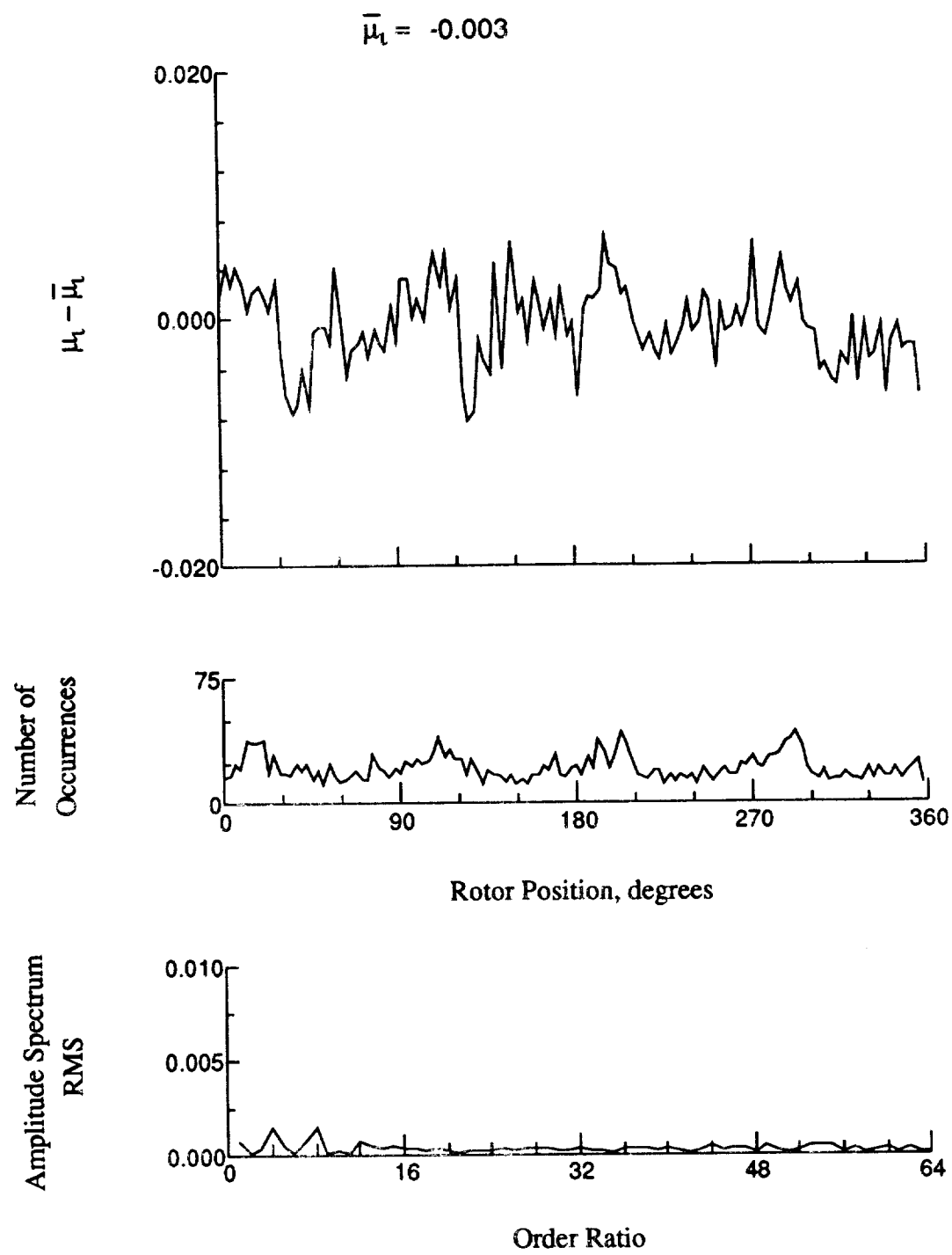


Figure 167. Induced inflow velocity measured at 300 degrees and r/R of 0.86.

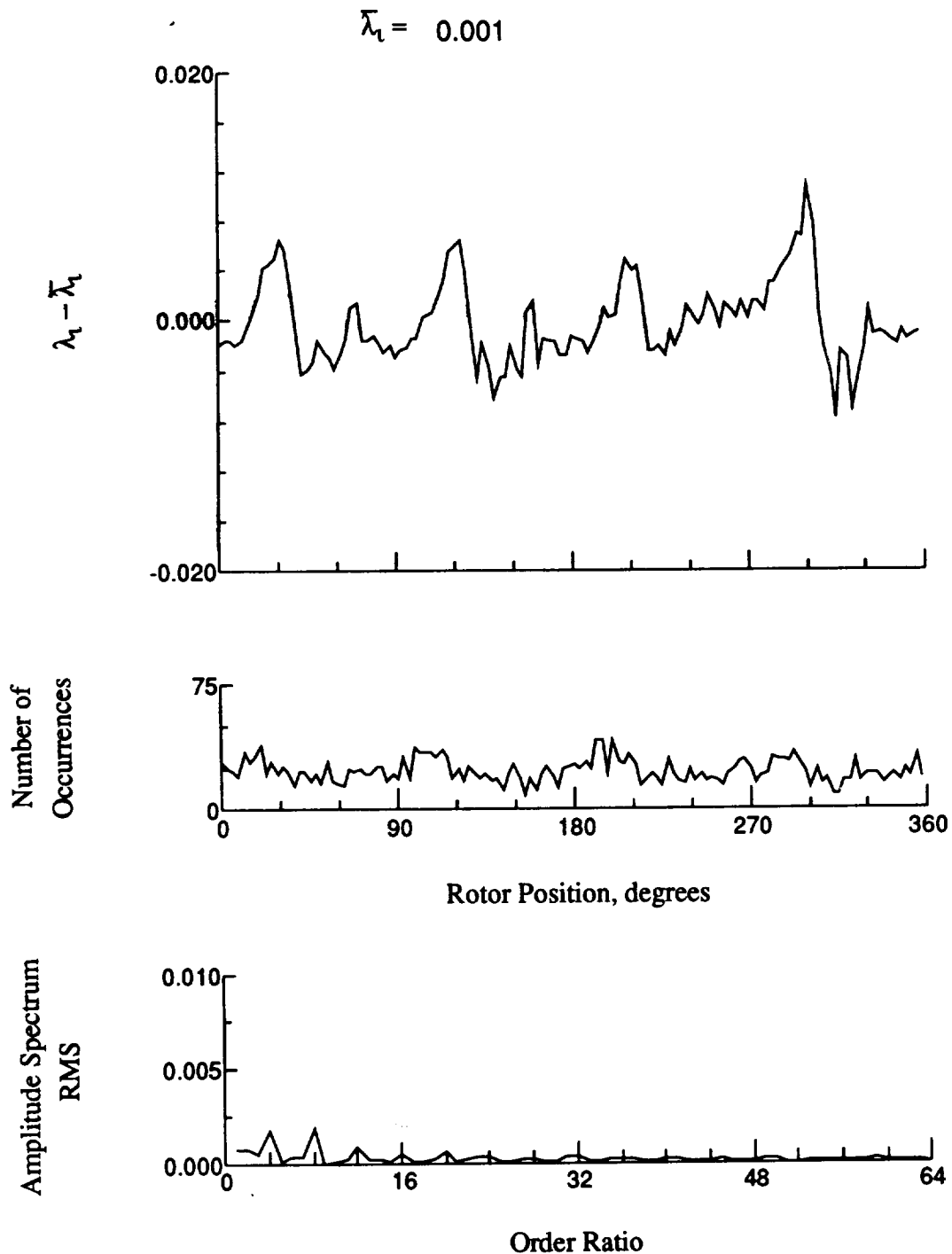


Figure 167.- Concluded.

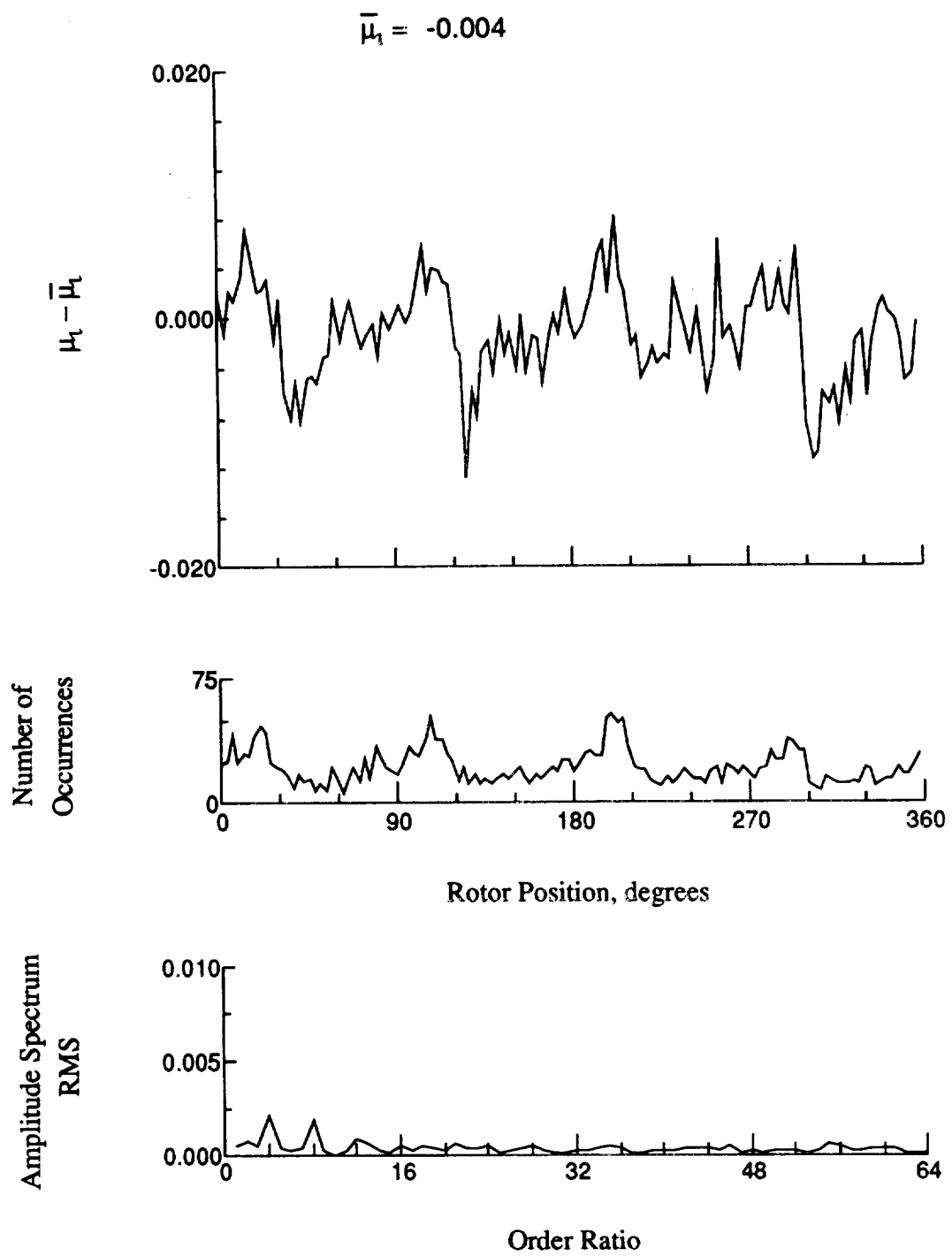


Figure 168.- Induced inflow velocity measured at 300 degrees and r/R of 0.90.

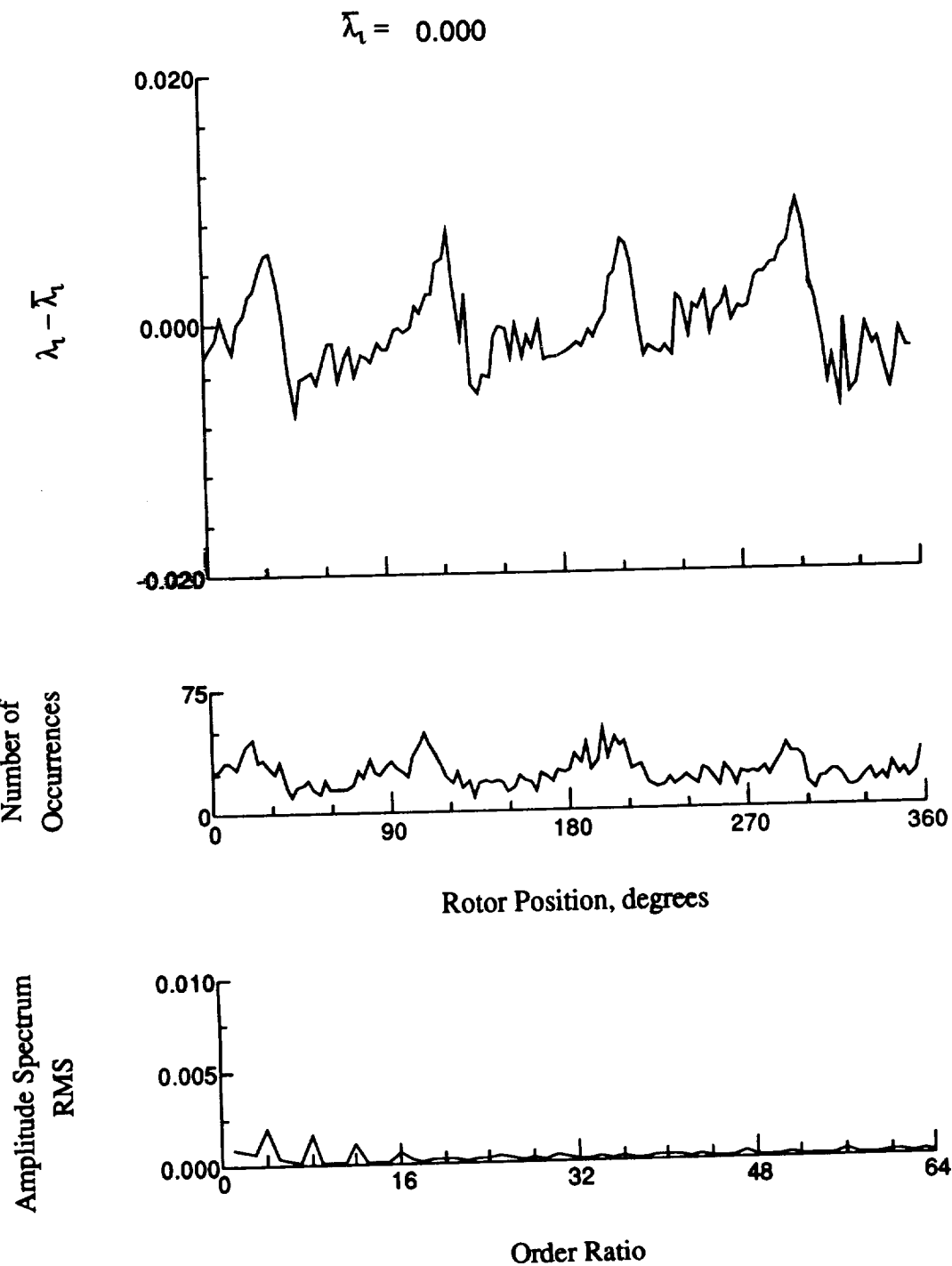


Figure 168.- Concluded.

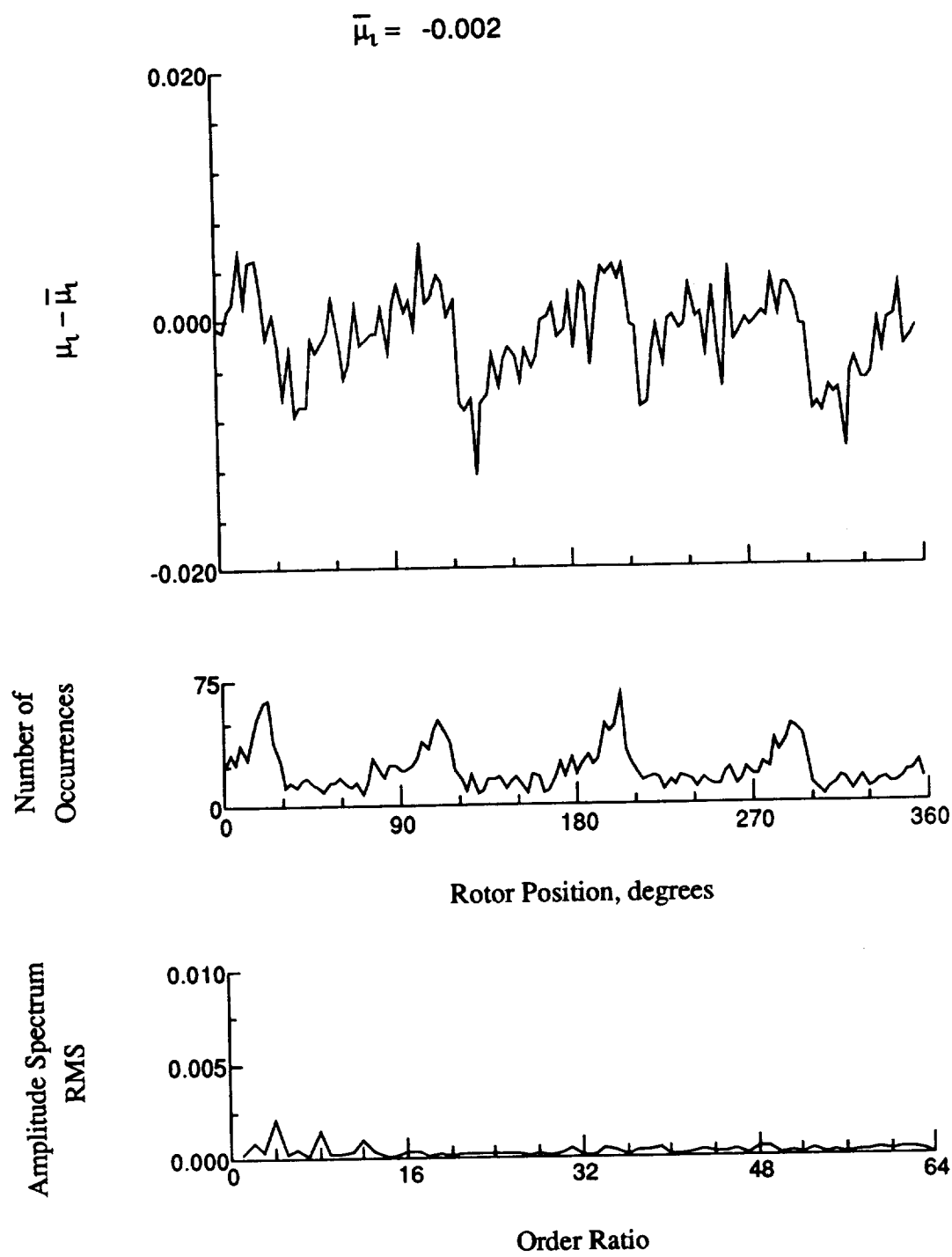


Figure 169.- Induced inflow velocity measured at 300 degrees and r/R of 0.94.

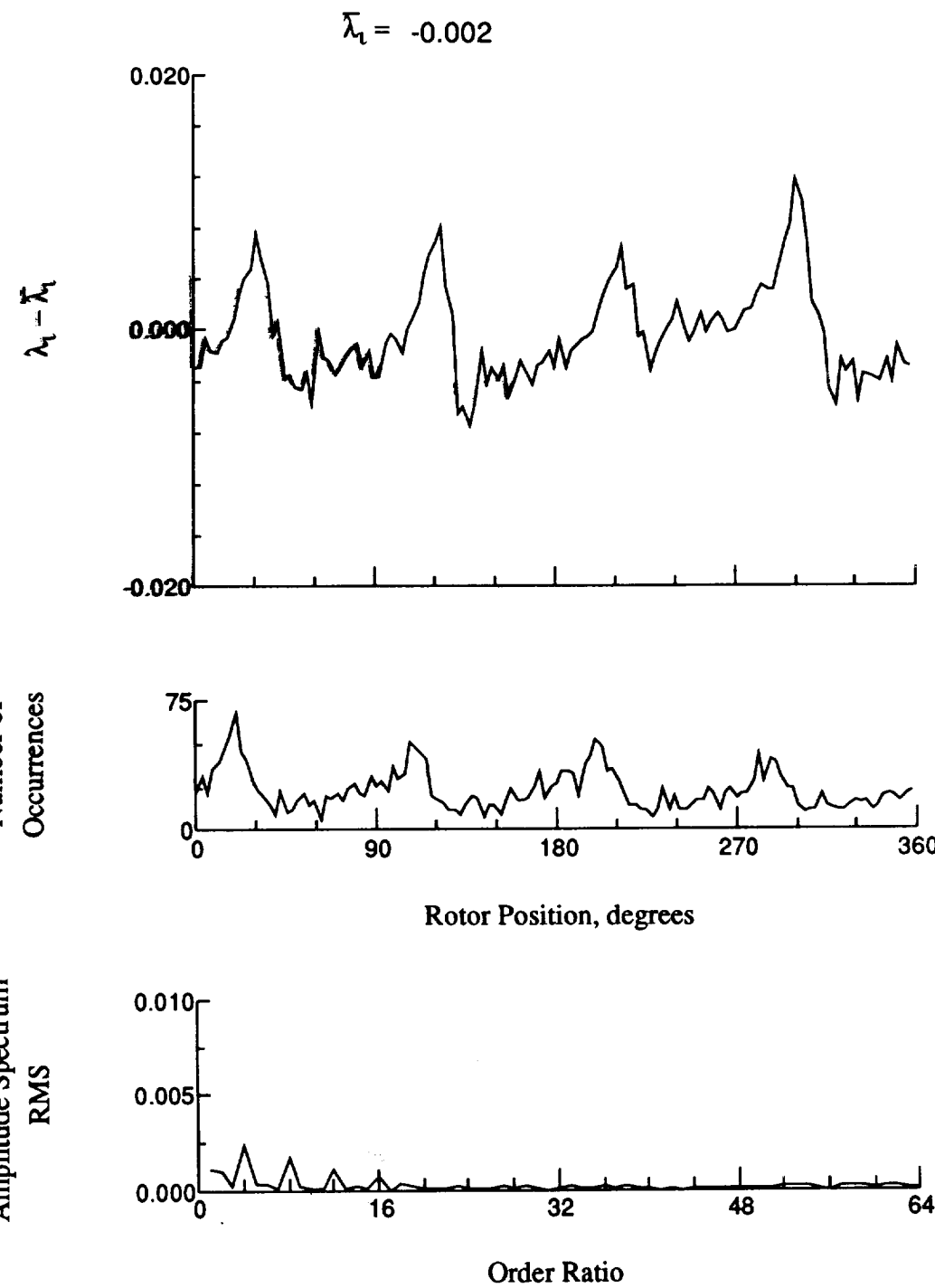


Figure 169.- Concluded.

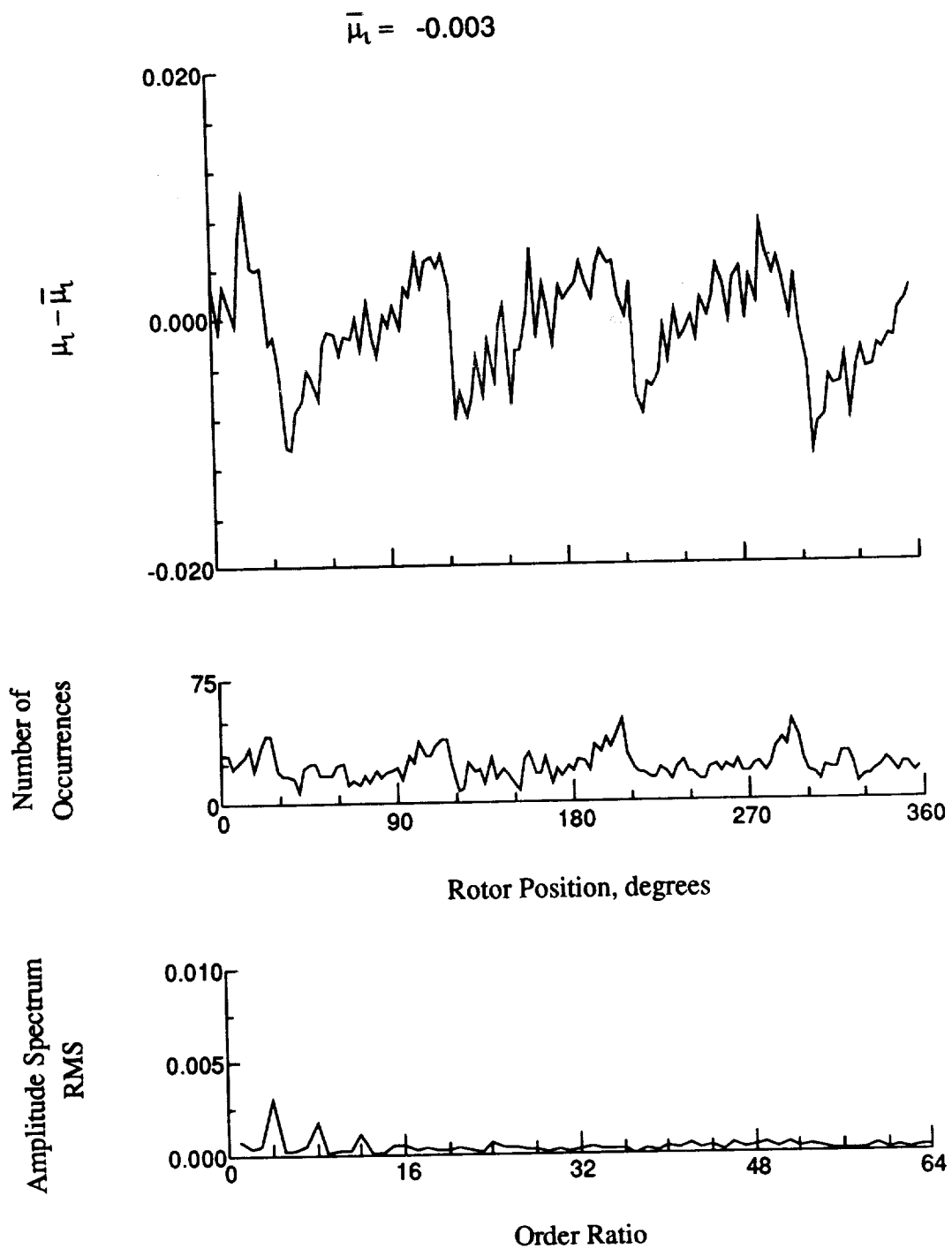


Figure 170.- Induced inflow velocity measured at 300 degrees and r/R of 0.96.

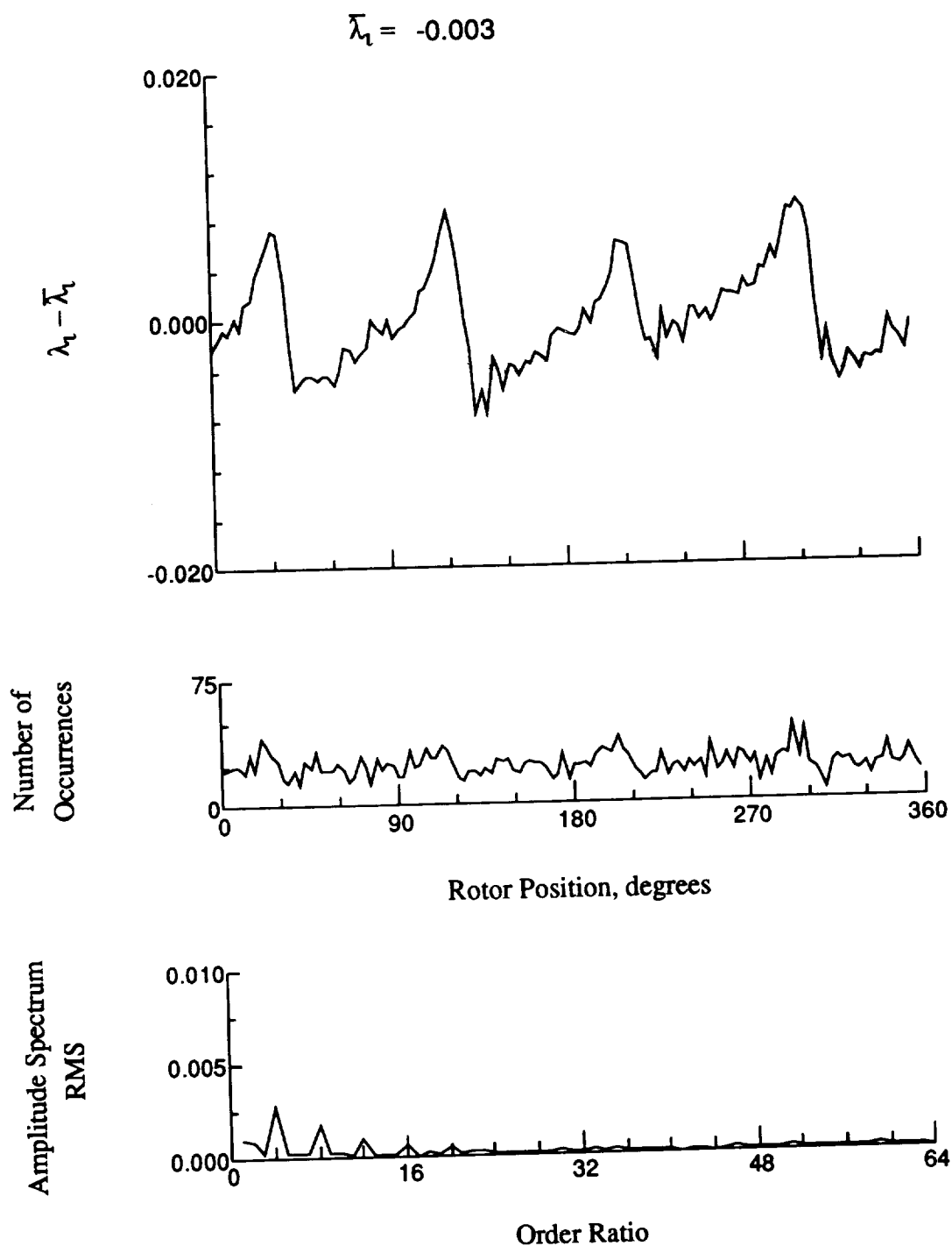


Figure 170.- Concluded.

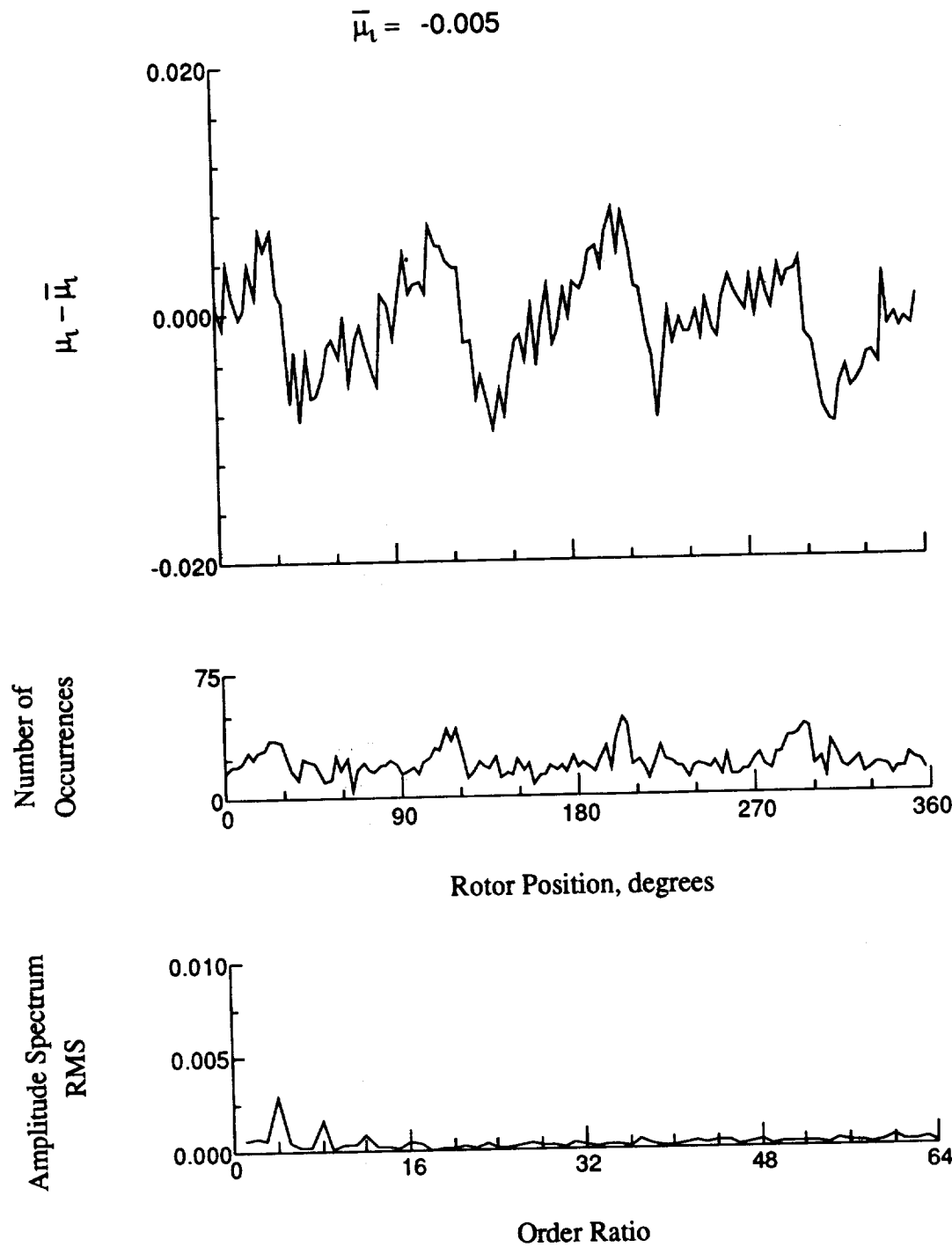


Figure 171.- Induced inflow velocity measured at 300 degrees and r/R of 1.00.

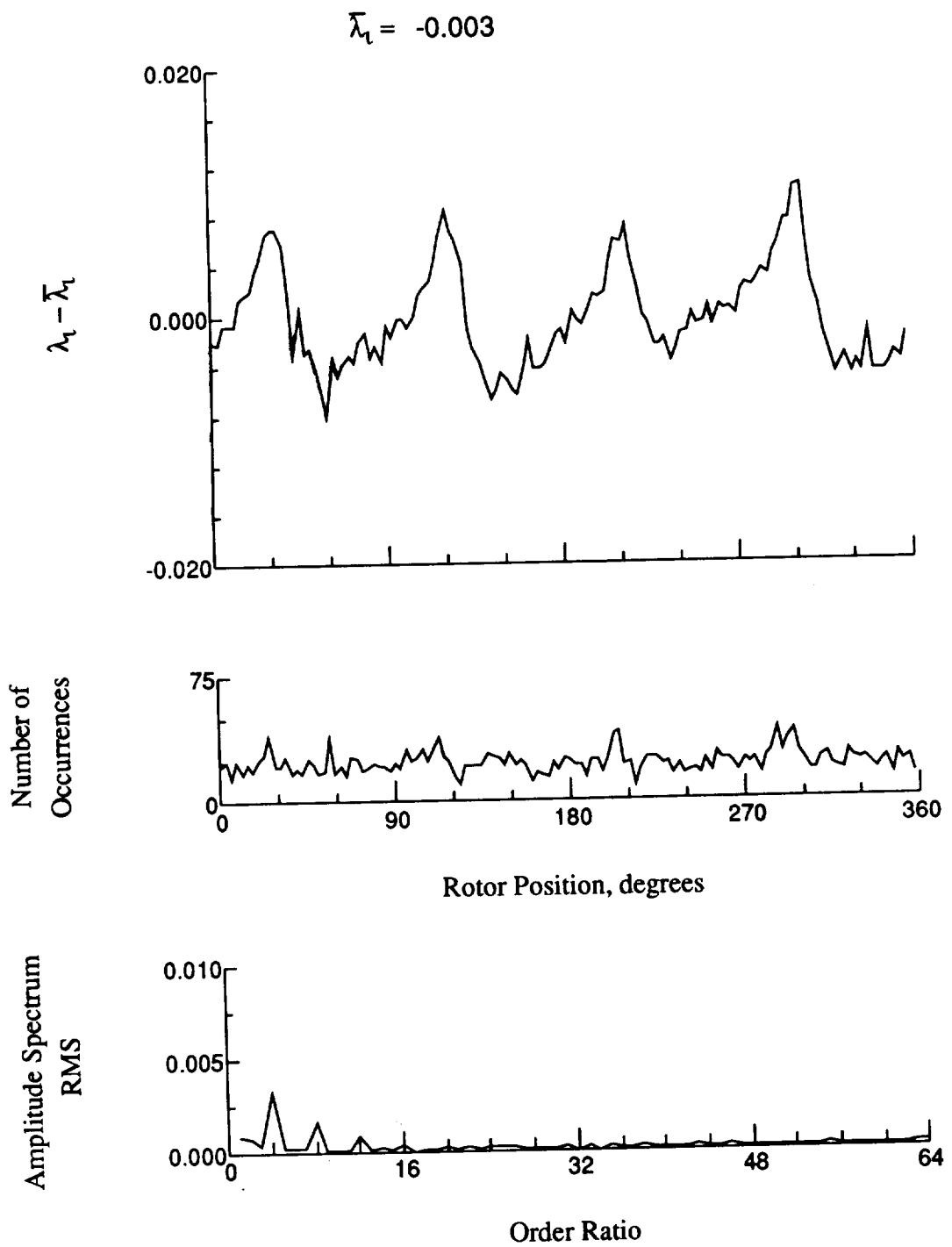


Figure 171.- Concluded.

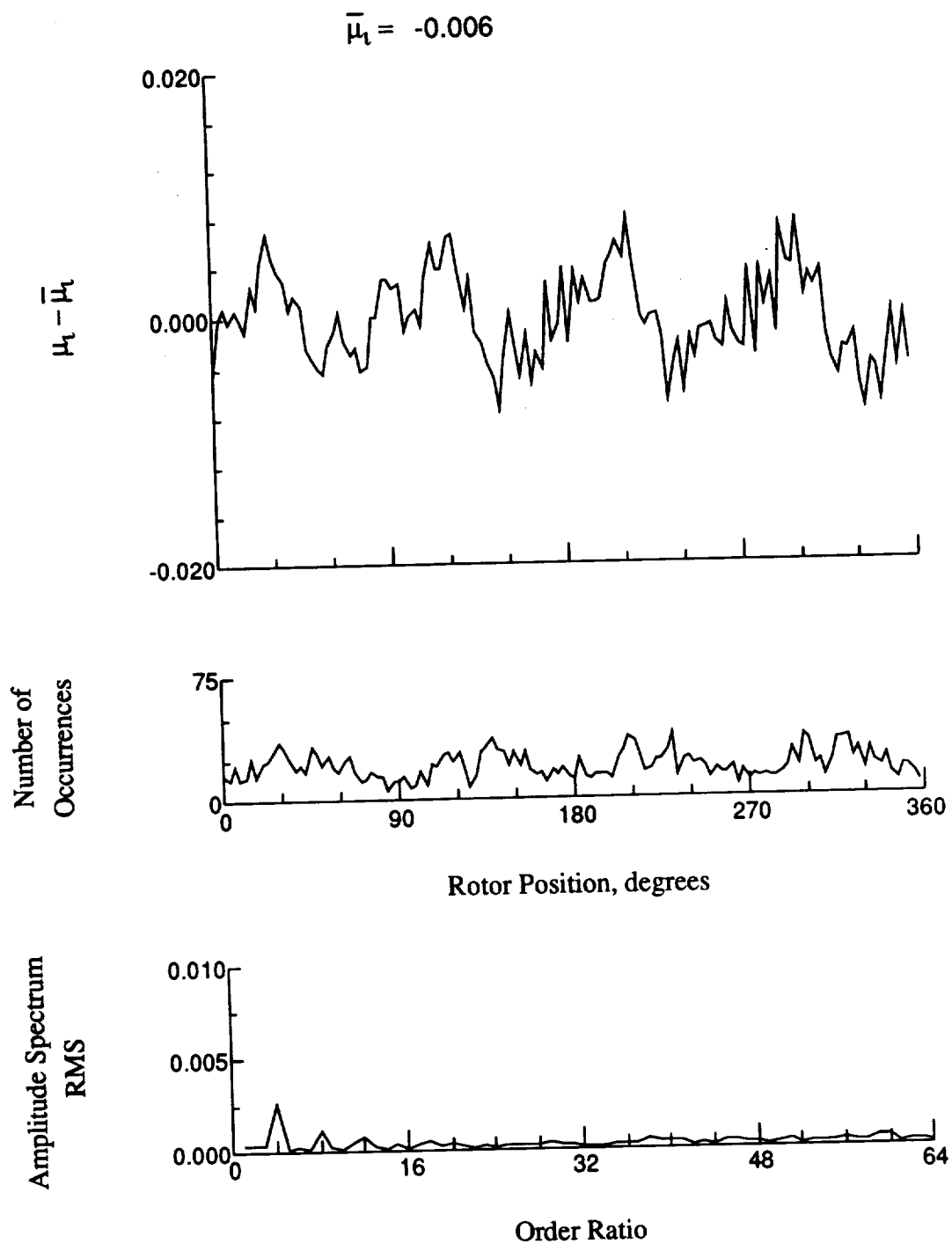


Figure 172.- Induced inflow velocity measured at 300 degrees and r/R of 1.10.

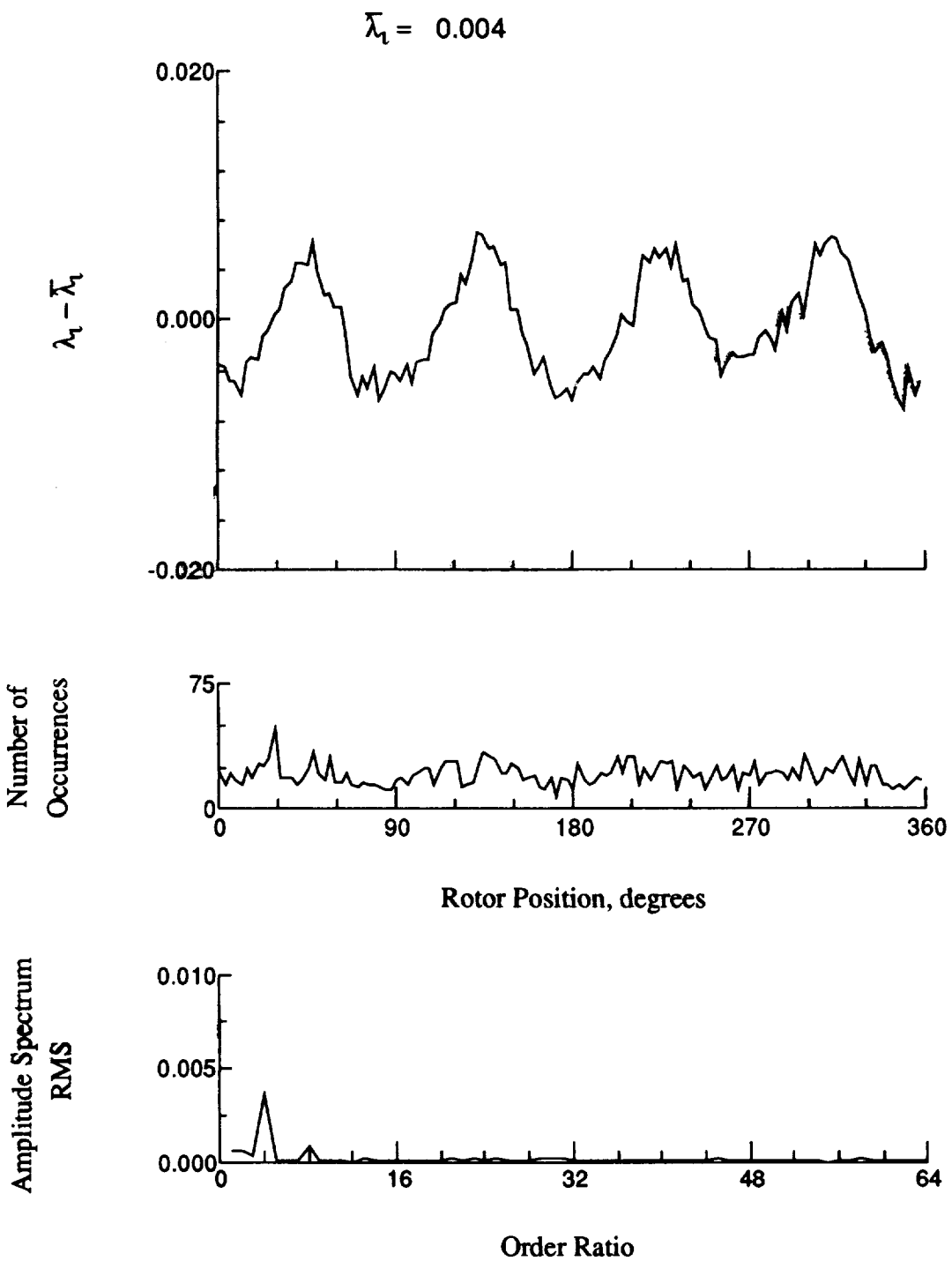


Figure 172.- Concluded.

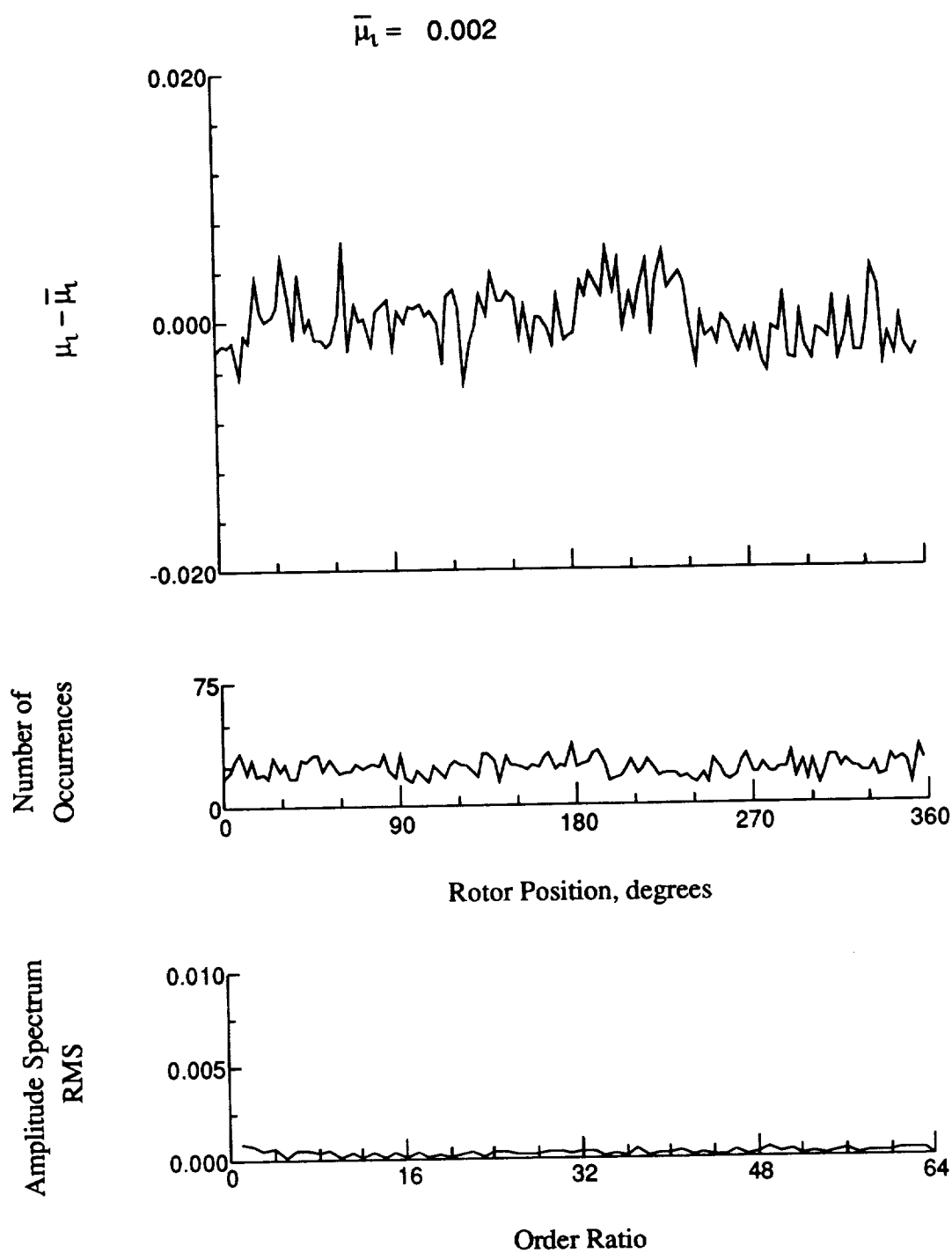


Figure 173.- Induced inflow velocity measured at 330 degrees and r/R of 0.20.

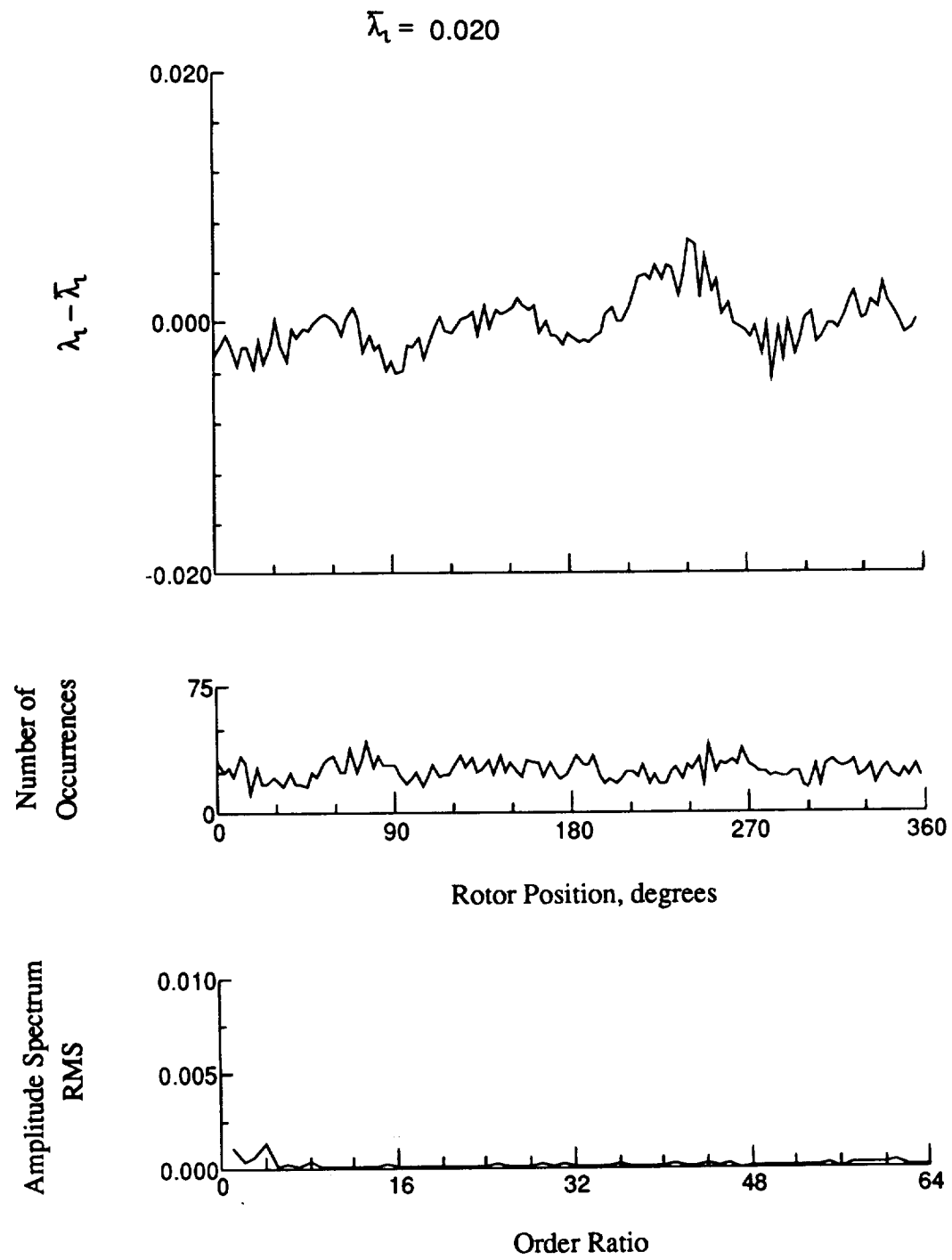


Figure 173.- Concluded.

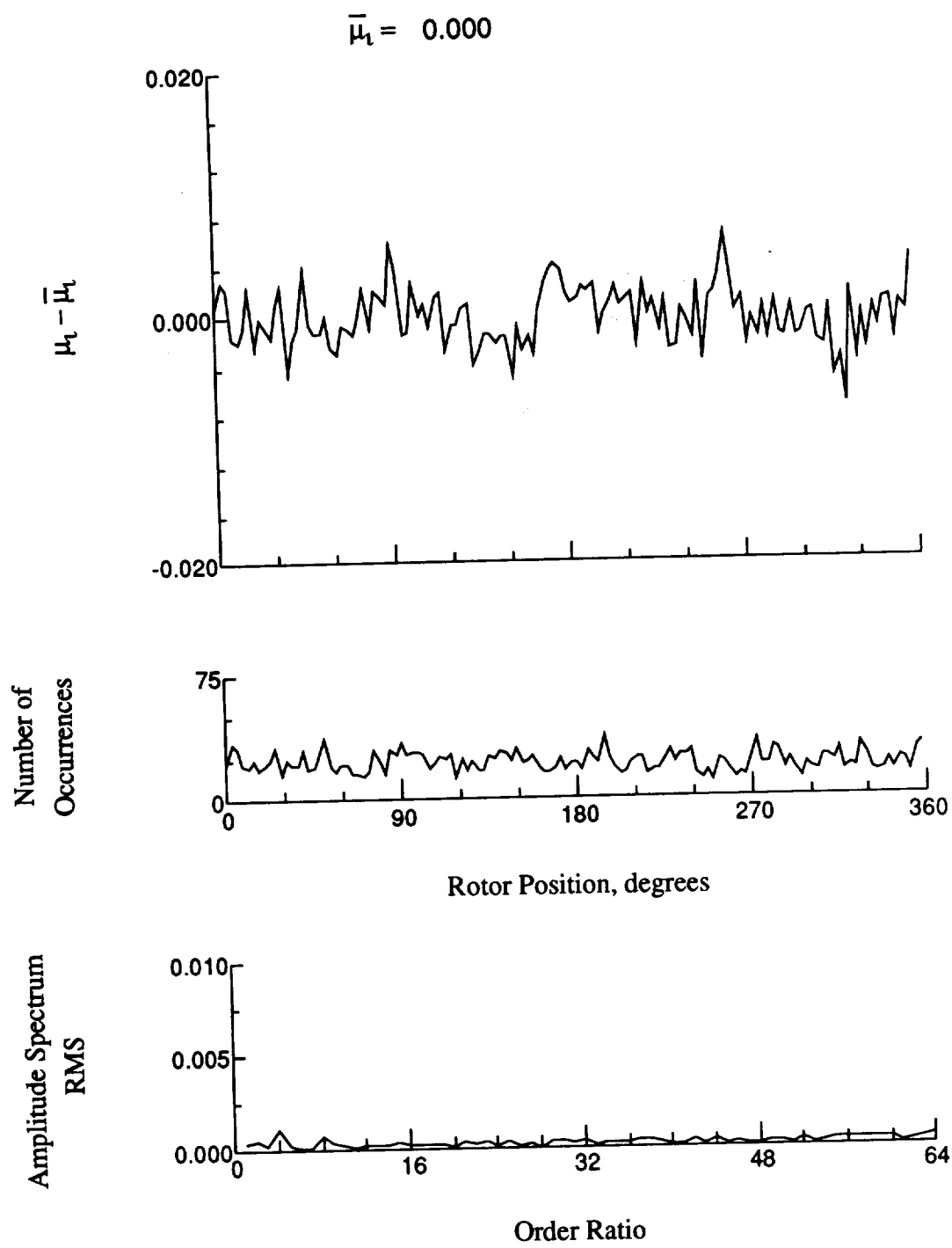


Figure 174.- Induced inflow velocity measured at 330 degrees and r/R of 0.32.

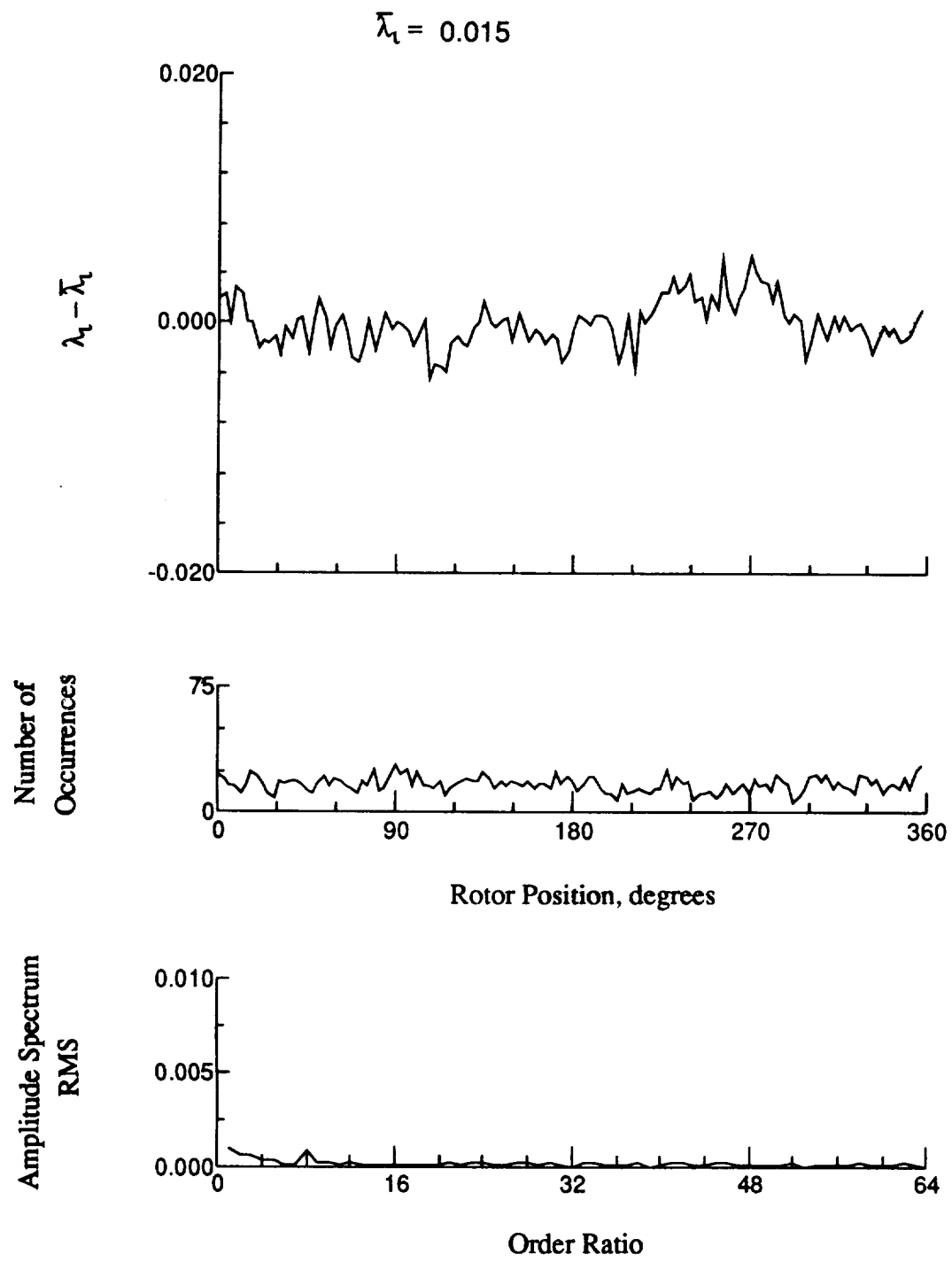


Figure 174.- Concluded.

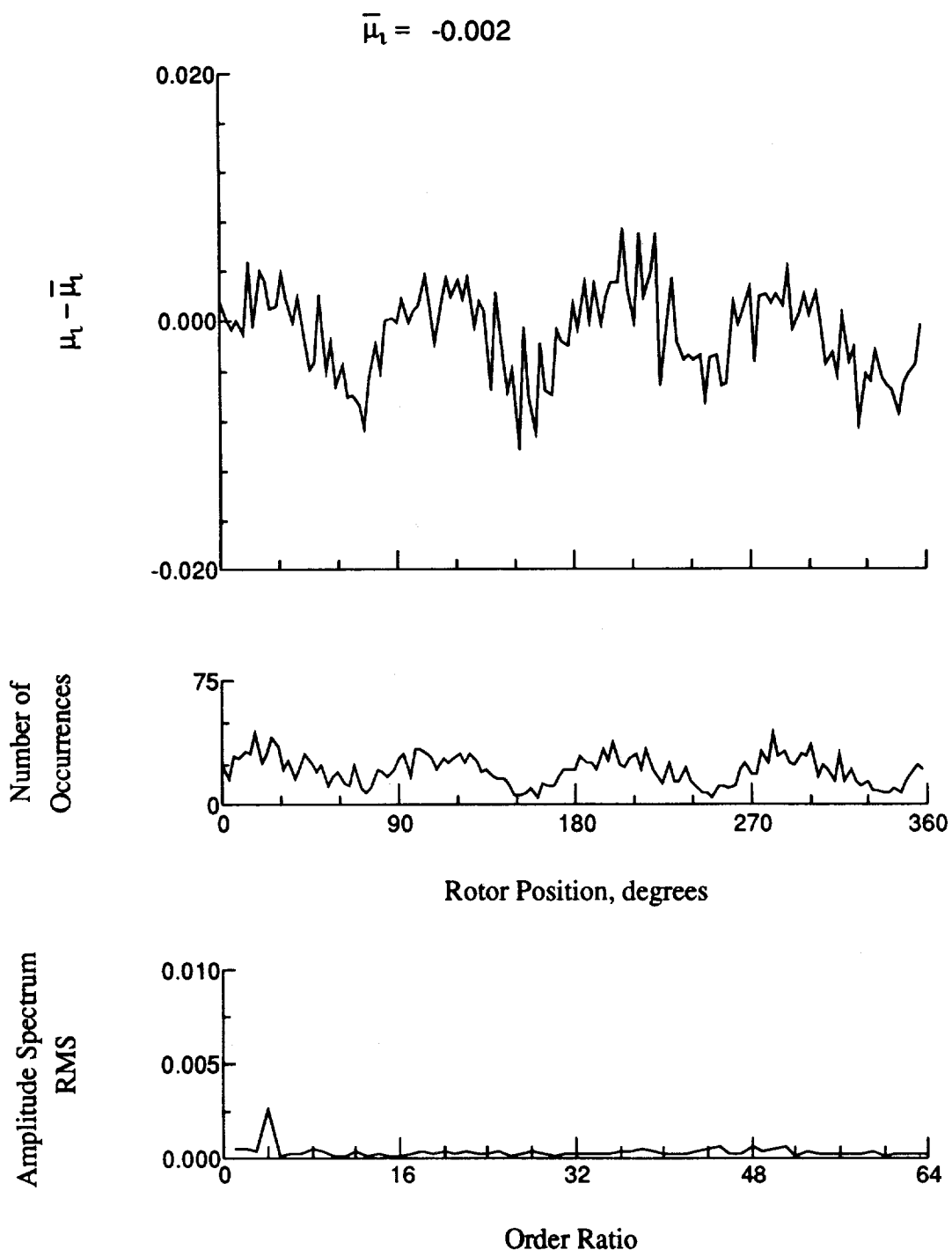


Figure 175.- Induced inflow velocity measured at 330 degrees and r/R of 0.50.

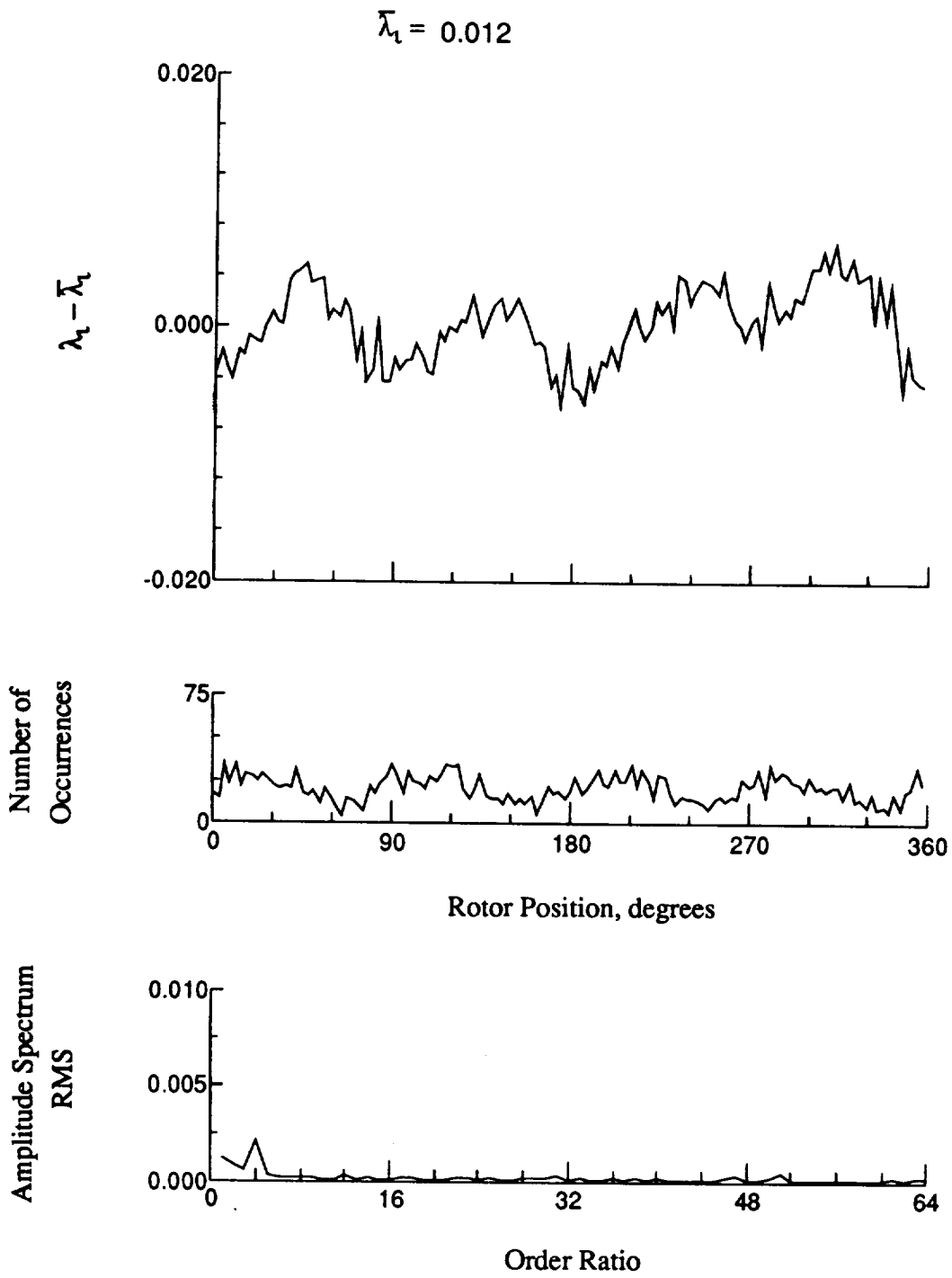


Figure 175.- Concluded.

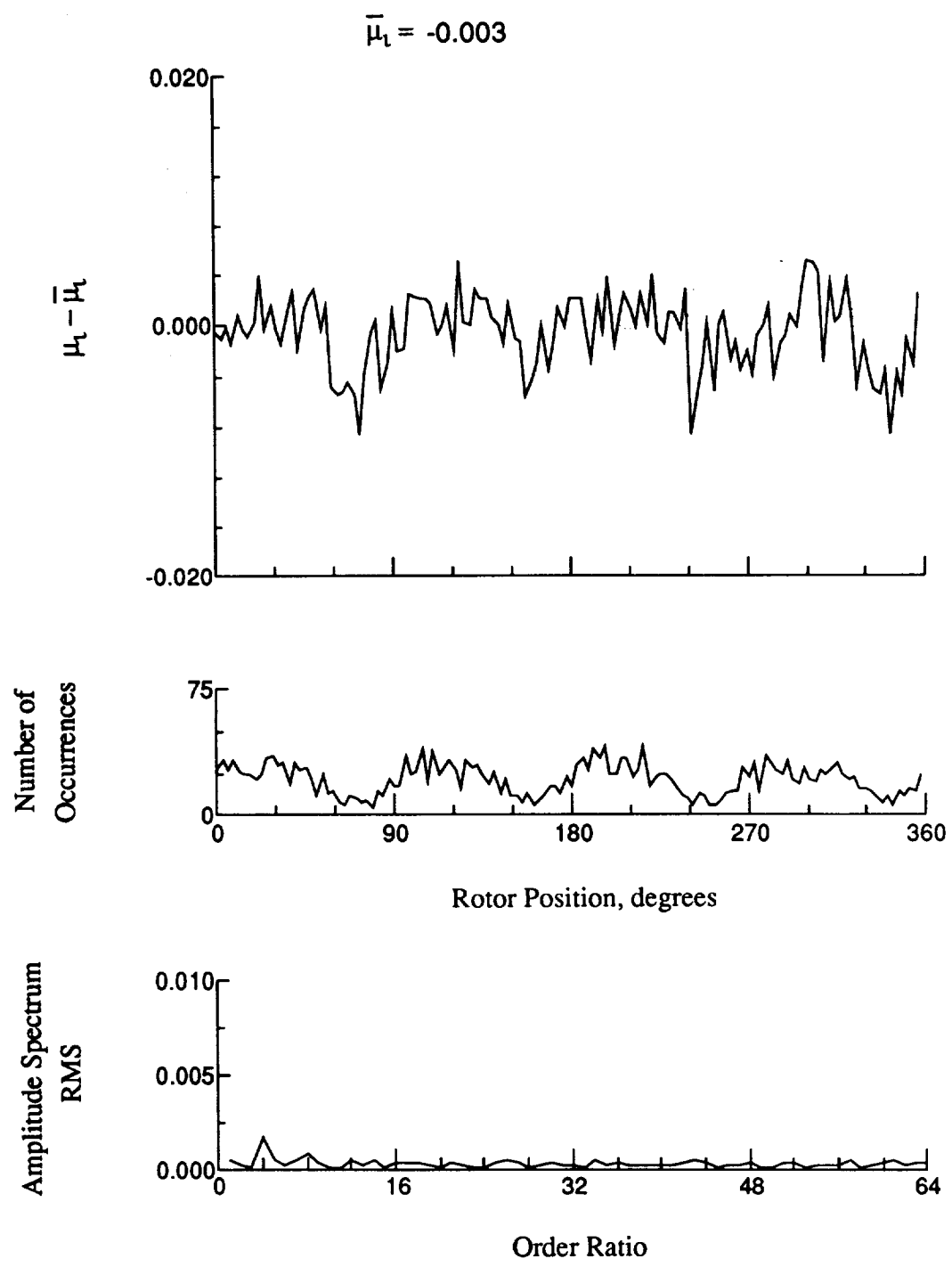


Figure 176.- Induced inflow velocity measured at 330 degrees and r/R of 0.58.

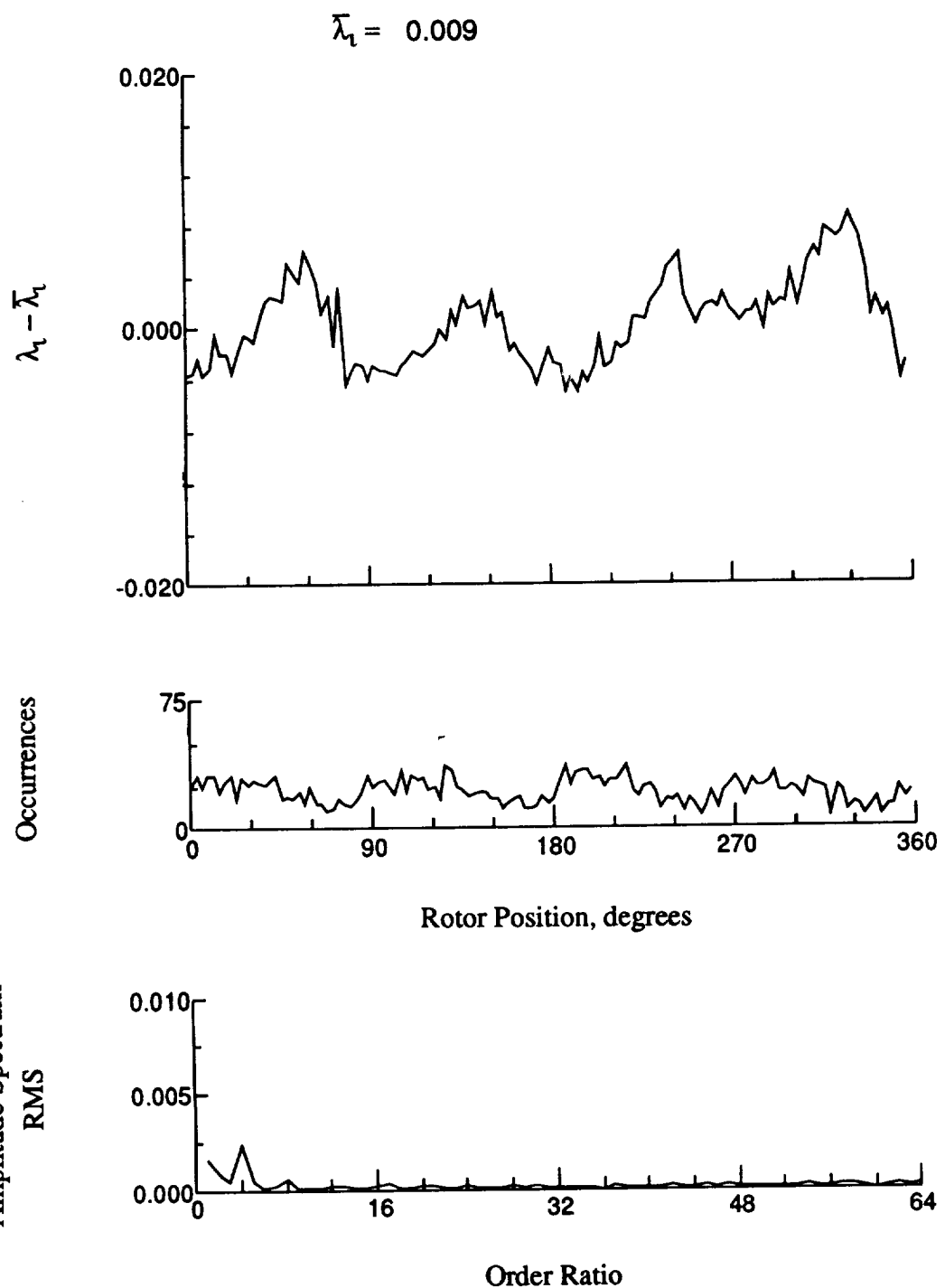


Figure 176.- Concluded.

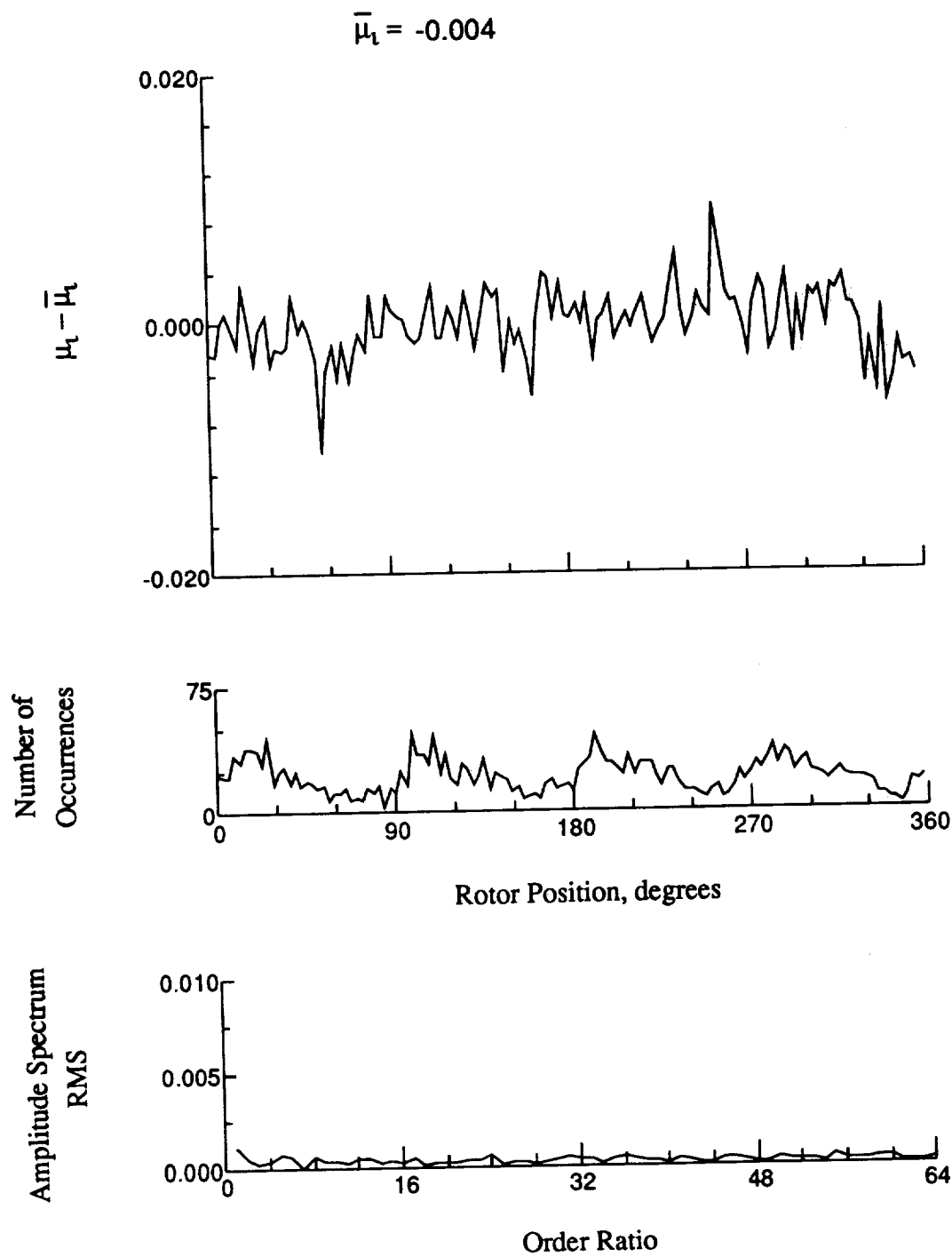


Figure 177.- Induced inflow velocity measured at 330 degrees and r/R of 0.69.

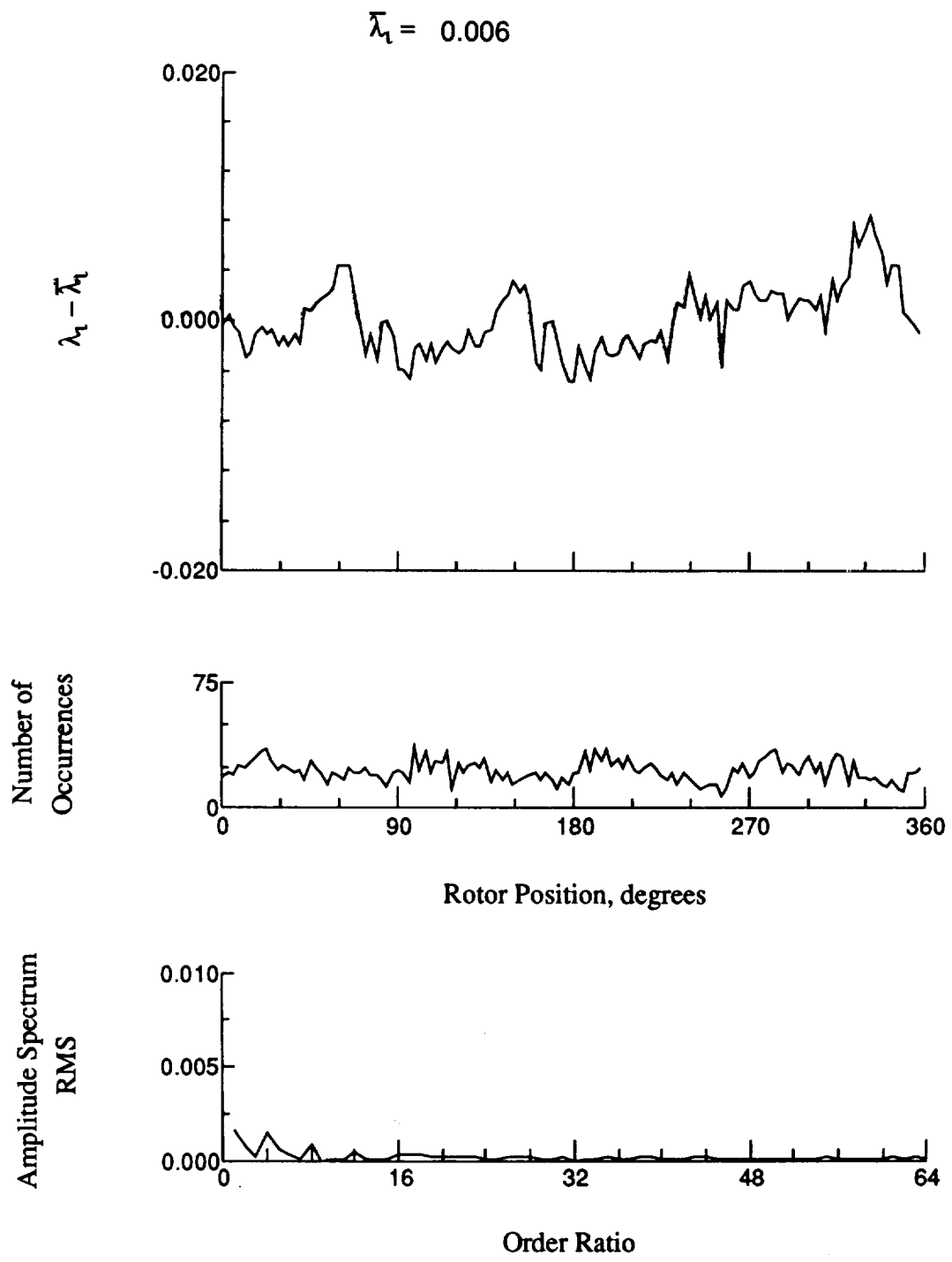


Figure 177.- Concluded.

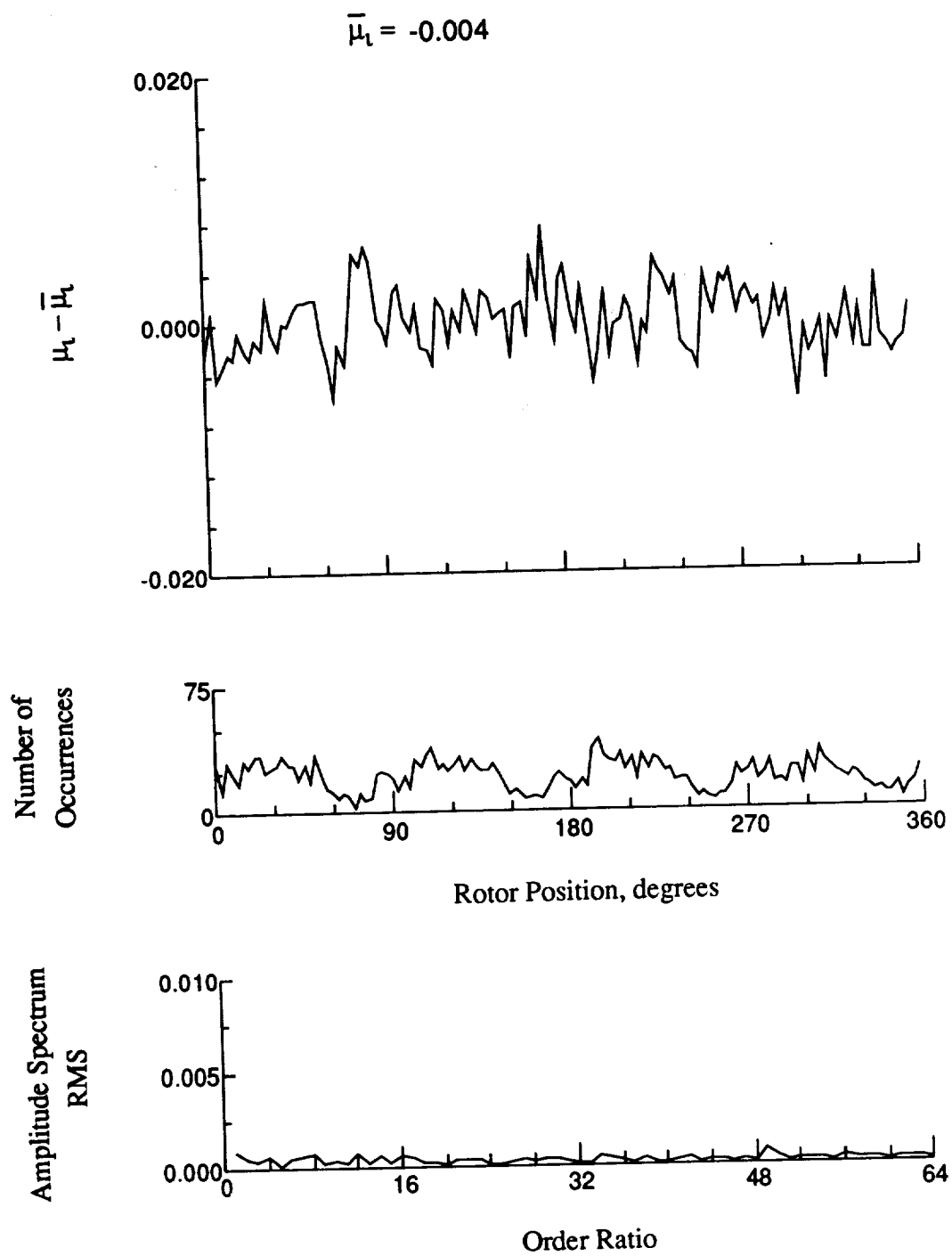


Figure 178.- Induced inflow velocity measured at 330 degrees and r/R of 0.73.

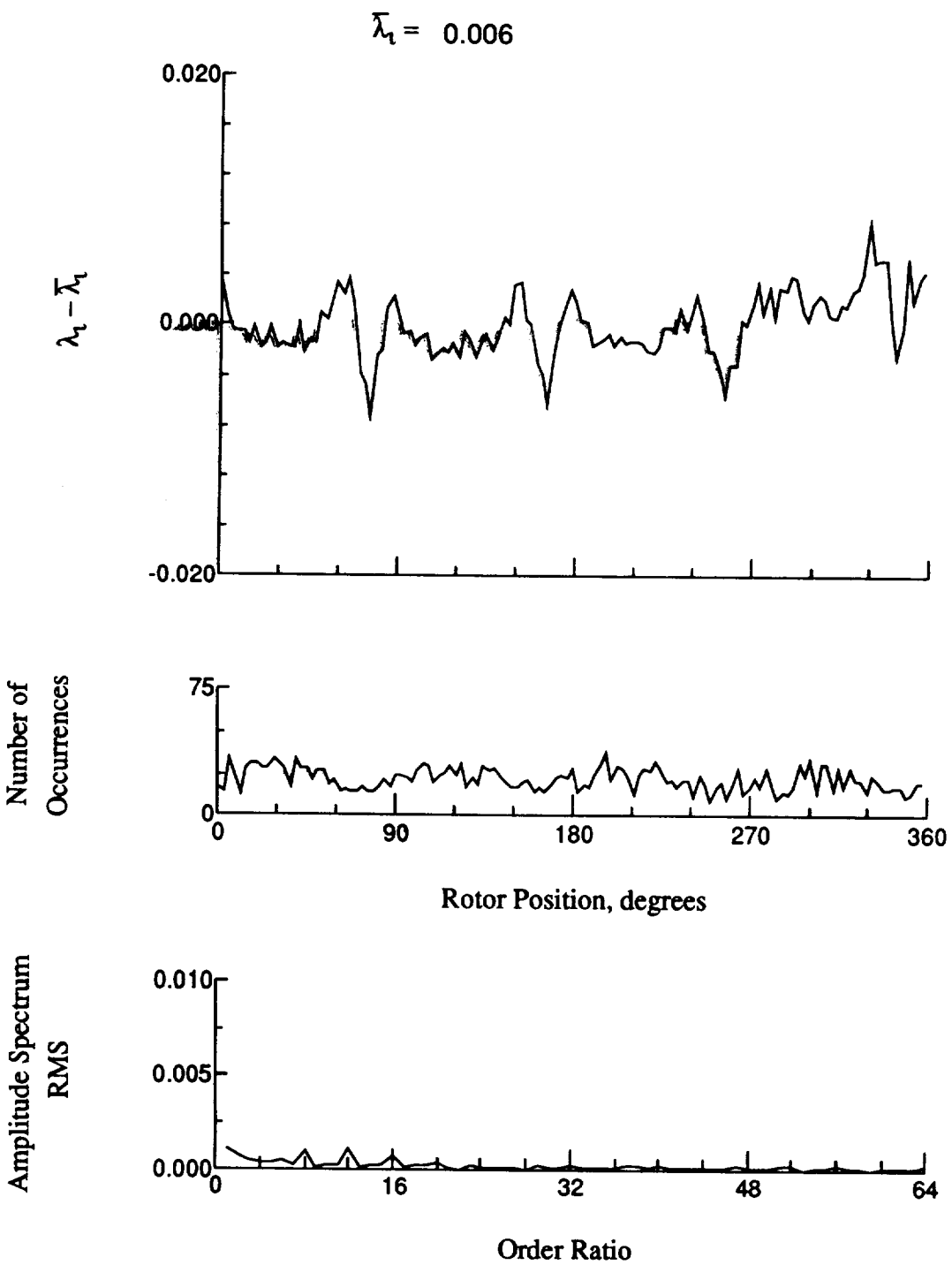


Figure 178.- Concluded.

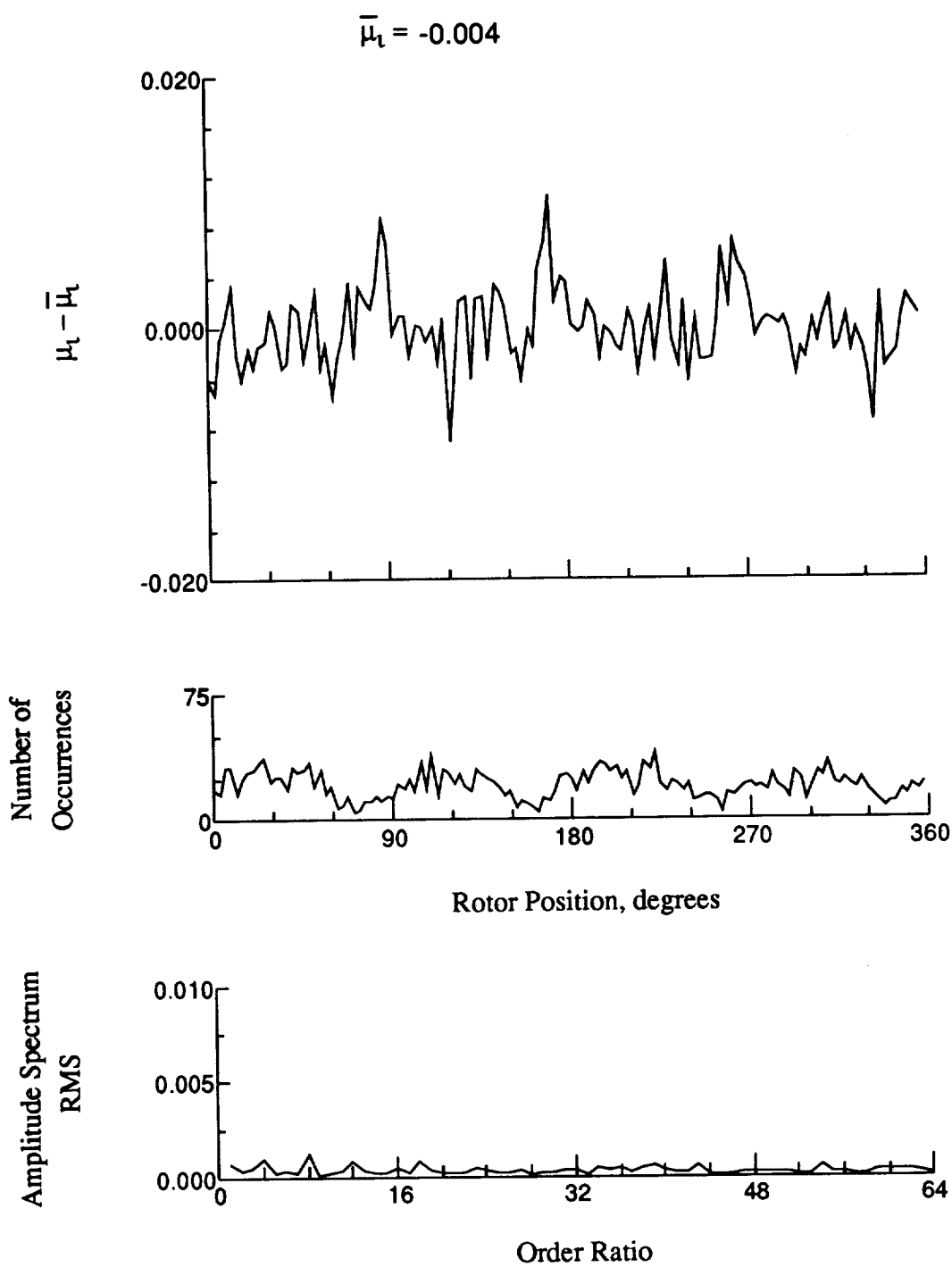


Figure 179.- Induced inflow velocity measured at 330 degrees and r/R of 0.75.

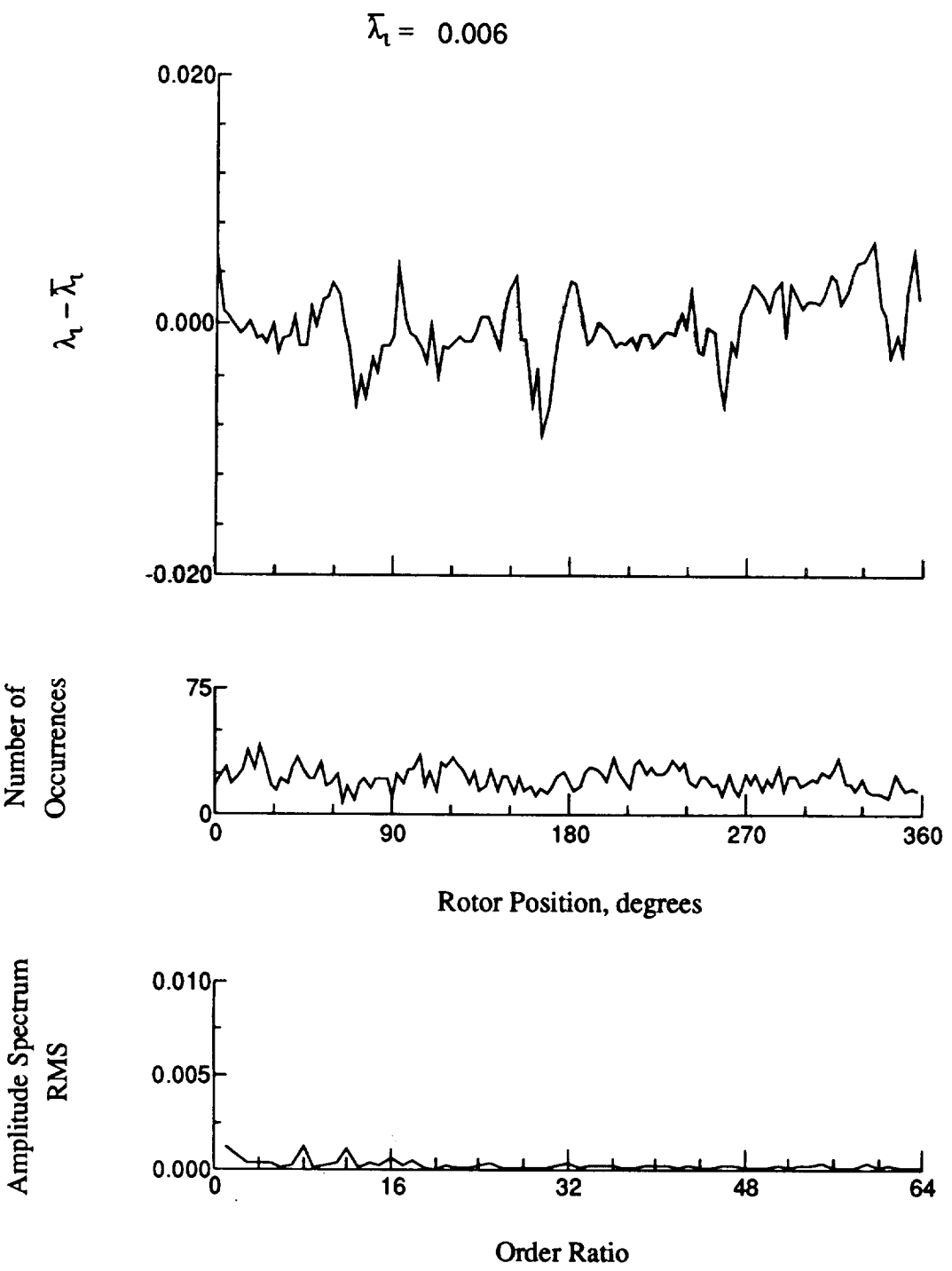


Figure 179.- Concluded.

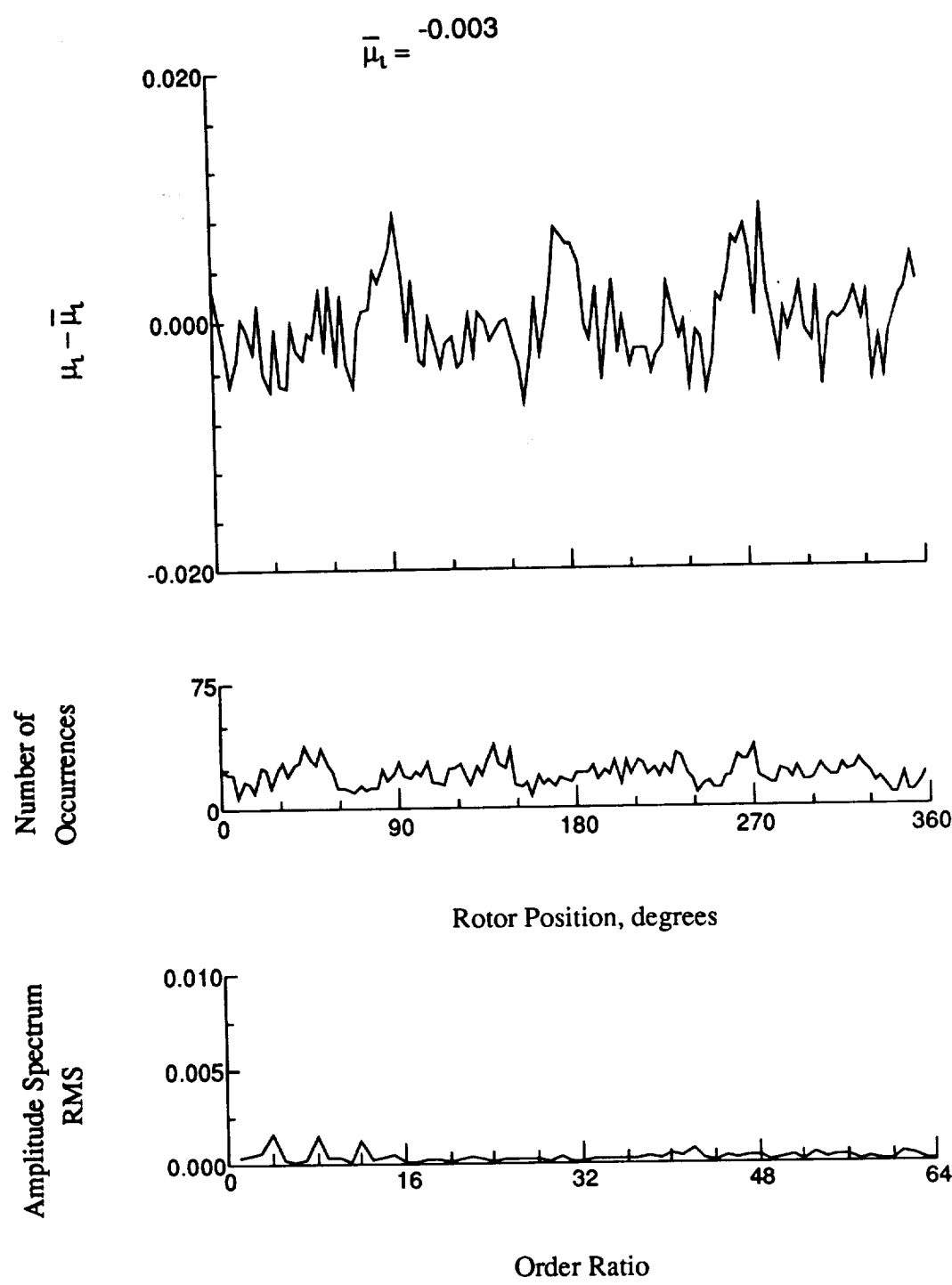


Figure 180.- Induced inflow velocity measured at 330 degrees and r/R of 0.81.

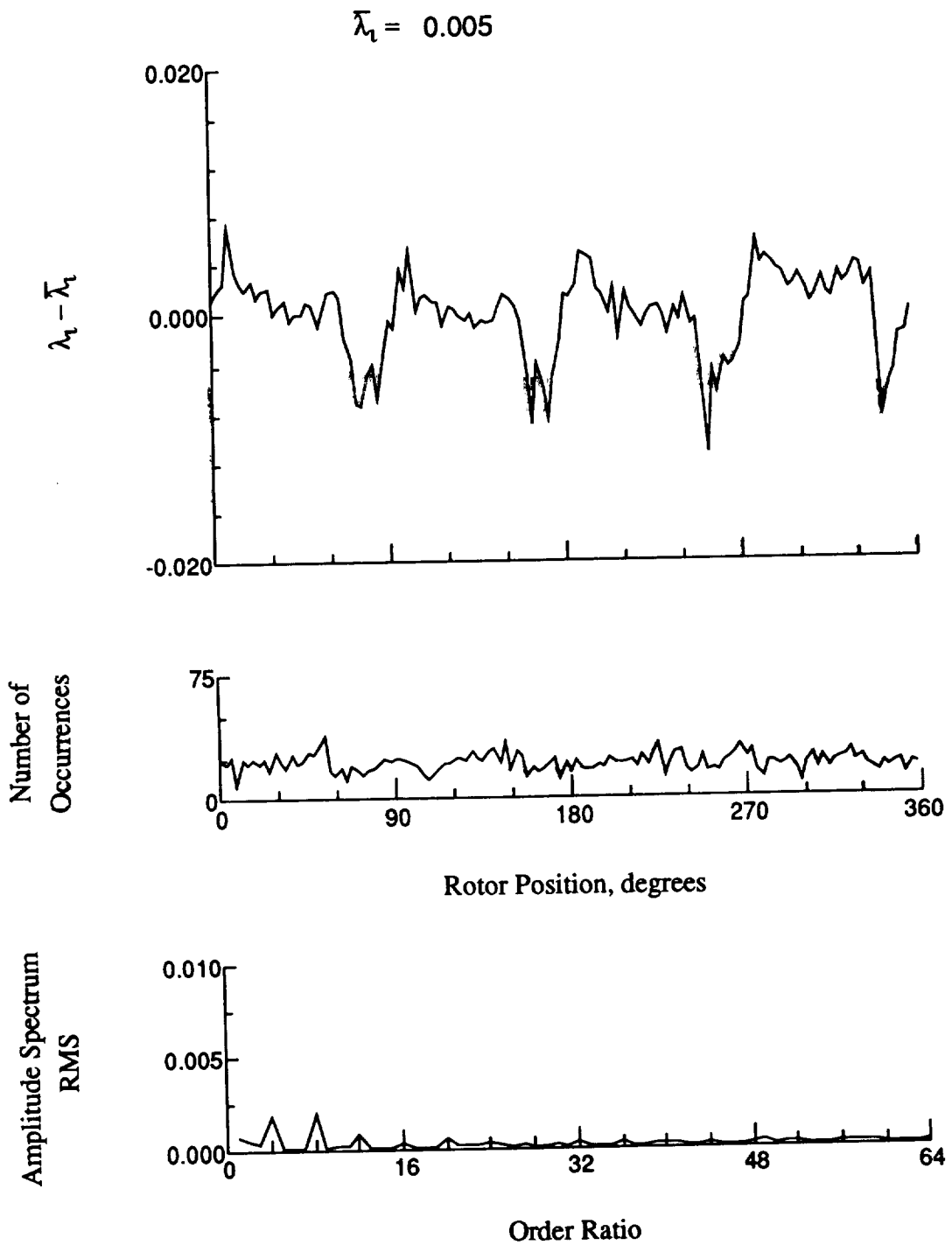


Figure 180.- Concluded.

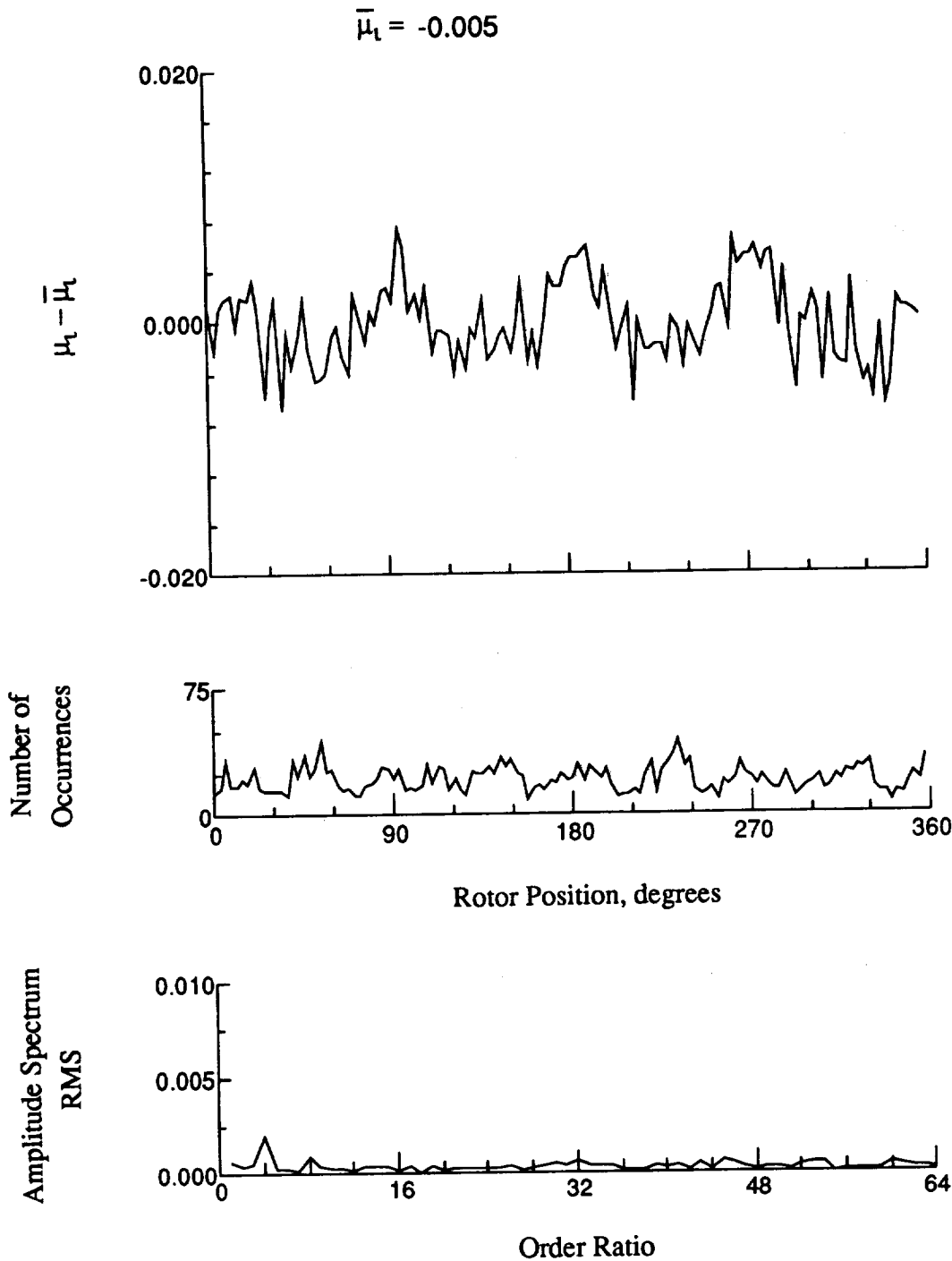


Figure 181.- Induced inflow velocity measured at 330 degrees and r/R of 0.86.

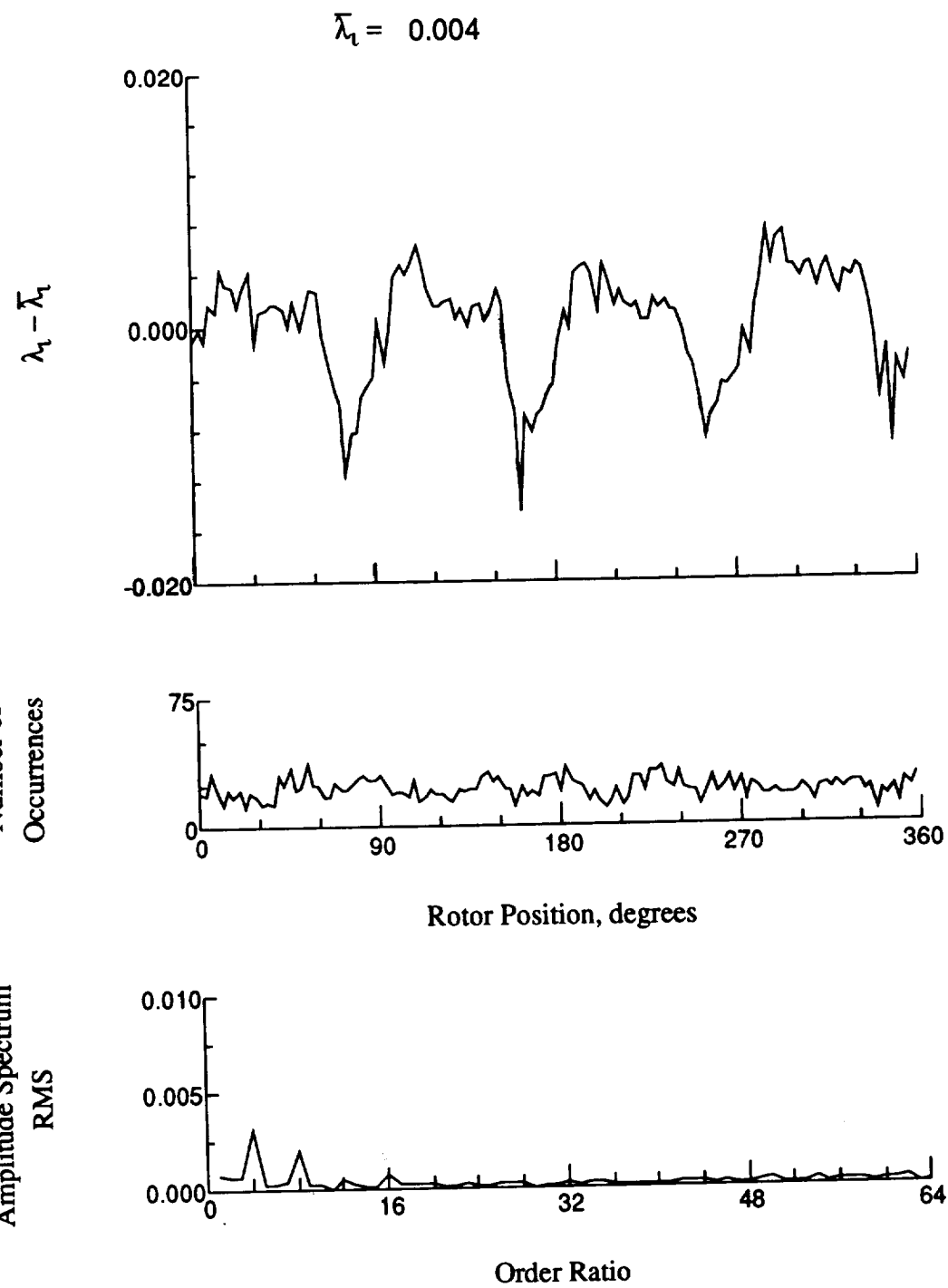


Figure 181.- Concluded.

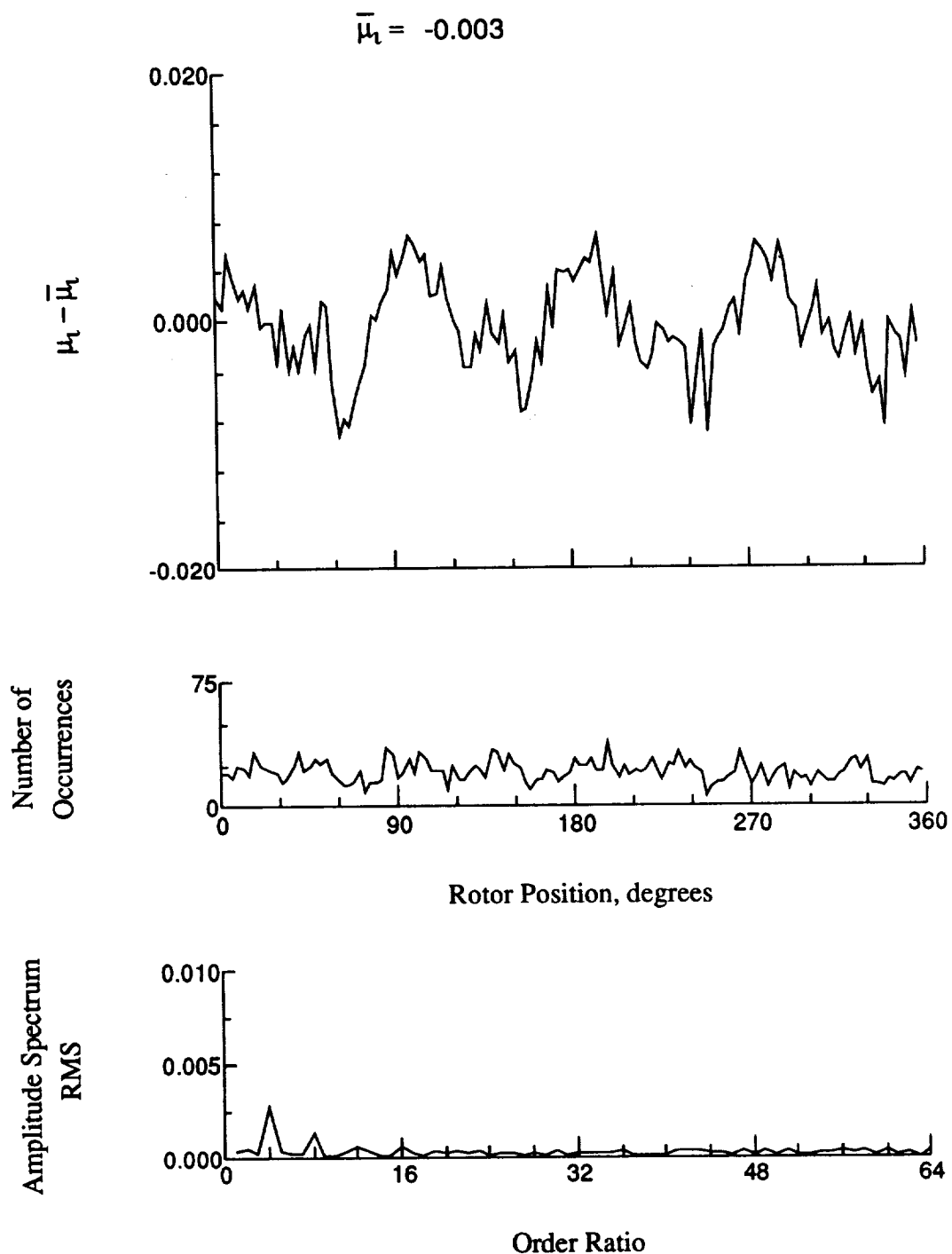


Figure 182.- Induced inflow velocity measured at 330 degrees and r/R of 0.90.

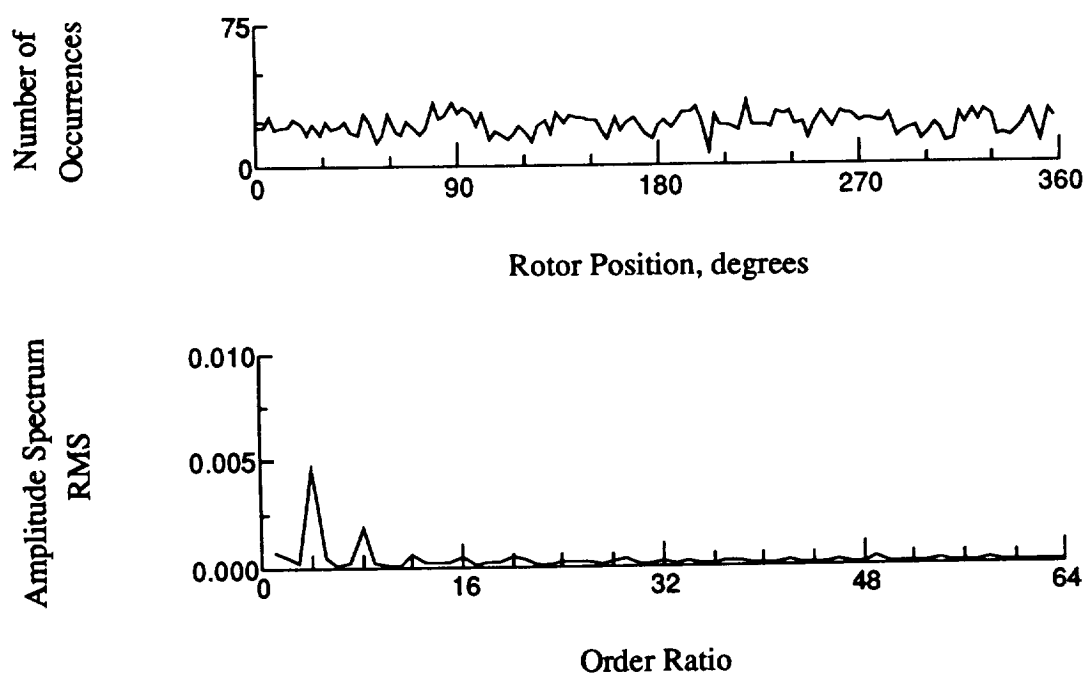
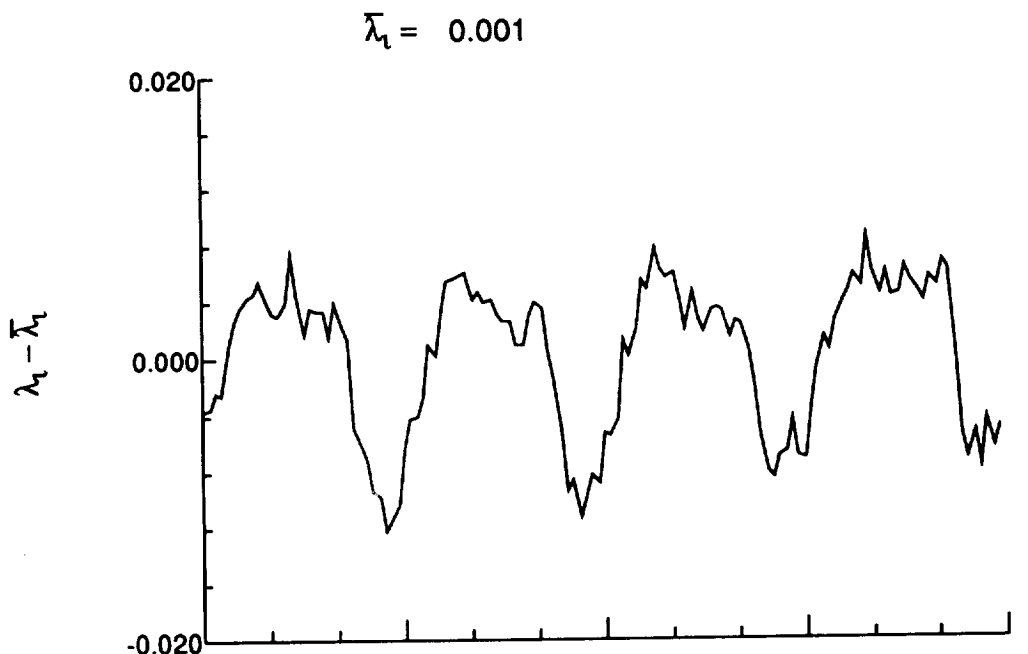


Figure 182.- Concluded.

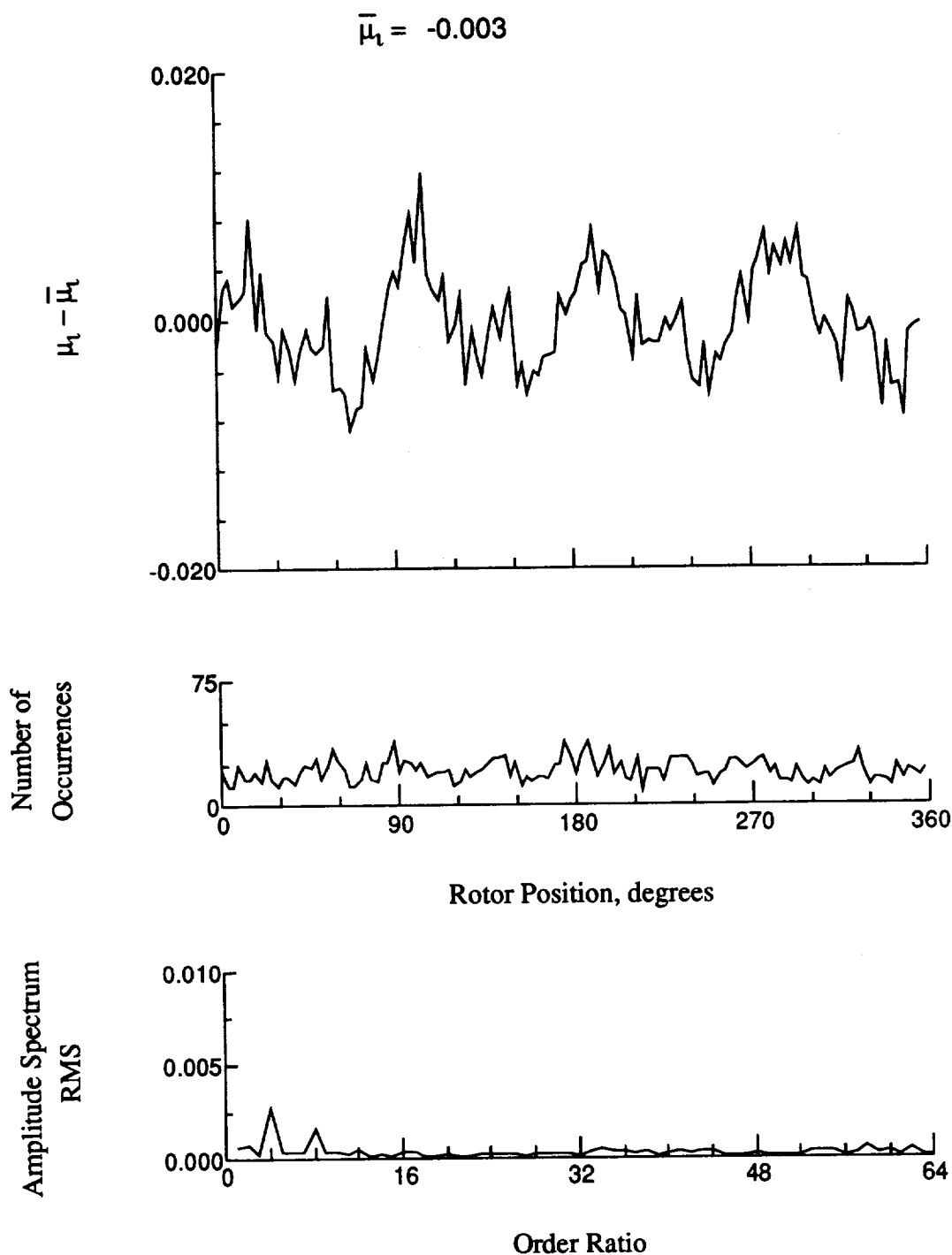


Figure 183.- Induced inflow velocity measured at 330 degrees and r/R of 0.94.

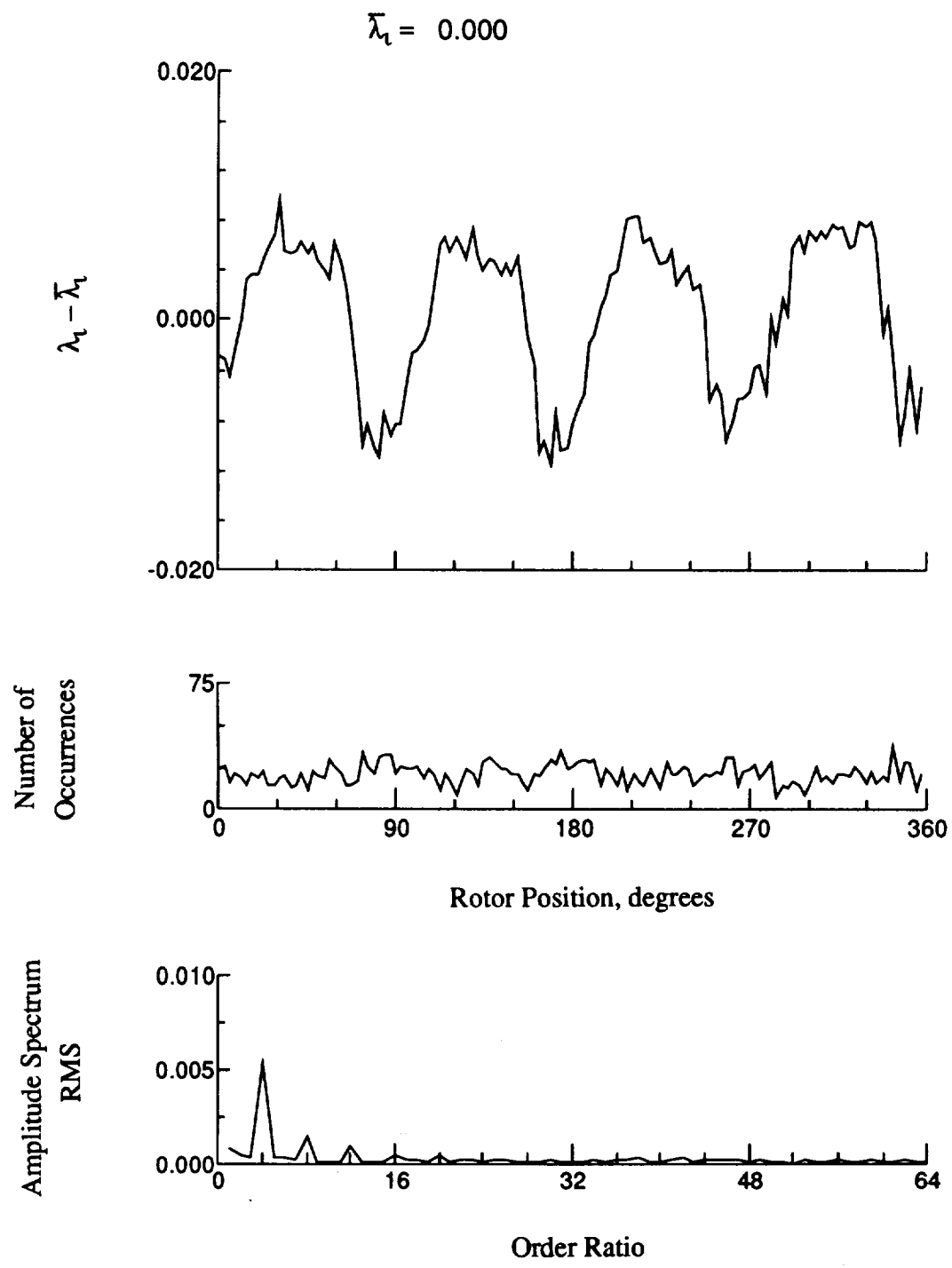


Figure 183.- Concluded.

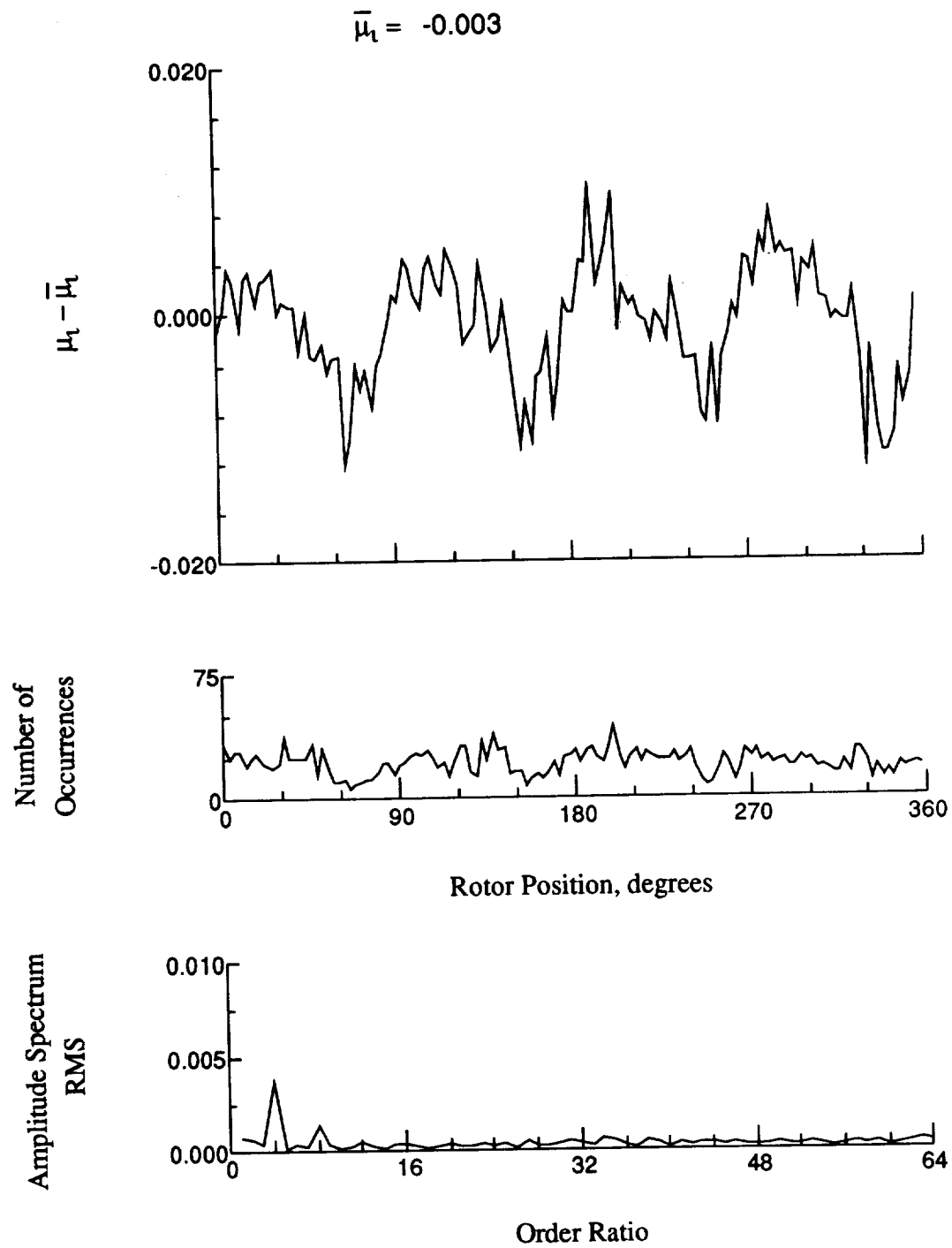


Figure 184.- Induced inflow velocity measured at 330 degrees and r/R of 0.96.

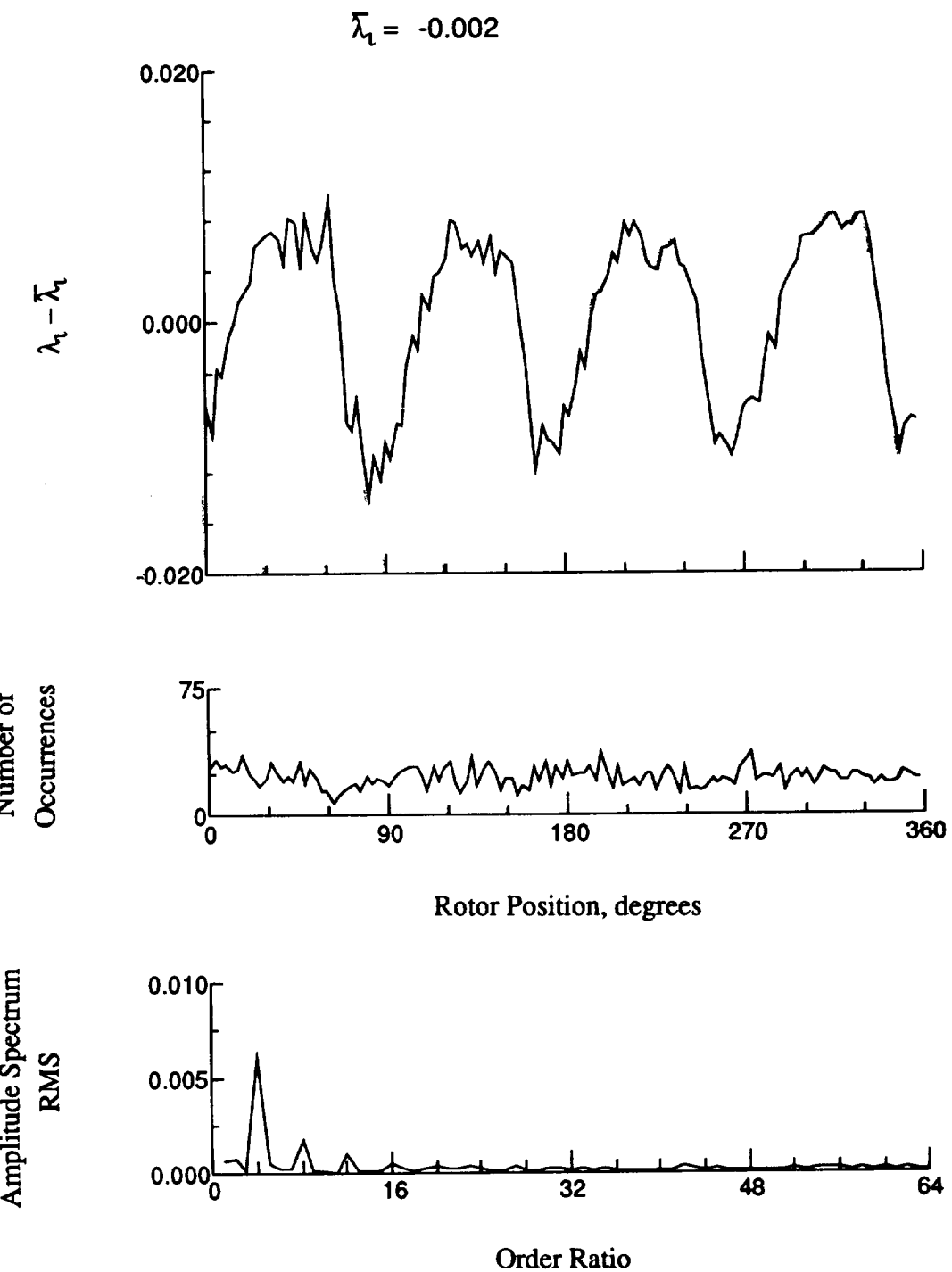


Figure 184.- Concluded.

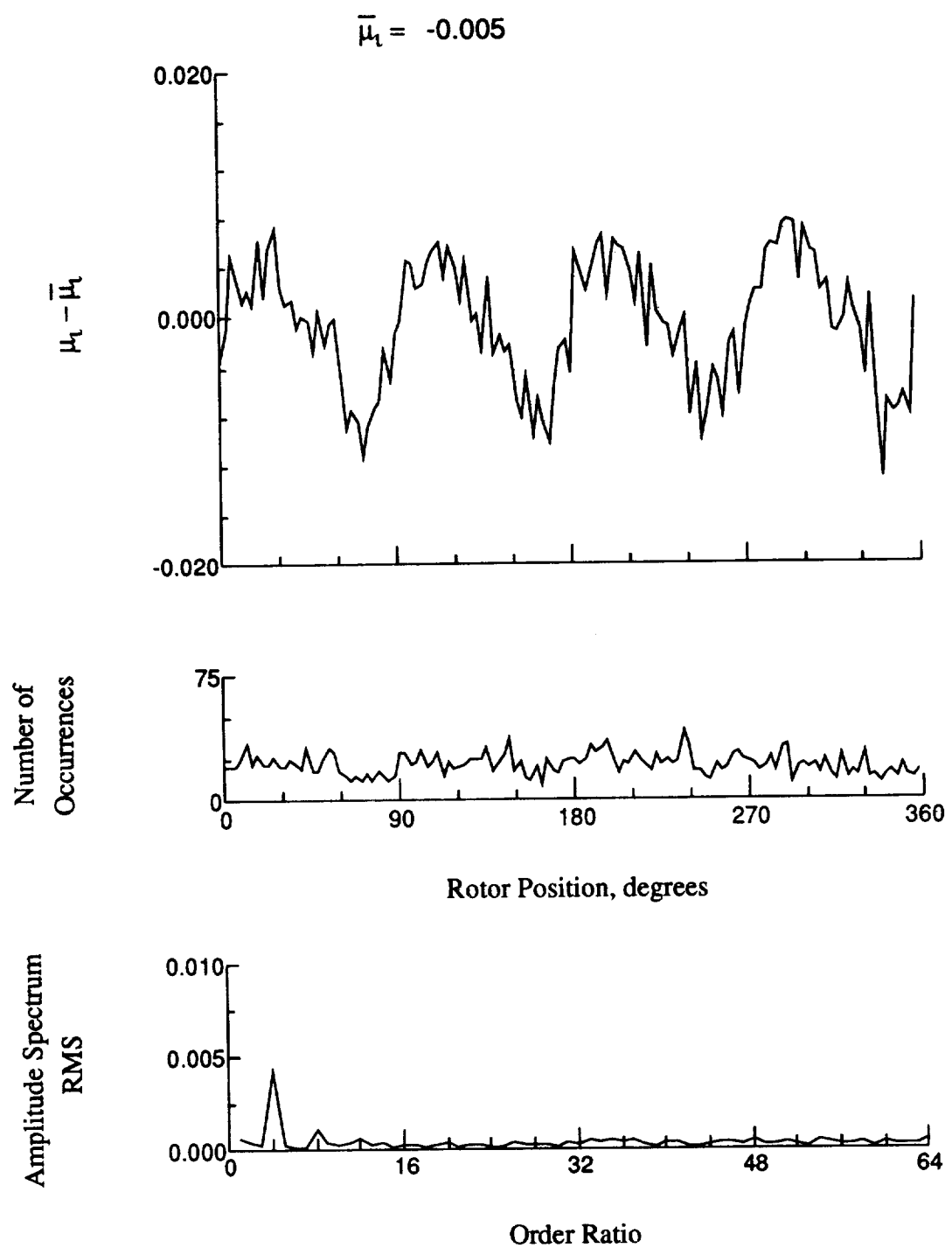


Figure 185.- Induced inflow velocity measured at 330 degrees and r/R of 1.00.

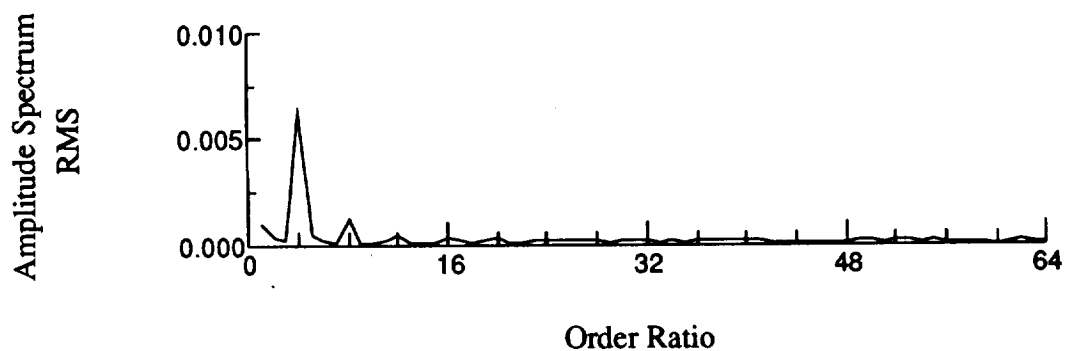
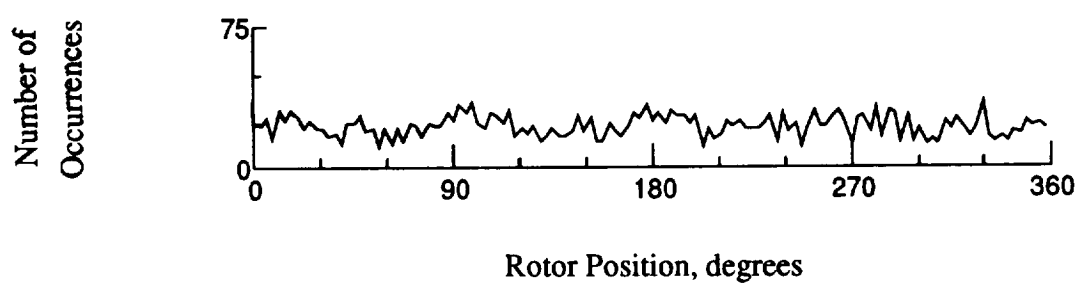
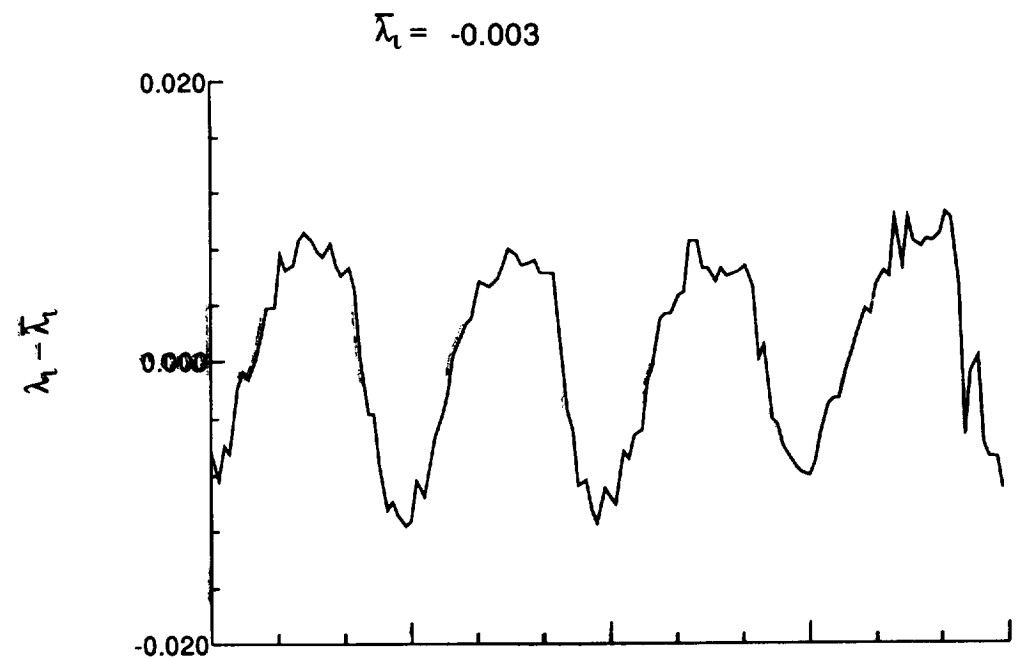


Figure 185.- Concluded.

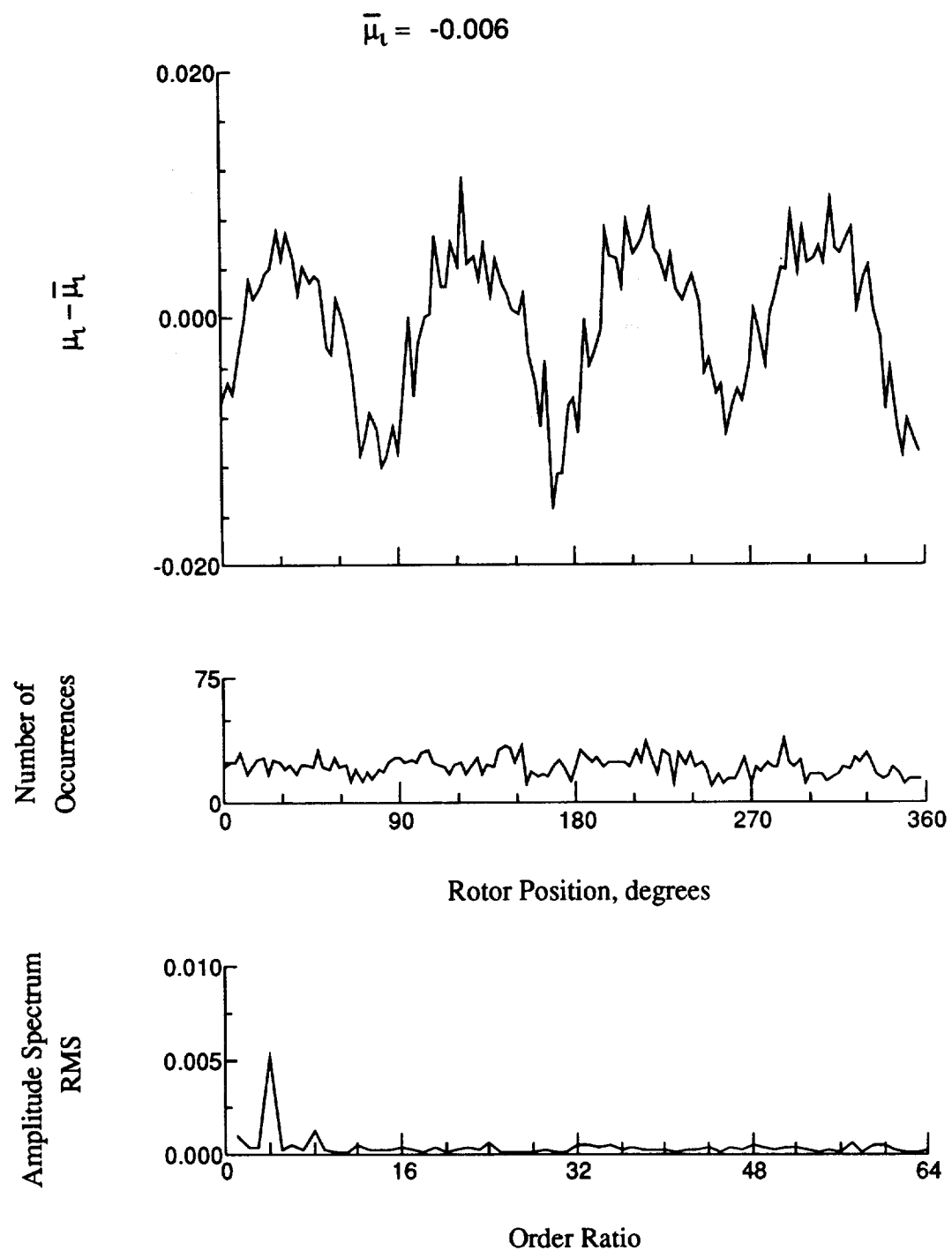


Figure 186.- Induced inflow velocity measured at 330 degrees and r/R of 1.10.

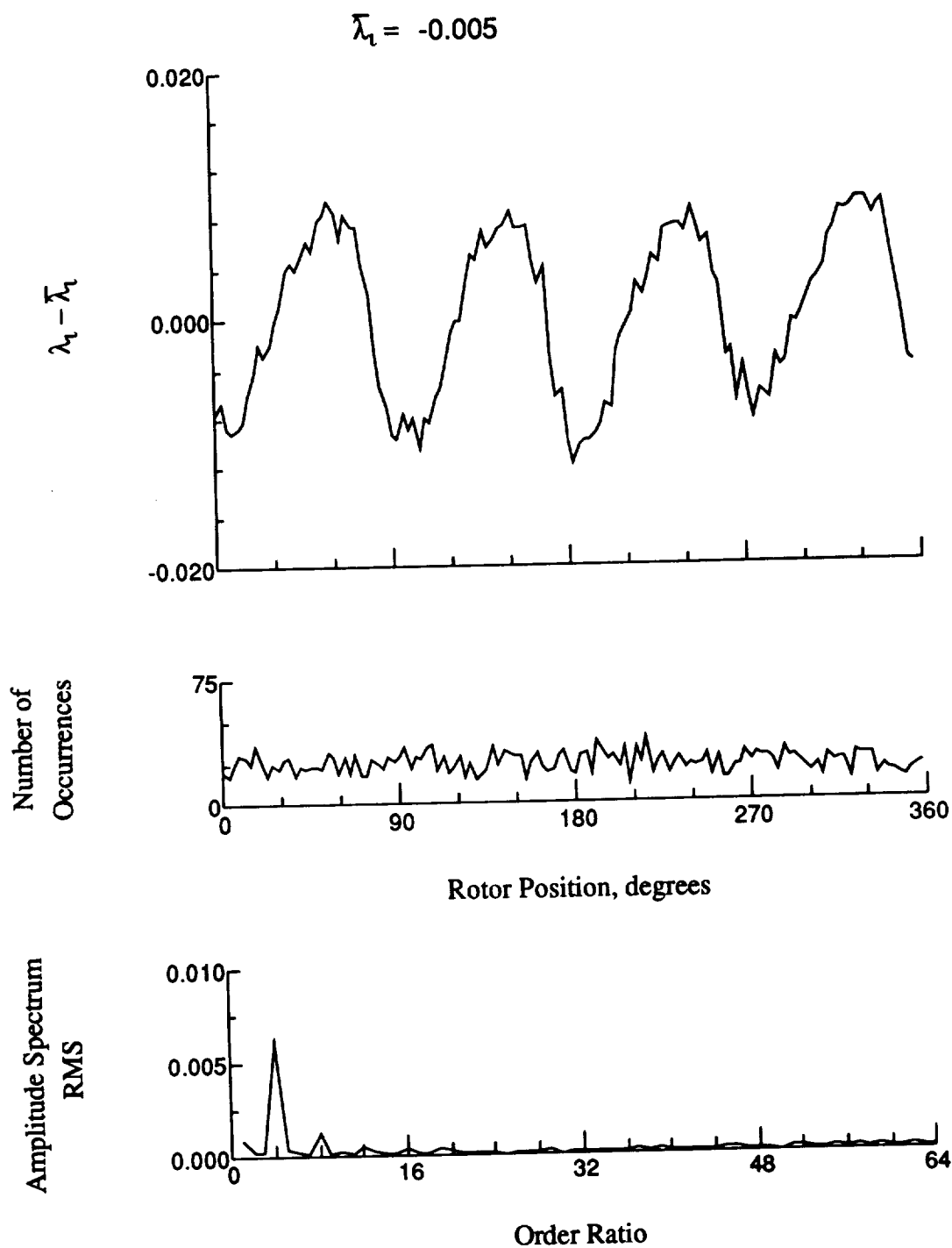


Figure 186.- Concluded.

REPORT DOCUMENTATION PAGE			Form Approved OMB No. 0704-0188
<p>Public reporting burden for this collection of information is estimated to average 1 hour per response, including the time for reviewing instructions, searching existing data sources, gathering and maintaining the data needed, and completing and reviewing the collection of information. Send comments regarding this burden estimate or any other aspect of this collection of information, including suggestions for reducing the burden, to Washington Headquarters Services, Directorate for Information Operations and Reports, 1215 Jefferson Davis Highway, Suite 1204, Arlington, VA 22202-4302, and to the Office of Management and Budget, Paperwork Reduction Project (0704-0188), Washington, DC 20503.</p>			
1. AGENCY USE ONLY (Leave blank)	2. REPORT DATE	3. REPORT TYPE AND DATES COVERED	
	November 1993	Technical Memorandum	
4. TITLE AND SUBTITLE Investigation of the Aerodynamic Environment for an Advanced Lightweight Rotor in Forward Flight. Volume 3: Laser Velocimeter Inflow Data, Advance Ratio of 0.37, Thrust Coefficient of 0.0064 and Hover Tip Speed of 603 Ft/Sec.			5. FUNDING NUMBERS WU 505-59-87-85 PR 1L161102AH45
6. AUTHOR(S) W. Derry Mace, Joe W. Elliott, Martin A. Peryea, Albert G. Brand, and Tom L. Wood			
7. PERFORMING ORGANIZATION NAME(S) AND ADDRESS(ES) NASA Langley Research Center Hampton, VA 23665-5225 and Aeroflightdynamics Directorate - JRPO NASA Langley Research Center Hampton, VA 23681-0001			8. PERFORMING ORGANIZATION REPORT NUMBER
9. SPONSORING / MONITORING AGENCY NAME(S) AND ADDRESS(ES) National Aeronautics and Space Administration Washington, DC 20546-0001 and U. S. Army Aviation and Troop Command St. Louis, MO 63120-1798			10. SPONSORING / MONITORING AGENCY REPORT NUMBER NASA TM-109040, Vol. 3 ATCOM TR-93-A-012, Vol. 3
11. SUPPLEMENTARY NOTES Floppy disks in Microsoft MS-DOS format included with report. Mace: Lockheed Engineering & Sciences Company, Hampton, VA Elliott: Aeroflightdynamics Directorate - JRPO, Langley Research Center, Hampton, VA Peryea, Brand, and Wood: Bell Helicopter Textron Inc., Fort Worth, TX			
12a. DISTRIBUTION / AVAILABILITY STATEMENT Unclassified-Unlimited Subject Category 02		12b. DISTRIBUTION CODE	
13. ABSTRACT (Maximum 200 words) An Advanced Lightweight Rotor (ALR) model was tested in high-speed forward flight, $\mu=0.37$, at the 14- by 22-Foot Subsonic Tunnel at the NASA Langley Research Center. A two-component laser velocimeter was used to obtain azimuthally dependent velocities in the inflow region and in the wake of the rotor. Data are presented here without analysis. To facilitate the use of the data sets, they are also provided on a 1.4 Mbyte 3.5 inch floppy disk in Microsoft Corporation MS-DOS format.			
14. SUBJECT TERMS Rotor model, Induced Inflow Measurements; Laser Velocimetry			15. NUMBER OF PAGES 382
			16. PRICE CODE A17
17. SECURITY CLASSIFICATION OF REPORT Unclassified	18. SECURITY CLASSIFICATION OF THIS PAGE Unclassified	19. SECURITY CLASSIFICATION OF ABSTRACT	20. LIMITATION OF ABSTRACT

NSN 7540-01-280-5500